The Oxidative Capacity of the Atmosphere around the Arabian Peninsula:

Ship-based Atmospheric Measurements of OH and HO_2 Radicals using Laser Induced Fluorescence Spectroscopy

Dissertation

Zur Erlangung des Grades

„Doktor der Naturwissenschaften

Im Promotionsfach Chemie“

Am Fachbereich Chemie, Pharmazie,

Geographie und Geowissenschaften

der Johannes Gutenberg-Universität, Mainz,

ausgeführt am

Max-Planck-Institut für Chemie,

Mainz

Vorgelegt von

Sebastian Manuel Tauer

Geboren in Trier

Mainz, 2022

1. Gutachter: [redacted]

2. Gutachter: [redacted]

Tag der Mündlichen Prüfung:

26.01.2023

Abstract

The oxidative capacity of the atmosphere is largely governed by the radicals OH and HO_2 (HO_x), which are the primary self-cleaning agents of the atmosphere. A measure for the strength of the self-cleaning is the recycling probability of HO_x, that varies strongly with atmospheric composition and temperature. Due to climate change, global temperatures are expected to rise, which will lead to a change in atmospheric composition from increased emissions of biogenic VOC. Coupled with decreasing NO_x emissions from combustion processes, it is important to understand the impact of these changes on the recycling probability and, thus, the oxidative capacity.

To study the oxidative capacity under high temperatures and VOC loading, the **A**ir **Q**uality and Climate Change in the **A**rabian **Ba**sin (AQABA) ship-based field campaign was conducted in the summer of 2017, starting in Toulon, France travelling around the Arabian Peninsula and back. The Arabian Gulf is characterized by intense solar radiation and high ambient temperatures, combined with strong emissions from the exploitation of its rich oil and gas reserves. As a comparison with the cooler and less polluted Mediterranean Sea, the Arabian Gulf can give insight into the impact of rising global temperatures on the recycling probability under conditions of large anthropogenic VOC emissions. The radicals OH and HO_2 were measured by the ground-based *H*ydr*O*xyl *R*adical Measurement *U*nit based on fluorescence *S*pectroscopy (HORUS).

Despite higher primary production in the Arabian Gulf ($2.3\pm0.2 \cdot 10^7$ molec cm^{-3} s^{-1}, Mediterranean Sea: $1.3\pm0.2 \cdot 10^7$ molec cm^{-3} s^{-1}), radical concentrations were lower by a factor of >1.5 and the recycling probability (15±10 % (1σ) @ 0.1 pptv NO) showed values greatly decreased compared to the Mediterranean Sea (57±5 % (1σ) @ 0.1 pptv NO). Box-model calculations, investigating the reason for the reduced recycling probability compared to the Mediterranean Sea, show an increased importance of radical-radical reactions in the Arabian Gulf, due to high concentrations of RO_2 radicals. These reactions can cause radical recycling or destruction. While radical destruction directly decreases the recycling probability through termination of the radical propagation, radical recycling from these reactions caused an indirect decrease, as they could not be included in the calculation.

Throughout the recycling of HO_x in the troposphere, tropospheric O_3 is produced, which causes plant stress and is harmful for the respiratory system of humans and animals. Therefore, the radical recycling probability has a direct impact on the net ozone production rate (NOPR). The NOPR was calculated using, measured NO and HO_2 and calculated RO_2 concentrations. It is expected, that the NOPR has a maximum at the crossover point between its NO_x-limited and VOC-limited regimes. However, no NO concentration was found throughout the AQABA campaign, where the NOPR peaked. Due to this finding, it was concluded that NOPR was NO_x-limited in the marine boundary layer during the whole campaign.

Kurzfassung

Die Oxidationskapazität der Atmosphäre wird größtenteils durch die Radikale OH und HO_2 (HO_x) bestimmt, welche die primären „Reinigungsmittel“ in der Atmosphäre sind. Ein Maß für die Stärke der Selbstreinigungskraft ist die Rezyklierungswahrscheinlichkeit (RZWK) von HO_x, welche abhängig von atmosphärischer Zusammensetzung und Temperatur stark schwanken kann. Durch den Klimawandel werden höhere globale Temperaturen erwartet, was zu einer Veränderung in der Zusammensetzung der Atmosphäre, durch erhöhte Emission von biogenen VOC, führt. Verbunden mit geringeren NO_x Emissionen aus Verbrennungsprozessen, ist es wichtig, den Einfluss dieser Veränderung auf die RZWK und die Oxidationskapazität zu verstehen.

Um die Oxidationskapazität bei hohen Temperaturen und VOC-Belastung zu untersuchen, fand die schiffbasierte **A**ir **Q**uality and Climate Change in the **A**rabian **Ba**sin (AQABA) Messkampagne im Sommer 2017 statt und wurde von Toulon, Frankreich um die Arabische Halbinsel und zurück durchgeführt. Der Arabische Golf wird charakterisiert durch intensive Sonneneinstrahlung und hohe Umgebungstemperaturen, gepaart mit starken Emissionen durch das Erschließen seiner reichen Öl- und Gasvorkommen. Im Vergleich zum kühleren und weniger verschmutzten Mittelmeer, kann der Arabische Golf Einblick auf den Einfluss von steigenden Temperaturen auf die RZWK bei hohen anthropogenen VOC Emissionen geben. Die Radikale OH und HO_2 wurden durch das *H*ydr*O*xyl *R*adical Measurement *U*nit based on fluorescence *S*pectroscopy (HORUS) gemessen.

Trotz hoher Primärproduktion im Arabischen Golf ($2.3\pm0.2 \cdot 10^7$ molec cm^{-3} s^{-1}, Mittelmeer: $1.3\pm0.2 \cdot 10^7$ molec cm^{-3} s^{-1}) waren die Radikalkonzentrationen um einen Faktor >1.5 geringer und die RZWK (15±10 % (1σ) @ 0.1 pptv NO) zeigte deutlich erniedrigte Werte verglichen mit dem Mittelmeer (57±5 % (1σ) @ 0.1 pptv NO). Modellrechnungen, zur Untersuchung der geringeren RZWK im Vergleich zum Mittelmeer, zeigen einen erhöhten Einfluss von Radikal-Radikal-Reaktionen im Arabischen Golf, welche durch hohe RO_2 Konzentrationen verursacht werden. Diese Reaktionen können Radikalrezyklierung und -zerstörung verursachen. Während Radikalzerstörung die RZWK durch Radikalkettenabbruch direkt verringert, kann Radikalrezyklierung dies durch diese Reaktionen indirekt, da sie in der Berechnung der RZWK nicht berücksichtigt werden konnten.

Während des Rezyklierens von HO_x in der Troposphäre kann troposphärisches O_3 produziert werden, welches Stress in Pflanzen hervorruft und für die Atmungsorgane von Menschen und Tieren schädlich ist. Dadurch hat die RZWK einen direkten Einfluss auf die Netto-Ozon-Produktionsrate NOPR. Die NOPR wurde mithilfe von NO und HO_2 Messungen und berechneten RO_2 Konzentrationen bestimmt. Es wird erwartet, dass die NOPR ein Maximum am Übergangspunkt zwischen NO_x-limitiertem und VOC-limitierten Regime aufweist. Während AQABA konnte allerdings keine NO Konzentration gefunden werden, bei der NOPR ein Maximum erreicht. Daraus folgt, dass NOPR während der gesamten Kampagne NO_x-limitiert war.

Contents

List of Tables

List of Figures

1 The Atmosphere

1.1 The oxidative capacity of the atmosphere

Earth's Atmosphere is mainly comprised of Nitrogen (~78 %), Oxygen (~21 %) and a variable amount of water (~ 0 - 2 %). Its chemical and physical properties are highly influenced by the remaining less than 1 % of trace gases (e.g. Ozone (O_3), Methane (CH_4), Carbon dioxide (CO_2)).

Gas	Molecular Weight	Average Mixing Ratio (ppm)	Cycle
Ar	39.948	9340	No cycle
Ne	20.179	18	
Kr	83.80	1.1	
Xe	131.30	0.09	
N_2	28.013	780,840	Biological and microbiological
O_2	32	209,460	
CH_4	16.043	1.72	Biogenic and chemical
CO_2	44.010	355	Anthropogenic and biogenic
CO	28.010	0.12 (NH) 0.06 (SH)	Anthropogenic and chemical
H_2	2.016	0.58	Biogenic and chemical
N_2O	44.012	0.311	Biogenic and chemical
SO_2	64.06	10^{-5}–10^{-4}	Anthropogenic, biogenic, chemical
NH_3	17	10^{-4}–10^{-3}	Biogenic and chemical
NO	30.006	10^{-6}–10^{-2}	Anthropogenic, biogenic, chemical
NO_2	46.006		
O_3	48	10^{-2}–10^{-1}	Chemical
H_2O	18.015	Variable	Physicochemical
He	4.003	5.2	

Figure 1.1 Composition of the Atmosphere, taken from Seinfeld (1998)

These trace gases are continuously emitted by or secondary products of biogenic, anthropogenic and geological processes (Seinfeld, 1998). Figure 1.1 gives an overview of atmospheric trace gases. Many trace gases can impact ecological and human health. Pollution is a leading cause of excess human mortality and lower life expectancy (Jos Lelieveld et al., 2020) and with expected increasing emissions on the African continent (Liousse, Assamoi, Criqui, Granier, & Rosset, 2014) and the Indian subcontinent (Ghude et al., 2013; Krotkov et al., 2016; Umezawa et al., 2018), this phenomenon is likely to become more and more prevalent. Without the property of cleaning by oxidative processes, trace gases would increase in atmospheric concentration to levels toxic to life. Through oxidative processes trace gases are successively oxidized to less toxic gases (e.g. CO_2, H_2O)

or polar or water soluble species (e.g. H_2SO_4, HNO_3), which in turn are removed from the atmosphere via dry or wet deposition. The most important oxidant in the atmosphere during daytime is the hydroxyl radical (OH), with ozone (O_3) and hydrogen peroxide (H_2O_2) having minor contributions to the oxidative capacity. The nitrate radical (NO_3) is due to its photo lability only important during nighttime oxidation. Even though with typical lifetimes of less than a second and average daytime concentrations in the sub pptv area, OH has the highest impact on atmospheric cleansing, due to its high reactivity towards many chemical species. This importance makes OH chemistry essential for understanding and predicting atmospheric chemistry as a whole. Closely related to OH is the hydroperoxyl radical (HO_2), which is a product of many reactions of OH with trace gases. HO_2 can reform OH through reaction with e.g. NO and O_3. This ability together with its much longer lifetime of ~ 100 s, HO_2 can act as reservoir for OH. Due to the fast turnover rate between OH and HO_2, the sum of both is known as HO_x.

A shift in the chemical make-up of the atmosphere due to environmental changes, such as urbanization or deforestation could have a significant impact on the cleansing capacity of the atmosphere. Despite these changes, global OH concentrations remained stable around 10^6 molecules/cm^3 during the past century (J. Lelieveld, Peters, Dentener, & Krol, 2002). This indicates a buffering system capable of stabilizing OH concentrations even though pollutants and therefore OH reactivity is high. Nevertheless, due to climate change, environmental changes might become more severe. Higher temperatures can induce stress in plants, which influences emission strength of monoterpenes and isoprene (Kesselmeier & Staudt, 1999), leading to changing volatile organic compound (VOC) composition as well as higher VOC concentrations. Coupled with reducing NO_x emissions due to more strict governmental emission guidelines, HO_x concentrations could be reduced through lower recycling production and increased loss from reaction with VOC (J. Lelieveld et al., 2002; Prinn, 2003). In addition, increasing temperatures are leading to changes in the water cycle, with generally lower relative humidity (RH) over land (IPCC et al., 2018), leading to a higher dust particle load in the atmosphere, potentially having an impact on HO_x concentrations.

1.2 Marine Boundary Layer

The lower troposphere is in close contact with the planetary surface. To a height of 1 – 5 km, roughness of the surface and thermal updrafts cause turbulent transport and mixing. This allows a separation of the troposphere in two distinct parts: the planetary boundary layer (PBL) and the free troposphere (FT). Figure 1.2 shows a schematic overview of the troposphere with PBL and FT (Möller, 2003). The PBL height can vary

from a few meters and 5 km, depending on location and time of year or day. The PBL itself can also be categorized in two distinct regions. The continental PBL (CBL) and the marine PBL (MBL). Since approx. 70% of earth's surface is covered in water, the MBL is a major part of the lower troposphere. With the oceans directly influencing the MBL, large amounts of heat and moisture are exchanged between ocean and atmosphere (Fairall, Bradley, Rogers, Edson, & Young, 1996). Additionally, phytoplankton are sources for biogenic VOC and dimethyl sulfide (DMS) (Millet et al., 2008; Moore, Oram, & Penkett, 1994; Shaw, Chisholm, & Prinn, 2003). Oxidation of VOCs or DMS can form secondary organic aerosols (SOA) and sulfate respectively, and in turn can lead to cloud condensation, influencing earth's radiative budget.

A strong interaction between CBL and MBL can be found in coastal areas. Due to temperature differences between land and sea, often times airmasses travel from land to sea. These air masses can introduce an immense amount of emissions in the MBL, originating on land. With approx. 40% of world's population living within 100 km of the coast, it is vital to get a closer understanding of processes in this special environment.

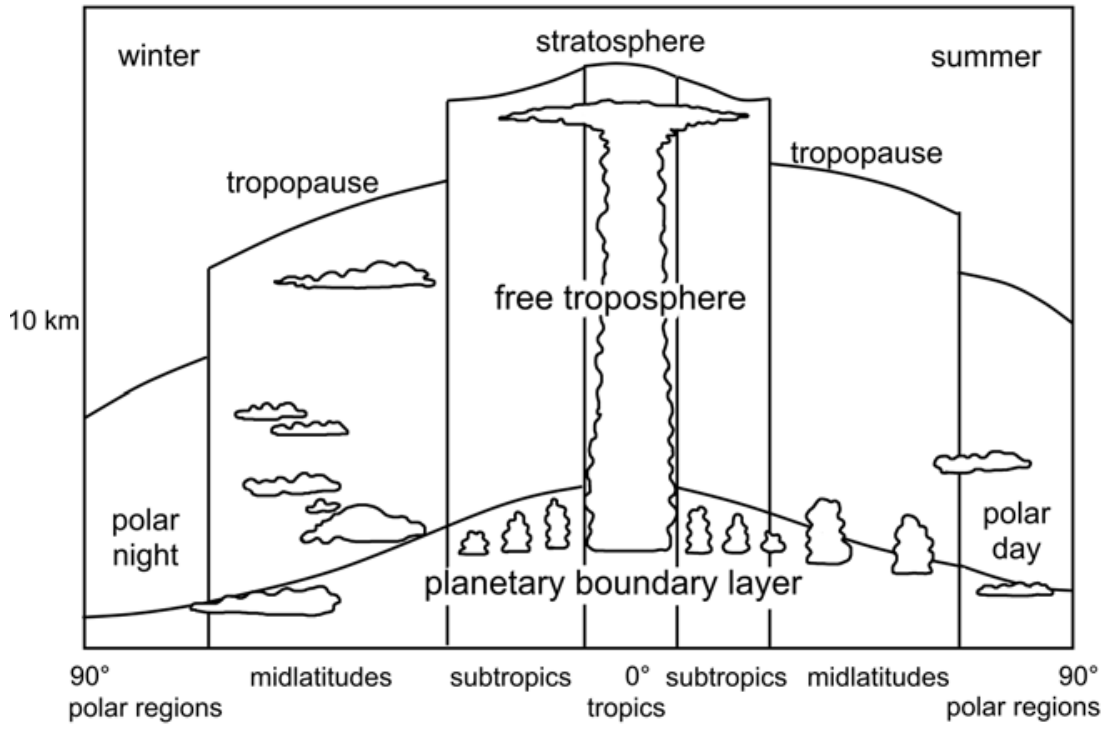

Figure 1.2 Schematic overview of the troposphere, taken from Möller (2003)

1.3 Hydroxyl- and Hydroperoxyl radical chemistry in the troposphere

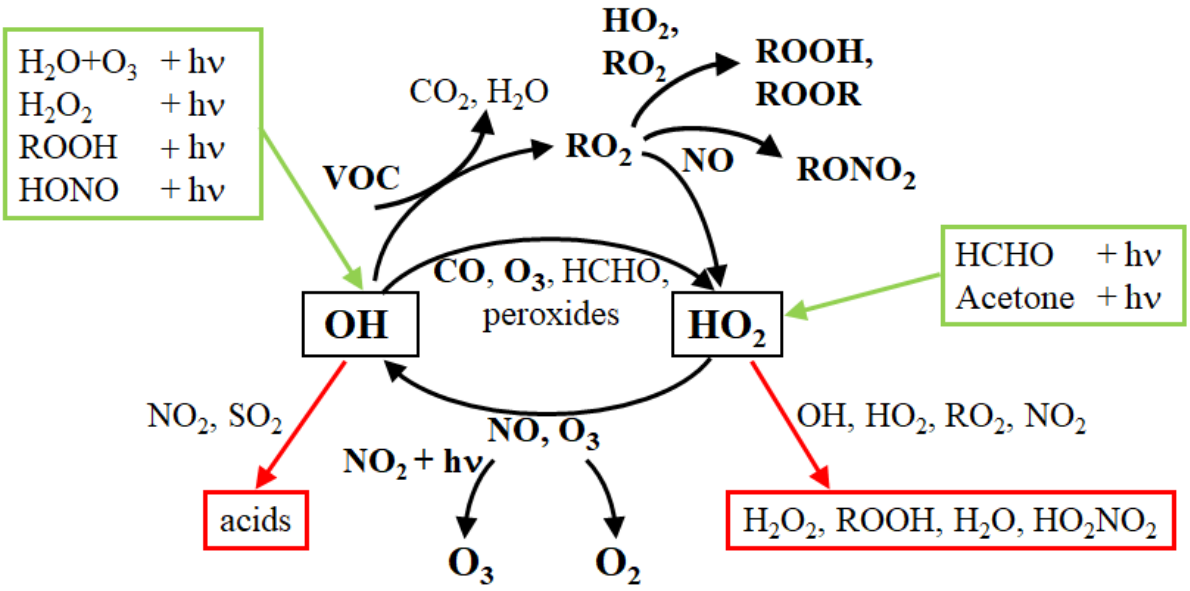

Figure 1.3 Simplified schematic of HO_x chemistry. Radical production (green), recycling (black) and loss (red) are indicated by arrows.

As the most important oxidant in the atmosphere during daytime, OH is at the center of a large amount of atmospheric reactions. Figure 1.3 shows a simplified schematic of the chemistry of OH and HO_2. In the lower troposphere, HO_x radicals are produced photochemically from precursor species, e.g. $O(^1D)$, H_2O_2, HONO. Via the reaction of OH with CO or O_3 and the reaction of HO_2 with NO and O_3, both HO_x species interchange within minutes and are in an equilibrium with each other (Levy, 1971). Additionally, reaction with most VOC lead to formation of organic peroxy radicals (RO_2), which can react with NO to form HO_2 or organic nitrates. While the former contributes to recycling of radicals, the latter leads to loss of radicals. Other loss processes of HO_x include reaction with NO_2 and NO, forming HNO_3 and HONO respectively, as well as recombination reactions with OH, HO_2 or RO_2, forming organic peroxide, H_2O_2 and water. Sources, sinks and recycling of HO_x will be discussed in more detail in the following chapter.

1.3.1 HO_x sources

The main source of OH in the lower, remote troposphere is the photolysis of O_3 (R.1a), producing an excited oxygen atom $O(^1D)$ and O_2. The majority of $O(^1D)$ will lose their excitation by reacting with O_2 and N_2, returning to ground state $O(^3P)$ (R.1b) and reforming O_3 (R.1c). The remaining $O(^1D)$ atoms react with water forming OH (R.1d). At 1 % water vapor content and 298 K this fraction is about 14 % (R. Atkinson et al., 2004).

$$O_3 + h\nu \rightarrow O_2 + O(^1D) \quad \text{(R.1a)}$$
$$O(^1D) + M \rightarrow O(^3P) + M \quad M=N_2, O_2 \quad \text{(R.1b)}$$
$$O(^3P) + O_2 + M \rightarrow O_3 + M \quad \text{(R.1c)}$$
$$O(^1D) + H_2O \rightarrow 2OH \quad \text{(R.1d)}$$

Since this source of OH is highly dependent on water vapor concentration, in regions with low water concentrations other sources of HO_x can be important. The photolysis of hydroperoxide and organic peroxides (R.2 & R.3) can be important especially in the upper troposphere, where water content in the atmosphere is reduced.

$$H_2O_2 + h\nu \rightarrow 2OH \quad \text{(R.2)}$$
$$ROOH + h\nu \rightarrow OH + RO \quad \text{(R.3)}$$

The photolysis of HONO often contributes to the production of OH during early morning hours (R.4). After accumulating during the night, HONO will decompose forming OH even before HO_x production via ozone photolysis starts (Hofzumahaus et al., 2009).

$$HONO + h\nu \rightarrow OH + NO \quad \text{(R.4)}$$
$$\text{Alkene} + O_3 \rightarrow OH + \text{products} \quad \text{(R.5)}$$

A non-photolytic source of OH is the ozonolysis of alkenes (R.5). During the reaction a Criegee Intermediate is formed, which can release OH during decomposition (Criegee, 1975).

$$HCHO + h\nu + 2O_2 \rightarrow 2HO_2 + CO \quad \text{(R.6)}$$

The major primary source of HO_2 in the atmosphere is the photolysis of Formaldehyde (HCHO).

1.3.2 HOx recycling

OH and HO_2 form an equilibrium with each other, through several recycling reactions. The most prevalent HO_2 production is via the reaction of OH with CO and O_2, forming CO_2 and HO_2 (R.7). Other channels, which produce HO_2 by reacting with OH are O_3, HCHO, H_2O_2 and SO_2 (R.8 - 11).

$$OH + CO + O_2 \rightarrow HO_2 + CO_2 \quad \text{(R.7)}$$
$$OH + O_3 \rightarrow HO_2 + O_2 \quad \text{(R.8)}$$
$$OH + HCHO + O_2 \rightarrow HO_2 + H_2O + CO \quad \text{(R.9)}$$
$$OH + H_2O_2 \rightarrow HO_2 + H_2O \quad \text{(R.10)}$$
$$OH + SO_2 + O_2 + H_2O \rightarrow HO_2 + H_2SO_4 \quad \text{(R.11)}$$

In turn, HO_2 can recycle to OH by the reaction with NO or O_3 (R.12 & 13).

$$HO_2 + O_3 \rightarrow OH + 2O_2 \quad \text{(R.12)}$$
$$HO_2 + NO \rightarrow OH + NO_2 \quad \text{(R.13)}$$

Another pathway to form HO_2 from OH is through the oxidation of VOC by OH (R.14). The forming organic peroxy radical (RO_2) can react with NO forming an alkoxy radical (RO) (R.15), which can produce HO_2 and an aldehyde (RCHO) through reaction with O_2 (R.16). RO_2 chemistry is described in further detail in 1.4.

$$RCH_3 + OH + O_2 \rightarrow RCH_2O_2 + H_2O \quad \text{(R.14)}$$
$$RCH_2O_2 + NO \rightarrow RCH_2O + NO_2 \quad \text{(R.15)}$$
$$RCH_2O + O_2 \rightarrow RCHO + HO_2 \quad \text{(R.16)}$$

where R denotes an organic group.

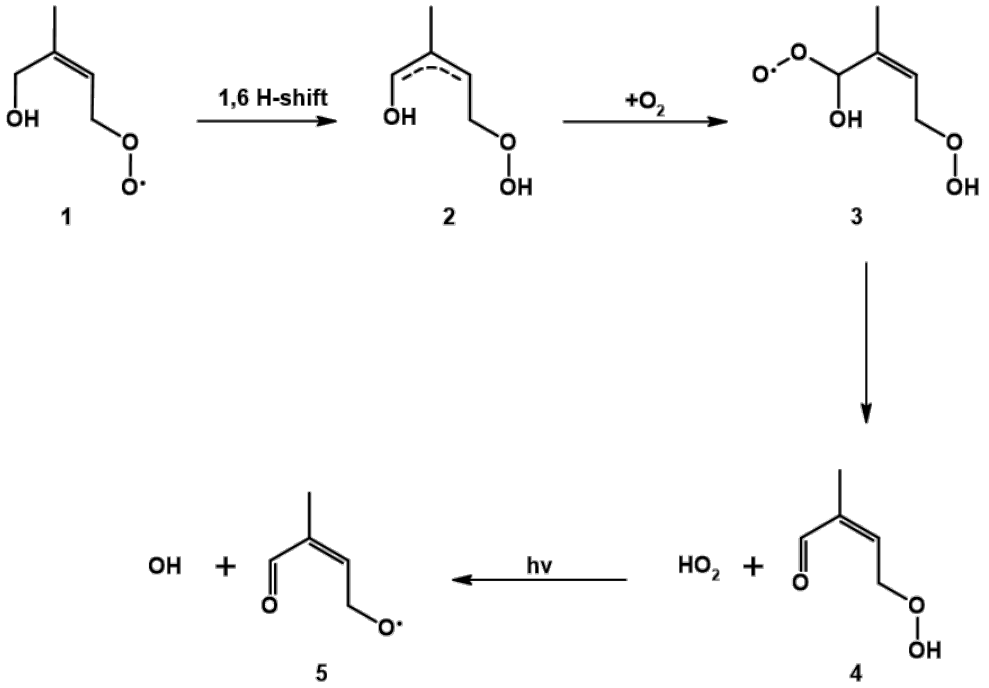

Figure 1.4 Recycling mechanism of RO_2 formed from isoprene under low-NO conditions. Different reaction pathways were omitted for simplicity and can be found in Peeters, Müller, Stavrakou, and Nguyen (2014)

Additionally, Peeters et al. (2014) reported a mechanism for OH recycling for isoprene oxidation (Figure 1.4). A produced Z-δ-hydroxy isoprenyl peroxy radical **1** can undergo a 1,6-H-shift to form an allylic hydroxy hydroperoxide **2**. Through addition of O_2, followed by fast unimolecular decomposition, a hydroperoxy aldehyde **4** (HPALD) is formed. Fast photolysis of HPALD reforms OH. This mechanism is relevant under very low-NO conditions.

1.3.3 HO_x sinks

The main sink of HO_x are radical self- or cross-reactions (R.17 - 19) producing peroxides or water and O_2.

$$HO_2 + HO_2 \rightarrow H_2O_2 + O_2 \quad \text{(R.17)}$$
$$HO_2 + RO_2 \rightarrow ROOH + O_2 \quad \text{(R.18)}$$
$$OH + HO_2 \rightarrow H_2O + O_2 \quad \text{(R.19)}$$

Another potential sink for HO_x are the formation of acids (R.20 - 22).

$$OH + NO + M \rightarrow HONO + M \quad \text{(R.20)}$$
$$OH + NO_2 + M \rightarrow HNO_3 + M \quad \text{(R.21)}$$
$$HO_2 + NO_2 + M \rightarrow HNO_4 + M \quad \text{(R.22)}$$

As mentioned above, photolysis of peroxides and HONO can lead to production of radicals, however a considerable portion of peroxides and acids is lost from the radical cycle through dry and wet deposition processes.

1.4 Organic peroxy radicals

1.4.1 Production

Organic peroxy radicals play a major role in the HO_x cycle (see 1.3.2). As mentioned above, the reaction of OH with VOC leads to the production of RO_2. The reaction pathway can be separated into two distinct groups. Alkanes and other saturated VOCs react with OH by H abstraction forming alkyl radicals, which react with oxygen to alkyl peroxy radicals (R.23 - 24). Unsaturated VOCs can react quickly by addition of OH with subsequent addition of oxygen to form β-hydroxy peroxy radicals (R.25 - 26) (R. Atkinson & Arey, 2003).

$$RCH_2R' + OH \rightarrow RCHR' + H_2O \quad \text{(R.23)}$$
$$RCHR' + O_2 \rightarrow RCHO_2R' \quad \text{(R.24)}$$
$$RCH = CHR' + OH \rightarrow RCH - CHOHR' \quad \text{(R.25)}$$
$$RCH - CHOHR' + O_2 \rightarrow RCHO_2 - CHOHR' \quad \text{(R.26)}$$

The production of RO_2 through OH oxidation of aromatics differs from the simple reactions of alkanes and alkenes. The oxidation mechanism of benzene is shown in Figure 1.5. Initial addition of OH forming alkyl radical **1**, which can react with O_2 either by H-abstraction forming phenol **2** or by addition forming a peroxy radical. The peroxy radical can produce phenol via an elimination reaction (~53 %) or form a bicyclic alkyl radical **3** through intramolecular (~47 %) (Xu, Møller, Crounse, Kjaergaard, & Wennberg, 2020). A small

amount of **3** (~1 %) can form a bicyclic epoxy alkoxy radical **5** via isomerization, however the reaction with O_2 dominates, forming a bicyclic peroxy radical **4**.

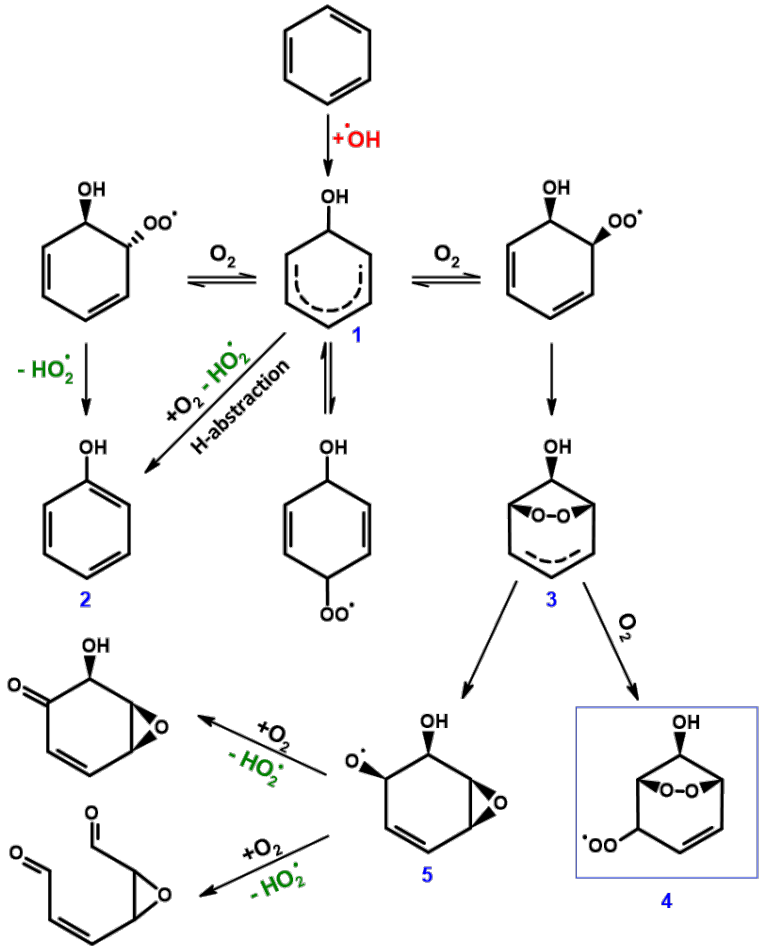

Figure 1.5 Production of RO_2 through oxidation of benzene. Taken and modified from Kunkler (2021).

Additionally, nitrate radicals can react with unsaturated VOC via addition, forming RO_2 (R.27 – 28) (Wayne et al., 1991).

$$RCH = CHR' + NO_3 \rightarrow RCH - CHNO_3R' \quad \text{(R.27)}$$

$$RCH - CHNO_3R' + O_2 \rightarrow RCHO_2 - CHNO_3R' \quad \text{(R.28)}$$

1.4.2 Loss

As mentioned in 1.3.2, RO_2 can be part of the HO_x cycle via the reaction with NO to reform HO_2 (R.14 - 16) and for RO_2 from isoprene via 1,6-H-shift. Depending on the production pathway reaction with NO can be followed by different reactions. Figure 1.6 shows the reaction scheme of RO_2 produced from saturated (left) and unsaturated VOCs (right) (Fuchs et al., 2011). Reaction of RO_2 from saturated VOC with NO forming alkoxy radicals is followed by H abstraction by oxygen producing HO_2 and a carbonyl compound. The

reaction of RO_2 from unsaturated VOC with NO is followed by unimolecular decomposition of the produced β-hydroxy alkoxy radical, forming a carbonyl compound and a hydroxy alkyl radical, which can rapidly react with oxygen forming another carbonyl compound and HO_2. Under atmospheric conditions, the reaction with NO is the rate-determining step for both types of RO_2.

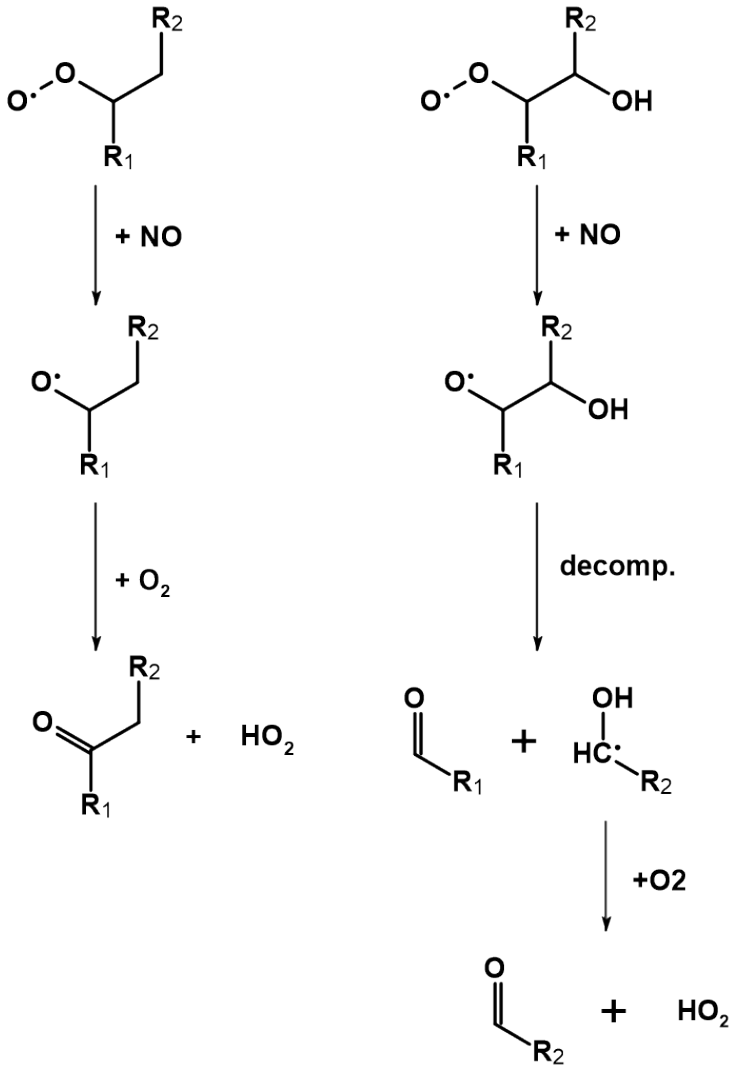

Figure 1.6 Reaction scheme of alkyl peroxy radical (left) and β-hydroxy alkyl peroxy radical (right). (taken and modified from Fuchs et al. (2011))

The reaction of RO_2 with NO has a second competing reaction branch. Instead of abstraction of an oxygen atom, NO can add to RO_2 to form an organic nitrate (R.29), leading to loss of radicals through this channel. The branching ratio of both reactions are dependent on the type of RO_2, with increasing chance of forming nitrate with higher number of atoms (excluding hydrogen) (Wennberg et al., 2018). Another loss process of RO_2 is the reaction with other radicals (R.18 & 30). These reactions remove two radicals form the HO_x cycle.

$$RO_2 + NO + M \rightarrow RONO_2 + M \quad \text{(R.29)}$$
$$RO_2 + R'O_2 \rightarrow \text{products} \quad \text{(R.30)}$$

1.5 Ozone production

Both OH and HO_2 play an important role in the production of tropospheric ozone. O_3 is mainly formed through the photochemical cycle of NO and NO_2 (R.31 - R.33).

$$NO_2 + h\nu \rightarrow NO + O(^3P) \quad \text{(R.31)}$$
$$O(^3P) + O_2 + M \rightarrow O_3 + M \quad \text{(R.32)}$$
$$O_3 + NO \rightarrow NO_2 + O_2 \quad \text{(R.33)}$$

This represents a "null-cycle", where net ozone production (NOP) is zero. However, NO can also be oxidized by HO_2 (R.13) and RO_2 (R.15), thus forming NO_2 without loss of O_3, which in turn leads to a O_3 production. If this production exceeds the loss through photolysis (R.1a), reaction with OH (R.8) and reaction with HO_2 (R.12), O_3 is produced and increases in concentration. At low NO_x mixing ratios, the formation of peroxides (R.17, R.18 & R.30) or recycling through ozone (R.12) dominates. Net ozone production rate (NOPR) in this regime is NO_x-limited. Increasing NO_x mixing ratios favor R.13 and R.15, thus increasing NOPR. With NO_x mixing ratios increasing further, the production of HNO_3 from OH and NO_2 (R.21) and production of organic nitrates (R.29) causes loss of HO_x and thus decreasing NOPR. NOPR in this regime is NO_x-saturated or VOC-limited. Figure 1.7 shows OH concentrations and NOPR as a function of NO_x mixing ratio. High NOPR can cause an accumulation of tropospheric O_3 to higher levels, which in turn are known to induce plant stress and can harm respiratory health in both animals and humans (Nuvolone, Petri, & Voller, 2018).

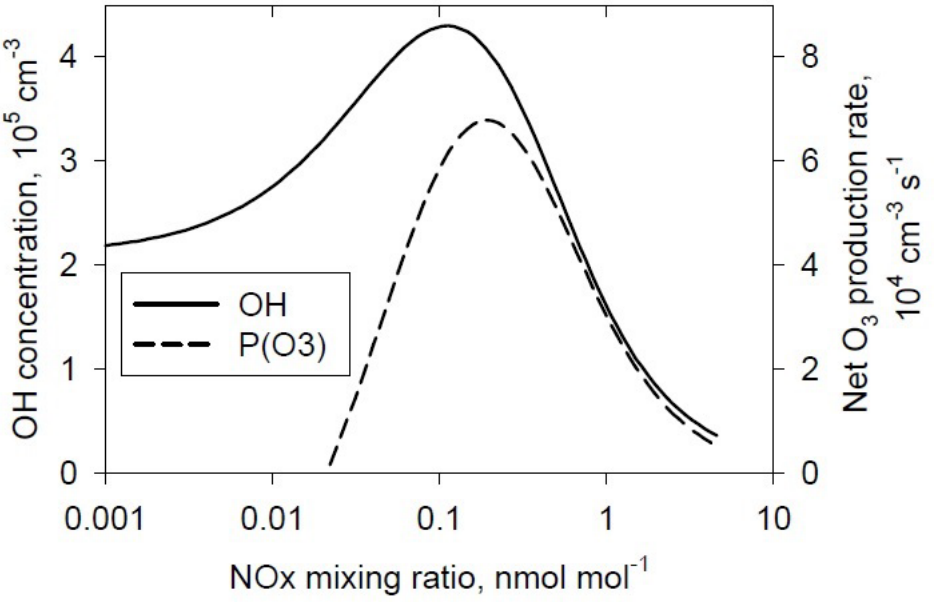

Figure 1.7 OH concentrations (solid line) and net ozone production rate (dashed line) as a function of NO mixing ratio. Taken from Schumann and Huntrieser (2007)

2 HO_x measurement techniques and the HORUS instrument

2.1 OH Measurement techniques

Due to its high reactivity towards many atmospheric trace gases, OH atmospheric lifetimes are typically shorter than one second. This makes measurements of OH rather difficult, since wall losses have to be minimized and a fast detection is required. In addition, low OH concentrations between $10^5 - 10^7$ molec/cm^3 cause the need for highly sensitive instrumentation. Three widely used techniques are: differential optical absorption spectroscopy (DOAS) via direct absorption by OH (Perner et al., 1987), chemical ionization mass spectrometry (CIMS) via detection of H_2SO_4 after oxidation of SO_2 by atmospheric OH (Eisele & Tanner, 1991), and by laser-induced fluorescence of OH molecules based on fluorescence assay by gas expansion (LIF-FAGE) via the detection of OH fluorescence after laser excitation (Hard, O'Brien, Chan, & Mehrabzadeh, 1984). DOAS uses wave-length dependent absorption of light following Lambert-Beer law to directly measure OH concentration. Its uncertainty is mostly dependent on the uncertainty of the absorption cross section of OH, and its limit of detection is affected by the pathlength of the light, scattering by aerosols, and absorption due to other trace gases. As an absolute measurement technique, it does not require calibration. CIMS measures OH indirectly after conversion of $^{34}SO_2$ into $H_2{}^{34}SO_4$. H_2SO_4 is ionized by NO_3^- through a charge-transfer reaction and the ratio of HSO_4^-/HNO_3 is measured by a mass spectrometer. Since the isotope ^{34}S makes up only about 4 % of the naturally occurring sulfur, atmospheric H_2SO_4 can be distinguished from in the sample air.

2.1.1 LIF FAGE

The first report of OH excited by a tunable laser source and successfully detecting the resulting fluorescence was by C. C. Wang and Davis (1974). OH radicals can be selectively excited by UV light with a wavelength of 282.58 nm which is in resonance with the $P_1(2)$ line within the $A^2\Sigma^+ - X^2\Pi$, $v'=1 \leftarrow v''=0$ transitions of OH. The relaxation to ground state occurs via rotationally and vibrationally excited states with fluorescence in the wavelength range of 307-315 nm (C. C. Wang & Davis, 1974) with a lifetime of around 700 ns. However, at atmospheric pressure, most of the excited OH molecules lose their energy by collision quenching with other molecules, leading to a collision lifetime of ~1 ns (Heard & Pilling, 2003). Additionally, laser scatter on aerosols, other molecules in the sample air and walls within the instrument cause large background signal, which together with poor fluorescence yield lead to a detection limit of only 5 x10^6 molec/cm^3 (C. C. Wang & Davis, 1974). Further limitations of measurements of OH by LIF as reported by C. C. Wang and Davis (1974) are photodissociation of O_3 caused by laser radiation at 282 nm, yielding $O(^1D)$ atoms. Subsequent reaction of $O(^1D)$ with atmospheric water vapor leads to

formation of OH radicals analog to R.1.1d, causing the laser radiation itself to be a source of OH (Ortgies, Gericke, & Comes, 1980).

The introduction of the fluorescence assay by gas expansion (FAGE) technique led to a significant improvement in the measurements of OH using LIF. By lowering the pressure inside the detection chamber to ~1 – 5 mbar, both disadvantages of LIF as described above can be reduced. Lower pressure reduces the number density of H_2O and O_3, thus decreasing the amount of laser-generated OH (Hard et al., 1984). Even though lower pressure also lowers the number density of detectable OH and increases wall losses due to longer mean free path for molecules within the detection chamber, the OH fluorescence yield is strongly increased due to decreasing collision quenching. Figure 2.1 shows an overview of the combined effects on detection sensitivity.

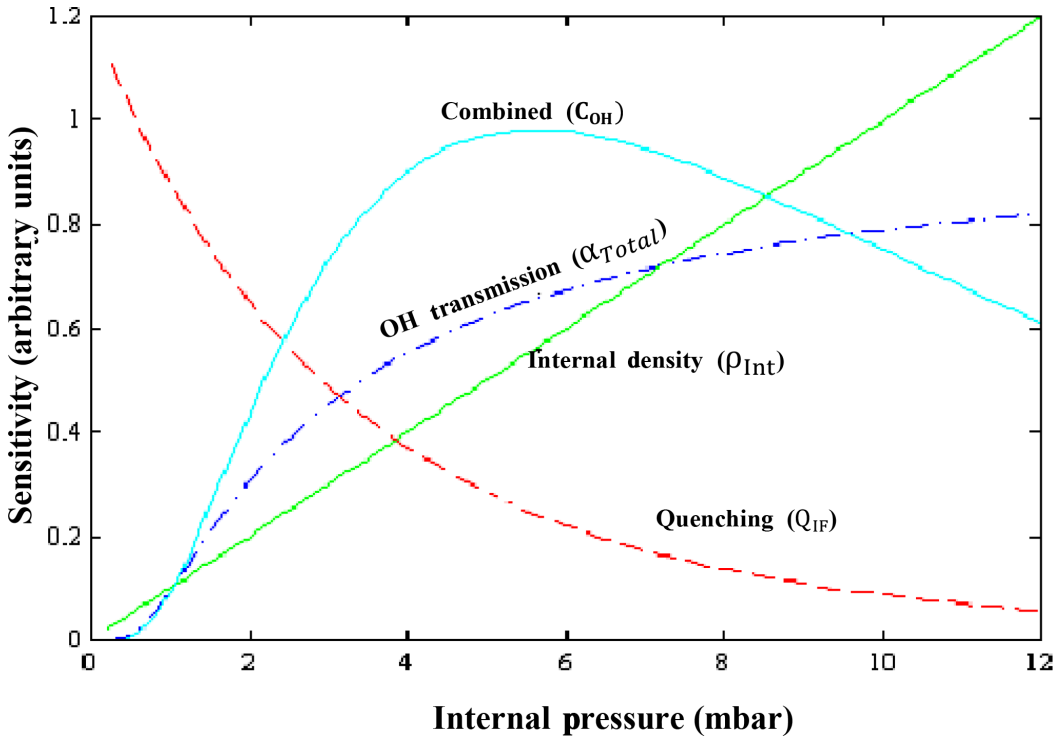

Figure 2.1 Schematic view of the pressure-dependent LIF-FAGE sensitivity as a function of internal pressure (light blue line), OH transmission (dotted-dashed dark blue line), internal density (green line) and quenching (dashed red line). (modified version of Faloona et al. (2004), taken from Marno et al. (2020)).

Further improvements were made to reduce background signals, such as installing baffles and black anodizing the internal walls in order to reduce scatter from internal reflections. To minimize the impact of fluorescence from aerosols and other molecules in the sample air, electronic detector gating times were introduced (Creasey, Halford-Maw, Heard, Spence, & Whitaker, 1998; Hard et al., 1984; Stevens, Mather, & Brune, 1994). During the laser pulse, the detector is switched off. After the initial laser pulse, the detectors are

switched on, and the detected signal is integrated over several hundred nanoseconds (see Figure 2.2).

Even though production of laser-generated OH was reduced due to lower pressure, it was still a significant source of uncertainty (Smith & Crosley, 1990). By changing the laser wavelength to 308 nm to excite the $A^2\Sigma^+$ - $X^2\Pi$, $v'=0 \leftarrow v''=0$ transition, both O_3 absorption cross section and $O(^1D)$ quantum yield are reduced, leading to a ~30 times lower interference by laser-generated OH. Additionally, the absorption cross section of OH at 308 nm is ~4 times higher than at 282 nm, therefore increasing the OH fluorescence signal (Chan, Hard, Mehrabzadeh, George, & O'Brien, 1990).

More recently, J. Mao et al. (2012) suggested that in some LIF-FAGE designs, an unknown source of OH, produced in the low pressure side, may cause interference in measurements of atmospheric OH. In order to account for such an interference, a scavenger, e.g. propane, is added to chemically remove atmospheric OH under atmospheric pressure (Novelli et al., 2014).

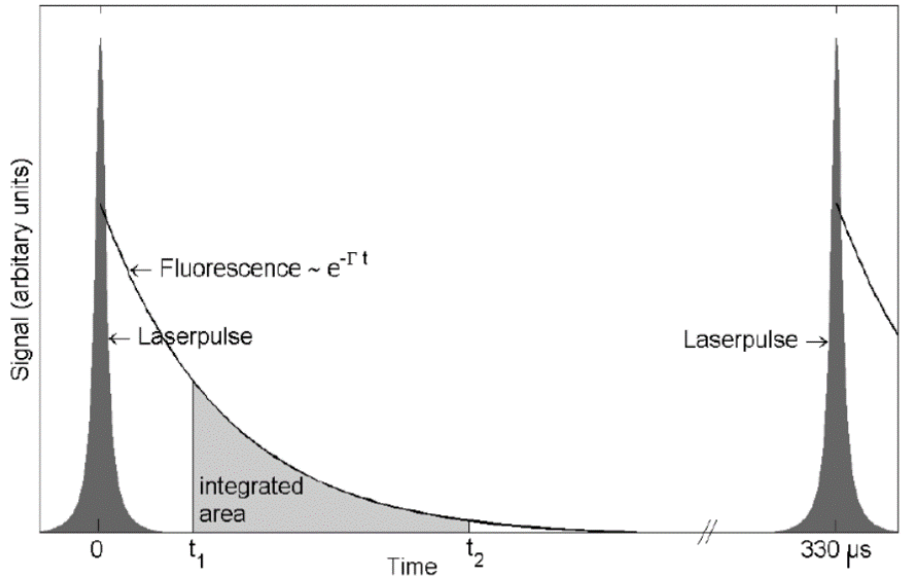

Figure 2.2 Schematic representation of the timing of photon counting process that is used to quantify OH concentrations by LIF-FAGE technique. The detectors are switched off during the laser pulse (dark grey areas) by electronic gating. The detector is switched on at t_1 and the integrated area (light grey) is proportional to OH number concentration. At t_2 the detector is switched off again before the next laser pulse (Taken from Faloona et al. (2004), modified).

2.2 HO_2 Measurement techniques

HO_2 typically reaches concentrations around 100 times higher than those of OH, with lifetimes of a few minutes and is often measured alongside OH. CIMS measures HO_2 and RO_2 indirectly by injection of NO to converting them into OH (Reiner, Hanke, & Arnold, 1997). Produced OH is measured as described above (2.1). By adding N_2 to the sample air, the reaction of RO to HO_2 (R.1.16) is suppressed, causing ~70 % produced H_2SO_4 stemming from HO_2 (Heard & Pilling, 2003).

2.2.1 LIF FAGE

Chemical conversion of HO_2 to OH by injection of excess NO (R.1.13), allows the LIF-FAGE technique to indirectly measure HO_2. The produced OH is then measured similarly as described in 2.1.1. Due to the short time between the point of NO injection and detection of produced OH radicals (a few milliseconds), high mixing ratios of NO are needed in order to reach high conversion efficiency. However, wall losses and efficient NO mixing during injection also impact conversion efficiency. Additionally, atmospheric RO_2 can react with NO producing detectable amounts of OH (R.14 – 16), therefore artificially increasing measured HO_2 concentrations. Measured HO_2 and internally produced HO_2 from RO_2 is called HO_2^*. Alkene-based RO_2 species can also decompose unimolecular, rapidly forming HO_2 under low pressure conditions (Fuchs et al., 2011). The interferences from RO_2 species can be reduced by shortening the reaction time and reducing NO concentrations at the expense of HO_2 conversion efficiency. The impact of RO_2 on the *H*ydr*O*xyl*R*adical measurement *U*nit based on fluorescence *S*pectroscopy (HORUS) LIF-FAGE instrument and its correction will be discussed in chapter 3.

2.3 HO_x observations using numerical box models

Atmospheric numerical models are a powerful tool to predict and simulate non-linear physical and chemical processes in the atmosphere. This allows the description of the influence of different environmental conditions on chemical composition and climatological effects. The reliability of such calculations depends on the choice and mathematical implementation of the relevant processes and their viability to describe reality. Validation is done through comparison with measured data, where significant discrepancies hint to an inaccurate or incomplete description of processes. To reduce complexity, often chemical and meteorological processes are separated. Due to the short tropospheric lifetime of HO_x, their concentrations are only influenced by local concentration of other trace gases and thus are only indirectly influenced by transport mechanisms. This makes numerical model calculation together with measurements a viable method to analyze atmospheric processes of HO_x and better understand their influence on the oxidation capacity of the atmosphere.

One such numerical model is CAABA/MECCA, which was developed at the Max Planck Institute for Chemistry, Mainz (Sander, Kerkweg, Jöckel, & Lelieveld, 2005). The chemical mechanism MECCA (**M**odule **E**fficiently **C**alculating the **C**hemistry of the **A**tmosphere) is used in the confines of the box model CAABA (**C**hemistry **A**s **A** **B**oxmodel **A**pplication). MECCA mechanism contains of about 600 species and 1600 reactions, including basic chemistry such as HO_x, O_3 and NO_x, as well as more complex organic oxidation chemistry in its subsection MOM (**M**ainz **O**rganic **M**echanism) (Cabrera-Perez, 2016; Hens et al., 2014; J. Lelieveld, 2016; Nölscher, 2014; Taraborrelli, 2012). CAABA/MECCA is written in Fortran90, with the KPP (**K**inetic **P**re**P**rocessor) software (Sandu & Sander, 2006) for numeric integration. CAABA/MECCA is described in more detail in Sander et al. (2005), R. Sander et al. (2011) and Sander et al. (2019).

In the scope of this work, CAABA/MECCA-4.0 (Sander et al., 2019) was employed for different uses throughout this work.

2.4 HORUS

The observations of OH and HO_2 discussed in this work were conducted using the ground-based *H*ydr*O*xyl *R*adical Measurement *U*nit based on fluorescence *S*pectroscopy (HORUS) by the Max Planck Institute for Chemistry (Mainz, Germany). HORUS is based on the aforementioned LIF-FAGE technique and is described further in Martinez et al. (2010). An *I*nlet *P*re-*I*njector (IPI) was used to account for any unknown source of OH causing interference in the measurement. The IPI system is described in further detail in Novelli et al. (2014). The instrument is comprised of laser system, low-pressure detection unit, IPI, vacuum system and instrument control and data acquisition unit (described below).

2.4.1 Instrument setup

Laser system

The UV light used for the excitation of OH is provided by a Nd:YAG pumped pulsed, tunable dye laser system (Martinez et al., 2010; Wennberg et al., 1994). A diode-pumped Nd:YAG laser (Type Navigator I, Spectra Physics) provides frequency-doubled light at 532 nm to a custom-made dye laser system. It is operated at a pulse frequency of ~3 kHz with a pulse length of ~25 ns. A tenfold beam expander and a collecting lens are used to focus the beam on the dye cell. Additionally, to counteract potential thermal and mechanical influences on misalignment, the incoupling of the green laser can be controlled by two piezo-actuated mirrors.

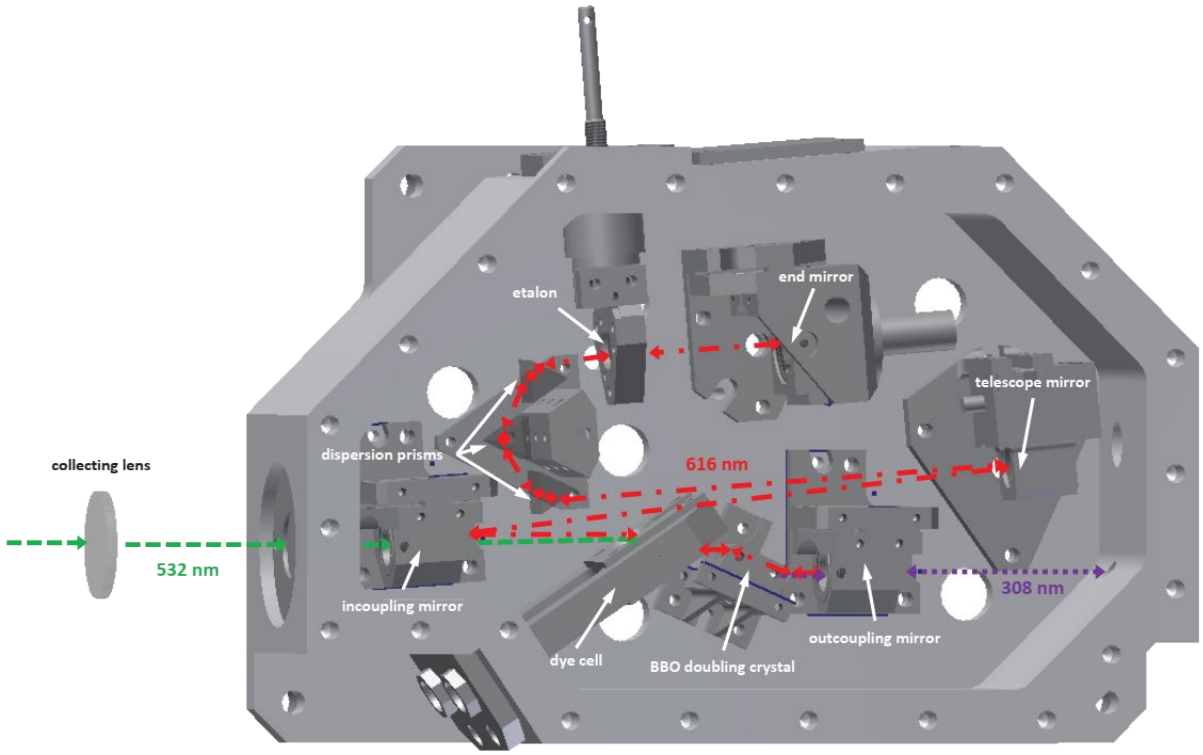

Figure 2.3 Schematic setup of the dye laser system. The incoming 532 nm wavelength laser beam is focused by the collecting lens onto the dye cell. The fluorescence from the pyrromethene-597 laser dye is selectively amplified at 616 nm inside the optical resonator. Using a nonlinear doubling crystal (BBO), UV light at 308 nm is produced. Taken from Hens (2013).

Figure 2.3 shows a schematic setup of the dye laser cavity (taken from Hens (2013)). The incoming expanded beam of the pump laser (532 nm) is focused by the collecting lens on the dye cell, hitting it at the Brewster angle. The laser dye is Pyrromethene-597 (Radiant Dyes Laser, Germany) dissolved in >99.9 % pure isopropanol. It absorbs the green laser light and fluoresces in the red wavelength range. The dye is circulated between a dye cell and a reservoir in order to prevent overheating and degradation of pyrromethene-597 and to prevent oversaturation of excited laser dye within the dye cell. The circulation rate is set to 1.6 - 1.7 liters per minute, which results in a complete exchange of dye within the cell after two laser pulses. The emitted light is then amplified within the cavity between the end mirror and the outcoupling mirror (see Figure 2.3). Since the dye emits a broad band of red light, two steps of wavelength selection are done. The combination of 3 dispersion prisms and a rotatable intracavity etalon achieves the selection of the required light at a wavelength of 616 nm. A β-barium borate (BBO) crystal is used to generate the second harmonic of the 616 nm beam to 308 nm. The UV light is then coupled out of the cavity via the outcoupling mirror and transported to the detection cells using optical fibers.

Low-pressure detection unit

The detection system of HORUS is shown in a schematic in Figure 2.4 (taken from Hens (2013)). Sample air is drawn through the Inlet-Pre-Injector (IPI) at a rate of ~50 SLM (p = 1013 hPa, T = 273.15 K). Propane can be added as a scavenging agent to remove atmospheric OH, allowing measurement of residual chemical background OH signal suggested by J. Mao et al. (2012).

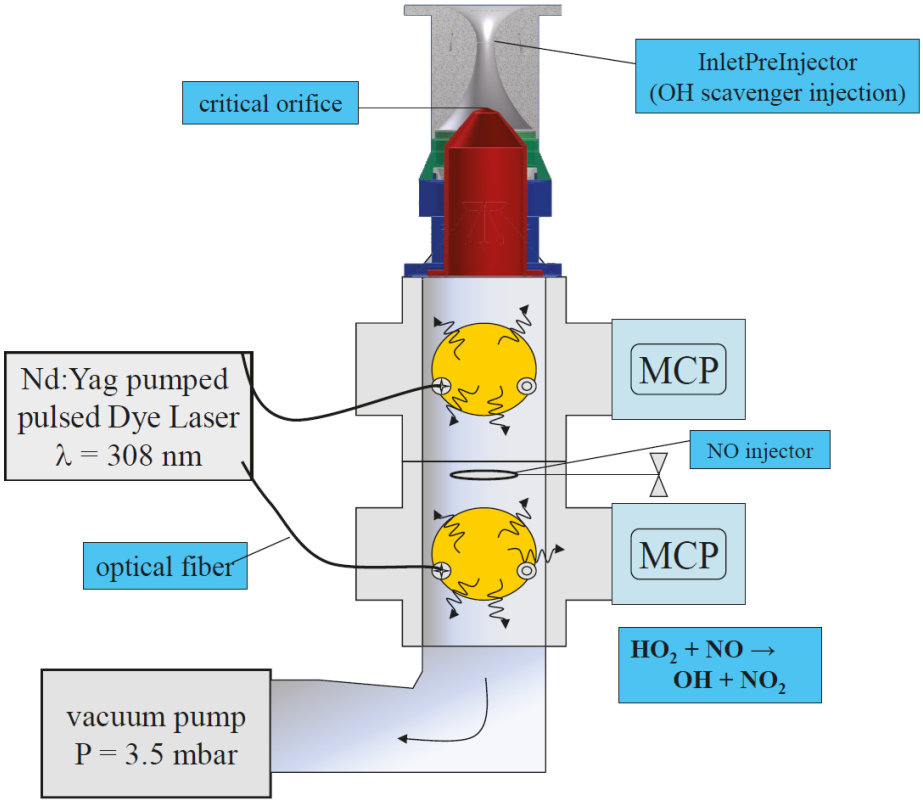

Figure 2.4 Schematic setup of the HORUS detection system. Sample air is drawn through the IPI at a rate of ~50 L/min. About 10 L/min is drawn through a critical orifice into the low-pressure detection cell. Laser light with a wavelength of 308 nm is used to excite OH radicals and fluorescence is detected by multi-channel plate detector (MCP). After adding excess amount of NO, HO_2 radicals are converted to OH and can be measured in the same way in the lower detection cell.

A critical orifice is used to guarantee a constant mass flow through the system. The internal pressure is kept between 2.5 - 4 mbar in order to assure high sensitivity. Additionally, this pressure difference results in an internal flow of ~10 SLM, which is necessary to avoid excitation of the same sample air by two consecutive laser pulses, producing laser-generated OH. Inside the detection cell, a White Cell setup (White, 1942) is used to maximize fluorescence signal and therefore instrument sensitivity.

Detection of OH is achieved by collecting fluorescence light on a multi-channel plate detector set up perpendicular to the direction of sample air flow and laser beam in order to minimize interference from scattered light. Atmospheric OH concentrations are measured in the upper detection cell of the HORUS setup (see Figure 2.4) HO_2 measurements are done via chemical conversion adding NO in excess downstream of the OH detection. The sum of remaining atmospheric OH and OH converted from HO_2 are measured in the lower detection cell. HO_2 concentrations can then be calculated by taking the OH measurements of the upper detection cell into account. Additionally, HO_2 measurements are influenced by the residence time inside the HORUS system, which can be calculated using the known mass flow from the critical orifice, the diameter and length of the tube between NO injector and point of measurement. This approach assumes perfect mixing of NO at the point of injection and gives the so-called physical residence time, which overestimates the time NO has to react with HO_2. Utilizing a simple NO calibration using a known amount of NO and HO_2, and the rate constant for the reaction of NO with HO_2, the chemical residence time can be calculated (Eq.1). It represents the actual reaction time of NO and HO_2 taking mixing into account and is shorter than the physical residence time. The chemical residence time inside HORUS is generally 6.5±0.5 ms.

$$[OH] = [HO_2] \cdot \left(1 - \exp\left(-k_{NO+HO_2} \cdot [NO] \cdot t\right)\right) \qquad \text{(Eq.1)}$$

The correlation between the measured fluorescence signal and OH radical concentrations is determined by the instrument sensitivity normalized for laser power. The instrument sensitivity is dependent on different factor (e.g. sensitivity of the detector, transmissivity of the White Cell setup, quenching effects of water vapor inside the sample air), some of which are difficult to quantify and can change over time. Calibrations of HORUS are therefore performed regularly and are described in chapter 2.4.2.

Scattering of light or possible fluorescence of other species in the sample air can cause a background signal, which elevates the fluorescence signal, and has to be accounted for. In the HORUS setup, this is done by tuning the laser off resonance for OH molecules and measuring the background signal periodically. After 5 seconds of online measurement, the frequency of the laser beam is alternately shifted to higher and lower frequencies (~37GHz) of the $Q_1(2)$ transition line of OH (Figure 2.5a). Figure 2.5b shows the typical “toggling” pattern of HORUS during measurements.

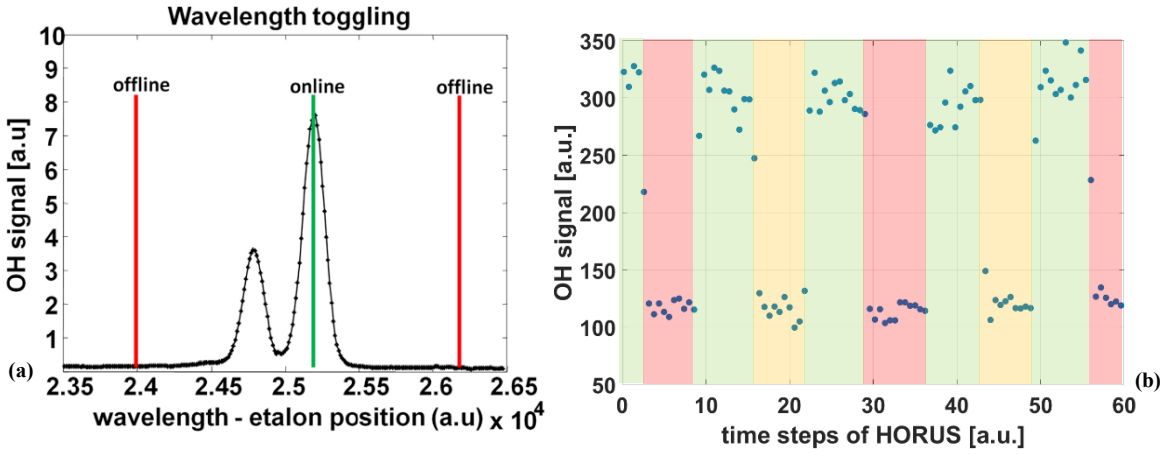

Figure 2.5(a) The laser beam is periodically tuned on (green line) and off OH resonance (red lines) to measured HORUS internal fluorescence background signal. (b) Measured signal of on-off resonance toggling. On (green areas) and off (red and yellow areas) resonance are alternated approx. every 5 sec. Off resonance is also alternated between frequency above (red area) and below (yellow) OH resonance line at 308 nm.

Vacuum system

The Vacuum needed for the HORUS system is created by a combination of a scroll pump (Type XDS-35, Edwards) with a roots blower (Type M90, Eaton). The air is compressed in front of the pump, leading to higher pumping efficiency, achieving the volume flow and low pressures required to operate the HORUS system.

Instrument control and data acquisition

The HORUS instrument is controlled by an embedded PC running a Debian LINUX operating system. Analog and digital sensors as well as stepper motors, mass flow controller and valves are connected to the data acquisition using a modular system of electronic cards, developed at the Max Planck-Institute for Chemistry, Mainz. An ISA bus is used to establish a connection to the PC. The HORUS software is based on a client-server model and programmed in "C". The server controls the communication with hardware and stores recorded data on a hard drive. The graphical user interface (GUI) is programmed in MatLab (Mathworks, Inc.) and is realized as a client, allowing continued data acquisition even during GUI malfunction.

2.4.2 Calibration

As an indirect measurement method, calculation of OH concentrations from LIF-FAGE data requires knowledge of the instrument sensitivity C_{OH}. To ensure stability over a period of time, regular calibrations are done by producing known concentrations of OH and HO_2 via photolysis of water vapor. Different mixtures of dry and humid air are produced in a range of 0-25 mmol mol^{-1}. The water vapor concentrations are measured by an infrared absorption instrument (LI-7000, LICOR), which is calibrated against a dew point generator

(LI-610, LICOR), which is in turn calibrated against NIST traceable pressure and temperature sensor. A mercury vapor lamp (Pen ray line source, LOT-QuantumDesign, Europe) is used to photolyze the water vapor to form OH and HO_2 (see R.34 - 36). The radical concentration can then be calculated according to equation Eq. 2 (Faloona et al., 2004).

$$H_2O + h\nu \xrightarrow{\lambda=184.9\ nm} OH + H^* \quad \text{(R.34)}$$

$$H^* \xrightarrow{M} H \quad \text{(R.35)}$$

$$H + O_2 \xrightarrow{M} HO_2 \quad \text{(R.36)}$$

$$[OH] = [HO_2] = \Phi_0 \sigma_{H_2O} [H_2O] t f_{O_2} \quad \text{(Eq.2)}$$

with the actinic flux density of the lamp Φ_0, the absorption cross section of water at 184.9 nm σ_{H_2O}, the residence time t under the lamp. Additionally, a correction factor f_{O_2} is applied to correct for absorption by oxygen and a resulting reduction of actinic flux density.

$$f_{O_2} = \int_0^h \frac{e^{-\sigma_{O_2}[O_2]x} dx}{h} \quad \text{(Eq.3)}$$

Figure 2.6 shows a schematic setup of the calibration unit of the HORUS instrument.

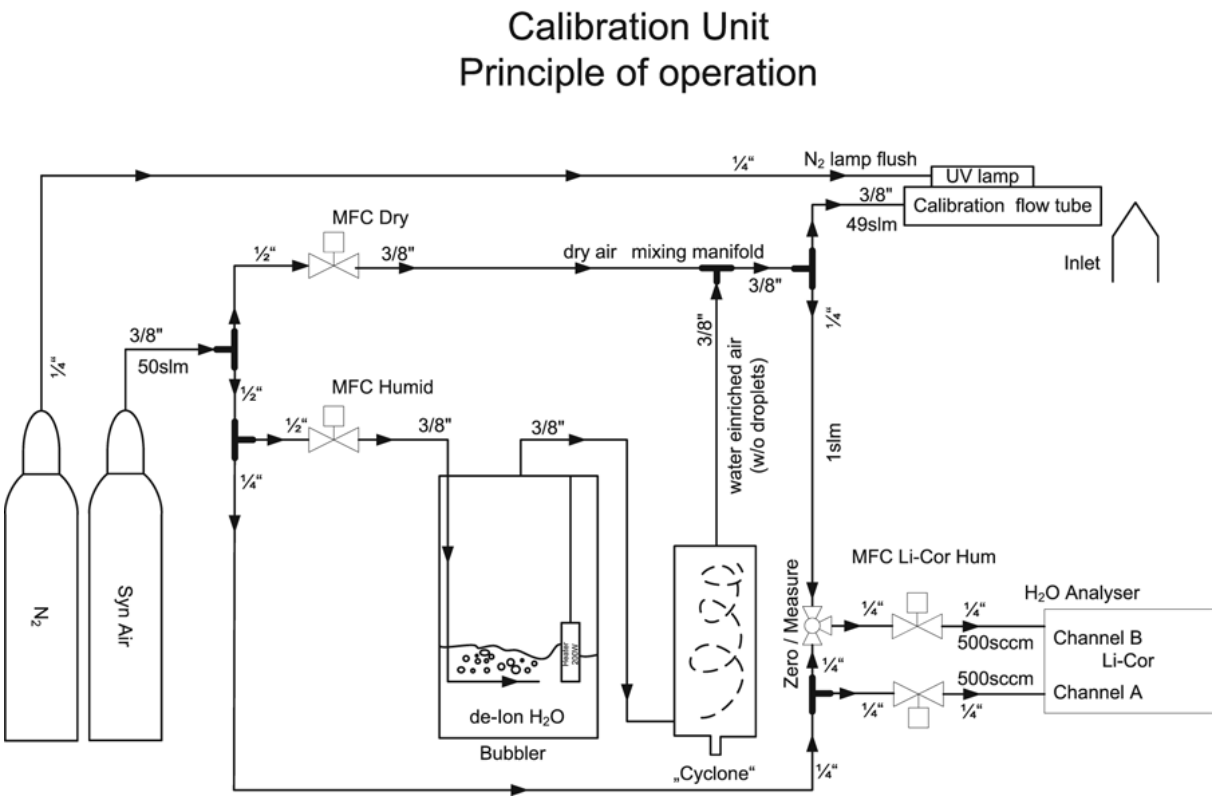

Figure 2.6 Schematic gas flow plan of the calibration setup used for the HORUS instrument. (Taken from Kubistin (2009))

The actinic flux density of the lamp is measured using the actinometric method by N_2O photolysis described by Martinez et al. (2010). $O(^1D)$ molecules produced by N_2O photolysis react with N_2O to form NO. The produced NO is measured by a NO_x chemiluminescence analyzer (C42, Thermo Environmental Instruments). The NO analyzer is calibrated using a NIST standard.

Interferences

In order to achieve reliable measurements of OH and HO_2, possible interferences have to be accounted for. In the LIF-FAGE method, interferences can be caused by processes inside the instrument itself, or atmospheric substances interacting with the laser light at the applied wavelength of 308 nm. One such substance is sulfur dioxide (SO_2), as it absorbs light around 308 nm. In the HORUS setup, this is accounted for by the aforementioned "toggling" during measurements. By shifting the wavelength of the laser beam off OH resonance, the spectral can be measured, allowing for subtraction of possible fluorescence caused by SO_2.

Internally generated OH were suspected to cause interference (J. Mao et al., 2012). In the HORUS setup, this is accounted for by using the IPI system (Novelli et al., 2014). By

adding propane to the sample air, atmospheric OH can be scavenged by more than 95 %, allowing measurements of internally produced OH only (Figure 2.7).

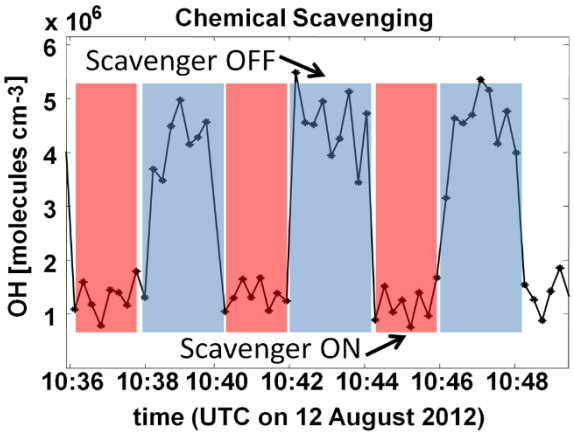

Figure 2.7 By injecting a scavenger into the sample air, background OH can be obtained (red shaded area). Atmospheric OH can be obtained from the difference of total OH (blue shaded area) and background OH. (taken from Novelli et al. (2014))

A known interference in the HO_2 measurements caused by organic peroxides RO_2 will be discussed in detail in chapter 3.

3 Characterization and correction of RO_2 interferences

The measurements of HO_2 in HORUS are based on the conversion of HO_2 to OH using an excess amount of NO (see 2.2.1 and R.13). As mentioned in 1.4, RO_2 can undergo similar reactions with NO. After subsequent reaction with oxygen, HO_2 is produced (R.16). Inside the HORUS setup, these reactions can occur after the injection of NO and therefore artificially increase HO_2. While relevant under atmospheric conditions, these reactions were expected to be negligible under the low pressure and short reaction time in the FAGE detection system compared to the reaction of HO_2 with NO (Heard & Pilling, 2003). Further studies showed, that the impact of RO_2 highly depends on the organic part of the molecule. For methyl peroxy radicals (CH_3O_2), interferences between 5 – 10 % had been reported (Hens, 2013; Holland, Hofzumahaus, Schäfer, Kraus, & Pätz, 2003). Fuchs et al. (2011) reported an interference of up to 80 % caused by RO_2 produced from unsaturated and aromatic VOCs. This is caused by the aforementioned different reaction pathways undergone by $RO_{2\ sat}$ and $RO_{2\ unsat}$ (see 1.4 and Figure 1.6). For $RO_{2\ sat}$, low-pressure and high-NO conditions inside the HORUS setup cause the reaction of the alkoxy radical RO with O_2 to be the rate-determining step. Other possible reactions of the alkoxy radical are reaction with NO and NO_2. However, both reactions do not produce OH and do not cause an additional OH signal. Therefore, these reactions are not relevant for the correction of RO_2 interference inside HORUS. For $RO_{2\ unsat}$, the unimolecular decomposition is favored by the low pressure inside HORUS, therefore the reaction of RO_2 with NO is rate-determining and highly favored under HORUS internal conditions. Due to these circumstances, it is necessary to correct for possible artificially produced HO_2 by RO_2 (further named RO_2 interference). The following chapter addresses this correction in detail.

3.1 Estimation of ambient RO_2

To quantify the interference caused by RO_2 on the HO_2 measurements, the RO_2 concentration in ambient air has to be estimated. Due to the large variety of RO_2, their measurements are difficult to conduct and it is necessary to estimate ambient RO_2 concentrations.

3.1.1 RO_2 Estimation using NO_x/O_3 PSS

One possible method to estimate ambient RO_2 concentrations is via the NO_x/O_3 photo stationary state (PSS) (Leighton, 1961). R.37 - 39 form a so-called null cycle for NO_x and O_3. Under the assumption of steady state and without the influence of VOC, the production and loss rate of NO_2 can be assumed as Eq.4.

$$j(NO_2) \cdot [NO_2] = k_{NO+O_3} \cdot [NO] \cdot [O_3] \quad \text{(Eq.4)}$$

where $j(NO_2)$ is the photolysis frequency of NO_2, and k_{NO+O_3} is the rate constant of $NO + O_3$.

$$NO_2 + h\nu \rightarrow NO + O(^3P) \quad \text{(R.37)}$$
$$O(^3P) + O_2 + M \rightarrow O_3 + M \quad \text{(R.38)}$$
$$O_3 + NO \rightarrow NO_2 + O_2 \quad \text{(R.39)}$$

Additionally, other atmospheric oxidizing agents can produce NO_2 by reaction with NO, namely HO_2 and RO_2 (R.13 & 15), expanding Eq.4 to Eq.5.

$$j(NO_2) \cdot [NO_2] = k_{NO+O_3} \cdot [NO] \cdot [O_3] + k_{NO+HO_2} \cdot [NO] \cdot [HO_2] + [NO] \cdot \sum_i k_{NO+R_iO_2} \cdot [R_iO_2] \quad \text{(Eq.5)}$$

where k_{NO+HO_2} is the rate constant of $NO+HO_2$, R_iO_2 is a particular organic peroxy radical, and $k_{NO+R_iO_2}$ is the rate constant of $NO+R_iO_2$.

Assuming the rate constant of each peroxy radical equals the rate constant k_{NO+HO_2} (Cantrell et al., 1997; Hauglustaine et al., 1996; J. A. Thornton et al., 2002), all peroxy radicals R_iO_2 can be described as RO_2 and estimated by solving Eq.5 for RO_2 yielding Eq.6.

$$[RO_2] = \frac{j(NO_2) \cdot [NO_2] - k_{NO+O_3} \cdot [NO] \cdot [O_3]}{k_{NO+HO_2} \cdot [NO]} - [HO_2] \quad \text{(Eq.6)}$$

However, this method of estimating ambient RO_2 concentrations using NO_x/O_3 PSS does not account for different VOC compositions present at the time of measurement. As mentioned above, the nature of VOC from which the peroxy radical derives from, determines further reactions. Therefore, inclusion of measured VOC data can give better insight of the RO_2 concentrations causing interferences inside the HORUS setup. This is accounted for in the second method presented here.

3.1.2 RO_2 estimation using HO_2 and OH reactivity

HO_2 can be used to describe ambient RO_2 concentrations by assuming similar reaction patterns for RO_2 and HO_2.

During daytime, steady state establishes within minutes for RO_2 and HO_2. This allows to describe their concentration as being only dependent on production and losses (Eq.7 - 8).

$$\sum[RO_2]_i = \frac{P_{\sum[RO_2]_i}}{L_{\sum[RO_2]_i}} \quad \text{(Eq.7)}$$

$$[HO_2] = \frac{P_{HO_2}}{L_{HO_2}} \quad \text{(Eq.8)}$$

where P_{RO_2} and L_{RO_2} are the production and loss rates of all RO_2, P_{HO_2} and L_{HO_2} are the production and loss rates of HO_2.

Assuming the production of RO_2 and HO_2 during daytime occurs predominantly by the reactions of OH with VOC (R.35-38) and CO, respectively, Eq.7 and Eq.8 can be expanded to Eq.9 and Eq.10.

$$\sum[VOC]_i \cdot [OH] \cdot k_{VOC_i} = \sum[RO_2]_i \cdot L_{RO_2} \quad \text{(Eq.9)}$$

$$[CO] \cdot [OH] \cdot k_{CO} = [HO_2] \cdot L_{HO_2} \quad \text{(Eq.10)}$$

where k_{VOC_i} and k_{CO} are the rate constant of the reaction of VOC_i with OH and of CO with OH.

Lastly, assuming the major loss of RO_2 and HO_2 occurs by similar reactions (see chapters 1.3.2 - 1.3.3), both the loss of RO_2 (L_{RO_2}) and HO_2 (L_{HO_2}) in Eq.9 and Eq. 10 are considered equal. Under these assumptions, the ratio of the RO_2 and HO_2 concentration is the ratio of their respective production rates (Eq.11). Subsequently, the RO_2 concentration can be expressed as the HO_2 concentration scaled by the ratio of the production rates resulting in Eq.12.

$$\frac{\sum[VOC]_i \cdot [OH] \cdot k_{VOC_i}}{\sum[RO_2]_i} = \frac{[CO] \cdot [OH] \cdot k_{CO}}{[HO_2]} \quad \text{(Eq.11)}$$

$$\sum[RO_2]_i = \frac{\sum[VOC]_i \cdot k_{VOC_i}}{[CO] \cdot k_{CO}} \cdot [HO_2] \quad \text{(Eq.12)}$$

Total uncertainty is calculated from the uncertainties of each variable according to Gauss error propagation.

This allows to estimate the RO_2 concentration based on the measured HO_2, CO and VOC concentrations under conditions where the assumptions made are feasible.

3.2 Analytical and numerical calculation of the HORUS-internal RO_2 conversion using NO titration

The calculation of the RO_2 interference in HORUS from ambient RO_2 concentrations is highly dependent on the type of peroxy radical present. As mentioned in 1.4.2, structural differences stemming from the VOC from which RO_2 was produced, possible conversion to HO_2 and interference in HORUS can vary greatly. Additionally, many rate constants of the reactions forming HO_2 from RO_2 are not studied yet and therefore unavailable to be used in calculations. A simplification is thusly needed in order to calculate HORUS-internal RO_2 interferences.

In the following section, two methods of calculating RO_2 interference are presented.

3.2.1 Cost effective estimate of the RO_2 conversion to OH efficiency based on the internal temperature and pressure in HORUS

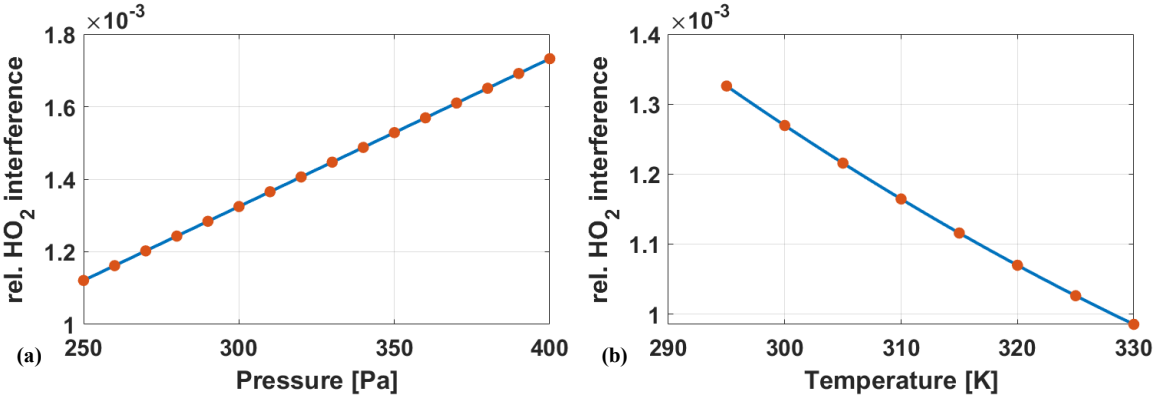

Figure 3.1 Relative HO_2 interference for $RO_{2\,sat}$ vs. pressure (a) and temperature (b), respectively. The data obtained from CAABA/MECCA (red) was fitted (blue) with Eq.13 for the pressure dependency and Eq.14 for the temperature dependency, respectively. The range of x was chosen to encompass conditions normally encountered during HORUS measurements. The NO concentration was $5.64 \cdot 10^{14}$ molec cm^{-3}.

With ambient RO_2 concentrations estimated, interference caused through internally produced OH can be calculated using the CAABA/MECCA box model. By initializing the box model with internal conditions of HORUS (2.5 – 4 mbar, 295 – 330 K, $5.64 \cdot 10^{14}$ molec cm^{-3} NO), chemistry inside the measurement system can be simulated and enables the calculation of internally produced OH, which is then normalized for the initial concentration of RO_2 and corresponds to the HO_2 interference relative to the RO_2 concentration (I_{rel}) inside of HORUS. The reaction rate constants used to describe the reactions are temperature and pressure dependent. Therefore, throughout the measurement by HORUS, the internal pressure and temperature are constantly monitored. They follow in general the variations of their ambient counterparts. Additionally, significant changes in pressure can occur, when the critical orifice at the inlet is obstructed, e.g. by crystallizing sea salt. However, the numerical simulation of each of the 2-min measurement interval

typically used during a multi-day measurement campaign is computational expensive. A more cost-effective approach is to parameterize the RO_2 to OH conversion as a function of the internal pressure and temperature.

Figure 3.1 shows the relative HO_2 interference by conversion of $RO_{2\ sat}$ versus pressure (a) and temperature (b) calculated by numerical simulations of CAABA/MECCA. A linear fit Eq.13 had been used to describe the pressure dependency ($I_{rel,p}$). The second order polynomial Eq.14 was used to describe the temperature dependency ($I_{rel,T}$). By normalizing $I_{rel,T}$ to the temperature used during calculation of $I_{rel,p}$ allows to combine both factors to Eq.15.

$$I_{rel,p}(p) = m_1 \cdot p + m_2 \quad \text{(Eq.13)}$$

$$I_{rel,T}(T) = n_1 \cdot T^2 + n_2 \cdot T + n_3 \quad \text{(Eq.14)}$$

$$I_{rel}(p,T) = I_{rel,p}(p) \cdot \left(\frac{I_{rel,T}(T)}{I_{rel,T}(295)} \right) \quad \text{(Eq.15)}$$

Table 3.1 Parameter for temperature and pressure dependency for relative HO_2 interference from $RO_{2\ sat}$ and $RO_{2\ unsat}$. Parameters were calculated for c(NO) = $5.64 \cdot 10^{14}$ molec cm^{-3}

Parameter	$RO_{2\ sat}$	$RO_{2\ unsat}$
m_1	$4.07 \cdot 10^{-6}$	$-7.11 \cdot 10^{-8}$
m_2	$1.02 \cdot 10^{-4}$	$3.39 \cdot 10^{-2}$
n_1	$5.16 \cdot 10^{-8}$	$2.56 \cdot 10^{-6}$
n_2	$-4.20 \cdot 10^{-5}$	$-1.92 \cdot 10^{-3}$
n_3	$9.22 \cdot 10^{-3}$	0.38

Figure 3.2a shows relative HO_2 interference $I_{rel\ sat}$ for $RO_{2\ sat}$ vs. internal pressure and temperature using the parameters from Table 3.1. The surface describes the interference inside HORUS for RO_2 from saturated VOC. Since the NO concentration has a major influence on the conversion of RO_2 to HO_2 and OH, the described surface is only applicable for the NO concentration used for these calculations (c(NO) = $5.64 \cdot 10^{14}$ molec cm^{-3}). For these conditions, the relative HO_2 interference $I_{rel\ sat}$ is between 0.08 – 0.17 %.

Similarly, $I_{rel\ unsat}$ can be calculated for $RO_{2\ unsat}$ (Figure 3.2b). Contrary to $I_{rel\ sat}$, $I_{rel\ unsat}$ only shows a negligible pressure dependency. As shown in 1.4.2, for $RO_{2\ unsat}$ only the reaction with NO is pressure dependent. Since the mass flow of NO injected into the detection axis, the concentration of NO is constant even with fluctuating pressures. For these conditions, the relative HO_2 interference $I_{rel\ unsat}$ is between 2.24 - 3.38 %.

The discrepancy between $I_{rel\ sat}$ and $I_{rel\ unsat}$ is expected, since the conversion of $RO_{2\ sat}$ to HO_2 inside HORUS occurs through two bimolecular reactions (R.23 - 24). Contrary, after of $RO_{2\ unsat}$ with NO, a fast, unimolecular decomposition precedes the formation of HO_2.

This decomposition rate was determined to be in the order of 10^4 to 10^6 s^{-1} (R. Atkinson, 1997; Orlando et al., 1998; Vereecken, Peeters, Orlando, Tyndall, & Ferronato, 1999). Total relative HO_2 interference I_{rel} is calculated using Eq. 16.

$$I_{rel} = [RO_2]_{sat} \cdot I_{rel\,sat} + [RO_2]_{unsat} \cdot I_{rel\,unsat} \qquad \text{(Eq.16)}$$

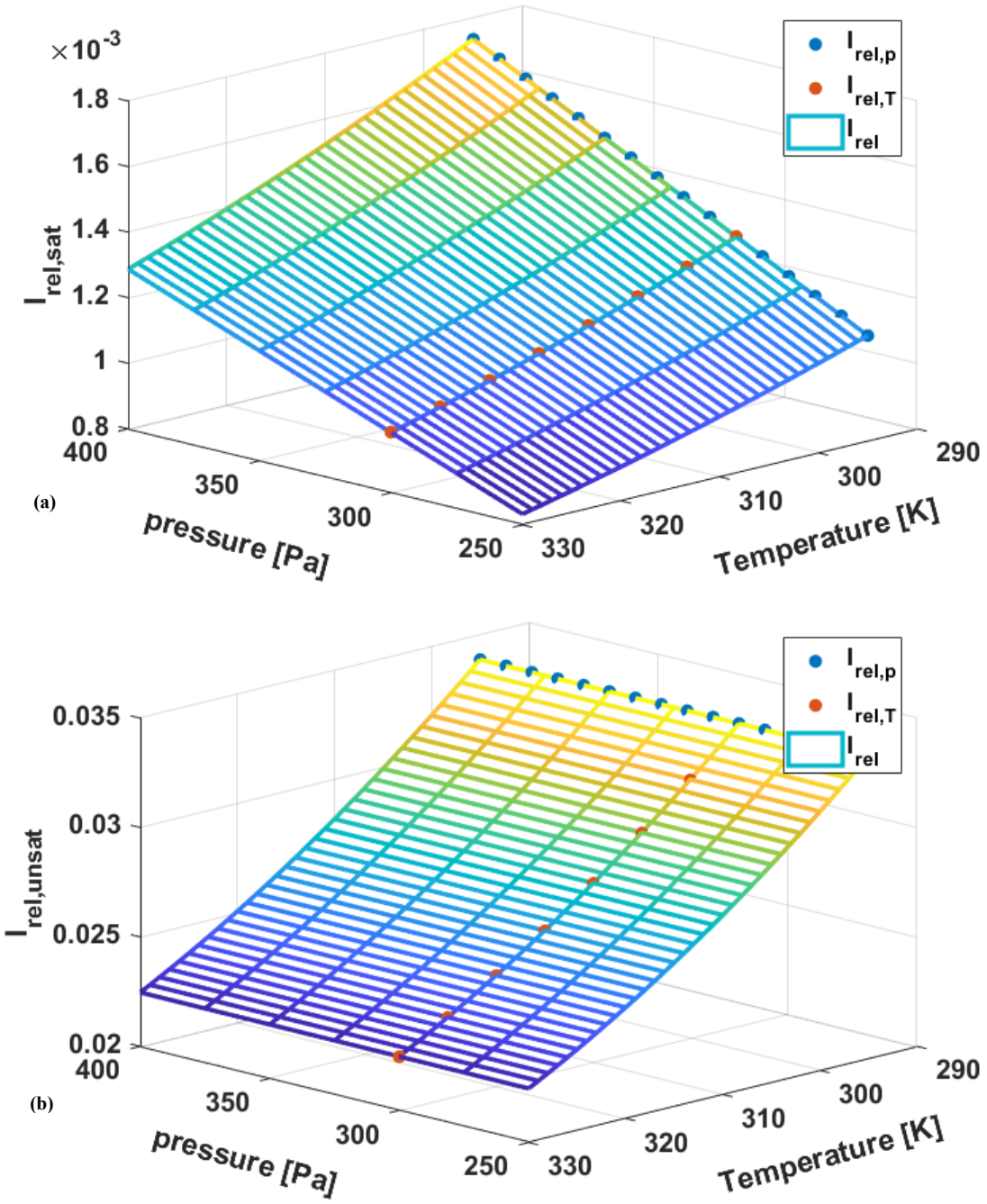

Figure 3.2 Combination of the equation describing $I_{rel,p}$ (blue dots)and $I_{rel,T}$ (red dots) spanning a surface, which characterizes I_{rel} for a given temperature and pressure. I_{rel} from $RO_{2\,sat}$ ($I_{rel\,sat}$) (a) shows a dependency of both pressure and temperature, while I_{rel} from $RO_{2\,unsat}$ ($I_{rel\,unsat}$) (b) only shows a temperature dependency and stays constant for different pressures.

As described in 2.4.1, the effective residence time inside HORUS includes the mixing efficiency of NO with the sample air and the transport from the NO-injection and detection of OH. Using the pump flow, tube length and diameter, the effective residence time is estimated to be 6.5±0.5 ms. To estimate the impact of the resulting uncertainty of the residence time in the conversion efficiency, model calculations based on the assumption of a residence time of 6 and 7 ms are performed.

Additionally, uncertainties in the rate constants used in the box model need to be accounted for by varying rate constants randomly using Monte-Carlo-simulations (MC). It is assumed, that all $RO_{2\ sat}$ can be described through CH_3O_2, and all $RO_{2\ unsat}$ can be described through $HOCH_2CH_2O_2$. However, since for each category of RO_2, reaction rate constants vary with each RO_2, a large additional uncertainty is introduced. To account for this, the error used in the MC simulations is changed to encompass rate constants of the RO_2 shown in Table 3.2. Table 3.3 shows rate constants and corresponding errors used.

Table 3.2 RO_2 used to estimate reaction rate constant uncertainty

		RO_2 included / origin VOC (for $RO_{2\ unsat}$)
$RO_{2\ sat}$	$RO_2 + NO \rightarrow RO + NO_2$	CH_3O_2*, $C_2H_5O_2$*, i-$C_3H_7O_2$*, n-$C_3H_7O_2$*, n-$C_4H_9O_2$*, t-$C_4H_9O_2$*
	$RO + O_2 \rightarrow HO_2 + products$	CH_3O*, $C_2H_5O^+$, 1-$C_3H_7O^+$, 2-$C_3H_7O^+$, 1-$C_4H_9O^+$
$RO_{2\ unsat}$	$RO_2 + NO \rightarrow RO + NO_2$	Ethen*, Propene#, 1-Butene#, 2-Butene#, 2-Methylpropene#, 1,3-Butadiene#, Isoprene#

* (Sander et al., 2019), + (R. Atkinson et al., 2006), # (Miller, Yeung, Kiep, & Elrod, 2004)

Table 3.3 Rate constants and errors used for CAABA/MECCA simulation. Errors do not represent literature uncertainty, but were chosen to account for RO_2 from different saturated or unsaturated VOC.

	reaction	Rate constant k *	log(f)
$RO_{2\ sat}$	$RO_2 + NO \rightarrow RO + NO_2$	$2.3 \cdot 10^{-12} \cdot \exp(360/temp)$	1.19
	$RO + O_2 \rightarrow HO_2 + products$	$1.3 \cdot 10^{-14} \cdot \exp(-663/temp)$	3.0
$RO_{2\ unsat}$	$RO_2 + NO \rightarrow RO + NO_2$	$2.54 \cdot 10^{-12} \cdot \exp(360/temp)$	1.10

* (R. Atkinson et al., 2006)

Due to the large differences in the rate constant for the reaction $RO+O_2$ for different VOC, the uncertainty for this reaction is chosen very large. Additionally, since this reaction is rate determining, it is a major contributor to the total uncertainty of $I_{rel\ sat}$. Since the uncertainties of the rate constants are described as a lognormal distribution, total uncertainty cannot be described with 1σ confidence interval. Instead, they are described with an upper and lower

error. Upper and lower total uncertainty for $I_{rel\ sat}$ and $I_{rel\ unsat}$ were then calculated using Gauss error propagation.

Table 3.4 Lower and upper error $I_{rel\ sat}$ and $I_{rel\ unsat}$.

	$\Delta I_{rel\ sat}$	$\Delta I_{rel\ unsat}$
Lower uncertainty	64.5 %	14.8 %
Upper uncertainty	181.6 %	17.3 %

The error margin for $I_{rel\ sat}$ is significantly larger than those of $I_{rel\ unsat}$. This is mostly caused by large uncertainties suggested for the reactions of $RO_{2\ sat}$ (see Table 3.3).

In order to calculate the total uncertainty for I_{rel}, the concentrations for $RO_{2\ sat}$ and $RO_{2\ unsat}$ have to be known (Eq. 16). To estimate the range and influence, Eq. 16 can be changed to

$$I_{rel} = [RO_2](f_{sat} \cdot I_{rel\ sat} + (1 - f_{sat}) \cdot I_{rel\ unsat}) \quad \text{(Eq.17)}$$

$$\frac{I_{rel}}{[RO_2]} = (f_{sat} \cdot I_{rel\ sat} + (1 - f_{sat}) \cdot I_{rel\ unsat}) \quad \text{(Eq.18)}$$

$$\Delta\left(\frac{I_{rel}}{[RO_2]}\right) = (f_{sat} \cdot \Delta I_{rel\ sat} + (1 - f_{sat}) \cdot \Delta I_{rel\ unsat}) \quad \text{(Eq.19)}$$

Eq. 17, with the fraction of saturated RO_2 f_{sat} of the total RO_2 concentration [RO_2]. By dividing with the total RO_2 concentration, the total interference relative to the total RO_2 concentration can be calculated (Eq. 18). Total uncertainty of I_{rel}/[RO_2] can be calculated using Eq.19.

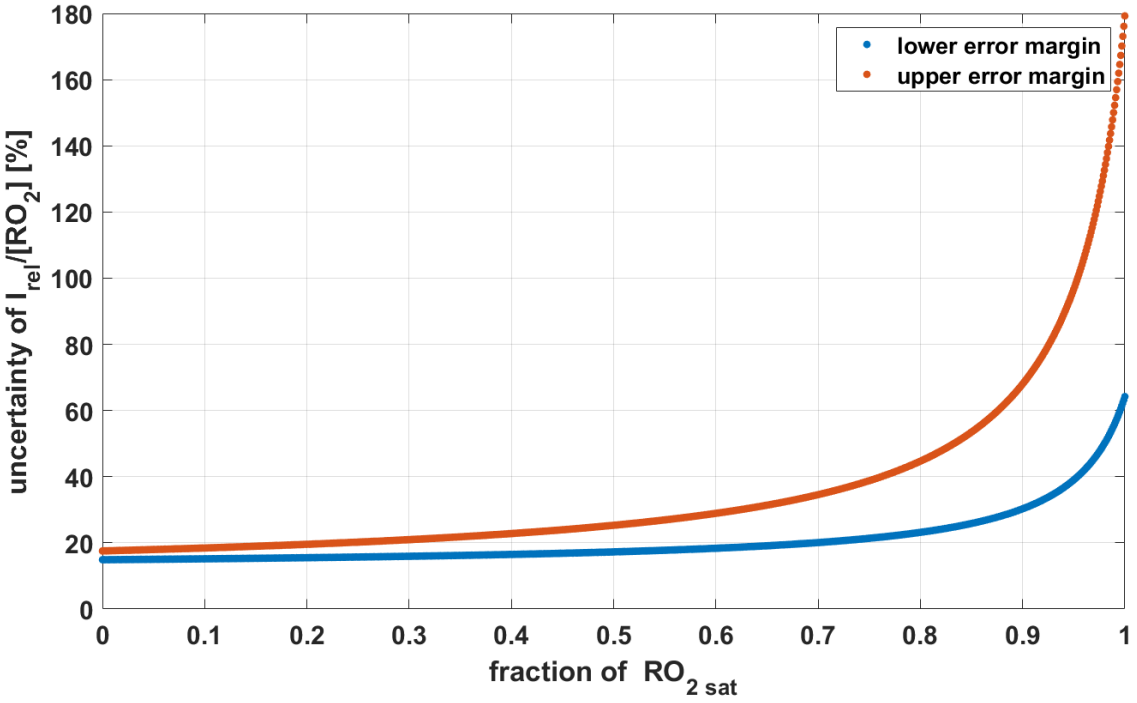

Figure 3.3 Lower (blue) and upper (red) relative error margin of $I_{rel}/[RO_2]$ vs. the fraction of $RO_{2\ sat}$.

Figure 3.3 shows the lower and upper relative error margin of $I_{rel}/[RO_2]$ vs. the fraction of $RO_{2\ sat}$. Due to the low overall interference caused by $RO_{2\ sat}$, the large error shown in Table 3.4 only significantly increases the total uncertainty above $f_{sat} = 0.6$.

3.2.2 Model based estimate of the ambient RO_2 concentration based on titration of RO_2 by NO

Measurement of HO_2 within HORUS is achieved by chemical conversion of HO_2 to OH by adding NO before the second detection axis (see Figure 2.4). In order to determine this chemical conversion efficiency within HORUS, NO titrations are periodically performed throughout the day. Besides HO_2, RO_2 is also converted by NO (see Figure 1.6) leading to artificial generated HO_2 which can further react with NO generating OH which is detected. The resulting data collected from NO titrations is therefore comprised of OH formed by HO_2 and RO_2 and thus contains information about momentary RO_2 interference at the time of measurement. Figure 3.4 exemplifies with the total internal OH (blue) and its fractions by HO_2 (red) and RO_2 (yellow). In order to retrieve the information about ambient HO_2 and RO_2 from these titrations the CAABA/MECCA box model is used.

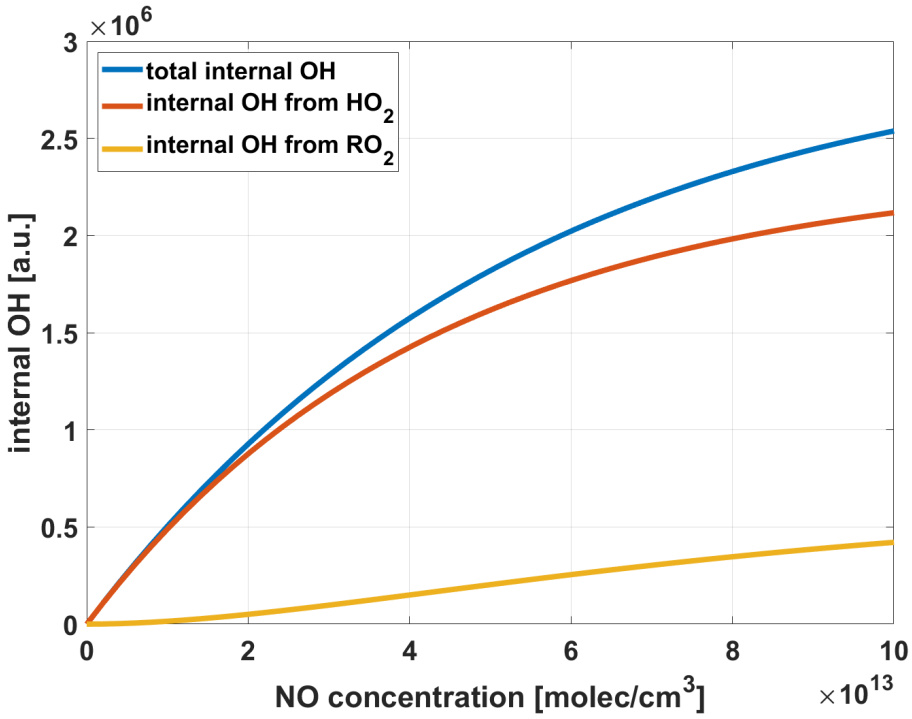

Figure 3.4 Internal OH produced by HO_2 and RO_2 as seen during NO titrations. Total internal OH (blue) consists of OH produced by HO_2 (red) and the sum of OH produced by all RO_2 present during measurement (yellow)

The model is initialized with HORUS internal conditions (see above) and estimated ambient RO_2 concentrations (as described in 3.1) are used as starting parameter in CAABA/MECCA. By varying HORUS-internal HO_2, $RO_{2\ sat}$ and $RO_{2\ unsat}$ and comparing the modeled titration with the measured one, a cost function is minimized utilizing the least square method. Figure 3.5 shows internal OH from a measured NO titration (blue), internal OH from CM model (red), and the fractions of internal OH from HO_2 (yellow), $RO_{2\ sat}$ (purple) and $RO_{2\ unsat}$ (green). By calculating the ratio of the OH signal derived from HO_2 of the total OH signal for the NO concentration injected into HORUS during regular measurements (~$0.7 \cdot 10^{13}$ molec/cm^3), interference caused by OH from RO_2 can be corrected (Figure 3.5, grey vertical line).

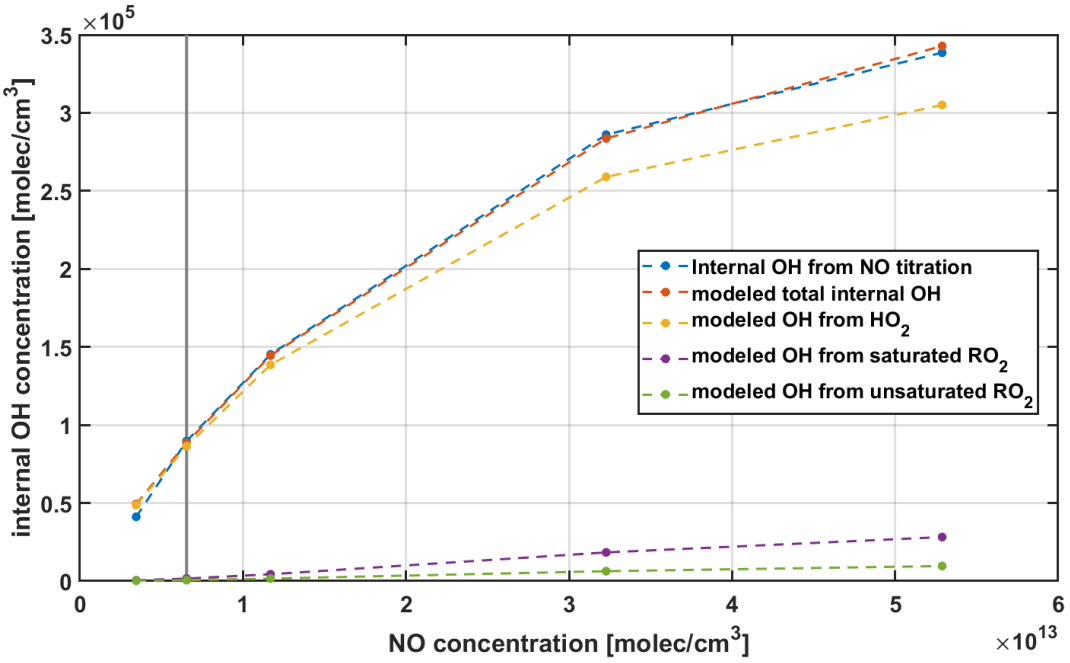

Figure 3.5 Example of NO titration measured with HORUS (blue), with total modeled internal OH (red), and modeled internal OH from HO_2 (yellow), $RO_{2\,sat}$ (purple) and $RO_{2\,unsat}$ (green). The vertical line set to the NO concentration injected during normal measurements.

In order to account for statistical variability during the measurement of NO titration, observation weights ($w = 1/\sigma^2$) are used to estimate the quality of the individual measurement of each titration. Additionally, a known problem of approximations using the least square method is the possibility of reaching different local minima of the cost function depending on initially used starting parameter. To account for this possibility, Monte Carlo simulations for each titration are conducted. Using a random number generator, initial parameters for HO_2, $RO_{2\,sat}$ and $RO_{2\,unsat}$ were varied 1000 times according to a normal distribution. Calculating a mean and standard deviation gives a measure of error for each titration. Total uncertainty is calculated by adding up both sources of error.

3.3 Validation of CAABA/MECCA estimates of HORUS internal conditions

To investigate the contribution of RO_2 to the HO_2 signal inside of HORUS, Kunkler (2021) performed a master thesis under the supervision and in close collaboration with this work. The results are the basis of this chapter.

As shown above, it is possible to estimate RO_2 interference in the HORUS instrument using the CAABA/MECCA box model. Though it has not been shown, that CAABA/MECCA can accurately describe HORUS internal conditions. Additionally, it is unknown, whether the separation of RO_2 into $RO_{2\,sat}$ and $RO_{2\,unsat}$ is sufficient to describe the large variety of

RO_2 in the atmosphere. Lab studies were performed in the scope of a master thesis (Kunkler, 2021). Several tests were conducted using different RO_2 in order to show the validity of this assumption. Known concentrations of RO_2 from several saturated (methane, propane and n-butane), unsaturated VOC (ethene, propene, but-1-ene and isoprene), and benzene were produced in situ. NO titrations were performed for each single RO_2 with the HORUS setup and simulated with CM. Figure 3.6, Figure 3.7 and Figure 3.10 show measured and simulated NO titrations for both $RO_{2\ sat}$ and $RO_{2\ unsat}$, respectively.

Interference from $RO_{2\ sat}$

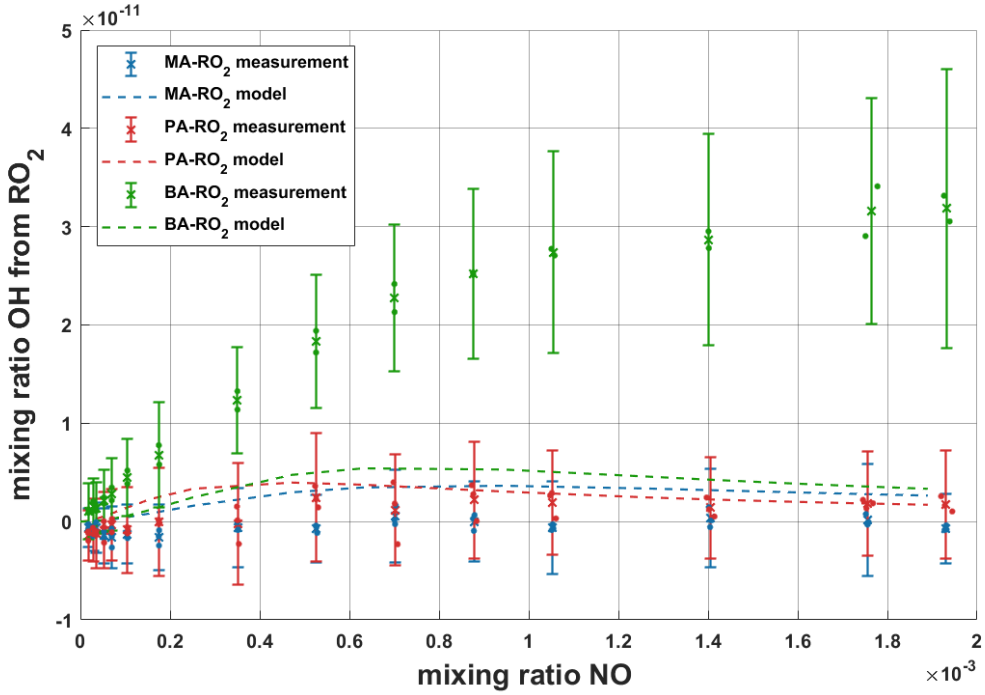

Figure 3.6 Mixing ratio of OH generated from different $RO_{2\ sat}$. Shown points represent measured NO titrations, while dotted lines represent modeled data. Modeled data of both MA-RO_2 and PA-RO_2 describe the measured NO titrations, while measurements of BA-RO_2 are underestimated by the corresponding model (taken from Kunkler (2021)).

Modeled data for RO_2 from propane (PA-RO_2) and methane (MA-RO_2) show great agreement with measured NO titration. Internal production of OH is very minor for these compounds, which indicates a small influence on RO_2 interference in HORUS. Modeled data for RO_2 from n-butane follows this trend, while measurements show higher production of internal OH. A possible cause for this increased internal OH are side products of the reaction of BA-RO_2 with NO. Jungkamp, Smith, and Seinfeld (1997) reported a significant amount of nitrites and acetaldehyde production. Since nitrites can also be produced from MA-RO_2 and PA-RO_2, and did not cause an interference for these RO_2, it is assumed, that no interference is caused by nitrites formed from BA-RO_2. Furthermore, for acetaldehyde no reactions are known, which can cause an interference inside a LIF-FAGE instrument.

According to Jungkamp et al. (1997), the alkoxy radical formed from BA-RO_2 can undergo a 1,5-H-shift, which can open up different reaction paths. However, it is unknown, if species are produced, which cause an interference in the HORUS system. Further investigations are needed to answer this question.

Interference from $RO_{2\ unsat}$

Modeled data for RO_2 from ethene (EE-RO_2) and isoprene (IE-RO_2) show good agreement with measured data, while modeled data for RO_2 from propene (PE-RO_2) and but-1-ene (BE-RO_2) underestimate measured data. For all $RO_{2\ unsat}$, modeled data underestimates OH mixing ratio for lower NO mixing ratios (between 0.1 - $0.5 \cdot 10^{-3}$). It is possible, that this caused by an offset of NO injected into the setup. Adding an offset of ~$0.04 \cdot 10^{-3}$ leads to improved agreement for lower NO mixing ratios (see Appendix A, Figure A.1, Kunkler (2021)). However, since it is unclear, what the cause of this discrepancy for low NO mixing ratios is, no NO offset correction was applied in further investigations.

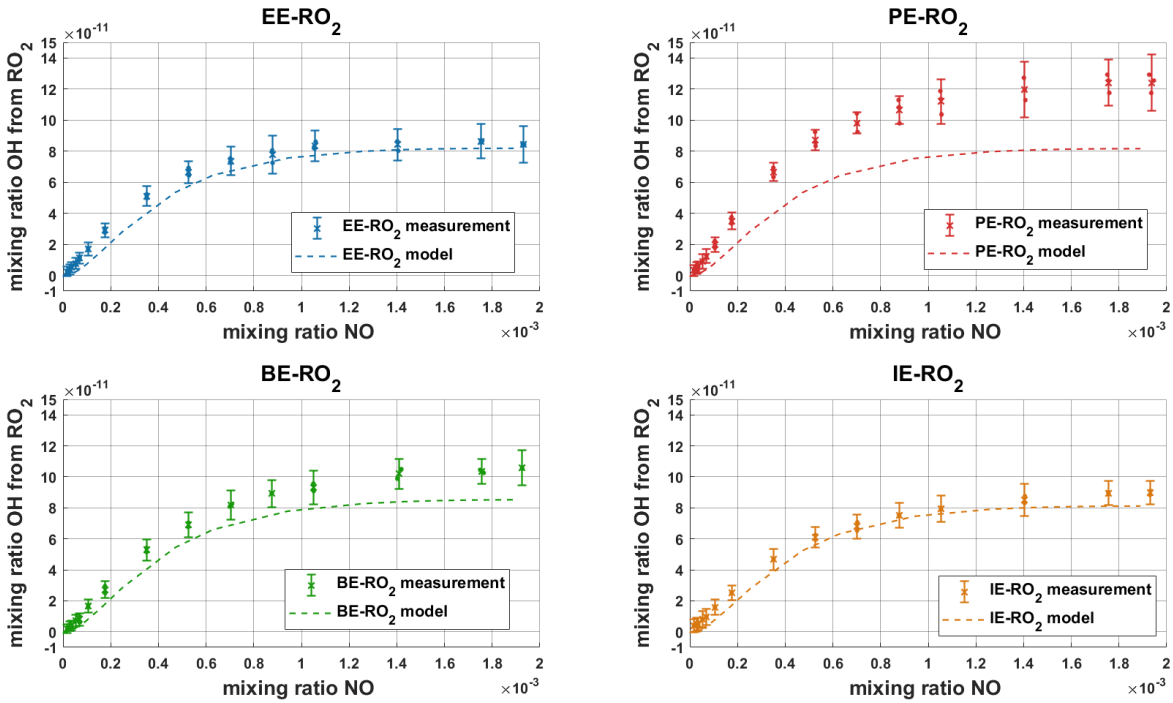

Figure 3.7 Mixing ratio of OH generated from different $RO_{2\ unsat}$. Shown points represent measured NO titrations, while dotted lines represent modeled data. Modeled data of PE-RO_2 and BE-RO_2 underestimates measured data, while modeled data of EE-RO_2 and IE-RO_2 describe measurements within error estimation (taken from Kunkler (2021)).

The measured NO titrations for PE-RO_2 and BE-RO_2 both show maximum conversion of RO_2 of over 100 % (143 % and 122 %, respectively). This indicates, that aside from expected conversion of RO_2 to OH, other reactions have taken place, which produced additional HO_2 or OH radicals. A possible source of additional radicals could be through laser generation. The photolysis of aldehydes inside the LIF-FAGE system is known to

cause an interference (Roger Atkinson, 2000). Since the photolysis of the aldehyde and the excitation of the resulting OH both need a photon, an interference caused from this reaction shows a squared dependency of the laser power inside the White cell of the HORUS system. Figure 3.8 shows the normalized OH signal vs. laser power inside the White cell. Both PE-RO_2 (red) and BE-RO_2 (blue) show a linear dependency on laser power within the error margins (2σ). Another possibility for additional OH signal is a laser repetition rate, which is chosen too high (3 kHz during HORUS measurements). This can cause more than one excitation-emission-cycle for OH radicals, leading to an increased fluorescence signal. Figure 3.9 shows the normalized OH signal vs. NO mixing ratios for repetition frequencies of 2 kHz, 3 kHz and 4 kHz. For all three frequencies similar OH signals were measured, indicating no increased signal through multiple excitation-emission-cycles.

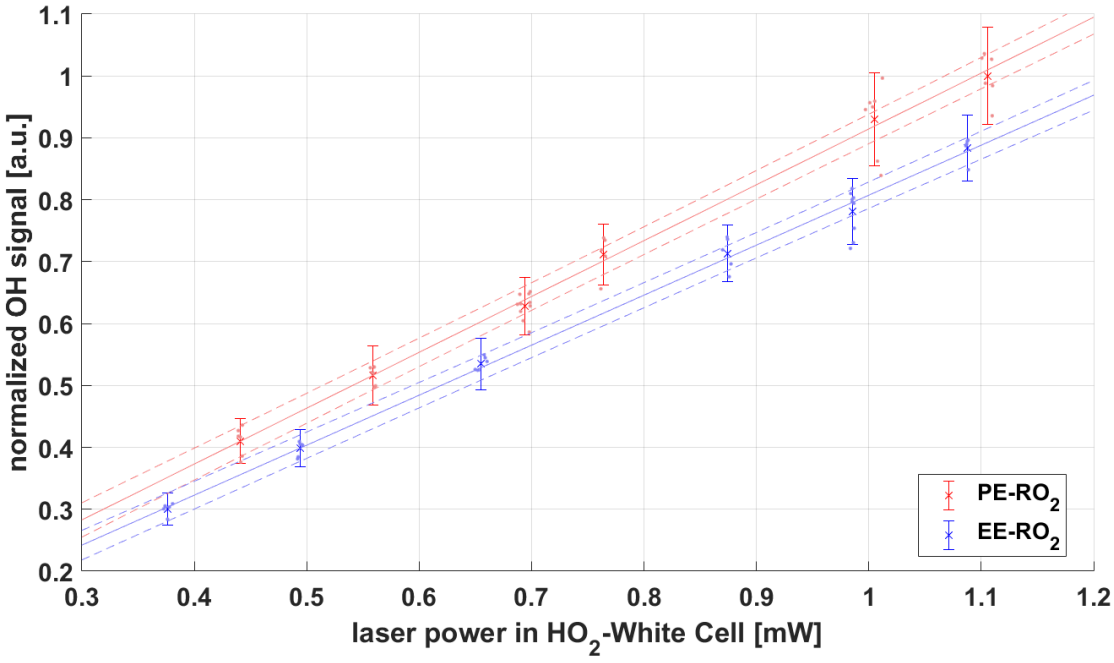

Figure 3.8 Normalized OH signal from PE-RO_2 (red) and BE-RO_2 (blue) vs. laser power inside of the White cell, with a NO mixing ratio of $9 \cdot 10^{-4}$. The lines show the linear fit for both RO_2 (solid line) and the 95 % confidence interval (dashed lines) (taken from Kunkler (2021)).

For EE-RO_2 and IE-RO_2, the model was able to describe the measured data within the margin of error. For BE-RO_2 and PE-RO_2 the model underestimated the measured results, with a yield of >100 % for both species. This indicates additional radical sources through reactions inside of HORUS, which are not considered.

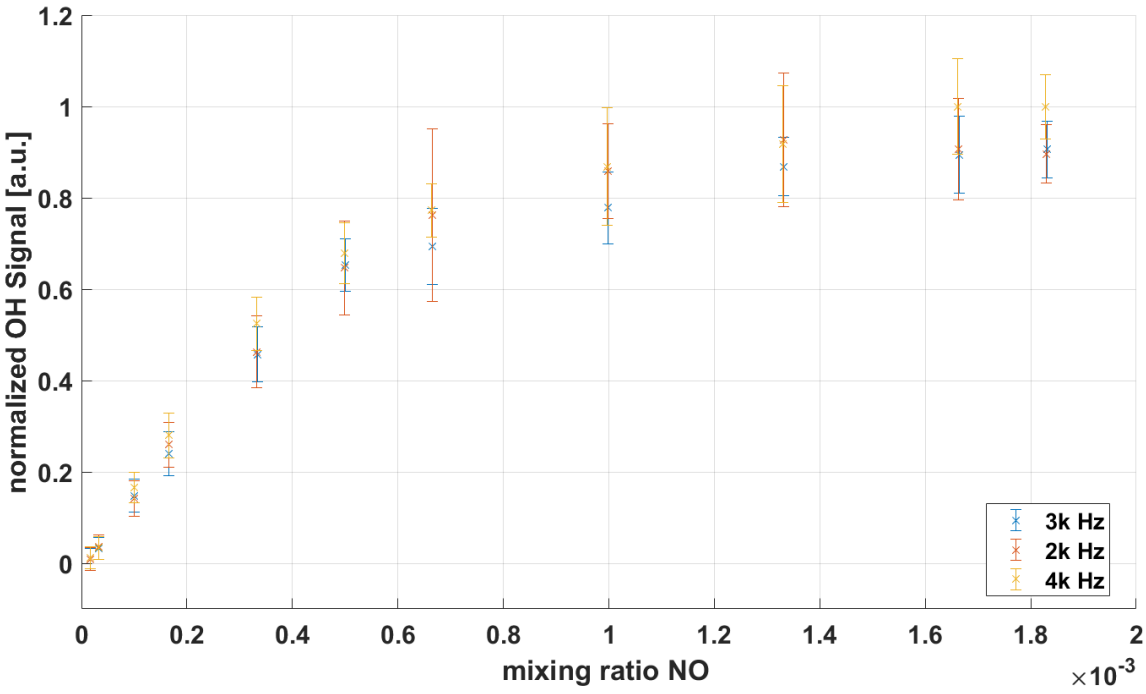

Figure 3.9 Normalized OH signal for PE-RO_2 vs. NO mixing ratio for different laser repetition rates (2000, 3000, 4000 Hz). The OH signal with 4k Hz repetition rate is slightly higher than with lower repetition rate, indicating multiple excitations of OH (taken from Kunkler (2021)).

Interference from RO_2 originating from benzene

Additionally, HO_2 interference from OH-initiated oxidation products of benzene were investigated. As described in 1.4.1, oxidation of benzene by OH can yield peroxy radicals as well as phenol, which produces HO_2 (see Figure 1.5). The produced HO_2 cannot be separated from the sample air. The measured OH is thusly a sum of OH produced from RO_2 and phenol. For the model calculations, it was assumed that only phenol (~53 %) and a bicyclic RO_2 (~47 %) were produced as reported by Xu et al. (2020). Figure 3.10 shows modelled and measured OH mixing ratios vs NO mixing ratio. Measured HO_2-generated OH is shown as blue x with 1σ error bars. OH, generated from RO_2 is shown as the green line, while OH from phenol production is shown as the yellow line. The sum of both is shown as the red line. According to the model calculation, at high NO mixing ratios the yield of generated OH reaches almost unity. The measured OH mixing ratios were ~28±7 % lower than the model results, indicating radical loss reactions. The reaction of RO_2 with HO_2 can produce bicyclic alcohols, epoxides and peroxides (Birdsall & Elrod, 2011). However, Xu et al. (2020) reported a ~47 % yield of the bicyclic alkoxy radical **6**, due to the almost quantitative conversion of the bicyclic RO_2 **4** to **6**.

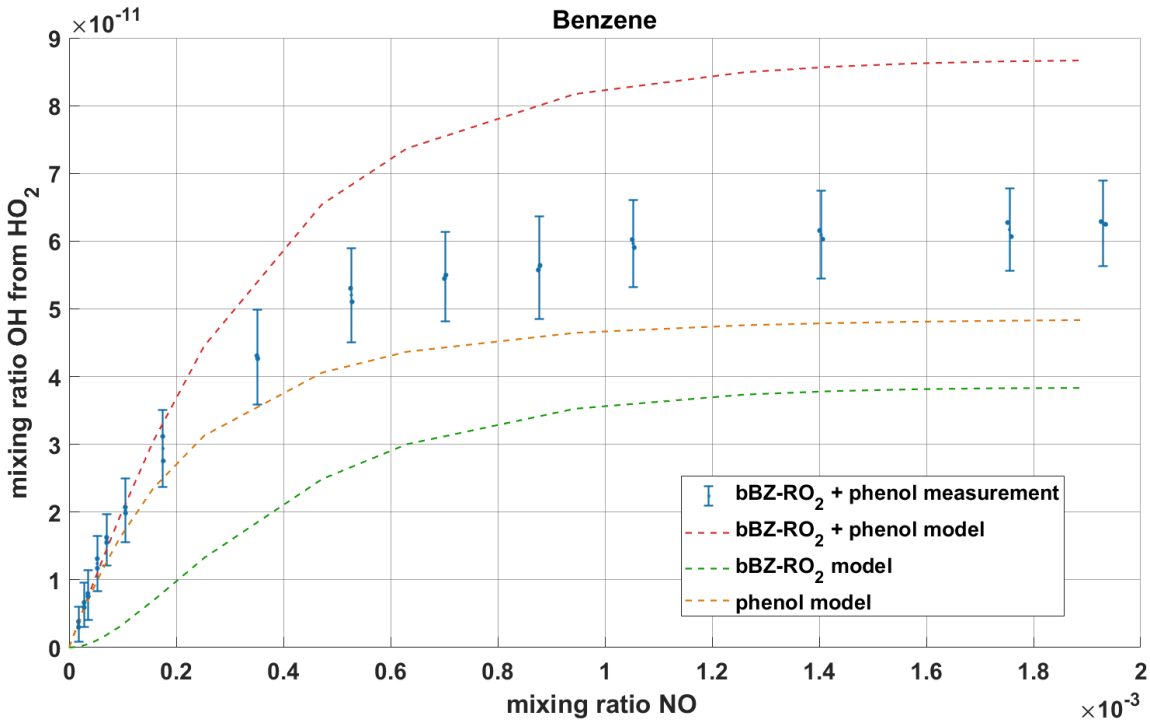

Figure 3.10 Mixing ratio of OH generated from the oxidation of benzene vs. NO mixing ratio. The shown points represent measured NO titrations, with 2σ error margin. The dotted lines show modeled data, with OH from the bicyclic RO_2 bBZ-RO_2 (green), OH from phenol (yellow) and the sum of both (red).

Other loss reactions include RO_2 self and cross reactions. However, a lower radical loss through these reactions is expected, since reaction rates of self and cross reactions of secondary and tertiary RO_2 are generally slower (Jenkin & Hayman, 1995) and the HO_2 mixing ratio during the measurement was higher than those of RO_2. Other loss reactions are the reaction of **4** or **6** with NO, both of which are reported to be insignificant as radical loss reactions. Since the unimolecular decomposition of **6** is pressure independent, while the reaction of **6** is a 3rd order reaction, the reaction rate of the unimolecular decomposition is expected to be 3-5 orders of magnitude faster than reaction of **6** with NO (Birdsall & Elrod, 2011; Jenkin & Hayman, 1995; Xu et al., 2020). Similarly, Xu et al. (2020) reported a radical loss for the reaction of **4** with NO of <0.1 %. Therefore, the known reaction pathways of the OH-initiated oxidation products of benzene cannot sufficiently explain the observed radical loss. It is suspected that long lived oxidation products may occur, which do not have sufficient time to form radical under the conditions inside the HORUS instrument.

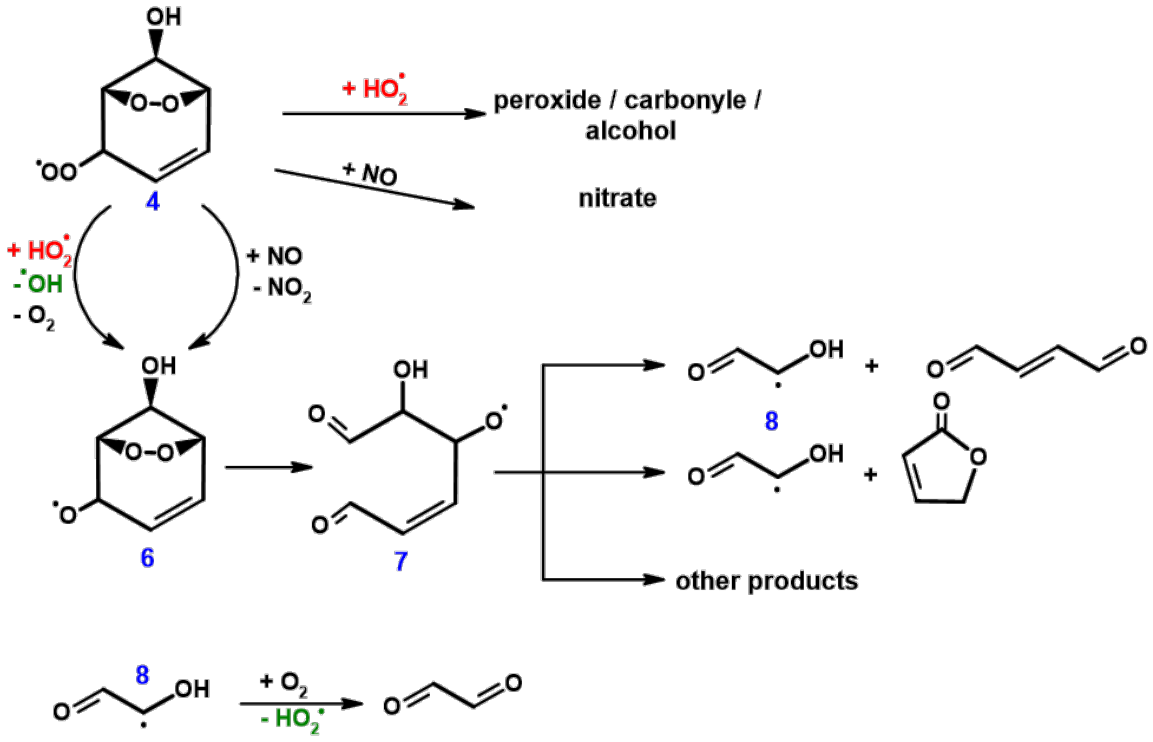

Figure 3.11 Schematic overview of the reaction pathway of bicyclic peroxy radical of benzene **4**. Produced HO_2 is shown in green, while HO_2, which is used up is shown in red (Taken from Kunkler (2021)).

Implications on RO_2 interference correction using CAABA/MECCA

The RO_2 interference of several $RO_{2\,sat}$, and $RO_{2\,unsat}$, as well as the RO_2 from benzene oxidation was investigated inside HORUS and compared to CAABA/MECCA model calculations. The interference caused by RO_2 from methane and propane was described by the model within the error margin. The model did underestimate the interference from BA-RO_2, which could not be explained with known products from the OH-initiated oxidation of butane. It is possible, that a 1,5-H-shift of the alkoxy radical of BA-RO_2 lead to reactions, which can produce OH. Further investigations are needed.

The interference caused by $RO_{2\,unsat}$ was investigated for the RO_2 of ethene, propene, but-1-ene and isoprene. Model calculations of interference caused by EE-RO_2 and IE-RO_2 were able to describe measured interference within the error margin. The model underestimated the interference caused by BE-RO_2 and PE-RO_2. The measured radical yield of >100 % indicates an additional radical source. Tests, to investigate, whether the additional interference is caused by laser generated OH or multiple excitation-emission-cycles, did not show positive results. This indicates, that during the test additional radical sources occur for these RO_2 within the HORUS system.

The interference caused by RO_2 from benzene was caused by HO_2 from the formation of phenol and from the RO_2 branch of the oxidation mechanism (see Figure 1.5 and Figure 3.11). The model calculation overestimated the total amount of OH produced through these reactions by ~28±7 %. The known radical loss reaction within the oxidation mechanism were not sufficient to explain the lower measured radical yield and it is therefore assumed, that some long-lived oxidation products occur. These long-lived products may not have enough time to produce radicals within the time frame of the injection of NO and the point of measurement.

The tests employed in this chapter showed that CAABA/MECCA calculations are able to describe RO_2 interference from certain RO_2 of the saturated and unsaturated groups within the margin of error. Some RO_2 showed discrepancies between the model and measurement, which are not explained by the known oxidation mechanisms. It is likely that the method of RO_2 production used for the tests, caused some of the discrepancies, since it was not possible to separate the produced RO_2 from reactants and possible side products. Due to the extensive OH-initiated oxidation mechanism of benzene, the RO_2 interference caused by benzene RO_2 cannot be sufficiently described and needs further investigation.

Additionally, it is unclear, whether these studies can describe more complex RO_2, e.g. from terpenes, or higher oxygenated RO_2 using the simple separation into $RO_{2\,sat}$ and $RO_{2\,unsat}$. Further studies are needed to investigate these groups of RO_2.

3.4 Summary

The knowledge of ambient RO_2 concentrations is important for LIF-FAGE measurements, as they cause an artificially increased HO_2 signal inside the instrument. Two methods to estimate RO_2 concentrations were reported. Using the NO/NO_2 photo stationary state assumption (Leighton, 1961), a sum of HO_2 and RO_2 can be calculated. The second method uses ambient HO_2 concentrations and OH reactivity. It is assumed, that the production of HO_2 and RO_2 during daytime is predominantly from the reaction of OH with VOC and CO, respectively. Additionally, by assuming that major loss for HO_2 and RO_2 are similar, the RO_2 concentration can be calculated by the HO_2 concentrations scaled by their respective production rates. This method allows the calculation of the RO_2 concentrations to be based on the measurements of HO_2, CO and VOC.

In order to correct for RO_2 interference, the efficiency of the conversion of RO_2 into OH inside the HORUS instrument was investigated. Two methods were employed. Firstly, a cost-effective estimate based on internal temperature and pressure was used by parameterizing temperature and pressure dependency of the conversion of $RO_{2\,sat}$ and $RO_{2\,unsat}$. Secondly, a model-based approach was used to estimate ambient RO_2

concentrations using titration of RO_2 by NO. By minimizing a cost function using the least squared method, it has been shown, that ambient concentrations of HO_2 and RO_2 can be extracted.

In order to validate the assumptions concerning the approach to correct RO_2 interference in HORUS, lab studies were conducted in the master thesis of Kunkler (2021). Several different RO_2 were produced in situ and used to perform NO titrations. CAABA/MECCA model calculations were done and compared with the measured NO titrations. It was shown that certain RO_2 of saturated and unsaturated origin are able to be described by the model with the margin of error. However, the model underestimated the interference caused by the RO_2 of butane, but-1-ene and pent-1-ene. It is unknown from which sources the additional radical originated, since known reaction pathways are not sufficient to explain the discrepancy. Additionally, the interference of the RO_2 of benzene was overestimated by the model. It is suspected that the short reaction time inside the HORUS system leads to long lived products of the oxidation not being able to produce radicals.

Furthermore, it is unclear, whether the separation used here is sufficient to describe more complex or higher oxygenated RO_2. Further studies are needed.

4 AQABA field campaign

Throughout the last century, the region around the Arabian Peninsula has seen strong economic development due to its rich oil and gas reserves. Extraction, industrialization and urbanization caused the Middle East to become a global hot spot for air pollution. Additionally, the region has exceptional environmental and meteorological conditions, with extensive deserts, intense solar radiation and high temperatures. Nonetheless, observational data is sparse and the Arabian Basin receives little attention, e.g. in report of the Intergovernmental Panel on Climate Change (IPCC).

The AQABA (**A**ir **Q**uality and Climate Change in the **A**rabian **Ba**sin) field campaign was a comprehensive ship borne experiment conducted in summer of 2017. A dataset including measurements of the oxidants OH and HO_2; trace gases such as O_3, CO, NO, NO_2, H_2O_2, HCHO, HONO; a range of VOCs and their oxidation products; aerosol size distribution, photolysis frequencies; and meteorological properties. From June to September 2017, the research and survey vessel *Kommandor Iona* (Hays Ships Ltd.) sailed from Toulon (France) to Kuwait and back (Figure 4.1), covering the Mediterranean Sea, Red Sea, Arabian Sea, and Arabian Gulf.

Figure 4.1 Map of the track covered by the AQABA field campaign in 2017. Starting in Toulon, France, measurements were taken through the Mediterranean Sea, Suez Canal, Red Sea, Arabian Sea and Arabian Gulf.

The general objective of the AQABA 2017 campaign was to comprehensively characterize the atmospheric physics and chemistry in the regions surrounding the Arabian Peninsula, as well as the Mediterranean Sea.

In order to measure OH and HO_2, the ground-based **H**ydr**O**xyl **R**adical Measurement **U**nit based on fluorescence **S**pectroscopy (HORUS) by the Max Planck Institute for Chemistry (Mainz, Germany) was deployed during the AQABA campaign.

4.1 Instrumentation

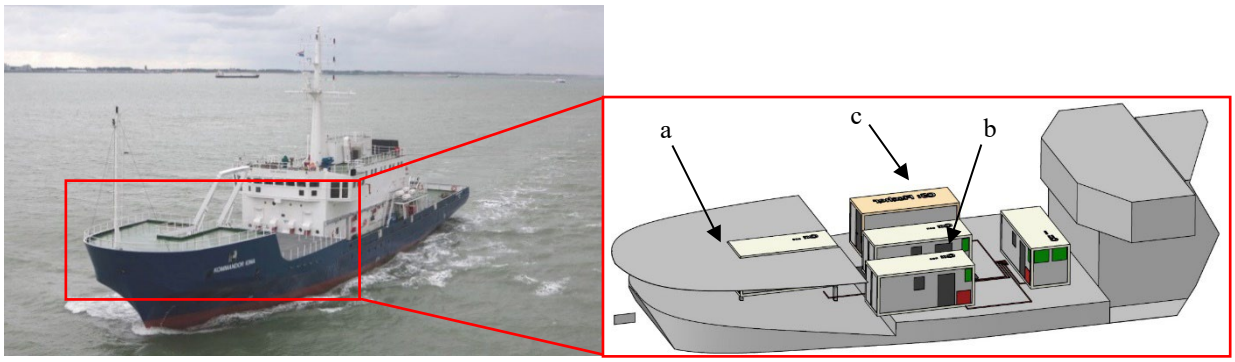

Figure 4.2 Kommandor Iona (Hays Ships Ltd.) (left) and CAD drawing of Main Deck and Forecastle Deck (right). The HO_x inlet was located on the forecastle deck (a). A 6 m high common inlet was used for measurements of NO_x, O_3, HCHO, H_2O_2, ROOH, SO_2, CO, VOC, OVOC and OH reactivity (b). For measurements of aerosol particles, a silica gel aerosol dryer was installed approx. 12 m above sea level (c) (Celik et al., 2020).

During the intensive measurement period of AQABA 2017 campaign, a broad set of instrumentation were installed on the research and survey vessel *Kommandor Iona* (Hays Ships Ltd.). Three positions were chosen to set up the inlets of instruments measuring trace gases, as well as photolysis frequencies. OH, and HO_2 were measured on the Forecastle Deck (a, see Figure 4.2) to reduce the impact of obstructions of the ship. A 6 m high cylindrical stainless-steel common inlet was installed for the measurements of O_3, NO_x, CO, H_2O_2, ROOH, HONO, VOC, OVOC, HCHO, and OH reactivity (b). A silica gel aerosol dryer was installed for sampling aerosol measurements (c). A brief summary of instrumentation, with time resolution, uncertainties and limits of detection are given in Table 4.1.

4.2 Regional characteristics

In order to simplify comparison between the many different environmental conditions sampled during AQABA, eight distinct regions along the ship's track were identified (Figure 4.3); the Mediterranean Sea, Suez Canal and Gulf of Suez, northern Red Sea,

southern Red Sea, Gulf of Aden, Arabian Sea, Gulf of Oman, and Arabian Gulf. The Arabian Gulf is well known for its extensive oil and gas industry as well as intensive ship traffic. High emissions of VOC, NO_x and CO are expected. Additionally, high photochemistry is expected due to intense solar radiation. Similar conditions, but to a lesser extent, are expected for the Gulf of Oman. The Arabian Sea is a comparably pristine environment, with low levels of NO_x, O_3 and VOC. Ship traffic in the Gulf of Aden is denser as it is funneled in and out of the Arabian Sea. Additionally, air masses from east of the horn of Africa are expected to bring aged biogenic and anthropogenic emissions. The Red Sea is separated in the southern and northern section, with extensive oil and gas extraction in both parts. Additionally, northern Red Sea is influenced strongly by the metropolitan areas along the northern Nile river. In both regions, high particle number concentrations are expected due to the surrounding Sahara and Arabian Deserts. The narrow Suez Canal can be characterized by its high density of ship traffic and strong influence from the Cairo metropolitan area. The Mediterranean Sea is mostly influenced by aged air from the European mainland.

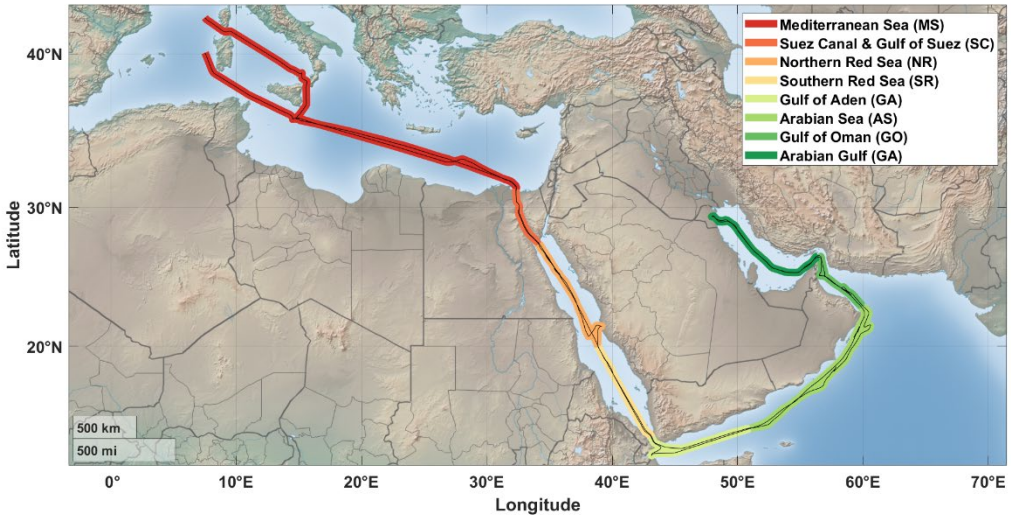

Figure 4.3 Ship track of the *Kommandor Iona* during AQABA (black). The cruise was separated into eight distinct regions.

4.2.1 Back-trajectories during AQABA

Back-trajectories of air parcels encountered along the ship track have been calculated using **Hy**brid **S**ingle-**P**article **L**agrangian **I**ntegrated **T**rajectory model (HYSPLIT). The general origin of air masses of leg 1 and leg 2 of the AQABA field campaign are shown in Figure 4.4 and Figure 4.5, respectively.

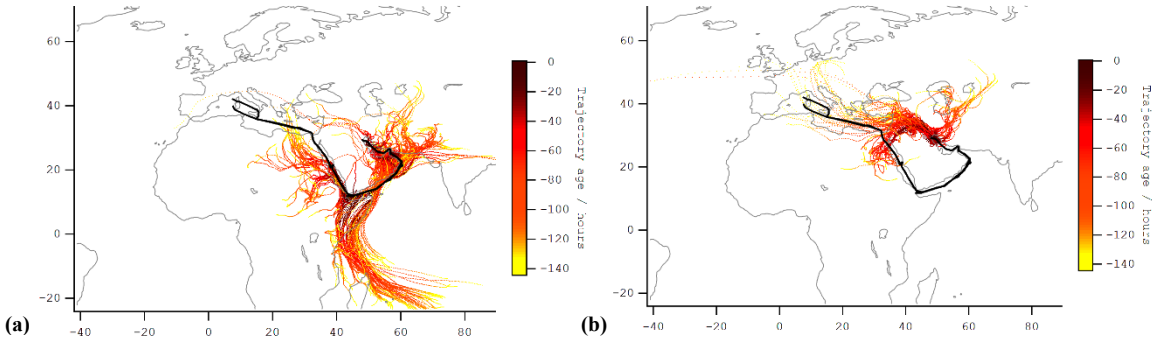

Figure 4.4 HYSPLIT back-trajectories of leg 1 of the Gulf of Aden, the Arabian Sea, and the Gulf of Oman (a), and the Arabian Gulf (b). The black line shows the ship track. The color of the trajectories shows the age of the air mass in hrs (D. Walter, personal communication, 23. Nov.2017).

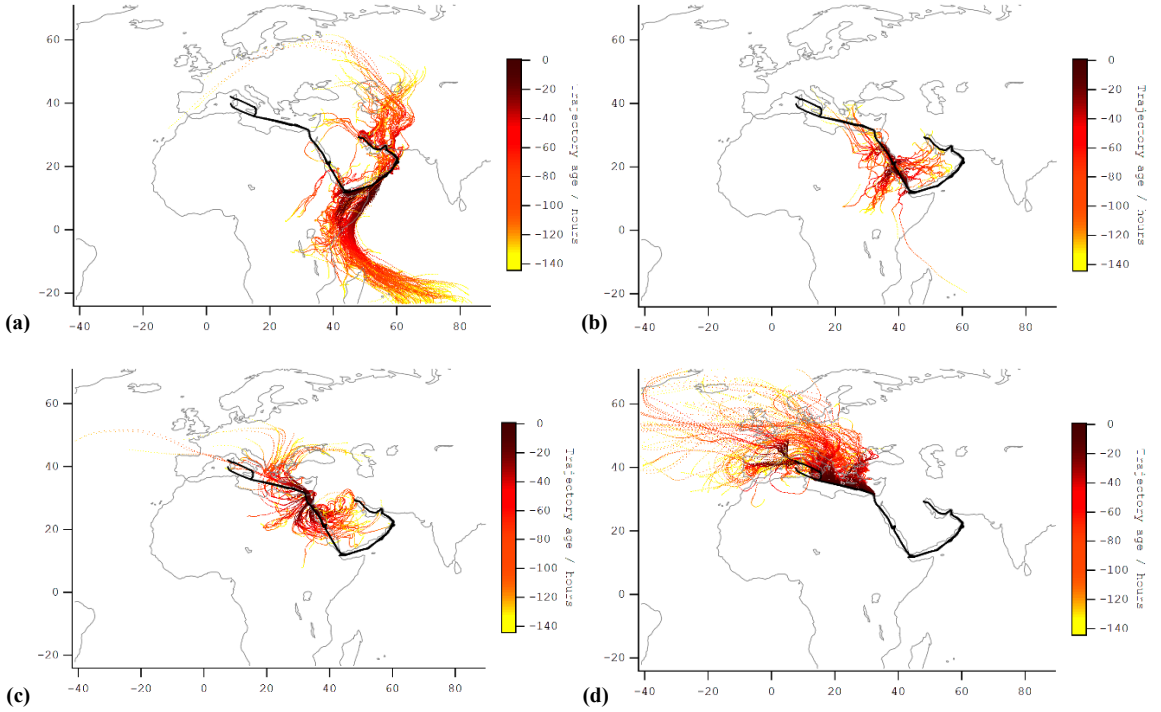

Figure 4.5 HYSPLIT back-trajectories of leg 2 of the AQABA campaign. The Arabian Gulf, the Gulf of Oman, the Arabian Sea, and the Gulf of Aden are shown in panel (a). The Red Sea is shown in panel (b). The Suez Canal is shown in panel (c), and the Mediterranean Sea is shown in panel (d). The black line shows the ship track. The color of the trajectories shows the age of the air mass in hrs (D. Walter, personal communication, 23. Nov.2017).

Table 4.1 Excerpt of instrumentation installed during AQABA 2017. Only species listed, which are used within this work.

Species	Time resolution	Accuracy (1σ)	Precision (1σ)	Limit of detection	Technique/ Instrument	Institution
OH	14 sec	17 %	0.065 – 0.26 pptv	0.03 – 0.15 pptv	IPI-LIF-FAGE	MPIC
HO_2	14 sec	20 %	0.95 – 10 pptv	0.22 – 2.01 pptv	IPI-LIF-FAGE	MPIC
NO	5 sec	5.61 % [#]	4.4 pptv [#]	10.5 pptv [#]	CLD analyzer	MPIC
NO_2	5 sec	7 % [#]	112.4 pptv [#]	26.1 pptv [#]		MPIC
O_3	5 sec	2 % [#]	2% [#]	3 ppbv [#]	Optical absorption	MPIC
HCHO	3 min	13.2 % [##]	6.8 % @ 8.59 ppbv [##]	0.128 ppbv [##]	Hantzsch monitor	MPIC
H_2O_2	3 min	3 % [##]	1.2 % @ 4.36 ppbv [##]	8 pptv [##]	HPLC	MPIC
ROOH	3 min	3 % [##]	1.8 % @ 4.49 ppbv [##]	6 pptv [##]		MPIC
SO_2	10 sec	20 %	4 %	163 pptv	CIMS	MPIC
CH_4	1 min	0.3 ppbv [*]	0.1 % [*]	N/A	CRDS/PICARRO	LSCE
CO	1 min	8 ppbv [*]	5 % [*]	N/A		LSCE
CO	1 sec	20 %	11 – 19 %	4.2 – 8.5 pptv	QCL spectrometer	MPIC
HONO	1 min	20 %	-	3 pptv	LOPAP	MPIC
VOC	50 min	-	- [**]	- [**]	GC-MS	MPIC1
OVOC		-	-	-	PTR-TOF-MS	MPIC
OH reactivity	5 min	26 – 35 % [+]	0.05 – 54.54 s^{-1} [+]	5.4 – 12.19 s^{-1} [+]	CRM	MPIC
Photolysis frequencies	10 sec	> 10 %	-	-	Spectral radiometry	MPIC
Aerosols	-	-	-	-	CNC, OPC, FMPS, AMS	MPIC

[#] (Tadic et al., 2020), [##] (Dienhart et al., 2022), [*] (Paris et al., 2021), [**] see (Bourtsoukidis et al., 2019) for full list of measured VOC, uncertainties and limit of detection have a range depending on VOC species, [+] (Pfannerstill et al., 2019)

Acronyms: **CLD** = Chemiluminescence Detector, **HPLC** = High Performance Liquid Chromatography, **CIMS** = Chemical Ionization Mass Spectrometry, **CRDS** = Cavity Ring-Down Spectroscopy, **QCL** = Quantum Cascade Laser, **LOPAP** = Long-Path Absorption Photometer, **GC** = Gas Chromatography, **PTR-TOF MS** = Proton Transfer Reaction Time-of-Flight Mass Spectrometry, **CRM** = Comparative reactivity method, **CNC** = Condensation Nuclei Counter, **OPC** = Optical Particle Counter, **FMPS** = Fast Mobility Particle Sizer, **AMS** = Aerosol Mass Spectrometer

4.3 Observations

4.3.1 NO_x and O_3

Since NO_x and O_3 are closely related with each other through NO_x/O_3 PSS (see 3.1.1), observations are shown together for both legs (Figure 4.6 a & b). A summary of median and respective quantiles for NO_x and O_3 during the AQABA campaign is shown in Table 4.2. Tadic et al. (2020) reported NO_x mixing ratios during AQABA range from less than 50 pptv in the pristine regions of the Arabian Sea to more than 10 ppbv in regions of high anthropogenic pollution. High NO_x medians were observed in the northern Red Sea (1.76 ppbv), the Gulf of Oman (2.74 ppbv) and the Arabian Gulf (1.26 ppbv). The air masses observed in these regions bring fresh pollution from nearby metropolitan areas. In combination with local point sources (e.g. oil rigs), NO_x levels are increased. The southern Red Sea, Mediterranean Sea and Arabian Sea showed median NO_x mixing ratios of 0.46, 0.25 and 0.19 ppbv, respectively.

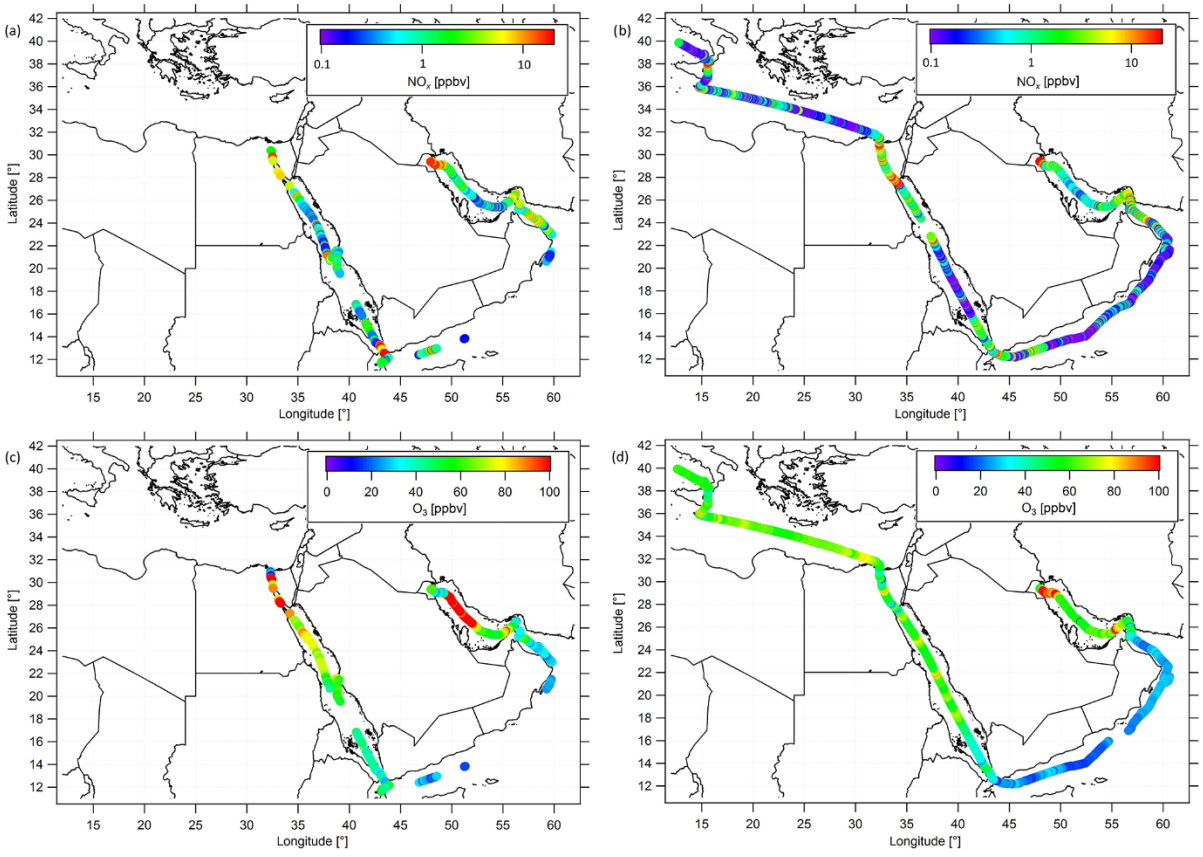

Figure 4.6 Ship cruises with color-scaled NOx mixing ratios (logarithmic scale) during (a) the first and (b) the second leg, and color-scaled O_3 mixing ratios (linear scale) during (c) the first and (d) the second leg. Note that both NO_x and O_3 have been filtered for contamination from the ship's stack. (taken from Tadic et al. (2020))

Figure 4.6 c & d show O_3 mixing ratios for both legs with a range between 20 to 170 ppbv, reported by Tadic et al. (2020). The lowest median O_3 mixing ratios were observed in the Arabian Sea (21.5 ppbv), which is the only region representing the remote MBL. Low median O_3 mixing ratios were also observed in the Gulf of Oman (31.5 ppbv), which in combination with NO_x mixing ratios suggest O_3 destruction by fresh NO emissions. In the Arabian Gulf, O_3 events of up to 170 ppbv were observed with a median of 62.5 ppbv. O_3 mixing ratios in the Mediterranean Sea, southern and northern Red Sea are 61.5, 64.2 and 46.9 ppbv, respectively. The air masses observed over the Mediterranean Sea was characterized as photochemically aged due to the northerly winds, which bring oxidized air masses from Turkey, Greece and the Balkans (Pfannerstill et al., 2019). This led to low variability in the O_3 mixing ratio in this region. Contrary, large amounts of pollution sources in the Arabian Gulf caused high variability in the measurements.

Table 4.2 Overview of measured NO_x (top panel) and O_3 (bottom panel) median mixing ratios in ppbv including 1st and 3rd quantile (taken from Tadic et al. (2020).

NO_x	Mediterranean Sea	Northern Red Sea	Southern Red Sea	Arabian Sea	Gulf of Oman	Arabian Gulf
1st quantile	0.12	0.68	0.18	0.10	1.03	0.52
median	0.25	1.76	0.46	0.19	2.74	1.26
3rd quantile	0.96	5.68	1.60	0.54	5.92	3.47
O_3	Mediterranean Sea	Northern Red Sea	Southern Red Sea	Arabian Sea	Gulf of Oman	Arabian Gulf
1st quantile	57.05	53.51	40.68	17.45	26.7	53.1
median	61.54	64.16	46.93	22.52	31.5	62.5
3rd quantile	66.48	75.51	60.28	26.19	38.0	90.4

4.3.2 HCHO, H_2O_2 and ROOH

Measurements of HCHO, H_2O_2 and ROOH were reported by Dienhart et al. (2022). A summary of median and respective quantiles for HCHO, H_2O_2 and ROOH during the AQABA campaign is shown in Table 4.3. Highest HCHO mixing ratios (Figure 4.7 a & b) were observed in the Arabian Gulf (12.6 ppbv) from air masses originating from Iraq and Kuwait, indicating fresh emissions from local sources. The lowest median mixing ratios were observed in the southern Red Sea (0.37 ppbv) from unpolluted air masses originating in Eritrea. Low mixing ratios were also found the Arabian Sea (0.86 ppbv) and the Mediterranean Sea (0.77 ppbv), indicating aged age masses with only minor fresh emissions from anthropogenic or biogenic sources. The highest median mixing ratios were reported for the Arabian Gulf (3.1 ppbv), the Suez Canal (1.5 ppbv) and the Gulf of

Oman (1.2 ppbv), which showed high levels of VOCs (Bourtsoukidis et al., 2019) and OH reactivity (Pfannerstill et al., 2019) while the lowest were observed in the southern Red Sea, Mediterranean Sea and Arabian Sea with 0.37, 0.77 and 0.86 ppbv, respectively.

Figure 4.7 c & d shows H_2O_2 mixing ratios for both leg 1 and 2. Compared to HCHO, lower variability in mixing ratios were observed for H_2O_2. Lowest median mixing ratio with 0.13 ppbv for the Gulf of Oman, while highest were found in the Mediterranean Sea (0.26 ppbv), the Suez Canal (0.25 ppbv) and southern Red Sea (0.25 ppbv). High H_2O_2 mixing ratios are generally associated with high HO_2 mixing ratios, since the reaction of HO_2 with itself is the major production channel for H_2O_2.

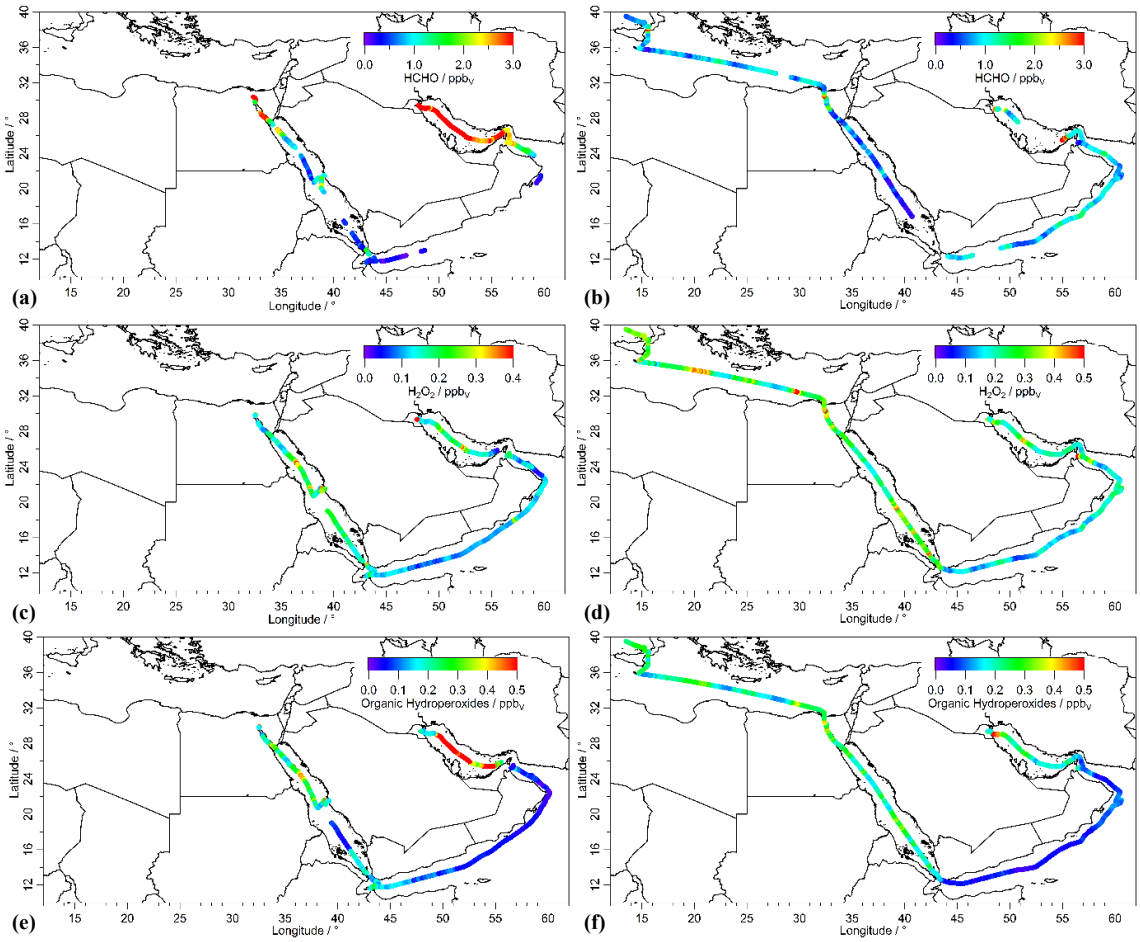

Figure 4.7 Overview and data coverage of HCHO, H_2O_2 and organic hydroperoxide measurements during both legs of the AQABA ship campaign (graphs on the left represent the first leg). Contaminated HCHO data (e.g. by ship exhausts) was removed from the dataset with a stack filter, therefore there is less HCHO data coverage during the first leg in the Arabian Sea. (taken from Dienhart et al. (2022))

Organic peroxides (ROOH) are shown in Figure 4.7 e & f. Overall variability is higher than H_2O_2 variability. The highest mixing ratio was observed during the first leg in the Arabian Gulf (2.26 ppbv). Highest median mixing ratios were observed in the Arabian Gulf

(0.23 ppbv). High VOC concentrations and strong solar radiation are likely to cause high levels of RO_2, which, in turn, result in high ROOH mixing ratios in this region. Lowest median mixing ratios were measured in the Arabian Sea (0.057 ppbv) and the Gulf of Oman (0.07 ppbv). Methyl hydroperoxide (MHP), peracetic acid (PAA) and ethyl hydroperoxide (EHP) were identified as the major contributors to organic peroxides. In the Arabian Gulf, significantly increased levels of EHP were detected.

Table 4.3 Overview of measured HCHO (top panel), H_2O_2 (middle panel) and ROOH (bottom panel) median mixing ratios in ppbv including 1st and 3rd quantile (taken from Dienhart et al. (2022)).

HCHO	Mediterranean Sea	Suez Canal	Northern Red Sea	Southern Red Sea	Arabian Sea	Gulf of Oman	Arabian Gulf
1st quantile	0.60	0.9	0.52	0.23	0.63	0.90	2.4
median	0.77	1.5	0.76	0.37	0.86	1.22	3.1
3rd quantile	0.99	2.9	1.26	0.57	1.05	2.33	4.5
H_2O_2	Mediterranean Sea	Suez Canal	Northern Red Sea	Southern Red Sea	Arabian Sea	Gulf of Oman	Arabian Gulf
1st quantile	0.20	0.19	0.14	0.18	0.12	0.08	0.17
median	0.26	0.25	0.19	0.25	0.15	0.13	0.21
3rd quantile	0.33	0.35	0.25	0.32	0.19	0.19	0.33
ROOH	Mediterranean Sea	Suez Canal	Northern Red Sea	Southern Red Sea	Arabian Sea	Gulf of Oman	Arabian Gulf
1st quantile	0.16	0.20	0.15	0.12	0.046	0.048	0.18
median	0.22	0.26	0.21	0.17	0.057	0.070	0.23
3rd quantile	0.27	0.33	0.28	0.23	0.084	0.097	0.43

4.3.3 Methane

Figure 4.8 shows methane mixing ratios from the first (a) and second leg (b), reported by Paris et al. (2021). Highest median mixing ratios were observed in the Arabian Gulf (1926 ppbv, 75% quantile: 1941 ppbv) and during the second leg in the Mediterranean Sea (1926 ppbv, 1937 ppbv). Median mixing ratios in the Mediterranean Sea during the first leg were significantly lower (1881 ppbv, 1884 ppbv). Lowest median methane mixing ratios were reported in the Arabian Sea (1813 ppbv, 1831 ppbv) and Gulf of Oman (1831 ppbv, 1853 ppbv).

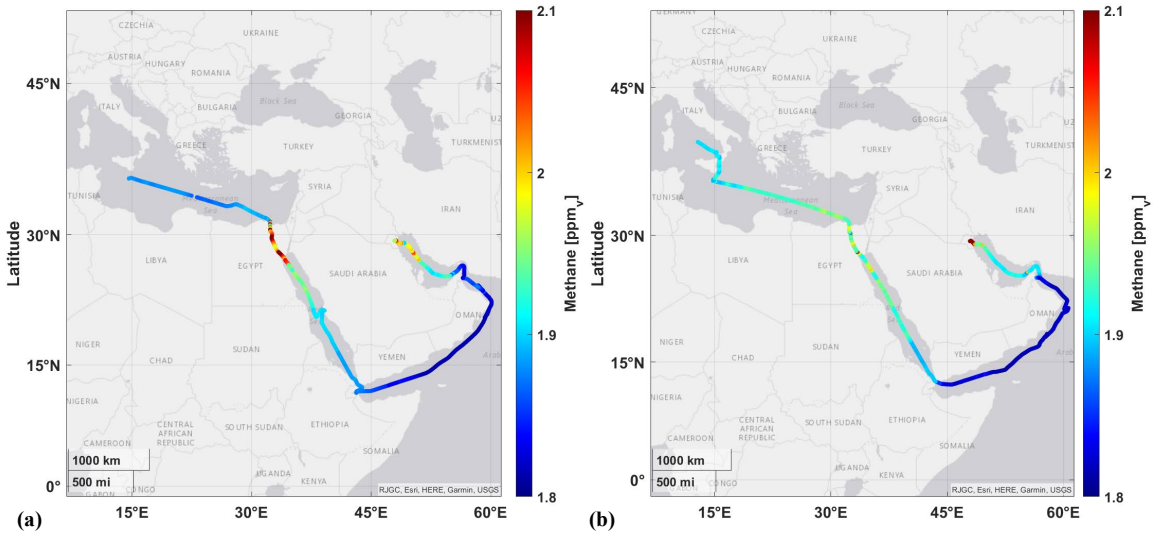

Figure 4.8 Overview of ship cruises with color-scaled mixing ratios of methane during the first (a) and the second leg (b). The data was filtered for contamination of the ship's own exhaust.

4.3.4 HONO

Measurements of HONO were conducted using a Long-Path-Absorption-Photometer. Data coverage and mixing ratios are shown in Figure 4.9. High mixing ratios were found in regions with high density of ship traffic, e.g. Suez Canal and near harbors. Highest median mixing ratios were observed during the first leg in the Suez Canal (0.38 ppbv, 75% quartile: 0.44 ppbv) and the Southern Red Sea (0.41 ppbv, 2.51 ppbv), while lowest mixing ratios were measured during the second leg in the Arabian Sea (0.005 ppbv, 0.019 ppbv) and Gulf of Aden (0.07 ppbv, 0.13 ppbv), which were both influenced by air masses originating in the Indian Ocean south of the Horn of Africa.

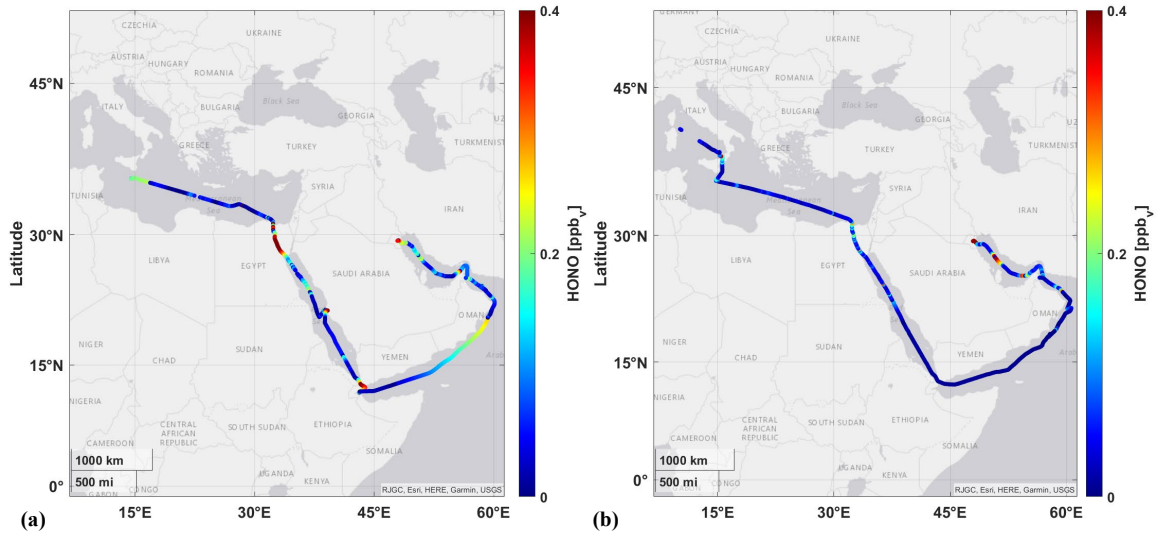

Figure 4.9 Overview of HONO data measured during AQABA. Color-scaling indicates the mixing ratio for the first (a) and second leg (b).

4.3.5 VOC / OVOC

Non-methane hydro carbons (NMHC) were reported by Bourtsoukidis et al. (2019). Figure 4.10 shows box plots of selected NMHC during the AQABA campaign. Overall lowest mixing ratios were found in the Arabian Sea, where the majority of NMHC were close to the limit of detection. Despite these clean conditions, ethene mixing ratios were elevated (0.09 ppbv), with a maximum of 0.24 ppbv. Since ethene is a highly reactive trace gas with relatively low lifetime, high mixing ratios indicate a local source. Similar conditions were observed in the Mediterranean Sea, with average values being slightly higher than in the Arabian Sea. High mixing ratios were found in the Suez Canal, due to intensive ship traffic and proximity to populated areas. The most abundant alkanes were n-butane (3 ppbv), ethane (2.64 ppbv) and i-butane (1.39 ppbv), while ethene (0.81 ppbv) dominated alkenes. The northern and southern part of the Red Sea showed very different NMHC mixing ratios. The northern Red Sea showed a strong influence from air coming from highly populated and industrialized north-eastern part of Africa (Egypt, Libya), causing NMHC mixing ratios to be higher than in the southern Red Sea. Both alkanes and alkenes were dominated by species of shorter chain length. In the southern Red Sea, air masses originating from central Africa led to lower overall mixing ratios, the southern part was mostly influenced by air coming from central Africa. This caused NMHC in the southern part of the Red Sea to be significantly lower than in the northern part. NMHC in the Arabian Gulf were on average higher, due to high ship traffic and petrochemical industries. C_2-C_5 alkanes and alkenes showed high values as well as high variability, which is attributed to the diverse influence of strong local petrochemical sources.

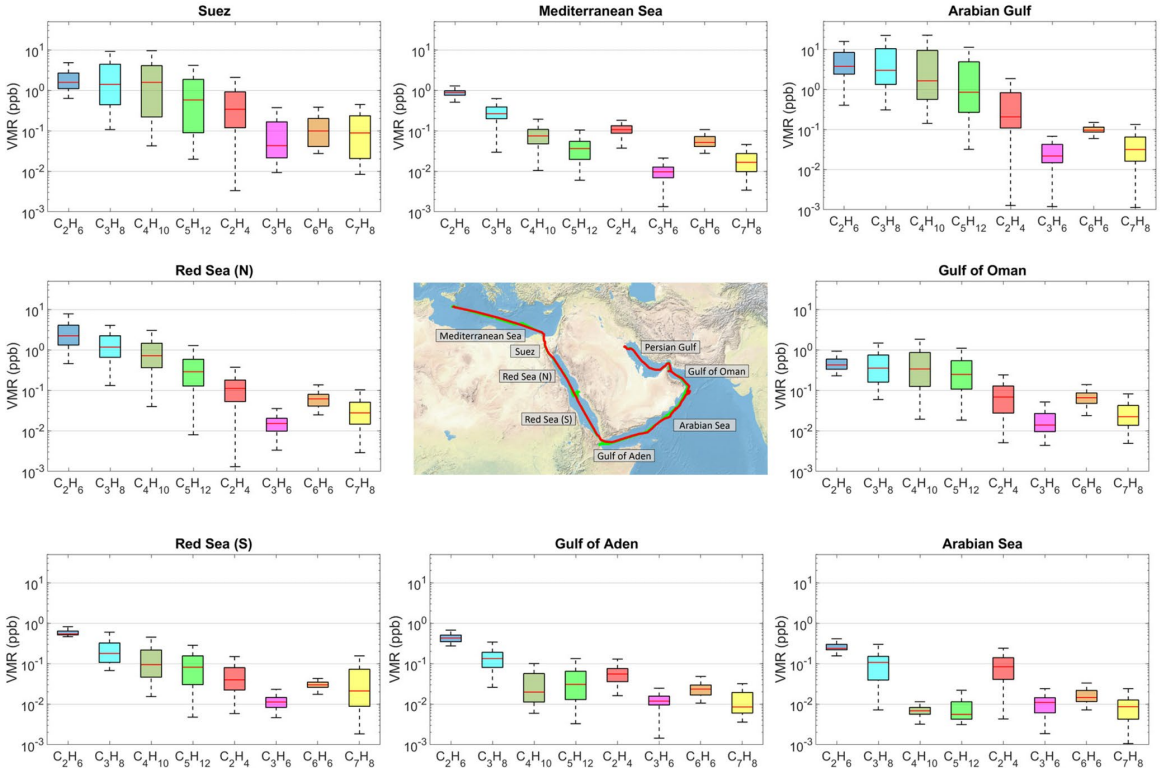

Figure 4.10 Volume mixing ratios of selected NMHC species over the eight regions. For each box, the central red line indicates the median mixing ratio for both campaign legs. The bottom and top edges of the box indicate the 25th (q1) and 75th (q3) percentiles respectively. The boxplot draws points as outliers if they are greater than q3+w×(q3–q1) or less than q1–w×(q3–q1). The whiskers correspond to ±2.7 σ and 99.3 % coverage if the data are normally distributed. The ship track of the first leg is shown in the map with the green line, the second leg with the red line. (Taken from Bourtsoukidis et al. (2019))

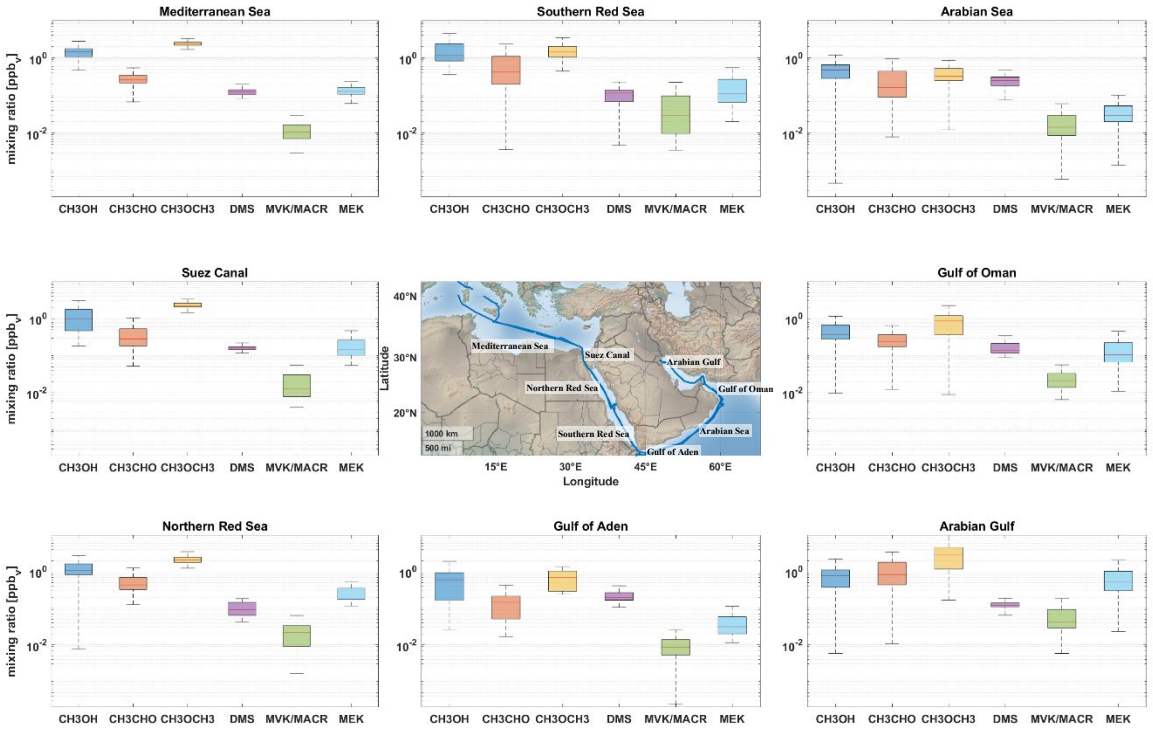

Figure 4.11 Mixing ratios of selected oxygenated VOC (OVOC) over the eight regions during the AQABA campaign. The top and bottom edges of each box indicate the 25th and 75th percentiles, respectively. The red line indicates the median for each box. The whiskers correspond to ±2.7 σ and 99.3 % coverage if the data is normally distributed. The ships track is shown in the middle panel.

Figure 4.11 shows box plots of selected OVOC for the regions during AQABA. Similar to NMHC, lowest median values of OVOC were observed in the Arabian Sea, with the exception of DMS (0.24 ppbv). This increase to the highest levels during the campaign indicates large amounts of phytoplankton, which can emit large amounts of DMS. In the Gulf of Oman and Gulf of Aden slightly higher mixing ratios for most OVOC were observed. Compared to the Arabian Sea, both gulf regions show higher acetone levels (Gulf of Oman, 0.87 ppbv, Gulf of Aden, 0.69 ppbv). Highest overall OVOC mixing ratios were found in the Arabian Gulf, with very high values for acetone (2.8 ppbv), acetaldehyde (0.81 ppbv) and methanol (0.77 ppbv). N. Wang et al. (2020) reported a good correlation between C_2-C_7 carbonyls during daytime, indicating ozone and carbonyls were co-produced via photochemical oxidation. The northern Red Sea, Suez Canal and Mediterranean Sea showed very similar mixing ratios of OVOC. Methanol and acetone show similar levels throughout the northern Red Sea, Suez Canal and Mediterranean Sea (~1 ppbv and ~2 ppbv, respectively), while decreasing mixing ratios were observed for acetaldehyde, MEK and MVK/MACR. Ketones can be released as a product of fuel combustion and the high concentrations in the Suez Canal are likely caused by the dense ship traffic in the narrow channel (Huang et al., 2018).

4.3.6 OH reactivity

OH reactivity was reported by Pfannerstill et al. (2019) and is shown in Figure 4.12. The range of OH reactivity during the AQABA campaign was from <5.4 s^{-1} (below detection limit) over the Arabian Sea up to 303.6 s^{-1} during fueling in Fujairah (UAE). As expected, regions with strong pollution like the Arabian Gulf and the Suez Canal had high median OH reactivity of 11.2 s^{-1} (75% quantile: 15.2 s^{-1}, Arabian Gulf) and 10.8 s^{-1} (18.8 s^{-1}, Suez Canal), respectively. The largest share in OH reactivity over the Arabian Gulf can be attributed to OVOC (35 %), followed by alkanes and alkenes (both 9 %). In the narrow Suez Canal, a strong influence of ship emissions can be seen by the large share of NO_x (10 %) in OH reactivity. OH reactivity in the northern Red Sea (median: 8.5 s^{-1}, 75% quantile: 15.0 s^{-1}), southern Red Sea (7.9 s^{-1}, 10.9 s^{-1}), Gulf of Aden (8.0 s^{-1}, 10.1 s^{-1}) and Gulf of Oman (8.4 s^{-1}, 10.5 s^{-1}) were in a similar range and are mostly attributed to emissions from ship traffic. Again, OVOC have the largest share of OH reactivity (12 – 21 %) followed by NO_x and alkenes (both 4 – 9 %) and inorganics (mostly SO_2 and CO) (4 – 6 %). Less reactive air was observed over the open seas of the Mediterranean (6.8 s^{-1}, 7.8 s^{-1}) and Arabian Sea (4.9 s^{-1}, 6.5 s^{-1}). Measurements over the Arabian Sea were often below the detection limit of 5.4 s^{-1}. OVOC were the largest contributors to OH reactivity with 11 – 12 %. Over the Mediterranean Sea, shipping emissions had a bigger influence compared to the Arabian Sea, evident from NO_x contribution of ~4 % in the Mediterranean and ~1 % in the Arabian Sea. In all regions, large fractions of OH reactivity (between 27±55 % in the Arabian Gulf, and 72±57 % in the Arabian Sea) could not be attributed to any trace gas.

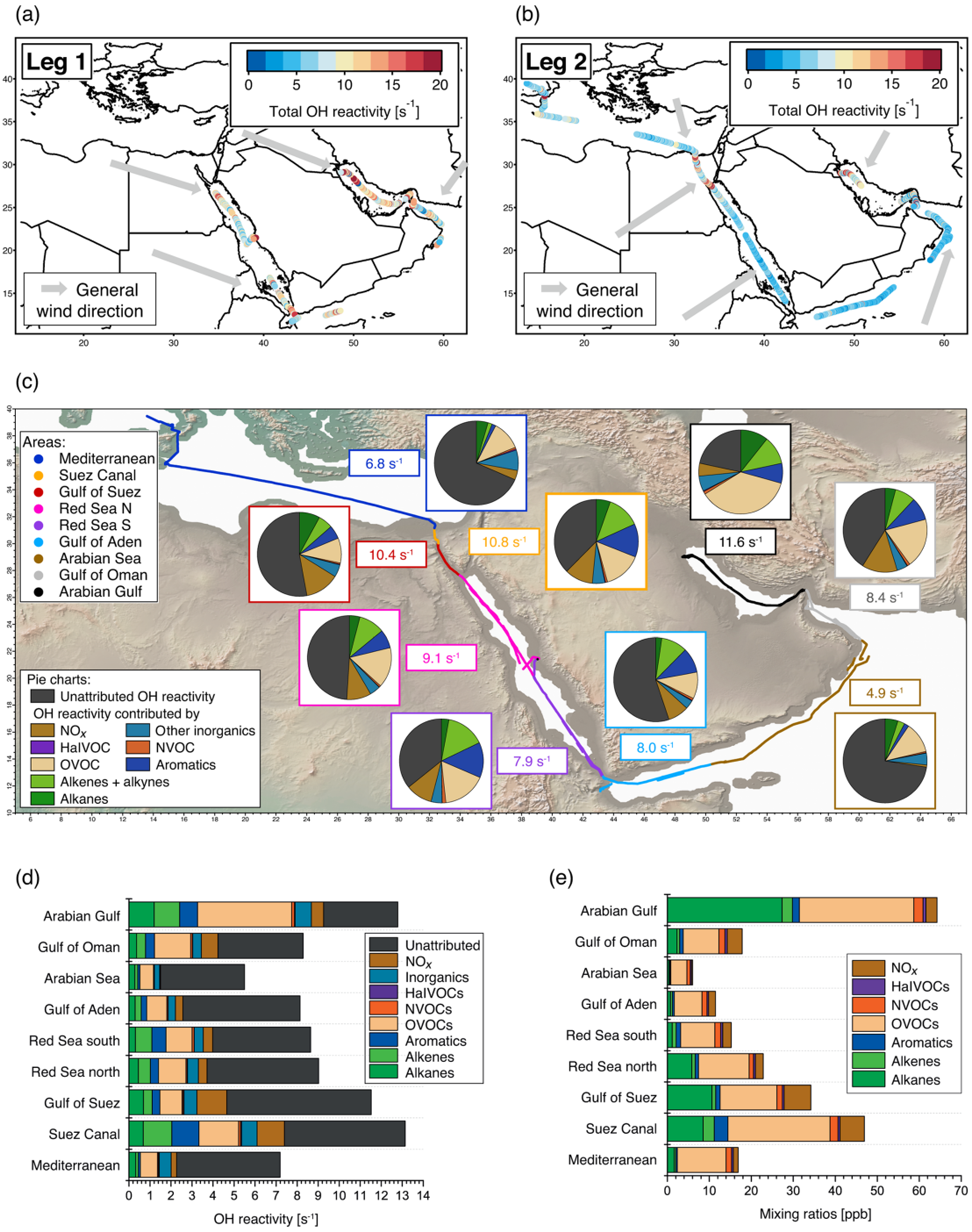

Figure 4.12 Overview of total OH reactivity around the Arabian Peninsula during the AQABA campaign. OH reactivity during (a) leg 1 (5–31 July 2017) and (b) leg 2 (3–31 August 2017). The maximum in the color scales is set to 20 s^{-1} for better visibility of differences, although there are a few data points above this value. Arrows depict general wind directions for the respective regions. (c) Total OH reactivity medians by region, and pie charts showing the contribution of compound classes for data points where speciated OH reactivity ≥ LOD (exception: pie charts of Mediterranean and Arabian seas show the average of all data points, due to the low number of points above LOD). (d) Average OH reactivity and speciation by region for all data points, including those where speciated OH reactivity was below the LOD. Error bars show the total uncertainty of the measurement. (e) Average mixing ratio of VOCs = trace gases in parts per billion by compound class and region (except for the class of inorganic compounds other than NO_x). Port calls and bunkering are excluded from all averages. (Taken from Pfannerstill et al. (2019))

4.4 OH and HO_2^*

4.4.1 Calibration

Determination of actinic flux density

In order to calibrate the HORUS system, it is necessary to know the actinic flux of the mercury vapor lamp used in the calibration, to calculate the OH and HO_2 concentration produced by the lamp. For this, the actinic flux measurement for the lamp used during AQABA was done according to 2.4.2.

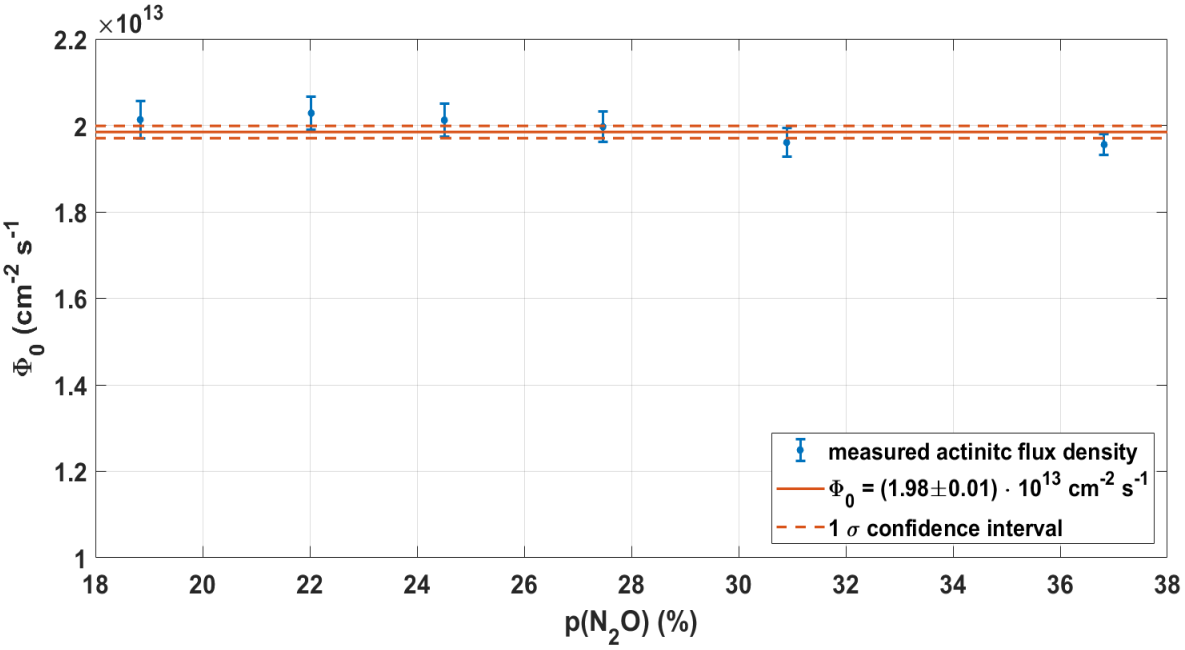

Figure 4.13 Actinic flux density of the pen ray lamp used in the calibration of the HORUS instrument. Error bars indicate the propagated statistical variability of the calculated flux density.

The resulting actinic flux density is shown in Figure 4.13. The measured actinic flux density was calculated to be $\Phi_0 = (1.98 \pm 0.01) \cdot 10^{13}$ $cm^{-2}s^{-1}$. The systematic error was calculated to be ~16.1 %. All contributing components are summarized in Table 4.4.

Table 4.4 Systematic uncertainties during actinometric measurement

Parameter	Uncertainty
NO Monitor (TEI)	7 %
NO standard (NIST)	1 %
Mass Flow Controller	2 %
Absorption cross section σ_{H_2O}	2 %
Quantum yield	1 %
Kinetic rate coefficients	12 %
Dimensions of reaction chamber	3 %
Pressure sensor	2 %
Variability of measured terms	5 %
Overall uncertainty	16.1 %

Calibration of the HORUS system

As an indirect measurement method, LIF-FAGE requires determination of instrument sensitivity. To ensure possible instability of the MCP detectors over a period of time as well as other factors impacting the sensitivity (e.g. wall losses, alignment of the White cell, etc.) regular calibrations of the HORUS system was done during AQABA, as described in 2.4.2. The sensitivity during AQABA vs. time is shown in Figure 4.14. c_{OH} (blue) is the sensitivity of the OH detector towards OH. c_{HO_2} (red) is the sensitivity of the HO_2 detector towards HO_2, and $c_{OH(HO_2)}$ (yellow) is the sensitivity of the HO_2 detector towards OH. $c_{OH(HO_2)}$ is used to correct the signal of the HO_2 detector for any remaining OH measured in the sample air. Calibrations were done after sun down to ensure maximum data coverage during daytime, as well as to avoid discontinuity of the data, due to an updated sensitivity factor.

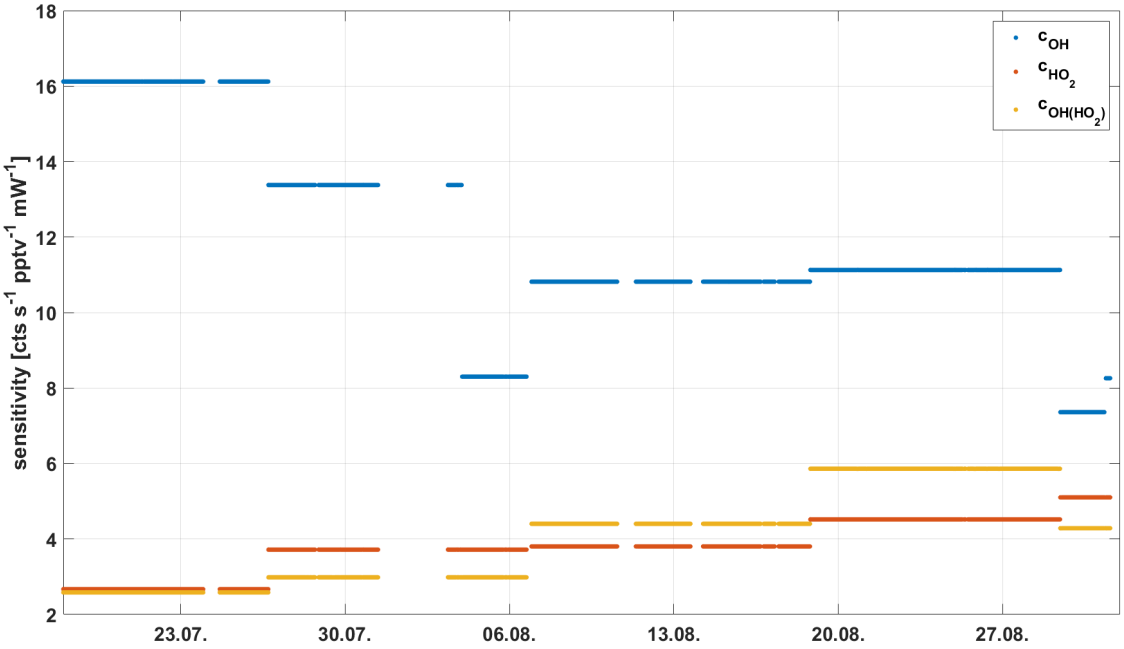

Figure 4.14 Sensitivity over time during AQABA. Two detectors were used during the campaign. c_{OH} (blue) is the sensitivity of the OH detector. c_{HO_2} (red) is the sensitivity of the HO_2 detector towards HO_2, and $c_{OH(HO_2)}$ (yellow) is the sensitivity of the HO_2 detector towards OH. $c_{OH(HO_2)}$ is necessary to correct for remaining atmospheric OH detected by the HO_2 detector.

4.4.2 Measurements of OH and HO_2^*

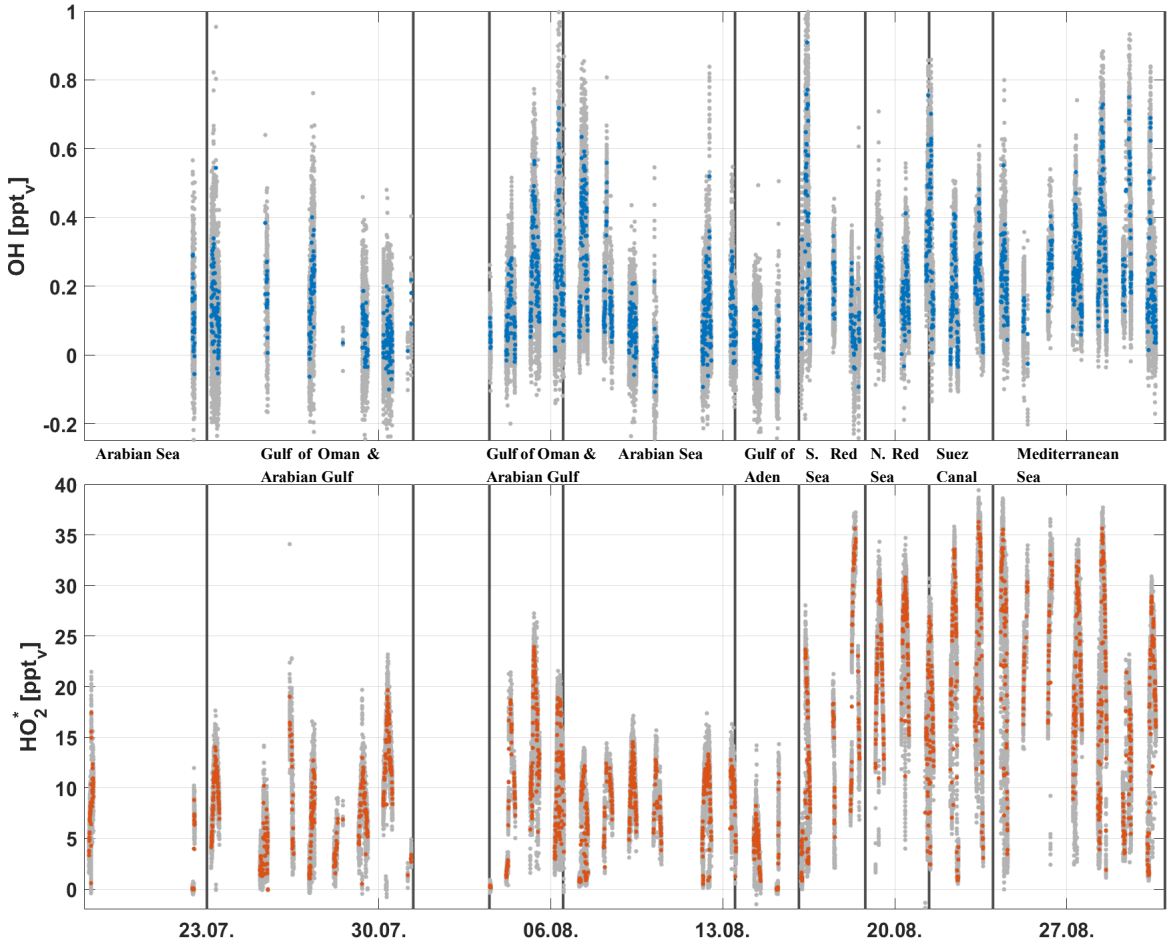

Figure 4.15 Overview of OH and HO_2^* measurements during AQABA 2017 campaign. Data shown is only during daytime and was filtered for the ship's own stack emissions. The top panel shows OH mixing ratio, the bottom panel shows HO_2 mixing ratio. Gray data shows 15 sec resolution and colored data shows 20 min averages (blue and red). Vertical lines separate the different regions during AQABA.

OH and HO_2 measurements are shown in Figure 4.15. The data shown is only during daytime ($J(O^1D) > 5 \cdot 10^{-6}$ s^{-1}) and filtered for the ship's own emissions. The top panel shows OH mixing ratios in 15 s resolution (gray) and 20 min averages (blue). The bottom panel shows HO_2 measurements not corrected for possible interference by RO_2 (further called HO_2^*). Similar to OH, HO_2^* is shown in 15 s resolution (gray) and 20 min averages (red). The typical diurnal cycle can be found for most days for both OH and HO_2^*, with low mixing ratios in the morning followed by a strong increase to a maximum during midday and a decrease in the afternoon to typical low levels in the evening/night. If not further specified, OH and HO_2^* mixing ratios discussed here represent the levels during noon.

Both OH and HO_2^* show low levels over the Gulf of Oman and Arabian Gulf during leg 1 (median: 0.08 pptv, 75% quantile: 0.14 pptv & 11.7 pptv, 14.6 pptv, respectively) in comparison to the remaining timeseries. During leg 2, OH increased from similar levels as

during leg 1 up to 0.40 pptv (75% quantile: 0.45 pptv). HO_2^* did not follow this trend with levels staying between ~20 pptv – 25 pptv. Over the Arabian Sea, mixing ratios of OH and HO_2 decreased, mainly caused by low NO_x and O_3, as well as the overall clean air indicated by low VOC concentration measured by the PTR-MS and GC. While OH gradually decreased from its high over the Gulf of Oman to a low close to the limit of detection (~0.1 pptv), HO_2^* stayed between ~ 13 – 15 pptv. OH levels over the Gulf of Aden were close to the limit of detection (~0.1 pptv), while HO_2^* levels were <10 pptv. Entering the southern Red Sea through the Bab al-Mandab strait, dense shipping traffic caused high NO_x and VOC levels, which in turn caused an increase in both OH and HO_2^* to 0.52 pptv (0.60 pptv) and 22.9 pptv (23.4 pptv), respectively. As the strait opens in to the much wider Red Sea, pollution decreased and OH decreased to close to the limit of detection. HO_2^* increased further to 33.6 pptv (34.0 pptv) and stayed at high levels above 25 pptv throughout the rest of the campaign. The northern Red Sea is influenced by regions with stronger anthropogenic emissions compared to the southern section. This was visible through the increase in OH mixing ratios to 0.29 pptv (0.37 pptv). As the ship approached the Gulf of Suez, a strong increase in NO_x from dense ship traffic traversing through the Gulf caused HO_2^* to decrease (25.4 pptv, 26.4 pptv) and OH to increase (0.57 pptv, 0.62 pptv). With decreasing NO_x, HO_x returned back to levels from before the event. Over the Mediterranean Sea, OH stayed at similar levels as over the Suez Canal, but increased in the latter half to 0.61 pptv (0.65 pptv). HO_2^* kept its high levels of 30.1 pptv (33.3 pptv).

4.5 RO_2 interference characterization during AQABA

4.5.1 Estimation of RO_2 mixing ratios

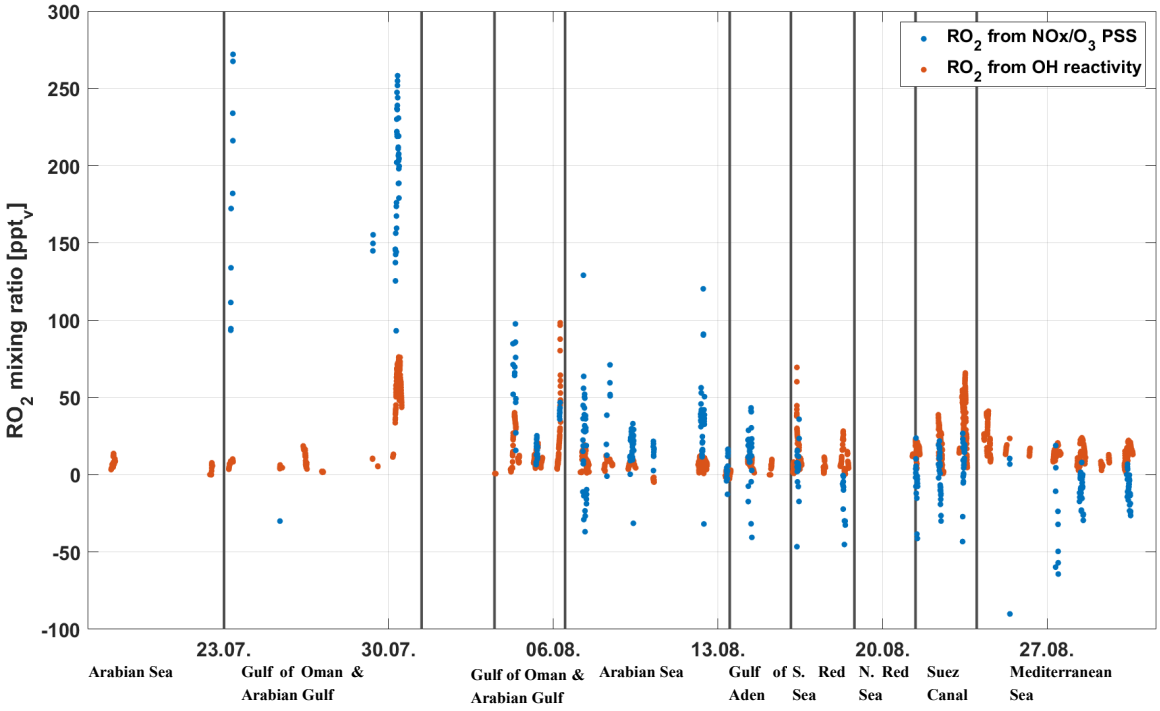

Figure 4.16 Calculated RO_2 mixing ratios during AQABA using NO_x/O_3 PSS (blue) (Tadic et al., 2020) and OH reactivity and HO_2 (red). From the calculated (HO_2 + RO_2) reported in Tadic et al. (2020), measured HO_2 concentrations were subtracted to obtain $RO_{2\,PSS}$. Vertical lines separate the different regions during AQABA.

As mentioned above, HO_2 measurements in a LIF-FAGE instrument are prone to interference caused by RO_2. Since there are no measurements of RO_2 during the AQABA campaign, mixing ratios are estimated using the methods described in section 3.1. Figure 4.16 shows RO_2 mixing ratios estimated using NO_x/O_3 photo stationary state ($RO_{2\,PSS}$), and OH reactivity and HO_2 ($RO_{2\,reac}$). In order to derive $RO_{2\,PSS}$, measured HO_2 was subtracted from RO_x (HO_2 + RO_2) reported by Tadic et al. (2020). This subtraction lead to negative mixing ratios in the southern Red Sea, Suez Canal and Mediterranean Sea, due to very low calculated RO_x mixing ratios throughout these regions. It is suspected, that RO_x mixing ratios derived using the NO_x/O_3 PSS are underestimated in these regions, possibly by an overestimation of the NO_2 offset. $RO_{2\,reac}$ were calculated using speciated reactivity reported by Pfannerstill et al. (2019). As shown above, up to 72 % of total reactivity could not be attributed to any trace gas. The estimated RO_2 concentrations are therefore only a lower boundary and were likely higher during the AQABA campaign. Additionally, total data coverage of all VOC and OVOC was limited. Therefore, the requirement for model calculations had been the availability of all VOC/OVOC, which contribute >90 % of speciated OH reactivity. This increased data coverage significantly, but exacerbate the underestimation of RO_2 with this method. Highest mixing ratios for both methods are found

over the Arabian Gulf on leg 1 with 260 pptv ($RO_{2\ PSS}$) and (98.3±34.6 pptv) ($RO_{2\ reac}$). Lowest estimated mixing ratios for $RO_{2\ reac}$ are in the Arabian Sea, while lowest levels for $RO_{2\ PSS}$ reach negative values from the southern Red Sea on for the remainder of the campaign. Due to this, $RO_{2\ reac}$ was used for further corrections of RO_2 interference. Total uncertainty of RO_2 was calculated from the individual uncertainties to be ~84 % (see Table 4.1, Δk_{CO}=5 %). Total uncertainty for $RO_{2\ PSS}$ was estimated to be 6 % (Tadic et al., 2020).

4.5.2 Correction of RO_2 interference in HO_2^*

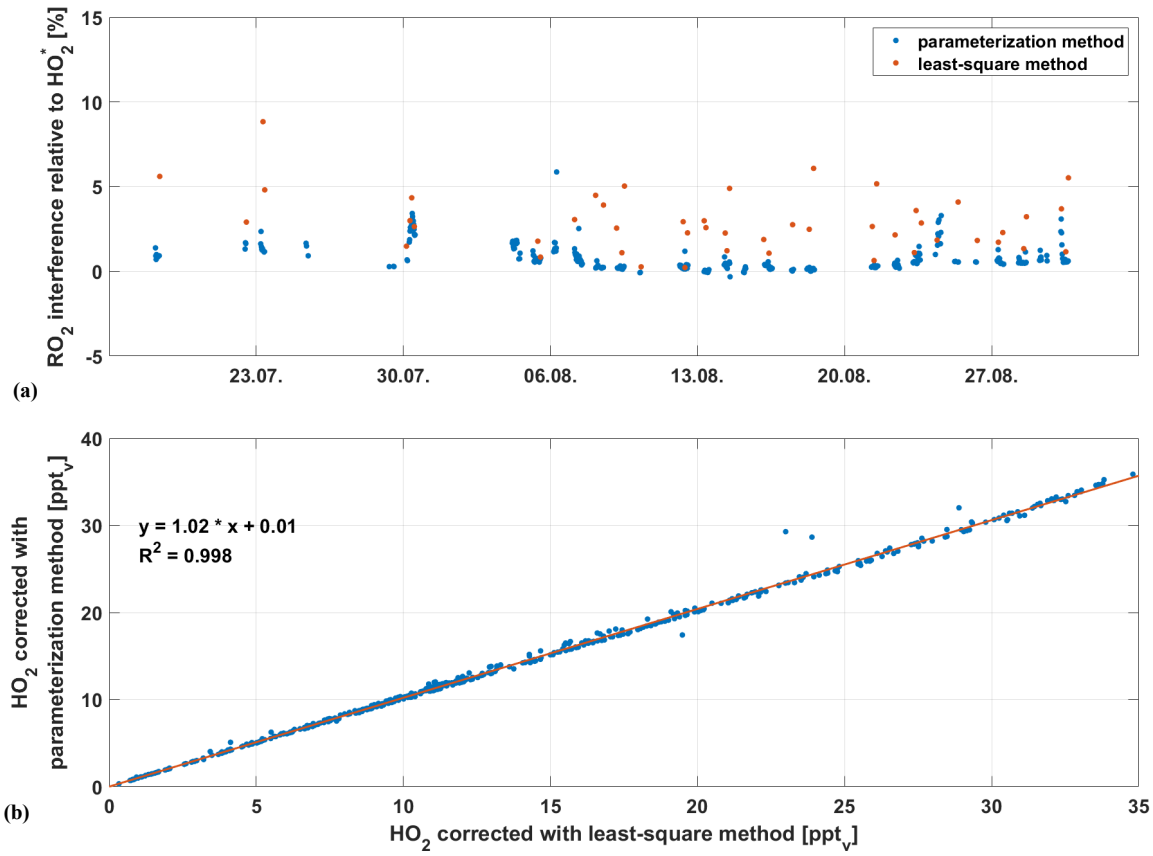

Figure 4.17(a) Fraction of HO_2 from RO_2 in HO_2^* calculated using least-square method (blue) and parameterization method (red) during the AQABA 2017 campaign. (b) Correlation of HO_2 corrected (10 min averages, blue dots) with both methods. Linear fit is shown as a red line.

To correct for RO_2 interference during the AQABA campaign, the methods described in sections 3.2.1 and 3.2.2 were applied to the measured HO_2^* data. The relative RO_2 interference of HO_2^* calculated with both methods is shown in the top frame of Figure 4.17. A correlation of correspondingly corrected HO_2 is shown in the bottom frame. Throughout the AQABA campaign, RO_2 interference was calculated to be <5 %, which is comparable to previous findings with the HORUS instrument (Hens, 2013) as well as the estimates by Fuchs et al. (2011). Estimations using the least-square method (3.2.2) yielded higher RO_2

interference values compared to estimates from the parameterization method (3.2.1). Calculation of HO_2 mixing ratios using both methods show a good correlation, with a slope of 1.02 and an $R^2 = 0.998$. Since the least-square method uses NO titrations, this method has information regarding the RO_2 composition at that time. However, this limits the resolution to a maximum of one every 2 h. Data coverage of the parameterization method is higher, since it is only affected by RO_2 data coverage and additionally, this method accounts for fast changes in internal pressure and temperature. A combination of both methods was used to correct for RO_2 interference during the AQABA campaign using slope and intercept of the correlation in Figure 4.17b. Total uncertainty for RO_2 interference was calculated to be + 156 % / - 102 %.

4.5.3 Corrected HO_2 mixing ratios

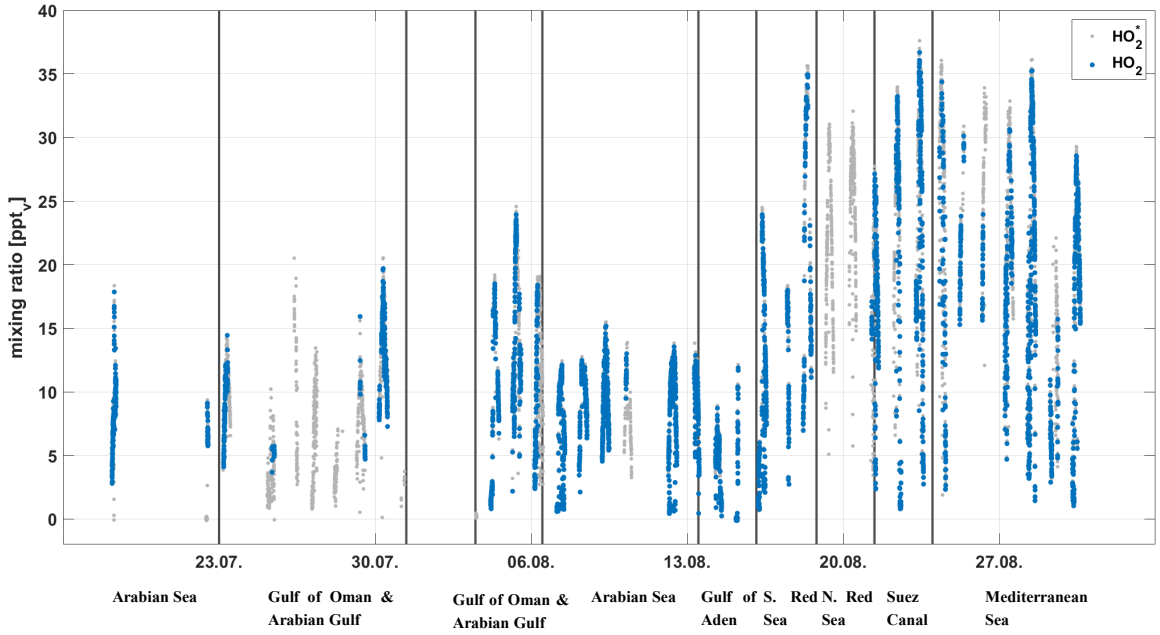

Figure 4.18 HO_2 data (blue) during AQABA campaign corrected for RO_2 interference. HO_2^* mixing ratios shown in gray. Vertical lines separate the different regions during AQABA.

HO_2 mixing ratios corrected for RO_2 interference are shown in Figure 4.18. The median interference caused by RO_2 is 2.4 % (75% quantile: 2.8%), with the lowest values found in the Arabian Sea, Gulf of Aden and southern Red Sea (~2 %) and the highest in the Arabian Gulf (~5 %).

5 Stability of tropospheric OH concentration

During daytime, OH has a major influence on atmospheric oxidative capacity. The production of OH can be separated in primary production, e.g. through the reaction of $O(^1D)$ with water vapor, and recycling processes (chapter 1.3.2). These recycling processes strongly affect the stability of tropospheric OH. Auto-catalytic conditions could lead to a built-up of HO_x, causing instability in the system, while the absence of recycling processes could cause an accumulation of pollutants and reduced gases (J. Lelieveld et al., 2002). Therefore, the recycling probability can be interpreted as a measure for the stability of tropospheric OH and its oxidative capacity. This chapter gives better insight on OH primary and secondary production rates as well as OH recycling probability during AQABA.

5.1 OH primary production

Using the observations described in chapter 4, OH primary production rates can be calculated considering reactions R.40 – 41.

$$O(^1D) + H_2O \rightarrow 2OH \quad \text{(R.40)}$$

$$HONO + h\nu \rightarrow OH + NO \quad \text{(R.41)}$$

$$OH + NO \rightarrow HONO \quad \text{(R.42)}$$

Their contributions to OH primary production rates during AQABA are shown in Figure 5.1. HONO was not measured during the Gulf of Aden and Southern Red Sea. The contribution of HONO photolysis to OH primary production was calculated by accounting for the backreaction of OH with NO (R.42), thus resulting in the net OH production rate from HONO photolysis. Calculated OH primary production rates during noon are in the range of $0.8 – 2.3 \cdot 10^7$ molec cm^{-3} s^{-1}. The reaction of $O(^1D)$ with H_2O is the most important source of OH and shows the expected diurnal cycle. The highest contribution was found in the Northern Red Sea with ~99 %. The highest contribution of HONO to the primary production was found in the Arabian Gulf (~10 %), while lowest was found in the Northern Red Sea (~1 %). OH production rate from photolysis of H_2O_2 and MHP (methyl hydroperoxide) were calculated. They contributed <1 % and were thus neglected.

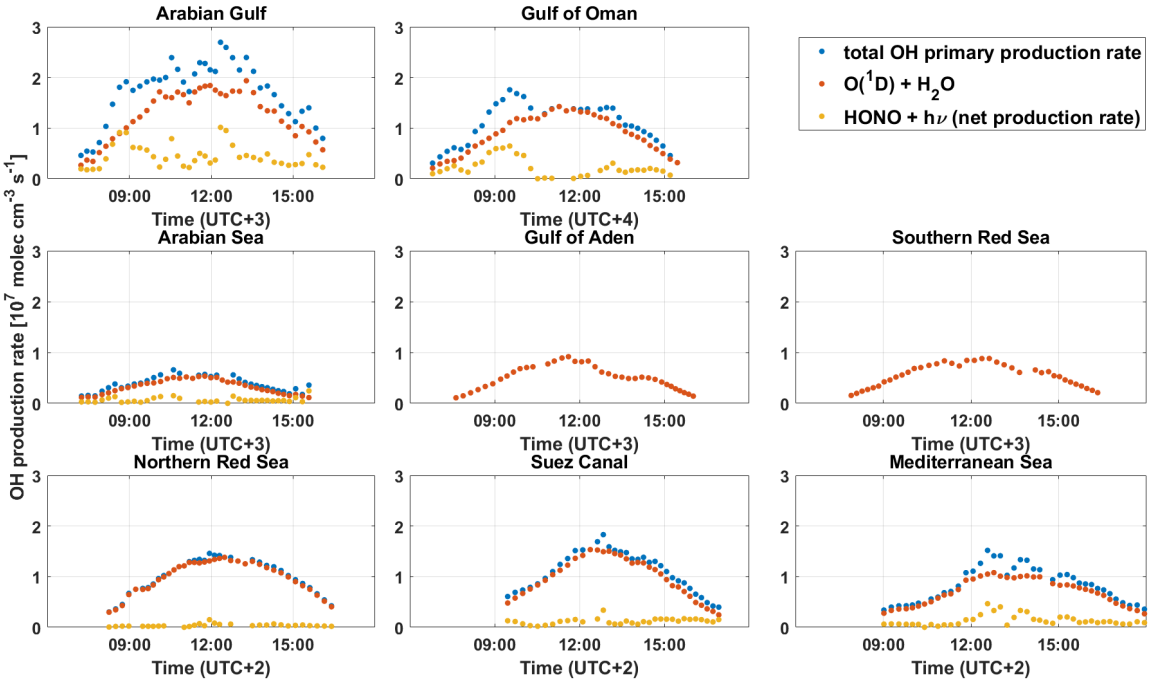

Figure 5.1 OH primary production versus time of day around the Arabian Peninsula and Mediterranean Sea during AQABA. Total OH primary production (blue) is comprised of OH production from O_3 photolysis (red) and HONO photolysis (yellow). Contributions from peroxide photolysis were <1 % and thus were neglected in this calculation. No HONO data was measured during the Gulf of Aden and Southern Red Sea, thus OH production from HONO is missing.

5.1.1 HO_x primary production

As shown above, the Arabian Gulf showed higher primary production of OH compared to the Mediterranean Sea, while simultaneously observed HO_x concentrations were lower by a factor of >1.5 in the Arabian Gulf. Utilizing the primary production of OH and adding primary production of HO_2 gives the total production of HO_x P_{HO_x}. Assuming steady state, P_{HO_x} can be used to determine the maximum HO_2 concentration at a given P_{HO_x}. Eq.25 describes the steady state assumption. Assuming only the reaction of HO_2 with itself is a viable radical loss reaction (R.17) allows to define a maximum HO_2 concentration using Eq.25 at a given production of HO_x P_{HO_x} (Eq.26). Additional loss reactions of HO_2, e.g., the reaction of HO_2 with RO_2, will, thusly, lower the HO_2 concentration at a constant P_{HO_x}. This relationship can give insight into the extent of additional radical loss rate in a specific region. Figure 5.7 shows the HO_2 concentration vs. HO_x production rates. Measured data for different regions during the AQABA campaign are shown as differently colored points. The yellow line defines an enveloping upper limit of the HO_2 concentration if the self-reaction is the only loss reaction (Eq.26). As expected, the measured HO_2 concentrations

are below the enveloping curve, which is caused by other radical loss reactions. At similar P_{HO_x}, the Arabian Gulf shows a much lower HO_2 concentration than the Mediterranean Sea. Even at higher P_{HO_x}, the HO_2 concentration shows values far below suggested by the enveloping curve. These low values indicate a significant additional radical loss in the Arabian Gulf. High VOC concentrations and primary OH production in the Gulf region indicate high concentrations of RO_2, leading to possible high loss rates through the reaction of HO_2 with RO_2. HYSPLIT trajectories (Figure 4.4 & Figure 4.5) showed air masses affecting the Arabian Gulf originating in the surrounding deserts. This could lead to high dust particle concentrations, and thus loss of HO_2 on the surface. These losses are investigated in further detail in chapter 5.3.2.

$$P_{HO_x} = [HO_2]\, L_{HO_2} + [OH] L_{OH} \quad \text{(Eq.25)}$$

$$[HO_2] = \sqrt{\frac{P_{HO_x}}{k_{HO_2+HO_2}}} \quad \text{(Eq.26)}$$

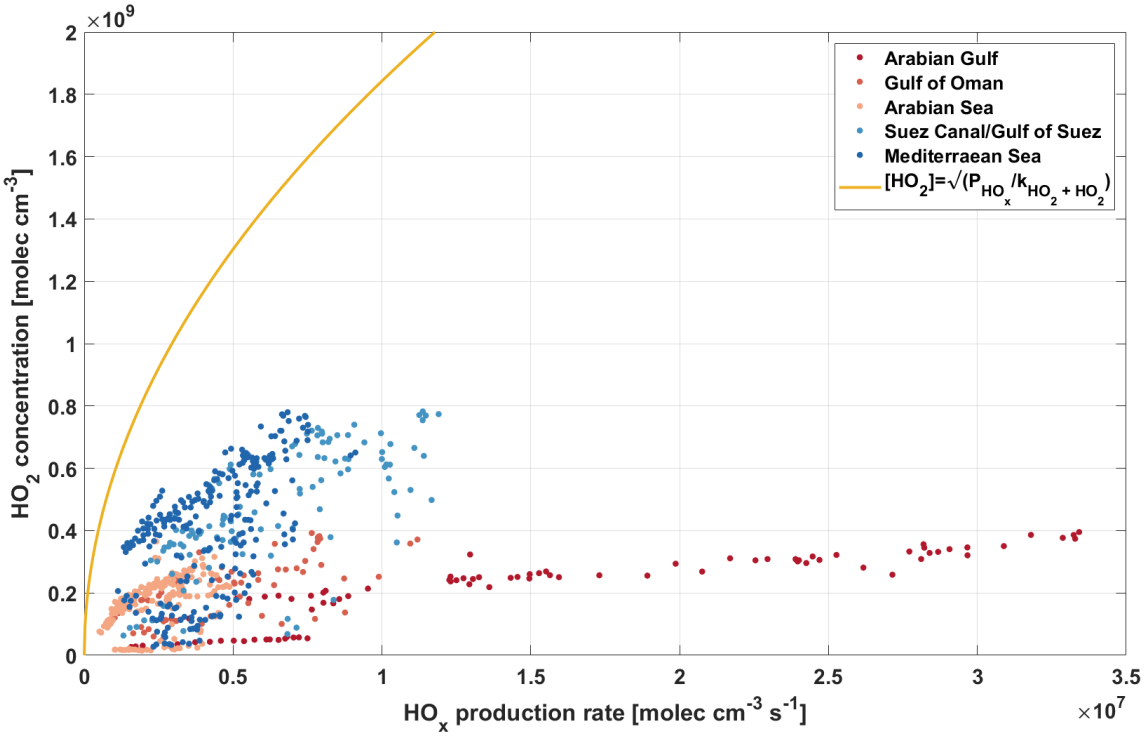

Figure 5.2 HO_2 concentrations vs. HO_x production rate. The points show measured data over different regions during the AQABA campaign. The yellow line shows the upper limit for HO_2, if the only loss reaction is the reaction of HO_2 with itself, neglecting other loss processes.

5.2 OH secondary production

After the initial production of OH, the recycling processes (see chapter 1.3.2) play an important role in maintaining the radical concentration. Oxidation of pollutants leads to the production of peroxy radicals (HO_2 and RO_2), which can be recycled back to OH (R.43 – 44). These reactions are considered secondary production.

$$HO_2 + NO \rightarrow OH + NO_2 \quad \text{(R.43)}$$

$$HO_2 + O_3 \rightarrow OH + 2\,O_2 \quad \text{(R.44)}$$

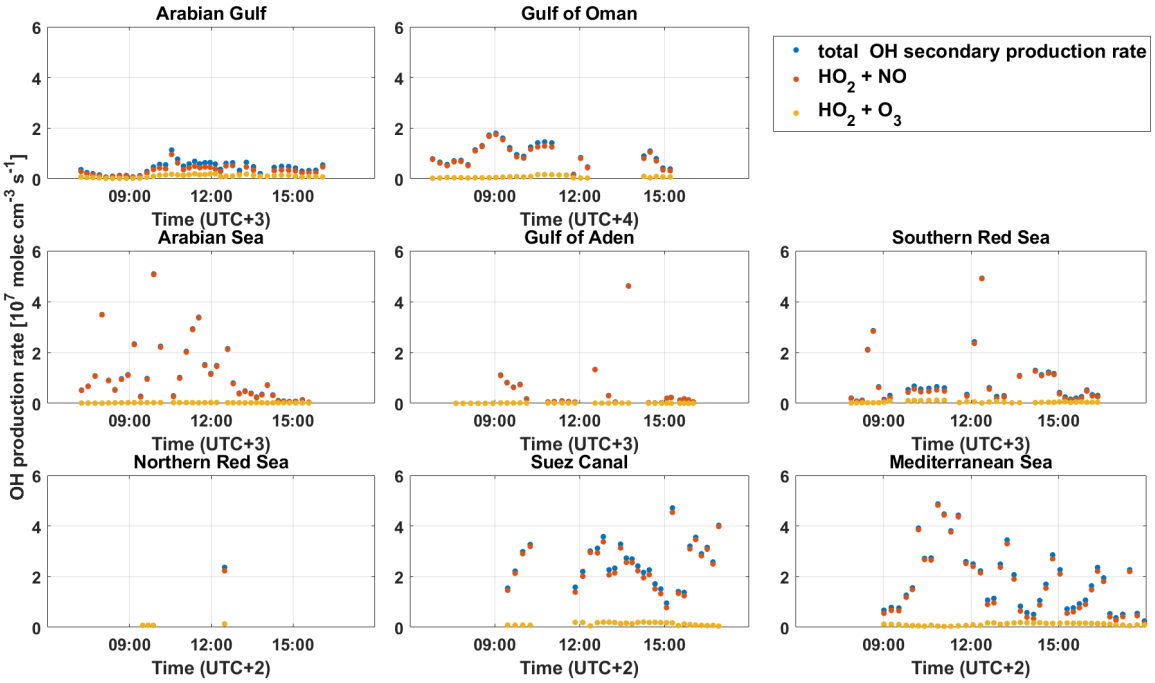

Figure 5.3 OH secondary production versus time of day around the Arabian Peninsula and Mediterranean Sea during AQABA. Total OH secondary production (blue) is comprised of OH production from HO_2 + NO (red) and HO_2 + O_3(yellow). Due to missing HO_2 measurements, data coverage in the Gulf of Aden and Northern Red Sea is low.

Contributions to OH secondary production rates are shown in Figure 5.2. Coverage of secondary production rates in the Gulf of Aden and Northern Red Sea regions are low, due to missing HO_2 data.

Secondary production rates are between ~0.2 - 5 · 10^7 molec cm^{-3} s^{-1}, with lowest levels in the Arabian Gulf and highest in the Mediterranean Sea. The reaction of HO_2 with NO was the most important source of OH through recycling processes, with contributions between ~65 – 99 % compared to total secondary production.

5.3 OH recycling probability

The OH recycling probability r is calculated from the ratio of secondary sources S to the total OH production $P+S$ (J. Lelieveld et al., 2002).

$$r = \frac{S}{S+P} \qquad \text{(Eq.20)}$$

As shown in 5.2, the reaction of HO_2 with NO is the major contributor in S. Since NO mixing ratios thusly contribute to both nominator and denominator in Eq.20, r can be parameterized as a function of NO. Figure 5.3 shows OH recycling probability as a function of NO mixing ratio for various measurement campaigns, including ground-based and ship-based measurements under rural and metropolitan conditions. Since no primary production through photolysis of O_3 or HONO occurs during nighttime, this data ($J_{O(^1D)} < 5 \cdot 10^{-6}$ s^{-1}) is omitted for all data sets.

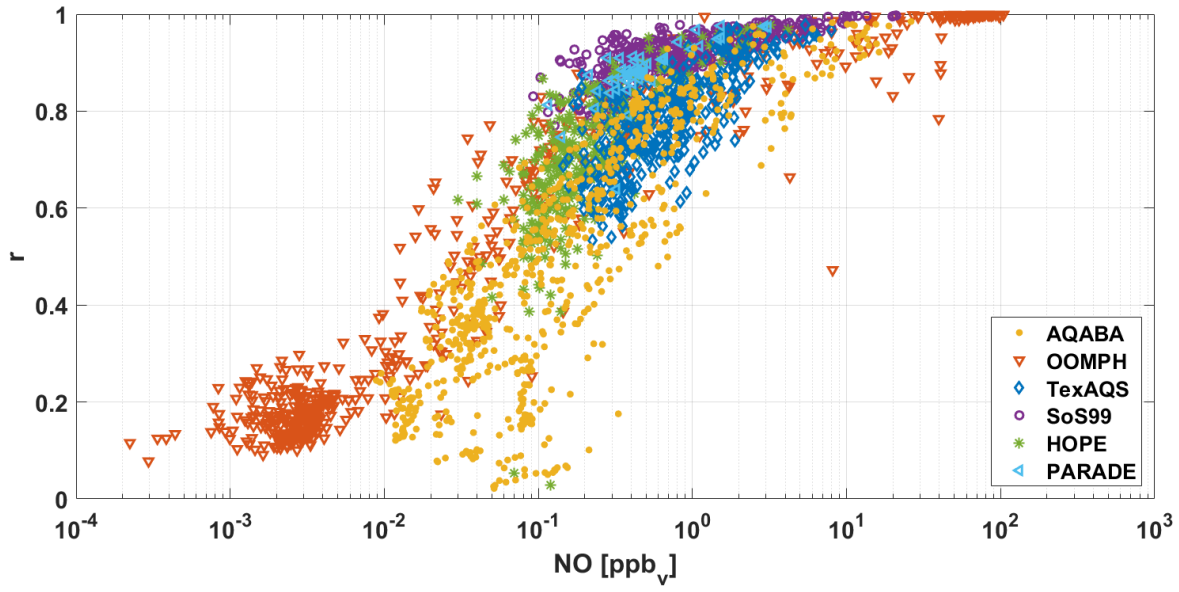

Figure 5.4 OH recycling probability r as a function of ambient NO mixing ratio in ppbv. Shown are measurement campaigns in different environments. OOMPH – marine boundary layer, ship stack plume; TexAQS – metropolitan, anthropogenic VOC; SOS99 – metropolitan, biogenic VOC; HOPE and PARADE – biogenic and anthropogenic VOC.

The dataset measured during OOMPH (**O**rganics over the **O**cean **M**odifying **P**articles in both **H**emispheres, red triangles) is dominated by remote marine boundary layer (MBL) in the southern Atlantic, which is characterized by low NO_x and VOC mixing ratios. However, due to wind direction sometimes the stack plume of the ship affected the measurement, which caused high NO_x conditions to be observed. The NO emissions lead to increased recycling of HO_2 to OH and thus increasing r values close to 1. Measurements in an environment with high anthropogenic VOC emissions and high NO_x mixing ratios (**Tex**as

Air **Q**uality **S**tudy, TexAQS, blue diamonds) show a decrease in the recycling probability. Depending on wind direction, the measurements were influenced by emissions from petrochemical industries and the Houston metropolitan area (Jingqiu Mao et al., 2010). Due to increased VOC emissions, at similar NO mixing ratios secondary production *S* is lower during the TexAQS compared to OOMPH. Measurements during SOS99 (**S**outhern **O**xidants **S**tudy, purple circles) are influenced by both biogenic emissions from surrounding deciduous forests and pastures, as well as anthropogenic emissions from nearby Nashville, Tennesee (Martinez et al., 2003) with high NO_x values >100 pptv. Observed *r* values are above TexAQS and OOMPH observations at similar NO mixing ratios. Measurements conducted during HOPE12 (**Ho**henpeißenberg **P**hotochemistry **E**xperiment, green stars) and PARADE (**Pa**rticles and **Ra**dicals: **D**iel observations of the impact of urban and biogenic **E**missions, light blue triangles) showed a strong influence by biogenic emissions from the surrounding forests as well as anthropogenic emissions from nearby settlements. Recycling probabilities for high NO_x conditions during both campaigns lie between SOS99 and TexAQS. For lower NO levels, *r* values during HOPE12 are lower than during OOMPH.

With NO mixing ratios <10 pptv, *r* values are typically low at around 0.2. When NO levels increase to around 1 ppbv, *r* can exceed levels of 0.95. If NO levels increase even further, high levels of NO_2 can be produced. This leads to a decrease in *r* due to the increasing relevancy of the reaction of OH + NO_2 (direct OH sink, producing HNO_3) (Cariolle et al., 2008; Crawford et al., 2000; Jaeglé, Jacob, Brune, & Wennberg, 2001).

In the case of the AQABA (yellow dots) dataset, a wide range of recycling probabilities were observed due to the wide range of regional conditions during the measurement, with values from <0.1 up to >0.9 depending on NO mixing ratio. Additionally, for similar NO levels, values of *r* can range from ~0.1 up to 0.7 between different regions during the campaign. For better insight, OH recycling probabilities separated by regions are shown in Figure 5.4. Observations over the Mediterranean Sea are in line with results from OOMPH and HOPE12, with *r* ranging from 0.2 up to >0.9 depending on NO mixing ratio. When NO mixing ratios are comparable, recycling probabilities in the Suez Canal/Gulf of Suez are slightly lower than in the Mediterranean Sea. The Arabian Sea was dominated by low NO mixing ratios, which in turn caused low recycling probabilities. The Arabian Sea is a remote region with low influence from anthropogenic emissions. Compared to the OOMPH dataset, NO mixing ratios in the Arabian Sea reach higher levels, while *r* is lower at similar NO. The higher NO is likely due to higher ship traffic in the region with the close by entry to the Red Sea and Gulf of Oman. The lower recycling probability indicate a higher primary production or reduced secondary production through recycling processes. Increased VOC concentrations could lead to lower *r* by offering an additional loss process through the

formation of organic nitrates (see chapter 1.4). High NO mixing ratios between 2 – 10 ppbv were observed with corresponding higher values of *r*. These observations were taken close to the Gulf of Oman, causing a high influence from increased ship traffic and overall anthropogenic emissions in this region. The recycling probabilities in the Gulf of Oman and the Arabian Gulf are significantly lower compared to the other datasets shown. Especially in the Arabian Gulf, the recycling probability was found to be lower by a factor of ~8 compared to the Mediterranean Sea and a factor of ~9 compared to the other datasets shown. The region showed the highest primary production rate throughout AQABA and low secondary production rate. The low recycling probability is an indicator for a low stability of tropospheric OH in the region and therefore oxidative capacity of the atmosphere (J. Lelieveld et al., 2002). In order to understand the conditions observed in the Arabian Gulf, the cause of the low secondary production is investigated further.

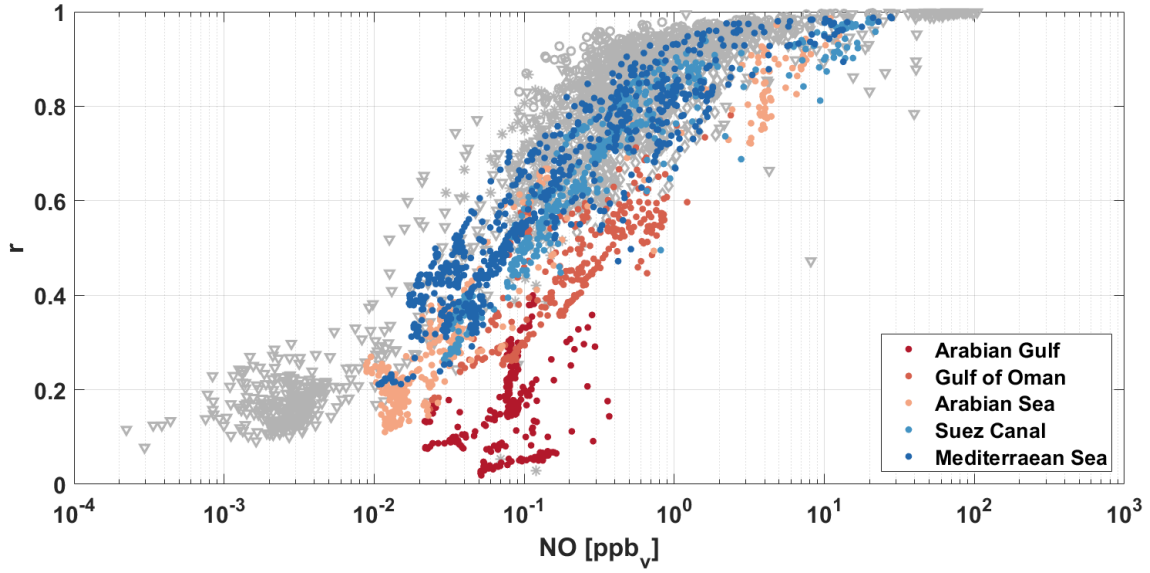

Figure 5.5 OH recycling probability during AQABA separated for different regions. The regions of the Red Sea and Gulf of Aden are not shown, since data coverage for *r* was low or non-existent, due to missing HO_2/HONO data. Data shown from other measurement campaigns are shown for comparison in gray in the background. See Figure 5.3for more information.

5.3.1 Missing secondary production rate

With observed high primary and low secondary production in the Arabian Gulf, it is vital to understand the loss processes that lead to the low, observed recycling probability. It is assumed that the low secondary production in the Arabian Gulf is caused by either a missing reaction contributing to secondary production, or increased RO_x loss processes competing with recycling reactions. By taking the Mediterranean Sea as a reference, a 'missing' secondary production rate α can be calculated (Eq.21 & 22). α is the rate of

secondary production needed in the Arabian Gulf to achieve recycling probabilities observed in the Mediterranean Sea. It is assumed, that α can either be recycling reactions, which are not accounted for in the calculation of r, or loss reactions, which are more important in the Arabian Gulf. In order to calculate α, the calculated recycling probabilities are partitioned into different NO mixing ratio bins. The bins were arbitrarily chosen to separate one order of magnitude into 10 bins.

$$r_{Med} = \frac{S_{Arab} + \alpha}{S_{Arab} + \alpha + P_{Arab}} \quad \text{(Eq.21)}$$

$$\Rightarrow \quad \alpha = \frac{P_{Arab} \cdot r_{Med}}{1 - r_{Med}} - S_{Arab} \quad \text{(Eq.22)}$$

with the recycling probability in the Mediterranean Sea r_{Med}, the primary and secondary production rate in the Arabian Sea S_{Arab} and P_{Arab}, and missing secondary production α.

Figure 5.5 shows α vs NO mixing ratio in ppbv (top panel). With increasing NO, α increases from ~0.7 up to $4.0 \cdot 10^7$ molec cm^{-3} s^{-1}, indicating an influence of NO levels on the loss processes leading to a lower recycling probability. However, this can be misleading, as the secondary production rate is also highly influenced by NO. A better indicator is the fraction of α of the total secondary production $S_{Arab} + \alpha$, which decreases with increasing NO mixing ratios from >0.85 to ~0.6 at ~0.5 ppbv (Figure 5.5, bottom panel). This decrease indicates a possible loss process independent on NO concentration. A sudden increase for high NO mixing ratios could indicate, that a NO influenced loss process increased in impact with increasing NO and overtook the non-NO loss process.

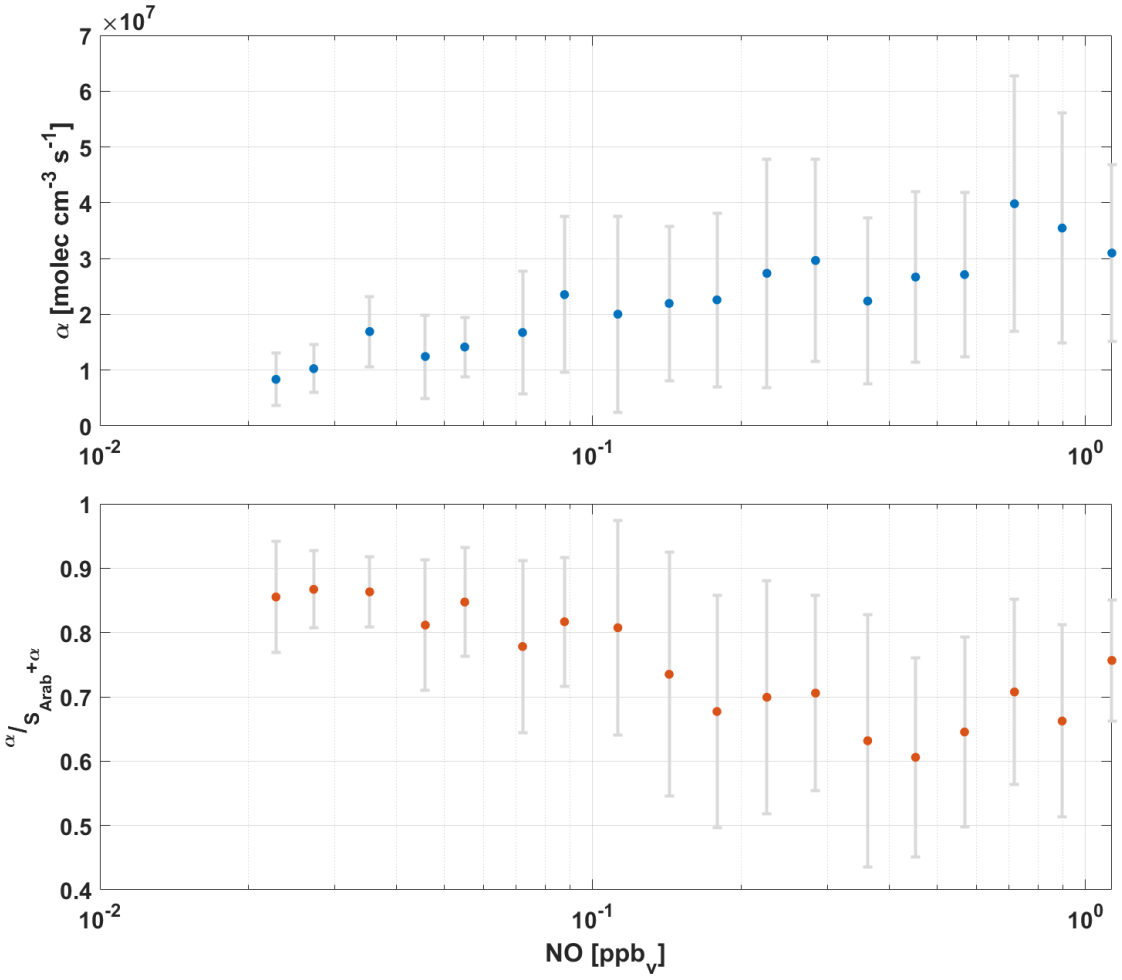

Figure 5.6 Missing secondary production rate α vs. NO mixing ratio (top). α represents additional secondary production needed to reach levels of r observed in the Mediterranean Sea for similar NO mixing ratios. The bottom panel shows the fraction of the missing secondary production rate α of the sum of S_{Arab} and α vs. NO mixing ratio.

5.3.2 Investigating RO_x losses

In order to identify possible sinks for RO_x, which caused the low recycling probability in the Arabian Gulf, several loss pathways were investigated using measurements and box model calculations.

Loss of HO_2 through deposition on particle surfaces

Heterogenous uptake on aerosol and dust particles can to be a significant sink for HO_2 (Carslaw et al., 2002; Carslaw et al., 1999; Jacob, 1986, 2000; J. Mao, Fan, Jacob, & Travis, 2013; Sommariva et al., 2004; Joel A. Thornton, Jaeglé, & McNeill, 2008). Its high solubility in water (Henry's law constant 6.8 mol m^{-3} Pa^{-1} (S. P. Sander et al., 2011)) and rapid dissociation (pK_a = 4.7) of HO_2 promote fast loss through uptake in aqueous aerosols and sea spray. During AQABA, it is expected, that mineral dust particles from surrounding

deserts can be a major fraction of the measured particle surface. HO_2 uptake has been observed for Cu-doped aerosols catalyzed by a Cu(I)/Cu(II) redox cycling, converting HO_2 to H_2O_2 (Cooper & Abbatt, 1996; Mozurkewich, McMurry, Gupta, & Calvert, 1987; Taketani, Kanaya, & Akimoto, 2008). A similar catalytic mechanism has been proposed involving Cu(I)/Cu(II) and Fe(II)/Fe(III) (J. Mao et al., 2013). As a measure of efficiency of heterogeneous HO_2 uptake, the reactive uptake coefficient γ_{HO_2} is used. γ_{HO_2} is defined as the fraction of HO_2 collisions with aerosol surface resulting in reaction (J. Mao et al., 2013). An excerpt of reported uptake coefficients for different surfaces is shown in Table 5.1.

Table 5.1 HO_2 uptake coefficients for different surfaces

Surface	Type of Surface	Uptake coefficient γ
H_2O	flowing liquid	>0.01 [a]
NaCl	solid dry film	0.01 [b]
$(NH_4)_2SO_4$ doped with Cu(II)	salt solution aerosol	0.52 [c]
Aerosols doped with Cu/Fe	model simulations	0.4 – 1 [d *]

[*] uptake coefficient is dependent on pH and Cu/Fe ratio

[a] (Hanson, Burkholder, Howard, & Ravishankara, 1992), [b] (Remorov, Gershenzon, Molina, & Molina, 2002), [c] (Taketani et al., 2008), [d] (J. Mao et al., 2013)

To calculate the loss rate from the reported uptake coefficients, a first-order loss to aerosol surfaces was used, see Eq.23 (Ravishankara, 1997).

$$L_{PS} = \frac{c_g A \gamma}{4} \cdot [\mathrm{HO_2}] \qquad \text{(Eq.23)}$$

$$\text{with} \quad c_g = \sqrt{\frac{8RT}{\pi M_{HO_2}}} \qquad \text{(Eq.24)}$$

c_g is the mean molecular speed of gas molecules (see Eq.24), A is the particle surface area per volume unit, γ is the uptake coefficient, R is the universal gas constant, T is the ambient temperature and M_{HO_2} is the molecular weight of HO_2. To calculate L_{PS} for loss on H_2O and NaCl surfaces, surface areas of particles below 10 µm were used. Since dust particles are generally larger, with a diameter in the range of 2.5 – 10 µm (Maring, Savoie, Izaguirre, Custals, & Reid, 2003), the surface area of these particles was used to calculate L_{PS} for Cu and Cu/Fe doped particles. Calculated L_{PS} is shown in the top panel of Figure 5.6, the bottom panel shows L_{PS} divided by missing production α. The highest loss was found on for Cu/Fe doped aerosols with a maximum of $2.7 \cdot 10^4$ molec cm^{-3} s^{-1} and a maximum ratio of α of 0.16 %. This indicates, that during the measurements observed here, uptake on

particle surfaces does not reduce HO_2 concentrations significantly, which, in turn, does not reduce secondary OH production in the Arabian Gulf.

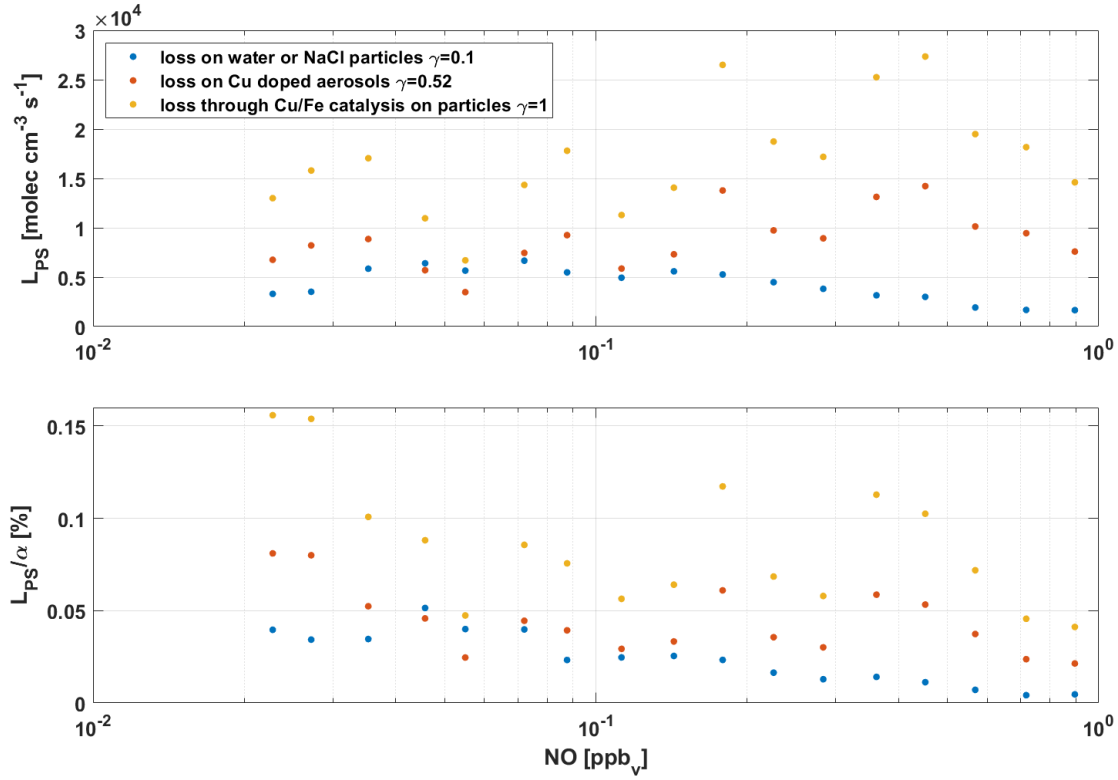

Figure 5.7 Loss rate on different surfaces L_{PS} vs. NO mixing ratio in ppbv (top panel). The particle surface of particles between 2.5 and 10 µm diameter were used to calculate for loss on Cu doped aerosols and loss through Cu/Fe catalysis. The particle surface of particles below 10 µm diameter were used to calculated loss on water or NaCl surfaces. Fraction of loss on different surfaces of the missing secondary production α vs. NO mixing ratio in ppbv (bottom panel).

Budget calculations and investigation of HO_2/RO_2 loss rates

Loss processes of peroxy radicals through chemical reactions with other trace gases can lead to either to recycling or loss of radicals (see chapters 1.3.3 and 1.4.2). In order to investigate these reactions and possible loss pathways in the Arabian Gulf, CAABA/MECCA box model calculations, constrained by measured trace gas concentrations had been performed. The measurements during AQABA were taken as boundary conditions. As mentioned in chapter 3.1.2, total data coverage of all VOC/OVOC was limited. Therefore, the requirement for model calculations had been the availability of all VOC/OVOC, which contribute >90 % of speciated OH reactivity (see Pfannerstill et al. (2019)). Loss rates were calculated for HO_2 and all RO_2. Due to the large number of possible reactions of HO_2 (236 reactions) and RO_2 (608 reactions), reaction groups were defined (Table 5.2). Loss reactions of HO_2 were separated into three groups: HL_{rad}, radical

loss through radical-radical reactions, HCC_{NO_x}, recycling reaction of HO_2 with NO, HCC_{other}, non-NO_x radical chain propagation, e.g. reaction of HO_2 with O_3 to form OH and O_2. Loss reactions of RO_2 were separated into six groups: RL_{NO_x}, radical loss through reaction with NO_x, RL_{rad}, radical loss through radical-radical reactions, RL_{other}, other radical loss, RCC_{NO_x}, radical chain propagation through reaction with NO_x, RCC_{HO_2}, radical chain propagation by reaction with HO_2, RCC_{other}, other radical chain propagation reactions, e.g. unimolecular reactions of RO_2.

Loss rates of RO_2 and HO_2 for regions during AQABA are shown in Figure 5.8. The Gulf of Aden and Northern Red Sea are not included due to lack of HO_x measurements. The highest and lowest overall radical loss rates were calculated for the Arabian Gulf with ~$6.6 \cdot 10^7$ molec cm^{-3} s^{-1}, and the Arabian Sea with ~$5.3 \cdot 10^6$ molec cm^{-3} s^{-1}, respectively. This is consistent with expectations, due to the high levels of pollution in the Arabian Gulf and the remote conditions observed in the Arabian Sea. In each region, the overall largest contributor to the loss rate are reactions with NO_x. Recycling reactions by reaction with NO_x (RCC_{NO_x} and HCC_{NO_x}) contribute up to 96 % of total loss rate in the Mediterranean Sea. However, due to limited data coverage during the Mediterranean Sea, the data used in the model calculations are during early morning, with very low HO_x concentrations. Thus, budget calculations are not representative for the whole region of the Mediterranean Sea. The Suez Canal showed similar recycling probabilities as the Mediterranean Sea, with NO_x recycling reactions contributing ~81 %. The lowest contribution is shown in the Arabian Sea and Arabian Gulf, with 38 % and 52 %, respectively, due to low NO mixing ratios. Additionally, high radical-radical reaction rates (RL_{rad} and HL_{rad}) lead to a higher radical loss in the Arabian Sea and Arabian Gulf compared to the Suez Canal.

In order to illustrate the impact of radical loss for each region, Figure 5.9 shows radical loss as a fraction of total loss rates.

Table 5.2 Groups of RO_x loss reactions, with number of reactions found in CAABA/MECCA and example for each group

Loss reactions of RO_2			
Type of reaction	**Abbrev.**	**reactions in this group**	**example**
Radical loss from reaction with NO_x	RL_{NO_x}	77	$CH_3C(O)O_2 + NO_2 \rightarrow PAN$
Radical loss from radical-radical reaction	RL_{rad}	146	$CH_3O_2 + HO_2 \rightarrow CH_3OOH + O_2$
Other radical loss	RL_{other}	52	$CH_3O_2 \rightarrow 0.5\ HCHO + 0.5\ CH_3OH + 0.5\ O_2$
Radical chain propagation by reaction with NO_x	RCC_{NO_x}	124	$CH_3O_2 + NO \rightarrow CH_3O + NO_2$
Radical chain propagation by reaction with HO_2	RCC_{HO_2}	72	$CH_3C(O)O_2 + HO_2 \rightarrow OH + +CH_3 + CO_2$
Other radical chain propagation reactions	RCC_{other}	137	$CH_3O_2 + OH \rightarrow CH_3O + HO_2$ $C_4H_7O_4 \rightarrow CH_3C(O)CH_2OH + CO + OH$
Loss reactions of HO_2			
Type of reaction	**Abbrev.**	**reactions in this group**	**example**
HO_2 loss through radical-radical reaction	HL_{rad}	146	$HO_2 + HO_2 \rightarrow H_2O_2 + O_2$
Radical chain propagation through reaction with NO_x	HCC_{NO_x}	1	$HO_2 + NO \rightarrow OH + NO_2$
Other radical chain propagation	HCC_{other}	89	$HO_2 + O_3 \rightarrow OH + 2\ O_2$

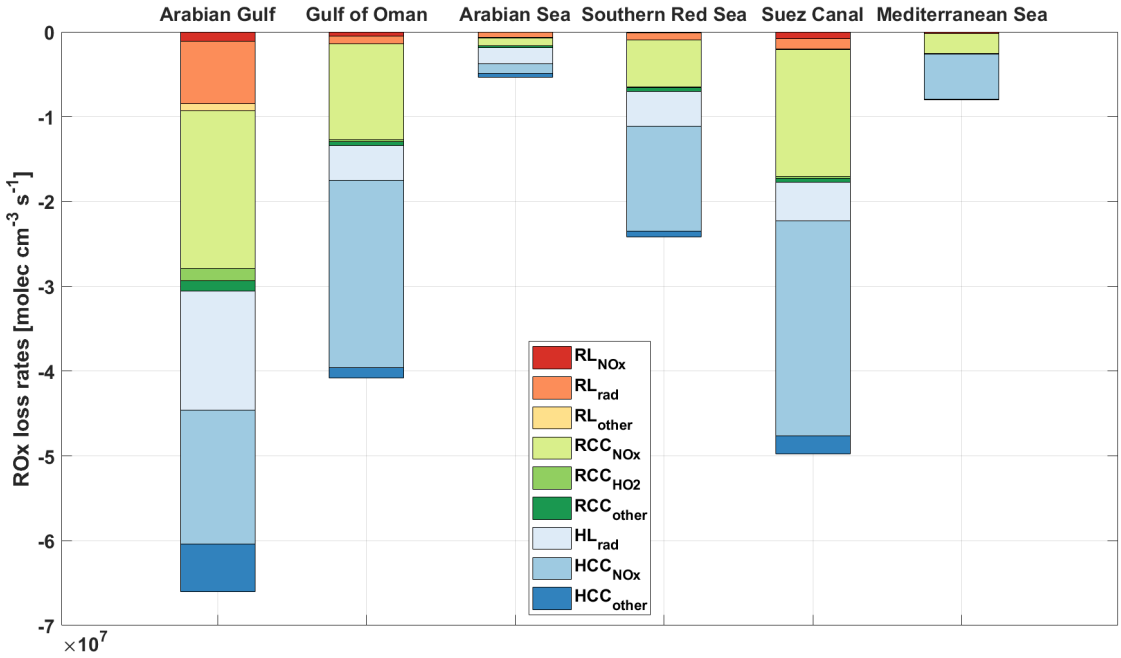

Figure 5.8 RO_x loss rates for regions during AQABA. Loss rates accounted for RO_2 radicals are shown in red to green and loss rates accounted to HO_2 are shown in different shades of blue. The low RO_x loss rates in the Mediterranean Sea are caused by low data coverage in this region. The obtained RO_x losses are therefore not representative for the whole region of the Mediterranean Sea.

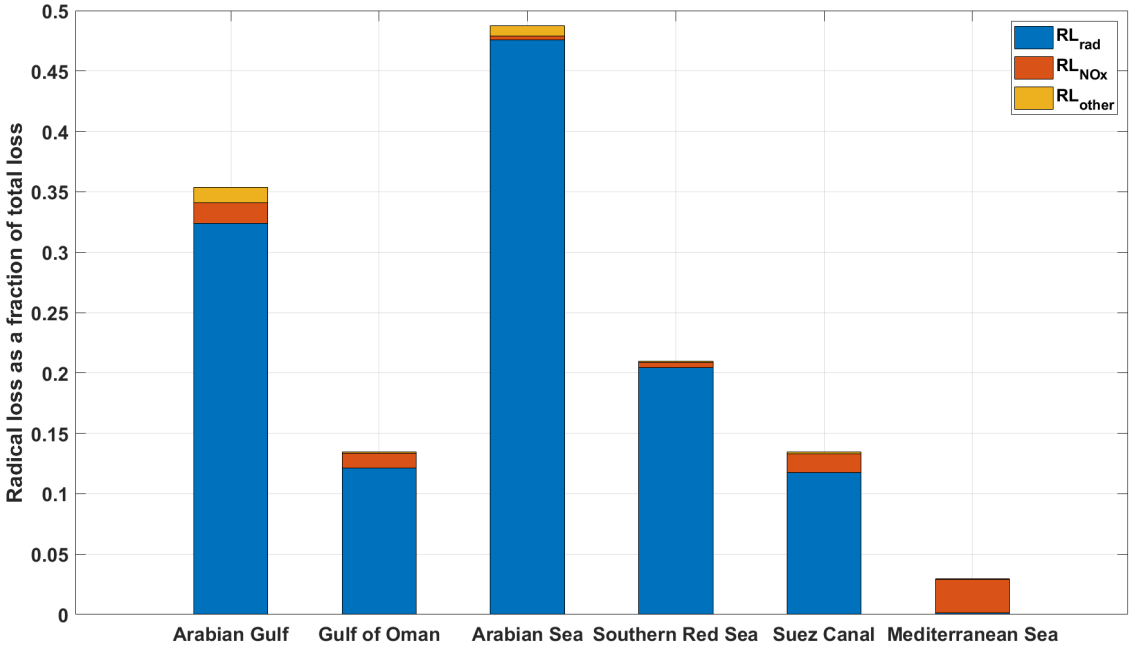

Figure 5.9 Radical loss of RO_x as a fraction of total loss during AQABA. Radical loss from radical-radical reaction is shown in blue (RL_{rad}), loss from nitrate formation is shown in red (RL_{NOx}), other radical loss is shown in yellow (RL_{other}).

Overall radical loss contributes between 3 % and 49 % of total RO_x loss rate. The highest fraction was calculated for the Arabian Sea and Arabian Gulf with 49 % and 35 %, respectively, suggesting a large fraction of radicals being lost instead of recycled in these two regions. RL_{rad} is the most important loss path way, with only minor contribution from RL_{NO_x} and RL_{other}. The Mediterranean Sea showed lowest contribution of radical loss to the total loss rate with 3 %, suggesting good recycling. Additionally, due to high NO_x and low RO_x concentrations in the Mediterranean Sea, the reaction with NO_x was the major radical loss, with radical-radical reactions only contributing insignificantly. However, as already mentioned, the data available for the Mediterranean Sea is only representative for the early morning in the region. Due to low radical concentrations in the early morning, the majority of loss rate is attribute of reaction with NO_x. With 13 % radical loss in the Suez Canal is significantly lower compared to the Arabian Gulf and Arabian Sea, indicating generally higher radical losses in both regions.

In the calculation of secondary production rates, only the reactions of HO_2 with NO and O_3, respectively, are considered as recycling reactions. In order to investigate additional recycling processes, non-NO_x radical recycling as a fraction of total RO_x loss rate for each region during AQABA is shown in Figure 5.10. Due to low NO_x mixing ratios in the Arabian Gulf and Arabian Sea, both regions show a high fraction of non-NO_x recycling. As expected, a large fraction of non-NO_x recycling is due to the reaction of HO_2 with O_3, which is already accounted for in the calculation of the recycling probability (see chapter 5.2). However, in the Arabian Gulf approx. 50 % of non-NO_x recycling is contributed by reactions from the groups RCC_{HO_2}, RCC_{other} and HCC_{other}, indicating a significant portion of recycling not accounted for in the calculation of *r*.

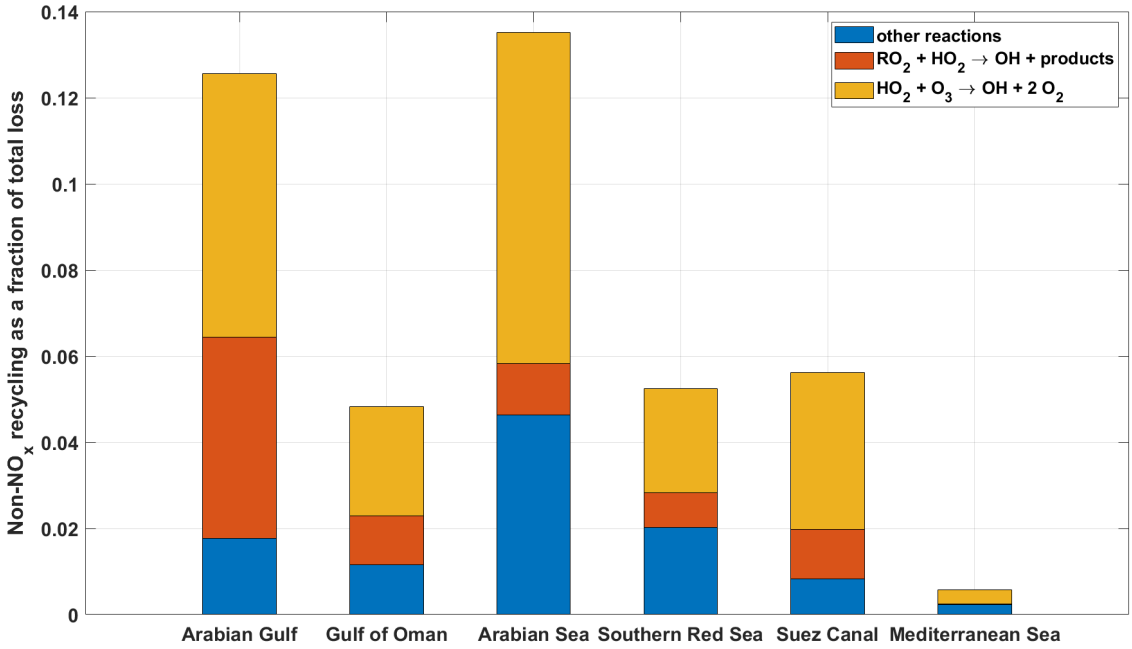

Figure 5.10 Non-NO_x radical recycling rate as a fraction of total loss rate of RO_x, separated in major contributing reactions. Recycling from $HO_2 + O_3$ is shown in yellow, radical-radical recycling is shown in red, and other recycling reactions, e.g. unimolecular decomposition of RO_2, is shown in blue.

Important reactions influencing non-NO_x recycling are unimolecular reactions of RO_2 and reaction of RO_2 with HO_2. In the Arabian Gulf, RCC_{HO_2} contributes ~37 % of total non-NO_x recycling and ~4.6 % of total RO_x loss rate. Since the reaction of RO_2 with HO_2 can act both as radical loss and radical recycling due to different reaction branches, it is important to investigate the branching ratios for RO_2 from different origin VOC. Hasson et al. (2012) found an increase in branching ratio towards recycling with increasing degree of substitution from primary to tertiary peroxy radicals. Additionally, due to the formation of a tetroxide (see Figure 5.11), RO_2 with a carbonyl in α- or β-position favor the production of the recycling reaction branch (R1c) or production of O_3 and an alcohol (R1b) over the production of a hydroperoxide (R1a). Hui, Fradet, Okumura, and Sander (2019) reported a temperature dependency for the branching ratio of the reaction of HO_2 and acetyl peroxy radical. R1b showed a negative temperature dependency, R1c showed a positive, while R1a showed no temperature dependency. The Arabian Gulf shows increased OVOC concentration and it is therefore likely, that the concentration of oxygenated RO_2 is increased. In combination with high temperatures, the recycling through RO_2 with HO_2 is expected to be relevant.

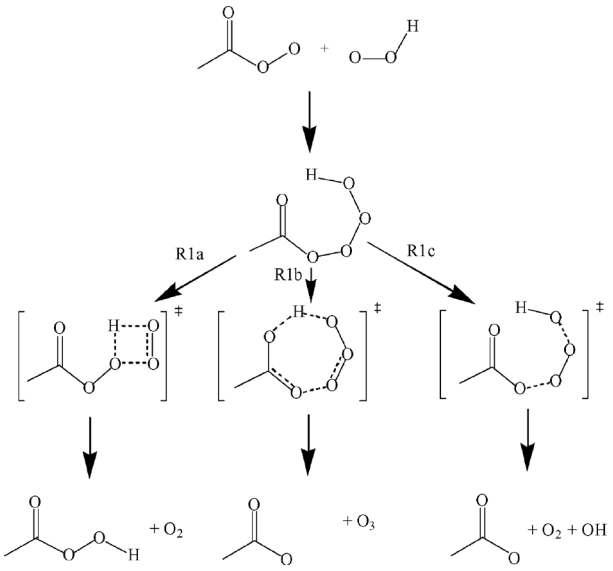

Figure 5.11 Proposed mechanism for the reaction of acetyl peroxy radical and HO_2. The tetroxide intermediate is formed to produce an acetic acid and ozone (R1b) or acetyl oxy radical oxygen and OH (R1c). Alternatively, a 4 membered ring intermediate can be formed to produce the hydroperoxide and oxygen (R1a). Taken from Hasson, Kuwata, Arroyo, and Petersen (2005)

This additional recycling together with the increased loss of radicals does not explain the low recycling probability observed in the Arabian Gulf. However, loss rates calculated with the model are only a lower boundary, since not all VOC were used in the calculation. It is to be expected, that higher loss rates are reached, when accounting for missing VOC. Comprehensive VOC and RO_2 measurements are needed to be able to quantify losses and additional recycling, which cause the low recycling probabilities calculated for the Arabian Gulf region.

5.4 Summary

Noontime values of the OH primary production rates ranged between $0.8 – 2.3 \cdot 10^7$ molec cm^{-3} s^{-1}, with the reaction of $O(^1D)$ with H_2O as most important source of OH. Secondary production rates ranged between $0.2 - 5 \cdot 10^7$ molec cm^{-3} s^{-1}. The most important recycling process is the reaction of HO_2 with NO, followed by the reaction of HO_2 with O_3. The highest levels of OH primary production was found in the Arabian Gulf, however this region also showed exceptionally small secondary production. This indicates a significant loss of radicals throughout the radical cycle (see Figure 1.3).

OH recycling probabilities during AQABA ranged between <0.1 up to >0.9, with distinct differences between regions during the campaign. For similar NO mixing ratios, *r* values between 0.1 to 0.7 were calculated. The Arabian Gulf region showed an especially low recycling probability, indicating higher radical loss and lower radical chain propagation. This suggests a low stability of tropospheric OH concentrations in this region.

A missing secondary production rate α for the Arabian Gulf was calculated using the Mediterranean Sea as a reference. With increasing NO mixing ratios, α increases, indicating a NO dependency of α. The fraction of α of the total secondary production $S_{Arab} + \alpha$ decreases, contradicting the first assessment.

Maximum calculated heterogeneous uptake of HO_2 on particle surfaces in the Arabian Gulf was found to be less than $2.7 \cdot 10^4$ molec cm^{-3} s^{-1}, contributing insignificantly to missing secondary production rate α. In the Arabian Gulf, HO_2 concentrations were lower compared to the Mediterranean Sea, despite high HO_x production rates. Box model calculations show, that low NO_x levels cause recycling reactions with NO to be less important. High RO_2 concentrations cause radical-radical reactions to take up a major role in the HO_x cycle, through radical loss and radical recycling reactions. Both these factors decrease the recycling probability. For regions with low NO_x conditions, it is necessary to include potential recycling through radical-radical reactions. For AQABA, this is not possible due to missing measurement of RO_2 and low data coverage of VOC.

6 Net Ozone Production Rate

The formation of NO_2 through the reaction of NO with HO_2 or RO_2 causes a net ozone production in the troposphere (see 1.5). If accumulated, these increased O_3 mixing ratios can cause plant stress and harm to the respiratory system of animals and humans (Nuvolone et al., 2018). As a precursor to O_3, much effort was put into mitigating NO_x (Miyazaki et al., 2017) emissions in Europe and America. However, NO_x emissions increased substantially in Asia, India, and the Middle East (Miyazaki et al., 2017). The following chapter characterizes net ozone production rates (NOPR) and compares the results to those obtained by Tadic et al. (2020). The influence of NO mixing ratios was investigated, and the crossover point between NO_x-limited and VOC-limited regimes was examined.

6.1 Net ozone production rate from measured HO_2 and estimated RO_2

The interconversion reactions between NO and NO_2 rapidly produce and destroy O_3 and thus form a null cycle (see 1.5, R.31 – 33). Any additional O_3 production is due to the reaction of peroxy radicals with NO forming NO_2. During daytime, NO_2 can, in turn, photolyze and the produced $O(^3P)$ reacts with O_2 to O_3. The production of O_3 can be described as shown in Eq.27. To calculate *NOPR*, O_3 loss L_{O_3} has to be subtracted from O_3 production P_{O_3}. The major loss channels are the photolysis of O_3, followed by the reaction of $O(^1D)$ with water vapor (R.1a & R.1d), the reaction with OH (R.8) and HO_2 (R.12). Other loss channels are the deposition of O_3 on the surface, reaction with the halogen monoxides BrO and IO and ozonolysis with alkenes. The surface deposition was estimated using surface iodide concentrations and the boundary layer height (Pound, Sherwen, Helmig, Carpenter, & Evans, 2020). The surface iodide concentrations were taken from Sherwen et al. (2019) and boundary layer height was taken from Dienhart et al. (2022). Since no halogen monoxide concentrations were available during AQABA, this O_3 loss pathway was not included. O_3 loss was calculated using Eq.28.

$$P_{O_3} = \left(k_{HO_2+NO}[HO_2] + \sum_i k_{R_iO_2+NO}[R_iO_2] \right) \cdot [NO] \quad \text{(Eq.27)}$$

$$L_{O_3} = [O_3] \cdot \left(\alpha j_{O^1D}[O_3] + k_{O_3+OH}[OH] + k_{HO_2+O_3}[HO_2] + \sum_i [Alkene_i] k_{Alkene_i+O_3} + \frac{[O_3]v_d}{h_{BL}} \right) \quad \text{(Eq.28)}$$

with $$\alpha = \frac{k_{O^1D+H_2O}[H_2O]}{k_{O^1D+H_2O}[H_2O] + k_{O^1D+N_2}[N_2] + k_{O^1D+O_2}[O_2]} \quad \text{(Eq.29)}$$

$$NOPR = P_{O_3} - L_{O_3} \quad \text{(Eq.30)}$$

R_iO_2 represents a particular RO_2, j_{O^1D} is the photolysis frequency for O_3 to $O(^1D)$, α is the fraction of $O(^1D)$, which reacts with H_2O, v_d is the deposition velocity, and h_{BL} is the boundary layer height. *NOPR* was calculated using measurements during AQABA and RO_2 concentrations estimated in chapter 3.1. Thus, R_iO_2 was separated into RO_2 from saturated VOC and RO_2 from unsaturated VOC. The rate constants of CH_3O_2 and $HOCH_2CH_2O_2$ were used for saturated and unsaturated, respectively. The unsaturated VOC ethene, propene, butene and isoprene were used to calculate O_3 loss from ozonolysis, as these species had the highest mixing ratios among measured unsaturated VOC. However, ozonolysis was only a significant loss in the Arabian Gulf and Gulf of Oman, where fresh emissions of these VOC caused ~11 % of total O_3 loss. The contribution of ozonolysis in other regions was <3 %. Thus, the loss from ozonolysis was only included for the Arabian Gulf and Gulf of Oman. This increased data coverage in the remaining regions significantly. *NOPR* calculated in this work is further named $NOPR_{calc}$.

Tadic et al. (2020) reported *NOPR* calculated from NO/NO_2 photo stationary state ($NOPR_{PSS}$). For the calculation of $NOPR_{PSS,}$ the production term P_{O_3} was simplified to Eq.32. Under the photo stationary state assumption of NO/NO_2, the sum of HO_2 and RO_2 can be calculated as shown in Eq.32. Since this assumption gives only a lump sum of HO_2 and RO_2, the rate constant for the reaction of HO_2 with NO is used to calculate P_{O_3}. Additionally, the data used for $NOPR_{PSS}$ was restricted to ±2 h around noontime to allow the best approximation of the photo stationary state assumption. The data reported by Tadic et al. (2020) is used as a comparison.

All used rate constants for calculating both *NOPR* variants are shown in Table 6.1.

$$P_{O_3} = k_{HO_2+NO}\,[NO] \cdot ([HO_2] + [RO_2]) \quad \text{(Eq.31)}$$

$$\text{with} \quad ([HO_2] + [RO_2]) = \frac{(j_{NO_2}\,[NO_2] - k_{NO+O_3}\,[NO][O_3])}{k_{NO+HO_2}\,[NO]} \quad \text{(Eq.32)}$$

Table 6.1 Rate constants used to calculate *NOPR* with measured data

	Reaction	**Rate constant**
k_{HO_2+NO}	$HO_2 + NO \rightarrow OH + NO_2$	$3.3{\cdot}10^{-12} \cdot \exp(270/T)$ *
$k_{CH_3O_2+NO}$	$CH_3O_2 + NO \rightarrow CH_3O + NO_2$	$1.8{\cdot}10^{-12} \cdot \exp(300/T)$ *
$k_{HOCH_2CH_2O_2+NO}$	$HOCH_2CH_2O_2 + NO \rightarrow HOCH_2CH_2O + NO_2$	$2.54{\cdot}10^{-12} \cdot \exp(360/T)$ +
k_{O_3+OH}	$OH + O_3 \rightarrow HO_2 + O_2$	$1.7{\cdot}10^{-12} \cdot \exp(-940/T)$ *
$k_{O_3+HO_2}$	$HO_2 + O_3 \rightarrow OH + 2\,O_2$	$1.0{\cdot}10^{-14} \cdot \exp(-490/T)$ *
$k_{O^1D+H_2O}$	$O^1D + H_2O \rightarrow 2OH$	$1.63{\cdot}10^{-10} \cdot \exp(60/T)$ *
$k_{O^1D+N_2}$	$O^1D + N_2 \rightarrow O^3P + N_2$	$2.15{\cdot}10^{-11} \cdot \exp(110/T)$ *
$k_{O^1D+O_2}$	$O^1D + O_2 \rightarrow O^3P + O_2$	$3.3{\cdot}10^{-11} \cdot \exp(55/T)$ *

* (J. B. Burkholder et al., 2019), + (Saunders, Jenkin, Derwent, & Pilling, 2003)

The relative uncertainty for $NOPR_{calc}$ was calculated through error propagation of Eq.27-29. The median relative uncertainty of $NOPR_{calc}$ obtained during AQABA is 57 %. The average relative uncertainty is 358 %, with a heavy bias towards single data outliers with very high or low values. Therefore, the relative uncertainty is estimated according to the median at 57 %. Tadic et al. (2020) reported a median relative uncertainty for $NOPR_{PSS}$ of 91 %.

$NOPR_{calc}$ (red) and $NOPR_{PSS}$ (blue, Tadic et al. (2020)) are shown in Figure 6.1. $NOPR_{calc}$ in the Arabian Sea and the southern Red Sea was generally low, with positive and negative values. Both regions show low concentrations of VOC and NO_x. Thus, leading to low production rates or O_3 destruction. A notable exception is the first day after exiting the Gulf of Oman on 07. Aug., when $NOPR_{calc}$ values peak at ~3.5 pptv s^{-1}. It is suspected that this is strongly influenced by dense ship traffic present within the Gulf of Oman. $NOPR_{PSS}$ and $NOPR_{calc}$ show good agreement for the Arabian Sea and the southern Red Sea regions. Additionally, when crossing the Bab al-Mandab strait between the Gulf of Aden and the southern Red Sea, dense ship traffic caused another peak in $NOPR_{calc}$, shortly increasing to values >5 pptv s^{-1}. Since this peak is not representative for the Gulf of Aden or southern Red Sea region, it was excluded from further investigations done with this dataset.

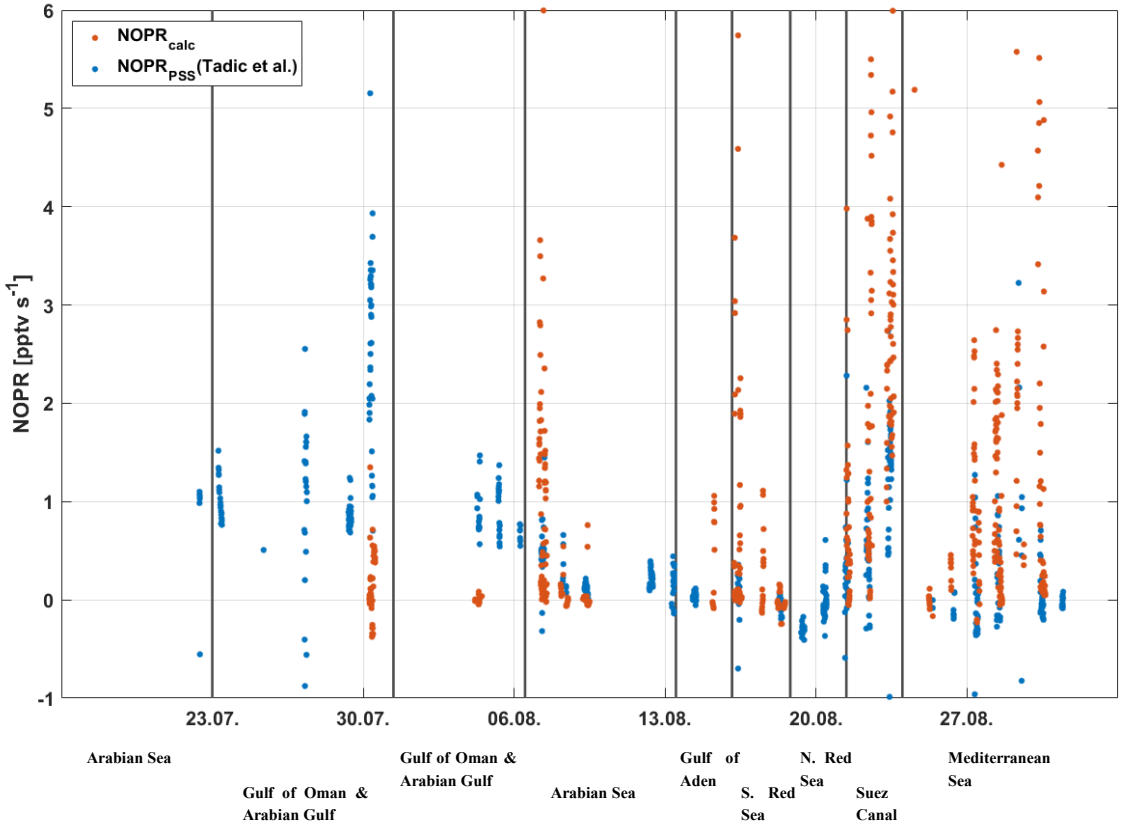

Figure 6.1 Timeline of *NOPR* calculated in this work (red) and by Tadic et al. (2020) (blue), shown in pptv s^{-1}. Gray, vertical lines indicate the separation between regions during AQABA.

In the Arabian Gulf and the Gulf of Oman, $NOPR_{calc}$ shows values around 0 pptv s^{-1}, with a median value of 0.06 pptv s^{-1} (75 % quantile: 0.42 pptv s^{-1}). Figure 6.2 shows the O_3 budget with production (positive bars) and loss rates (negative bars). In the Arabian Gulf and Gulf of Oman, the budget is balanced between production and loss. Due to high water vapor concentrations (4.0±0.2 %), the reaction of $O(^1D)$ with water vapor leads to high O_3 loss, while low NO_x concentrations lead to only small production of O_3 by peroxy radicals. The high O_3 mixing ratios of up to 170 ppbv are thus likely produced closer to sources of fresh NO_x, such as the surrounding cities. Due to high RO_2 concentrations in the region, NO_x quickly depletes further away from the sources. This leads to the conditions, in which the O_3 concentrations can only barely be maintained, as observed along the ship track. Figure 6.2 shows the O_3 budget with production (positive bars) and loss rates (negative bars). Contrary to $NOPR_{calc}$, $NOPR_{PSS}$ shows high values up to >5 pptv s^{-1} in this region. This discrepancy is likely due to an overestimation of $NOPR_{PSS}$ and an underestimation of $NOPR_{calc}$. $NOPR_{PSS}$ can be overestimated due to another null cycle, which was not accounted for in the calculation. The reaction of halogen oxides with NO can form NO_2 and a halogen radical. The formed NO_2 can photolyze and produce O_3 in the subsequent reactions. Then, the formed halogen radical reacts with O_3, which establishes a null cycle

(R.45 & 46). Sources of reactive halogen in the marine boundary layer during AQABA could be marine biota, which is known to emit organohalogen species. These species are photolabile and produce halogen radicals (Simpson, 2015). Another source is the reaction of the nocturnal NO_x species, N_2O_5 with HCl or NaCl. This reaction produces $ClNO_2$, which photolyzes to produce Cl radicals (Finlayson-Pitts, 1990; Finlayson-Pitts, 1989; Tolbert). Using the PSS assumption to calculate the sum of HO_2 and RO_2 disregards this null cycle, which results in artificially increased $NOPR_{PSS}$ values. The $NOPR_{calc}$ described within this work represents a minimum boundary, because the RO_2 estimates used are considered a lower boundary (see 3.1.2). However, it is suspected, that the RO_2 concentrations in the Arabian Gulf are underestimated by ~40 %. This is not enough to compensate for the discrepancy.

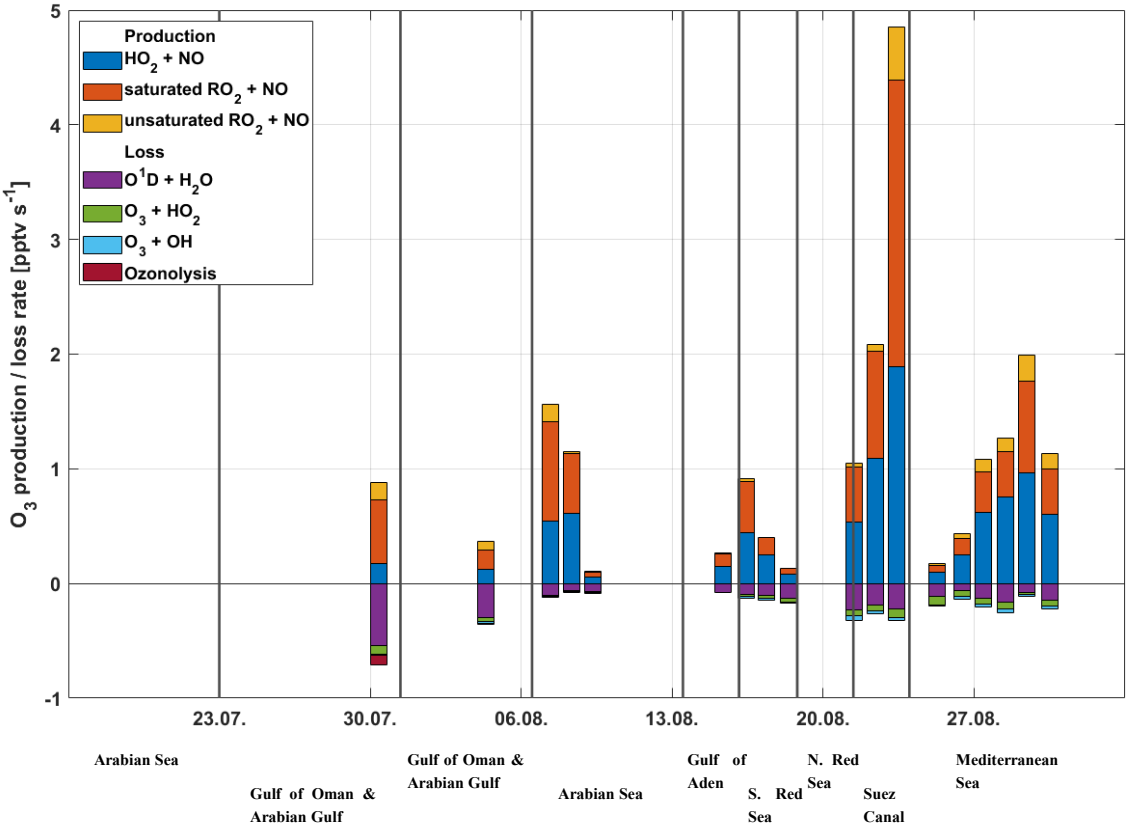

Figure 6.2 O_3 budget during the AQABA campaign. Production rates are shown as positive bars, while loss rates are shown as negative bars. Gray, vertical lines indicate the separation between regions during AQABA.

$$NO + XO \rightarrow NO_2 + X \quad \text{with X=F, Cl, Br, I} \qquad \text{(R.45)}$$

$$X + O_3 \rightarrow X + O_2 \qquad \text{(R.46)}$$

Significant O_3 production rates can be found in the Suez Canal and Gulf of Suez region, with values exceeding >5 pptv s^{-1}. The $NOPR_{calc}$ shows a latitudinal gradient with the highest values at the northern exit of the Suez Canal. Anthropogenic influence increased from two factors throughout the Suez Canal region. First, the narrowing of the shipping lane from the Northern Red Sea to the Gulf of Suez, followed by the Suez Canal itself, caused higher ship emissions through dense traffic. Additionally, northwestern winds introduced emissions from the Cairo metropolitan area in the northern part of this region. Both factors lead to increasing $NOPR_{calc}$. $NOPR_{PSS}$ is in good agreement during the Suez Canal. This indicates that the possible overestimation of $NOPR_{PSS}$ from halogen oxides and underestimation of $NOPR_{calc}$, due to RO_2 estimation, are less significant in this region.

In the Mediterranean Sea, $NOPR_{calc}$ shows values ranging from -0.2-+4.8 pptv s^{-1}, with a median of 0.56 pptv s^{-1} (1.76 pptv s^{-1}). $NOPR_{PSS}$ shows good agreement for most of the $NOPR_{calc}$ data over the Mediterranean Sea. During the time before noon on 30.08., $NOPR_{calc}$ exceeded values of 4 pptv s^{-1} as the ship passed through the strait of Messina. Fresh NO_x and VOC emissions from the nearby city of Messina showed a peak in $NOPR_{calc}$ (Figure 6.1). The passage is not included in $NOPR_{PSS}$ since it happened outside the ±2 h time interval (see above). Since this peak in $NOPR_{calc}$ is not representative of the region of the Mediterranean Sea, it was excluded from the following analysis.

6.2 NOPR dependence on NO and HO_x production

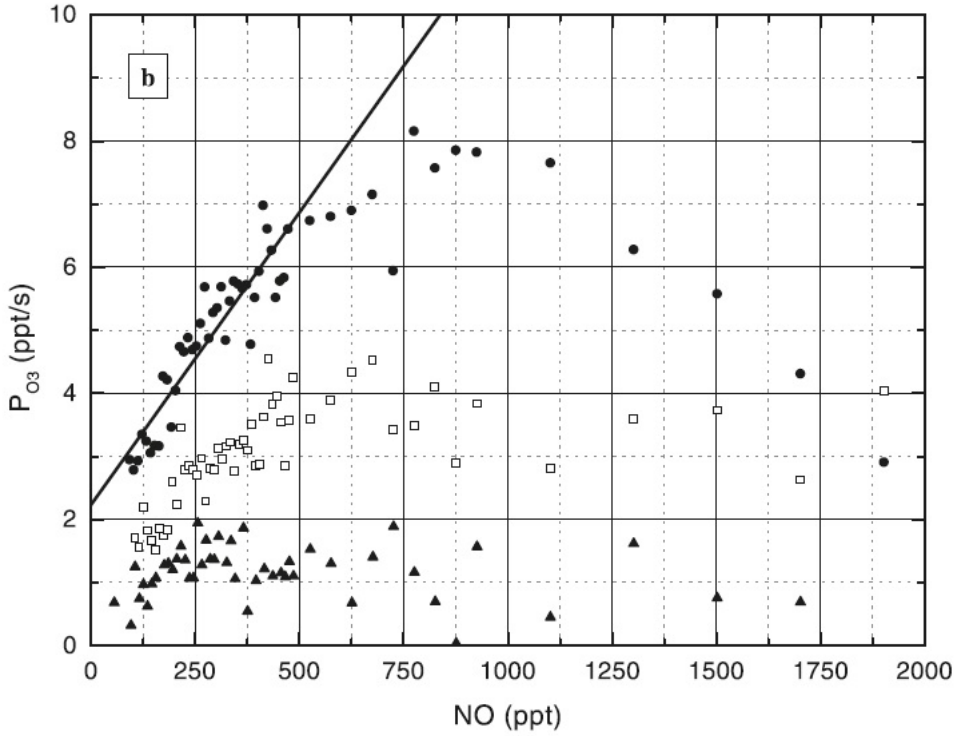

Figure 6.3 Averaged P_{O_3} plotted versus [NO]. P_{O_3} data were placed into three P_{HOx} bins: high ($0.5 < P_{HOx} < 0.7$ ppt/s, circles), moderate ($0.2 < P_{HOx} < 0.3$ ppt/s, squares), and low ($0.03 < P_{HOx} < 0.07$ ppt/s, triangles), and then averaged as a function of NO. All three P_{HOx} regimes demonstrate the expected generic dependence on NO, P_{O_3} increases linearly with NO for low NO (<600 ppt NO), and then P_{O_3} becomes independent of NO for high NO (>600 ppt NO). The crossover point between NO_x-limited and VOC-limited O_3 production occurs at different levels of NO in the three P_{HOx} regimes. (taken from J. A. Thornton et al. (2002)

During measurements in Nashville, Tennessee, in 1999, J. A. Thornton et al. (2002) found significantly different O_3 production rates for different times of the day. These differences were caused by changing emissions from the surrounding environment throughout the day. To mitigate a potential systematic error, P_{O_3} was separated by P_{HOx} (see Figure 6.3). During AQABA, this dependency on P_{HOx} was not observed. Figure 6.4 exemplifies this by separating the calculated $NOPR_{calc}$ values for the Arabian Sea into high (yellow triangles, 0.1-0.25 pptv s^{-1}), moderate (red squares, 0.04-0.1 pptv s^{-1}), and low (blue dots, 0.016-0.04 pptv s^{-1}) P_{HOx}. During AQABA, primary emission sources were ship traffic and petrochemical industries, which did not cause significant diurnal variations. Therefore, all levels of P_{HOx} in Figure 6.3 show similar $NOPR_{calc}$ for similar NO mixing ratios. Accordingly, no separation by P_{HOx} was necessary for the AQABA dataset. Similar plots for other regions can be found in Appendix A.

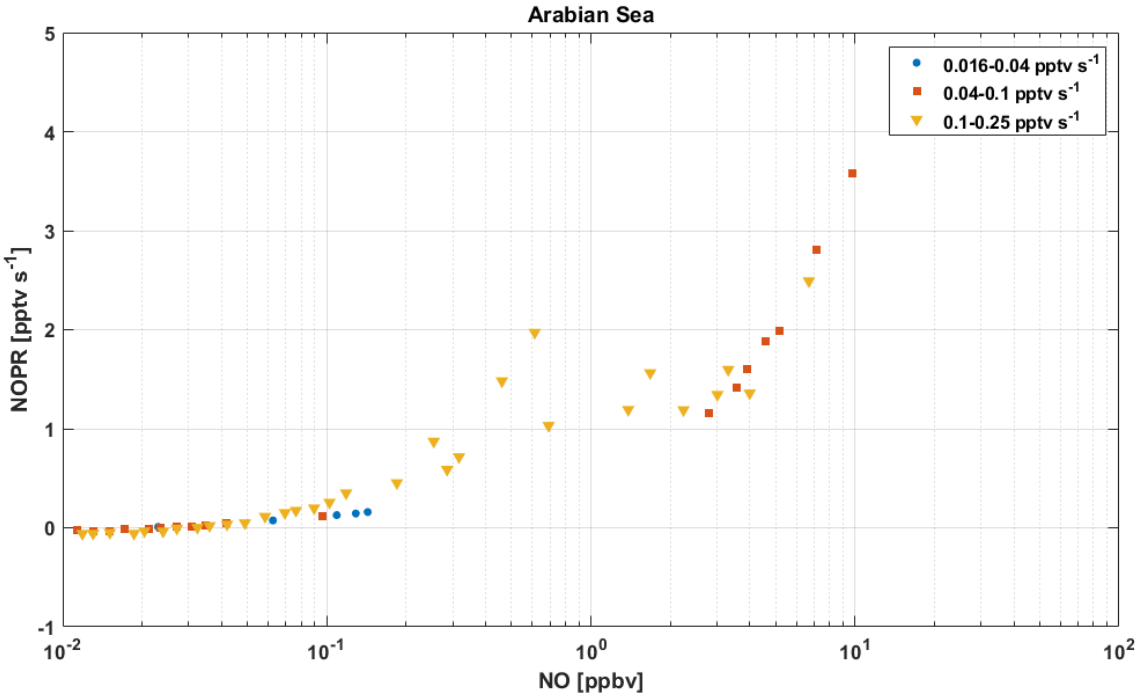

Figure 6.4 $NOPR_{calc}$ over the Arabian Sea as a function of NO mixing ratio. The blue dots show $NOPR_{calc}$ at low P_{HOx}, red squares at moderate P_{HOx}, and yellow triangles at high P_{HOx}. All three P_{HOx} regimes show similar NOPR, indicating no significant fluctuations of conditions throughout the day.

As NO is a reaction partner with RO_x, the dependency of *NOPR* can be sorted into two regimes. Under low NO_x conditions, radical-radical reactions are the dominant chain termination reactions. The most important loss reactions are R.17-19 & R.30. As NO mixing ratios increase, *NOPR* increases until the formation of nitrates exceeds radical-radical reactions. At this point, a further increase of NO yields decreasing *NOPR*. Under these conditions, the reaction of OH with NO_2 (R.21) and nitrate formation of RO_2 (R.29) become dominant chain termination reactions. O_3 production is called NO_x-limited in the low NO regime, and VOC-limited in the high NO regime. The crossover point of NO_x-limited and VOC-limited regimes corresponds to a NO mixing ratio where *NOPR* has a maximum (J. A. Thornton et al., 2002).

RO_2 concentrations estimated in chapter 3.1.2 were used to calculate the radical loss. Therefore, loss reactions involving RO_2 are calculated using CH_3O_2 and $HOCH_2CH_2O_2$ as a proxy for RO_2 from saturated ($RO_{2\ sat}$) and unsaturated VOC ($RO_{2\ unsat}$), respectively.

The total loss of RO_x L_{ROx} is assumed as the sum of chain termination rates (Eq.33), with *HHloss* as RO_x self-reactions and *NHloss* as RO_x-NO_x reactions. The reaction of RO_2 with NO has two reaction pathways. Since only chain termination reactions are used, a yield β of 3 % for R.29 relative to R.15 is assumed (Mellouki et al., 2021). Rate constants used in this calculation are summarized in Table 6.1 and Table 6.2.

$$L_{HO_x} = HHloss + NHloss \quad \text{(Eq.33)}$$

$$\begin{aligned} HHloss &= 2\,k_{HO_2+HO_2}[HO_2]^2 + 2\,k_{CH_3O_2+HO_2}[HO_2][CH_3O_2] \\ &+ 2\,k_{HOCH_2CH_2O_2+HO_2}[HO_2][HOCH_2CH_2O_2] \\ &+ 2\,k_{OH+HO_2}[HO_2][OH] + 2\,k_{CH_3O_2+CH_3O_2}[CH_3O_2][CH_3O_2] \\ &+ 2k_{HOCH_2CH_2O_2+HOCH_2CH_2O_2}[HOCH_2CH_2O_2][HOCH_2CH_2O_2] \end{aligned} \quad \text{(Eq.34)}$$

$$\begin{aligned} NHloss = {} & k_{OH+NO_2}[OH][NO_2] + \\ & \beta\,k_{CH_3O_2+NO}[NO][CH_3O_2] + \\ & \beta\,k_{HOCH_2CH_2O_2+NO}[NO][HOCH_2CH_2O_2] \end{aligned} \quad \text{(Eq.35)}$$

Table 6.2 Rate constants used to calculate *HHloss* and *NHloss*

	Reaction	**Rate constant**
$k_{HO_2+HO_2}$	$HO_2 + HO_2 \rightarrow H_2O_2 + O_2$	$3.0\cdot10^{-13}\cdot\exp(-490/T)$ *
k_{OH+HO_2}	$OH + HO_2 \rightarrow H_2O + O_2$	$4.8\cdot10^{-11}\cdot\exp(250/T)$ *
$k_{CH_3O_2+HO_2}$	$CH_3O_2 + HO_2 \rightarrow CH_3OOH + O_2$	$3.8\cdot10^{-13}\cdot\exp(780/T)$ *
$k_{HOCH_2CH_2O_2+HO_2}$	$HOCH_2CH_2O_2 + HO_2 \rightarrow HOCH_2CH_2OOH + O_2$	$1.53\cdot10^{-13}\cdot\exp(1300/T)$ +
$k_{CH_3O_2+CH_3O_2}$	$CH_3O_2 + CH_3O_2 \rightarrow CH_3OH + HCHO + O_2$	$1.03\cdot10^{-13}\cdot\exp(365/T)$ *
$k_{HOCH_2CH_2O_2+HOCH_2CH_2O_2}$	$HOCH_2CH_2O_2 + HOCH_2CH_2O_2 \rightarrow HOCH_2CH_2OH + HOCH_2CHO + O_2$	$7.8\cdot10^{-14}\cdot\exp(1000/T)$ *
k_{OH+NO_2}	$OH + NO_2 \rightarrow HNO_3$	$1.63\cdot10^{-10}\cdot\exp(60/T)$ *

* (J. B. Burkholder et al., 2019), + (Saunders et al., 2003)

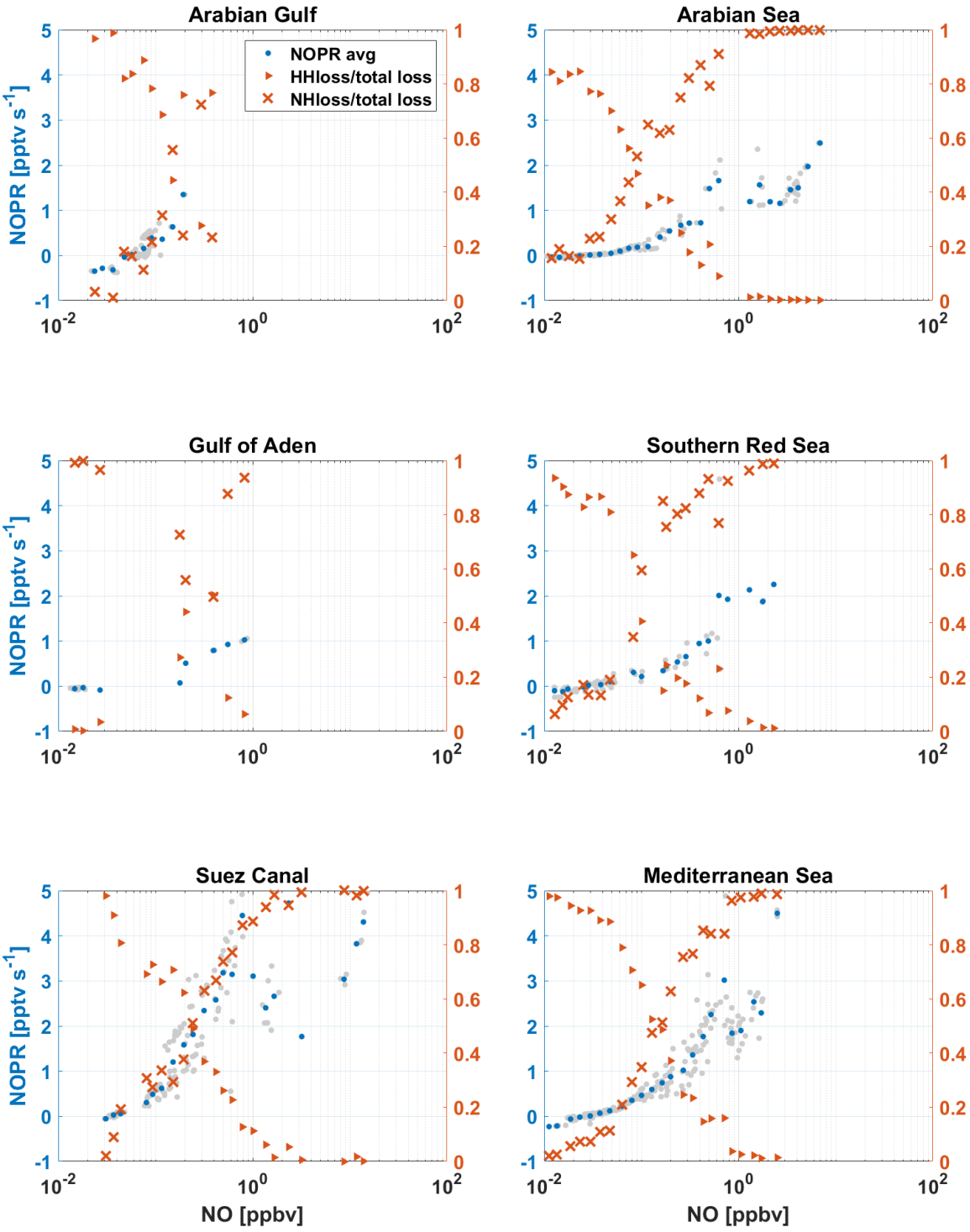

Figure 6.5 The left axis shows $NOPR_{calc}$ for different regions during AQABA vs. NO mixing ratio in ppbv. The gray dots show non-averaged $NOPR_{calc}$, while the blue dots show averaged $NOPR_{calc}$. The right axis shows the fraction of total radical loss vs. NO mixing ratio. The fractional loss through *HHloss* is shown in red triangles, and the fractional loss through *NHloss* is shown in red crosses.

$NOPR_{calc}$ and radical losses *HHloss* and *NHloss* are shown side by side for different regions in Figure 6.5. $NOPR_{calc}$ vs. NO mixing ratio are shown on the left axis. Gray dots represent unaveraged data, while blue dots show averaged data. The right axis shows relative radical loss through radical-radical reactions *HHloss*/total loss (red triangles) and nitrate formation *NHloss*/total loss (red crosses).

$NOPR_{calc}$ for all regions shows an increase with an increasing NO mixing ratio. However, even at the highest levels of NO, no maximum of $NOPR_{calc}$ can be seen. Since a crossover point between *HHloss* and *NHloss* can be seen in every region, it does not correspond with the maximum of $NOPR_{calc}$. RO_2 estimations are considered a lower boundary. Since RO_2 affects *HHloss* quadratically, an increase in RO_2 would shift the crossover point further to higher NO mixing ratios. To improve the results for *HHloss* and *NHloss*, measurements of RO_2 and their speciation would be needed.

As discussed above, the lowest $NOPR_{calc}$ was found in the Arabian Gulf, with rates around 0 pptv s^{-1}. High variability in the data also suggests close proximity to NO_x and VOC sources. In the Suez Canal region, similarly high variability can be seen, especially for NO mixing ratios >1 ppbv. It is suspected that air masses with different origins and compositions have been observed in this region. The HYSPLIT trajectories (Figure 4.5) show airmasses from southern Egypt in the southern part of the Suez Canal, while the northern part of the Suez Canal was influenced by air masses from northern Egypt and south eastern Europe.

Since no maximum in $NOPR_{calc}$ can be observed for any region during AQABA, it is assumed that $NOPR_{calc}$ is NO_x-limited throughout the campaign. This is consistent with the findings of Tadic et al. (2020) and Pfannerstill et al. (2019). Tadic et al. (2020) used a ratio of HCHO and NO_2 as an indicator and found only tendencies of VOC-limitation in the Suez Canal region (Tadic et al. (2020) label the Suez Canal as the Northern Red Sea). Pfannerstill et al. (2019) based their study on OH reactivity measurements and classified most regions as being in a transition between NO_x- and VOC-limited, with a tendency towards NO_x-limited. An exception was the Suez Canal, which showed a slight tendency towards VOC-limitation.

6.3 Summary

Net ozone production rates were calculated using measured HO_2 and calculated RO_2 mixing ratios. Throughout AQABA, the values ranged from -0.3 to >5 pptv s^{-1}, with significant differences in the regions. A budget analysis of the Arabian Gulf and Gulf of Oman showed a balanced O_3 budget. High water concentrations and fresh emissions of unsaturated VOC caused a high loss of O_3, while low NO_x concentrations lead to only a

low O_3 production from peroxy radicals. The discrepancy between $NOPR_{calc}$ and $NOPR_{PSS}$ is likely due to an overestimation of $NOPR_{PSS}$ from halogen oxide formation, as well as an underestimation of $NOPR_{calc}$ due to calculated RO_2 concentrations being a lower boundary. A peak in $NOPR_{calc}$ in the Mediterranean Sea is caused by higher NO_x mixing ratios from fresh emissions encountered in the Strait of Messina.

No P_{HOx} dependency for $NOPR_{calc}$ was found during AQABA, since the strength of significant emission sources during AQABA did not show diurnal variations. As a consequence, a separation of $NOPR_{calc}$ based on P_{HOx} was not needed.

The finding of the crossover point between NO_x-limited and VOC-limited regimes of O_3 production was attempted, using radical-radical loss and nitrate formation. However, equations Eq.34 & 35 could not describe radical losses adequately. For all regions, an increase in $NOPR_{calc}$ with increasing NO was reached. However, no maximum was found. This indicates that all regions are NO_x-limited, which is largely consistent with findings from Tadic et al. (2020) and Pfannerstill et al. (2019). The exception being the Suez Canal region, where conditions were found to have tendencies towards VOC-limitation.

7 Summary and Conclusions

The region around the Arabian Peninsula is synonymous with intense solar radiation and high ambient temperatures. Combined with strong sources of VOC from oil and gas extraction and processing, these conditions have a major impact on the oxidative capacity of the atmosphere. To investigate the oxidative capacity under the conditions of high photochemistry and anthropogenic pollution, the AQABA ship-based measurement campaign was conducted in the summer of 2017. As part of a large ensemble of instrumentation, the OH and HO_2 radicals were measured using the HORUS system.

Since OH can also be recycled through RO_2, their quantification is important to characterize the oxidative potential. Due to missing RO_2 measurements during AQABA, lower boundaries of ambient RO_2 concentrations were calculated utilizing measurement-constrained CAABA/MECCA box-model calculations and measured OH reactivity. The highest average mixing ratios were found in the Suez Canal (23.8±14.7 pptv) and the Arabian Gulf (23.2±22.4 pptv), followed by the Mediterranean Sea (15.0±7.4 pptv). With 4.9±3.7 pptv and 6.8±4.9 pptv, respectively, the Gulf of Aden and the Arabian Sea showed the lowest mixing ratio.

As a measure of the oxidative potential, an investigation of the OH recycling probability was conducted for the AQABA dataset. The Arabian Gulf (15±10 % (1σ) @ 0.1 pptv NO) showed significantly lower recycling probability compared to the Mediterranean Sea (57±5 % (1σ) @ 0.1 pptv NO). Possible radical losses were investigated. HO_2 loss on particle surfaces was negligible over the Arabian Gulf, being less than 0.16 % of missing secondary production. Peroxy radical losses had been studied using the constrained CAABA/MECCA box model. The calculations showed, that due to low NO_x (0.09±0.05 pptv) and high radical mixing ratios in the Arabian Gulf, the importance of the recycling reaction of HO_2/RO_2 and NO is decreased. In contrast, the significance of radical-radical reactions increased, which led to an increase in the destruction of radicals from peroxide formation by a factor of ~ 2 in the Arabian Gulf (32.4 % of total RO_x loss). At similar VOC load but higher NO_x levels, the Gulf of Oman and Suez Canal showed a lower contribution of 12.1 % and 11.7 %, respectively. The pristine air masses in the Arabian Sea showed that 47.6 % of total RO_x loss can be contributed to radical-radical reactions. Due to very low NO_x and VOC mixing ratios, the reaction of HO_2 with itself is the major contributor to radical loss. The contribution in the Mediterranean Sea was <0.2 %. However, this is only representable for the early morning period, where radical levels were generally low. An increased destruction of radicals through radical-radical reactions leads directly to a decrease of the recycling probability *r*. Additionally, high radical concentrations cause radical-radical recycling reactions to be more important in the Arabian

Gulf. This is particularly the case given that they could not be accounted for in the calculation of the OH recycling probability, thus indirectly lowering *r*.

As a side product of radical recycling, tropospheric O_3 is directly impacted by the recycling probability. The net ozone production rate $NOPR_{calc}$ was calculated using HO_2 measurements and RO_2 concentrations determined in this work. $NOPR_{calc}$ along the ship track in the Arabian Gulf and Gulf of Oman showed production rates around 0 pptv s^{-1}. High measured water vapor concentrations (4.0±0.2 %) caused a high loss of O_3 through the reaction of $O(^1D)$ with H_2O. Additionally, high radical concentrations depleted NO_x concentrations, leading to low production of O_3. Throughout AQABA, there were no observable condition where $NOPR_{calc}$ peaked at a specific NO concentration. Therefore, the NOPR in this work is categorized as NO_x-limited. These findings are consistent with Tadic et al. (2020) and Pfannerstill et al. (2019).

To conclude, the results show an increased shift in importance towards radical-radical reactions for the recycling probability in low NO_x/high VOC regions. In the Arabian Gulf, this is due to the high RO_2 concentrations. The reaction of RO_2 with HO_2 is the biggest contributor and add to radical destruction and recycling. Both reduce the recycling probability either directly or indirectly. It is, thus, important to include RO_2 observations and speciation in future measurements. Despite high radical concentrations in the Arabian Gulf, *NOPR* was around 0 pptv s^{-1}. High water vapor and low NO_x concentrations caused both high O_3 destruction and low production, respectively. In the Mediterranean Sea, future exploitation of natural gas reservoirs in Turkish and Greek waters could lead to high VOC loads similar to the Arabian Gulf. However, due to lower primary radical production it is expected, that NO_x will remain higher, which in turn will lead to higher *NOPR* compared to the Arabian Gulf.

8 Bibliography

Atkinson, R. (1997). Gas-Phase Tropospheric Chemistry of Volatile Organic Compounds: 1. Alkanes and Alkenes. *Journal of Physical and Chemical Reference Data, 26*(2), 215-290. doi:10.1063/1.556012

Atkinson, R. (2000). Atmospheric chemistry of VOCs and NOx. *Atmospheric Environment, 34*(12), 2063-2101. doi:https://doi.org/10.1016/S1352-2310(99)00460-4

Atkinson, R., & Arey, J. (2003). Atmospheric Degradation of Volatile Organic Compounds. *Chemical Reviews, 103*(12), 4605-4638. doi:10.1021/cr0206420

Atkinson, R., Baulch, D. L., Cox, R. A., Crowley, J. N., Hampson, R. F., Hynes, R. G., Jenkin, M. E., Rossi, M. J., & Troe, J. (2004). Evaluated kinetic and photochemical data for atmospheric chemistry: Volume I - gas phase reactions of O_x, HO_x, NO_x and SO_x species. *Atmos. Chem. Phys., 4*(6), 1461-1738. doi:10.5194/acp-4-1461-2004

Atkinson, R., Baulch, D. L., Cox, R. A., Crowley, J. N., Hampson, R. F., Hynes, R. G., Jenkin, M. E., Rossi, M. J., Troe, J., & Subcommittee, I. (2006). Evaluated kinetic and photochemical data for atmospheric chemistry: Volume II – gas phase reactions of organic species. *Atmos. Chem. Phys., 6*(11), 3625-4055. doi:10.5194/acp-6-3625-2006

Birdsall, A. W., & Elrod, M. J. (2011). Comprehensive NO-Dependent Study of the Products of the Oxidation of Atmospherically Relevant Aromatic Compounds. *The Journal of Physical Chemistry A, 115*(21), 5397-5407. doi:10.1021/jp2010327

Bourtsoukidis, E., Ernle, L., Crowley, J. N., Lelieveld, J., Paris, J. D., Pozzer, A., Walter, D., & Williams, J. (2019). Non-methane hydrocarbon (C2–C8) sources and sinks around the Arabian Peninsula. *Atmos. Chem. Phys., 19*(10), 7209-7232. doi:10.5194/acp-19-7209-2019

Cabrera-Perez, D. (2016). Global atmospheric budget of simple monocyclic aromatic compounds. *Atmos. Chem. Phys., 16*(11), 6931-6947. doi:10.5194/acp-16-6931-2016

Cantrell, C., Shetter, R., Calvert, J., Eisele, F., Williams, E., Baumann, K., Brune, W., Stevens, P., & Mather, J. (1997). Peroxy radicals from photostationary state deviations and steady state calculations during the Tropospheric OH Photochemistry Experiment at Idaho Hill, Colorado, 1993. *J. Geophys. Res.-Atmos., 102*, 6369-6378. doi:10.1029/96JD01703

Cariolle, D., Evans, M. J., Chipperfield, M. P., Butkovskaya, N., Kukui, A., & Le Bras, G. (2008). Impact of the new HNO₃-forming channel of the HO₂+NO reaction on tropospheric HNO₃, NO_x, HO_x and ozone. *Atmos. Chem. Phys., 8*(14), 4061-4068. doi:10.5194/acp-8-4061-2008

Carslaw, N., Creasey, D. J., Heard, D. E., Jacobs, P. J., Lee, J. D., Lewis, A. C., McQuaid, J. B., Pilling, M. J., Bauguitte, S., Penkett, S. A., Monks, P. S., & Salisbury, G. (2002). Eastern Atlantic Spring Experiment 1997 (EASE97) 2. Comparisons of model concentrations of OH, HO2, and RO2 with measurements. *Journal of Geophysical Research: Atmospheres, 107*(D14), ACH 5-1-ACH 5-16. doi:https://doi.org/10.1029/2001JD001568

Carslaw, N., Creasey, D. J., Heard, D. E., Lewis, A. C., McQuaid, J. B., Pilling, M. J., Monks, P. S., Bandy, B. J., & Penkett, S. A. (1999). Modeling OH, HO2, and RO2 radicals in the marine boundary layer: 1. Model construction and comparison with field measurements. *Journal of Geophysical Research: Atmospheres, 104*(D23), 30241-30255. doi:https://doi.org/10.1029/1999JD900783

Celik, S., Drewnick, F., Fachinger, F., Brooks, J., Darbyshire, E., Coe, H., Paris, J. D., Eger, P. G., Schuladen, J., Tadic, I., Friedrich, N., Dienhart, D., Hottmann, B., Fischer, H., Crowley, J. N., Harder, H., & Borrmann, S. (2020). Influence of vessel characteristics and atmospheric processes on the gas and particle phase of ship emission plumes: in situ measurements in the Mediterranean Sea and around the Arabian Peninsula. *Atmos. Chem. Phys., 20*(8), 4713-4734. doi:10.5194/acp-20-4713-2020

Chan, C. Y., Hard, T. M., Mehrabzadeh, A. A., George, L. A., & O'Brien, R. J. (1990). Third-generation FAGE instrument for tropospheric hydroxyl radical measurement. *Journal of Geophysical Research: Atmospheres, 95*(D11), 18569-18576. doi:https://doi.org/10.1029/JD095iD11p18569

Cooper, P. L., & Abbatt, J. P. D. (1996). Heterogeneous Interactions of OH and HO2 Radicals with Surfaces Characteristic of Atmospheric Particulate Matter. *The Journal of Physical Chemistry, 100*(6), 2249-2254. doi:10.1021/jp952142z

Crawford, J., Davis, D., Olson, J., Chen, G., Liu, S., Fuelberg, H., Hannan, J., Kondo, Y., Anderson, B., Gregory, G., Sachse, G., Talbot, R., Viggiano, A., Heikes, B., Snow, J., Singh, H., & Blake, D. (2000). Evolution and chemical consequences of lightning-produced NO x observed in the North Atlantic upper troposphere. *Journal of Geophysical Research: Atmospheres, 105*(D15), 19795-19809. doi:https://doi.org/10.1029/2000JD900183

Creasey, D. J., Halford-Maw, P. A., Heard, D. E., Spence, J. E., & Whitaker, B. J. (1998). Fast photomultiplier tube gating system for photon counting applications. *Review of Scientific Instruments, 69*(12), 4068-4073. doi:Doi 10.1063/1.1149252

Criegee, R. (1975). Mechanism of Ozonolysis. *Angewandte Chemie International Edition in English, 14*(11), 745-752. doi:https://doi.org/10.1002/anie.197507451

Dienhart, D., Brendel, B., Crowley, J. N., Eger, P. G., Harder, H., Martinez, M., Pozzer, A., Rohloff, R., Schuladen, J., Tauer, S., Lelieveld, J., & Fischer, H. (2022). Formaldehyde and hydroperoxide distribution around the Arabian Peninsula - evaluation of EMAC model results with ship-based measurements. *Atmos. Chem. Phys. Discuss., 2022*, 1-40. doi:10.5194/acp-2022-580

Eisele, F. L., & Tanner, D. J. (1991). Ion-assisted tropospheric OH measurements. *Journal of Geophysical Research: Atmospheres, 96*(D5), 9295-9308. doi:https://doi.org/10.1029/91JD00198

Fairall, C. W., Bradley, E. F., Rogers, D. P., Edson, J. B., & Young, G. S. (1996). Bulk parameterization of air-sea fluxes for Tropical Ocean-Global Atmosphere Coupled-Ocean Atmosphere Response Experiment. *Journal of Geophysical Research: Oceans, 101*(C2), 3747-3764. doi:https://doi.org/10.1029/95JC03205

Faloona, I. C., Tan, D., Lesher, R. L., Hazen, N. L., Frame, C. L., Simpas, J. B., Harder, H., Martinez, M., Di Carlo, P., Ren, X. R., & Brune, W. H. (2004). A laser-induced fluorescence instrument for detecting tropospheric OH and HO2: Characteristics and calibration. *Journal of Atmospheric Chemistry, 47*(2), 139-167. doi:DOI 10.1023/B:JOCH.0000021036.53185.0e

Finlayson-Pitts, B. J. (1990). Ozone destruction and bromine photochemistry at ground level in the Arctic spring. *Nature, 343*(6259), 622-625. doi:10.1038/343622a0

Finlayson-Pitts, B. J. (1989). Formation of chemically active chlorine compounds by reactions of atmospheric NaCl particles with gaseous N2O5 and ClONO2. *337*, 241-244.

Fuchs, H., Bohn, B., Hofzumahaus, A., Holland, F., Lu, K. D., Nehr, S., Rohrer, F., & Wahner, A. (2011). Detection of HO₂ by laser-induced fluorescence: calibration and interferences from RO₂ radicals. *Atmos. Meas. Tech., 4*(6), 1209-1225. doi:10.5194/amt-4-1209-2011

Ghude, S. D., Kulkarni, S. H., Jena, C., Pfister, G. G., Beig, G., Fadnavis, S., & van der A, R. J. (2013). Application of satellite observations for identifying regions of dominant sources of nitrogen oxides over the Indian Subcontinent. *Journal of Geophysical Research: Atmospheres, 118*(2), 1075-1089. doi:https://doi.org/10.1029/2012JD017811

Hanson, D. R., Burkholder, J. B., Howard, C. J., & Ravishankara, A. R. (1992). Measurement of hydroxyl and hydroperoxy radical uptake coefficients on water and sulfuric acid surfaces. *The Journal of Physical Chemistry, 96*(12), 4979-4985. doi:10.1021/j100191a046

Hard, T. M., O'Brien, R. J., Chan, C. Y., & Mehrabzadeh, A. A. (1984). Tropospheric free radical determination by fluorescence assay with gas expansion. *Environmental Science & Technology, 18*(10), 768-777. doi:10.1021/es00128a009

Hasson, A. S., Kuwata, K. T., Arroyo, M. C., & Petersen, E. B. (2005). Theoretical studies of the reaction of hydroperoxy radicals (HO2) with ethyl peroxy (CH3CH2O2), acetyl peroxy (CH3C(O)O2), and acetonyl peroxy (CH3C(O)CH2O2) radicals. *Journal of Photochemistry and Photobiology A: Chemistry, 176*(1), 218-230. doi:https://doi.org/10.1016/j.jphotochem.2005.08.012

Hasson, A. S., Tyndall, G. S., Orlando, J. J., Singh, S., Hernandez, S. Q., Campbell, S., & Ibarra, Y. (2012). Branching Ratios for the Reaction of Selected Carbonyl-Containing Peroxy Radicals with Hydroperoxy Radicals. *The Journal of Physical Chemistry A, 116*(24), 6264-6281. doi:10.1021/jp211799c

Hauglustaine, D. A., Madronich, S., Ridley, B. A., Walega, J. G., Cantrell, C. A., Shetter, R. E., & Hübler, G. (1996). Observed and model-calculated photostationary state at Mauna Loa Observatory during MLOPEX 2. *Journal of Geophysical Research: Atmospheres, 101*(D9), 14681-14696. doi:https://doi.org/10.1029/95JD03612

Heard, D. E., & Pilling, M. J. (2003). Measurement of OH and HO2 in the Troposphere. *Chemical Reviews, 103*(12), 5163-5198. doi:10.1021/cr020522s

Hens, K. (2013). OH and HO2 radical measurements in a boreal forest environment using laser induced fluorescence spectroscopy. *Dissertation*.

Hens, K., Novelli, A., Martinez, M., Auld, J., Axinte, R., Bohn, B., Fischer, H., Keronen, P., Kubistin, D., Nölscher, A. C., Oswald, R., Paasonen, P., Petäjä, T., Regelin, E., Sander, R., Sinha, V., Sipilä, M., Taraborrelli, D., Tatum Ernest, C., Williams, J., Lelieveld, J., & Harder, H. (2014). Observation and modelling of HO_x radicals in a boreal forest. *Atmos. Chem. Phys., 14*(16), 8723-8747. doi:10.5194/acp-14-8723-2014

Hofzumahaus, A., Rohrer, F., Lu, K., Bohn, B., Brauers, T., Chang, C.-C., Fuchs, H., Holland, F., Kita, K., Kondo, Y., Li, X., Lou, S., Shao, M., Zeng, L., Wahner, A.,

& Zhang, Y. (2009). Amplified Trace Gas Removal in the Troposphere. *Science, 324*(5935), 1702-1704. doi:10.1126/science.1164566

Holland, F., Hofzumahaus, A., Schäfer, J., Kraus, A., & Pätz, H.-W. (2003). Measurements of OH and HO2 radical concentrations and photolysis frequencies during BERLIOZ. *Journal of Geophysical Research: Atmospheres, 108*(D4), PHO 2-1-PHO 2-23. doi:https://doi.org/10.1029/2001JD001393

Huang, C., Hu, Q., Wang, H., Qiao, L., Jing, S. a., Wang, H., Zhou, M., Zhu, S., Ma, Y., Lou, S., Li, L., Tao, S., Li, Y., & Lou, D. (2018). Emission factors of particulate and gaseous compounds from a large cargo vessel operated under real-world conditions. *Environmental Pollution, 242*, 667-674. doi:https://doi.org/10.1016/j.envpol.2018.07.036

Hui, A. O., Fradet, M., Okumura, M., & Sander, S. P. (2019). Temperature Dependence Study of the Kinetics and Product Yields of the HO2 + CH3C(O)O2 Reaction by Direct Detection of OH and HO2 Radicals Using 2f-IR Wavelength Modulation Spectroscopy. *The Journal of Physical Chemistry A, 123*(17), 3655-3671. doi:10.1021/acs.jpca.9b00442

IPCC, Masson-Delmotte, V., Zhai, P., Pörtner, H.-O., Roberts, D., Skea, J., Shukla, P., Pirani, A., Moufouma-Okia, W., Péan, C., Pidcock, R., Connors, S., Matthews, R., Chen, Y., Zhou, X., Gomis, M., Lonnoy, E., Maycock, T., Tignor, M., & Tabatabaei, M. (2018). *Global warming of 1.5°C. An IPCC Special Report on the impacts of global warming of 1.5°C above pre-industrial levels and related global greenhouse gas emission pathways, in the context of strengthening the global response to the threat of climate change, sustainable development, and efforts to eradicate poverty*.

J. B. Burkholder, S. P. Sander, J. Abbatt, J. R. B., C. Cappa, J. D. Crounse, T. S. Dibble, R. E. Huie, C. E. Kolb, M. J. Kurylo, V. L. Orkin, C. J. Percival, D. M. Wilmouth, and P. H. Wine Jet Propulsion Laboratory, P., & http://jpldataeval.jpl.nasa.gov. (2019). Chemical Kinetics and Photochemical Data for Use in Atmospheric Studies, Evaluation No. 19. *JPL Publication 19-5, Jet Propulsion Laboratory, Pasadena*.

Jacob, D. J. (1986). Chemistry of OH in remote clouds and its role in the production of formic acid and peroxymonosulfate. *Journal of Geophysical Research: Atmospheres, 91*(D9), 9807-9826. doi:https://doi.org/10.1029/JD091iD09p09807

Jacob, D. J. (2000). Heterogeneous chemistry and tropospheric ozone. *Atmospheric Environment, 34*(12), 2131-2159. doi:https://doi.org/10.1016/S1352-2310(99)00462-8

Jaeglé, L., Jacob, D. J., Brune, W. H., & Wennberg, P. O. (2001). Chemistry of HOx radicals in the upper troposphere. *Atmospheric Environment, 35*(3), 469-489. doi:https://doi.org/10.1016/S1352-2310(00)00376-9

Jenkin, M. E., & Hayman, G. D. (1995). Kinetics of reactions of primary, secondary and tertiary β-hydroxy peroxyl radicals. *Journal of the Chemical Society, Faraday Transactions, 91*(13), 1911-1922. doi:10.1039/FT9959101911

Jungkamp, T. P. W., Smith, J. N., & Seinfeld, J. H. (1997). Atmospheric Oxidation Mechanism of n-Butane: The Fate of Alkoxy Radicals. *The Journal of Physical Chemistry A, 101*(24), 4392-4401. doi:10.1021/jp970212r

Kesselmeier, J., & Staudt, M. (1999). Biogenic Volatile Organic Compounds (VOC): An Overview on Emission, Physiology and Ecology. *Journal of Atmospheric Chemistry, 33*(1), 23-88. doi:10.1023/A:1006127516791

Krotkov, N. A., McLinden, C. A., Li, C., Lamsal, L. N., Celarier, E. A., Marchenko, S. V., Swartz, W. H., Bucsela, E. J., Joiner, J., Duncan, B. N., Boersma, K. F., Veefkind, J. P., Levelt, P. F., Fioletov, V. E., Dickerson, R. R., He, H., Lu, Z., & Streets, D. G. (2016). Aura OMI observations of regional SO2 and NO2 pollution changes from 2005 to 2015. *Atmos. Chem. Phys., 16*(7), 4605-4629. doi:10.5194/acp-16-4605-2016

Kubistin, D. (2009). OH-HO2-Radikale über dem tropischen Regenwald.

Kunkler, F. (2021). Quantifizierung der RO2-Interferenz auf das HORUS-HO2-Messsignal.

Leighton, P. A. (1961). Photochemistry of air pollution. *Physical chemistry, Academic Press, New York 9*, 300 p. pp.

Lelieveld, J. (2016). Global tropospheric hydroxyl distribution, budget and reactivity. *Atmos. Chem. Phys., 16*(19), 12477-12493. doi:10.5194/acp-16-12477-2016

Lelieveld, J., Peters, W., Dentener, F. J., & Krol, M. C. (2002). Stability of tropospheric hydroxyl chemistry. *Journal of Geophysical Research: Atmospheres, 107*(D23), ACH 17-11-ACH 17-11. doi:10.1029/2002jd002272

Lelieveld, J., Pozzer, A., Pöschl, U., Fnais, M., Haines, A., & Munzel, T. (2020). Loss of life expectancy from air pollution compared to other risk factors: A worldwide perspective. *Cardiovascular research, 116*. doi:10.1093/cvr/cvaa025

Levy, H. (1971). Normal Atmosphere: Large Radical and Formaldehyde Concentrations Predicted. *Science, 173*, 141-143.

Liousse, C., Assamoi, E., Criqui, P., Granier, C., & Rosset, R. (2014). Explosive growth in African combustion emissions from 2005 to 2030. *Environmental Research Letters, 9*(3), 035003. doi:10.1088/1748-9326/9/3/035003

Mao, J., Fan, S., Jacob, D. J., & Travis, K. R. (2013). Radical loss in the atmosphere from Cu-Fe redox coupling in aerosols. *Atmos. Chem. Phys., 13*(2), 509-519. doi:10.5194/acp-13-509-2013

Mao, J., Ren, X., Chen, S., Brune, W. H., Chen, Z., Martinez, M., Harder, H., Lefer, B., Rappenglück, B., Flynn, J., & Leuchner, M. (2010). Atmospheric oxidation capacity in the summer of Houston 2006: Comparison with summer measurements in other metropolitan studies. *Atmospheric Environment, 44*(33), 4107-4115. doi:https://doi.org/10.1016/j.atmosenv.2009.01.013

Mao, J., Ren, X., Zhang, L., Van Duin, D. M., Cohen, R. C., Park, J. H., Goldstein, A. H., Paulot, F., Beaver, M. R., Crounse, J. D., Wennberg, P. O., DiGangi, J. P., Henry, S. B., Keutsch, F. N., Park, C., Schade, G. W., Wolfe, G. M., Thornton, J. A., & Brune, W. H. (2012). Insights into hydroxyl measurements and atmospheric oxidation in a California forest. *Atmos. Chem. Phys., 12*(17), 8009-8020. doi:10.5194/acp-12-8009-2012

Maring, H., Savoie, D. L., Izaguirre, M. A., Custals, L., & Reid, J. S. (2003). Mineral dust aerosol size distribution change during atmospheric transport. *Journal of Geophysical Research: Atmospheres, 108*(D19). doi:https://doi.org/10.1029/2002JD002536

Marno, D., Ernest, C., Hens, K., Javed, U., Klimach, T., Martinez, M., Rudolf, M., Lelieveld, J., & Harder, H. (2020). Calibration of an airborne HOx instrument using the All Pressure Altitude-based Calibrator for HOx Experimentation (APACHE). *Atmos. Meas. Tech., 13*(5), 2711-2731. doi:10.5194/amt-13-2711-2020

Martinez, M., Harder, H., Kovacs, T. A., Simpas, J. B., Bassis, J., Lesher, R., Brune, W. H., Frost, G. J., Williams, E. J., Stroud, C. A., Jobson, B. T., Roberts, J. M., Hall, S. R., Shetter, R. E., Wert, B., Fried, A., Alicke, B., Stutz, J., Young, V. L., White, A. B., & Zamora, R. J. (2003). OH and HO2 concentrations, sources, and loss rates during the Southern Oxidants Study in Nashville, Tennessee, summer 1999. *Journal of Geophysical Research: Atmospheres, 108*(D19). doi:https://doi.org/10.1029/2003JD003551

Martinez, M., Harder, H., Kubistin, D., Rudolf, M., Bozem, H., Eerdekens, G., Fischer, H., Klüpfel, T., Gurk, C., Königstedt, R., Parchatka, U., Schiller, C. L., Stickler, A., Williams, J., & Lelieveld, J. (2010). Hydroxyl radicals in the tropical troposphere over the Suriname rainforest: airborne measurements. *Atmos. Chem. Phys., 10*(8), 3759-3773. doi:10.5194/acp-10-3759-2010

Mellouki, A., Ammann, M., Cox, R. A., Crowley, J. N., Herrmann, H., Jenkin, M. E., McNeill, V. F., Troe, J., & Wallington, T. J. (2021). Evaluated kinetic and photochemical data for atmospheric chemistry: volume VIII – gas-phase reactions of organic species with four, or more, carbon atoms (≥ C4). *Atmos. Chem. Phys., 21*(6), 4797-4808. doi:10.5194/acp-21-4797-2021

Miller, A. M., Yeung, L. Y., Kiep, A. C., & Elrod, M. J. (2004). Overall rate constant measurements of the reactions of alkene-derived hydroxyalkylperoxy radicals with nitric oxide. *Physical Chemistry Chemical Physics, 6*(13), 3402-3407. doi:10.1039/B402110J

Millet, D. B., Jacob, D. J., Custer, T. G., de Gouw, J. A., Goldstein, A. H., Karl, T., Singh, H. B., Sive, B. C., Talbot, R. W., Warneke, C., & Williams, J. (2008). New constraints on terrestrial and oceanic sources of atmospheric methanol. *Atmos. Chem. Phys., 8*(23), 6887-6905. doi:10.5194/acp-8-6887-2008

Miyazaki, K., Eskes, H., Sudo, K., Boersma, K. F., Bowman, K., & Kanaya, Y. (2017). Decadal changes in global surface NOx emissions from multi-constituent satellite data assimilation. *Atmos. Chem. Phys., 17*(2), 807-837. doi:10.5194/acp-17-807-2017

Möller, D. (2003). *Luft: Chemie, Physik, Biologie, Reinhaltung, Recht*: De Gruyter.

Moore, R. M., Oram, D. E., & Penkett, S. A. (1994). Production of isoprene by marine phytoplankton cultures. *Geophysical Research Letters, 21*(23), 2507-2510. doi:https://doi.org/10.1029/94GL02363

Mozurkewich, M., McMurry, P. H., Gupta, A., & Calvert, J. G. (1987). Mass accommodation coefficient for HO2 radicals on aqueous particles. *Journal of Geophysical Research: Atmospheres, 92*(D4), 4163-4170. doi:https://doi.org/10.1029/JD092iD04p04163

Nölscher, A. C. (2014). Using total OH reactivity to assess isoprene photooxidation via measurement and model. *Atmospheric Environment, 89*, 453-463. doi:https://doi.org/10.1016/j.atmosenv.2014.02.024

Novelli, A., Hens, K., Tatum Ernest, C., Kubistin, D., Regelin, E., Elste, T., Plass-Dülmer, C., Martinez, M., Lelieveld, J., & Harder, H. (2014). Characterisation of an inlet pre-injector laser-induced fluorescence instrument for the measurement of atmospheric hydroxyl radicals. *Atmos. Meas. Tech., 7*(10), 3413-3430. doi:10.5194/amt-7-3413-2014

Nuvolone, D., Petri, D., & Voller, F. (2018). The effects of ozone on human health. *Environmental Science and Pollution Research, 25*(9), 8074-8088. doi:10.1007/s11356-017-9239-3

Orlando, J. J., Tyndall, G. S., Bilde, M., Ferronato, C., Wallington, T. J., Vereecken, L., & Peeters, J. (1998). Laboratory and Theoretical Study of the Oxy Radicals in the OH- and Cl-Initiated Oxidation of Ethene. *The Journal of Physical Chemistry A, 102*(42), 8116-8123. doi:10.1021/jp981937d

Ortgies, G., Gericke, K. H., & Comes, F. J. (1980). Is UV laser induced fluorescence a method to monitor tropospheric OH? *Geophysical Research Letters, 7*, 905-908. doi:10.1029/GL007i011p00905

Paris, J. D., Riandet, A., Bourtsoukidis, E., Delmotte, M., Berchet, A., Williams, J., Ernle, L., Tadic, I., Harder, H., & Lelieveld, J. (2021). Shipborne measurements of methane and carbon dioxide in the Middle East and Mediterranean areas and the contribution from oil and gas emissions. *Atmos. Chem. Phys., 21*(16), 12443-12462. doi:10.5194/acp-21-12443-2021

Peeters, J., Müller, J.-F., Stavrakou, T., & Nguyen, V. S. (2014). Hydroxyl Radical Recycling in Isoprene Oxidation Driven by Hydrogen Bonding and Hydrogen Tunneling: The Upgraded LIM1 Mechanism. *The Journal of Physical Chemistry A, 118*(38), 8625-8643. doi:10.1021/jp5033146

Perner, D., Platt, U., Trainer, M., Hübler, G., Drummond, J., Junkermann, W., Rudolph, J., Schubert, B., Volz, A., Ehhalt, D. H., Rumpel, K. J., & Helas, G. (1987). Measurements of tropospheric OH concentrations: A comparison of field data with model predictions. *Journal of Atmospheric Chemistry, 5*(2), 185-216. doi:10.1007/BF00048859

Pfannerstill, E. Y., Wang, N. J., Edtbauer, A., Bourtsoukidis, E., Crowley, J. N., Dienhart, D., Eger, P. G., Ernle, L., Fischer, H., Hottmann, B., Paris, J. D., Stonner, C., Tadic, I., Walter, D., & Williams, J. (2019). Shipborne measurements of total OH reactivity around the Arabian Peninsula and its role in ozone chemistry. *Atmospheric Chemistry and Physics, 19*(17), 11501-11523. doi:10.5194/acp-19-11501-2019

Pound, R. J., Sherwen, T., Helmig, D., Carpenter, L. J., & Evans, M. J. (2020). Influences of oceanic ozone deposition on tropospheric photochemistry. *Atmos. Chem. Phys., 20*(7), 4227-4239. doi:10.5194/acp-20-4227-2020

Prinn, R. G. (2003). The Cleansing Capacity of the Atmosphere. *Annual Review of Environment and Resources, 28*(1), 29-57. doi:10.1146/annurev.energy.28.011503.163425

Ravishankara, A. R. (1997). Heterogeneous and Multiphase Chemistry in the Troposphere. *Science, 276*(5315), 1058-1065. doi:10.1126/science.276.5315.1058

Reiner, T., Hanke, M., & Arnold, F. (1997). Atmospheric peroxy radical measurements by ion molecule reaction-mass spectrometry: A novel analytical method using amplifying chemical conversion to sulfuric acid. *Journal of Geophysical Research: Atmospheres, 102*(D1), 1311-1326. doi:https://doi.org/10.1029/96JD02963

Remorov, R. G., Gershenzon, Y. M., Molina, L. T., & Molina, M. J. (2002). Kinetics and Mechanism of HO2 Uptake on Solid NaCl. *The Journal of Physical Chemistry A, 106*(18), 4558-4565. doi:10.1021/jp013179o

Sander, R., Baumgaertner, A., Cabrera-Perez, D., Frank, F., Gromov, S., Grooß, J. U., Harder, H., Huijnen, V., Jöckel, P., Karydis, V. A., Niemeyer, K. E., Pozzer, A.,

Riede, H., Schultz, M. G., Taraborrelli, D., & Tauer, S. (2019). The community atmospheric chemistry box model CAABA/MECCA-4.0. *Geosci. Model Dev., 12*(4), 1365-1385. doi:10.5194/gmd-12-1365-2019

Sander, R., Baumgaertner, A., Gromov, S., Harder, H., Jöckel, P., Kerkweg, A., Kubistin, D., Regelin, E., Riede, H., Sandu, A., Taraborrelli, D., Tost, H., & Xie, Z. Q. (2011). The atmospheric chemistry box model CAABA/MECCA-3.0. *Geosci. Model Dev., 4*(2), 373-380. doi:10.5194/gmd-4-373-2011

Sander, R., Kerkweg, A., Jöckel, P., & Lelieveld, J. (2005). Technical note: The new comprehensive atmospheric chemistry module MECCA. *Atmos. Chem. Phys., 5*(2), 445-450. doi:10.5194/acp-5-445-2005

Sander, S. P., J. Abbatt, J. R. Barker, J. B. Burkholder, R. R. Friedl, D. M. Golden, R. E. Huie, C. E. Kolb, M. J. Kurylo, G., K. Moortgat, and, V. L. O., & Wine, P. H. (2011). Chemical Kinetics and Photochemical Data for Use in Atmospheric Studies,

Evaluation No. 17,. *JPL Publication 10-6, Jet Propulsion Laboratory, Pasadena*.

Sandu, A., & Sander, R. (2006). Technical note: Simulating chemical systems in Fortran90 and Matlab with the Kinetic PreProcessor KPP-2.1. *Atmos. Chem. Phys., 6*(1), 187-195. doi:10.5194/acp-6-187-2006

Saunders, S. M., Jenkin, M. E., Derwent, R. G., & Pilling, M. J. (2003). Protocol for the development of the Master Chemical Mechanism, MCM v3 (Part A): tropospheric degradation of non-aromatic volatile organic compounds. *Atmos. Chem. Phys., 3*(1), 161-180. doi:10.5194/acp-3-161-2003

Schumann, U., & Huntrieser, H. (2007). The global lightning-induced nitrogen oxides source. *Atmos. Chem. Phys., 7*(14), 3823-3907. doi:10.5194/acp-7-3823-2007

Seinfeld, J. H., Pandis, S. N. (1998). Atmospheric Chemistry and Physics - From Air Pollution to Climate Change. *John Wiley & Sons*.

Shaw, S. L., Chisholm, S. W., & Prinn, R. G. (2003). Isoprene production by Prochlorococcus, a marine cyanobacterium, and other phytoplankton. *Marine Chemistry, 80*(4), 227-245. doi:https://doi.org/10.1016/S0304-4203(02)00101-9

Sherwen, T., Chance, R. J., Tinel, L., Ellis, D., Evans, M. J., & Carpenter, L. J. (2019). A machine-learning-based global sea-surface iodide distribution. *Earth Syst. Sci. Data, 11*(3), 1239-1262. doi:10.5194/essd-11-1239-2019

Simpson, W. R. (2015). Tropospheric Halogen Chemistry: Sources, Cycling, and Impacts. *Chemical Reviews, 115*(10), 4035-4062. doi:10.1021/cr5006638

Smith, G. P., & Crosley, D. R. (1990). A photochemical model of ozone interference effects in laser detection of tropospheric OH. *Journal of Geophysical Research: Atmospheres, 95*(D10), 16427-16442. doi:https://doi.org/10.1029/JD095iD10p16427

Sommariva, R., Haggerstone, A. L., Carpenter, L. J., Carslaw, N., Creasey, D. J., Heard, D. E., Lee, J. D., Lewis, A. C., Pilling, M. J., & Zádor, J. (2004). OH and HO₂ chemistry in clean marine air during SOAPEX-2. *Atmos. Chem. Phys., 4*(3), 839-856. doi:10.5194/acp-4-839-2004

Stevens, P. S., Mather, J. H., & Brune, W. H. (1994). Measurement of tropospheric OH and HO2 by laser-induced fluorescence at low pressure. *Journal of Geophysical Research: Atmospheres, 99*(D2), 3543-3557. doi:https://doi.org/10.1029/93JD03342

Tadic, I., Crowley, J. N., Dienhart, D., Eger, P., Harder, H., Hottmann, B., Martinez, M., Parchatka, U., Paris, J. D., Pozzer, A., Rohloff, R., Schuladen, J., Shenolikar, J.,

Tauer, S., Lelieveld, J., & Fischer, H. (2020). Net ozone production and its relationship to nitrogen oxides and volatile organic compounds in the marine boundary layer around the Arabian Peninsula. *Atmospheric Chemistry and Physics, 20*(11), 6769-6787. doi:10.5194/acp-20-6769-2020

Taketani, F., Kanaya, Y., & Akimoto, H. (2008). Kinetics of Heterogeneous Reactions of HO2 Radical at Ambient Concentration Levels with (NH4)2SO4 and NaCl Aerosol Particles. *The Journal of Physical Chemistry A, 112*(11), 2370-2377. doi:10.1021/jp0769936

Taraborrelli, D. (2012). Hydroxyl radical buffered by isoprene oxidation over tropical forests. *Nature Geoscience, 5*(3), 190-193. doi:10.1038/ngeo1405

Thornton, J. A., Jaeglé, L., & McNeill, V. F. (2008). Assessing known pathways for HO2 loss in aqueous atmospheric aerosols: Regional and global impacts on tropospheric oxidants. *Journal of Geophysical Research: Atmospheres, 113*(D5). doi:https://doi.org/10.1029/2007JD009236

Thornton, J. A., Wooldridge, P. J., Cohen, R. C., Martinez, M., Harder, H., Brune, W. H., Williams, E. J., Roberts, J. M., Fehsenfeld, F. C., Hall, S. R., Shetter, R. E., Wert, B. P., & Fried, A. (2002). Ozone production rates as a function of NOx abundances and HOx production rates in the Nashville urban plume. *Journal of Geophysical Research: Atmospheres, 107*(D12), ACH 7-1-ACH 7-17. doi:https://doi.org/10.1029/2001JD000932

Tolbert, M. (1988). Science1988, 240, 1018− 1021.

Umezawa, T., Matsueda, H., Sawa, Y., Niwa, Y., Machida, T., & Zhou, L. (2018). Seasonal evaluation of tropospheric CO2 over the Asia-Pacific region observed by the CONTRAIL commercial airliner measurements. *Atmos. Chem. Phys., 18*(20), 14851-14866. doi:10.5194/acp-18-14851-2018

Vereecken, L., Peeters, J., Orlando, J. J., Tyndall, G. S., & Ferronato, C. (1999). Decomposition of β-Hydroxypropoxy Radicals in the OH-Initiated Oxidation of Propene. A Theoretical and Experimental Study. *The Journal of Physical Chemistry A, 103*(24), 4693-4702. doi:10.1021/jp990046i

Wang, C. C., & Davis, L. I. (1974). Measurement of Hydroxyl Concentrations in Air Using a Tunable uv Laser Beam. *Physical Review Letters, 32*(7), 349-352. doi:10.1103/PhysRevLett.32.349

Wang, N., Edtbauer, A., Stönner, C., Pozzer, A., Bourtsoukidis, E., Ernle, L., Dienhart, D., Hottmann, B., Fischer, H., Schuladen, J., Crowley, J. N., Paris, J. D., Lelieveld, J., & Williams, J. (2020). Measurements of carbonyl compounds around the Arabian Peninsula: overview and model comparison. *Atmos. Chem. Phys., 20*(18), 10807-10829. doi:10.5194/acp-20-10807-2020

Wayne, R. P., Barnes, I., Biggs, P., Burrows, J. P., Canosa-Mas, C. E., Hjorth, J., Le Bras, G., Moortgat, G. K., Perner, D., Poulet, G., Restelli, G., & Sidebottom, H. (1991). The nitrate radical: physics, chemistry, and the atmosphere. *Atmospheric Environment, 25*(1), 1-203.

Wennberg, P. O., Bates, K. H., Crounse, J. D., Dodson, L. G., McVay, R. C., Mertens, L. A., Nguyen, T. B., Praske, E., Schwantes, R. H., Smarte, M. D., St Clair, J. M., Teng, A. P., Zhang, X., & Seinfeld, J. H. (2018). Gas-Phase Reactions of Isoprene and Its Major Oxidation Products. *Chemical Reviews, 118*(7), 3337-3390. doi:10.1021/acs.chemrev.7b00439

Wennberg, P. O., Cohen, R. C., Hazen, N. L., Lapson, L. B., Allen, N. T., Hanisco, T. F., Oliver, J. F., Lanham, N. W., Demusz, J. N., & Anderson, J. G. (1994). Aircraft-Borne, Laser-Induced Fluorescence Instrument for the in-Situ Detection of Hydroxyl and Hydroperoxyl Radicals. *Review of Scientific Instruments, 65*(6), 1858-1876. doi:Doi 10.1063/1.1144835

White, J. U. (1942). Long Optical Paths of Large Aperture. *Journal of the Optical Society of America, 32*(5), 285-288. doi:10.1364/JOSA.32.000285

Xu, L., Møller, K. H., Crounse, J. D., Kjaergaard, H. G., & Wennberg, P. O. (2020). New Insights into the Radical Chemistry and Product Distribution in the OH-Initiated Oxidation of Benzene. *Environmental Science & Technology, 54*(21), 13467-13477. doi:10.1021/acs.est.0c04780

A. Supplementary Data

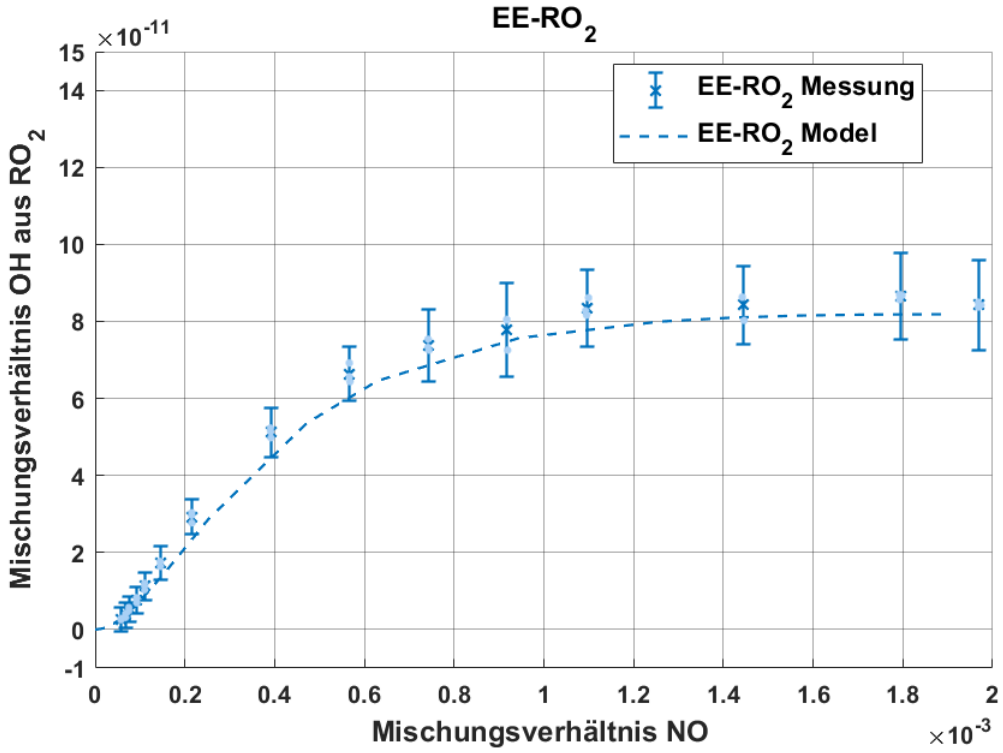

Figure A.1 Measurement of peroxy radicals from ethene under the assumption of a NO offset of $+0.04 \cdot 10^{-3}$ s^{-1}. Dots represent the measurement and the dotted line represent box model results.

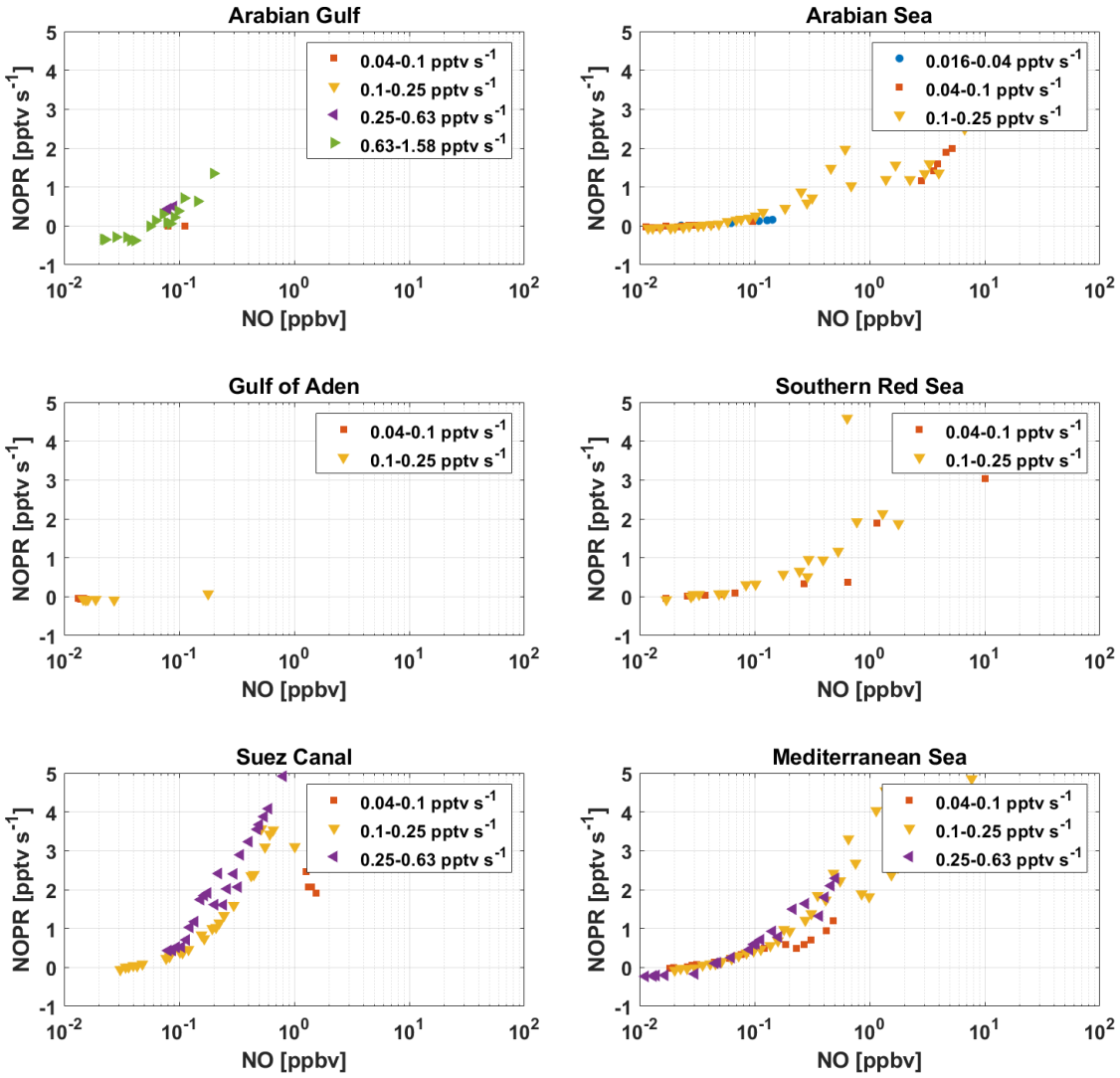

Figure A.2 $NOPR_{calc}$ over the Arabian Sea as a function of NO mixing ratio. The differently colored markers show different levels of P_{HOx} during the AQABA campaign. All regimes of P_{HOx} show similar NOPR, indicating no significant fluctuations of conditions throughout the day.

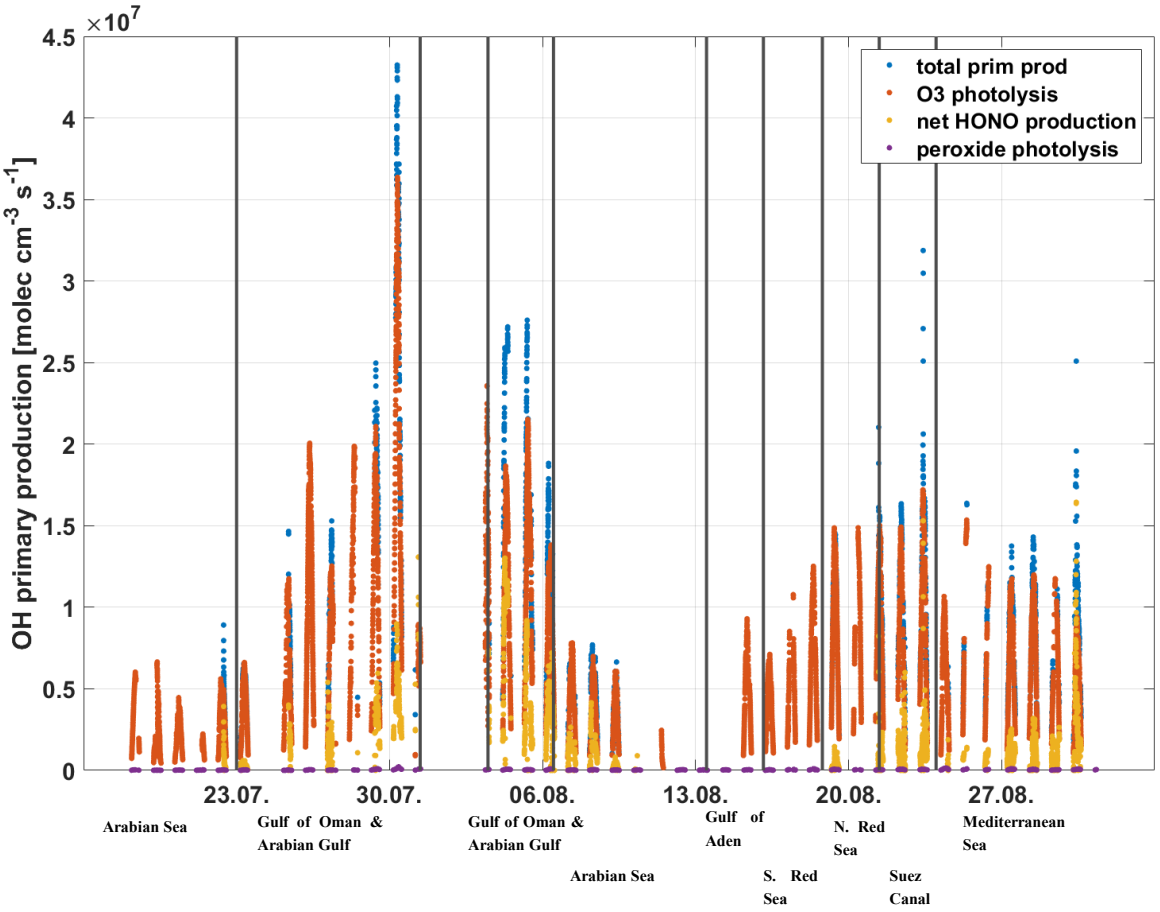

Figure A.3 Timeseries of total OH primary production and the individual contributing reactions. The blue dots show the total primary production, the red dots show the production from the photolysis of ozone, yellow dots show the net production from HONO photolysis and the purple dots show the OH production from H_2O_2 and ROOH.

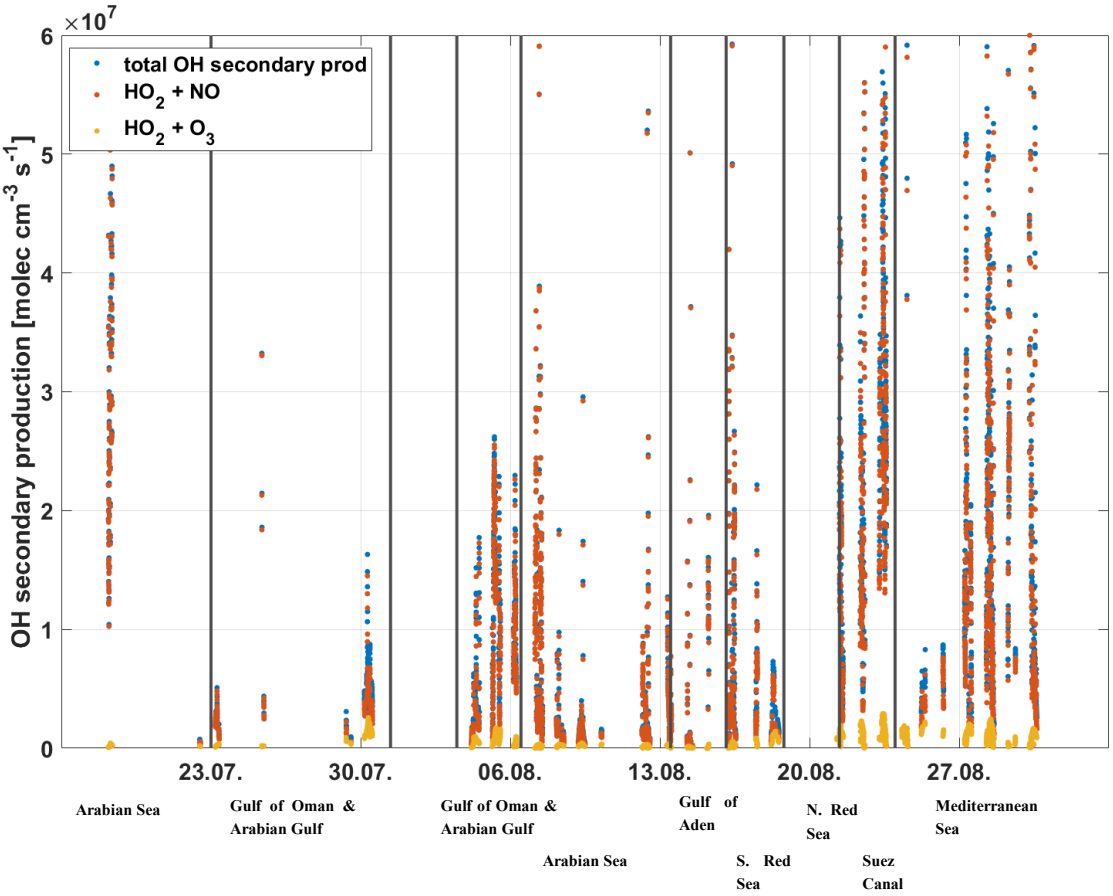

Figure A.4 Timeseries of total OH secondary production and the individual contributing reactions. The blue dots show the total secondary production, the red dots show the production from the reaction of HO_2 with NO, yellow dots show the production from the reaction of HO_2 with O_3.

B. CAABA/MECCA chemical mechanism

Table 1: Gas phase reactions

#	labels	reaction	rate coefficient	reference
G1000	UpStTrG	$O_2 + O(^1D) \rightarrow O(^3P) + O_2$	3.3E-11*EXP(55./temp)	Burkholder et al. (2015)
G1001	UpStTrG	$O_2 + O(^3P) \rightarrow O_3$	6.0E-34*((temp/300.)**(-2.4)) *cair	Burkholder et al. (2015)
G1002a	UpStG	$O_3 + O(^1D) \rightarrow 2\ O_2$	1.2E-10	Burkholder et al. (2015)*
G1002b	UpG	$O_3 + O(^1D) \rightarrow O_2 + 2\ O(^3P)$	1.2E-10	Burkholder et al. (2015)
G1003	UpStG	$O_3 + O(^3P) \rightarrow 2\ O_2$	8.0E-12*EXP(-2060./temp)	Burkholder et al. (2015)
G1004	UpG	$O_2 + O^+ \rightarrow O_2^+ + O(^3P)$	k_Op_O2(temp,temp_ion)	Fuller-Rowell (1993)
G1101	UpG	$O_2^+ + e^- \rightarrow 2\ O(^3P)$	2.7E-7*(300./temp_elec)**(.7)	Fuller-Rowell (1993)
G2100	UpStTrG	$H + O_2 \rightarrow HO_2$	k_3rd(temp,cair,4.4E-32,1.3, 7.5E-11,-0.2,0.6)	Burkholder et al. (2015)
G2101	UpStG	$H + O_3 \rightarrow OH + O_2$	1.4E-10*EXP(-470./temp)	Burkholder et al. (2015)
G2102	UpStG	$H_2 + O(^1D) \rightarrow H + OH$	1.2E-10	Burkholder et al. (2015)
G2103	UpStG	$OH + O(^3P) \rightarrow H + O_2$	1.8E-11*EXP(180./temp)	Burkholder et al. (2015)
G2104	UpStTrG	$OH + O_3 \rightarrow HO_2 + O_2$	1.7E-12*EXP(-940./temp)	Burkholder et al. (2015)
G2105	UpStTrG	$OH + H_2 \rightarrow H_2O + H$	2.8E-12*EXP(-1800./temp)	Burkholder et al. (2015)
G2106	UpStG	$HO_2 + O(^3P) \rightarrow OH + O_2$	3.E-11*EXP(200./temp)	Burkholder et al. (2015)
G2107	UpStTrG	$HO_2 + O_3 \rightarrow OH + 2\ O_2$	1.E-14*EXP(-490./temp)	Burkholder et al. (2015)
G2108a	UpStG	$HO_2 + H \rightarrow 2\ OH$	7.2E-11	Burkholder et al. (2015)
G2108b	UpStG	$HO_2 + H \rightarrow H_2 + O_2$	6.9E-12	Burkholder et al. (2015)
G2108c	UpStG	$HO_2 + H \rightarrow O(^3P) + H_2O$	1.6E-12	Burkholder et al. (2015)
G2109	UpStTrG	$HO_2 + OH \rightarrow H_2O + O_2$	4.8E-11*EXP(250./temp)	Burkholder et al. (2015)
G2110	UpStTrG	$HO_2 + HO_2 \rightarrow H_2O_2 + O_2$	k_HO2_HO2	Burkholder et al. (2015)*
G2111	UpStTrG	$H_2O + O(^1D) \rightarrow 2\ OH$	1.63E-10*EXP(60./temp)	Burkholder et al. (2015)
G2112	UpStTrG	$H_2O_2 + OH \rightarrow H_2O + HO_2$	1.8E-12	Burkholder et al. (2015)
G2113	UpG	$H_2 + O(^3P) \rightarrow H + OH$	1.60E-11*EXP(-4570./temp)	Roble (1995)
G2114a	UpG	$OH + OH \rightarrow H_2O + O(^3P)$	4.20E-12*EXP(-240./temp)	Sander et al. (2003)
G2114b	UpG	$OH + OH \rightarrow H_2O_2$	k_3rd(temp,cair,6.9E-31,1.0, 2.6E-11,0.,0.6)	Burkholder et al. (2015)
G2115	UpG	$H + H \rightarrow H_2$	5.7E-32*(300./temp)**(1.6)*cair	Roble (1995)
G2116	UpG	$H_2O_2 + O(^3P) \rightarrow OH + HO_2$	1.40E-12*EXP(-2000./temp)	Sander et al. (2003)
G2117	UpStTrG	$H_2O + H_2O \rightarrow (H_2O)_2$	6.521E-26*temp*EXP(1851.09/temp) *EXP(-5.10485E-3*temp)	Scribano et al. (2006)*
G2118	UpStTrG	$(H_2O)_2 \rightarrow H_2O + H_2O$	1.E0	see note*
G3001	UpGN	$NO^+ + e^- \rightarrow .15\ N + .85\ N(^2D) + O(^3P)$	4.2E-7*(300./temp_elec)**(0.85)	Bailey et al. (2002)

Table 1: Gas phase reactions (... continued)

#	labels	reaction	rate coefficient	reference
G3002	UpGN	$N_2^+ + e^- \rightarrow .88\ N + 1.12\ N(^2D)$	1.8E-7*(temp_elec/300.)**(-0.39)	Swaminathan et al. (1998)
G3003	UpGN	$N(^2D) + e^- \rightarrow N + e^-$	3.8E-12*(temp_elec)**(.81)	Swaminathan et al. (1998)
G3100	UpStGN	$N + O_2 \rightarrow NO + O(^3P)$	1.5E-11*EXP(-3600./temp)	Burkholder et al. (2015)
G3101	UpStTrGN	$N_2 + O(^1D) \rightarrow O(^3P) + N_2$	2.15E-11*EXP(110./temp)	Burkholder et al. (2015)
G3102a	UpStGN	$N_2O + O(^1D) \rightarrow 2\ NO$	7.259E-11*EXP(20./temp)	Burkholder et al. (2015)
G3102b	StGN	$N_2O + O(^1D) \rightarrow N_2 + O_2$	4.641E-11*EXP(20./temp)	Burkholder et al. (2015)
G3103	UpStTrGN	$NO + O_3 \rightarrow NO_2 + O_2$	3.0E-12*EXP(-1500./temp)	Burkholder et al. (2015)
G3104	UpStGN	$NO + N \rightarrow O(^3P) + N_2$	2.1E-11*EXP(100./temp)	Burkholder et al. (2015)
G3105	UpStGN	$NO_2 + O(^3P) \rightarrow NO + O_2$	5.1E-12*EXP(210./temp)	Burkholder et al. (2015)
G3106	StTrGN	$NO_2 + O_3 \rightarrow NO_3 + O_2$	1.2E-13*EXP(-2450./temp)	Burkholder et al. (2015)
G3107	UpStGN	$NO_2 + N \rightarrow N_2O + O(^3P)$	5.8E-12*EXP(220./temp)	Burkholder et al. (2015)
G3108	StTrGN	$NO_3 + NO \rightarrow 2\ NO_2$	1.5E-11*EXP(170./temp)	Burkholder et al. (2015)
G3109	UpStTrGN	$NO_3 + NO_2 \rightarrow N_2O_5$	k_NO3_NO2	Burkholder et al. (2015)*
G3110	StTrGN	$N_2O_5 \rightarrow NO_2 + NO_3$	k_NO3_NO2/(5.8E-27*EXP(10840./ temp))	Burkholder et al. (2015)*
G3111	UpGN	$N(^2D) + NO \rightarrow N_2 + O(^3P)$	6.70E-11	Fuller-Rowell (1993)
G3112	UpGN	$N(^2D) + O_2 \rightarrow NO + O(^3P)$	6.20E-12*(temp/300.)	Duff et al. (2003)
G3113	UpGN	$N(^2D) + O(^3P) \rightarrow N + O(^3P)$	6.90E-13	Fell et al. (1990)
G3114	UpGN	$N(^2D) + O_3 \rightarrow NO + O_2$	0.80E-16	Sander et al. (2003)
G3115	UpGN	$NO + O(^3P) \rightarrow NO_2$	k_3rd(temp,cair,9.0E-32,1.5, 3.0E-11,0.0,0.6)	Burkholder et al. (2015)
G3116	UpGN	$NO_2 + O(^3P) \rightarrow NO_3$	k_3rd(temp,cair,2.5E-31,1.8, 2.2E-11,0.7,0.6)	Burkholder et al. (2015)
G3117	UpGN	$N(^2D) \rightarrow N$	10.6	Fuller-Rowell (1993)
G3118	UpGN	$N^+ + O_2 \rightarrow NO + O^+$	3.66E-11	Barth (1992)
G3119	UpGN	$N_2^+ + O(^3P) \rightarrow NO^+ + N(^2D)$	k_N2_O(temp,temp_ion)	Fuller-Rowell (1993)
G3120a	UpGN	$N^+ + O_2 \rightarrow NO^+ + O(^3P)$	2.60E-10	Fuller-Rowell (1993)
G3120b	UpGN	$N^+ + O_2 \rightarrow O_2^+ + N$	3.10E-10	Swaminathan et al. (1998)
G3121	UpGN	$N^+ + O(^3P) \rightarrow O^+ + N$	1.00E-12	Fuller-Rowell (1993)
G3122	UpGN	$O_2^+ + N \rightarrow NO^+ + O(^3P)$	1.20E-10	Fuller-Rowell (1993)
G3123	UpGN	$O_2^+ + NO \rightarrow NO^+ + O_2$	4.40E-10	Fuller-Rowell (1993)
G3124	UpGN	$O^+ + N_2 \rightarrow NO^+ + N$	k_Op_N2(temp,temp_ion)	Fuller-Rowell (1993)
G3125	UpGN	$N_2^+ + O_2 \rightarrow N_2 + O_2^+$	5.10E-11*(temp/300.)**(-0.8)	Fuller-Rowell (1993)
G3200	TrGN	$NO + OH \rightarrow HONO$	k_3rd(temp,cair,7.0E-31,2.6, 3.6E-11,0.1,0.6)	Burkholder et al. (2015)

Table 1: Gas phase reactions (... continued)

#	labels	reaction	rate coefficient	reference
G3201	UpStTrGN	$NO + HO_2 \rightarrow NO_2 + OH$	3.3E-12*EXP(270./temp)	Burkholder et al. (2015)
G3202a	UpStTrGN	$NO_2 + OH \rightarrow HNO_3$	(1.-alpha_HOONO) * k_NO2_OH	Amedro et al. (2020)
G3202b	UpStTrGN	$NO_2 + OH \rightarrow HOONO$	alpha_HOONO * k_NO2_OH	Amedro et al. (2020)
G3203	StTrGN	$NO_2 + HO_2 \rightarrow HNO_4$	k_NO2_HO2	Burkholder et al. (2015)*
G3204	TrGN	$NO_3 + HO_2 \rightarrow NO_2 + OH + O_2$	3.5E-12	Burkholder et al. (2015)
G3205	TrGN	$HONO + OH \rightarrow NO_2 + H_2O$	1.8E-11*EXP(-390./temp)	Burkholder et al. (2015)
G3206	StTrGN	$HNO_3 + OH \rightarrow H_2O + NO_3$	k_HNO3_OH	Dulitz et al. (2018)*
G3207	StTrGN	$HNO_4 \rightarrow NO_2 + HO_2$	k_NO2_HO2/(2.1E-27*EXP(10900./temp))	Burkholder et al. (2015)*
G3208	StTrGN	$HNO_4 + OH \rightarrow NO_2 + H_2O$	1.3E-12*EXP(380./temp)	Burkholder et al. (2015)
G3209	TrGN	$NH_3 + OH \rightarrow NH_2 + H_2O$	1.7E-12*EXP(-710./temp)	Kohlmann and Poppe (1999)
G3210	TrGN	$NH_2 + O_3 \rightarrow NH_2O + O_2$	4.3E-12*EXP(-930./temp)	Kohlmann and Poppe (1999)
G3211	TrGN	$NH_2 + HO_2 \rightarrow NH_2O + OH$	4.8E-07*EXP(-628./temp)*(temp)**(-1.32)	Kohlmann and Poppe (1999)
G3212	TrGN	$NH_2 + HO_2 \rightarrow HNO + H_2O$	9.4E-09*EXP(-356./temp)*(temp)**(-1.12)	Kohlmann and Poppe (1999)
G3213	TrGN	$NH_2 + NO \rightarrow HO_2 + OH + N_2$	1.92E-12*((temp/298.)**(-1.5))	Kohlmann and Poppe (1999)
G3214	TrGN	$NH_2 + NO \rightarrow N_2 + H_2O$	1.41E-11*((temp/298.)**(-1.5))	Kohlmann and Poppe (1999)
G3215	TrGN	$NH_2 + NO_2 \rightarrow N_2O + H_2O$	1.2E-11*((temp/298.)**(-2.0))	Kohlmann and Poppe (1999)
G3216	TrGN	$NH_2 + NO_2 \rightarrow NH_2O + NO$	0.8E-11*((temp/298.)**(-2.0))	Kohlmann and Poppe (1999)
G3217	TrGN	$NH_2O + O_3 \rightarrow NH_2 + O_2$	1.2E-14	Kohlmann and Poppe (1999)
G3218	TrGN	$NH_2O \rightarrow NHOH$	1.3E3	Kohlmann and Poppe (1999)
G3219	TrGN	$HNO + OH \rightarrow NO + H_2O$	8.0E-11*EXP(-500./temp)	Kohlmann and Poppe (1999)
G3220	TrGN	$HNO + NHOH \rightarrow NH_2OH + NO$	1.66E-12*EXP(-1500./temp)	Kohlmann and Poppe (1999)
G3221	TrGN	$HNO + NO_2 \rightarrow HONO + NO$	1.0E-12*EXP(-1000./temp)	Kohlmann and Poppe (1999)
G3222	TrGN	$NHOH + OH \rightarrow HNO + H_2O$	1.66E-12	Kohlmann and Poppe (1999)
G3223	TrGN	$NH_2OH + OH \rightarrow NHOH + H_2O$	4.13E-11*EXP(-2138./temp)	Kohlmann and Poppe (1999)
G3224	TrGN	$HNO + O_2 \rightarrow HO_2 + NO$	3.65E-14*EXP(-4600./temp)	Kohlmann and Poppe (1999)
G3225	UpGN	$N + OH \rightarrow NO + H$	5.00E-11	Roble (1995)
G3226	UpGN	$NO_2 + H \rightarrow NO + OH$	4.00E-10*EXP(-340./temp)	Sander et al. (2003)
G3227	UpStTrGN	$HOONO \rightarrow NO_2 + OH$	(alpha_HOONO*k_NO2_OH) /(3.5E-27*EXP(10135./temp))	see note*
G3228	UpStTrGN	$HOONO + OH \rightarrow H_2O + NO_3$	1.3E-12*EXP(380./temp)	Burkholder et al. (2015)*
G4100	UpStG	$CH_4 + O(^1D) \rightarrow .75\ CH_3 + .75\ OH + .25\ HCHO + .4\ H + .05\ H_2$	1.75E-10	Burkholder et al. (2015)

Table 1: Gas phase reactions (... continued)

#	labels	reaction	rate coefficient	reference
G4101	StTrG	$CH_4 + OH \rightarrow CH_3 + H_2O$	1.85E-20*EXP(2.82*LOG(temp) -987./temp)	Atkinson (2003)
G4102	TrG	$CH_3OH + OH \rightarrow .85\ HCHO + .85\ HO_2 + .15\ CH_3O + H_2O$	6.38E-18*((temp)**2)*EXP(144./temp)	Atkinson et al. (2006)
G4103a	StTrG	$CH_3O_2 + HO_2 \rightarrow CH_3OOH + O_2$	3.8E-13*EXP(780./temp)/(1.+1./498.*EXP(1160./temp))	Atkinson et al. (2006)
G4103b	StTrG	$CH_3O_2 + HO_2 \rightarrow HCHO + H_2O + O_2$	3.8E-13*EXP(780./temp)/(1.+498.*EXP(-1160./temp))	Atkinson et al. (2006)
G4104a	StTrGN	$CH_3O_2 + NO \rightarrow CH_3O + NO_2$	2.3E-12*EXP(360./temp)*(1.-beta_CH3NO3)	Atkinson et al. (2006), Butkovskaya et al. (2012), Flocke et al. (1998)
G4104b	StTrGN	$CH_3O_2 + NO \rightarrow CH_3ONO_2$	2.3E-12*EXP(360./temp)*beta_CH3NO3	Atkinson et al. (2006), Butkovskaya et al. (2012), Flocke et al. (1998)*
G4105	TrGN	$CH_3O_2 + NO_3 \rightarrow CH_3O + NO_2 + O_2$	1.2E-12	Atkinson et al. (2006)
G4106a	StTrG	$CH_3O_2 \rightarrow CH_3O + .5\ O_2$	7.4E-13*EXP(-520./temp)*RO2*2.	Atkinson et al. (2006)
G4106b	StTrG	$CH_3O_2 \rightarrow .5\ HCHO + .5\ CH_3OH + .5\ O_2$	(k_CH3O2-7.4E-13*EXP(-520./temp)) *RO2*2.	Atkinson et al. (2006)
G4107	StTrG	$CH_3OOH + OH \rightarrow .6\ CH_3O_2 + .4\ HCHO + .4\ OH + H_2O$	k_CH3OOH_OH	Wallington et al. (2018)
G4108	StTrG	$HCHO + OH \rightarrow CO + H_2O + HO_2$	9.52E-18*EXP(2.03*LOG(temp) +636./temp)	Sivakumaran et al. (2003)
G4109	TrGN	$HCHO + NO_3 \rightarrow HNO_3 + CO + HO_2$	3.4E-13*EXP(-1900./temp)	Burkholder et al. (2015)*
G4110	UpStTrG	$CO + OH \rightarrow H + CO_2$	(1.57E-13+cair*3.54E-33)	McCabe et al. (2001)
G4111	TrG	$HCOOH + OH \rightarrow CO_2 + HO_2 + H_2O$	2.94E-14*exp(786./temp) +9.85E-13*EXP(-1036./temp)	Paulot et al. (2011)
G4112	UpStG	$CO + O(^3P) \rightarrow CO_2$	6.60E-33*EXP(-1103./temp)	Roble (1995)
G4113	UpStG	$CH_4 + O(^3P) \rightarrow .51\ CH_3 + .51\ OH + .49\ CH_3O + .49\ H$	6.03E-18*(temp)**(2.17) *EXP(-3619./temp)	Roble (1995), Garton et al. (2003), Espinosa-Garcia and Garcia-Bernáldez (2000)
G4114	StTrGN	$CH_3O_2 + NO_2 \rightarrow CH_3O_2NO_2$	k_NO2_CH3O2	Burkholder et al. (2015)
G4115	StTrGN	$CH_3O_2NO_2 \rightarrow CH_3O_2 + NO_2$	k_NO2_CH3O2/(9.5E-29*EXP(11234./temp))	Burkholder et al. (2015)*
G4116	StTrGN	$CH_3O_2NO_2 + OH \rightarrow HCHO + NO_3 + H_2O$	3.00E-14	see note*
G4117	StTrGN	$CH_3ONO_2 + OH \rightarrow H_2O + HCHO + NO_2$	4.0E-13*EXP(-845./temp)	Atkinson et al. (2006)
G4118	StTrG	$CH_3O \rightarrow HO_2 + HCHO$	1.3E-14*exp(-663./temp)*c(ind_O2)	Chai et al. (2014)

Table 1: Gas phase reactions (... continued)

#	labels	reaction	rate coefficient	reference
G4119a	StTrGN	$CH_3O + NO_2 \rightarrow CH_3ONO_2$	k_3rd_iupac(temp,cair,8.1E-29, 4.5,2.1E-11,0.,0.44)	Atkinson et al. (2006)
G4119b	StTrGN	$CH_3O + NO_2 \rightarrow HCHO + HONO$	9.6E-12*EXP(-1150./temp)	Atkinson et al. (2006)
G4120a	StTrGN	$CH_3O + NO \rightarrow CH_3ONO$	k_3rd_iupac(temp,cair,2.6E-29, 2.8,3.3E-11,0.6,REAL(EXP(-temp/ 900.),SP))	Atkinson et al. (2006)
G4120b	StTrGN	$CH_3O + NO \rightarrow HCHO + HNO$	2.3E-12*(temp/300.)**(0.7)	Atkinson et al. (2006)
G4121	StTrG	$CH_3O_2 + O_3 \rightarrow CH_3O + 2\ O_2$	2.9E-16*exp(-1000./temp)	Burkholder et al. (2015)
G4122	StTrGN	$CH_3ONO + OH \rightarrow H_2O + HCHO + NO$	1.E-10*exp(-1764./temp)	Nielsen et al. (1991)
G4123	StTrG	$HCHO + HO_2 \rightarrow HOCH_2O_2$	9.7E-15*EXP(625./temp)	Atkinson et al. (2006)
G4124	StTrG	$HOCH_2O_2 \rightarrow HCHO + HO_2$	2.4E12*EXP(-7000./temp)	Atkinson et al. (2006)
G4125	StTrG	$HOCH_2O_2 + HO_2 \rightarrow .5\ HOCH_2OOH + .5\ HCOOH + .2\ OH + .2\ HO_2 + .3\ H_2O + .8\ O_2$	5.6E-15*EXP(2300./temp)	Atkinson et al. (2006)
G4126	StTrGN	$HOCH_2O_2 + NO \rightarrow NO_2 + HO_2 + HCOOH$	0.7275*2.3E-12*EXP(360./temp)	Atkinson et al. (2006)*
G4127	StTrGN	$HOCH_2O_2 + NO_3 \rightarrow NO_2 + HO_2 + HCOOH$	1.2E-12	see note*
G4129a	StTrG	$HOCH_2O_2 \rightarrow HCOOH + HO_2$	(k_CH3O2*5.5E-12)**(0.5)*RO2*2.	Atkinson et al. (2006)
G4129b	StTrG	$HOCH_2O_2 \rightarrow .5\ HCOOH + .5\ HOCH_2OH + .5\ O_2$	(k_CH3O2*5.7E-14*EXP(750./temp)) **(0.5)*RO2*2.	Atkinson et al. (2006)
G4130a	StTrG	$HOCH_2OOH + OH \rightarrow HOCH_2O_2 + H_2O$	k_ROOHRO	Taraborrelli (2010)*
G4130b	StTrG	$HOCH_2OOH + OH \rightarrow HCOOH + H_2O + OH$	k_ROHRO + k_s*f_sOOH*f_sOH	Taraborrelli (2010)*
G4132	StTrG	$HOCH_2OH + OH \rightarrow HO_2 + HCOOH + H_2O$	2.*k_ROHRO + k_s*f_sOH*f_sOH	Taraborrelli (2010)*
G4133	StTrG	$CH_3O_2 + OH \rightarrow CH_3O + HO_2$	1.4E-10	Bossolasco et al. (2014)*
G4134	StTrG	$CH_2OO \rightarrow CO + HO_2 + OH$	1.124E+14*EXP(-10000./temp)	see note*
G4135	StTrG	$CH_2OO + H_2O \rightarrow HOCH_2OOH$	k_CH2OO_NO2*3.6E-6	Ouyang et al. (2013)*
G4136	StTrG	$CH_2OO + (H_2O)_2 \rightarrow HOCH_2OOH + H_2O$	5.2E-12	Chao et al. (2015), Lewis et al. (2015)*
G4137	StTrGN	$CH_2OO + NO \rightarrow HCHO + NO_2$	6.E-14	Welz et al. (2012)*
G4138	StTrGN	$CH_2OO + NO_2 \rightarrow HCHO + NO_3$	k_CH2OO_NO2	Welz et al. (2012), Stone et al. (2014)*
G4140	StTrG	$CH_2OO + CO \rightarrow HCHO + CO_2$	3.6E-14	Vereecken et al. (2012)
G4141	StTrG	$CH_2OO + HCOOH \rightarrow 2\ HCOOH$	1.E-10	Welz et al. (2014)*
G4142	StTrG	$CH_2OO + HCHO \rightarrow 2\ LCARBON$	1.7E-12	Stone et al. (2014)*
G4143	StTrG	$CH_2OO + CH_3OH \rightarrow 2\ LCARBON$	5.E-12	Vereecken et al. (2012)*
G4144	StTrG	$CH_2OO + CH_3O_2 \rightarrow 2\ LCARBON$	5.E-12	Vereecken et al. (2012)*
G4145	StTrG	$CH_2OO + HO_2 \rightarrow LCARBON$	5.E-12	Vereecken et al. (2012)

Table 1: Gas phase reactions (... continued)

#	labels	reaction	rate coefficient	reference
G4146	StTrG	$CH_2OO + O_3 \rightarrow HCHO + 2\ O_2$	1.E-12	Vereecken et al. (2014)
G4147	StTrG	$CH_2OO + CH_2OO \rightarrow 2\ HCHO + O_2$	6.E-11	Buras et al. (2014)
G4148	StTrGN	$HOCH_2O_2 + NO_2 \rightarrow HOCH_2O_2NO_2$	k_NO2_CH3O2	see note*
G4149	StTrGN	$HOCH_2O_2NO_2 \rightarrow HOCH_2O_2 + NO_2$	k_NO2_CH3O2/(9.5E-29*EXP(11234./ temp))	Barnes et al. (1985)*
G4150	StTrGN	$HOCH_2O_2NO_2 + OH \rightarrow HCOOH + NO_3 + H_2O$	9.50E-13*EXP(-650./temp)*f_sOH	see note*
G4151	StTrG	$CH_3 + O_2 \rightarrow CH_3O_2$	k_3rd_iupac(temp,cair,7.0E-31, 3.,1.8E-12,-1.1,0.33)	Atkinson et al. (2006)
G4152	StTrG	$CH_3 + O_3 \rightarrow .956\ HCHO + .956\ H + .044\ CH_3O + O_2$	5.1E-12*exp(-210./temp)	Albaladejo et al. (2002), Ogryzlo et al. (1981)
G4153	StTrG	$CH_3 + O(^3P) \rightarrow .83\ HCHO + .83\ H + .17\ CO + .17\ H_2 + .17\ H$	1.3E-10	Atkinson et al. (2006)
G4154	StTrG	$CH_3O + O_3 \rightarrow CH_3O_2 + O_2$	2.53E-14	Albaladejo et al. (2002)*
G4155	StTrG	$CH_3O + O(^3P) \rightarrow .75\ CH_3 + .75\ O_2 + .25\ HCHO + .25\ OH$	2.5E-11	Baulch et al. (2005)
G4156	StTrG	$CH_3O_2 + O(^3P) \rightarrow CH_3O + O_2$	4.3E-11	Zellner et al. (1988)
G4157	StTrG	$HCHO + O(^3P) \rightarrow .7\ OH + .7\ CO + .3\ H + .3\ CO_2 + HO_2$	3.4E-11*EXP(-1600./temp)	Burkholder et al. (2015)
G4158	TrG	$CH_2OO^* \rightarrow .37\ CH_2OO + .47\ CO + .47\ H_2O + .16\ HO_2 + .16\ CO + .16\ OH$	KDEC	Atkinson et al. (2006)
G4159	TrGN	$HCN + OH \rightarrow H_2O + CN$	k_3rd(temp,cair,4.28E-33,1.0, REAL(4.25E-13*EXP(-1150./temp) ,SP),1.0,0.8)	Kleinböhl et al. (2006)
G4160a	TrGN	$HCN + O(^1D) \rightarrow O(^3P) + HCN$	1.08E-10*EXP(105./temp) *0.15*EXP(200./temp)	Strekowski et al. (2010)
G4160b	TrGN	$HCN + O(^1D) \rightarrow H + NCO$	1.08E-10*EXP(105./temp)*0.68/2.	Strekowski et al. (2010)*
G4160c	TrGN	$HCN + O(^1D) \rightarrow OH + CN$	1.08E-10*EXP(105./temp)*(1.-(0.68/ 2.+0.15*EXP(200./temp)))	Strekowski et al. (2010)*
G4161	TrGN	$HCN + O(^3P) \rightarrow H + NCO$	1.0E-11*EXP(-4000./temp)	Burkholder et al. (2015)*
G4162	TrGN	$CN + O_2 \rightarrow NCO + O(^3P)$	1.2E-11*EXP(210./temp)*0.75	Baulch et al. (2005)
G4163	TrGN	$CN + O_2 \rightarrow CO + NO$	1.2E-11*EXP(210./temp)*0.25	Baulch et al. (2005)
G4164	TrGN	$NCO + O_2 \rightarrow CO_2 + NO$	7.E-15	Becker et al. (2000)*
G42000	TrGC	$C_2H_6 + OH \rightarrow C_2H_5O_2 + H_2O$	1.49E-17*temp*temp*EXP(-499./ temp)	Atkinson et al. (2006)
G42001	TrGC	$C_2H_4 + O_3 \rightarrow HCHO + CH_2OO^*$	9.1E-15*EXP(-2580./temp)	Atkinson et al. (2006)*

Table 1: Gas phase reactions (... continued)

#	labels	reaction	rate coefficient	reference
G42002	TrGC	$C_2H_4 + OH \rightarrow HOCH_2CH_2O_2$	k_3rd_iupac(temp,cair,8.6E-29, 3.1,9.E-12,0.85,0.48)	Atkinson et al. (2006), Rickard and Pascoe (2009)
G42003	TrGC	$C_2H_5O_2 + HO_2 \rightarrow C_2H_5OOH$	7.5E-13*EXP(700./temp)	Burkholder et al. (2015)
G42004a	TrGCN	$C_2H_5O_2 + NO \rightarrow CH_3CHO + HO_2 + NO_2$	2.55E-12*EXP(380./temp)*(1.-beta_C2H5NO3)	Atkinson et al. (2006), Butkovskaya et al. (2010)
G42004b	TrGCN	$C_2H_5O_2 + NO \rightarrow C_2H_5ONO_2$	2.55E-12*EXP(380./temp)*beta_C2H5NO3	Atkinson et al. (2006), Butkovskaya et al. (2010)
G42005	TrGCN	$C_2H_5O_2 + NO_3 \rightarrow CH_3CHO + HO_2 + NO_2$	2.3E-12	Wallington et al. (2018)
G42006	TrGC	$C_2H_5O_2 \rightarrow .8\ CH_3CHO + .6\ HO_2 + .2\ C_2H_5OH$	2.*(7.6E-14*k_CH3O2)**(.5)*RO2	Sander et al. (2019), Atkinson et al. (2006)
G42007a	TrGC	$C_2H_5OOH + OH \rightarrow C_2H_5O_2 + H_2O$	k_ROOHRO	Sander et al. (2019)
G42007b	TrGC	$C_2H_5OOH + OH \rightarrow CH_3CHO + OH$	k_s*f_sOOH	Sander et al. (2019)
G42008a	TrGC	$CH_3CHO + OH \rightarrow CH_3C(O) + H_2O$	4.4E-12*EXP(365./temp)*0.95	Atkinson et al. (2006)
G42008b	TrGC	$CH_3CHO + OH \rightarrow HCOCH_2O_2 + H_2O$	4.4E-12*EXP(365./temp)*0.05	Atkinson et al. (2006)
G42009	TrGCN	$CH_3CHO + NO_3 \rightarrow CH_3C(O) + HNO_3$	KNO3AL	Rickard and Pascoe (2009)
G42010	TrGC	$CH_3COOH + OH \rightarrow CH_3 + CO_2 + H_2O$	k_CH3CO2H_OH	Atkinson et al. (2006)*
G42011a	TrGC	$CH_3C(O)OO + HO_2 \rightarrow OH + CH_3 + CO_2$	5.20E-13*EXP(980./temp)*1.507*0.61	Groß et al. (2014)
G42011b	TrGC	$CH_3C(O)OO + HO_2 \rightarrow CH_3C(O)OOH$	5.20E-13*EXP(980./temp)*1.507*0.23	Groß et al. (2014)
G42011c	TrGC	$CH_3C(O)OO + HO_2 \rightarrow CH_3COOH + O_3$	5.20E-13*EXP(980./temp)*1.507*0.16	Groß et al. (2014)
G42012	TrGCN	$CH_3C(O)OO + NO \rightarrow CH_3 + CO_2 + NO_2$	8.1E-12*EXP(270./temp)	Tyndall et al. (2001a)
G42013	TrGCN	$CH_3C(O)OO + NO_2 \rightarrow PAN$	k_CH3CO3_NO2	Burkholder et al. (2015)*
G42014	TrGCN	$CH_3C(O)OO + NO_3 \rightarrow CH_3 + NO_2 + CO_2$	4.E-12	Canosa-Mas et al. (1996)
G42017a	TrGC	$CH_3C(O)OO \rightarrow CH_3 + CO_2$	k1_RO2RCO3*0.9	Sander et al. (2019)
G42017b	TrGC	$CH_3C(O)OO \rightarrow CH_3COOH$	k1_RO2RCO3*0.1	Sander et al. (2019)
G42018	TrGC	$CH_3C(O)OOH + OH \rightarrow CH_3C(O)OO + H_2O$	k_ROOHRO	Rickard and Pascoe (2009)*
G42020	TrGCN	$PAN + OH \rightarrow HCHO + CO + NO_2 + H_2O$	3.00E-14	Rickard and Pascoe (2009)
G42021	TrGCN	$PAN \rightarrow CH_3C(O)OO + NO_2$	k_PAN_M	Burkholder et al. (2015)*
G42022a	TrGC	$C_2H_2 + OH \rightarrow GLYOX + OH$	k_3rd(temp,cair,5.5e-30,0.0, 8.3e-13,-2.,0.6)*0.71	Burkholder et al. (2015)*
G42022b	TrGC	$C_2H_2 + OH \rightarrow HCOOH + CO + HO_2$	k_3rd(temp,cair,5.5e-30,0.0, 8.3e-13,-2.,0.6)*0.29	Burkholder et al. (2015)*
G42023a	TrGC	$HOCH_2CHO + OH \rightarrow HOCH2CO + H_2O$	8.00E-12*0.80	Atkinson et al. (2006)
G42023b	TrGC	$HOCH_2CHO + OH \rightarrow HOCHCHO + H_2O$	8.00E-12*0.20	Atkinson et al. (2006)
G42024a	TrGC	$HOCH2CO + O_2 \rightarrow HOCH_2CO_3$	5.1E-12*(1.-1./(1+1.85E-18*cair))	Atkinson et al. (2006), Beyersdorf et al. (2010)*

Table 1: Gas phase reactions (... continued)

#	labels	reaction	rate coefficient	reference
G42024b	TrGC	$HOCH2CO + O_2 \rightarrow OH + HCHO + CO_2$	5.1E-12*1./(1+1.85E-18*cair)	Atkinson et al. (2006), Beyersdorf et al. (2010)*
G42025	TrGC	$HOCHCHO \rightarrow GLYOX + HO_2$	KDEC	Sander et al. (2019)
G42026	TrGCN	$HOCH_2CHO + NO_3 \rightarrow HOCH2CO + HNO_3$	KNO3AL	Rickard and Pascoe (2009)
G42027a	TrGC	$HOCH_2CO_3 \rightarrow HCHO + CO_2 + HO_2$	k1_RO2RCO3*0.9	Sander et al. (2019)
G42027b	TrGC	$HOCH_2CO_3 \rightarrow HOCH_2CO_2H$	k1_RO2RCO3*0.1	Sander et al. (2019)
G42028a	TrGC	$HOCH_2CO_3 + HO_2 \rightarrow HCHO + HO_2 + OH + CO_2$	KAPHO2*r_CO3_OH	Sander et al. (2019), Groß et al. (2014)
G42028b	TrGC	$HOCH_2CO_3 + HO_2 \rightarrow HOCH_2CO_3H$	KAPHO2*r_CO3_OOH	Sander et al. (2019), Groß et al. (2014)
G42028c	TrGC	$HOCH_2CO_3 + HO_2 \rightarrow HOCH_2CO_2H + O_3$	KAPHO2*r_CO3_O3	Sander et al. (2019), Groß et al. (2014)
G42029	TrGCN	$HOCH_2CO_3 + NO \rightarrow NO_2 + HO_2 + HCHO + CO_2$	KAPNO	Rickard and Pascoe (2009)
G42030	TrGCN	$HOCH_2CO_3 + NO_2 \rightarrow PHAN$	k_CH3CO3_NO2	Rickard and Pascoe (2009)
G42031	TrGCN	$HOCH_2CO_3 + NO_3 \rightarrow NO_2 + HO_2 + HCHO + CO_2$	KRO2NO3*1.74	Rickard and Pascoe (2009)
G42032	TrGC	$HOCH_2CO_2H + OH \rightarrow .09\ HCHO + .09\ CO_2 + .91\ HCOCO_3H + HO_2 + H_2O$	k_CO2H+k_s*f_sOH*f_CO2H	Sander et al. (2019)
G42033a	TrGC	$HOCH_2CO_3H + OH \rightarrow HOCH_2CO_3 + H_2O$	k_ROOHRO	Sander et al. (2019)
G42033b	TrGC	$HOCH_2CO_3H + OH \rightarrow HCOCO_3H + HO_2$	k_s*f_sOH*f_CO2H	Sander et al. (2019)
G42034	TrGCN	$PHAN \rightarrow HOCH_2CO_3 + NO_2$	k_PAN_M	Rickard and Pascoe (2009)
G42035	TrGCN	$PHAN + OH \rightarrow HCHO + CO + NO_2 + H_2O$	k_s*f_sOH*f_cpan+k_ROHRO	Sander et al. (2019)
G42036	TrGC	$GLYOX + OH \rightarrow HCOCO + H_2O$	3.1E-12*EXP(340./temp)	Atkinson et al. (2006), Orlando and Tyndall (2001), Lockhart et al. (2013)
G42037	TrGCN	$GLYOX + NO_3 \rightarrow HCOCO + HNO_3$	KNO3AL	Rickard and Pascoe (2009)
G42038a	TrGC	$HCOCO \rightarrow CO + CO + HO_2$	7.E11*EXP(-3160./temp) +5.E-12*c(ind_O2)	Orlando and Tyndall (2001), Lockhart et al. (2013), Rickard and Pascoe (2009)
G42037b	TrGC	$HCOCO \rightarrow HCOCO_3$	5.E-12*c(ind_O2)*3.2*exp(-550./temp)	Lockhart et al. (2013), Rickard and Pascoe (2009)
G42037c	TrGC	$HCOCO \rightarrow OH + CO + CO_2$	5.E-12*c(ind_O2) *(1.-3.2*exp(-550./temp))	Lockhart et al. (2013), Rickard and Pascoe (2009)
G42039a	TrGC	$HCOCO_3 \rightarrow CO + HO_2 + CO_2$	k1_RO2RCO3*0.9	Sander et al. (2019)
G42039b	TrGC	$HCOCO_3 \rightarrow HCOCO_2H$	k1_RO2RCO3*0.1	Sander et al. (2019)

Table 1: Gas phase reactions (... continued)

#	labels	reaction	rate coefficient	reference
G42040	TrGC	$HCOCO_3 + HO_2 \rightarrow HO_2 + CO + CO_2 + OH$	KAPHO2	Feierabend et al. (2008), Sander et al. (2019)
G42041	TrGCN	$HCOCO_3 + NO \rightarrow HO_2 + CO + NO_2 + CO_2$	KAPNO	Rickard and Pascoe (2009)
G42042	TrGCN	$HCOCO_3 + NO_3 \rightarrow HO_2 + CO + NO_2 + CO_2$	KRO2NO3*1.74	Rickard and Pascoe (2009)
G42043	TrGCN	$HCOCO_3 + NO_2 \rightarrow HO_2 + CO + NO_3 + CO_2$	k_CH3CO3_NO2	Orlando and Tyndall (2001), Sander et al. (2019)
G42044	TrGC	$HCOCO_2H + OH \rightarrow CO + HO_2 + CO_2 + H_2O$	k_CO2H+k_t*f_O*f_CO2H	Sander et al. (2019)
G42045a	TrGC	$HCOCO_3H + OH \rightarrow HCOCO_3 + H_2O$	k_ROOHRO	Sander et al. (2019)
G42045b	TrGC	$HCOCO_3H + OH \rightarrow CO + CO_2 + H_2O + OH$	k_t*f_O*f_CO2H	Sander et al. (2019)
G42046	TrGC	$HOCH_2CH_2O_2 \rightarrow .6\ HOCH_2CH_2O + .2\ HOCH_2CHO + .2$ ETHGLY	2.*(7.8E-14*EXP(1000./temp) *k_CH3O2)**(.5)*RO2	Atkinson et al. (2006), Rickard and Pascoe (2009)
G42047	TrGCN	$HOCH_2CH_2O_2 + NO \rightarrow .25\ HO_2 + .5\ HCHO + .75\ HOCH_2CH_2O + NO_2$	KRO2NO*(1.-alpha_AN(3,1,0,0,0, temp,cair))	Rickard and Pascoe (2009)*
G42048	TrGCN	$HOCH_2CH_2O_2 + NO \rightarrow$ ETHOHNO3	KRO2NO*alpha_AN(3,1,0,0,0,temp, cair)	Sander et al. (2019)
G42049a	TrGC	$HOCH_2CH_2O_2 + HO_2 \rightarrow$ HYETHO2H	1.53E-13*EXP(1300./temp) *(1.-r_CHOHCH2O2_OH)	Rickard and Pascoe (2009)
G42049b	TrGC	$HOCH_2CH_2O_2 + HO_2 \rightarrow HOCH_2CH_2O + OH$	1.53E-13*EXP(1300./temp) *r_CHOHCH2O2_OH	Rickard and Pascoe (2009)
G42050	TrGCN	$ETHOHNO3 + OH \rightarrow .93\ NO_3CH2CHO + .93\ HO_2 + .07\ HOCH_2CHO + .07\ NO_2 + H_2O$	k_s*(f_sOH*f_CH2ONO2+f_ONO2*f_ pCH2OH)+k_ROHRO	Sander et al. (2019)
G42051a	TrGC	$HYETHO2H + OH \rightarrow HOCH_2CH_2O_2 + H_2O$	k_ROOHRO	Rickard and Pascoe (2009)*
G42051b	TrGC	$HYETHO2H + OH \rightarrow HOCH_2CHO + OH + H_2O$	k_s*f_sOOH*f_pCH2OH	Sander et al. (2019)
G42051c	TrGC	$HYETHO2H + OH \rightarrow HOOCH2CHO + HO_2 + H_2O$	k_s*f_sOH*f_pCH2OH+k_ROHRO	Sander et al. (2019)
G42052a	TrGC	$HOCH_2CH_2O \rightarrow HO_2 + HOCH_2CHO$	6.00E-14*EXP(-550./temp) *C(ind_O2)	Rickard and Pascoe (2009)
G42052b	TrGC	$HOCH_2CH_2O \rightarrow HO_2 + HCHO + HCHO$	9.50E13*EXP(-5988./temp)	Rickard and Pascoe (2009)
G42053	TrGC	$ETHGLY + OH \rightarrow HOCH_2CHO + HO_2 + H_2O$	2.*k_s*f_sOH*f_pCH2OH+2.*k_ROHRO	Sander et al. (2019)
G42054	TrGC	$HCOCH_2O_2 \rightarrow .6\ HCHO + .6\ CO + .6\ HO_2 + .2$ GLYOX $+ .2\ HOCH_2CHO$	k1_RO2pORO2	Sander et al. (2019)
G42055a	TrGC	$HCOCH_2O_2 + HO_2 \rightarrow$ HOOCH2CHO	k_RO2_HO2(temp,2)*r_COCH2O2_OOH	Sander et al. (2019)
G42055b	TrGC	$HCOCH_2O_2 + HO_2 \rightarrow HCHO + CO + HO_2 + OH$	k_RO2_HO2(temp,2)*r_COCH2O2_OH	Sander et al. (2019)
G42056a	TrGCN	$HCOCH_2O_2 + NO \rightarrow NO_2 + HCHO + CO + HO_2$	KRO2NO*(1.-alpha_AN(3,1,1,0,0, temp,cair))	Sander et al. (2019)

Table 1: Gas phase reactions (... continued)

#	labels	reaction	rate coefficient	reference
G42056b	TrGCN	$HCOCH_2O_2 + NO \rightarrow NO_3CH2CHO$	KRO2NO*alpha_AN(3,1,1,0,0,temp, cair)	Sander et al. (2019)
G42057	TrGCN	$HCOCH_2O_2 + NO_3 \rightarrow HCHO + CO + HO_2 + NO_2$	KRO2NO3	Sander et al. (2019)
G42058a	TrGC	$HOOCH2CHO + OH \rightarrow HCOCH_2O_2$	k_ROOHRO	Sander et al. (2019)
G42058b	TrGC	$HOOCH2CHO + OH \rightarrow HCHO + CO + OH$	0.8*8.E-12	Sander et al. (2019)*
G42058c	TrGC	$HOOCH2CHO + OH \rightarrow$ GLYOX $+ OH$	k_s*f_sOOH*f_CHO	Sander et al. (2019)
G42059	TrGCN	$HOOCH2CHO + NO_3 \rightarrow OH + HCHO + CO + HNO_3$	KNO3AL	Rickard and Pascoe (2009)
G42060	TrGCN	$HOOCH_2CO_3 + NO \rightarrow NO_2 + OH + HCHO + CO_2$	KAPNO	Sander et al. (2019)
G42061	TrGCN	$HOOCH_2CO_3 + NO_3 \rightarrow NO_2 + OH + HCHO + CO_2$	KRO2NO3*1.74	Sander et al. (2019)
G42062a	TrGC	$HOOCH_2CO_3 + HO_2 \rightarrow 2\ OH + HCHO + CO_2$	KAPHO2*r_CO3_OH	Sander et al. (2019)
G42062b	TrGC	$HOOCH_2CO_3 + HO_2 \rightarrow$ HOOCH2CO3H	KAPHO2*r_CO3_OOH	Sander et al. (2019)
G42062c	TrGC	$HOOCH_2CO_3 + HO_2 \rightarrow$ HOOCH2CO2H $+ O_3$	KAPHO2*r_CO3_O3	Sander et al. (2019)
G42063a	TrGC	$HOOCH_2CO_3 \rightarrow OH + HCHO + CO_2$	k1_RO2RCO3*0.9	Sander et al. (2019)
G42063b	TrGC	$HOOCH_2CO_3 \rightarrow$ HOOCH2CO2H	k1_RO2RCO3*0.1	Sander et al. (2019)
G42064a	TrGC	$HOOCH2CO3H + OH \rightarrow HOOCH_2CO_3 + H_2O$	2.*k_ROOHRO	Sander et al. (2019)
G42064b	TrGC	$HOOCH2CO3H + OH \rightarrow HCOCO_3H + OH + H_2O$	k_s*f_sOOH*f_CO2H	Sander et al. (2019)
G42065	TrGC	$HOOCH2CO2H + OH \rightarrow HCOCO_2H + OH + H_2O$	k_s*f_sOOH*f_CO2H+k_CO2H	Sander et al. (2019)
G42066	TrGC	$CH2CO + OH \rightarrow .6\ HCHO + .6\ HO_2 + .6\ CO + .4$ HOOCH2CO2H	2.8E-12*exp(510./temp)	Baulch et al. (2005), Sander et al. (2019)
G42067a	TrGC	$CH3CHOHOOH + OH \rightarrow CH_3COOH + OH$	(k_t*f_tOOH*f_tOH + k_ROHRO)	Sander et al. (2019)
G42067b	TrGC	$CH3CHOHOOH + OH \rightarrow$ CH3CHOHO2	k_ROOHRO	Sander et al. (2019)
G42068	TrGC	$CH3CHOHO2 \rightarrow CH_3CHO + HO_2$	3.46E12*EXP(-12500./(1.98*temp))	Hermans et al. (2005), Sander et al. (2019)
G42069	TrGC	$CH_3CHO + HO_2 \rightarrow$ CH3CHOHO2	3.46E12*EXP(-12500./(1.98*temp)) /(6.34E26*EXP(-14700./ (1.98*temp)))	Hermans et al. (2005), Sander et al. (2019)
G42070	TrGC	$CH3CHOHO2 + HO_2 \rightarrow .5$ CH3CHOHOOH $+ .3\ CH_3COOH + .2\ CH_3 + .2$ HCOOH $+ .2$ OH	5.6E-15*EXP(2300./temp)	Sander et al. (2019)
G42071	TrGC	$CH3CHOHO2 \rightarrow CH_3 + HCOOH + OH$	k1_RO2sORO2	Sander et al. (2019)
G42072	TrGCN	$CH3CHOHO2 + NO \rightarrow CH_3 + HCOOH + OH + NO_2$	KRO2NO	Sander et al. (2019)
G42073	TrGCN	$C_2H_5ONO_2 + OH \rightarrow CH_3CHO + H_2O + NO_2$	6.7E-13*EXP(-395./temp)	Atkinson et al. (2006)
G42074a	TrGCN	$NO_3CH2CHO + OH \rightarrow$ GLYOX $+ NO_2 + H_2O$	k_s*f_CH2ONO2*f_CHO	Paulot et al. (2009a), Sander et al. (2019)*
G42074b	TrGCN	$NO_3CH2CHO + OH \rightarrow NO_3CH2CO_3 + H_2O$	k_t*f_O*f_CH2ONO2*3.	Paulot et al. (2009a), Sander et al. (2019)*

Table 1: Gas phase reactions (... continued)

#	labels	reaction	rate coefficient	reference
G42075	TrGCN	$NO_3CH2CO_3 + HO_2 \rightarrow HCHO + NO_2 + CO_2 + OH$	KAPHO2	Rickard and Pascoe (2009)*
G42076	TrGCN	$NO_3CH2CO_3 + NO \rightarrow HCHO + NO_2 + CO_2 + NO_2$	KAPNO	Rickard and Pascoe (2009)
G42077	TrGCN	$NO_3CH2CO_3 + NO_2 \rightarrow NO_3CH2CHO$	k_CH3CO3_NO2	Rickard and Pascoe (2009)
G42078	TrGCN	$NO_3CH2CO_3 \rightarrow HCHO + NO_2 + CO_2$	k1_RO2RCO3	Rickard and Pascoe (2009)*
G42079	TrGCN	$NO_3CH2CHO \rightarrow NO_3CH2CO_3 + NO_2$	k_PAN_M	Rickard and Pascoe (2009)
G42080	StTrGCN	$C_2H_5O_2 + NO_2 \rightarrow C_2H_5O_2NO_2$	k_3rd_iupac(temp,cair,1.3E-29, 6.2,8.8E-12,0.0,0.31)	Atkinson et al. (2006)
G42081	StTrGCN	$C_2H_5O_2NO_2 \rightarrow C_2H_5O_2 + NO_2$	k_3rd_iupac(temp,cair, REAL(4.8E-4*EXP(-9285./temp) ,SP),0.0,REAL(8.8E15*EXP(-10440./ temp),SP),0.0,0.31)	Atkinson et al. (2006)
G42082	StTrGCN	$C_2H_5O_2NO_2 + OH \rightarrow CH_3CHO + NO_3 + H_2O$	9.50E-13*EXP(-650./temp)	Sander et al. (2019)*
G42083a	TrGC	$CH_3C(O) + O_2 \rightarrow CH_3C(O)OO$	5.1E-12*(1. - 1./(1.+ 9.4E-18*cair))	Atkinson et al. (2006), Beyersdorf et al. (2010)*
G42083b	TrGC	$CH_3C(O) + O_2 \rightarrow OH + HCHO + CO$	5.1E-12*1./(1.+9.4E-18*cair)	Atkinson et al. (2006), Beyersdorf et al. (2010)*
G42084	TrGC	$C_2H_5OH + OH \rightarrow .95\ C_2H_5O_2 + .95\ HO_2 + .05\ HOCH_2CH_2O_2 + H_2O$	3.0E-12*EXP(20./temp)	Sander et al. (2019), Atkinson et al. (2006)
G42085a	TrGCN	$CH_3CN + OH \rightarrow NCCH_2O_2 + H_2O$	8.1E-13*EXP(-1080./temp)*0.40	Atkinson et al. (2006), Tyndall et al. (2001b)*
G42085b	TrGCN	$CH_3CN + OH \rightarrow OH + CH_3C(O) + NO$	8.1E-13*EXP(-1080./temp)*(1.-0.40)	Atkinson et al. (2006), Tyndall et al. (2001b)*
G42086a	TrGCN	$CH_3CN + O(^1D) \rightarrow O(^3P) + CH_3CN$	2.54E-10*EXP(-24./temp) *0.0269*EXP(137./temp)	Strekowski et al. (2010)
G42086b	TrGCN	$CH_3CN + O(^1D) \rightarrow 2\ H + CO + HCN$	2.54E-10*EXP(-24./temp)*0.16	Strekowski et al. (2010)*
G42086c	TrGCN	$CH_3CN + O(^1D) \rightarrow .5\ CH_3 + .5\ NCO + .5\ NCCH_2O_2 + .5\ OH$	2.54E-10*EXP(-24./temp)*(1.-(0.16+ 0.0269*EXP(137./temp)))	Strekowski et al. (2010)*
G42087	TrGCN	$NCCH_2O_2 + NO \rightarrow HCN + CO_2 + HO_2 + NO_2$	KRO2NO	see note*
G42088	TrGCN	$NCCH_2O_2 + HO_2 \rightarrow HCN + CO_2 + HO_2$	k_RO2_HO2(temp,2)	see note*
G42089a	TrGC	$CH_2CHOH + OH \rightarrow HCOOH + OH + HCHO$	k_CH2CHOH_OH_HCOOH	Sander et al. (2019), So et al. (2014)*
G42089b	TrGC	$CH_2CHOH + OH \rightarrow HOCH_2CHO + HO_2$	k_CH2CHOH_OH_ALD	Sander et al. (2019), So et al. (2014)
G42090	TrGC	$CH_2CHOH + HCOOH \rightarrow CH_3CHO + HCOOH$	k_CH2CHOH_HCOOH	Sander et al. (2019), da Silva (2010)*

12

Table 1: Gas phase reactions (... continued)

#	labels	reaction	rate coefficient	reference
G42091	TrGC	$CH_3CHO + HCOOH \rightarrow CH_2CHOH + HCOOH$	k_ALD_HCOOH	Sander et al. (2019), da Silva (2010)*
G43000a	TrGC	$C_3H_8 + OH \rightarrow iC_3H_7O_2 + H_2O$	k_s	Sander et al. (2019)
G43000b	TrGC	$C_3H_8 + OH \rightarrow C_3H_7O_2 + H_2O$	2.*k_p	Sander et al. (2019)
G43001a	TrGC	$C_3H_6 + O_3 \rightarrow HCHO + .16\ CH3CHOHOOH + .50\ OH + .50\ HCOCH_2O_2 + .05\ CH2CO + .09\ CH_3OH + .09\ CO + .2\ CH_4 + .2\ CO_2$	5.5E-15*EXP(-1880./temp)*.57	Atkinson et al. (2006)*
G43001b	TrGC	$C_3H_6 + O_3 \rightarrow CH_3CHO + CH_2OO^*$	5.5E-15*EXP(-1880./temp)*.43	Atkinson et al. (2006)*
G43002	TrGC	$C_3H_6 + OH \rightarrow HYPROPO2$	k_3rd_iupac(temp,cair,8.6E-27, 3.5,3.E-11,1.,0.5)	Atkinson et al. (2006), Rickard and Pascoe (2009)
G43003	TrGCN	$C_3H_6 + NO_3 \rightarrow PRONO3BO2$	4.6E-13*EXP(-1155./temp)	Wallington et al. (2018)
G43004	TrGC	$iC_3H_7O_2 + HO_2 \rightarrow iC_3H_7OOH$	1.9E-13*EXP(1300./temp)	Atkinson (1997)*
G43005a	TrGCN	$iC_3H_7O_2 + NO \rightarrow CH_3COCH_3 + HO_2 + NO_2$	2.7E-12*EXP(360./temp)*(1.-alpha_ AN(3,2,0,0,0,temp,cair))	Wallington et al. (2018)
G43005b	TrGCN	$iC_3H_7O_2 + NO \rightarrow iC_3H_7ONO_2$	2.7E-12*EXP(360./temp)*alpha_ AN(3,2,0,0,0,temp,cair)	Wallington et al. (2018)
G43006	TrGC	$iC_3H_7O_2 \rightarrow .8\ CH_3COCH_3 + .2$ IPROPOL $+ .6\ HO_2$	2.*(1.6E-12*EXP(-2200./temp) *k_CH3O2)**(.5)*RO2	Rickard and Pascoe (2009), Atkinson et al. (2006)
G43007a	TrGC	$iC_3H_7OOH + OH \rightarrow iC_3H_7O_2 + H_2O$	k_ROOHRO	Sander et al. (2019)
G43007b	TrGC	$iC_3H_7OOH + OH \rightarrow CH_3COCH_3 + H_2O + OH$	k_t*f_tOOH	Sander et al. (2019)
G43008	TrGC	$C_3H_7O_2 + HO_2 \rightarrow C_3H_7OOH$	1.9E-13*EXP(1300./temp)	Atkinson (1997)*
G43009a	TrGCN	$C_3H_7O_2 + NO \rightarrow C_2H_5CHO + HO_2 + NO_2$	2.7E-12*EXP(360./temp)*(1.-alpha_ AN(3,1,0,0,0,temp,cair))	Wallington et al. (2018)
G43009b	TrGCN	$C_3H_7O_2 + NO \rightarrow C_3H_7ONO_2$	2.7E-12*EXP(360./temp)*alpha_ AN(3,1,0,0,0,temp,cair)	Wallington et al. (2018)
G43010	TrGC	$C_3H_7O_2 \rightarrow .8\ CH_3COCH_3 + .2$ NPROPOL $+ .6\ HO_2$	2.*(k_CH3O2*3.E-13)**(.5)*RO2	Rickard and Pascoe (2009), Atkinson et al. (2006)
G43011	TrGC	$CH_3COCH_3 + OH \rightarrow CH_3COCH_2O_2 + H_2O$	(8.8E-12*EXP(-1320./temp) +1.7E-14*EXP(423./temp))	Atkinson et al. (2006)*
G43012a	TrGC	$CH_3COCH_2O_2 + HO_2 \rightarrow CH_3COCH_2O_2H$	8.6E-13*EXP(700./temp)*r_COCH2O2_ OOH	Tyndall et al. (2001a), Sander et al. (2019)
G43012b	TrGC	$CH_3COCH_2O_2 + HO_2 \rightarrow OH + CH_3C(O) + HCHO$	8.6E-13*EXP(700./temp)*r_COCH2O2_ OH	Tyndall et al. (2001a), Sander et al. (2019)
G43013a	TrGCN	$CH_3COCH_2O_2 + NO \rightarrow CH_3C(O) + HCHO + NO_2$	2.9E-12*EXP(300./temp)*(1.-alpha_ AN(4,1,1,0,0,temp,cair))	Burkholder et al. (2015)

13

Table 1: Gas phase reactions (... continued)

#	labels	reaction	rate coefficient	reference
G43013b	TrGCN	$CH_3COCH_2O_2 + NO \rightarrow NOA$	2.9E-12*EXP(300./temp)*alpha_AN(4,1,1,0,0,temp,cair)	Burkholder et al. (2015)
G43014	TrGC	$CH_3COCH_2O_2 \rightarrow .3\ CH_3C(O) + .3\ HCHO + .5\ MGLYOX + .2\ CH_3COCH_2OH$	k1_RO2pORO2	Orlando and Tyndall (2012)
G43015a	TrGC	$CH_3COCH_2O_2H + OH \rightarrow CH_3COCH_2O_2 + H_2O$	k_ROOHRO	see note*
G43015b	TrGC	$CH_3COCH_2O_2H + OH \rightarrow MGLYOX + OH + H_2O$	k_s*f_sOOH*f_CO	Sander et al. (2019)
G43016	TrGC	$CH_3COCH_2OH + OH \rightarrow MGLYOX + HO_2 + H_2O$	1.6E-12*EXP(305./temp)	Atkinson et al. (2006)
G43017	TrGC	$MGLYOX + OH \rightarrow .4\ CH_3 + .6\ CH_3C(O) + 1.4\ CO + H_2O$	1.9E-12*EXP(575./temp)	Baeza-Romero et al. (2007), Atkinson et al. (2006)
G43020	TrGCN	$iC_3H_7ONO_2 + OH \rightarrow CH_3COCH_3 + NO_2$	6.2E-13*EXP(-230./temp)	Wallington et al. (2018)
G43021	TrGCN	$CH_3COCH_2O_2 + NO_3 \rightarrow CH_3C(O) + HCHO + NO_2$	KRO2NO3	Rickard and Pascoe (2009)
G43022	TrGC	$HYPROPO2 \rightarrow CH_3CHO + HCHO + HO_2$	k1_RO2sORO2	Rickard and Pascoe (2009)
G43023a	TrGC	$HYPROPO2 + HO_2 \rightarrow HYPROPO2H$	k_RO2_HO2(temp,3)*(1.-r_CHOHCH2O2_OH)	Rickard and Pascoe (2009)
G43023b	TrGC	$HYPROPO2 + HO_2 \rightarrow CH_3CHO + HCHO + HO_2 + OH$	k_RO2_HO2(temp,3)*r_CHOHCH2O2_OH	Rickard and Pascoe (2009)
G43024a	TrGCN	$HYPROPO2 + NO \rightarrow CH_3CHO + HCHO + HO_2 + NO_2$	KRO2NO*(1.-alpha_AN(4,1,0,0,0,temp,cair))	Rickard and Pascoe (2009)
G43024b	TrGCN	$HYPROPO2 + NO \rightarrow PROPOLNO3$	KRO2NO*alpha_AN(4,1,0,0,0,temp,cair)	Rickard and Pascoe (2009)
G43025	TrGCN	$HYPROPO2 + NO_3 \rightarrow CH_3CHO + HCHO + HO_2 + NO_2$	KRO2NO3	Rickard and Pascoe (2009)
G43026a	TrGC	$HYPROPO2H + OH \rightarrow HYPROPO2$	k_ROOHRO	Rickard and Pascoe (2009)
G43026b	TrGC	$HYPROPO2H + OH \rightarrow CH_3COCH_2OH + OH$	(k_s*f_sOH*f_pCH2OH+k_t*f_tOOH*f_pCH2OH)	Sander et al. (2019)
G43027	TrGCN	$PRONO3BO2 + HO_2 \rightarrow PR2O2HNO3$	k_RO2_HO2(temp,3)	Rickard and Pascoe (2009)
G43028	TrGCN	$PRONO3BO2 + NO \rightarrow NOA + HO_2 + NO_2$	KRO2NO	Rickard and Pascoe (2009)*
G43029	TrGCN	$PRONO3BO2 + NO_3 \rightarrow NOA + HO_2 + NO_2$	KRO2NO3	Rickard and Pascoe (2009)
G43030a	TrGCN	$PR2O2HNO3 + OH \rightarrow PRONO3BO2$	k_ROOHRO	Rickard and Pascoe (2009)
G43030b	TrGCN	$PR2O2HNO3 + OH \rightarrow NOA + OH$	k_t*f_tOOH*f_CH2ONO2	Sander et al. (2019)
G43031	TrGCN	$MGLYOX + NO_3 \rightarrow CH_3C(O) + CO + HNO_3$	KNO3AL*2.4	Rickard and Pascoe (2009)
G43032	TrGCN	$NOA + OH \rightarrow MGLYOX + NO_2$	(k_s*f_CO*f_ONO2+k_p*f_CO)	Sander et al. (2019)
G43033	TrGC	$HOCH2COCHO + OH \rightarrow .8609\ HOCH2CO + .8609\ CO + .1391\ HCOCOCHO + .1391\ HO_2$	(1.9E-12*EXP(575./temp)+k_s*f_sOH*f_CO)	Sander et al. (2019)
G43034	TrGCN	$HOCH2COCHO + NO_3 \rightarrow HOCH2CO + CO + HNO_3$	KNO3AL*2.4	Sander et al. (2019)
G43035	TrGC	$CH_3COCO_2H + OH \rightarrow CH_3C(O) + H_2O + CO_2$	4.9E-14*EXP(276./temp)	Mellouki and Mu (2003), Sander et al. (2019)

Table 1: Gas phase reactions (... continued)

#	labels	reaction	rate coefficient	reference
G43036	TrGC	$HCOCOCH_2O_2 \rightarrow .6\ HCOCO + .6\ HCHO + .2\ HCOCOCHO + .2\ HOCH2COCHO$	k1_RO2pORO2	Sander et al. (2019)
G43037	TrGCN	$HCOCOCH_2O_2 + NO \rightarrow HCOCO + HCHO + NO_2$	KRO2NO	Sander et al. (2019)*
G43038a	TrGC	$HCOCOCH_2O_2 + HO_2 \rightarrow HCOCOCH2OOH$	k_RO2_HO2(temp,3)*r_COCH2O2_OOH	Sander et al. (2019)
G43038b	TrGC	$HCOCOCH_2O_2 + HO_2 \rightarrow HCOCO + HCHO + OH$	k_RO2_HO2(temp,3)*r_COCH2O2_OH	Sander et al. (2019)
G43039	TrGCN	$HCOCOCH_2O_2 + NO_3 \rightarrow HCOCO + HCHO + NO_2$	KRO2NO3	Sander et al. (2019)
G43040a	TrGC	$HCOCOCH_2OOH + OH \rightarrow HOOCH_2CO_3 + CO + H_2O$	k_t*f_CO*f_O	Sander et al. (2019)*
G43040b	TrGC	$HCOCOCH_2OOH + OH \rightarrow HCOCOCHO + H_2O + OH$	k_s*f_sOOH*f_CO	Sander et al. (2019)*
G43040c	TrGC	$HCOCOCH_2OOH + OH \rightarrow HCOCOCH_2O_2 + H_2O$	k_ROOHRO	Sander et al. (2019)
G43041	TrGCN	$HCOCOCH_2OOH + NO_3 \rightarrow HOOCH_2CO_3 + CO + HNO_3$	KNO3AL*2.4	Sander et al. (2019)
G43042	TrGC	$HOCH2COCH2O2 \rightarrow HCHO + HOCH2CO$	k1_RO2pORO2	Sander et al. (2019)
G43043a	TrGC	$HOCH2COCH2O2 + HO_2 \rightarrow HOCH2COCH2OOH$	k_RO2_HO2(temp,3)*r_COCH2O2_OOH	Sander et al. (2019)
G43043b	TrGC	$HOCH2COCH2O2 + HO_2 \rightarrow HCHO + HOCH2CO + OH$	k_RO2_HO2(temp,3)*r_COCH2O2_OH	Sander et al. (2019)
G43044	TrGCN	$HOCH2COCH2O2 + NO \rightarrow HCHO + HOCH2CO + NO_2$	KRO2NO	Sander et al. (2019)*
G43045a	TrGC	$HOCH2COCH2OOH + OH \rightarrow HOCH2COCHO + OH$	k_s*f_sOOH*f_CO	Sander et al. (2019)
G43045b	TrGC	$HOCH2COCH2OOH + OH \rightarrow HOCH2COCH2O2$	k_ROOHRO	Sander et al. (2019)
G43045c	TrGC	$HOCH2COCH2OOH + OH \rightarrow HCOCOCH_2OOH + HO_2$	1.60E-12*EXP(305./temp)	Sander et al. (2019)*
G43046	TrGC	$CH3CHCO + OH \rightarrow .72\ CO + .72\ CH_3CHO + .72\ HO_2 + .21\ CH_3COCO_2H + .07\ CH_3CHO + .07\ HO_2 + .07\ CO_2$	7.6E-11	Hatakeyama et al. (1985), Sander et al. (2019)
G43047	TrGCN	$PROPOLNO3 + OH \rightarrow CH_3COCH_2OH + NO_2$	k_t*f_ONO2*f_pCH2OH+k_s*f_sOH*f_CH2ONO2	Sander et al. (2019)
G43048	TrGCN	$CH_3COCH_2O_2 + NO_2 \rightarrow CH_3COCH_2OONO_2$	2.3E-12*EXP(300./temp)	Tyndall et al. (2001a)*
G43049	TrGCN	$CH_3COCH_2OONO_2 \rightarrow CH_3COCH_2O_2 + NO_2$	1.9E16*EXP(-10830./temp)	Sehested et al. (1998)*
G43050	TrGCN	$CH_3COCH_2OONO_2 + OH \rightarrow MGLYOX + NO_3 + H_2O$	9.50E-13*EXP(-650./temp)*f_CO	Sander et al. (2019)*
G43051a	TrGC	$C_3H_7OOH + OH \rightarrow C_3H_7O_2 + H_2O$	k_ROOHRO	Sander et al. (2019)
G43051b	TrGC	$C_3H_7OOH + OH \rightarrow C_2H_5CHO + H_2O + OH$	k_s*f_sOOH	Sander et al. (2019)
G43051c	TrGC	$C_3H_7OOH + OH \rightarrow C_2H_5CHO + HO_2 + H_2O$	k_s*f_pCH2OH	Sander et al. (2019)*
G43052	TrGC	$C_2H_5CHO + OH \rightarrow C_2H_5CO_3 + H_2O$	4.9E-12*EXP(405./temp)	Atkinson et al. (2006)*
G43053	TrGCN	$C_2H_5CHO + NO_3 \rightarrow C_2H_5CO_3 + HNO_3$	6.3E-15	Atkinson et al. (2006)
G43054a	TrGC	$C_2H_5CO_3 \rightarrow C_2H_5O_2 + CO_2$	k1_RO2RCO3*0.9	Sander et al. (2019)
G43054b	TrGC	$C_2H_5CO_3 \rightarrow C_2H_5CO_2H$	k1_RO2RCO3*0.1	Sander et al. (2019)
G43055a	TrGC	$C_2H_5CO_3 + HO_2 \rightarrow C_2H_5O_2 + CO_2 + OH$	KAPHO2*r_CO3_OH	Sander et al. (2019), Groß et al. (2014)
G43055b	TrGC	$C_2H_5CO_3 + HO_2 \rightarrow C_2H_5CO_3H$	KAPHO2*r_CO3_OOH	Sander et al. (2019), Groß et al. (2014)

Table 1: Gas phase reactions (... continued)

#	labels	reaction	rate coefficient	reference
G43055c	TrGC	$C_2H_5CO_3 + HO_2 \rightarrow C_2H_5CO_2H + O_3$	KAPHO2*r_CO3_O3	Sander et al. (2019), Groß et al. (2014)
G43056	TrGCN	$C_2H_5CO_3 + NO \rightarrow NO_2 + C_2H_5O_2 + CO_2$	KAPNO	Rickard and Pascoe (2009)
G43057	TrGCN	$C_2H_5CO_3 + NO_2 \rightarrow PPN$	k_CH3CO3_NO2	Rickard and Pascoe (2009)
G43058	TrGCN	$PPN \rightarrow C_2H_5CO_3 + NO_2$	k_PAN_M	Rickard and Pascoe (2009)
G43059	TrGC	$C_2H_5CO_2H + OH \rightarrow CH_3CHO + CO_2 + H_2O$	k_CO2H+k_p+k_s*f_CO2H	Sander et al. (2019)*
G43060a	TrGC	$C_2H_5CO_3H + OH \rightarrow C_2H_5CO_3 + H_2O$	k_ROOHRO	Sander et al. (2019)
G43060b	TrGC	$C_2H_5CO_3H + OH \rightarrow CH_3CHO + CO_2 + H_2O$	k_s*f_CO2H+k_p	Sander et al. (2019)*
G43061	TrGCN	$PPN + OH \rightarrow CH_3CHO + CO_2 + NO_2 + H_2O$	k_s*f_cpan+k_p	Sander et al. (2019)*
G43062	TrGC	$CH_3COCO_3H + OH \rightarrow CH_3COCO_3 + H_2O$	k_ROOHRO	Sander et al. (2019)
G43063a	TrGC	$CH_3COCO_3 + HO_2 \rightarrow CH_3C(O) + CO_2 + OH$	KAPHO2*r_CO3_OH	Sander et al. (2019)
G43063b	TrGC	$CH_3COCO_3 + HO_2 \rightarrow CH_3COCO_3H$	KAPHO2*(r_CO3_OOH+r_CO3_O3)	Sander et al. (2019)
G43064	TrGCN	$CH_3COCO_3 + NO \rightarrow CH_3C(O) + CO_2 + NO_2$	KAPNO	Sander et al. (2019)
G43065	TrGCN	$CH_3COCO_3 + NO_2 \rightarrow CH_3C(O) + CO_2 + NO_3$	k_CH3CO3_NO2	Sander et al. (2019)*
G43066	TrGCN	$CH_3COCO_3 + NO_3 \rightarrow CH_3C(O)OO + CO_2 + NO_2$	KRO2NO3*1.74	Sander et al. (2019)
G43067	TrGC	$CH_3COCO_3 \rightarrow CH_3C(O)OO + CO_2$	k1_RO2RCO3	Sander et al. (2019)
G43068	TrGC	$HCOCOCHO + OH \rightarrow 3\ CO + HO_2$	2.*k_t*f_CO*f_O	Sander et al. (2019)
G43069	TrGC	$IPROPOL + OH \rightarrow CH_3COCH_3 + HO_2 + H_2O$	2.6E-12*EXP(200./temp)	Atkinson et al. (2006)
G43070a	TrGC	$NPROPOL + OH \rightarrow C_2H_5CHO + HO_2 + H_2O$	4.6E-12*EXP(70./temp)*(k_s*f_sOH/(k_p+k_s*f_pCH2OH+k_s*f_sOH))	Atkinson et al. (2006), Sander et al. (2019)*
G43070b	TrGC	$NPROPOL + OH \rightarrow HYPROPO2 + H_2O$	4.6E-12*EXP(70./temp)*((k_p+k_s*f_pCH2OH)/(k_p+k_s*f_pCH2OH+k_s*f_sOH))	Atkinson et al. (2006), Sander et al. (2019)*
G43071a	TrGC	$CH_2CHCH_2OH + OH \rightarrow HCOOH + OH + CH_3CHO$	k_CH2CHOH_OH_HCOOH	Sander et al. (2019), So et al. (2014)*
G43072	TrGC	$CH_2CHCH_2OH + HCOOH \rightarrow C_2H_5CHO + HCOOH$	k_CH2CHOH_HCOOH	Sander et al. (2019), da Silva (2010)*
G43073	TrGC	$C_2H_5CHO + HCOOH \rightarrow CH_2CHCH_2OH + HCOOH$	k_ALD_HCOOH	Sander et al. (2019), da Silva (2010)*
G43074	TrGC	$HCOCOCH_2OOH + OH \rightarrow HCOCO + CO + HO_2 + OH$	k_s*f_sOOH*f_CO+k_ROOHRO	Sander et al. (2019)*
G43202	TrGTerC	$HCOCH2CHO + OH \rightarrow HCOCH2CO3$	4.29E-11	Rickard and Pascoe (2009)
G43203	TrGTerCN	$HCOCH2CHO + NO_3 \rightarrow HCOCH2CO3 + HNO_3$	2.*KNO3AL*2.4	Rickard and Pascoe (2009)
G43204a	TrGTerC	$HCOCH2CO3 \rightarrow HCOCH_2O_2 + CO_2$	k1_RO2RCO3*0.9	Sander et al. (2019)
G43204b	TrGTerC	$HCOCH2CO3 \rightarrow HCOCH2CO2H$	k1_RO2RCO3*0.1	Sander et al. (2019)
G43205	TrGTerCN	$HCOCH2CO3 + NO \rightarrow HCOCH_2O_2 + CO_2 + NO_2$	KAPNO	Rickard and Pascoe (2009)

Table 1: Gas phase reactions (... continued)

#	labels	reaction	rate coefficient	reference
G43206	TrGTerCN	$HCOCH2CO3 + NO_2 \rightarrow C_3PAN2$	k_CH3CO3_NO2	Rickard and Pascoe (2009)
G43207a	TrGTerC	$HCOCH2CO3 + HO_2 \rightarrow HCOCH2CO3H$	KAPHO2*r_CO3_OOH	Rickard and Pascoe (2009)
G43207b	TrGTerC	$HCOCH2CO3 + HO_2 \rightarrow HCOCH2CO2H + O_3$	KAPHO2*r_CO3_O3	Rickard and Pascoe (2009)
G43207c	TrGTerC	$HCOCH2CO3 + HO_2 \rightarrow HCOCH_2O_2 + CO_2 + OH$	KAPHO2*r_CO3_OH	Rickard and Pascoe (2009)
G43210	TrGTerCN	$C_3PAN2 \rightarrow HCOCH2CO3 + NO_2$	k_PAN_M	Rickard and Pascoe (2009)
G43211	TrGTerCN	$C_3PAN2 + OH \rightarrow GLYOX + CO + NO_2$	2.10E-11	Rickard and Pascoe (2009)
G43212	TrGTerC	$HCOCH2CO2H + OH \rightarrow HCOCH_2O_2 + CO_2$	2.14E-11	Rickard and Pascoe (2009)
G43213a	TrGTerC	$HOC_2H_4CO_3 \rightarrow HOCH_2CH_2O_2 + CO_2$	k1_RO2RCO3*0.9	Sander et al. (2019)
G43213b	TrGTerC	$HOC_2H_4CO_3 \rightarrow HOC2H4CO2H$	k1_RO2RCO3*0.1	Sander et al. (2019)
G43214	TrGTerCN	$HOC_2H_4CO_3 + NO \rightarrow HOCH_2CH_2O_2 + CO_2 + NO_2$	KAPNO	Rickard and Pascoe (2009)
G43215a	TrGTerC	$HOC_2H_4CO_3 + HO_2 \rightarrow HOC2H4CO3H$	KAPHO2*r_CO3_OOH	Rickard and Pascoe (2009)
G43215b	TrGTerC	$HOC_2H_4CO_3 + HO_2 \rightarrow HOCH_2CH_2O_2 + CO_2 + OH$	KAPHO2*r_CO3_OH	Rickard and Pascoe (2009)
G43215c	TrGTerC	$HOC_2H_4CO_3 + HO_2 \rightarrow HOC2H4CO2H + O_3$	KAPHO2*r_CO3_O3	Rickard and Pascoe (2009)
G43218	TrGTerCN	$HOC_2H_4CO_3 + NO_2 \rightarrow C_3PAN1$	k_CH3CO3_NO2	Rickard and Pascoe (2009)
G43219	TrGTerC	$HOC2H4CO2H + OH \rightarrow HOCH_2CH_2O_2 + CO_2$	1.39E-11	Rickard and Pascoe (2009)
G43220	TrGTerC	$HOC2H4CO3H + OH \rightarrow HOC_2H_4CO_3$	1.73E-11	Rickard and Pascoe (2009)
G43221	TrGTerCN	$C_3PAN1 \rightarrow HOC_2H_4CO_3 + NO_2$	k_PAN_M	Rickard and Pascoe (2009)
G43222	TrGTerCN	$C_3PAN1 + OH \rightarrow HOCH_2CHO + CO + NO_2$	4.51E-12	Rickard and Pascoe (2009)
G43223	TrGTerC	$HCOCH2CO3H + OH \rightarrow HCOCH_2O_2 + CO_2 + H_2O$	2.49E-11	Rickard and Pascoe (2009)*
G43415	TrGAroC	$C3DIALOOH + OH \rightarrow HCOCOCHO + OH$	1.44E-10	Rickard and Pascoe (2009)
G43418a	TrGAroC	$C3DIALO2 + HO_2 \rightarrow C3DIALOOH$	k_RO2_HO2(temp,3)*(r_CO3_OOH+r_CO3_O3)	Rickard and Pascoe (2009)
G43418b	TrGAroC	$C3DIALO2 + HO_2 \rightarrow GLYOX + CO + HO_2 + OH$	k_RO2_HO2(temp,3)*r_CO3_OH	Rickard and Pascoe (2009)
G43419	TrGAroCN	$C3DIALO2 + NO \rightarrow GLYOX + CO + HO_2 + NO_2$	KRO2NO	Rickard and Pascoe (2009)*
G43420	TrGAroCN	$C3DIALO2 + NO_3 \rightarrow GLYOX + CO + HO_2 + NO_2$	KRO2NO3	Rickard and Pascoe (2009)*
G43421	TrGAroC	$C3DIALO2 \rightarrow GLYOX + CO + HO_2$	k1_RO2sOR02	Rickard and Pascoe (2009)*
G43422a	TrGAroC	$HCOCOHCO3 + HO_2 \rightarrow GLYOX + CO_2 + HO_2 + OH$	KAPHO2*r_CO3_OH	Rickard and Pascoe (2009)
G43422b	TrGAroC	$HCOCOHCO3 + HO_2 \rightarrow HCOCOHCO3H$	KAPHO2*(r_CO3_OOH+r_CO3_O3)	Rickard and Pascoe (2009)
G43424	TrGAroCN	$HCOCOHCO3 + NO \rightarrow GLYOX + CO_2 + HO_2 + NO_2$	KAPNO	Rickard and Pascoe (2009)
G43425	TrGAroCN	$HCOCOHCO3 + NO_2 \rightarrow HCOCOHPAN$	k_CH3CO3_NO2	Rickard and Pascoe (2009)
G43426	TrGAroCN	$HCOCOHCO3 + NO_3 \rightarrow GLYOX + CO_2 + HO_2 + NO_2$	KRO2NO3*1.74	Rickard and Pascoe (2009)
G43427	TrGAroC	$HCOCOHCO3 \rightarrow GLYOX + CO_2 + HO_2$	k1_RO2RCO3	Rickard and Pascoe (2009)
G43428	TrGAroC	$METACETHO + OH \rightarrow CH_3C(O) + CO_2$	9.82E-11	Rickard and Pascoe (2009)
G43442	TrGAroCN	$HCOCOHPAN + OH \rightarrow GLYOX + CO + NO_2$	6.97E-11	Rickard and Pascoe (2009)
G43443	TrGAroCN	$HCOCOHPAN \rightarrow HCOCOHCO3 + NO_2$	k_PAN_M	Rickard and Pascoe (2009)

Table 1: Gas phase reactions (... continued)

#	labels	reaction	rate coefficient	reference
G43444	TrGAroC	C32OH13CO + OH → HCOCOHCO3	1.36E-10	Rickard and Pascoe (2009)
G43446	TrGAroC	HCOCOHCO3H + OH → HCOCOHCO3	7.33E-11	Rickard and Pascoe (2009)
G44000	TrGC	C_4H_{10} + OH → $LC_4H_9O_2$ + H_2O	2.03E-17*temp*temp*EXP(78./temp)	Atkinson et al. (2006)*
G44001a	TrGC	$LC_4H_9O_2$ → C_3H_7CHO + HO_2	(k1_RO2pRO2*0.1273+k1_RO2sRO2*0.8727)*0.1273	Rickard and Pascoe (2009), Sander et al. (2019)
G44001b	TrGC	$LC_4H_9O_2$ → .636 MEK + .636 HO_2 + .364 CH_3CHO + .364 $C_2H_5O_2$	(k1_RO2pRO2*0.1273+k1_RO2sRO2*0.8727)*0.8727	Rickard and Pascoe (2009), Sander et al. (2019)*
G44002	TrGC	$LC_4H_9O_2$ + HO_2 → LC_4H_9OOH	k_RO2_HO2(temp,4)	Rickard and Pascoe (2009)
G44003a	TrGCN	$LC_4H_9O_2$ + NO → NO_2 + C_3H_7CHO + HO_2	KRO2NO*(1.-(0.1273*alpha_AN(4,1,0,0,0,temp,cair)+0.8727*alpha_AN(4,2,0,0,0,temp,cair)))*0.1273	Rickard and Pascoe (2009), Sander et al. (2019)
G44003b	TrGCN	$LC_4H_9O_2$ + NO → NO_2 + .636 MEK + .636 HO_2 + .364 CH_3CHO + .364 $C_2H_5O_2$	KRO2NO*(1.-(0.1273*alpha_AN(4,1,0,0,0,temp,cair)+0.8727*alpha_AN(4,2,0,0,0,temp,cair)))*0.8727	Rickard and Pascoe (2009), Sander et al. (2019)
G44003c	TrGCN	$LC_4H_9O_2$ + NO → LC4H9NO3	KRO2NO*(0.1273*alpha_AN(4,1,0,0,0,temp,cair)+0.8727*alpha_AN(4,2,0,0,0,temp,cair))	Rickard and Pascoe (2009)*
G44004a	TrGCN	$LC_4H_9O_2$ + NO_3 → NO_2 + C_3H_7CHO + HO_2	KRO2NO3*0.1273	Rickard and Pascoe (2009), Sander et al. (2019)
G44004b	TrGCN	$LC_4H_9O_2$ + NO_3 → NO_2 + .636 MEK + .636 HO_2 + .364 CH_3CHO + .364 $C_2H_5O_2$	KRO2NO3*0.8727	Rickard and Pascoe (2009), Sander et al. (2019)
G44005a	TrGC	LC_4H_9OOH + OH → $LC_4H_9O_2$ + H_2O	k_ROOHRO	Sander et al. (2019)
G44005b	TrGC	LC_4H_9OOH + OH → C_3H_7CHO + H_2O + OH	k_s*f_tOOH*f_alk*(k_p/(k_p+k_s))	Sander et al. (2019)
G44005c	TrGC	LC_4H_9OOH + OH → MEK + H_2O + OH	k_t*f_tOOH*f_alk*(k_s/(k_p+k_s))	Sander et al. (2019)
G44006a	TrGC	iC_4H_{10} + OH → $TC_4H_9O_2$ + H_2O	1.17E-17*temp*temp*EXP(213./temp)*k_t/(3.*k_p+k_t)	Atkinson (2003)
G44006b	TrGC	iC_4H_{10} + OH → $IC_4H_9O_2$ + H_2O	1.17E-17*temp*temp*EXP(213./temp)*3.*k_p/(3.*k_p+k_t)	Atkinson (2003)
G44007	TrGC	$TC_4H_9O_2$ → CH_3COCH_3 + CH_3	k1_RO2tRO2	Rickard and Pascoe (2009), Sander et al. (2019)
G44008	TrGC	$TC_4H_9O_2$ + HO_2 → TC_4H_9OOH	k_RO2_HO2(temp,4)	Rickard and Pascoe (2009)
G44009a	TrGCN	$TC_4H_9O_2$ + NO → NO_2 + CH_3COCH_3 + CH_3	KRO2NO*(1.-alpha_AN(4,3,0,0,0,temp,cair))	Rickard and Pascoe (2009), Sander et al. (2019)
G44009b	TrGCN	$TC_4H_9O_2$ + NO → TC4H9NO3	KRO2NO*alpha_AN(4,3,0,0,0,temp,cair)	Rickard and Pascoe (2009)

18

Table 1: Gas phase reactions (... continued)

#	labels	reaction	rate coefficient	reference
G44010a	TrGC	TC_4H_9OOH + OH → $TC_4H_9O_2$ + H_2O	k_ROOHRO	Sander et al. (2019)
G44010b	TrGC	TC_4H_9OOH + OH → CH_3COCH_3 + HCHO + OH + H_2O	3.*k_p*f_tCH2OH	Sander et al. (2019)*
G44011	TrGCN	TC4H9NO3 + OH → CH_3COCH_3 + HCHO + NO_2 + H_2O	3.*k_p*f_CH2ONO2	Sander et al. (2019)*
G44012	TrGC	$IC_4H_9O_2$ → IPRCHO	k1_RO2sRO2	Rickard and Pascoe (2009), Sander et al. (2019)
G44013	TrGC	$IC_4H_9O_2$ + HO_2 → IC_4H_9OOH	k_RO2_HO2(temp,4)	Rickard and Pascoe (2009)
G44014a	TrGCN	$IC_4H_9O_2$ + NO → NO_2 + IPRCHO	KRO2NO*(1.-alpha_AN(4,2,0,0,0,temp,cair))	Rickard and Pascoe (2009), Sander et al. (2019)
G44014b	TrGCN	$IC_4H_9O_2$ + NO → IC4H9NO3	KRO2NO*alpha_AN(4,2,0,0,0,temp,cair)	Rickard and Pascoe (2009)
G44015a	TrGC	IC_4H_9OOH + OH → $IC_4H_9O_2$ + H_2O	k_ROOHRO	Sander et al. (2019)
G44015b	TrGC	IC_4H_9OOH + OH → IPRCHO + OH + H_2O	k_s*f_sOOH+2.*k_s+k_t*f_pCH2OH	Sander et al. (2019)*
G44016	TrGCN	IC4H9NO3 + OH → IPRCHO + NO_2 + H_2O	k_s*f_ONO2+2.*k_p+k_t*f_CH2ONO2	Sander et al. (2019)*
G44017	TrGC	MVK + O_3 → .87 MGLYOX + .5481 CO + .1392 HO_2 + .1392 OH + .3219 CH_2OO + .13 HCHO + .04680 OH + .04680 CO + .07280 $CH_3C(O)$ + .026 CH_3CHO + .026 CO_2 + .026 HCHO + .026 HO_2 + .02402 MGLYOX + .02402 H_2O_2 + .00718 CH_3COCO_2H	8.5E-16*EXP(-1520./temp)	Sander et al. (2019)
G44018	TrGC	MVK + OH → LHMVKABO2	2.6E-12*EXP(610./temp)	Sander et al. (2019), Atkinson et al. (2006)*
G44019	TrGC	MEK + OH → LMEKO2 + H_2O	1.5E-12*EXP(-90./temp)	Atkinson et al. (2006), Sander et al. (2019)*
G44020	TrGC	LMEKO2 + HO_2 → LMEKOOH	k_RO2_HO2(temp,4)	Sander et al. (2019)
G44021a	TrGCN	LMEKO2 + NO → .62 CH_3CHO + .62 $CH_3C(O)$ + .38 HCHO + .38 CO_2 + .38 $HOCH_2CH_2O_2$ + NO_2	KRO2NO*(1.-(.62*alpha_AN(4,2,1,0,0,temp,cair)+.38*alpha_AN(4,1,0,1,0,temp,cair)))	Sander et al. (2019)*
G44021b	TrGCN	LMEKO2 + NO → LMEKNO3	KRO2NO*(.62*alpha_AN(4,2,1,0,0,temp,cair)+.38*alpha_AN(4,1,0,1,0,temp,cair))	Sander et al. (2019)
G44022a	TrGC	LMEKOOH + OH → LMEKO2 + H_2O	k_ROOHRO	Sander et al. (2019)
G44022b	TrGC	LMEKOOH + OH → .62 BIACET + .38 HCHO + .38 CO_2 + .38 $HOCH_2CH_2O_2$ + H_2O + OH	(.62*k_t*f_tOOH*f_CO+.38*k_s*f_sOOH)	Sander et al. (2019)
G44023a	TrGCN	LC4H9NO3 + OH → MEK + NO_2 + H_2O	(k_t*f_ONO2*f_alk+k_p*f_alk+k_s*f_CH2ONO2+k_p)*(k_s/(k_p+k_s))	Sander et al. (2019)*

19

Table 1: Gas phase reactions (... continued)

#	labels	reaction	rate coefficient	reference
G44023b	TrGCN	LC4H9NO3 + OH → C_3H_7CHO + NO_2 + H_2O	(k_p+k_s*(1.+f_CH2ONO2+f_ONO2) *f_alk)*(k_p/(k_p+k_s))	Sander et al. (2019)*
G44024	TrGCN	MPAN + OH → CH_3COCH_2OH + CO + NO_2	3.2E-11	Orlando et al. (2002)
G44025	TrGCN	MPAN → MACO3 + NO_2	k_PAN_M	see note*
G44026	TrGC	LMEKO2 → .538 HCHO + .538 CO_2 + .459 $HOCH_2CH_2O_2$ + .079 $C_2H_5O_2$ + .462 $CH_3C(O)$ + .462 CH_3CHO	(.62*k1_RO2sORO2+.38*k1_RO2pORO2)	Rickard and Pascoe (2009)*
G44027	TrGC	MACR + OH → .45 MACO3 + .55 MACRO2	8.E-12*EXP(380./temp)	Orlando et al. (1999b), Sander et al. (2019)
G44028	TrGC	MACR + O_3 → .5481 CO + .1392 HO_2 + .1392 OH + .3219 CH_2OO + .87 MGLYOX + .13 HCHO + .13 OH + .065 $HCOCOCH_2O_2$ + .065 CO + .065 $CH_3C(O)$	1.36E-15*EXP(-2112./temp)	Sander et al. (2019)
G44029	TrGCN	MACR + NO_3 → MACO3 + HNO_3	KNO3AL*2.0	Rickard and Pascoe (2009)
G44030a	TrGC	MACO3 → $CH_3C(O)$ + HCHO + CO_2	k1_RO2RCO3*0.9	Sander et al. (2019)
G44030b	TrGC	MACO3 → MACO2H	k1_RO2RCO3*0.1	Sander et al. (2019)
G44031a	TrGC	MACO3 + HO_2 → MACO2 + OH	KAPHO2*r_CO3_OH	Sander et al. (2019)
G44031b	TrGC	MACO3 + HO_2 → MACO3H	KAPHO2*r_CO3_OOH	Sander et al. (2019)
G44031c	TrGC	MACO3 + HO_2 → MACO2H + O_3	KAPHO2*r_CO3_O3	Sander et al. (2019)
G44032	TrGCN	MACO3 + NO → MACO2 + NO_2	8.70E-12*EXP(290./temp)	Sander et al. (2019)
G44033	TrGCN	MACO3 + NO_2 → MPAN	k_CH3CO3_NO2	Rickard and Pascoe (2009)
G44034	TrGCN	MACO3 + NO_3 → MACO2 + NO_2	KRO2NO3*1.74	Sander et al. (2019)
G44035	TrGC	MACRO2 → .7 CH_3COCH_2OH + .7 HCHO + .7 HO_2 + .3 MACROH	k1_RO2tORO2	Rickard and Pascoe (2009)*
G44036a	TrGC	MACRO2 + HO_2 → MACRO + OH	k_RO2_HO2(temp,4)*r_COCH2O2_OH	Sander et al. (2019)
G44036b	TrGC	MACRO2 + HO_2 → MACROOH	k_RO2_HO2(temp,4)*r_COCH2O2_OOH	Sander et al. (2019)
G44037a	TrGCN	MACRO2 + NO → MACRO + NO_2	KRO2NO*(1.-alpha_AN(6,3,1,0,0, temp,cair))	Sander et al. (2019)
G44037b	TrGCN	MACRO2 + NO → MACRNO3	KRO2NO*alpha_AN(6,3,1,0,0,temp, cair)	Sander et al. (2019)
G44038	TrGCN	MACRO2 + NO_3 → MACRO + NO_2	KRO2NO3	Sander et al. (2019)
G44039a	TrGC	MACROOH + OH → MACRO2	k_ROOHRO	Sander et al. (2019)
G44039b	TrGC	MACROOH + OH → CO + CH_3COCH_2OH + OH	k_t*f_O*f_tCH2OH*f_alk	Sander et al. (2019)
G44039c	TrGC	MACROOH + OH → CO + MGLYOX + HO_2	(k_s*f_sOH*f_pCH2OH + k_ROHRO)	Sander et al. (2019)
G44040	TrGC	MACROH + OH → CH_3COCH_2OH + CO + HO_2	k_t*f_O*f_tCH2OH*f_alk	Sander et al. (2019)

Table 1: Gas phase reactions (... continued)

#	labels	reaction	rate coefficient	reference
G44041	TrGC	MACRO → .885 CH_3COCH_2OH + .885 CO + .115 MGLYOX + .115 HCHO + HO_2	KDEC	Sander et al. (2019)
G44042	TrGC	MACO2H + OH → CH_3COCH_2OH + HO_2 + CO_2	((k_adt+k_adp)*a_CO2H+k_CO2H)	Sander et al. (2019)
G44043a	TrGC	MACO3H + OH → CH_3COCH_2OH + CO_2 + OH	(k_adt+k_adp)*a_CO2H	Sander et al. (2019)
G44043b	TrGC	MACO3H + OH → MACO3	k_ROOHRO	Sander et al. (2019)
G44044	TrGC	LHMVKABO2 → .024 CO2H3CHO + .072 MGLYOX + .072 HO_2 + .072 HCHO + .5280 $CH_3C(O)$ + .5280 $HOCH_2CHO$ + .176 BIACETOH + .2 HO12CO3C4	(.12*k1_RO2pORO2+.88*k1_RO2sORO2)	Sander et al. (2019)
G44045a	TrGC	LHMVKABO2 + HO_2 → OH + $HOCH_2CHO$ + $CH_3C(O)$	k_RO2_HO2(temp,4)*.88*r_COCH2O2_ OH	Sander et al. (2019)
G44045b	TrGC	LHMVKABO2 + HO_2 → LHMVKABOOH	k_RO2_HO2(temp,4)*(.12+.88*r_ COCH2O2_OOH)	Sander et al. (2019)
G44046a	TrGCN	LHMVKABO2 + NO → .12 MGLYOX + .12 HO_2 + .88 $HOCH_2CHO$ + .88 $CH_3C(O)$ + .12 HCHO + NO_2	KRO2NO*(1.-(.12*alpha_AN(6,1,0, 1,0,temp,cair)+.88*alpha_AN(6,2, 1,0,0,temp,cair)))	Sander et al. (2019)
G44046b	TrGCN	LHMVKABO2 + NO → MVKNO3	KRO2NO*(.12*alpha_AN(6,1,0,1,0, temp,cair)+.88*alpha_AN(6,2,1,0, 0,temp,cair))	Sander et al. (2019)*
G44047	TrGCN	LHMVKABO2 + NO_3 → .12 MGLYOX + .12 HO_2 + .88 $HOCH_2CHO$ + .88 $CH_3C(O)$ + .12 HCHO + .12 HO_2 + NO_2	KRO2NO3	Sander et al. (2019)
G44048a	TrGC	LHMVKABOOH + OH → LHMVKABO2	k_ROOHRO	Sander et al. (2019)
G44048b	TrGC	LHMVKABOOH + OH → .12 CO2H3CHO + .88 BIACETOH + OH	(.12*k_s*f_sOOH*f_pCH2OH+.88*k_ t*f_tOOH*f_pCH2OH*f_CO)	Sander et al. (2019)
G44049a	TrGC	CO2H3CHO + OH → CO2H3CO3	k_t*f_O*f_alk	Sander et al. (2019)
G44049b	TrGC	CO2H3CHO + OH → $CH_3COCOCHO$ + HO_2 + H_2O	k_t*f_CO*f_tOH*f_CHO	Sander et al. (2019)
G44050	TrGCN	CO2H3CHO + NO_3 → CO2H3CO3 + HNO_3	KNO3AL*4.0	Rickard and Pascoe (2009)
G44051	TrGC	CO2H3CO3 → MGLYOX + HO_2 + CO_2	k1_RO2RCO3	Sander et al. (2019)
G44052a	TrGC	CO2H3CO3 + HO_2 → OH + MGLYOX + HO_2 + CO_2	KAPHO2*r_CO3_OH	Sander et al. (2019)
G44052b	TrGC	CO2H3CO3 + HO_2 → CO2H3CO2H + O_3	KAPHO2*r_CO3_O3	Sander et al. (2019)
G44052c	TrGC	CO2H3CO3 + HO_2 → CO2H3CO3H	KAPHO2*r_CO3_OOH	Sander et al. (2019)
G44053	TrGCN	CO2H3CO3 + NO → MGLYOX + HO_2 + NO_2 + CO_2	KAPNO	Sander et al. (2019)
G44054	TrGCN	CO2H3CO3 + NO_3 → MGLYOX + HO_2 + NO_2 + CO_2	KRO2NO3*1.74	Sander et al. (2019)
G44055a	TrGC	CO2H3CO3H + OH → CO2H3CO3	k_ROOHRO	Sander et al. (2019)
G44055b	TrGC	CO2H3CO3H + OH → $CH_3C(O)$ + CO + CO_2 + OH	(k_t*f_CO2H*f_CO*f_tOH)	Sander et al. (2019)

Table 1: Gas phase reactions (... continued)

#	labels	reaction	rate coefficient	reference
G44056	TrGC	CO2H3CO2H + OH → CH3COCOCO2H + HO_2	k_t*f_CO2H*f_CO*f_tOH+k_CO2H	Sander et al. (2019)
G44057a	TrGC	HO12CO3C4 + OH → BIACETOH + HO_2	k_t*f_tOH*f_alk*f_CO	Sander et al. (2019)
G44057b	TrGC	HO12CO3C4 + OH → CO2H3CHO + HO_2	k_s*f_sOH*f_alk	Sander et al. (2019)
G44058	TrGC	MACO2 → .65 CH_3 + .65 CO + .65 HCHO + .35 OH + .35 $CH_3COCH_2O_2$ + CO_2	KDEC	Sander et al. (2019)
G44059	TrGC	LHMVKABO2 → .88 MGLYOX + .88 HCHO + .12 HOOCH2CHO + .12 $CH_3C(O)$ + OH	k_hsd	Sander et al. (2019)
G44060	TrGC	MACRO2 → MGLYOX + HCHO + OH	k_hsb	Sander et al. (2019)
G44061a	TrGCN	MVKNO3 + OH → MGLYOX + CO_2 + HO_2 + NO_2 + H_2O	k_s*f_sOOH*f_CH2ONO2+k_ROHRO	Sander et al. (2019)*
G44061b	TrGCN	MVKNO3 + OH → BIACETOH + NO_2 + H_2O	k_t*f_ONO2*f_CO*f_pCH2OH	Sander et al. (2019)*
G44062a	TrGCN	MACRNO3 + OH → CH_3COCH_2OH + CO_2 + NO_2 + H_2O	k_t*f_O*f_CH2ONO2	Sander et al. (2019)*
G44062b	TrGCN	MACRNO3 + OH → MGLYOX + CO + NO_2 + H_2O	k_ROHRO+k_s*f_sOOH*f_CH2ONO2	Sander et al. (2019)*
G44063	TrGC	MACRO2 → CH_3COCH_2OH + OH + CO	k_14hsal	Sander et al. (2019)
G44064	TrGC	EZCH3CO2CHCHO → .9 $CH_3COCHCO$ + .1 $CH_3C(O)$ + .01 GLYOX + .18 CO + .09 HO_2 + OH	k_15hs24vynal	Sander et al. (2019)
G44065	TrGC	EZCH3CO2CHCHO + HO_2→ $CH_3COOHCHCHO$	k_RO2_HO2(temp,4)	Sander et al. (2019)
G44066	TrGCN	EZCH3CO2CHCHO + NO → CH_3COCHO_2CHO + NO_2	KRO2NO	Sander et al. (2019)*
G44067	TrGCN	EZCH3CO2CHCHO + NO_3→ CH_3COCHO_2CHO + NO_2	KRO2NO3	Sander et al. (2019)
G44068	TrGC	EZCH3CO2CHCHO → CH_3COCHO_2CHO	k1_RO2sORO2	Sander et al. (2019)
G44069	TrGC	EZCHOCCH3CHO2 → $HCOCCH_3CO$ + OH	k_15hs24vynal	Sander et al. (2019)
G44070	TrGCN	EZCHOCCH3CHO2 + NO → $HCOCO_2CH_3CHO$ + NO_2	KRO2NO	Sander et al. (2019)*
G44071	TrGC	EZCHOCCH3CHO2 + HO_2→ $HCOCCH_3CHOOH$	k_RO2_HO2(temp,4)	Sander et al. (2019)
G44072	TrGCN	EZCHOCCH3CHO2 + NO_3→ $HCOCO_2CH_3CHO$ + NO_2	KRO2NO3	Sander et al. (2019)
G44073	TrGC	EZCHOCCH3CHO2 → $HCOCO_2CH_3CHO$	k1_RO2pORO2	Sander et al. (2019)
G44074	TrGC	$CH_3COOHCHCHO$ → CH_3COCHO_2CHO + OH	k_hydec	Sander et al. (2019)
G44075	TrGC	$HCOCCH_3CHOOH$ → $HCOCO_2CH_3CHO$ + OH	k_hydec	Sander et al. (2019)
G44076	TrGCN	CH_3COCHO_2CHO + NO → $CH_3C(O)$ + GLYOX + NO_2	KRO2NO	Sander et al. (2019)*
G44077	TrGCN	CH_3COCHO_2CHO + NO_3 → $CH_3C(O)$ + GLYOX + NO_2	KRO2NO3	Sander et al. (2019)
G44078	TrGC	CH_3COCHO_2CHO + HO_2 → $CH_3C(O)$ + GLYOX + OH	k_RO2_HO2(temp,4)	Sander et al. (2019)*
G44079	TrGC	CH_3COCHO_2CHO → $CH_3C(O)$ + GLYOX	k1_RO2sORO2	Sander et al. (2019)
G44080	TrGC	$HCOCO_2CH_3CHO$ → MGLYOX + CO + HO_2	k1_RO2tORO2	Sander et al. (2019)
G44081	TrGCN	$HCOCO_2CH_3CHO$ + NO → MGLYOX + CO + HO_2 + NO_2	KRO2NO	Sander et al. (2019)*

Table 1: Gas phase reactions (... continued)

#	labels	reaction	rate coefficient	reference
G44082	TrGC	$HCOCO_2CH_3CHO$ + HO_2 → MGLYOX + CO + HO_2 + OH	k_RO2_HO2(temp,4)	Sander et al. (2019)*
G44083	TrGCN	$HCOCO_2CH_3CHO$ + NO_3 → MGLYOX + CO + HO_2 + NO_2	KRO2NO3	Sander et al. (2019)
G44084	TrGC	$HCOCCH_3CO$ + OH → CO + MGLYOX + HO_2	1E-10*a_CHO	Hatakeyama et al. (1985), Sander et al. (2019)
G44085	TrGC	$CH_3COCHCO$ + OH → CO + MGLYOX + HO_2	7.6E-11*a_COCH3	Hatakeyama et al. (1985), Sander et al. (2019)*
G44086	TrGCN	LMEKNO3 + OH → .62 MGLYOX + .62 HCHO + .62 HO_2 + .62 NO_2 + .38 $CH_3C(O)$ + .38 $NO_3CH2CHO$	.62*(k_p*(f_CO+f_CH2ONO2)) +.38*(k_s*f_CH2ONO2*f_CO)	Sander et al. (2019)*
G44087	TrGC	MEPROPENE + OH → IBUTOLBO2	9.4E-12*EXP(505./temp)	Atkinson et al. (2006)
G44088a	TrGC	MEPROPENE + O_3 → CH_3COCH_3 + CH_2OO*	2.7E-15*EXP(-1630./temp)*0.33	Atkinson et al. (2006), Sander et al. (2019)
G44088b	TrGC	MEPROPENE + O_3 → $CH_3COCH_2O_2$ + OH + HCHO	2.7E-15*EXP(-1630./temp)*0.67	Atkinson et al. (2006), Sander et al. (2019)
G44089	TrGCN	MEPROPENE + NO_3 → CH_3COCH_3 + HCHO + NO_2	3.4E-13	Atkinson et al. (2006), Sander et al. (2019)*
G44090	TrGC	IBUTOLBO2 → CH_3COCH_3 + HCHO + HO_2	k1_RO2tORO2	Sander et al. (2019)
G44091a	TrGC	IBUTOLBO2 + HO_2 → IBUTOLBOOH	k_RO2_HO2(temp,4)*r_COCH2O2_OOH	Sander et al. (2019)
G44091b	TrGC	IBUTOLBO2 + HO_2 → CH_3COCH_3 + HCHO + HO_2 + OH	k_RO2_HO2(temp,4)*r_COCH2O2_OH	Sander et al. (2019)
G44092a	TrGCN	IBUTOLBO2 + NO → CH_3COCH_3 + HCHO + HO_2 + NO_2	KRO2NO*(1.-alpha_AN(5,3,0,0,0, temp,cair))	Sander et al. (2019)
G44092b	TrGCN	IBUTOLBO2 + NO → IBUTOLBNO3	KRO2NO*alpha_AN(5,3,0,0,0,temp, cair)	Sander et al. (2019)
G44093	TrGCN	IBUTOLBO2 + NO_3 → CH_3COCH_3 + HCHO + HO_2 + NO_2	KRO2NO3	Sander et al. (2019)
G44094a	TrGC	IBUTOLBOOH + OH → IBUTOLBO2	k_ROOHRO	Sander et al. (2019)
G44094b	TrGC	IBUTOLBOOH + OH → CH_3COCH_3 + HCHO + HO_2	k_s*f_sOOH*f_pCH2OH	Sander et al. (2019)
G44095	TrGCN	IBUTOLBNO3 + OH → CH_3COCH_3 + HCHO + HO_2 + NO_2	3.*k_p	Sander et al. (2019)
G44096	TrGC	BUT1ENE + OH → LBUT1ENO2	6.6E-12*EXP(465./temp)	Atkinson et al. (2006)*
G44097a	TrGC	BUT1ENE + O_3 → HCHO + .5 C_2H_5CHO + .5 H_2O_2 + .5 CH_3CHO + .5 CO + .5 HO_2	3.35E-15*EXP(-1745./temp)*.57	Atkinson et al. (2006), Sander et al. (2019)*

Table 1: Gas phase reactions (... continued)

#	labels	reaction	rate coefficient	reference
G44097b	TrGC	BUT1ENE + O_3 → C_2H_5CHO + CH_2OO^*	3.35E-15*EXP(-1745./temp)*.43	Atkinson et al. (2006), Sander et al. (2019)*
G44098	TrGCN	BUT1ENE + NO_3 → C_2H_5CHO + HCHO + NO_2	3.2E-13*EXP(-950./temp)	Atkinson et al. (2006), Sander et al. (2019)*
G44099	TrGC	LBUT1ENO2 → C_2H_5CHO + HCHO + HO_2	k1_RO2sORO2	Sander et al. (2019)
G44100a	TrGC	LBUT1ENO2 + HO_2 → LBUT1ENOOH	k_RO2_HO2(temp,4)*r_COCH2O2_OOH	Sander et al. (2019)
G44100b	TrGC	LBUT1ENO2 + HO_2 → C_2H_5CHO + HCHO + HO_2 + OH	k_RO2_HO2(temp,4)*r_COCH2O2_OH	Sander et al. (2019)
G44101a	TrGCN	LBUT1ENO2 + NO → C_2H_5CHO + HCHO + HO_2 + NO_2	KRO2NO*(1.-alpha_AN(5,2,0,0,0, temp,cair))	Sander et al. (2019)
G44101b	TrGCN	LBUT1ENO2 + NO → LBUT1ENNO3	KRO2NO*alpha_AN(5,2,0,0,0,temp, cair)	Sander et al. (2019)
G44102	TrGCN	LBUT1ENO2 + NO_3 → C_2H_5CHO + HCHO + HO_2 + NO_2	KRO2NO3	Sander et al. (2019)
G44103a	TrGC	LBUT1ENOOH + OH → LBUT1ENO2	k_ROOHRO	Sander et al. (2019)
G44103b	TrGC	LBUT1ENOOH + OH → $C_2H_5CO_3$ + HCHO + HO_2	k_t*f_tOOH*f_pCH2OH	Sander et al. (2019)*
G44104	TrGCN	LBUT1ENNO3 + OH → C_2H_5CHO + CO + HO_2 + NO_2	k_s*f_sOH*f_CH2ONO2	Sander et al. (2019)*
G44105	TrGC	CBUT2ENE + OH → BUT2OLO2	1.1E-11*EXP(485./temp)	Atkinson et al. (2006)
G44106	TrGC	CBUT2ENE + O_3 → CH_3CHO + .16 CH3CHOHOOH + .50 OH + .50 $HCOCH_2O_2$ + .05 CH2CO + .09 CH_3OH + .09 CO + .2 CH_4 + .2 CO_2	3.2E-15*EXP(-965./temp)	Atkinson et al. (2006), Sander et al. (2019)*
G44107	TrGCN	CBUT2ENE + NO_3 → 2 CH_3CHO + NO_2	3.5E-13	Atkinson et al. (2006), Sander et al. (2019)*
G44108	TrGC	TBUT2ENE + OH → BUT2OLO2	1.0E-11*EXP(553./temp)	Atkinson et al. (2006)
G44109	TrGC	TBUT2ENE + O_3 → CH_3CHO + .16 CH3CHOHOOH + .50 OH + .50 $HCOCH_2O_2$ + .05 CH2CO + .09 CH_3OH + .09 CO + .2 CH_4 + .2 CO_2	6.6E-15*EXP(-1060./temp)	Atkinson et al. (2006), Sander et al. (2019)
G44110	TrGCN	TBUT2ENE + NO_3 → 2 CH_3CHO + NO_2	1.78E-12*EXP(-530./temp) +1.28E-14*EXP(570./temp)	Atkinson et al. (2006), Sander et al. (2019)*
G44111	TrGC	BUT2OLO2 → C_2H_5CHO + HCHO + HO_2	k1_RO2sORO2	Sander et al. (2019)
G44112a	TrGC	BUT2OLO2 + HO_2 → BUT2OLOOH	k_RO2_HO2(temp,4)*r_COCH2O2_OOH	Sander et al. (2019)
G44112b	TrGC	BUT2OLO2 + HO_2 → 2 CH_3CHO + HO_2 + OH	k_RO2_HO2(temp,4)*r_COCH2O2_OH	Sander et al. (2019)
G44113a	TrGCN	BUT2OLO2 + NO → 2 CH_3CHO + HO_2 + NO_2	KRO2NO*(1.-alpha_AN(5,2,0,0,0, temp,cair))	Sander et al. (2019)

Table 1: Gas phase reactions (... continued)

#	labels	reaction	rate coefficient	reference
G44113b	TrGCN	BUT2OLO2 + NO → BUT2OLNO3	KRO2NO*alpha_AN(5,2,0,0,0,temp, cair)	Sander et al. (2019)
G44114	TrGCN	BUT2OLO2 + NO_3 → 2 CH_3CHO + HO_2 + NO_2	KRO2NO3	Sander et al. (2019)
G44115a	TrGC	BUT2OLOOH + OH → BUT2OLO2	k_ROOHRO	Sander et al. (2019)
G44115b	TrGC	BUT2OLOOH + OH → LMEKOOH + HO_2	k_t*f_tOH*f_pCH2OH	Sander et al. (2019)
G44115c	TrGC	BUT2OLOOH + OH → BUT2OLO + OH	k_t*f_tOOH*f_pCH2OH	Sander et al. (2019)
G44116	TrGCN	BUT2OLNO3 + OH → LMEKNO3 + HO_2	k_t*f_tOH*f_CH2ONO2	Sander et al. (2019)
G44117	TrGC	BUT2OLO + OH → BIACET + HO_2	k_t*f_tOH*f_CO	Sander et al. (2019)
G44118	TrGC	IPRCHO + OH → IPRCO3 + H_2O	6.8E-12*EXP(410./temp)	Atkinson et al. (2006)
G44119	TrGCN	IPRCHO + NO_3 → IPRCO3 + HNO_3	1.67E-12*EXP(-1460./temp)	Atkinson et al. (2006)
G44120	TrGC	IPRCO3 → $iC_3H_7O_2$ + CO_2	k1_RO2RCO3	Rickard and Pascoe (2009)
G44121a	TrGC	IPRCO3 + HO_2 → PERIBUACID	KAPHO2*r_CO3_OOH	Rickard and Pascoe (2009), Sander et al. (2019)
G44121b	TrGC	IPRCO3 + HO_2 → $iC_3H_7O_2$ + CO_2 + OH	KAPHO2*(1.-r_CO3_OOH)	Rickard and Pascoe (2009), Sander et al. (2019)
G44122	TrGCN	IPRCO3 + NO_2 → PIPN	k_CH3CO3_NO2	Rickard and Pascoe (2009)
G44123	TrGCN	IPRCO3 + NO → $iC_3H_7O_2$ + CO_2 + NO_2	KAPNO	Rickard and Pascoe (2009)
G44124a	TrGC	PERIBUACID + OH → IPRCO3 + H_2O	k_ROOHRO	Rickard and Pascoe (2009)
G44124b	TrGC	PERIBUACID + OH → CH_3COCH_3 + H_2O + CO_2	k_s*f_CO2H	Sander et al. (2019)*
G44125	TrGCN	PIPN → IPRCO3 + NO_2	k_PAN_M	Rickard and Pascoe (2009)
G44126	TrGCN	PIPN + OH → CH_3COCH_3 + CO_2 + NO_2	k_s*f_cpan	Sander et al. (2019)*
G44127	TrGC	MPROPENOL + OH → HCOOH + OH + CH_3COCH_3	k_CH2CHOH_OH_HCOOH	Sander et al. (2019), So et al. (2014)*
G44128	TrGC	MPROPENOL + HCOOH → IPRCHO + HCOOH	k_CH2CHOH_HCOOH	Sander et al. (2019), da Silva (2010)*
G44129	TrGC	IPRCHO + HCOOH → MPROPENOL + HCOOH	k_ALD_HCOOH	Sander et al. (2019), da Silva (2010)*
G44130	TrGC	BUTENOL + OH → HCOOH + OH + C_2H_5CHO	k_CH2CHOH_OH_HCOOH	Sander et al. (2019), So et al. (2014)*
G44131	TrGC	BUTENOL + HCOOH → C_3H_7CHO + HCOOH	k_CH2CHOH_HCOOH	Sander et al. (2019), da Silva (2010)*
G44132	TrGC	C_3H_7CHO + HCOOH → BUTENOL + HCOOH	k_ALD_HCOOH	Sander et al. (2019), da Silva (2010)*
G44133	TrGC	HVMK + OH → HCOOH + OH + MGLYOX	8.8E-11	Sander et al. (2019), So et al. (2014), Messaadia et al. (2015)*

Table 1: Gas phase reactions (... continued)

#	labels	reaction	rate coefficient	reference
G44134	TrGC	HVMK + HCOOH → CO2C3CHO + HCOOH	k_CH2CHOH_HCOOH	Sander et al. (2019), da Silva (2010)*
G44135	TrGC	CO2C3CHO + HCOOH → HVMK + HCOOH	k_ALD_HCOOH	Sander et al. (2019), da Silva (2010)*
G44136	TrGC	HMAC + OH → HCOOH + OH + MGLYOX	8.8E-11	Sander et al. (2019), So et al. (2014), Messaadia et al. (2015)*
G44137	TrGC	HMAC + HCOOH → IBUTDIAL + HCOOH	k_CH2CHOH_HCOOH	Sander et al. (2019), da Silva (2010)*
G44138	TrGC	IBUTDIAL + HCOOH → HMAC + HCOOH	k_ALD_HCOOH	Sander et al. (2019), da Silva (2010)*
G44139	TrGC	CO2C3CHO + OH → $CH_3COCH_2O_2$ + CO_2 + H_2O	k_t*f_O*f_alk+k_s*f_CHO*f_CO	Sander et al. (2019)*
G44140	TrGCN	CO2C3CHO + NO_3 → $CH_3COCH_2O_2$ + CO_2 + HNO_3	KNO3AL*4.0	Sander et al. (2019)*
G44141	TrGC	IBUTDIAL + OH → CH_3CHO + CO + HO_2 + CO_2 + H_2O	2.*k_t*f_O*f_alk+k_t*f_CHO*f_CHO	Sander et al. (2019)*
G44142	TrGCN	IBUTDIAL + NO_3 → CH_3CHO + CO + HO_2 + CO_2 + HNO_3	2.*KNO3AL*4.0	Sander et al. (2019)*
G44200	TrGTerC	$CH_3COCOCH_2O_2$ → $CH_3C(O)$ + HCHO + CO	k1_RO2pORO2	Rickard and Pascoe (2009)
G44201	TrGTerC	$CH_3COCOCH_2O_2$ + HO_2 → $CH_3COCOCH_2OOH$	k_RO2_HO2(temp,4)	Rickard and Pascoe (2009)
G44202	TrGTerCN	$CH_3COCOCH_2O_2$ + NO → $CH_3C(O)$ + HCHO + CO + NO_2	KRO2NO	Rickard and Pascoe (2009)*
G44203a	TrGTerC	$CH_3COCOCH_2OOH$ + OH → $CH_3COCOCHO$ + OH	k_s*f_CO*f_sOOH	Rickard and Pascoe (2009)*
G44203b	TrGTerC	$CH_3COCOCH_2OOH$ + OH → $CH_3COCOCH_2O_2$	k_ROOHRO	Rickard and Pascoe (2009)
G44204	TrGTerC	C44O2 + HO_2 → C44OOH	k_RO2_HO2(temp,4)	Rickard and Pascoe (2009)
G44205	TrGTerCN	C44O2 + NO → HCOCH2CHO + CO_2 + HO_2 + NO_2	KRO2NO	Rickard and Pascoe (2009)*
G44206	TrGTerC	C44O2 → HCOCH2CHO + CO_2 + HO_2	k1_RO2sORO2	Rickard and Pascoe (2009)
G44207	TrGTerC	C44OOH + OH → C44O2	7.46E-11	Rickard and Pascoe (2009)
G44208	TrGTerC	CHOC3COO2 → HCOCH2CO3 + HCHO	k1_RO2pORO2	Rickard and Pascoe (2009)
G44209	TrGTerC	CHOC3COO2 + HO_2 → C413COOOH	k_RO2_HO2(temp,4)	Rickard and Pascoe (2009)
G44210	TrGTerCN	CHOC3COO2 + NO → HCOCH2CO3 + HCHO + NO_2	KRO2NO	Rickard and Pascoe (2009)*
G44211	TrGTerC	C413COOOH + OH → CHOC3COO2	8.33E-11	Rickard and Pascoe (2009)
G44212	TrGTerC	C4CODIAL + OH → C312COCO3	3.39E-11	Rickard and Pascoe (2009)
G44213	TrGTerCN	C4CODIAL + NO_3 → C312COCO3 + HNO_3	2.*KNO3AL*4.0	Rickard and Pascoe (2009)
G44214	TrGTerC	C312COCO3 → $HCOCOCH_2O_2$ + CO_2	k1_RO2RCO3	Rickard and Pascoe (2009)
G44215a	TrGTerC	C312COCO3 + HO_2 → C312COCO3H	KAPHO2*r_CO3_OOH	Rickard and Pascoe (2009)
G44215b	TrGTerC	C312COCO3 + HO_2 → $HCOCOCH_2O_2$ + CO_2 + OH	KAPHO2*(1.-r_CO3_OOH)	Rickard and Pascoe (2009)

Table 1: Gas phase reactions (... continued)

#	labels	reaction	rate coefficient	reference
G44216	TrGTerCN	C312COCO3 + NO_2 → C312COPAN	k_CH3CO3_NO2	Rickard and Pascoe (2009)
G44217	TrGTerCN	C312COCO3 + NO → $HCOCOCH_2O_2$ + CO_2 + NO_2	KAPNO	Rickard and Pascoe (2009)
G44218	TrGTerC	C312COCO3H + OH → C312COCO3	1.63E-11	Rickard and Pascoe (2009)
G44219	TrGTerCN	C312COPAN → C312COCO3 + NO_2	k_PAN_M	Rickard and Pascoe (2009)
G44220	TrGTerCN	C312COPAN + OH → HCOCOCHO + CO + NO_2	1.27E-11	Rickard and Pascoe (2009)
G44221	TrGTerC	$CH_3COCOCHO$ + OH → $CH_3C(O)$ + 2 CO	8.4E-13*EXP(830./temp)	Sander et al. (2019)*
G44222	TrGTerCN	$CH_3COCOCHO$ + NO_3 → $CH_3C(O)$ + 2 CO + HNO_3	KNO3AL*4.0	Rickard and Pascoe (2009)
G44223	TrGTerC	IBUTALOH + OH → IPRHOCO3	1.4E-11	Rickard and Pascoe (2009)
G44224a	TrGTerC	IPRHOCO3 + HO_2 → CH_3COCH_3 + CO_2 + HO_2 + OH	KAPHO2*r_CO3_OH	Rickard and Pascoe (2009), Sander et al. (2019)
G44224b	TrGTerC	IPRHOCO3 + HO_2 → IPRHOCO2H + O_3	KAPHO2*r_CO3_O3	Rickard and Pascoe (2009), Sander et al. (2019)
G44224c	TrGTerC	IPRHOCO3 + HO_2 → IPRHOCO3H	KAPHO2*r_CO3_OOH	Rickard and Pascoe (2009), Sander et al. (2019)
G44225	TrGTerCN	IPRHOCO3 + NO → CH_3COCH_3 + CO_2 + HO_2 + NO_2	KAPNO	Rickard and Pascoe (2009)
G44226	TrGTerCN	IPRHOCO3 + NO_2 → C4PAN5	k_CH3CO3_NO2	Rickard and Pascoe (2009)
G44227	TrGTerCN	IPRHOCO3 + NO_3 → CH_3COCH_3 + CO_2 + HO_2 + NO_2	KRO2NO3*1.74	Rickard and Pascoe (2009)
G44228a	TrGTerC	IPRHOCO3 → CH_3COCH_3 + CO_2 + HO_2	k1_RO2RCO3*0.7	Rickard and Pascoe (2009)
G44228b	TrGTerC	IPRHOCO3 → IPRHOCO2H	k1_RO2RCO3*0.3	Rickard and Pascoe (2009)
G44229	TrGTerC	IPRHOCO2H + OH → CH_3COCH_3 + CO_2 + HO_2 + H_2O	1.72E-12	Rickard and Pascoe (2009)
G44230	TrGTerC	OH + IPRHOCO3H → IPRHOCO3	4.80E-12	Rickard and Pascoe (2009)
G44231	TrGTerCN	C4PAN5 → IPRHOCO3 + NO_2	k_PAN_M	Rickard and Pascoe (2009)
G44232	TrGTerCN	C4PAN5 + OH → CH_3COCH_3 + CO + NO_2	4.75E-13	Rickard and Pascoe (2009)
G44233a	TrGTerC	MBOOO → IPRHOCO2H	1.60E-17*C(ind_H2O)*(0.08+0.15)	Rickard and Pascoe (2009), Sander et al. (2019)
G44233b	TrGTerC	MBOOO → IBUTALOH + H_2O_2	1.60E-17*C(ind_H2O)*0.77	Rickard and Pascoe (2009), Sander et al. (2019)
G44234	TrGTerC	MBOOO + CO → IBUTALOH + CO_2	1.20E-15	Rickard and Pascoe (2009)
G44235	TrGTerCN	MBOOO + NO → IBUTALOH + NO_2	1.00E-14	Rickard and Pascoe (2009)
G44236	TrGTerCN	MBOOO + NO_2 → IBUTALOH + NO_3	1.00E-15	Rickard and Pascoe (2009)
G44400	TrGAroC	MALANHY + OH → MALANHYO2	1.4E-12	Rickard and Pascoe (2009)
G44401a	TrGAroC	MALDIALOOH + OH → HOCOC4DIAL + OH	1.22E-10	Rickard and Pascoe (2009)
G44401b	TrGAroC	MALDIALOOH + OH → MALDIALO2	k_ROOHRO	Rickard and Pascoe (2009)
G44402	TrGAroCN	NC4DCO2H + OH → MALANHY + NO_2	k_ROOHRO	Rickard and Pascoe (2009)*
G44403	TrGAroC	CO14O3CO2H + OH → $HCOCH_2O_2$ + 2 CO_2	2.19E-11	Rickard and Pascoe (2009)

Table 1: Gas phase reactions (... continued)

#	labels	reaction	rate coefficient	reference
G44404	TrGAroC	BZFUOOH + OH → BZFUO2	3.68E-11	Rickard and Pascoe (2009)
G44405	TrGAroC	HOCOC4DIAL + OH → CO2C4DIAL + HO_2	3.67E-11	Rickard and Pascoe (2009)
G44406a	TrGAroC	MALDIALCO3 + HO_2 → MALDALCO2H + O_3	KAPHO2*r_CO3_O3	Rickard and Pascoe (2009)
G44406b	TrGAroC	MALDIALCO3 + HO_2 → MALDALCO3H	KAPHO2*r_CO3_OOH	Rickard and Pascoe (2009)
G44406c	TrGAroC	MALDIALCO3 + HO_2 → .6 MALANHY + HO_2 + .4 GLYOX + .4 CO + .4 CO_2 + OH	KAPHO2*r_CO3_OH	Rickard and Pascoe (2009)*
G44407	TrGAroCN	MALDIALCO3 + NO → .6 MALANHY + HO_2 + .4 GLYOX + .4 CO + .4 CO_2 + NO_2	KAPNO	Rickard and Pascoe (2009)*
G44408	TrGAroCN	MALDIALCO3 + NO_2 → MALDIALPAN	k_CH3CO3_NO2	Rickard and Pascoe (2009)
G44409	TrGAroCN	MALDIALCO3 + NO_3 → .6 MALANHY + HO_2 + .4 GLYOX + .4 CO + .4 CO_2 + NO_2	KRO2NO3*1.74	Rickard and Pascoe (2009)*
G44410	TrGAroC	MALDIALCO3 → .6 MALANHY + HO_2 + .4 GLYOX + .4 CO + .4 CO_2	k1_RO2RCO3	Rickard and Pascoe (2009)*
G44411	TrGAroCN	BZFUONE + NO_3 → NBZFUO2	3.00E-13	Rickard and Pascoe (2009)
G44412	TrGAroC	BZFUONE + O_3 → .3125 CO14O3CO2H + .1875 CO14O3CHO + .1875 H_2O_2 + .5 CO + .5 CO_2 + .5 $HCOCH_2O_2$ + .5 OH	2.20E-19	see note*
G44413	TrGAroC	BZFUONE + OH → BZFUO2	4.45E-11	Rickard and Pascoe (2009)
G44414	TrGAroCN	NBZFUOOH + OH → NBZFUO2	6.18E-12	Rickard and Pascoe (2009)
G44415	TrGAroC	MALDALCO3H + OH → MALDIALCO3	4.00E-11	Rickard and Pascoe (2009)
G44416	TrGAroC	EPXDLCO2H + OH → C3DIALO2 + CO_2	2.31E-11	Rickard and Pascoe (2009)
G44417a	TrGAroC	EPXDLCO3 + HO_2 → C3DIALO2 + CO_2 + OH	KAPHO2*r_CO3_OH	Rickard and Pascoe (2009)
G44417b	TrGAroC	EPXDLCO3 + HO_2 → EPXDLCO2H + O_3	KAPHO2*r_CO3_O3	Rickard and Pascoe (2009)
G44417c	TrGAroC	EPXDLCO3 + HO_2 → EPXDLCO3H	KAPHO2*r_CO3_OOH	Rickard and Pascoe (2009)
G44418	TrGAroCN	EPXDLCO3 + NO → C3DIALO2 + CO_2 + NO_2	KAPNO	Rickard and Pascoe (2009)
G44419	TrGAroCN	EPXDLCO3 + NO_2 → EPXDLPAN	k_CH3CO3_NO2	Rickard and Pascoe (2009)
G44420	TrGAroCN	EPXDLCO3 + NO_3 → C3DIALO2 + CO_2 + NO_2	KRO2NO3*1.74	Rickard and Pascoe (2009)
G44421	TrGAroC	EPXDLCO3 → C3DIALO2 + CO_2	k1_RO2RCO3	Rickard and Pascoe (2009)*
G44422	TrGAroC	MALNHYOHCO + OH → CO + CO + CO + CO_2 + HO_2	5.68E-12	Rickard and Pascoe (2009)
G44423	TrGAroCN	MALDIAL + NO_3 → MALDIALCO3 + HNO_3	2.*KNO3AL*2.0	Rickard and Pascoe (2009)
G44424	TrGAroC	MALDIAL + O_3 → 1.0675 GLYOX + .125 HCHO + .1125 $HCOCO_2H$ + .0675 H_2O_2 + .82 HO_2 + .57 OH + 1.265 CO + .25 CO_2	2.00E-18	Rickard and Pascoe (2009)*
G44425	TrGAroC	MALDIAL + OH → .83 MALDIALCO3 + .17 MALDIALO2	5.20E-11	Rickard and Pascoe (2009)*

Table 1: Gas phase reactions (... continued)

#	labels	reaction	rate coefficient	reference
G44426	TrGAroC	MALANHYOOH + OH → MALNHYOHCO + OH	4.66E-11	Rickard and Pascoe (2009)
G44427	TrGAroCN	MALDIALPAN + OH → GLYOX + CO + CO + NO_2	3.70E-11	Rickard and Pascoe (2009)
G44428	TrGAroCN	MALDIALPAN → MALDIALCO3 + NO_2	k_PAN_M	Rickard and Pascoe (2009)
G44429a	TrGAroC	MALANHYO2 + HO_2 → MALANHYOOH	k_RO2_HO2(temp,4)*(1.-r_COCH2O2_OH-r_CHOHCH2O2_OH)	Rickard and Pascoe (2009), Sander et al. (2019)
G44429b	TrGAroC	MALANHYO2 + HO_2 → HCOCOHCO3 + CO_2 + OH	k_RO2_HO2(temp,4)*(r_COCH2O2_OH+r_CHOHCH2O2_OH)	Rickard and Pascoe (2009), Sander et al. (2019)
G44430	TrGAroCN	MALANHYO2 + NO → HCOCOHCO3 + CO_2 + NO_2	KRO2NO	Rickard and Pascoe (2009)*
G44431	TrGAroCN	MALANHYO2 + NO_3 → HCOCOHCO3 + CO_2 + NO_2	KRO2NO3	Rickard and Pascoe (2009)*
G44432	TrGAroC	MALANHYO2 → HCOCOHCO3 + CO_2	k1_RO2sORO2	Rickard and Pascoe (2009)*
G44433	TrGAroC	EPXDLCO3H + OH → EPXDLCO3	2.62E-11	Rickard and Pascoe (2009)
G44434	TrGAroC	CO2C4DIAL + OH → CO + CO + CO + CO + HO_2	2.45E-11	Rickard and Pascoe (2009)
G44435a	TrGAroCN	NBZFUO2 + HO_2 → NBZFUOOH	k_RO2_HO2(temp,4)*(1.-r_COCH2O2_OH)	Rickard and Pascoe (2009), Sander et al. (2019)
G44435b	TrGAroCN	NBZFUO2 + HO_2 → .5 CO14O3CHO + .5 NO_2 + .5 NBZFUONE + .5 HO_2 + OH	k_RO2_HO2(temp,4)*r_COCH2O2_OH	Rickard and Pascoe (2009), Sander et al. (2019)
G44436	TrGAroCN	NBZFUO2 + NO → .5 CO14O3CHO + .5 NO_2 + .5 NBZFUONE + .5 HO_2 + NO_2	KRO2NO	Rickard and Pascoe (2009)*
G44437	TrGAroCN	NBZFUO2 + NO_3 → .5 CO14O3CHO + .5 NO_2 + .5 NBZFUONE + .5 HO_2 + NO_2	KRO2NO3	Rickard and Pascoe (2009)*
G44438	TrGAroCN	NBZFUO2 → .5 CO14O3CHO + .5 NO_2 + .5 NBZFUONE + .5 HO_2	k1_RO2sORO2	Rickard and Pascoe (2009)*
G44439	TrGAroC	MALDALCO2H + OH → .6 MALANHY + HO_2 + .4 GLYOX + .4 CO + .4 CO_2	3.70E-11	Rickard and Pascoe (2009)*
G44440	TrGAroCN	EPXC4DIAL + NO_3 → EPXDLCO3 + HNO_3	2.*KNO3AL*4.0	Rickard and Pascoe (2009)
G44441	TrGAroC	EPXC4DIAL + OH → EPXDLCO3	4.32E-11	Rickard and Pascoe (2009)
G44442a	TrGAroC	MECOACETO2 + HO_2 → MECOACEOOH	k_RO2_HO2(temp,4)*(1.-r_COCH2O2_OH)	Rickard and Pascoe (2009), Sander et al. (2019)
G44442b	TrGAroC	MECOACETO2 + HO_2 → $CH_3C(O)OO$ + HCHO + CO_2 + OH	k_RO2_HO2(temp,4)*r_COCH2O2_OH	Rickard and Pascoe (2009), Sander et al. (2019)
G44443	TrGAroCN	MECOACETO2 + NO → $CH_3C(O)OO$ + HCHO + CO_2 + NO_2	KRO2NO	Rickard and Pascoe (2009)*
G44444	TrGAroCN	MECOACETO2 + NO_3 → $CH_3C(O)OO$ + HCHO + CO_2 + NO_2	KRO2NO3	Rickard and Pascoe (2009)*
G44445	TrGAroC	MECOACETO2 → $CH_3C(O)OO$ + HCHO + CO_2	k1_RO2pORO2	Rickard and Pascoe (2009)*

Table 1: Gas phase reactions (... continued)

#	labels	reaction	rate coefficient	reference
G44446	TrGAroCN	CO14O3CHO + NO_3 → CO + $HCOCH_2O_2$ + CO_2 + HNO_3	KNO3AL*8.0	Rickard and Pascoe (2009)
G44447	TrGAroC	CO14O3CHO + OH → CO + $HCOCH_2O_2$ + CO_2	3.44E-11	Rickard and Pascoe (2009)
G44448	TrGAroCN	NBZFUONE + OH → BZFUCO + NO_2	1.16E-12	Rickard and Pascoe (2009)
G44449a	TrGAroC	BZFUO2 + HO_2 → BZFUOOH	k_RO2_HO2(temp,4)*(1.-r_COCH2O2_OH-r_CHOHCH2O2_OH)	Rickard and Pascoe (2009), Sander et al. (2019)
G44449b	TrGAroC	BZFUO2 + HO_2 → CO14O3CHO + HO_2 + OH	k_RO2_HO2(temp,4)*(r_COCH2O2_OH+r_CHOHCH2O2_OH)	Rickard and Pascoe (2009), Sander et al. (2019)
G44450	TrGAroCN	BZFUO2 + NO → CO14O3CHO + HO_2 + NO_2	KRO2NO	Rickard and Pascoe (2009)*
G44451	TrGAroCN	BZFUO2 + NO_3 → CO14O3CHO + HO_2 + NO_2	KRO2NO3	Rickard and Pascoe (2009)*
G44452	TrGAroC	BZFUO2 → CO14O3CHO + HO_2	k1_RO2sORO2	Rickard and Pascoe (2009)*
G44453	TrGAroC	BZFUCO + OH → CO14O3CHO + HO_2	1.78E-11	Rickard and Pascoe (2009)
G44456a	TrGAroC	MALDIALO2 + HO_2 → MALDIALOOH	k_RO2_HO2(temp,4)*(1.-r_COCH2O2_OH-r_CHOHCH2O2_OH)	Rickard and Pascoe (2009)
G44456b	TrGAroC	MALDIALO2 + HO_2 → GLYOX + GLYOX + HO_2 + OH	k_RO2_HO2(temp,4)*(r_COCH2O2_OH+r_CHOHCH2O2_OH)	Rickard and Pascoe (2009)
G44457	TrGAroCN	MALDIALO2 + NO → GLYOX + GLYOX + HO_2 + NO_2	KRO2NO	Rickard and Pascoe (2009)*
G44458	TrGAroCN	MALDIALO2 + NO_3 → GLYOX + GLYOX + HO_2 + NO_2	KRO2NO3	Rickard and Pascoe (2009)*
G44459	TrGAroC	MALDIALO2 → GLYOX + GLYOX + HO_2	k1_RO2sORO2	Rickard and Pascoe (2009)*
G44460	TrGAroCN	EPXDLPAN + OH → HCOCOCHO + CO + NO_2	2.29E-11	Rickard and Pascoe (2009)
G44461	TrGAroCN	EPXDLPAN → EPXDLCO3 + NO_2	k_PAN_M	Rickard and Pascoe (2009)*
G44462	TrGAroC	MECOACEOOH + OH → MECOACETO2	3.59E-12	Rickard and Pascoe (2009)
G45000	TrGC	C_5H_8 + O_3 → .3508 MACR + .01518 MACO2H + .2440 MVK + .7085 HCHO + .11 CH_2OO + .1275 C_3H_6 + .1575 $CH_3C(O)$ + .0510 CH_3 + .2625 HO_2 + .27 OH + .09482 H_2O_2 + .255 CO_2 + .522 CO + .07182 HCHO + .03618 $HCOCH_2O_2$ + .01782 CO + 0.05408 LCARBON	1.03E-14*EXP(-1995./temp)	Atkinson et al. (2006), Sander et al. (2019)
G45001	TrGC	C_5H_8 + OH → .63 LISOPAB + .30 LISOPCD + .07 LISOPEFO2	2.7E-11*EXP(390./temp)	Atkinson et al. (2006), Sander et al. (2019)
G45002	TrGCN	C_5H_8 + NO_3 → NISOPO2	3.0E-12*EXP(-450./temp)	Atkinson et al. (2006)
G45003a	TrGC	LISOPAB + O_2 → LISOPACO2	5.530E-13	Sander et al. (2019)
G45003b	TrGC	LISOPAB + O_2 → ISOPBO2	3.E-12	Sander et al. (2019)
G45004a	TrGC	LISOPCD + O_2 → LDISOPACO2	6.780E-13	Sander et al. (2019)
G45004b	TrGC	LISOPCD + O_2 → ISOPDO2	3.E-12	Sander et al. (2019)

Table 1: Gas phase reactions (... continued)

#	labels	reaction	rate coefficient	reference
G45005	TrGC	LISOPACO2 → LISOPAB + O_2	3.1E12*exp(-7900./temp)*.6+7.8E13*exp(-8600./temp)*.4	Sander et al. (2019)
G45006	TrGC	ISOPBO2 → LISOPAB + O_2	3.7E14*exp(-9570./temp)+4.2E14*exp(-9970./temp)	Sander et al. (2019)
G45007	TrGC	LDISOPACO2 → LISOPCD + O_2	5.65E12*exp(-8410./temp)*.42+1.4E14*exp(-9110./temp)*.58	Sander et al. (2019)
G45008	TrGC	ISOPDO2 → LISOPCD + O_2	5.0E14*exp(-10120./temp)+8.25E14*exp(-10220./temp)	Sander et al. (2019)
G45009a	TrGC	LISOPACO2 → C1ODC2O2C4OOH	k_16hsz14 * 2./3.*(1.-f_HPAL)	Sander et al. (2019)
G45009b	TrGC	LISOPACO2 → LZCODC23DBCOOH + HO_2	k_16hsz14 * (2./3.*f_HPAL + 1./3.)	Sander et al. (2019)
G45010a	TrGC	LDISOPACO2 → C1OOHC3O2C4OD	k_16hsz41 * 2./3.*(1.-f_HPAL)	Sander et al. (2019)
G45010b	TrGC	LDISOPACO2 → LZCODC23DBCOOH + HO_2	k_16hsz41 * (2./3.*f_HPAL + 1./3.)	Sander et al. (2019)
G45011	TrGC	LISOPACO2 → .9 LISOPACO + .1 ISOPAOH	k1_RO2LISOPACO2	Rickard and Pascoe (2009), Sander et al. (2019)
G45012	TrGC	LISOPACO2 + HO_2 → LISOPACOOH	k_RO2_HO2(temp,5)	Rickard and Pascoe (2009)
G45013a	TrGCN	LISOPACO2 + NO → LISOPACO + NO_2	KRO2NO*(1.-alpha_AN(6,1,0,0,0,temp,cair))	Lockwood et al. (2010), Paulot et al. (2009a), Sander et al. (2019)
G45013b	TrGCN	LISOPACO2 + NO → LISOPACNO3	KRO2NO*alpha_AN(6,1,0,0,0,temp,cair)	Lockwood et al. (2010), Paulot et al. (2009a), Sander et al. (2019)
G45014	TrGCN	LISOPACO2 + NO_3 → LISOPACO + NO_2	KRO2NO3	Rickard and Pascoe (2009)
G45015	TrGC	LDISOPACO2 → .9 LISOPACO + .1 ISOPAOH	k1_RO2LISOPACO2	Rickard and Pascoe (2009), Sander et al. (2019)
G45016	TrGC	LDISOPACO2 + HO_2 → LISOPACOOH	k_RO2_HO2(temp,5)	Rickard and Pascoe (2009)
G45017a	TrGCN	LDISOPACO2 + NO → LISOPACO + NO_2	KRO2NO*(1.-alpha_AN(6,1,0,0,0,temp,cair))	Lockwood et al. (2010), Paulot et al. (2009a), Sander et al. (2019)
G45017b	TrGCN	LDISOPACO2 + NO → LISOPACNO3	KRO2NO*alpha_AN(6,1,0,0,0,temp,cair)	Lockwood et al. (2010), Paulot et al. (2009a), Sander et al. (2019)
G45018	TrGCN	LDISOPACO2 + NO_3 → LISOPACO + NO_2	KRO2NO3	Rickard and Pascoe (2009)
G45019a	TrGC	LISOPACOOH + OH → LISOPACO2	k_ROOHRO	Sander et al. (2019)
G45019b	TrGC	LISOPACOOH + OH → LZCODC23DBCOOH + HO_2	k_s*f_allyl*f_sOH	Sander et al. (2019)
G45019c	TrGC	LISOPACOOH + OH → LHC4ACCHO + OH	(k_s*f_sOOH*f_allyl+ k_ROHRO)	Sander et al. (2019)

Table 1: Gas phase reactions (... continued)

#	labels	reaction	rate coefficient	reference
G45019d	TrGC	LISOPACOOH + OH → LIEPOX + OH	(k_adt+k_ads)*a_CH2OH*a_CH2OOH	Sander et al. (2019)*
G45020	TrGC	ISOPAOH + OH → LHC4ACCHO + HO_2	(k_adt+k_ads)*a_CH2OH*a_CH2OH+k_s*f_sOH*f_allyl+k_ROHRO	Sander et al. (2019)
G45021	TrGCN	LISOPACNO3 + OH → LISOPACNO3O2	(k_adt+k_ads)*a_CH2ONO2*a_CH2OH	Sander et al. (2019)*
G45022	TrGC	ISOPBO2 → .8 MVK + .8 HCHO + .8 HO_2 + .2 ISOPBOH	k1_RO2ISOPBO2	Rickard and Pascoe (2009)
G45023a	TrGC	ISOPBO2 + HO_2 → ISOPBOOH	k_RO2_HO2(temp,5)*(1.-r_CHOHCH2O2_OH)	Sander et al. (2019)
G45023b	TrGC	ISOPBO2 + HO_2 → MVK + HCHO + HO_2 + OH	k_RO2_HO2(temp,5)*r_CHOHCH2O2_OH	Sander et al. (2019)
G45024a	TrGCN	ISOPBO2 + NO → MVK + HCHO + HO_2 + NO_2	KRO2NO*(1.-alpha_AN(6,3,0,0,0,temp,cair))	Lockwood et al. (2010), Sander et al. (2019)
G45024b	TrGCN	ISOPBO2 + NO → ISOPBNO3	KRO2NO*alpha_AN(6,3,0,0,0,temp,cair)	Lockwood et al. (2010), Sander et al. (2019)
G45025	TrGCN	ISOPBO2 + NO_3 → MVK + .75 HCHO + .75 HO_2 + .25 CH_3 + NO_2	KRO2NO3	Rickard and Pascoe (2009)
G45026a	TrGC	ISOPBOOH + OH → LIEPOX + OH	(k_ads+k_adp)*a_CH2OOH	Paulot et al. (2009b), Sander et al. (2019)
G45026b	TrGC	ISOPBOOH + OH → ISOPBO2	k_ROOHRO	Sander et al. (2019)
G45026c	TrGC	ISOPBOOH + OH → MGLYOX + $HOCH_2CHO$	k_ROHRO+k_s*f_alk*f_sOH	Sander et al. (2019)
G45027	TrGC	ISOPBOOH + O_3 → .1368 MACROOH + .1368 H_2O_2 + .2280 HO_2 + .4332 CH_3COCH_2OH + .2280 CO_2 + .6384 OH + .2052 CO + .57 HCHO + .43 MACROOH + .06880 HO_2 + .06880 OH + .2709 CO + .1591 CH_2OO	1.E-17	Sander et al. (2019)
G45028	TrGC	ISOPBOH + OH → MVK + .75 HCHO + .75 HO_2 + .25 CH_3	k_s*f_alk*f_sOH+(k_adp+k_ads)*a_CH2OH	Sander et al. (2019)
G45029	TrGCN	ISOPBNO3 + OH → ISOPBDNO3O2	(k_adt+k_adp)*f_CH2ONO2	Sander et al. (2019)
G45030	TrGC	ISOPDO2 → .8 MACR + .8 HCHO + .8 HO_2 + .1 HCOC5 + .1 ISOPDOH	k1_RO2ISOPDO2	Rickard and Pascoe (2009)
G45031a	TrGC	ISOPDO2 + HO_2 → ISOPDOOH	k_RO2_HO2(temp,5)*(1.-r_CHOHCH2O2_OH)	Sander et al. (2019)
G45031b	TrGC	ISOPDO2 + HO_2 → MACR + HCHO + HO_2 + OH	k_RO2_HO2(temp,5)*r_CHOHCH2O2_OH	Sander et al. (2019)
G45032a	TrGCN	ISOPDO2 + NO → MACR + HCHO + HO_2 + NO_2	KRO2NO*(1.-alpha_AN(6,2,0,0,0,temp,cair))	Lockwood et al. (2010), Sander et al. (2019)
G45032b	TrGCN	ISOPDO2 + NO → ISOPDNO3	KRO2NO*alpha_AN(6,2,0,0,0,temp,cair)	Lockwood et al. (2010), Sander et al. (2019)
G45033	TrGCN	ISOPDO2 + NO_3 → MACR + HCHO + HO_2 + NO_2	KRO2NO3	Rickard and Pascoe (2009)

Table 1: Gas phase reactions (... continued)

#	labels	reaction	rate coefficient	reference
G45034a	TrGC	ISOPDOOH + OH → LIEPOX + OH	(k_adt+k_adp)*a_CH2OOH	Paulot et al. (2009b), Sander et al. (2019)
G45034b	TrGC	ISOPDOOH + OH → ISOPDO2	k_ROOHRO	Sander et al. (2019)
G45034c	TrGC	ISOPDOOH + OH → HCOC5 + OH	k_t*f_tOOH*f_allyl*f_pCH2OH	Sander et al. (2019)
G45034d	TrGC	ISOPDOOH + OH → CH_3COCH_2OH + GLYOX + OH	k_s*f_pCH2OH*f_sOH	Sander et al. (2019)
G45035	TrGC	ISOPDOOH + O_3 → 1.393 OH + BIACETOH + .67 HCHO + .05280 HO_2 + .2079 CO + .1221 CH_2OO	1.E-17	Sander et al. (2019)
G45036	TrGC	ISOPDOH + OH → HCOC5 + HO_2	2.*k_ROHRO+(k_t*f_tOH*f_allyl+k_s*f_sOH)*f_pCH2OH+(k_adt+k_adp)*a_CH2OH	Sander et al. (2019)
G45037	TrGCN	ISOPDNO3 + OH → ISOPBDNO3O2	(k_adp+k_ads)*a_CH2ONO2	Sander et al. (2019)*
G45038	TrGCN	NISOPO2 → .8 NC4CHO + .6 HO_2 + .2 LISOPACNO3	k1_RO2LISOPACO2	Rickard and Pascoe (2009)
G45039	TrGCN	NISOPO2 + HO_2 → NISOPOOH	k_RO2_HO2(temp,5)	Rickard and Pascoe (2009)
G45040	TrGCN	NISOPO2 + NO → NC4CHO + HO_2 + NO_2	KRO2NO	Rickard and Pascoe (2009)*
G45041	TrGCN	NISOPO2 + NO_3 → NC4CHO + HO_2 + NO_2	KRO2NO3	Rickard and Pascoe (2009)
G45042	TrGCN	NISOPOOH + OH → NC4CHO + OH	1.03E-10	Rickard and Pascoe (2009)
G45043	TrGCN	NC4CHO + OH → LNISO3	(k_adt+k_ads)*a_CHO*a_CH2ONO2	Sander et al. (2019)*
G45044	TrGCN	NC4CHO + O_3 → .27 NOA + .027 $HCOCO_2H$ + .0162 GLYOX + .0162 H_2O_2 + .1458 HCOCO + .0405 HCOOH + .0405 CO + .8758 OH + .365 MGLYOX + .73 NO_2 + 0.7705 HCHO + .4055 CO_2 + .73 GLYOX	2.40E-17	Sander et al. (2019)
G45045	TrGCN	NC4CHO + NO_3 → LNISO3 + HNO_3	KNO3AL*4.25	Rickard and Pascoe (2009)
G45046	TrGCN	LNISO3 + HO_2 → LNISOOH	0.5*k_RO2_HO2(temp,5)+0.5*KAPHO2	Rickard and Pascoe (2009)
G45047	TrGCN	LNISO3 + NO → NOA + .5 HOCHCHO + .5 CO + .5 HO_2 + NO_2 + .5 CO_2	0.5*KAPNO+0.5*KRO2NO	Rickard and Pascoe (2009)*
G45048	TrGCN	LNISO3 + NO_3 → NOA + .5 HOCHCHO + .5 CO + .5 HO_2 + NO_2 + .5 CO_2	KRO2NO3*1.37	Rickard and Pascoe (2009)
G45049	TrGCN	LNISOOH + OH → LNISO3	2.65E-11	Rickard and Pascoe (2009)
G45050a	TrGC	LHC4ACCHO + OH → LC578O2	(k_adtertprim+k_ads)*a_CHO*a_CH2OH	Sander et al. (2019)
G45050b	TrGC	LHC4ACCHO + OH → LHC4ACCO3	k_t*f_0	Sander et al. (2019)
G45050c	TrGC	LHC4ACCHO + OH → C4MDIAL + HO_2	k_s*f_sOH*f_allyl	Sander et al. (2019)

Table 1: Gas phase reactions (... continued)

#	labels	reaction	rate coefficient	reference
G45051	TrGC	LHC4ACCHO + O_3 → .2225 $CH_3C(O)$ + .89 CO + .0171875 $HOCH_2CO_2H$ + .075625 H_2O_2 + .0171875 $HCOCO_2H$ + .2775 CH_3COCH_2OH + .6675 HO_2 + .2603125 GLYOX + .2225 HCHO + .89 OH + .2603125 $HOCH_2CHO$ + .5 MGLYOX	2.40E-17	Rickard and Pascoe (2009)
G45052	TrGCN	LHC4ACCHO + NO_3 → LHC4ACCO3 + HNO_3	KNO3AL*4.25	Rickard and Pascoe (2009)
G45053	TrGC	LC578O2 → .25 CH_3COCH_2OH + .75 MGLYOX + .25 HOCHCHO + .75 $HOCH_2CHO$ + .75 HO_2	k1_RO2tORO2	Rickard and Pascoe (2009)
G45054a	TrGC	LC578O2 + HO_2 → MGLYOX + $HOCH_2CHO$ + OH	k_RO2_HO2(temp,5)*r_COCH2O2_OH	Rickard and Pascoe (2009)
G45054b	TrGC	LC578O2 + HO_2 → LC578OOH	k_RO2_HO2(temp,5)*r_COCH2O2_OOH	Rickard and Pascoe (2009)
G45055	TrGCN	LC578O2 + NO → .25 CH_3COCH_2OH + .75 MGLYOX + .25 HOCHCHO + .75 $HOCH_2CHO$ + .75 HO_2 + NO_2	KRO2NO	Rickard and Pascoe (2009)*
G45056	TrGCN	LC578O2 + NO_3 → .25 CH_3COCH_2OH + .75 MGLYOX + .25 HOCHCHO + .75 $HOCH_2CHO$ + .75 HO_2 + NO_2	KRO2NO3	Rickard and Pascoe (2009)
G45057	TrGC	LC578O2 → .25 CH_3COCH_2OH + .75 MGLYOX + .25 $HOCH_2CHO$ + .75 $HOCH_2CHO$ + HO_2 + OH	k_hsb	Sander et al. (2019)
G45058a	TrGC	LC578OOH + OH → LC578O2	k_ROOHRO	Sander et al. (2019)
G45058b	TrGC	LC578OOH + OH → C1ODC2OOHC4OD + HO_2	k_t*f_O*f_tCH2OH*f_alk+k_t*f_tOH*f_pCH2OH*f_pCH2OH+k_s*f_sOH*f_pCH2OH	Sander et al. (2019)
G45059a	TrGC	LHC4ACCO3 → OH + .5 MACRO2 + .5 LHMVKABO2 + CO_2	k1_RO2RCO3*0.9	Sander et al. (2019)
G45059b	TrGC	LHC4ACCO3 → LHC4ACCO2H	k1_RO2RCO3*0.1	Sander et al. (2019)
G45060a	TrGC	LHC4ACCO3 + HO_2 → 2 OH + .5 MACRO2 + .5 LHMVKABO2 + CO_2	KAPHO2*r_CO3_OH	Sander et al. (2019)
G45060b	TrGC	LHC4ACCO3 + HO_2 → LHC4ACCO3H	KAPHO2*r_CO3_OOH	Sander et al. (2019)
G45060c	TrGC	LHC4ACCO3 + HO_2 → LHC4ACCO2H + O_3	KAPHO2*r_CO3_O3	Sander et al. (2019)
G45061	TrGCN	LHC4ACCO3 + NO → .5 MACRO2 + .5 LHMVKABO2 + NO_2 + CO_2	KAPNO	Sander et al. (2019)
G45062	TrGCN	LHC4ACCO3 + NO_2 → LC5PAN1719	k_CH3CO3_NO2	Rickard and Pascoe (2009)
G45063	TrGCN	LHC4ACCO3 + NO_3 → .5 MACRO2 + .5 LHMVKABO2 + NO_2 + CO_2	KRO2NO3*1.74	Sander et al. (2019)
G45064a	TrGC	LHC4ACCO2H + OH → OH + .5 MACRO2 + .5 LHMVKABO2 + CO_2	2.52E-11	Sander et al. (2019)
G45064b	TrGC	LHC4ACCO3H + OH → LHC4ACCO3	2.88E-11	Rickard and Pascoe (2009)

Table 1: Gas phase reactions (... continued)

#	labels	reaction	rate coefficient	reference
G45065	TrGCN	LC5PAN1719 → LHC4ACCO3 + NO_2	k_PAN_M	Rickard and Pascoe (2009)
G45066	TrGCN	LC5PAN1719 + OH → .5 MACROH + .5 HO12CO3C4 + CO + NO_2	2.52E-11	Rickard and Pascoe (2009)
G45067	TrGC	HCOC5 + OH → C59O2	3.81E-11	Rickard and Pascoe (2009)
G45068	TrGC	HCOC5 + O_3 → BIACETOH + .335 H_2O_2 + .67 HCHO + .2079 CO + .1221 CH_2OO + .05280 OH	7.51E-16*EXP(-1521./temp)	Sander et al. (2019)
G45069	TrGC	C59O2 → CH_3COCH_2OH + HOCH2CO	k1_RO2tORO2	Sander et al. (2019)
G45070a	TrGC	C59O2 + HO_2 → OH + CH_3COCH_2OH + HOCH2CO	k_RO2_HO2(temp,5)*r_COCH2O2_OH	Sander et al. (2019)
G45070b	TrGC	C59O2 + HO_2 → C59OOH	k_RO2_HO2(temp,5)*r_COCH2O2_OOH	Sander et al. (2019)
G45071	TrGCN	C59O2 + NO → CH_3COCH_2OH + HOCH2CO + NO_2	KRO2NO	Sander et al. (2019)*
G45072	TrGCN	C59O2 + NO_3 → CH_3COCH_2OH + HOCH2CO + NO_2	KRO2NO3	Sander et al. (2019)
G45073	TrGC	C59OOH + OH → C59O2	9.7E-12	Rickard and Pascoe (2009)
G45074	TrGC	LIEPOX + OH → DB1O2 + H_2O	5.78E-11*EXP(-400./temp) *(1.52/3.+0.98*2./3.)/1.51	Paulot et al. (2009b), Bates et al. (2014), Sander et al. (2019)*
G45075	TrGC	ISOPBO2 → MVK + HCHO + OH	k_hsb	Sander et al. (2019)
G45076	TrGC	ISOPDO2 → MACR + HCHO + OH	k_hsd	Sander et al. (2019)
G45077a	TrGC	LZCODC23DBCOOH + OH → .6 C1ODC2O2C4OOH + .4 C1OOHC2O2C4OD	k_adt*a_CHO*a_CH2OOH	Sander et al. (2019)
G45077b	TrGC	LZCODC23DBCOOH + OH → .6 C1ODC3O2C4OOH + .4 C1OOHC3O2C4OD	k_ads*a_CHO*a_CH2OOH	Sander et al. (2019)
G45077c	TrGC	LZCODC23DBCOOH + OH → LZCO3HC23DBCOD	k_t*f_O*f_alk+k_ROOHRO	Sander et al. (2019)
G45077d	TrGC	LZCODC23DBCOOH + OH → C4MDIAL + OH	k_s*f_sOOH*f_allyl	Sander et al. (2019)
G45078	TrGC	LZCODC23DBCOOH + O_3 → .4672 OH + .2336 $HCOCOCH_2O_2$ + .2336 CO + .2336 $CH_3C(O)$ + .4672 HOOCH2CHO + .1728 MGLYOX + .1901 OH + .0864 GLYOX + .02765 HOOCH2CHO + .02765 H_2O_2 + .02592 CH_3OOH + .02592 CO_2 + .01037 HCOCO + .01555 CH_2OO + .01555 CO + .006908 $HOOCH_2CO_3$ + .2628 OH + .1314 MGLYOX + .1314 OH + .1314 $HCOCOCH_2OOH$ + .2628 GLYOX + .0972 $CH_3COCH_2O_2H$ + .00972 $HCOCO_3H$ + .005832 GLYOX + .005832 H_2O_2 + .05249 OH + .05249 HCOCO + .01458 HCHO + .01458 CO_2 + .01458 HCOOH + .01458 CO	2.4E-17	Sander et al. (2019)
G45079	TrGC	C1OOHC2O2C4OD → .78 $CH_3COCH_2O_2H$ + .78 HOCHCHO + .22 CO2H3CHO + .22 HCHO + .22 OH	k1_RO2tORO2	Sander et al. (2019)

Table 1: Gas phase reactions (... continued)

#	labels	reaction	rate coefficient	reference
G45080	TrGCN	C1OOHC2O2C4OD + NO → .78 $CH_3COCH_2O_2H$ + .78 HOCHCHO + .22 CO2H3CHO + .22 HCHO + .22 OH + NO_2	KRO2NO	Sander et al. (2019)*
G45081a	TrGC	C1OOHC2O2C4OD + HO_2 → C1OOHC2OOHC4OD	k_RO2_HO2(temp,5)*r_COCH2O2_OOH	Sander et al. (2019)
G45081b	TrGC	C1OOHC2O2C4OD + HO_2 → .78 $CH_3COCH_2O_2H$ + .78 HOCHCHO + .22 CO2H3CHO + .22 HCHO + 1.22 OH	k_RO2_HO2(temp,5)*r_COCH2O2_OH	Sander et al. (2019)
G45082	TrGC	C1OOHC2O2C4OD → $CH_3COCH_2O_2H$ + GLYOX + OH	k_hsb	Sander et al. (2019)
G45083	TrGC	C1ODC2O2C4OOH → OH + C1ODC2OOHC4OD	k_15hsdhb	Sander et al. (2019)
G45084a	TrGC	C1OOHC2OOHC4OD + OH → C1ODC2OOHC4OD + OH	2.*k_s*f_sOOH*f_tCH2OH	Sander et al. (2019)
G45084b	TrGC	C1OOHC2OOHC4OD + OH → $CH_3COCH_2O_2H$ + 2 CO + 2 HO_2 + OH	k_t*f_tOH*f_pCH2OH*f_pCH2OH	Sander et al. (2019)
G45084c	TrGC	C1OOHC2OOHC4OD + OH → C1OOHC2O2C4OD	k_ROOHRO	Sander et al. (2019)
G45085	TrGC	C1ODC2OOHC4OD + OH → CO2H3CHO + CO + H_2O + OH	k_t*f_O*f_tCH2OH+k_t*f_tOH*f_tOH*f_CHO	Sander et al. (2019)
G45086	TrGC	C1ODC3O2C4OOH → MGLYOX + HOOCH2CHO + HO_2	k1_RO2sORO2	Sander et al. (2019)
G45087	TrGCN	C1ODC3O2C4OOH + NO → MGLYOX + HOOCH2CHO + HO_2 + NO_2	KRO2NO	Sander et al. (2019)
G45088	TrGC	C1ODC3O2C4OOH + HO_2 → .5 $CH_3C(O)$ + .5 CO + .5 MGLYOX + .5 HO_2 + $HOOCH_2CO_3$	k_RO2_HO2(temp,5)	Sander et al. (2019)
G45089	TrGC	C1ODC3O2C4OOH → MGLYOX + OH + HOOCH2CHO	k_hsd	Sander et al. (2019)
G45090	TrGC	C1OOHC3O2C4OD → .625 MGLYOX + 2 CO + 1.625 HO_2 + .375 $CH_3C(O)$ + .375 CO_2 + OH	k_15hsdhb	Sander et al. (2019)
G45091	TrGC	LHC4ACCO3 → LZCO3HC23DBCOD + HO_2	k_16hs	Sander et al. (2019)
G45092a	TrGC	C4MDIAL + OH → C1ODC2O2C4OD	(k_adt+k_ads)*a_CHO*a_CHO	Sander et al. (2019)*
G45092b	TrGC	C4MDIAL + OH → LZCO3C23DBCOD	2.*k_t*f_O*f_alk	Sander et al. (2019)*
G45093	TrGCN	C4MDIAL + NO_3 → LZCO3C23DBCOD + HNO_3	KNO3AL*4.25*2.	Sander et al. (2019)*
G45094a	TrGC	C1ODC2O2C4OD + HO_2 → OH + MGLYOX + HOCHCHO	k_RO2_HO2(temp,5)*r_COCH2O2_OH	Sander et al. (2019)
G45094b	TrGC	C1ODC2O2C4OD + HO_2 → C1ODC2OOHC4OD	k_RO2_HO2(temp,5)*r_COCH2O2_OOH	Sander et al. (2019)
G45095	TrGCN	C1ODC2O2C4OD + NO → NO_2 + MGLYOX + HOCHCHO	KRO2NO	Sander et al. (2019)*
G45096	TrGC	C1ODC2O2C4OD → MGLYOX + HOCHCHO	k1_RO2tORO2	Sander et al. (2019)

Table 1: Gas phase reactions (... continued)

#	labels	reaction	rate coefficient	reference
G45097a	TrGC	C1ODC2OOHC4OD + OH → MGLYOX + 2 CO	(2.*k_t*f_O*f_tCH2OH*f_alk+k_t*f_tOH*f_CHO*f_pCH2OH)*.5	Sander et al. (2019)
G45097b	TrGC	C1ODC2OOHC4OD + OH → MGLYOX + 2 CO + OH	(2.*k_t*f_O*f_tCH2OH*f_alk+k_t*f_tOH*f_CHO*f_pCH2OH)*.5	Sander et al. (2019)
G45098	TrGCN	LISOPACNO3O2 + NO → .21 NOA + .21 $HOCH_2CHO$ + .21 HO_2 + .49 HO12CO3C4 + .49 HCHO + .49 NO_2 + .045 MVKNO3 + .045 HCHO + .255 CH_3COCH_2OH + .255 $NO_3CH2CHO$ + .225 H_2O_2 + NO_2	KRO2NO	Sander et al. (2019)*
G45099	TrGCN	LISOPACNO3O2 → .21 NOA + .21 $HOCH_2CHO$ + .21 HO_2 + .49 HO12CO3C4 + .49 HCHO + .49 NO_2 + .045 MVKNO3 + .045 HCHO + .255 CH_3COCH_2OH + .255 $NO_3CH2CHO$ + .225 H_2O_2	k1_RO2tORO2+k_RO2_HO2(temp,5)*c(ind_HO2)	Sander et al. (2019)
G45100	TrGCN	ISOPBDNO3O2 + NO → .6 CH_3COCH_2OH + .6 $HOCH_2CHO$ + .26 MACRNO3 + .14 MVKNO3 + .4 HCHO + .4 HO_2 + 1.6 NO_2	KRO2NO	Sander et al. (2019)*
G45101	TrGCN	ISOPBDNO3O2 → .6 CH_3COCH_2OH + .6 $HOCH_2CHO$ + .26 MACRNO3 + .14 MVKNO3 + .4 HCHO + .4 HO_2 + .6 NO_2	k1_RO2sORO2+k_RO2_HO2(temp,5)*c(ind_HO2)	Sander et al. (2019)
G45102	TrGCN	LISOPACNO3 + O_3 → .8704 OH + .365 HO_2 + .73 MGLYOX + .4325 $NO_3CH2CHO$ + .135 CH_3COCH_2OH + .0675 GLYOX + .4325 NO_2 + .0891 H_2O_2 + .135 NOA + .0675 HOCHCHO + .3866 $HOCH_2CHO$ + .0405 CH_3OH + .0405 CO + .0054 HOCH2CO	2.8E-17	Feierabend et al. (2008), Sander et al. (2019)
G45103	TrGC	DB1O2 → DB1O2	k1_RO2sORO2	Sander et al. (2019)
G45104a	TrGC	DB1O2 + HO_2 → DB1OOH	k_RO2_HO2(temp,5)*(1.-r_CHOHCH2O2_OH)	Sander et al. (2019)*
G45104b	TrGC	DB1O2 + HO_2 → DB1O2 + OH	k_RO2_HO2(temp,5)*r_CHOHCH2O2_OH	Sander et al. (2019)
G45105a	TrGCN	DB1O2 + NO → DB1O2 + NO_2	KRO2NO*(1.-alpha_AN(7,2,0,0,0,temp,cair))	Sander et al. (2019)
G45105b	TrGCN	DB1O2 + NO → DB1NO3	KRO2NO*alpha_AN(7,2,0,0,0,temp,cair)	Sander et al. (2019)
G45106	TrGCN	DB1O2 + NO_3 → DB1O2 + NO_2	KRO2NO3	Sander et al. (2019)
G45107	TrGC	DB1O2 → DB1O2 + OH	1.E4	Peeters and Nguyen (2012)*
G45108a	TrGC	DB1O2 → DB1O2	KDEC*0.72	see note*
G45108b	TrGC	DB1O2 → .5 HVMK + .5 HMAC + HCHO + HO_2	KDEC*0.28	see note*

Table 1: Gas phase reactions (... continued)

#	labels	reaction	rate coefficient	reference
G45109	TrGC	DB1O2 → .48 CH_3COCH_2OH + .52 $HOCH_2CHO$ + .52 MGLYOX + .48 GLYOX + HO_2	k1_RO2sORO2	Sander et al. (2019)
G45110a	TrGC	DB1O2 + HO_2 → DB2OOH	k_RO2_HO2(temp,5)*(1.-r_CHOHCH2O2_OH)	Sander et al. (2019)
G45110b	TrGC	DB1O2 + HO_2 → .48 CH_3COCH_2OH + .52 $HOCH_2CHO$ + .52 MGLYOX + .48 GLYOX + HO_2 + OH	k_RO2_HO2(temp,5)*r_CHOHCH2O2_OH	Sander et al. (2019)
G45111	TrGCN	DB1O2 + NO → .48 CH_3COCH_2OH + .52 $HOCH_2CHO$ + .52 MGLYOX + .48 GLYOX + HO_2 + NO_2	KRO2NO	see note*
G45112	TrGCN	DB1O2 + NO_3 → .48 CH_3COCH_2OH + .52 $HOCH_2CHO$ + .52 MGLYOX + .48 GLYOX + HO_2 + NO_2	KRO2NO3	Sander et al. (2019)
G45113	TrGC	DB1O2 → .48 MACROOH + .52 LHMVKABOOH + CO + OH	k_14hsal	Sander et al. (2019)
G45114a	TrGC	DB1OOH + OH → DB1O2	k_ROOHRO	Sander et al. (2019)
G45114b	TrGC	DB1OOH + OH → HCOOH + HO_2 + CH_3COCHO_2CHO	k_adt	Sander et al. (2019)*
G45115	TrGC	DB1OOH + HCOOH → C1ODC2OOHC4OD + HCOOH	4.67E-26*(temp)**(3.286)*EXP(4509./(1.987*temp))	Sander et al. (2019), da Silva (2010)*
G45116	TrGCN	DB1NO3 + OH → HCOOH + NO_2 + CH_3COCHO_2CHO	k_adt	Sander et al. (2019)*
G45117	TrGC	DB2OOH + OH → DB1O2	k_ROOHRO	Sander et al. (2019)*
G45118	TrGC	LISOPACOOH + O_3 → 1.3272 OH + .36986 HO_2 + .0432 H_2O_2 + .08422 CO + .2025 CH_3OOH + .01215 CH_2OO + .3704 HCHO + .00405 CH_3OH + .0405 CO_2 + .1825 HOCH2COCH2O2 + .365 MGLYOX + .3866 HOOCH2CHO + .135 CH_3COCH_2OH + .0675 GLYOX + .00324 HCOCO + .3866 $HOCH_2CHO$ + .135 $CH_3COCH_2O_2H$ + .0675 HOCHCHO + .0054 HOCH2CO	4.829E-16	Sander et al. (2019)
G45119a	TrGC	LZCO3HC23DBCOD + OH → .62 CO2H3CHO + .62 OH + .62 CO_2 + .38 MGLYOX + .38 $HCOCO_3H$ + .38 HO_2	k_adt*a_CHO*a_CO2H	Sander et al. (2019)
G45119b	TrGC	LZCO3HC23DBCOD + OH → .62 CH_3COCO_3H + 1.24 CO + 1.24 HO_2 + .38 MGLYOX + .38 HO_2 + .38 CO + .38 HO_2 + .38 OH + .38 CO_2	k_ads*a_CHO*a_CO2H	Sander et al. (2019)
G45120	TrGC	LISOPEFO2 → LISOPEFO	k1_RO2pORO2	Sander et al. (2019)
G45121a	TrGCN	LISOPEFO2 + NO → LISOPEFO + NO_2	KRO2NO*(1.-alpha_AN(6,1,0,0,0,temp,cair))	Sander et al. (2019)
G45121b	TrGCN	LISOPEFO2 + NO → ISOPDNO3	KRO2NO*alpha_AN(6,1,0,0,0,temp,cair)	Sander et al. (2019)*

Table 1: Gas phase reactions (... continued)

#	labels	reaction	rate coefficient	reference
G45122a	TrGC	LISOPEFO2 + HO_2 → .7143 ISOPDOOH + .2857 ISOPBOOH	k_RO2_HO2(temp,5)*(1.-r_CHOHCH2O2_OH)	Sander et al. (2019)
G45122b	TrGC	LISOPEFO2 + HO_2 → LISOPEFO + OH	k_RO2_HO2(temp,5)*r_CHOHCH2O2_OH	Sander et al. (2019)
G45123	TrGCN	LISOPEFO2 + NO_3 → LISOPEFO + NO_2	KRO2NO3	Sander et al. (2019)
G45124	TrGC	LISOPEFO2 → .7143 MACR + .2857 MVK + HCHO + OH	0.7143*k_hsd+.2857*k_hsb	Sander et al. (2019)
G45125	TrGC	LISOPEFO → .7143 MACR + .2857 MVK + HCHO + HO_2	KDEC	Sander et al. (2019)
G45126a	TrGC	LISOPACO → 3METHYLFURAN + HO_2	KDEC*0.37	Sander et al. (2019), Paulot et al. (2009a), Francisco-Marquez et al. (2003)
G45126b	TrGC	LISOPACO → .65 LHC4ACCHO + .65 HO_2 + .35 DB1O2	KDEC*(1.-0.37)	Sander et al. (2019), Paulot et al. (2009a), Francisco-Marquez et al. (2003)
G45127a	TrGC	LISOPACO → 3METHYLFURAN + HO_2	KDEC*0.37	Sander et al. (2019), Paulot et al. (2009a), Francisco-Marquez et al. (2003)
G45127b	TrGC	LISOPACO → .65 LHC4ACCHO + .65 HO_2 + .35 DB1O2	KDEC*(1.-0.37)	Sander et al. (2019), Paulot et al. (2009a), Francisco-Marquez et al. (2003)
G45128	TrGC	3METHYLFURAN + OH → L3METHYLFURANO2	3.2E-11*EXP(310./temp)	Sander et al. (2019)*
G45129	TrGCN	3METHYLFURAN + NO_3 → L3METHYLFURANO2 + NO_2	1.9E-11	Sander et al. (2019), Atkinson et al. (2006)*
G45130	TrGC	L3METHYLFURANO2 → C4MDIAL + HO_2	k1_RO2sORO2	Sander et al. (2019)
G45131	TrGCN	L3METHYLFURANO2 + NO → C4MDIAL + HO_2 + NO_2	KRO2NO	Sander et al. (2019)*
G45132	TrGC	L3METHYLFURANO2 + HO_2 → C4MDIAL + HO_2	k_RO2_HO2(temp,5)	Sander et al. (2019)*
G45133	TrGC	LZCO3C23DBCOD → .62 EZCH3CO2CHCHO + .38 EZCHOCCH3CHO2 + CO_2	k1_RO2RCO3	Sander et al. (2019)
G45134a	TrGC	LZCO3C23DBCOD + HO_2 → .62 EZCH3CO2CHCHO + .38 EZCHOCCH3CHO2 + CO_2 + OH	KAPHO2*r_CO3_OH	Sander et al. (2019)
G45134b	TrGC	LZCO3C23DBCOD + HO_2 → LZCO3HC23DBCOD	KAPHO2*(r_CO3_OOH+r_CO3_O3)	Sander et al. (2019)*
G45135	TrGCN	LZCO3C23DBCOD + NO → .62 EZCH3CO2CHCHO + .38 EZCHOCCH3CHO2 + CO_2 + NO_2	KAPNO	Sander et al. (2019)
G45136	TrGCN	LZCO3C23DBCOD + NO_2 → LZCPANC23DBCOD	k_CH3CO3_NO2	Rickard and Pascoe (2009)

Table 1: Gas phase reactions (... continued)

#	labels	reaction	rate coefficient	reference
G45137	TrGCN	LZCO3C23DBCOD + NO_3 → .62 EZCH3CO2CHCHO + .38 EZCHOCCH3CHO2 + CO_2 + NO_2	KRO2NO3*1.74	Sander et al. (2019)
G45138	TrGCN	LZCPANC23DBCOD → LZCO3C23DBCOD + NO_2	k_PAN_M	Rickard and Pascoe (2009)
G45139	TrGCN	LZCPANC23DBCOD + OH → .62 EZCH3CO2CHCHO + .38 EZCHOCCH3CHO2 + CO_2 + NO_2	2.52E-11	Sander et al. (2019)*
G45200	TrGTerC	C511O2 → $CH_3C(O)$ + HCOCH2CHO	k1_RO2sORO2	Rickard and Pascoe (2009)
G45201	TrGTerCN	C511O2 + NO → $CH_3C(O)$ + HCOCH2CHO + NO_2	KRO2NO	Rickard and Pascoe (2009)*
G45202a	TrGTerC	C511O2 + HO_2 → C511OOH	k_RO2_HO2(temp,5)*r_COCH2O2_OOH	Rickard and Pascoe (2009), Sander et al. (2019)
G45202b	TrGTerC	C511O2 + HO_2 → $CH_3C(O)$ + HCOCH2CHO + OH	k_RO2_HO2(temp,5)*r_COCH2O2_OH	Rickard and Pascoe (2009), Sander et al. (2019)
G45203	TrGTerC	C511OOH + OH → C511O2	7.49E-11	Rickard and Pascoe (2009)
G45204	TrGTerC	CO23C4CHO + OH → CO23C4CO3	6.65E-11	Rickard and Pascoe (2009)
G45205	TrGTerCN	CO23C4CHO + NO_3 → CO23C4CO3 + HNO_3	KNO3AL*5.5	Rickard and Pascoe (2009)
G45206	TrGTerC	CO23C4CO3 → $CH_3COCOCH_2O_2$ + CO_2	k1_RO2RCO3	Rickard and Pascoe (2009)
G45207	TrGTerCN	CO23C4CO3 + NO → $CH_3COCOCH_2O_2$ + CO_2 + NO_2	KAPNO	Rickard and Pascoe (2009)*
G45208	TrGTerCN	CO23C4CO3 + NO_2 → C5PAN9	k_CH3CO3_NO2	Rickard and Pascoe (2009)
G45209a	TrGTerC	CO23C4CO3 + HO_2 → CO23C4CO3H	KAPHO2*(r_CO3_OOH+r_CO3_O3)	Rickard and Pascoe (2009)
G45209b	TrGTerC	CO23C4CO3 + HO_2 → $CH_3COCOCH_2O_2$ + CO_2 + OH	KAPHO2*r_CO3_OH	Rickard and Pascoe (2009)
G45210	TrGTerCN	C5PAN9 → CO23C4CO3 + NO_2	k_PAN_M	Rickard and Pascoe (2009)
G45211	TrGTerCN	C5PAN9 + OH → $CH_3COCOCHO$ + CO + NO_2	3.12E-13	Rickard and Pascoe (2009)
G45212	TrGTerC	C512O2 → C513O2	k1_RO2pRO2	Rickard and Pascoe (2009)
G45213	TrGTerC	C512O2 + HO_2 → C512OOH	k_RO2_HO2(temp,5)	Rickard and Pascoe (2009)
G45214	TrGTerCN	C512O2 + NO → C513O2 + NO_2	KRO2NO	Rickard and Pascoe (2009)*
G45215	TrGTerC	C512OOH + OH → CO13C4CHO + OH	1.01E-10	Rickard and Pascoe (2009)
G45216	TrGTerC	C513O2 → GLYOX + $HOC_2H_4CO_3$	k1_RO2sORO2	Rickard and Pascoe (2009)
G45217	TrGTerCN	C513O2 + NO → GLYOX + $HOC_2H_4CO_3$ + NO_2	KRO2NO	Rickard and Pascoe (2009)*
G45218a	TrGTerC	C513O2 + HO_2 → C513OOH	k_RO2_HO2(temp,5)*r_COCH2O2_OOH	Rickard and Pascoe (2009), Sander et al. (2019)
G45218b	TrGTerC	C513O2 + HO_2 → GLYOX + $HOC_2H_4CO_3$ + OH	k_RO2_HO2(temp,5)*r_COCH2O2_OH	Rickard and Pascoe (2009), Sander et al. (2019)
G45219	TrGTerC	CO13C4CHO + OH → CHOC3COCO3	1.33E-10	Rickard and Pascoe (2009)
G45220	TrGTerCN	CO13C4CHO + NO_3 → CHOC3COCO3 + HNO_3	2.*KNO3AL*5.5	Rickard and Pascoe (2009)
G45221	TrGTerC	C513OOH + OH → C513CO + OH	9.23E-11	Rickard and Pascoe (2009)
G45222	TrGTerC	CHOC3COCO3 → CHOC3COO2 + CO_2	k1_RO2RCO3	Rickard and Pascoe (2009)

Table 1: Gas phase reactions (... continued)

#	labels	reaction	rate coefficient	reference
G45223	TrGTerC	CHOC3COCO3 + HO_2 → CHOC3COOOH	KAPHO2	Rickard and Pascoe (2009)
G45224	TrGTerCN	CHOC3COCO3 + NO_2 → CHOC3COPAN	k_CH3CO3_NO2	Rickard and Pascoe (2009)
G45225	TrGTerCN	CHOC3COCO3 + NO → CHOC3COO2 + CO_2 + NO_2	KAPNO	Rickard and Pascoe (2009)*
G45226	TrGTerC	C513CO + OH → $HOC_2H_4CO_3$ + CO + CO	2.64E-11	Rickard and Pascoe (2009)
G45227	TrGTerC	C514O2 + HO_2 → C514OOH	k_RO2_HO2(temp,5)	Rickard and Pascoe (2009)
G45228a	TrGTerCN	C514O2 + NO → CO13C4CHO + HO_2 + NO_2	KRO2NO*(1.-alpha_AN(7,2,0,1,0,temp,cair))	Rickard and Pascoe (2009), Sander et al. (2019)
G45228b	TrGTerCN	C514O2 + NO → C514NO3	KRO2NO*alpha_AN(7,2,0,1,0,temp,cair)	Rickard and Pascoe (2009), Sander et al. (2019)
G45229	TrGTerCN	C514O2 + NO_3 → CO13C4CHO + HO_2 + NO_2	KRO2NO3	Rickard and Pascoe (2009)
G45230	TrGTerC	C514O2 → CO13C4CHO + HO_2	k1_RO2sRO2	Rickard and Pascoe (2009)
G45231	TrGTerC	C514OOH + OH → CO13C4CHO + OH	1.10E-10	Rickard and Pascoe (2009)
G45232	TrGTerCN	C514NO3 + OH → CO13C4CHO + NO_2	4.33E-11	Rickard and Pascoe (2009)
G45233	TrGTerC	CHOC3COOOH + OH → CHOC3COCO3	7.55E-11	Rickard and Pascoe (2009)
G45234	TrGTerCN	CHOC3COPAN → CHOC3COCO3 + NO_2	k_PAN_M	Rickard and Pascoe (2009)
G45235	TrGTerCN	CHOC3COPAN + OH → C4CODIAL + CO + NO_2	7.19E-11	Rickard and Pascoe (2009)
G45236	TrGTerC	MBO + OH → LMBOABO2	8.1E-12*EXP(610./temp)	Rickard and Pascoe (2009), Sander et al. (2019)*
G45237a	TrGTerC	MBO + O_3 → HCHO + .16 CH_3COCH_3 + .16 HO_2 + .16 CO + .16 OH + .84 MBOOO	1.0E-17*0.57	Rickard and Pascoe (2009), Sander et al. (2019)
G45237b	TrGTerC	MBO + O_3 → IBUTALOH + .63 CO + .37 $HOCH_2OOH$ + .16 OH + .16 HO_2	1.0E-17*0.43	Rickard and Pascoe (2009), Sander et al. (2019)
G45238	TrGTerCN	MBO + NO_3 → LNMBOABO2	4.6E-14*EXP(-400./temp)	Rickard and Pascoe (2009), Sander et al. (2019)
G45239	TrGTerC	LMBOABO2 + HO_2 → LMBOABOOH	k_RO2_HO2(temp,5)	Rickard and Pascoe (2009), Sander et al. (2019)
G45240a	TrGTerCN	LMBOABO2 + NO → LMBOABNO3	KRO2NO*(.67*alpha_AN(7,2,0,0,0,temp,cair)+.33*alpha_AN(7,1,0,0,0,temp,cair))	Rickard and Pascoe (2009), Sander et al. (2019)
G45240b	TrGTerCN	LMBOABO2 + NO → $HOCH_2CHO$ + CH_3COCH_3 + HO_2 + NO_2	KRO2NO*(1.-(.67*alpha_AN(7,2,0,0,0,temp,cair)+.33*alpha_AN(7,1,0,0,0,temp,cair)))*.67	Rickard and Pascoe (2009), Sander et al. (2019)
G45240c	TrGTerCN	LMBOABO2 + NO → IBUTALOH + HCHO + HO_2 + NO_2	KRO2NO*(1.-(.67*alpha_AN(7,2,0,0,0,temp,cair)+.33*alpha_AN(7,1,0,0,0,temp,cair)))*.33	Rickard and Pascoe (2009), Sander et al. (2019)

Table 1: Gas phase reactions (... continued)

#	labels	reaction	rate coefficient	reference
G45241a	TrGTerC	LMBOABO2 → $HOCH_2CHO + CH_3COCH_3 + HO_2$	k1_RO2sORO2*.67	Rickard and Pascoe (2009), Sander et al. (2019)
G45241b	TrGTerC	LMBOABO2 → IBUTALOH + HCHO + HO_2	k1_RO2pORO2*.33	Rickard and Pascoe (2009), Sander et al. (2019)
G45242a	TrGTerC	LMBOABOOH + OH → MBOACO	0.67*2.93E-11+.33*2.05E-12	Rickard and Pascoe (2009), Sander et al. (2019)
G45242b	TrGTerC	LMBOABOOH + OH → LMBOABO2	k_ROOHRO	Rickard and Pascoe (2009), Sander et al. (2019)
G45243	TrGTerCN	LMBOABNO3 + OH → MBOACO + NO_2	0.67*1.75E-12+.33*2.69E-12	Rickard and Pascoe (2009), Sander et al. (2019)
G45244	TrGTerC	MBOACO + OH → MBOCOCO + HO_2	3.79E-12	Rickard and Pascoe (2009)
G45245	TrGTerC	MBOCOCO + OH → CO + IPRHOCO3	1.38E-11	Rickard and Pascoe (2009)
G45246	TrGTerCN	LNMBOABO2 + HO_2 → LNMBOABOOH	k_RO2_HO2(temp,5)	Rickard and Pascoe (2009), Sander et al. (2019)
G45247	TrGTerCN	LNMBOABO2 + NO → .65 $NO_3CH2CHO$ + .65 CH_3COCH_3 + .65 HO_2 + .35 IBUTALOH + .35 HCHO + .35 NO_2 + NO_2	KRO2NO	Rickard and Pascoe (2009), Sander et al. (2019)*
G45248	TrGTerCN	LNMBOABO2 + NO_3 → .65 $NO_3CH2CHO$ + .65 CH_3COCH_3 + .65 HO_2 + .35 IBUTALOH + .35 HCHO + .35 NO_2 + NO_2	KRO2NO3	Rickard and Pascoe (2009), Sander et al. (2019)
G45249	TrGTerCN	LNMBOABO2 → .65 $NO_3CH2CHO$ + .65 CH_3COCH_3 + .65 HO_2 + .35 IBUTALOH + .35 HCHO + .35 NO_2	k1_RO2sORO2	Rickard and Pascoe (2009), Sander et al. (2019)
G45250a	TrGTerCN	LNMBOABOOH + OH → .65 C4MCONO3OH + .35 NMBOBCO	0.65*4.89E-12+.35*2.52E-12	Rickard and Pascoe (2009), Sander et al. (2019)
G45250b	TrGTerCN	LNMBOABOOH + OH → LNMBOABO2	k_ROOHRO	Rickard and Pascoe (2009), Sander et al. (2019)
G45251	TrGTerCN	NMBOBCO + OH → NC4OHCO3	4.26E-12	Rickard and Pascoe (2009)
G45252a	TrGTerCN	NC4OHCO3 + HO_2 → IBUTALOH + CO_2 + NO_2 + OH	KAPHO2*r_CO3_OH	Rickard and Pascoe (2009), Sander et al. (2019)
G45252b	TrGTerCN	NC4OHCO3 + HO_2 → NC4OHCO3H	KAPHO2*(r_CO3_O3+r_CO3_OOH)	Rickard and Pascoe (2009), Sander et al. (2019)
G45253	TrGTerCN	NC4OHCO3 + NO → IBUTALOH + CO_2 + NO_2 + NO_2	KAPNO	Rickard and Pascoe (2009)
G45254	TrGTerCN	NC4OHCO3 + NO_2 → NC4OHCPAN	k_CH3CO3_NO2	Rickard and Pascoe (2009)
G45255	TrGTerCN	NC4OHCO3 + NO_3 → IBUTALOH + CO_2 + NO_2 + NO_2	KRO2NO3*1.74	Rickard and Pascoe (2009)
G45256	TrGTerCN	NC4OHCO3 → IBUTALOH + CO_2 + NO_2	k1_RO2RCO3	Rickard and Pascoe (2009)

Table 1: Gas phase reactions (... continued)

#	labels	reaction	rate coefficient	reference
G45257	TrGTerCN	NC4OHCO3H + OH → NC4OHCO3	4.50E-12	Rickard and Pascoe (2009)
G45258	TrGTerCN	NC4OHCPAN + OH → IBUTALOH + CO + NO_2 + NO_2	1.27E-12	Rickard and Pascoe (2009)
G45259	TrGTerCN	NC4OHCPAN → NC4OHCO3 + NO_2	k_PAN_M	Rickard and Pascoe (2009)
G45260	TrGTerCN	C4MCONO3OH + OH → CH_3COCH_3 + HCHO + CO_2 + NO_2	1.23E-12	Rickard and Pascoe (2009), Sander et al. (2019)
G45400	TrGAroCN	NC4MDCO2HN + OH → MMALANHY + NO_2	k_ROOHRO	Rickard and Pascoe (2009)*
G45401	TrGAroCN	C54CO + NO_3 → 3 CO + $CH_3C(O)OO$ + HNO_3	KNO3AL*5.5	Rickard and Pascoe (2009)
G45402	TrGAroC	C54CO + OH → 3 CO + $CH_3C(O)OO$	1.72E-11	Rickard and Pascoe (2009)
G45403a	TrGAroCN	NTLFUO2 + HO_2 → NTLFUOOH	k_RO2_HO2(temp,5)*(1.-r_COCH2O2_OH)	Rickard and Pascoe (2009)
G45403b	TrGAroCN	NTLFUO2 + HO_2 → ACCOMECHO + NO_2 + OH	k_RO2_HO2(temp,5)*r_COCH2O2_OH	Rickard and Pascoe (2009)
G45404	TrGAroCN	NTLFUO2 + NO → ACCOMECHO + NO_2 + NO_2	KRO2NO	Rickard and Pascoe (2009)*
G45405	TrGAroCN	NTLFUO2 + NO_3 → ACCOMECHO + NO_2 + NO_2	KRO2NO3	Rickard and Pascoe (2009)*
G45406	TrGAroCN	NTLFUO2 → ACCOMECHO + NO_2	k1_RO2tORO2	Rickard and Pascoe (2009)*
G45407	TrGAroC	C5134CO2OH + OH → C54CO + HO_2	7.48E-11	Rickard and Pascoe (2009)
G45408	TrGAroCN	C5COO2NO2 + OH → MGLYOX + CO + CO + NO_2	5.43E-11	Rickard and Pascoe (2009)
G45409	TrGAroCN	C5COO2NO2 → C5CO14O2 + NO_2	k_PAN_M	Rickard and Pascoe (2009)*
G45410	TrGAroC	C5DIALOOH + OH → C5DIALCO + OH	7.52E-11	Rickard and Pascoe (2009)
G45411a	TrGAroC	C4CO2DBCO3 + HO_2 → C4CO2DCO3H	KAPHO2*(r_CO3_OOH+r_CO3_O3)	Rickard and Pascoe (2009)
G45411b	TrGAroC	C4CO2DBCO3 + HO_2 → HO_2 + CO + HCOCOCHO + CO_2 + OH	KAPHO2*r_CO3_OH	Rickard and Pascoe (2009), Sander et al. (2019)
G45412	TrGAroCN	C4CO2DBCO3 + NO → HO_2 + CO + HCOCOCHO + CO_2 + NO_2	KAPNO	Rickard and Pascoe (2009)
G45413	TrGAroCN	C4CO2DBCO3 + NO_2 → C4CO2DBPAN	k_CH3CO3_NO2	Rickard and Pascoe (2009)*
G45414	TrGAroCN	C4CO2DBCO3 + NO_3 → HO_2 + CO + HCOCOCHO + CO_2 + NO_2	KRO2NO3*1.74	Rickard and Pascoe (2009)
G45415	TrGAroC	C4CO2DBCO3 → HO_2 + CO + HCOCOCHO + CO_2	k1_RO2RCO3	Rickard and Pascoe (2009)
G45416	TrGAroC	MMALANHY + OH → MMALANHYO2	1.50E-12	Rickard and Pascoe (2009)
G45421a	TrGAroC	MMALANHYO2 + HO_2 → MMALNHYOOH	k_RO2_HO2(temp,5)*(1.-r_COCH2O2_OH-r_CHOHCH2O2_OH)	Rickard and Pascoe (2009), Sander et al. (2019)
G45421b	TrGAroC	MMALANHYO2 + HO_2 → CO2H3CO3 + CO_2 + OH	k_RO2_HO2(temp,5)*(r_COCH2O2_OH+r_CHOHCH2O2_OH)	Rickard and Pascoe (2009), Sander et al. (2019)
G45422	TrGAroCN	MMALANHYO2 + NO → CO2H3CO3 + CO_2 + NO_2	KRO2NO	Rickard and Pascoe (2009)*
G45423	TrGAroCN	MMALANHYO2 + NO_3 → CO2H3CO3 + CO_2 + NO_2	KRO2NO3	Rickard and Pascoe (2009)*
G45424	TrGAroC	MMALANHYO2 → CO2H3CO3 + CO_2	k1_RO2tORO2	Rickard and Pascoe (2009)*

Table 1: Gas phase reactions (... continued)

#	labels	reaction	rate coefficient	reference
G45428	TrGAroCN	C4CO2DBPAN + OH → HCOCOCHO + CO_2 + CO + NO_2	2.74E-11	Rickard and Pascoe (2009)
G45429	TrGAroCN	C4CO2DBPAN → C4CO2DBCO3 + NO_2	k_PAN_M	Rickard and Pascoe (2009)*
G45430a	TrGAroC	C5CO14O2 + HO_2 → .83 MALANHY + .83 CH_3 + .17 MGLYOX + .17 HO_2 + .17 CO + .17 CO_2 + OH	KAPHO2*r_CO3_OH	Rickard and Pascoe (2009)*
G45430b	TrGAroC	C5CO14O2 + HO_2 → C5CO14OH + O_3	KAPHO2*r_CO3_O3	Rickard and Pascoe (2009)
G45430c	TrGAroC	C5CO14O2 + HO_2 → C5CO14OOH	KAPHO2*r_CO3_OOH	Rickard and Pascoe (2009)
G45431	TrGAroCN	C5CO14O2 + NO → .83 MALANHY + .83 CH_3 + .17 MGLYOX + .17 HO_2 + .17 CO + .17 CO_2 + NO_2	KAPNO	Rickard and Pascoe (2009)*
G45432	TrGAroCN	C5CO14O2 + NO_2 → C5COO2NO2	k_CH3CO3_NO2	Rickard and Pascoe (2009)*
G45433	TrGAroCN	C5CO14O2 + NO_3 → .83 MALANHY + .83 CH_3 + .17 MGLYOX + .17 HO_2 + .17 CO + .17 CO_2 + NO_2	KRO2NO3*1.74	Rickard and Pascoe (2009)*
G45434	TrGAroC	C5CO14O2 → .83 MALANHY + .83 CH_3 + .17 MGLYOX + .17 HO_2 + .17 CO + .17 CO_2	k1_RO2RCO3	Rickard and Pascoe (2009)*
G45436	TrGAroC	C5CO14OH + OH → .83 MALANHY + .83 CH_3 + .17 MGLYOX + .17 HO_2 + .17 CO + .17 CO_2	5.44E-11	Rickard and Pascoe (2009)*
G45441	TrGAroCN	C5DICARB + NO_3 → C5CO14O2 + HNO_3	KNO3AL*2.75	Rickard and Pascoe (2009)
G45442	TrGAroC	C5DICARB + O_3 → .5338 GLYOX + .063 CH_3CHO + .348 $CH_3C(O)OO$ + .918 CO + .57 OH + .473 HO_2 + .0563 CH_3COCO_2H + .5338 MGLYOX + .676 H_2O_2 + .063 HCHO + .0563 $HCOCO_2H$ + .2465 CO_2	2.00E-18	Rickard and Pascoe (2009)
G45443	TrGAroC	C5DICARB + OH → .48 C5CO14O2 + .52 C5DICARBO2	6.2E-11	Rickard and Pascoe (2009)
G45444	TrGAroC	MC3ODBCO2H + OH → .35 GLYOX + .35 CH_3 + .35 CO + .35 CO_2 + .65 MMALANHY + .65 HO_2	4.38E-11	Rickard and Pascoe (2009)*
G45451	TrGAroCN	TLFUONE + NO_3 → NTLFUO2	1.00E-12	Rickard and Pascoe (2009)
G45452	TrGAroC	TLFUONE + O_3 → .5 CO + .5 OH + .5 MECOACETO2 + .3125 C24O3CCO2H + .1875 ACCOMECHO + .1875 H_2O_2	8.00E-19	see note*
G45453	TrGAroC	TLFUONE + OH → TLFUO2	6.90E-11	Rickard and Pascoe (2009)
G45454a	TrGAroC	ACCOMECO3 + HO_2 → ACCOMECO3H	KAPHO2*(r_CO3_OOH+r_CO3_O3)	Rickard and Pascoe (2009)
G45454b	TrGAroC	ACCOMECO3 + HO_2 → MECOACETO2 + CO_2 + OH	KAPHO2*r_CO3_OH	Rickard and Pascoe (2009)
G45455	TrGAroCN	ACCOMECO3 + NO → MECOACETO2 + CO_2 + NO_2	KAPNO	Rickard and Pascoe (2009)
G45456	TrGAroCN	ACCOMECO3 + NO_2 → ACCOMEPAN	k_CH3CO3_NO2	Rickard and Pascoe (2009)*
G45457	TrGAroCN	ACCOMECO3 + NO_3 → MECOACETO2 + CO_2 + NO_2	KRO2NO3*1.74	Rickard and Pascoe (2009)
G45458	TrGAroC	ACCOMECO3 → MECOACETO2 + CO_2	k1_RO2RCO3	Rickard and Pascoe (2009)

Table 1: Gas phase reactions (... continued)

#	labels	reaction	rate coefficient	reference
G45459	TrGAroC	C4CO2DCO3H + OH → C4CO2DBCO3	3.06E-11	Rickard and Pascoe (2009)
G45464	TrGAroCN	ACCOMECHO + NO_3 → ACCOMECO3 + HNO_3	KNO3AL*5.5	Rickard and Pascoe (2009)
G45465	TrGAroC	ACCOMECHO + OH → ACCOMECO3	7.09E-11	Rickard and Pascoe (2009)
G45466	TrGAroC	MMALNHYOOH + OH → MMALANHYO2	1.69E-11	Rickard and Pascoe (2009)
G45467a	TrGAroC	C5DICAROOH + OH → C5134CO2OH + OH	1.21E-10	Rickard and Pascoe (2009)
G45467b	TrGAroC	C5DICAROOH + OH → C5DICARBO2	k_ROOHRO	Rickard and Pascoe (2009)
G45468	TrGAroC	C24O3CCO2H + OH → MECOACETO2 + CO_2	8.76E-13	Rickard and Pascoe (2009)
G45469	TrGAroCN	NTLFUOOH + OH → NTLFUO2	4.44E-12	Rickard and Pascoe (2009)
G45470	TrGAroCN	ACCOMEPAN + OH → METACETHO + CO + CO + NO_2	1.00E-14	Rickard and Pascoe (2009)
G45471	TrGAroCN	ACCOMEPAN → ACCOMECO3 + NO_2	k_PAN_M	Rickard and Pascoe (2009)
G45476a	TrGAroC	TLFUO2 + HO_2 → TLFUOOH	k_RO2_HO2(temp,5)*(1.-r_COCH2O2_OH-r_CHOHCH2O2_OH)	Rickard and Pascoe (2009)
G45476b	TrGAroC	TLFUO2 + HO_2 → ACCOMECHO + HO_2 + OH	k_RO2_HO2(temp,5)*(r_COCH2O2_OH+r_CHOHCH2O2_OH)	Rickard and Pascoe (2009)*
G45477	TrGAroCN	TLFUO2 + NO → ACCOMECHO + HO_2 + NO_2	KRO2NO	Rickard and Pascoe (2009)*
G45478	TrGAroCN	TLFUO2 + NO_3 → ACCOMECHO + HO_2 + NO_2	KRO2NO3	Rickard and Pascoe (2009)*
G45479	TrGAroC	TLFUO2 → ACCOMECHO + HO_2	k1_RO2tORO2	Rickard and Pascoe (2009)*
G45480	TrGAroC	C5CO14OOH + OH → C5CO14O2	3.59E-12	Rickard and Pascoe (2009)
G45483	TrGAroC	TLFUOOH + OH → TLFUO2	2.53E-11	Rickard and Pascoe (2009)
G45485	TrGAroC	ACCOMECO3H + OH → ACCOMECO3	3.59E-12	Rickard and Pascoe (2009)
G45486a	TrGAroC	C5DIALO2 + HO_2 → C5DIALOOH	k_RO2_HO2(temp,5)*(1.-r_COCH2O2_OH)	Rickard and Pascoe (2009)
G45486b	TrGAroC	C5DIALO2 + HO_2 → MALDIAL + CO + HO_2 + OH	k_RO2_HO2(temp,5)*r_COCH2O2_OH	Rickard and Pascoe (2009)*
G45487	TrGAroCN	C5DIALO2 + NO → MALDIAL + CO + HO_2 + NO_2	KRO2NO	Rickard and Pascoe (2009)*
G45488	TrGAroCN	C5DIALO2 + NO_3 → MALDIAL + CO + HO_2 + NO_2	KRO2NO3	Rickard and Pascoe (2009)*
G45489	TrGAroC	C5DIALO2 → MALDIAL + CO + HO_2	k1_RO2sORO2	Rickard and Pascoe (2009)*
G45490a	TrGAroC	C5DICARBO2 + HO_2 → C5DICAROOH	k_RO2_HO2(temp,5)*(r_CO3_OOH+r_CO3_O3)	Rickard and Pascoe (2009)
G45491b	TrGAroC	C5DICARBO2 + HO_2 → MGLYOX + GLYOX + HO_2 + OH	k_RO2_HO2(temp,5)*r_CO3_OH	Rickard and Pascoe (2009)*
G45492	TrGAroCN	C5DICARBO2 + NO → MGLYOX + GLYOX + HO_2 + NO_2	KRO2NO	Rickard and Pascoe (2009)*
G45493	TrGAroCN	C5DICARBO2 + NO_3 → MGLYOX + GLYOX + HO_2 + NO_2	KRO2NO3	Rickard and Pascoe (2009)*

Table 1: Gas phase reactions (... continued)

#	labels	reaction	rate coefficient	reference
G45494	TrGAroC	C5DICARBO2 → MGLYOX + GLYOX + HO_2	k1_RO2sORO2	Rickard and Pascoe (2009)*
G46200a	TrGTerC	CO235C6O2 + HO_2 → CO235C6OOH	k_RO2_HO2(temp,6)*r_COCH2O2_OOH	Rickard and Pascoe (2009), Sander et al. (2019)
G46200b	TrGTerC	CO235C6O2 + HO_2 → CO23C4CO3 + HCHO + OH	k_RO2_HO2(temp,6)*r_COCH2O2_OH	Rickard and Pascoe (2009), Sander et al. (2019)
G46201	TrGTerCN	CO235C6O2 + NO → CO23C4CO3 + HCHO + NO_2	KRO2NO	Rickard and Pascoe (2009)*
G46202	TrGTerC	CO235C6O2 → CO23C4CO3 + HCHO	k1_RO2pORO2	Rickard and Pascoe (2009)
G46203	TrGTerC	CO235C6OOH + OH → CO235C6O2	1.01E-11	Rickard and Pascoe (2009)
G46204	TrGTerC	C614O2 → CO23C4CHO + HCHO + HO_2	k1_RO2sORO2	Rickard and Pascoe (2009)
G46205a	TrGTerCN	C614O2 + NO → CO23C4CHO + HCHO + HO_2 + NO_2	KRO2NO*(1.-alpha_AN(9,2,0,1,0, temp,cair))	Rickard and Pascoe (2009)
G46205b	TrGTerCN	C614O2 + NO → C614NO3	KRO2NO*alpha_AN(9,2,0,1,0,temp, cair)	Rickard and Pascoe (2009)
G46206a	TrGTerC	C614O2 + HO_2 → C614OOH	k_RO2_HO2(temp,6)*(1.-r_ CHOHCH2O2_OH)	Rickard and Pascoe (2009), Sander et al. (2019)
G46206b	TrGTerC	C614O2 + HO_2 → CO23C4CHO + HCHO + HO_2 + OH	k_RO2_HO2(temp,6)*r_CHOHCH2O2_OH	Rickard and Pascoe (2009), Sander et al. (2019)
G46207	TrGTerCN	C614NO3 + OH → C614CO + NO_2	7.11E-12	Rickard and Pascoe (2009)
G46208	TrGTerC	C614OOH + OH → C614CO + OH	8.69E-11	Rickard and Pascoe (2009)
G46209	TrGTerC	C614CO + OH → CO235C5CHO + HO_2	3.22E-12	Rickard and Pascoe (2009)
G46210	TrGTerC	CO235C5CHO + OH → CO23C4CO3 + CO	1.33E-11	Rickard and Pascoe (2009)
G46211	TrGTerCN	CO235C5CHO + NO_3 → CO23C4CO3 + CO + HNO_3	KNO3AL*5.5	Rickard and Pascoe (2009)
G46400	TrGAroC	PHENOOH + OH → PHENO2	1.16E-10	Rickard and Pascoe (2009)
G46401	TrGAroC	C6CO4DB + OH → CO + CO + HO_2 + CO + HCOCOCHO	7.70E-11	Rickard and Pascoe (2009)
G46402	TrGAroC	C5CO2DCO3H + OH → C5CO2DBCO3	3.60E-11	Rickard and Pascoe (2009)
G46403	TrGAroCN	NDNPHENOOH + OH → NDNPHENO2	k_ROOHRO	Rickard and Pascoe (2009)
G46404a	TrGAroC	C615CO2O2 + HO_2 → C615CO2OOH	k_RO2_HO2(temp,6)*(1.-r_COCH2O2_ OH)	Rickard and Pascoe (2009)
G46404b	TrGAroC	C615CO2O2 + HO_2 → C5DICARB + CO + HO_2 + OH	k_RO2_HO2(temp,6)*r_COCH2O2_OH	Rickard and Pascoe (2009)*
G46405	TrGAroCN	C615CO2O2 + NO → C5DICARB + CO + HO_2 + NO_2	KRO2NO	Rickard and Pascoe (2009)*
G46406	TrGAroCN	C615CO2O2 + NO_3 → C5DICARB + CO + HO_2 + NO_2	KRO2NO3	Rickard and Pascoe (2009)*
G46407	TrGAroC	C615CO2O2 → C5DICARB + CO + HO_2	k1_RO2sORO2	Rickard and Pascoe (2009)*
G46408	TrGAroCN	BZEMUCPAN + OH → MALDIAL + CO + CO_2 + NO_2	4.05E-11	Rickard and Pascoe (2009)
G46409	TrGAroCN	BZEMUCPAN → BZEMUCCO3 + NO_2	k_PAN_M	Rickard and Pascoe (2009)

Table 1: Gas phase reactions (... continued)

#	labels	reaction	rate coefficient	reference
G46410	TrGAroCN	BZBIPERNO3 + OH → BZOBIPEROH + NO_2	7.30E-11	Rickard and Pascoe (2009)
G46411	TrGAroCN	HOC6H4NO2 + NO_3 → NPHEN1O + HNO_3	9.00E-14	Rickard and Pascoe (2009)
G46412	TrGAroCN	HOC6H4NO2 + OH → NPHEN1O	9.00E-13	Rickard and Pascoe (2009)
G46413a	TrGAroCN	NDNPHENO2 + HO_2 → NDNPHENOOH	k_RO2_HO2(temp,6)*(1.-r_ CHOHCH2O2_OH)	Rickard and Pascoe (2009)
G46413b	TrGAroCN	NDNPHENO2 + HO_2 → NC4DCO2H + HNO_3 + CO + CO + NO_2 + OH	k_RO2_HO2(temp,6)*r_CHOHCH2O2_OH	Rickard and Pascoe (2009)*
G46414	TrGAroCN	NDNPHENO2 + NO → NC4DCO2H + HNO_3 + CO + CO + NO_2 + NO_2	KRO2NO	Rickard and Pascoe (2009)*
G46415	TrGAroCN	NDNPHENO2 + NO_3 → NC4DCO2H + HNO_3 + CO + CO + NO_2 + NO_2	KRO2NO3	Rickard and Pascoe (2009)*
G46416	TrGAroCN	NDNPHENO2 → NC4DCO2H + HNO_3 + CO + CO + NO_2	k1_RO2ISOPDO2	Rickard and Pascoe (2009)*
G46417	TrGAroC	PBZQCO + OH → C5CO2OHCO3	6.07E-11	Rickard and Pascoe (2009)
G46418	TrGAroCN	CATECHOL + NO_3 → CATEC1O + HNO_3	9.9E-11	Rickard and Pascoe (2009)*
G46419	TrGAroC	CATECHOL + O_3 → MALDALCO2H + $HCOCO_2H$ + HO_2 + OH	9.2E-18	Rickard and Pascoe (2009)
G46420	TrGAroC	CATECHOL + OH → CATEC1O	1.0E-10	Rickard and Pascoe (2009)
G46421	TrGAroC	C5COOHCO3H + OH → C5CO2OHCO3	8.01E-11	Rickard and Pascoe (2009)
G46422	TrGAroCN	NCATECHOL + NO_3 → NNCATECO2	2.60E-12	Rickard and Pascoe (2009)
G46423	TrGAroCN	NCATECHOL + OH → NCATECO2	3.47E-12	Rickard and Pascoe (2009)
G46424a	TrGAroC	C5CO2OHCO3 + HO_2 → C5COOHCO3H	KAPHO2*(r_CO3_OOH+r_CO3_O3)	Rickard and Pascoe (2009)
G46424b	TrGAroC	C5CO2OHCO3 + HO_2 → HOCOC4DIAL + HO_2 + CO + CO_2 + OH	KAPHO2*r_CO3_OH	Rickard and Pascoe (2009)
G46425	TrGAroCN	C5CO2OHCO3 + NO → HOCOC4DIAL + HO_2 + CO + CO_2 + NO_2	KAPNO	Rickard and Pascoe (2009)
G46426	TrGAroCN	C5CO2OHCO3 + NO_2 → C5CO2OHPAN	k_CH3CO3_NO2	Rickard and Pascoe (2009)*
G46427	TrGAroCN	C5CO2OHCO3 + NO_3 → HOCOC4DIAL + HO_2 + CO + CO_2 + NO_2	KRO2NO3*1.74	Rickard and Pascoe (2009)
G46428	TrGAroC	C5CO2OHCO3 → HOCOC4DIAL + HO_2 + CO + CO_2	k1_RO2RCO3	Rickard and Pascoe (2009)
G46429	TrGAroCN	BZEPOXMUC + NO_3 → BZEMUCCO3 + HNO_3	2.*KNO3AL*2.75	Rickard and Pascoe (2009)
G46430	TrGAroC	BZEPOXMUC + O_3 → EPXC4DIAL + .125 HCHO + .1125 $HCOCO_2H$ + .0675 GLYOX + .0675 H_2O_2 + .82 HO_2 + .57 OH + 1.265 CO + .25 CO_2	2.00E-18	Rickard and Pascoe (2009)*

Table 1: Gas phase reactions (... continued)

#	labels	reaction	rate coefficient	reference
G46431	TrGAroC	BZEPOXMUC + OH → .31 BZEMUCCO3 + .69 BZEMUCO2	6.08E-11	Rickard and Pascoe (2009)
G46432a	TrGAroCN	NCATECO2 + HO_2 → NCATECOOH	k_RO2_HO2(temp,6)*(1.-r_CHOHCH2O2_OH)	Rickard and Pascoe (2009)
G46432b	TrGAroCN	NCATECO2 + HO_2 → NC4DCO2H + $HCOCO_2H$ + HO_2 + OH	k_RO2_HO2(temp,6)*r_CHOHCH2O2_OH	Rickard and Pascoe (2009)*
G46433	TrGAroCN	NCATECO2 + NO → NC4DCO2H + $HCOCO_2H$ + HO_2 + NO_2	KRO2NO	Rickard and Pascoe (2009)*
G46434	TrGAroCN	NCATECO2 + NO_3 → NC4DCO2H + $HCOCO_2H$ + HO_2 + NO_2	KRO2NO3	Rickard and Pascoe (2009)*
G46435	TrGAroCN	NCATECO2 → NC4DCO2H + $HCOCO_2H$ + HO_2	k1_RO2ISOPDO2	Rickard and Pascoe (2009)*
G46436	TrGAroCN	NPHEN1OOH + OH → NPHEN1O2	9.00E-13	Rickard and Pascoe (2009)
G46437a	TrGAroCN	NPHENO2 + HO_2 → NPHENOOH	k_RO2_HO2(temp,6)*(1.-r_CHOHCH2O2_OH)	Rickard and Pascoe (2009)
G46437b	TrGAroCN	NPHENO2 + HO_2 → MALDALCO2H + GLYOX + NO_2 + OH	k_RO2_HO2(temp,6)*r_CHOHCH2O2_OH	Rickard and Pascoe (2009)*
G46438	TrGAroCN	NPHENO2 + NO → MALDALCO2H + GLYOX + NO_2 + NO_2	KRO2NO	Rickard and Pascoe (2009)*
G46439	TrGAroCN	NPHENO2 + NO_3 → MALDALCO2H + GLYOX + NO_2 + NO_2	KRO2NO3	Rickard and Pascoe (2009)*
G46440	TrGAroCN	NPHENO2 → MALDALCO2H + GLYOX + NO_2	k1_RO2ISOPDO2	Rickard and Pascoe (2009)*
G46441	TrGAroC	BENZENE + OH → .352 BZBIPERO2 + .118 BZEPOXMUC + .118 HO_2 + .53 PHENOL + .53 HO_2	2.3E-12*EXP(-190./temp)	Rickard and Pascoe (2009)*
G46442	TrGAroCN	C5CO2OHPAN + OH → HOCOC4DIAL + CO + CO + NO_2	7.66E-11	Rickard and Pascoe (2009)
G46443	TrGAroCN	C5CO2OHPAN → C5CO2OHCO3 + NO_2	k_PAN_M	Rickard and Pascoe (2009)
G46444	TrGAroCN	CATEC1O + NO_2 → NCATECHOL	k_C6H5O_NO2	Rickard and Pascoe (2009), Platz et al. (1998)
G46445	TrGAroC	CATEC1O + O_3 → CATEC1O2	k_C6H5O_O3	Rickard and Pascoe (2009), Tao and Li (1999)
G46446	TrGAroC	BZEMUCCO + OH → EPXDLCO3 + GLYOX	9.20E-11	Rickard and Pascoe (2009)
G46447a	TrGAroCN	NNCATECO2 + HO_2 → NNCATECOOH	k_RO2_HO2(temp,6)*(1.-r_CHOHCH2O2_OH)	Rickard and Pascoe (2009)
G46447b	TrGAroCN	NNCATECO2 + HO_2 → NC4DCO2H + $HCOCO_2H$ + NO_2 + OH	k_RO2_HO2(temp,6)*r_CHOHCH2O2_OH	Rickard and Pascoe (2009)*

Table 1: Gas phase reactions (... continued)

#	labels	reaction	rate coefficient	reference
G46448	TrGAroCN	NNCATECO2 + NO → NC4DCO2H + $HCOCO_2H$ + NO_2 + NO_2	KRO2NO	Rickard and Pascoe (2009)*
G46449	TrGAroCN	NNCATECO2 + NO_3 → NC4DCO2H + $HCOCO_2H$ + NO_2 + NO_2	KRO2NO3	Rickard and Pascoe (2009)*
G46450	TrGAroCN	NNCATECO2 → NC4DCO2H + $HCOCO_2H$ + NO_2	k1_RO2ISOPDO2	Rickard and Pascoe (2009)*
G46451	TrGAroC	BZEMUCCO2H + OH → C5DIALO2 + CO_2	4.06E-11	Rickard and Pascoe (2009)
G46452	TrGAroCN	NNCATECOOH + OH → NNCATECO2	k_ROOHRO	Rickard and Pascoe (2009)
G46453	TrGAroCN	NPHEN1O + NO_2 → DNPHEN	k_C6H5O_NO2	Rickard and Pascoe (2009), Platz et al. (1998)
G46454	TrGAroCN	NPHEN1O + O_3 → NPHEN1O2	k_C6H5O_O3	Rickard and Pascoe (2009), Tao and Li (1999)
G46455	TrGAroCN	DNPHEN + NO_3 → NDNPHENO2	2.25E-15	Rickard and Pascoe (2009)
G46456	TrGAroCN	DNPHEN + OH → DNPHENO2	3.00E-14	Rickard and Pascoe (2009)
G46457	TrGAroCN	PHENOL + NO_3 → .742 C6H5O + .742 HNO_3 + .258 NPHENO2	3.8E-12	Rickard and Pascoe (2009)*
G46458	TrGAroC	PHENOL + OH → .06 C6H5O + .8 CATECHOL + .8 HO_2 + .14 PHENO2	4.7E-13*EXP(1220./temp)	Rickard and Pascoe (2009)*
G46459	TrGAroCN	PBZQONE + NO_3 → NBZQO2	3.00E-13	Rickard and Pascoe (2009)
G46460	TrGAroC	PBZQONE + OH → PBZQO2	4.6E-12	Rickard and Pascoe (2009)
G46461a	TrGAroC	PHENO2 + HO_2 → PHENOOH	k_RO2_HO2(temp,6)*(1.-r_CHOHCH2O2_OH)	Rickard and Pascoe (2009)
G46461b	TrGAroC	PHENO2 + HO_2 → .71 MALDALCO2H + .71 GLYOX + .29 PBZQONE + HO_2 + OH	k_RO2_HO2(temp,6)*r_CHOHCH2O2_OH	Rickard and Pascoe (2009)*
G46462	TrGAroCN	PHENO2 + NO → .71 MALDALCO2H + .71 GLYOX + .29 PBZQONE + HO_2 + NO_2	KRO2NO	Rickard and Pascoe (2009)*
G46463	TrGAroCN	PHENO2 + NO_3 → .71 MALDALCO2H + .71 GLYOX + .29 PBZQONE + HO_2 + NO_2	KRO2NO3	Rickard and Pascoe (2009)*
G46464	TrGAroC	PHENO2 → .71 MALDALCO2H + .71 GLYOX + .29 PBZQONE + HO_2	k1_RO2ISOPDO2	Rickard and Pascoe (2009)*
G46465	TrGAroC	C615CO2OOH + OH → C6125CO + OH	9.42E-11	Rickard and Pascoe (2009)
G46466a	TrGAroC	C5CO2DBCO3 + HO_2 → C5CO2DCO3H	KAPHO2*(r_CO3_OOH+r_CO3_O3)	Rickard and Pascoe (2009)
G46466b	TrGAroC	C5CO2DBCO3 + HO_2 → $CH_3C(O)$ + HCOCOCHO + CO_2 + OH	KAPHO2*r_CO3_OH	Rickard and Pascoe (2009)
G46467	TrGAroCN	C5CO2DBCO3 + NO → $CH_3C(O)$ + HCOCOCHO + CO_2 + NO_2	KAPNO	Rickard and Pascoe (2009)

Table 1: Gas phase reactions (... continued)

#	labels	reaction	rate coefficient	reference
G46468	TrGAroCN	C5CO2DBCO3 + NO_2 → C5CO2DBPAN	k_CH3CO3_NO2	Rickard and Pascoe (2009)*
G46469	TrGAroCN	C5CO2DBCO3 + NO_3 → $CH_3C(O)$ + HCOCOCHO + CO_2 + NO_2	KRO2NO3*1.74	Rickard and Pascoe (2009)
G46470	TrGAroC	C5CO2DBCO3 → $CH_3C(O)$ + HCOCOCHO + CO_2	k1_RO2RCO3	Rickard and Pascoe (2009)
G46471	TrGAroCN	NPHEN1O2 + HO_2 → NPHEN1OOH	k_RO2_HO2(temp,6)	Rickard and Pascoe (2009)
G46472a	TrGAroCN	NPHEN1O2 + NO → NPHEN1O + NO_2	KRO2NO	Rickard and Pascoe (2009)
G46472b	TrGAroCN	NPHEN1O2 + NO_2 → NPHEN1O + NO_3	k_C6H5O2_NO2	Jagiella and Zabel (2007)*
G46473	TrGAroCN	NPHEN1O2 + NO_3 → NPHEN1O + NO_2	KRO2NO3	Rickard and Pascoe (2009)
G46474	TrGAroCN	NPHEN1O2 → NPHEN1O	k1_RO2sRO2	Rickard and Pascoe (2009)
G46475	TrGAroCN	NPHENOOH + OH → NPHENO2	1.07E-10	Rickard and Pascoe (2009)
G46476	TrGAroCN	C6H5O + NO_2 → HOC6H4NO2	k_C6H5O_NO2	Rickard and Pascoe (2009), Platz et al. (1998)*
G46477	TrGAroC	C6H5O + O_3 → C6H5O2	k_C6H5O_O3	Rickard and Pascoe (2009), Tao and Li (1999)
G46478	TrGAroCN	NCATECOOH + OH → NCATECO2	k_ROOHRO	Rickard and Pascoe (2009)
G46479	TrGAroC	PBZQOOH + OH → PBZQCO + OH	1.23E-10	Rickard and Pascoe (2009)
G46480a	TrGAroC	PBZQO2 + HO_2 → PBZQOOH	k_RO2_HO2(temp,6)*(1.-r_CHOHCH2O2_OH-r_COCH2O2_OH)	Rickard and Pascoe (2009)
G46480b	TrGAroC	PBZQO2 + HO_2 → C5CO2OHCO3 + OH	k_RO2_HO2(temp,6)*(r_CHOHCH2O2_OH+r_COCH2O2_OH)	Rickard and Pascoe (2009)*
G46481	TrGAroCN	PBZQO2 + NO → C5CO2OHCO3 + NO_2	KRO2NO	Rickard and Pascoe (2009)*
G46482	TrGAroCN	PBZQO2 + NO_3 → C5CO2OHCO3 + NO_2	KRO2NO3	Rickard and Pascoe (2009)*
G46483	TrGAroC	PBZQO2 → C5CO2OHCO3	k1_RO2sORO2	Rickard and Pascoe (2009)*
G46484	TrGAroC	BZOBIPEROH + OH → MALDIALCO3 + GLYOX	8.16E-11	Rickard and Pascoe (2009)
G46485a	TrGAroCN	DNPHENO2 + HO_2 → DNPHENOOH	k_RO2_HO2(temp,6)*(1.-r_CHOHCH2O2_OH)	Rickard and Pascoe (2009)
G46485b	TrGAroCN	DNPHENO2 + HO_2 → NC4DCO2H + $HCOCO_2H$ + NO_2 + OH	k_RO2_HO2(temp,6)*r_CHOHCH2O2_OH	Rickard and Pascoe (2009)*
G46486	TrGAroCN	DNPHENO2 + NO → NC4DCO2H + $HCOCO_2H$ + NO_2 + NO_2	KRO2NO	Rickard and Pascoe (2009)*
G46487	TrGAroCN	DNPHENO2 + NO_3 → NC4DCO2H + $HCOCO_2H$ + NO_2 + NO_2	KRO2NO3	Rickard and Pascoe (2009)*
G46488	TrGAroCN	DNPHENO2 → NC4DCO2H + $HCOCO_2H$ + NO_2	k1_RO2ISOPDO2	Rickard and Pascoe (2009)*
G46489	TrGAroC	BZBIPEROOH + OH → BZOBIPEROH + OH	9.77E-11	Rickard and Pascoe (2009)
G46490a	TrGAroC	BZEMUCO2 + HO_2 → BZEMUCOOH	k_RO2_HO2(temp,6)	Rickard and Pascoe (2009)

Table 1: Gas phase reactions (... continued)

#	labels	reaction	rate coefficient	reference
G46490b	TrGAroC	BZEMUCO2 + HO_2 → .5 EPXC4DIAL + .5 GLYOX + .5 HO_2 + .5 C3DIALO2 + .5 C32OH13CO + OH	k_RO2_HO2(temp,6)	Rickard and Pascoe (2009)*
G46491a	TrGAroCN	BZEMUCO2 + NO → BZEMUCNO3	KRO2NO*alpha_AN(10,2,0,1,0,temp,cair)	Rickard and Pascoe (2009)
G46491b	TrGAroCN	BZEMUCO2 + NO → .5 EPXC4DIAL + .5 GLYOX + .5 HO_2 + .5 C3DIALO2 + .5 C32OH13CO + NO_2	KRO2NO*(1.-alpha_AN(10,2,0,1,0,temp,cair))	Rickard and Pascoe (2009)*
G46492	TrGAroCN	BZEMUCO2 + NO_3 → .5 EPXC4DIAL + .5 GLYOX + .5 HO_2 + .5 C3DIALO2 + .5 C32OH13CO + NO_2	KRO2NO3	Rickard and Pascoe (2009)*
G46493	TrGAroC	BZEMUCO2 → .5 EPXC4DIAL + .5 GLYOX + .5 HO_2 + .5 C3DIALO2 + .5 C32OH13CO	k1_RO2sORO2	Rickard and Pascoe (2009)*
G46494	TrGAroCN	C5CO2DBPAN + OH → HCOCOCHO + CH_3CHO + CO_2 + NO_2	3.28E-11	Rickard and Pascoe (2009)
G46495	TrGAroCN	C5CO2DBPAN → C5CO2DBCO3 + NO_2	k_PAN_M	Rickard and Pascoe (2009)
G46496	TrGAroCN	NBZQOOH + OH → NBZQO2	6.68E-11	Rickard and Pascoe (2009)
G46497	TrGAroC	CATEC1OOH + OH → CATEC1O2	k_ROOHRO	Rickard and Pascoe (2009)
G46498	TrGAroC	C6125CO + OH → C5CO14O2 + CO	6.45E-11	Rickard and Pascoe (2009)
G46499a	TrGAroCN	NBZQO2 + HO_2 → NBZQOOH	k_RO2_HO2(temp,6)*(1.-r_COCH2O2_OH)	Rickard and Pascoe (2009)
G46499b	TrGAroCN	NBZQO2 + HO_2 → C6CO4DB + NO_2 + OH	k_RO2_HO2(temp,6)*r_COCH2O2_OH	Rickard and Pascoe (2009)*
G46500	TrGAroCN	NBZQO2 + NO → C6CO4DB + NO_2 + NO_2	KRO2NO	Rickard and Pascoe (2009)*
G46501	TrGAroCN	NBZQO2 + NO_3 → C6CO4DB + NO_2 + NO_2	KRO2NO3	Rickard and Pascoe (2009)*
G46502	TrGAroCN	NBZQO2 → C6CO4DB + NO_2	k1_RO2sORO2	Rickard and Pascoe (2009)*
G46503	TrGAroCN	DNPHENOOH + OH → DNPHENO2	k_ROOHRO	Rickard and Pascoe (2009)
G46504	TrGAroC	CATEC1O2 + HO_2 → CATEC1OOH	k_RO2_HO2(temp,6)	Rickard and Pascoe (2009)
G46505a	TrGAroCN	CATEC1O2 + NO → CATEC1O + NO_2	KRO2NO	Rickard and Pascoe (2009)
G46505b	TrGAroCN	CATEC1O2 + NO_2 → CATEC1O + NO_3	k_C6H5O2_NO2	Jagiella and Zabel (2007)*
G46506	TrGAroCN	CATEC1O2 + NO_3 → CATEC1O + NO_2	KRO2NO3	Rickard and Pascoe (2009)
G46507	TrGAroC	CATEC1O2 → CATEC1O	k1_RO2sORO2	Rickard and Pascoe (2009)
G46508	TrGAroC	BZEMUCCO3H + OH → BZEMUCCO3	4.37E-11	Rickard and Pascoe (2009)
G46509	TrGAroC	C6H5OOH + OH → C6H5O2	3.60E-12	Rickard and Pascoe (2009)
G46510	TrGAroC	BZEMUCOOH + OH → BZEMUCCO + OH	1.31E-10	Rickard and Pascoe (2009)
G46511a	TrGAroC	BZEMUCCO3 + HO_2 → BZEMUCCO2H + O_3	KAPHO2*r_CO3_O3	Rickard and Pascoe (2009)
G46511b	TrGAroC	BZEMUCCO3 + HO_2 → BZEMUCCO3H	KAPHO2*r_CO3_OOH	Rickard and Pascoe (2009)
G46511c	TrGAroC	BZEMUCCO3 + HO_2 → C5DIALO2 + CO_2 + OH	KAPHO2*r_CO3_OH	Rickard and Pascoe (2009)
G46512	TrGAroCN	BZEMUCCO3 + NO → C5DIALO2 + CO_2 + NO_2	KAPNO	Rickard and Pascoe (2009)

Table 1: Gas phase reactions (... continued)

#	labels	reaction	rate coefficient	reference
G46513	TrGAroCN	BZEMUCCO3 + NO_2 → BZEMUCPAN	k_CH3CO3_NO2	Rickard and Pascoe (2009)
G46514	TrGAroCN	BZEMUCCO3 + NO_3 → C5DIALO2 + CO_2 + NO_2	KRO2NO3*1.74	Rickard and Pascoe (2009)
G46515	TrGAroC	BZEMUCCO3 → C5DIALO2 + CO_2	k1_RO2RCO3	Rickard and Pascoe (2009)*
G46516	TrGAroC	C6H5O2 + HO_2 → C6H5OOH	k_RO2_HO2(temp,6)	Rickard and Pascoe (2009)
G46517	TrGAroCN	C6H5O2 + NO → C6H5O + NO_2	KRO2NO	Rickard and Pascoe (2009)
G46518	TrGAroCN	C6H5O2 + NO_3 → C6H5O + NO_2	KRO2NO3	Rickard and Pascoe (2009)
G46519	TrGAroC	C6H5O2 → C6H5O	k1_RO2sRO2	Rickard and Pascoe (2009)
G46520	TrGAroCN	C6H5O2 + NO_2 → C6H5O + NO_3	k_C6H5O2_NO2	Jagiella and Zabel (2007)
G46521	TrGAroCN	BZEMUCNO3 + OH → BZEMUCCO + NO_2	4.38E-11	Rickard and Pascoe (2009)
G46522a	TrGAroC	BZBIPERO2 + HO_2 → BZBIPEROOH	k_RO2_HO2(temp,6)*(1.-r_BIPERO2_OH)	Rickard and Pascoe (2009)
G46522b	TrGAroC	BZBIPERO2 + HO_2 → OH + GLYOX + HO_2 + .5 BZFUONE + .5 BZFUONE	k_RO2_HO2(temp,6)*r_BIPERO2_OH	Rickard and Pascoe (2009), Birdsall et al. (2010)*
G46523a	TrGAroCN	BZBIPERO2 + NO → BZBIPERNO3	KRO2NO*alpha_AN(9,2,0,0,1,temp,cair)	Rickard and Pascoe (2009)
G46523b	TrGAroCN	BZBIPERO2 + NO → NO_2 + GLYOX + HO_2 + .5 BZFUONE + .5 BZFUONE	KRO2NO*(1.-alpha_AN(9,2,0,0,1,temp,cair))	Rickard and Pascoe (2009)*
G46524	TrGAroCN	BZBIPERO2 + NO_3 → NO_2 + GLYOX + HO_2 + .5 BZFUONE + .5 BZFUONE	KRO2NO3	Rickard and Pascoe (2009)*
G46525	TrGAroC	BZBIPERO2 → GLYOX + HO_2 + BZFUONE	k1_RO2sORO2	Rickard and Pascoe (2009)*
G47200	TrGTerCN	CO235C6CHO + NO_3 → CO235C6CO3 + HNO_3	KNO3AL*5.5	Rickard and Pascoe (2009)
G47201	TrGTerC	CO235C6CHO + OH → CO235C6CO3	6.70E-11	Rickard and Pascoe (2009)
G47202a	TrGTerC	CO235C6CO3 + HO_2 → C235C6CO3H	KAPHO2*(r_CO3_OOH+r_CO3_O3)	Rickard and Pascoe (2009)
G47202b	TrGTerC	CO235C6CO3 + HO_2 → CO235C6O2 + CO_2 + OH	KAPHO2*r_CO3_OH	Rickard and Pascoe (2009)
G47203	TrGTerCN	CO235C6CO3 + NO → CO235C6O2 + CO_2 + NO_2	KAPNO	Rickard and Pascoe (2009)
G47204	TrGTerCN	CO235C6CO3 + NO_2 → C7PAN3	k_CH3CO3_NO2	Rickard and Pascoe (2009)
G47205	TrGTerC	CO235C6CO3 → CO235C6O2 + CO_2	k1_RO2RCO3	Rickard and Pascoe (2009)
G47206	TrGTerC	C235C6CO3H + OH → CO235C6CO3	4.75E-12	Rickard and Pascoe (2009)
G47207	TrGTerCN	C7PAN3 + OH → CO235C5CHO + CO + NO_2	8.83E-13	Rickard and Pascoe (2009)
G47208	TrGTerCN	C7PAN3 → CO235C6CO3 + NO_2	k_PAN_M	Rickard and Pascoe (2009)
G47209a	TrGTerC	C716O2 + HO_2 → C716OOH	k_RO2_HO2(temp,7)*r_COCH2O2_OOH	Rickard and Pascoe (2009), Sander et al. (2019)
G47209b	TrGTerC	C716O2 + HO_2 → CO13C4CHO + $CH_3C(O)$ + OH	k_RO2_HO2(temp,7)*r_COCH2O2_OH	Rickard and Pascoe (2009), Sander et al. (2019)
G47210	TrGTerCN	C716O2 + NO → CO13C4CHO + $CH_3C(O)$ + NO_2	KRO2NO	Rickard and Pascoe (2009)*

Table 1: Gas phase reactions (... continued)

#	labels	reaction	rate coefficient	reference
G47211	TrGTerC	C716O2 → CO13C4CHO + $CH_3C(O)$	k1_RO2sORO2	Rickard and Pascoe (2009)
G47212	TrGTerC	C716OOH + OH → CO235C6CHO + OH	1.20E-10	Rickard and Pascoe (2009)
G47213	TrGTerC	C721O2 + HO_2 → C721OOH	k_RO2_HO2(temp,7)	Rickard and Pascoe (2009)
G47214	TrGTerCN	C721O2 + NO → C722O2 + NO_2	KRO2NO	Rickard and Pascoe (2009)*
G47215	TrGTerC	C721O2 → C722O2	k1_RO2pRO2	Rickard and Pascoe (2009)
G47216	TrGTerC	C721OOH + OH → C721O2	1.27E-11	Rickard and Pascoe (2009)
G47217	TrGTerC	C722O2 + HO_2 → C722OOH	k_RO2_HO2(temp,7)	Rickard and Pascoe (2009)
G47218	TrGTerCN	C722O2 + NO → CH_3COCH_3 + C44O2 + NO_2	KRO2NO	Rickard and Pascoe (2009)*
G47219	TrGTerC	C722O2 → CH_3COCH_3 + C44O2	k1_RO2tRO2	Rickard and Pascoe (2009)
G47220	TrGTerC	C722OOH + OH → C722O2	3.31E-11	Rickard and Pascoe (2009)
G47221	TrGTerC	ROO6R3O2 → ROO6R5O2	5.68E10*EXP(-8745./temp)	Vereecken and Peeters (2012)
G47222	TrGTerCN	ROO6R3O2 + NO → ROO6R3O + NO_2	KRO2NO	Vereecken and Peeters (2012)*
G47223	TrGTerC	ROO6R3O2 + HO_2 → 7 LCARBON	k_RO2_HO2(temp,7)	Vereecken and Peeters (2012)*
G47224	TrGTerC	ROO6R3O2 → ROO6R3O	k1_RO2sRO2	Vereecken and Peeters (2012)
G47225	TrGTerC	ROO6R3O → 7 LCARBON + HO_2	5.7E10*EXP(-2949./temp)	Vereecken and Peeters (2012)*
G47226	TrGTerC	ROO6R5O2 → 7 LCARBON + OH	9.17E10*EXP(-8706./temp)	Vereecken and Peeters (2012)*
G47400	TrGAroC	TOLUENE + OH → .07 C6H5CH2O2 + .18 CRESOL + .18 HO_2 + .65 TLBIPERO2 + .10 TLEPOXMUC + .10 HO_2	1.8E-12*EXP(340./temp)	Rickard and Pascoe (2009)*
G47401	TrGAroC	C6H5CH2O2 + HO_2 → C6H5CH2OOH	1.5E-13*EXP(1310./temp)	Rickard and Pascoe (2009)
G47402a	TrGAroCN	C6H5CH2O2 + NO → C6H5CH2NO3	KRO2NO*alpha_AN(7,1,0,0,0,temp,cair)	Rickard and Pascoe (2009)*
G47402b	TrGAroCN	C6H5CH2O2 + NO → BENZAL + HO_2 + NO_2	KRO2NO*(1.-alpha_AN(7,1,0,0,0,temp,cair))	Rickard and Pascoe (2009)*
G47403	TrGAroCN	C6H5CH2O2 + NO_3 → BENZAL + HO_2 + NO_2	KRO2NO3	Rickard and Pascoe (2009)*
G47404	TrGAroC	C6H5CH2O2 → BENZAL + HO_2	2.*(k_CH3O2*2.4E-14*EXP(1620./temp))**(0.5)*RO2	Rickard and Pascoe (2009)*
G47405	TrGAroCN	CRESOL + NO_3 → .103 CRESO2 + .103 HNO_3 + .506 NCRESO2 + .391 TOL1O + .391 HNO_3	1.4E-11	Rickard and Pascoe (2009)*
G47406	TrGAroC	CRESOL + OH → .2 CRESO2 + .727 MCATECHOL + .727 HO_2 + .073 TOL1O	4.65E-11	Rickard and Pascoe (2009)*
G47407a	TrGAroC	TLBIPERO2 + HO_2 → TLBIPEROOH	k_RO2_HO2(temp,7)*(1.-r_BIPERO2_OH)	Rickard and Pascoe (2009)

Table 1: Gas phase reactions (... continued)

#	labels	reaction	rate coefficient	reference
G47407b	TrGAroC	TLBIPERO2 + HO_2 → OH + .6 GLYOX + .4 MGLYOX + HO_2 + .2 C4MDIAL + .2 C5DICARB + .2 TLFUONE + .2 BZFUONE + .2 MALDIAL	k_RO2_HO2(temp,7)*r_BIPERO2_OH	Rickard and Pascoe (2009), Birdsall et al. (2010)*
G47408a	TrGAroCN	TLBIPERO2 + NO → NO_2 + .6 GLYOX + .4 MGLYOX + HO_2 + .2 C4MDIAL + .2 C5DICARB + .2 TLFUONE + .2 BZFUONE + .2 MALDIAL	KRO2NO*(1.-alpha_AN(11,2,0,0,1, temp,cair))	Rickard and Pascoe (2009)*
G47408b	TrGAroCN	TLBIPERO2 + NO → TLBIPERNO3	KRO2NO*alpha_AN(11,2,0,0,1, temp,cair)	Rickard and Pascoe (2009)*
G47409	TrGAroCN	TLBIPERO2 + NO_3 → NO_2 + .6 GLYOX + .4 MGLYOX + HO_2 + .2 C4MDIAL + .2 C5DICARB + .2 TLFUONE + .2 BZFUONE + .2 MALDIAL	KRO2NO3	Rickard and Pascoe (2009)*
G47410	TrGAroC	TLBIPERO2 → .6 GLYOX + .4 MGLYOX + HO_2 + .2 C4MDIAL + .2 C5DICARB + .2 TLFUONE + .2 BZFUONE + .2 MALDIAL	k1_RO2sORO2	Rickard and Pascoe (2009)*
G47411	TrGAroCN	TLEPOXMUC + NO_3 → TLEMUCCO3 + HNO_3	KNO3AL*2.75	Rickard and Pascoe (2009)
G47412	TrGAroC	TLEPOXMUC + O_3 → EPXC4DIAL + .125 CH_3CHO + .695 $CH_3C(O)$ + .57 CO + .57 OH + .125 HO_2 + .1125 CH_3COCO_2H + .0675 MGLYOX + .0675 H_2O_2 + .25 CO_2	5.00E-18	Rickard and Pascoe (2009)*
G47413	TrGAroC	TLEPOXMUC + OH → .31 TLEMUCCO3 + .69 TLEMUCO2	7.99E-11	Rickard and Pascoe (2009)*
G47414	TrGAroC	C6H5CH2OOH + OH → BENZAL + OH	2.05E-11	Rickard and Pascoe (2009)
G47415	TrGAroCN	C6H5CH2NO3 + OH → BENZAL + NO_2	6.03E-12	Rickard and Pascoe (2009)
G47416	TrGAroCN	BENZAL + NO_3 → C6H5CO3 + HNO_3	2.40E-15	Rickard and Pascoe (2009)
G47417	TrGAroC	BENZAL + OH → C6H5CO3	5.9E-12*EXP(225./temp)	Rickard and Pascoe (2009)
G47418a	TrGAroC	CRESO2 + HO_2 → CRESOOH	k_RO2_HO2(temp,7)*(1.-r_CHOHCH2O2_OH)	Rickard and Pascoe (2009)
G47418b	TrGAroC	CRESO2 + HO_2 → .68 C5CO14OH + .68 GLYOX + HO_2 + .32 PTLQONE + OH	k_RO2_HO2(temp,7)*r_CHOHCH2O2_OH	Rickard and Pascoe (2009)*
G47419	TrGAroCN	CRESO2 + NO → .68 C5CO14OH + .68 GLYOX + HO_2 + .32 PTLQONE + NO_2	KRO2NO	Rickard and Pascoe (2009)*
G47420	TrGAroCN	CRESO2 + NO_3 → .68 C5CO14OH + .68 GLYOX + HO_2 + .32 PTLQONE + NO_2	KRO2NO3	Rickard and Pascoe (2009)*
G47421	TrGAroC	CRESO2 → .68 C5CO14OH + .68 GLYOX + HO_2 + .32 PTLQONE	k1_RO2ISOPDO2	Rickard and Pascoe (2009)*

Table 1: Gas phase reactions (... continued)

#	labels	reaction	rate coefficient	reference
G47422a	TrGAroCN	NCRESO2 + HO_2 → NCRESOOH	k_RO2_HO2(temp,7)*(1.-r_CHOHCH2O2_OH)	Rickard and Pascoe (2009)
G47422b	TrGAroCN	NCRESO2 + HO_2 → C5CO14OH + GLYOX + NO_2 + OH	k_RO2_HO2(temp,7)*r_CHOHCH2O2_OH	Rickard and Pascoe (2009)*
G47423	TrGAroCN	NCRESO2 + NO → C5CO14OH + GLYOX + NO_2 + NO_2	KRO2NO	Rickard and Pascoe (2009)*
G47424	TrGAroCN	NCRESO2 + NO_3 → C5CO14OH + GLYOX + NO_2 + NO_2	KRO2NO3	Rickard and Pascoe (2009)*
G47425	TrGAroCN	NCRESO2 → C5CO14OH + GLYOX + NO_2	k1_RO2ISOPDO2	Rickard and Pascoe (2009)*
G47426	TrGAroCN	TOL1O + NO_2 → TOL1OHNO2	k_C6H5O_NO2	Rickard and Pascoe (2009), Platz et al. (1998)*
G47427	TrGAroC	TOL1O + O_3 → OXYL1O2	k_C6H5O_O3	Rickard and Pascoe (2009), Tao and Li (1999)
G47428	TrGAroCN	MCATECHOL + NO_3 → MCATEC1O + HNO_3	1.7E-10*1.0	Rickard and Pascoe (2009)
G47429	TrGAroC	MCATECHOL + O_3 → MC3ODBCO2H + $HCOCO_2H$ + HO_2 + OH	2.8E-17	Rickard and Pascoe (2009)*
G47430	TrGAroC	MCATECHOL + OH → MCATEC1O	2.0E-10*1.0	Rickard and Pascoe (2009)
G47431	TrGAroC	TLBIPEROOH + OH → TLOBIPEROH + OH	9.64E-11	Rickard and Pascoe (2009)
G47432	TrGAroCN	TLBIPERNO3 + OH → TLOBIPEROH + NO_2	7.16E-11	Rickard and Pascoe (2009)
G47433	TrGAroC	TLOBIPEROH + OH → C5CO14O2 + GLYOX	7.99E-11	Rickard and Pascoe (2009)
G47434a	TrGAroC	TLEMUCCO3 + HO_2 → C615CO2O2 + CO_2 + OH	KAPHO2*r_CO3_OH	Rickard and Pascoe (2009)
G47434b	TrGAroC	TLEMUCCO3 + HO_2 → TLEMUCCO2H + O_3	KAPHO2*r_CO3_O3	Rickard and Pascoe (2009)
G47434c	TrGAroC	TLEMUCCO3 + HO_2 → TLEMUCCO3H	KAPHO2*r_CO3_OOH	Rickard and Pascoe (2009)
G47435	TrGAroCN	TLEMUCCO3 + NO → C615CO2O2 + CO_2 + NO_2	KAPNO	Rickard and Pascoe (2009)
G47436	TrGAroCN	TLEMUCCO3 + NO_2 → TLEMUCPAN	k_CH3CO3_NO2	Rickard and Pascoe (2009)*
G47437	TrGAroCN	TLEMUCCO3 + NO_3 → C615CO2O2 + CO_2 + NO_2	KRO2NO3*1.74	Rickard and Pascoe (2009)
G47438	TrGAroC	TLEMUCCO3 → C615CO2O2 + CO_2	k1_RO2RCO3	Rickard and Pascoe (2009)*
G47439a	TrGAroC	TLEMUCO2 + HO_2 → TLEMUCOOH	k_RO2_HO2(temp,7)*(1.-r_CHOHCH2O2_OH-r_COCH2O2_OH)	Rickard and Pascoe (2009)
G47439b	TrGAroC	TLEMUCO2 + HO_2 → .5 C3DIALO2 + .5 CO2H3CHO + .5 EPXC4DIAL + .5 MGLYOX + .5 HO_2 + OH	k_RO2_HO2(temp,7)*(r_CHOHCH2O2_OH+r_COCH2O2_OH)	Rickard and Pascoe (2009)*
G47440a	TrGAroCN	TLEMUCO2 + NO → TLEMUCNO3	KRO2NO*alpha_AN(11,2,1,0,0, temp,cair)	Rickard and Pascoe (2009)
G47440b	TrGAroCN	TLEMUCO2 + NO → .5 C3DIALO2 + .5 CO2H3CHO + .5 EPXC4DIAL + .5 MGLYOX + .5 HO_2 + NO_2	KRO2NO*(1.-alpha_AN(11,2,1,0,0, temp,cair))	Rickard and Pascoe (2009)*

Table 1: Gas phase reactions (... continued)

#	labels	reaction	rate coefficient	reference
G47441	TrGAroCN	TLEMUCO2 + NO_3 → .5 C3DIALO2 + .5 CO2H3CHO + .5 EPXC4DIAL + .5 MGLYOX + .5 HO_2 + NO_2	KRO2NO3	Rickard and Pascoe (2009)*
G47442	TrGAroC	TLEMUCO2 → .5 C3DIALO2 + .5 CO2H3CHO + .5 EPXC4DIAL + .5 MGLYOX + .5 HO_2	k1_RO2sORO2	Rickard and Pascoe (2009)*
G47443a	TrGAroC	C6H5CO3 + HO_2 → C6H5CO3H	1.1E-11*EXP(364./temp)*0.65	Roth et al. (2010)
G47443b	TrGAroC	C6H5CO3 + HO_2 → C6H5O2 + CO_2 + OH	1.1E-11*EXP(364./temp)*0.20	Roth et al. (2010)
G47443c	TrGAroC	C6H5CO3 + HO_2 → PHCOOH + O_3	1.1E-11*EXP(364./temp)*0.15	Roth et al. (2010)
G47444	TrGAroCN	C6H5CO3 + NO → C6H5O2 + CO_2 + NO_2	KAPNO	Rickard and Pascoe (2009)
G47445	TrGAroCN	C6H5CO3 + NO_2 → PBZN	k_CH3CO3_NO2	Rickard and Pascoe (2009)*
G47446	TrGAroCN	C6H5CO3 + NO_3 → C6H5O2 + CO_2 + NO_2	KRO2NO3*1.74	Rickard and Pascoe (2009)
G47447	TrGAroC	C6H5CO3 → C6H5O2 + CO_2	k1_RO2RCO3	Rickard and Pascoe (2009)*
G47448	TrGAroC	CRESOOH + OH → CRESO2	1.15E-10	Rickard and Pascoe (2009)
G47449	TrGAroCN	NCRESOOH + OH → NCRESO2	1.07E-10	Rickard and Pascoe (2009)
G47450	TrGAroCN	TOL1OHNO2 + NO_3 → NCRES1O + HNO_3	3.13E-13*1.0	Rickard and Pascoe (2009)
G47451	TrGAroCN	TOL1OHNO2 + OH → NCRES1O	2.8E-12	Rickard and Pascoe (2009)
G47452	TrGAroC	OXYL1O2 + HO_2 → OXYL1OOH	k_RO2_HO2(temp,7)	Rickard and Pascoe (2009)
G47453	TrGAroCN	OXYL1O2 + NO → TOL1O + NO_2	KRO2NO	Rickard and Pascoe (2009)
G47454	TrGAroCN	OXYL1O2 + NO_2 → TOL1O + NO_3	k_C6H5O2_NO2	Jagiella and Zabel (2007)*
G47455	TrGAroCN	OXYL1O2 + NO_3 → TOL1O + NO_2	KRO2NO3	Rickard and Pascoe (2009)
G47456	TrGAroC	OXYL1O2 → TOL1O	k1_RO2sRO2	Rickard and Pascoe (2009)
G47457	TrGAroCN	MCATEC1O + NO_2 → MNCATECH	k_C6H5O_NO2	Rickard and Pascoe (2009), Platz et al. (1998)
G47458	TrGAroC	MCATEC1O + O_3 → MCATEC1O2	k_C6H5O_O3	Rickard and Pascoe (2009), Tao and Li (1999)
G47459	TrGAroC	TLEMUCCO2H + OH → C615CO2O2 + CO_2	5.98E-11	Rickard and Pascoe (2009)
G47460	TrGAroC	TLEMUCCO3H + OH → TLEMUCCO3	6.29E-11	Rickard and Pascoe (2009)
G47461	TrGAroCN	TLEMUCPAN + OH → C5DICARB + CO + CO_2 + NO_2	5.96E-11	Rickard and Pascoe (2009)
G47462	TrGAroCN	TLEMUCPAN → TLEMUCCO3 + NO_2	k_PAN_M	Rickard and Pascoe (2009)
G47463	TrGAroC	TLEMUCOOH + OH → TLEMUCCO + OH	7.04E-11	Rickard and Pascoe (2009)
G47464	TrGAroCN	TLEMUCNO3 + OH → TLEMUCCO + NO_2	3.06E-11	Rickard and Pascoe (2009)
G47465	TrGAroC	TLEMUCCO + OH → $CH_3C(O)$ + EPXC4DIAL + CO	4.06E-11	Rickard and Pascoe (2009)
G47466	TrGAroC	C6H5CO3H + OH → C6H5CO3	4.66E-12	Rickard and Pascoe (2009)
G47467	TrGAroC	PHCOOH + OH → C6H5O2 + CO_2	1.10E-12	Rickard and Pascoe (2009)
G47468	TrGAroCN	PBZN + OH → C6H5OOH + CO + NO_2	1.06E-12	Rickard and Pascoe (2009)
G47469	TrGAroCN	PBZN → C6H5CO3 + NO_2	k_PAN_M*0.67	Rickard and Pascoe (2009)

Table 1: Gas phase reactions (... continued)

#	labels	reaction	rate coefficient	reference
G47470	TrGAroCN	PTLQONE + NO_3 → NPTLQO2	1.00E-12	Rickard and Pascoe (2009)
G47471	TrGAroC	PTLQONE + OH → PTLQO2	2.3E-11	Rickard and Pascoe (2009)
G47472	TrGAroCN	NCRES1O + NO_2 → DNCRES	k_C6H5O_NO2	Rickard and Pascoe (2009), Platz et al. (1998)
G47473	TrGAroCN	NCRES1O + O_3 → NCRES1O2	k_C6H5O_O3	Rickard and Pascoe (2009), Tao and Li (1999)
G47474	TrGAroC	OXYL1OOH + OH → OXYL1O2	4.65E-11	Rickard and Pascoe (2009)
G47475	TrGAroCN	MNCATECH + NO_3 → MNNCATECO2	5.03E-12	Rickard and Pascoe (2009)
G47476	TrGAroCN	MNCATECH + OH → MNCATECO2	6.83E-12	Rickard and Pascoe (2009)
G47477	TrGAroC	MCATEC1O2 + HO_2 → MCATEC1OOH	k_RO2_HO2(temp,7)	Rickard and Pascoe (2009)
G47478	TrGAroCN	MCATEC1O2 + NO → MCATEC1O + NO_2	KRO2NO	Rickard and Pascoe (2009)
G47479	TrGAroCN	MCATEC1O2 + NO_2 → MCATEC1O + NO_3	k_C6H5O2_NO2	Jagiella and Zabel (2007)*
G47480	TrGAroCN	MCATEC1O2 + NO_3 → MCATEC1O + NO_2	KRO2NO3	Rickard and Pascoe (2009)
G47481	TrGAroC	MCATEC1O2 → MCATEC1O	k1_RO2sORO2	Rickard and Pascoe (2009)
G47482a	TrGAroCN	NPTLQO2 + HO_2 → NPTLQOOH	k_RO2_HO2(temp,7)*(1.-r_COCH2O2_OH)	Rickard and Pascoe (2009)
G47482b	TrGAroCN	NPTLQO2 + HO_2 → C7CO4DB + NO_2 + OH	k_RO2_HO2(temp,7)*r_COCH2O2_OH	Rickard and Pascoe (2009)*
G47483	TrGAroCN	NPTLQO2 + NO → C7CO4DB + NO_2 + NO_2	KRO2NO	Rickard and Pascoe (2009)*
G47484	TrGAroCN	NPTLQO2 + NO_3 → C7CO4DB + NO_2 + NO_2	KRO2NO3	Rickard and Pascoe (2009)*
G47485	TrGAroCN	NPTLQO2 → C7CO4DB + NO_2	k1_RO2sORO2	Rickard and Pascoe (2009)*
G47486a	TrGAroC	PTLQO2 + HO_2 → PTLQOOH	k_RO2_HO2(temp,7)*(1.-r_CHOHCH2O2_OH-r_COCH2O2_OH)	Rickard and Pascoe (2009)
G47486b	TrGAroC	PTLQO2 + HO_2 → C6CO2OHCO3 + OH	k_RO2_HO2(temp,7)*(r_CHOHCH2O2_OH+r_COCH2O2_OH)	Rickard and Pascoe (2009)*
G47487	TrGAroCN	PTLQO2 + NO → C6CO2OHCO3 + NO_2	KRO2NO	Rickard and Pascoe (2009)*
G47488	TrGAroCN	PTLQO2 + NO_3 → C6CO2OHCO3 + NO_2	KRO2NO3	Rickard and Pascoe (2009)*
G47489	TrGAroC	PTLQO2 → C6CO2OHCO3	k1_RO2sORO2	Rickard and Pascoe (2009)*
G47490	TrGAroCN	DNCRES + NO_3 → NDNCRESO2	7.83E-15	Rickard and Pascoe (2009)
G47491	TrGAroCN	DNCRES + OH → DNCRESO2	5.10E-14	Rickard and Pascoe (2009)
G47492	TrGAroCN	NCRES1O2 + HO_2 → NCRES1OOH	k_RO2_HO2(temp,7)	Rickard and Pascoe (2009)
G47493	TrGAroCN	NCRES1O2 + NO → NCRES1O + NO_2	KRO2NO	Rickard and Pascoe (2009)
G47494	TrGAroCN	NCRES1O2 + NO_2 → NCRES1O + NO_3	k_C6H5O2_NO2	Jagiella and Zabel (2007)*
G47495	TrGAroCN	NCRES1O2 + NO_3 → NCRES1O + NO_2	KRO2NO3	Rickard and Pascoe (2009)
G47496	TrGAroCN	NCRES1O2 → NCRES1O	k1_RO2sRO2	Rickard and Pascoe (2009)

Table 1: Gas phase reactions (... continued)

#	labels	reaction	rate coefficient	reference
G47497a	TrGAroCN	MNNCATECO2 + HO_2 → MNNCATCOOH	k_RO2_HO2(temp,7)*(1.-r_CHOHCH2O2_OH)	Rickard and Pascoe (2009)
G47497b	TrGAroCN	MNNCATECO2 + HO_2 → NC4MDCO2HN + $HCOCO_2H$ + NO_2 + OH	k_RO2_HO2(temp,7)*r_CHOHCH2O2_OH	Rickard and Pascoe (2009)*
G47498	TrGAroCN	MNNCATECO2 + NO → NC4MDCO2HN + $HCOCO_2H$ + NO_2 + NO_2	KRO2NO	Rickard and Pascoe (2009)*
G47499	TrGAroCN	MNNCATECO2 + NO_3 → NC4MDCO2HN + $HCOCO_2H$ + NO_2 + NO_2	KRO2NO3	Rickard and Pascoe (2009)*
G47500	TrGAroCN	MNNCATECO2 → NC4MDCO2HN + $HCOCO_2H$ + NO_2	k1_RO2ISOPDO2	Rickard and Pascoe (2009)
G47501a	TrGAroCN	MNCATECO2 + HO_2 → MNCATECOOH	k_RO2_HO2(temp,7)*(1.-r_CHOHCH2O2_OH)	Rickard and Pascoe (2009)
G47501b	TrGAroCN	MNCATECO2 + HO_2 → NC4MDCO2HN + $HCOCO_2H$ + HO_2 + OH	k_RO2_HO2(temp,7)*r_CHOHCH2O2_OH	Rickard and Pascoe (2009)*
G47502	TrGAroCN	MNCATECO2 + NO → NC4MDCO2HN + $HCOCO_2H$ + HO_2 + NO_2	KRO2NO	Rickard and Pascoe (2009)*
G47503	TrGAroCN	MNCATECO2 + NO_3 → NC4MDCO2HN + $HCOCO_2H$ + HO_2 + NO_2	KRO2NO3	Rickard and Pascoe (2009)*
G47504	TrGAroCN	MNCATECO2 → NC4MDCO2HN + $HCOCO_2H$ + HO_2	k1_RO2ISOPDO2	Rickard and Pascoe (2009)*
G47505	TrGAroC	MCATEC1OOH + OH → MCATEC1O2	2.05E-10	Rickard and Pascoe (2009)
G47506	TrGAroCN	NPTLQOOH + OH → NPTLQO2	8.56E-11	Rickard and Pascoe (2009)
G47507	TrGAroC	PTLQOOH + OH → PTLQCO + OH	1.42E-10	Rickard and Pascoe (2009)
G47508	TrGAroC	PTLQCO + OH → C6CO2OHCO3	7.95E-11	Rickard and Pascoe (2009)
G47509a	TrGAroCN	NDNCRESO2 + HO_2 → NDNCRESOOH	k_RO2_HO2(temp,7)*(1.-r_CHOHCH2O2_OH)	Rickard and Pascoe (2009)
G47509b	TrGAroCN	NDNCRESO2 + HO_2 → NC4MDCO2HN + HNO_3 + 2 CO + NO_2 + OH	k_RO2_HO2(temp,7)*r_CHOHCH2O2_OH	Rickard and Pascoe (2009)*
G47510	TrGAroCN	NDNCRESO2 + NO → NC4MDCO2HN + HNO_3 + 2 CO + NO_2 + NO_2	KRO2NO	Rickard and Pascoe (2009)*
G47511	TrGAroCN	NDNCRESO2 + NO_3 → NC4MDCO2HN + HNO_3 + 2 CO + NO_2 + NO_2	KRO2NO3	Rickard and Pascoe (2009)*
G47512	TrGAroCN	NDNCRESO2 → NC4MDCO2HN + HNO_3 + 2 CO + NO_2	k1_RO2ISOPDO2	Rickard and Pascoe (2009)*
G47513a	TrGAroCN	DNCRESO2 + HO_2 → DNCRESOOH	k_RO2_HO2(temp,7)*(1.-r_CHOHCH2O2_OH)	Rickard and Pascoe (2009)
G47513b	TrGAroCN	DNCRESO2 + HO_2 → NC4MDCO2HN + $HCOCO_2H$ + NO_2 + OH	k_RO2_HO2(temp,7)*r_CHOHCH2O2_OH	Rickard and Pascoe (2009)*

Table 1: Gas phase reactions (... continued)

#	labels	reaction	rate coefficient	reference
G47514	TrGAroCN	DNCRESO2 + NO → NC4MDCO2HN + $HCOCO_2H$ + NO_2 + NO_2	KRO2NO	Rickard and Pascoe (2009)*
G47515	TrGAroCN	DNCRESO2 + NO_3 → NC4MDCO2HN + $HCOCO_2H$ + NO_2 + NO_2	KRO2NO3	Rickard and Pascoe (2009)*
G47516	TrGAroCN	DNCRESO2 → NC4MDCO2HN + $HCOCO_2H$ + NO_2	k1_RO2ISOPDO2	Rickard and Pascoe (2009)*
G47517	TrGAroCN	NCRES1OOH + OH → NCRES1O2	1.53E-12	Rickard and Pascoe (2009)
G47518	TrGAroCN	MNNCATCOOH + OH → MNNCATECO2	k_ROOHRO	Rickard and Pascoe (2009)
G47519	TrGAroCN	MNCATECOOH + OH → MNCATECO2	k_ROOHRO	Rickard and Pascoe (2009)
G47520	TrGAroC	C7CO4DB + OH → CO + CO + $CH_3C(O)$ + HCOCOCHO	9.58E-11	Rickard and Pascoe (2009)
G47521a	TrGAroC	C6CO2OHCO3 + HO_2 → C5134CO2OH + HO_2 + CO + CO_2 + OH	KAPHO2*r_CO3_OH	Rickard and Pascoe (2009)
G47521b	TrGAroC	C6CO2OHCO3 + HO_2 → C6COOHCO3H	KAPHO2*(r_CO3_OOH+r_CO3_O3)	Rickard and Pascoe (2009)
G47522	TrGAroCN	C6CO2OHCO3 + NO → C5134CO2OH + HO_2 + CO + CO_2 + NO_2	KAPNO	Rickard and Pascoe (2009)
G47523	TrGAroCN	C6CO2OHCO3 + NO_2 → C6CO2OHPAN	k_CH3CO3_NO2	Rickard and Pascoe (2009)
G47524	TrGAroCN	C6CO2OHCO3 + NO_3 → C5134CO2OH + HO_2 + CO + CO_2 + NO_2	KRO2NO3*1.74	Rickard and Pascoe (2009)
G47525	TrGAroC	C6CO2OHCO3 → C5134CO2OH + HO_2 + CO + CO_2	k1_RO2RCO3	Rickard and Pascoe (2009)
G47526	TrGAroCN	NDNCRESOOH + OH → NDNCRESO2	k_ROOHRO	Rickard and Pascoe (2009)
G47527	TrGAroCN	DNCRESOOH + OH → DNCRESO2	k_ROOHRO	Rickard and Pascoe (2009)
G47528	TrGAroC	C6COOHCO3H + OH → C6CO2OHCO3	9.29E-11	Rickard and Pascoe (2009)
G47529	TrGAroCN	C6CO2OHPAN + OH → C5134CO2OH + CO + CO + NO_2	8.96E-11	Rickard and Pascoe (2009)
G47530	TrGAroCN	C6CO2OHPAN → C6CO2OHCO3 + NO_2	k_PAN_M	Rickard and Pascoe (2009)
G48200	TrGTerC	C85O2 → C86O2	k1_RO2tRO2	Rickard and Pascoe (2009)
G48201	TrGTerC	C85O2 + HO_2 → C85OOH	k_RO2_HO2(temp,8)	Rickard and Pascoe (2009)
G48202	TrGTerCN	C85O2 + NO → C86O2 + NO_2	KRO2NO	Rickard and Pascoe (2009)*
G48203	TrGTerC	C85OOH + OH → C85O2	1.29E-11	Rickard and Pascoe (2009)
G48204	TrGTerC	C86O2 → C511O2 + CH_3COCH_3	k1_RO2tRO2	Rickard and Pascoe (2009)
G48205	TrGTerCN	C86O2 + NO → C511O2 + CH_3COCH_3 + NO_2	KRO2NO	Rickard and Pascoe (2009)*
G48206	TrGTerC	C86O2 + HO_2 → C86OOH	k_RO2_HO2(temp,8)	Rickard and Pascoe (2009)
G48207	TrGTerC	C86OOH + OH → C86O2	3.45E-11	Rickard and Pascoe (2009)
G48208	TrGTerC	C811O2 → C812O2	k1_RO2pRO2	Rickard and Pascoe (2009)
G48209	TrGTerC	C811O2 + HO_2 → 8 LCARBON	k_RO2_HO2(temp,8)	Rickard and Pascoe (2009)

Table 1: Gas phase reactions (... continued)

#	labels	reaction	rate coefficient	reference
G48210	TrGTerCN	C811O2 + NO → C812O2 + NO_2	KRO2NO	Rickard and Pascoe (2009)*
G48211	TrGTerC	C812O2 → C813O2	k1_RO2tORO2	Rickard and Pascoe (2009)
G48212	TrGTerCN	C812O2 + NO → C813O2 + NO_2	KRO2NO	Rickard and Pascoe (2009)*
G48213	TrGTerC	C812O2 + HO_2 → C812OOH	k_RO2_HO2(temp,8)	Rickard and Pascoe (2009)
G48214	TrGTerC	C812OOH + OH → C812O2	1.09E-11	Rickard and Pascoe (2009)
G48215	TrGTerC	C813O2 → CH_3COCH_3 + C512O2	k1_RO2tRO2	Rickard and Pascoe (2009)
G48216	TrGTerCN	C813O2 + NO → CH_3COCH_3 + C512O2 + NO_2	KRO2NO	Rickard and Pascoe (2009)*
G48217	TrGTerC	C813O2 + HO_2 → C813OOH	k_RO2_HO2(temp,8)	Rickard and Pascoe (2009)
G48218	TrGTerC	C813OOH + OH → C813O2	1.86E-11	Rickard and Pascoe (2009)
G48219	TrGTerCN	C721CHO + NO_3 → C721CO3 + HNO_3	KNO3AL*8.5	Rickard and Pascoe (2009)
G48220	TrGTerC	C721CHO + OH → C721CO3	2.63E-11	Rickard and Pascoe (2009)
G48221a	TrGTerC	C721CO3 + HO_2 → C721CO3H	KAPHO2*r_CO3_OOH	Rickard and Pascoe (2009)
G48221b	TrGTerC	C721CO3 + HO_2 → C721O2 + CO_2 + OH	KAPHO2*r_CO3_OH	Rickard and Pascoe (2009)
G48221c	TrGTerC	C721CO3 + HO_2 → NORPINIC + O_3	KAPHO2*r_CO3_O3	Rickard and Pascoe (2009)
G48222	TrGTerCN	C721CO3 + NO → C721O2 + CO_2 + NO_2	KAPNO	Rickard and Pascoe (2009)*
G48223	TrGTerCN	C721CO3 + NO_2 → C721PAN	k_CH3CO3_NO2	Rickard and Pascoe (2009)
G48224	TrGTerCN	C721CO3 + NO_3 → C721O2 + CO_2 + NO_2	KRO2NO3*1.74	Rickard and Pascoe (2009)
G48225	TrGTerC	C721CO3 → C721O2 + CO_2	k1_RO2RCO3*0.9	Sander et al. (2019)
G48226	TrGTerC	C721CO3 → NORPINIC	k1_RO2RCO3*0.1	Sander et al. (2019)
G48227	TrGTerC	C721CO3H + OH → C721CO3	9.65E-12	Rickard and Pascoe (2009)
G48228	TrGTerC	NORPINIC + OH → C721O2 + CO_2	6.57E-12	Rickard and Pascoe (2009)
G48229	TrGTerCN	C721PAN + OH → C721OOH + CO + NO_2	2.96E-12	Rickard and Pascoe (2009)
G48230	TrGTerCN	C721PAN → C721CO3 + NO_2	k_PAN_M	Rickard and Pascoe (2009)
G48231	TrGTerC	C8BC + OH → C8BCO2	3.04E-12	Rickard and Pascoe (2009)
G48232	TrGTerC	C8BCO2 + HO_2 → C8BCOOH	k_RO2_HO2(temp,8)	Rickard and Pascoe (2009)
G48233a	TrGTerCN	C8BCO2 + NO → C89O2 + NO_2	KRO2NO*(1.-alpha_AN(8,2,0,0,0, temp,cair))	Rickard and Pascoe (2009)
G48233b	TrGTerCN	C8BCO2 + NO → C8BCNO3	KRO2NO*alpha_AN(8,2,0,0,0,temp, cair)	Rickard and Pascoe (2009)
G48234	TrGTerC	C8BCO2 → C89O2	k1_RO2sRO2	Rickard and Pascoe (2009)
G48235	TrGTerC	C8BCOOH + OH → C8BCCO + OH	1.62E-11	Rickard and Pascoe (2009)
G48236	TrGTerCN	C8BCNO3 + OH → C8BCCO + NO_2	1.84E-12	Rickard and Pascoe (2009)
G48237	TrGTerC	C8BCCO + OH → C89O2	3.94E-12	Rickard and Pascoe (2009)
G48238	TrGTerC	C89O2 + HO_2 → C89OOH	k_RO2_HO2(temp,8)	Rickard and Pascoe (2009)

Table 1: Gas phase reactions (... continued)

#	labels	reaction	rate coefficient	reference
G48239a	TrGTerCN	C89O2 + NO → C810O2 + NO_2	KRO2NO*(1.-alpha_AN(7,2,0,0,0, temp,cair))	Rickard and Pascoe (2009)
G48239b	TrGTerCN	C89O2 + NO → C89NO3	KRO2NO*alpha_AN(7,2,0,0,0,temp, cair)	Rickard and Pascoe (2009)
G48240	TrGTerCN	C89O2 + NO_3 → C810O2 + NO_2	KRO2NO3	Rickard and Pascoe (2009)
G48241	TrGTerC	C89O2 → C810O2	k1_RO2tRO2	Rickard and Pascoe (2009)
G48242	TrGTerC	C89OOH + OH → C89O2	3.61E-11	Rickard and Pascoe (2009)
G48243	TrGTerCN	C89NO3 + OH → CH_3COCH_3 + CO13C4CHO + NO_2	2.56E-11	Rickard and Pascoe (2009)
G48244	TrGTerC	C810O2 + HO_2 → C810OOH	k_RO2_HO2(temp,8)	Rickard and Pascoe (2009)
G48245a	TrGTerCN	C810O2 + NO → CH_3COCH_3 + C514O2 + NO_2	KRO2NO*(1.-alpha_AN(10,3,0,0,0, temp,cair))	Rickard and Pascoe (2009)
G48245b	TrGTerCN	C810O2 + NO → C810NO3	KRO2NO*alpha_AN(10,3,0,0,0, temp,cair)	Rickard and Pascoe (2009)
G48246	TrGTerCN	C810O2 + NO_3 → CH_3COCH_3 + C514O2 + NO_2	KRO2NO3	Rickard and Pascoe (2009)
G48247	TrGTerC	C810O2 → CH_3COCH_3 + C514O2	k1_RO2tRO2	Rickard and Pascoe (2009)
G48248	TrGTerC	C810OOH + OH → C810O2	8.35E-11	Rickard and Pascoe (2009)
G48249	TrGTerCN	C810NO3 + OH → CH_3COCH_3 + CO13C4CHO + NO_2	4.96E-11	Rickard and Pascoe (2009)
G48400a	TrGAroC	LXYL + OH → TLEPOXMUC + HO_2 + LCARBON	0.401E-11	Rickard and Pascoe (2009)*
G48400b	TrGAroC	LXYL + OH → C6H5CH2O2 + LCARBON	0.101E-11	Rickard and Pascoe (2009)*
G48400c	TrGAroC	LXYL + OH → CRESOL + LCARBON	0.261E-11	Rickard and Pascoe (2009)*
G48400d	TrGAroC	LXYL + OH → TLBIPERO2 + HO_2 + LCARBON	0.932E-11	Rickard and Pascoe (2009)*
G48401	TrGAroCN	LXYL + NO_3 → C6H5CH2O2 + HNO_3 + LCARBON	3.9E-16	Rickard and Pascoe (2009)*
G48402	TrGAroC	EBENZ + OH → .10 TLEPOXMUC + .07 C6H5CH2O2 + .18 CRESOL + .65 TLBIPERO2 + .28 HO_2 + LCARBON	7.00E-12	Rickard and Pascoe (2009)*
G48403	TrGAroCN	EBENZ + NO_3 → C6H5CH2O2 + HNO_3 + LCARBON	1.20E-16	Rickard and Pascoe (2009)*
G48404	TrGAroCN	STYRENE + NO_3 → NSTYRENO2	1.50E-12	Rickard and Pascoe (2009)
G48405	TrGAroC	STYRENE + O_3 → .545 HCHO + .1 BENZENE + .28 C6H5O2 + .56 CO + .36 OH + .28 HO_2 + .075 PHCOOH + .545 BENZAL + .09 H_2O_2 + .075 HCOOH + .2 CO_2	1.70E-17	Rickard and Pascoe (2009)*
G48406	TrGAroC	STYRENE + OH → STYRENO2	5.80E-11	Rickard and Pascoe (2009)
G48407	TrGAroCN	NSTYRENO2 + HO_2 → NSTYRENOOH	k_RO2_HO2(temp,8)	Rickard and Pascoe (2009)
G48408	TrGAroCN	NSTYRENO2 + NO → NO_2 + NO_2 + HCHO + BENZAL	KRO2NO	Rickard and Pascoe (2009)*
G48409	TrGAroCN	NSTYRENO2 + NO_3 → NO_2 + NO_2 + HCHO + BENZAL	KRO2NO3	Rickard and Pascoe (2009)*
G48410	TrGAroCN	NSTYRENO2 → NO_2 + HCHO + BENZAL	k1_RO2sRO2	Rickard and Pascoe (2009)*

Table 1: Gas phase reactions (... continued)

#	labels	reaction	rate coefficient	reference
G48411	TrGAroCN	NSTYRENOOH + OH → NSTYRENO2	6.16E-11	Rickard and Pascoe (2009)
G48412a	TrGAroC	STYRENO2 + HO_2 → STYRENOOH	k_RO2_HO2(temp,8)*(1.-r_CHOHCH2O2_OH)	Rickard and Pascoe (2009)
G48412b	TrGAroC	STYRENO2 + HO_2 → HO_2 + OH + HCHO + BENZAL	k_RO2_HO2(temp,8)*r_CHOHCH2O2_OH	Rickard and Pascoe (2009)*
G48413	TrGAroCN	STYRENO2 + NO → NO_2 + HO_2 + HCHO + BENZAL	KRO2NO	Rickard and Pascoe (2009)*
G48414	TrGAroCN	STYRENO2 + NO_3 → NO_2 + HO_2 + HCHO + BENZAL	KRO2NO3	Rickard and Pascoe (2009)*
G48415	TrGAroC	STYRENO2 → HO_2 + HCHO + BENZAL	k1_RO2sRO2	Rickard and Pascoe (2009)*
G48416	TrGAroC	STYRENOOH + OH → STYRENO2	6.16E-11	Rickard and Pascoe (2009)
G49200	TrGTerC	C96O2 → C97O2	k1_RO2pRO2	Rickard and Pascoe (2009)
G49201	TrGTerC	C96O2 + HO_2 → C96OOH	k_RO2_HO2(temp,9)	Rickard and Pascoe (2009)
G49202a	TrGTerCN	C96O2 + NO → C97O2 + NO_2	KRO2NO*(1.-alpha_AN(10,1,0,0,0,temp,cair))	Rickard and Pascoe (2009)
G49202b	TrGTerCN	C96O2 + NO → C96NO3	KRO2NO*alpha_AN(10,1,0,0,0,temp,cair)	Rickard and Pascoe (2009)
G49203	TrGTerCN	C96NO3 + OH → NORPINAL + NO_2	2.88E-12	Rickard and Pascoe (2009)
G49204a	TrGTerC	C96OOH + OH → C96O2	k_ROOHRO	Rickard and Pascoe (2009)
G49205b	TrGTerC	C96OOH + OH → NORPINAL + OH	1.30E-11	Rickard and Pascoe (2009)
G49206	TrGTerC	C97O2 → C98O2	k1_RO2tRO2	Rickard and Pascoe (2009)
G49207	TrGTerCN	C97O2 + NO → C98O2 + NO_2	KRO2NO	Rickard and Pascoe (2009)*
G49208a	TrGTerC	C97O2 + HO_2 → C97OOH	k_RO2_HO2(temp,9)*r_COCH2O2_OOH	Rickard and Pascoe (2009), Sander et al. (2019)
G49208b	TrGTerC	C97O2 + HO_2 → C98O2 + OH	k_RO2_HO2(temp,9)*r_COCH2O2_OH	Rickard and Pascoe (2009), Sander et al. (2019)
G49209	TrGTerC	C97OOH + OH → C97O2	1.05E-11	Rickard and Pascoe (2009)
G49210	TrGTerC	C98O2 → C614O2 + CH_3COCH_3	k1_RO2tRO2	Rickard and Pascoe (2009)
G49211a	TrGTerCN	C98O2 + NO → C614O2 + CH_3COCH_3 + NO_2	KRO2NO*(1.-alpha_AN(12,3,0,0,0,temp,cair))	Rickard and Pascoe (2009)
G49211b	TrGTerCN	C98O2 + NO → 9 LCARBON + LNITROGEN	KRO2NO*alpha_AN(12,3,0,0,0,temp,cair)	Rickard and Pascoe (2009)
G49212	TrGTerC	C98O2 + HO_2 → C98OOH	k_RO2_HO2(temp,9)	Rickard and Pascoe (2009)
G49213	TrGTerC	C98OOH + OH → C98O2	2.05E-11	Rickard and Pascoe (2009)
G49214	TrGTerC	NORPINAL + OH → C85CO3	2.64E-11	Rickard and Pascoe (2009)
G49215	TrGTerCN	NORPINAL + NO_3 → C85CO3 + HNO_3	KNO3AL*8.5	Rickard and Pascoe (2009)
G49216	TrGTerC	C85CO3 → C85O2 + CO_2	k1_RO2RCO3	Rickard and Pascoe (2009)
G49217	TrGTerCN	C85CO3 + NO → C85O2 + CO_2 + NO_2	KAPNO	Rickard and Pascoe (2009)

62

Table 1: Gas phase reactions (... continued)

#	labels	reaction	rate coefficient	reference
G49218	TrGTerCN	C85CO3 + NO_2 → C9PAN2	k_CH3CO3_NO2	Rickard and Pascoe (2009)
G49219a	TrGTerC	C85CO3 + HO_2 → C85CO3H	KAPHO2*(r_CO3_OOH+r_CO3_O3)	Rickard and Pascoe (2009)
G49219b	TrGTerC	C85CO3 + HO_2 → C85O2 + CO_2 + OH	KAPHO2*r_CO3_OH	Rickard and Pascoe (2009)
G49220	TrGTerCN	C9PAN2 → C85CO3 + NO_2	k_PAN_M	Rickard and Pascoe (2009)
G49221	TrGTerCN	C9PAN2 + OH → C85OOH + CO + NO_2	6.60E-12	Rickard and Pascoe (2009)
G49222	TrGTerC	C85CO3H + OH → C85CO3	1.02E-11	Rickard and Pascoe (2009)
G49223a	TrGTerC	C89CO3 → .8 C811CO3 + .2 C89O2 + .2 CO_2	k1_RO2RCO3*0.9	Sander et al. (2019)
G49223b	TrGTerC	C89CO3 → C89CO2H	k1_RO2RCO3*0.1	Sander et al. (2019)
G49224a	TrGTerC	C89CO3 + HO_2 → C89CO3H	KAPHO2*r_CO3_OOH	Rickard and Pascoe (2009)
G49224b	TrGTerC	C89CO3 + HO_2 → C89CO2H + O_3	KAPHO2*r_CO3_O3	Rickard and Pascoe (2009)
G49224c	TrGTerC	C89CO3 + HO_2 → .80 C811CO3 + .20 C89O2 + .2 CO_2 + OH	KAPHO2*r_CO3_OH	Rickard and Pascoe (2009)
G49225	TrGTerCN	C89CO3 + NO_2 → C89PAN	k_CH3CO3_NO2	Rickard and Pascoe (2009)
G49226	TrGTerCN	C89CO3 + NO → .8 C811CO3 + .2 C89O2 + .2 CO_2 + NO_2	KAPNO	Rickard and Pascoe (2009)
G49227	TrGTerC	C89CO2H + OH → .8 C811CO3 + .2 C89O2 + .2 CO_2	2.69E-11	Rickard and Pascoe (2009)
G49228	TrGTerC	C89CO3H + OH → C89CO3	3.00E-11	Rickard and Pascoe (2009)
G49229	TrGTerCN	C89PAN → C89CO3 + NO_2	k_PAN_M	Rickard and Pascoe (2009)
G49230	TrGTerCN	C89PAN + OH → CH_3COCH_3 + CO13C4CHO + CO + NO_2	2.52E-11	Rickard and Pascoe (2009)
G49231a	TrGTerC	C811CO3 → C811O2 + CO_2	k1_RO2RCO3*0.9	Sander et al. (2019)
G49231b	TrGTerC	C811CO3 → PINIC	k1_RO2RCO3*0.1	Sander et al. (2019)
G49232a	TrGTerC	C811CO3 + HO_2 → C811CO3H	KAPHO2*r_CO3_OOH	Rickard and Pascoe (2009)
G49232b	TrGTerC	C811CO3 + HO_2 → PINIC + O_3	KAPHO2*r_CO3_O3	Rickard and Pascoe (2009)
G49232c	TrGTerC	C811CO3 + HO_2 → C811O2 + CO_2 + OH	KAPHO2*r_CO3_OH	Rickard and Pascoe (2009)
G49233	TrGTerCN	C811CO3 + NO → C811O2 + CO_2 + NO_2	KAPNO	Rickard and Pascoe (2009)
G49234	TrGTerCN	C811CO3 + NO_2 → C811PAN	k_CH3CO3_NO2	Rickard and Pascoe (2009)
G49235	TrGTerC	PINIC + OH → C811O2 + CO_2	7.29E-12	Rickard and Pascoe (2009)
G49236	TrGTerC	NOPINONE + OH → NOPINDO2	1.55E-11	Capouet et al. (2008), Rickard and Pascoe (2009)
G49237a	TrGTerC	NOPINDO2 + HO_2 → NOPINDOOH	k_RO2_HO2(temp,9)*r_COCH2O2_OOH	Rickard and Pascoe (2009), Sander et al. (2019)
G49237b	TrGTerC	NOPINDO2 + HO_2 → C89CO3 + OH	k_RO2_HO2(temp,9)*r_COCH2O2_OH	Rickard and Pascoe (2009), Sander et al. (2019)
G49238	TrGTerCN	NOPINDO2 + NO → C89CO3 + NO_2	KRO2NO	Rickard and Pascoe (2009)*

63

Table 1: Gas phase reactions (... continued)

#	labels	reaction	rate coefficient	reference
G49239	TrGTerC	NOPINDO2 → C89CO3	k1_RO2pORO2	Rickard and Pascoe (2009)
G49240	TrGTerC	NOPINDOOH → NOPINDCO	2.63E-11	Rickard and Pascoe (2009)
G49241	TrGTerC	NOPINDCO + OH → C89CO3	3.07E-12	Rickard and Pascoe (2009)
G49242	TrGTerC	NOPINOO → NOPINONE + H_2O_2	6.00E-18*c(ind_H2O)	Rickard and Pascoe (2009)
G49243	TrGTerC	NOPINOO + CO → NOPINONE + CO_2	1.2E-15	Rickard and Pascoe (2009)
G49244	TrGTerCN	NOPINOO + NO → NOPINONE + NO_2	1.E-14	Rickard and Pascoe (2009)
G49245	TrGTerCN	NOPINOO + NO_2 → NOPINONE + NO_3	1.E-15	Rickard and Pascoe (2009)
G49246	TrGTerC	NORPINENOL + OH → HCOOH + OH + C86O2	k_CH2CHOH_OH_HCOOH	Sander et al. (2019), So et al. (2014)*
G49247	TrGTerC	NORPINENOL + HCOOH → NORPINAL + HCOOH	k_CH2CHOH_HCOOH	Sander et al. (2019), da Silva (2010)*
G49248	TrGTerC	NORPINAL + HCOOH → NORPINENOL + HCOOH	k_ALD_HCOOH	Sander et al. (2019), da Silva (2010)*
G49249	TrGTerC	C811CO3H + OH → C811CO3	1.04E-11	Rickard and Pascoe (2009)
G49250	TrGTerCN	C811PAN → C811CO3 + NO_2	k_PAN_M	Rickard and Pascoe (2009)
G49251	TrGTerCN	C811PAN + OH → C721CHO + CO + NO_2	6.77E-12	Rickard and Pascoe (2009)
G49400a	TrGAroC	LTMB + OH → TLEPOXMUC + HO_2 + 2 LCARBON	0.827E-11	Rickard and Pascoe (2009)*
G49400b	TrGAroC	LTMB + OH → C6H5CH2O2 + 2 LCARBON	0.189E-11	Rickard and Pascoe (2009)*
G49400c	TrGAroC	LTMB + OH → CRESOL + 2 LCARBON	0.141E-11	Rickard and Pascoe (2009)*
G49400d	TrGAroC	LTMB + OH → TLBIPERO2 + HO_2 + 2 LCARBON	2.917E-11	Rickard and Pascoe (2009)*
G49401	TrGAroCN	LTMB + NO_3 → C6H5CH2O2 + HNO_3 + 2 LCARBON	1.52E-15	Rickard and Pascoe (2009)*
G40200	TrGTerC	APINENE + OH → .75 LAPINABO2 + .15 MENTHEN6ONE + .15 HO_2 + .10 ROO6R1O2	1.2E-11*EXP(440./temp)	Atkinson et al. (2006)*
G40201a	TrGTerCN	LAPINABO2 + NO → PINAL + HO_2 + NO_2	KRO2NO*(1.-(.65*alpha_AN(11,3,0,0,0,temp,cair)+.35*alpha_AN(11,2,0,0,0,temp,cair)))	Rickard and Pascoe (2009), Sander et al. (2019)
G40201b	TrGTerCN	LAPINABO2 + NO → LAPINABNO3	KRO2NO*(.65*alpha_AN(11,3,0,0,0,temp,cair)+.35*alpha_AN(11,2,0,0,0,temp,cair))	Rickard and Pascoe (2009), Sander et al. (2019)
G40202a	TrGTerC	LAPINABO2 + HO_2 → LAPINABOOH	k_RO2_HO2(temp,10)*(1.-r_CHOHCH2O2_OH)	Rickard and Pascoe (2009), Sander et al. (2019)
G40202b	TrGTerC	LAPINABO2 + HO_2 → PINAL + HO_2 + OH	k_RO2_HO2(temp,10)*r_CHOHCH2O2_OH	Rickard and Pascoe (2009), Sander et al. (2019)
G40203	TrGTerC	LAPINABO2 → PINAL + HO_2	RO2*(0.65*k1_RO2tORO2+.35*k1_RO2sORO2)	Rickard and Pascoe (2009)*

Table 1: Gas phase reactions (... continued)

#	labels	reaction	rate coefficient	reference
G40204	TrGTerC	LAPINABOOH + OH → .35 LAPINABO2 + .65 C96CO3	2.77E-11	Rickard and Pascoe (2009)*
G40205	TrGTerCN	LAPINABNO3 + OH → .35 PINAL + .65 C96CO3 + NO_2	4.29E-12	Rickard and Pascoe (2009)*
G40206	TrGTerC	MENTHEN6ONE + OH → OHMENTHEN6ONEO2	6.46E-11	Vereecken et al. (2007)*
G40207	TrGTerCN	OHMENTHEN6ONEO2 + NO → 2OHMENTHEN6ONE + HO_2 + NO_2	KRO2NO	Vereecken et al. (2007)*
G40208	TrGTerC	OHMENTHEN6ONEO2 + HO_2 → 2OHMENTHEN6ONE	k_RO2_HO2(temp,10)	Vereecken et al. (2007)
G40209	TrGTerC	OHMENTHEN6ONEO2 → 2OHMENTHEN6ONE + HO_2	k1_RO2tORO2	Vereecken et al. (2007)
G40210	TrGTerC	2OHMENTHEN6ONE + OH → 10 LCARBON	1E-11	Vereecken et al. (2007)
G40211	TrGTerC	PINAL + OH → .772 C96CO3 + .228 PINALO2	5.2E-12*EXP(600./temp)	Wallington et al. (2018)*
G40212	TrGTerCN	PINAL + NO_3 → C96CO3 + HNO_3	2.0E-14	Wallington et al. (2018)*
G40213a	TrGTerC	C96CO3 → C96O2 + CO_2	k1_RO2RCO3*0.9	Rickard and Pascoe (2009)
G40213b	TrGTerC	C96CO3 → PINONIC	k1_RO2RCO3*0.1	Rickard and Pascoe (2009)
G40214a	TrGTerC	C96CO3 + HO_2 → PERPINONIC	KAPHO2*r_CO3_OOH	Rickard and Pascoe (2009)
G40214b	TrGTerC	C96CO3 + HO_2 → PINONIC + O_3	KAPHO2*r_CO3_O3	Rickard and Pascoe (2009)
G40214c	TrGTerC	C96CO3 + HO_2 → C96O2 + OH + CO_2	KAPHO2*r_CO3_OH	Rickard and Pascoe (2009)
G40215	TrGTerCN	C96CO3 + NO_2 → C10PAN2	k_CH3CO3_NO2	Rickard and Pascoe (2009)
G40216	TrGTerCN	C96CO3 + NO → C96O2 + NO_2 + CO_2	KAPNO	Rickard and Pascoe (2009)
G40217	TrGTerCN	C96CO3 + NO_3 → C96O2 + NO_2 + CO_2	KRO2NO3*1.74	Rickard and Pascoe (2009)
G40218	TrGTerCN	C10PAN2 → C96CO3 + NO_2	k_PAN_M	Rickard and Pascoe (2009)
G40219	TrGTerCN	C10PAN2 + OH → NORPINAL + CO + NO_2	3.66E-12	Rickard and Pascoe (2009)
G40220	TrGTerC	PINONIC + OH → C96O2 + CO_2	6.65E-12	Rickard and Pascoe (2009)
G40221	TrGTerC	PERPINONIC + OH → C96CO3	9.73E-12	Rickard and Pascoe (2009)
G40222	TrGTerC	PINALO2 + HO_2 → PINALOOH	k_RO2_HO2(temp,10)	Rickard and Pascoe (2009)
G40223a	TrGTerCN	PINALO2 + NO → C106O2 + NO_2	KRO2NO*(1.-alpha_AN(12,3,0,1,0,temp,cair))	Rickard and Pascoe (2009), Sander et al. (2019)
G40223b	TrGTerCN	PINALO2 + NO → PINALNO3	KRO2NO*alpha_AN(12,3,0,1,0,temp,cair)	Rickard and Pascoe (2009), Sander et al. (2019)
G40224	TrGTerC	PINALO2 → C106O2	k1_RO2tRO2	Rickard and Pascoe (2009)
G40225	TrGTerC	PINALOOH + OH → PINALO2	2.75E-11	Rickard and Pascoe (2009)
G40226	TrGTerCN	PINALNO3 + OH → CO235C6CHO + CH_3COCH_3 + NO_2	2.25E-11	Rickard and Pascoe (2009)
G40227	TrGTerC	C106O2 + HO_2 → C106OOH	k_RO2_HO2(temp,10)	Rickard and Pascoe (2009)
G40228a	TrGTerCN	C106O2 + NO → C716O2 + CH_3COCH_3 + NO_2	KRO2NO*0.875*(1.-alpha_AN(13,3,0,0,0,temp,cair))	Rickard and Pascoe (2009), Sander et al. (2019)

Table 1: Gas phase reactions (... continued)

#	labels	reaction	rate coefficient	reference
G40228b	TrGTerCN	C106O2 + NO → C106NO3	KRO2NO*0.875*alpha_AN(13,3,0,0,0,temp,cair)	Rickard and Pascoe (2009), Sander et al. (2019)
G40229	TrGTerC	C106O2 → C716O2 + CH_3COCH_3	k1_RO2tRO2	Rickard and Pascoe (2009)
G40230	TrGTerC	C106OOH + OH → C106O2	8.01E-11	Rickard and Pascoe (2009)
G40231	TrGTerCN	C106NO3 + OH → CO235C6CHO + CH_3COCH_3 + NO_2	7.03E-11	Rickard and Pascoe (2009)
G40232	TrGTerC	APINENE + O_3 → .09 APINBOO + .08 PINONIC + .77 OH + .33 NORPINAL + .33 CO + .33 HO_2 + .06 APINAOO + .44 C109O2	8.05E-16*EXP(-640./temp)	Wallington et al. (2018)*
G40233	TrGTerC	APINAOO → PINAL + H_2O_2	1.00E-17*c(ind_H2O)	Rickard and Pascoe (2009)
G40234	TrGTerC	APINAOO + CO → PINAL + CO_2	1.20E-15	Rickard and Pascoe (2009)
G40235	TrGTerCN	APINAOO + NO → PINAL + NO_2	1.00E-14	Rickard and Pascoe (2009)
G40236	TrGTerCN	APINAOO + NO_2 → PINAL + NO_3	1.00E-15	Rickard and Pascoe (2009)
G40237a	TrGTerC	APINBOO → PINONIC	1.00E-17*c(ind_H2O)*(0.08+0.15)	Rickard and Pascoe (2009)
G40237b	TrGTerC	APINBOO → PINAL + H_2O_2	1.00E-17*c(ind_H2O)*0.77	Rickard and Pascoe (2009)
G40238	TrGTerC	APINBOO + CO → PINAL + CO_2	1.20E-15	Rickard and Pascoe (2009)
G40239	TrGTerCN	APINBOO + NO → PINAL + NO_2	1.00E-14	Rickard and Pascoe (2009)
G40240	TrGTerCN	APINBOO + NO_2 → PINAL + NO_3	1.00E-15	Rickard and Pascoe (2009)
G40241	TrGTerC	C109O2 → C89CO3 + HCHO	k1_RO2pORO2	Rickard and Pascoe (2009)
G40242	TrGTerCN	C109O2 + NO → C89CO3 + HCHO + NO_2	KRO2NO	Rickard and Pascoe (2009)*
G40243a	TrGTerC	C109O2 + HO_2 → C109OOH	k_RO2_HO2(temp,10)*r_COCH2O2_OOH	Rickard and Pascoe (2009), Sander et al. (2019)
G40243b	TrGTerC	C109O2 + HO_2 → C89CO3 + HCHO + OH	k_RO2_HO2(temp,10)*r_COCH2O2_OH	Rickard and Pascoe (2009), Sander et al. (2019)
G40244	TrGTerC	C109OOH + OH → C109CO + OH	5.47E-11	Rickard and Pascoe (2009)
G40245	TrGTerC	C109CO + OH → C89CO3 + CO	5.47E-11	Rickard and Pascoe (2009)
G40246	TrGTerCN	APINENE + NO_3 → LNAPINABO2	1.2E-12*EXP(490./temp)	Wallington et al. (2018)*
G40247	TrGTerCN	LNAPINABO2 → PINAL + NO_2	(0.65*k1_RO2tRO2 + 0.35*k1_RO2sRO2)	Rickard and Pascoe (2009)
G40248	TrGTerCN	LNAPINABO2 + NO → PINAL + NO_2 + NO_2	KRO2NO	Rickard and Pascoe (2009)*
G40249	TrGTerCN	LNAPINABO2 + HO_2 → LNAPINABOOH	k_RO2_HO2(temp,10)	Rickard and Pascoe (2009)
G40250	TrGTerCN	LNAPINABO2 + NO_3 → PINAL + NO_2 + NO_2	KRO2NO3	Rickard and Pascoe (2009)
G40251	TrGTerCN	LNAPINABOOH + OH → LNAPINABO2	(.65*6.87E-12+.35*1.23E-11)	Rickard and Pascoe (2009)
G40252a	TrGTerC	BPINENE + OH → BPINAO2	1.47E-11*EXP(467./temp) *(0.8326*0.3+0.068)/(0.8326+0.068)	Gill and Hites (2002)*

Table 1: Gas phase reactions (... continued)

#	labels	reaction	rate coefficient	reference
G40252b	TrGTerC	BPINENE + OH → ROO6R1O2	1.47E-11*EXP(467./temp) *0.8326*0.7/(0.8326+0.068)	Gill and Hites (2002)*
G40253a	TrGTerC	BPINAO2 + HO_2 → BPINAOOH	k_RO2_HO2(temp,10)*r_COCH2O2_OOH	Rickard and Pascoe (2009), Sander et al. (2019)
G40253b	TrGTerC	BPINAO2 + HO_2 → NOPINONE + HCHO + HO_2 + OH	k_RO2_HO2(temp,10)*r_COCH2O2_OH	Rickard and Pascoe (2009), Sander et al. (2019)
G40254a	TrGTerCN	BPINAO2 + NO → NOPINONE + HCHO + HO_2 + NO_2	KRO2NO*(1.-alpha_AN(11,3,0,0,0,temp,cair))	Rickard and Pascoe (2009), Sander et al. (2019)
G40254b	TrGTerCN	BPINAO2 + NO → BPINANO3	KRO2NO*alpha_AN(11,3,0,0,0,temp,cair)	Rickard and Pascoe (2009), Sander et al. (2019)
G40255	TrGTerC	BPINAO2 → NOPINONE + HCHO + HO_2	k1_RO2tORO2	Rickard and Pascoe (2009)
G40256	TrGTerC	BPINAOOH + OH → BPINAO2	1.33E-11	Rickard and Pascoe (2009)
G40257	TrGTerCN	BPINANO3 + OH → NOPINONE + HCHO + NO_2	4.70E-12	Rickard and Pascoe (2009)
G40258a	TrGTerCN	ROO6R1O2 + NO → ROO6R3O2 + CH_3COCH_3 + NO_2	KRO2NO*(1.-alpha_AN(13,3,0,0,0,temp,cair))	Vereecken and Peeters (2012)
G40258b	TrGTerCN	ROO6R1O2 + NO → ROO6R1NO3	KRO2NO*alpha_AN(13,3,0,0,0,temp,cair)	Vereecken and Peeters (2012)
G40259	TrGTerC	ROO6R1O2 + HO_2 → 10 LCARBON	k_RO2_HO2(temp,10)	Vereecken and Peeters (2012)*
G40260	TrGTerC	ROO6R1O2 → ROO6R3O2 + CH_3COCH_3	k1_RO2tORO2	Vereecken and Peeters (2012)
G40261a	TrGTerCN	RO6R1O2 + NO → RO6R3O2 + NO_2	KRO2NO*(1.-alpha_AN(12,3,0,0,0,temp,cair))	Vereecken and Peeters (2012)
G40261b	TrGTerCN	RO6R1O2 + NO → RO6R1NO3	KRO2NO*alpha_AN(12,3,0,0,0,temp,cair)	Vereecken and Peeters (2012)
G40262	TrGTerC	RO6R1O2 + HO_2 → 10 LCARBON	k_RO2_HO2(temp,10)	Vereecken and Peeters (2012)*
G40263	TrGTerC	RO6R1O2 → RO6R3O2	k1_RO2sORO2	Vereecken and Peeters (2012)
G40264a	TrGTerCN	RO6R3O2 + NO → 9 LCARBON + HCHO + HO_2 + NO_2	KRO2NO*(1.-alpha_AN(12,3,0,0,0,temp,cair))	Vereecken and Peeters (2012)
G40264b	TrGTerCN	RO6R3O2 + NO → 10 LCARBON + LNITROGEN	KRO2NO*alpha_AN(12,3,0,0,0,temp,cair)	Vereecken and Peeters (2012)
G40265	TrGTerC	RO6R3O2 + HO_2 → 10 LCARBON	k_RO2_HO2(temp,10)	Vereecken and Peeters (2012)
G40266	TrGTerC	RO6R3O2 → 9 LCARBON + HCHO + HO_2	k1_RO2sRO2	Vereecken and Peeters (2012)*
G40267a	TrGTerC	BPINENE + O_3 → NOPINONE + .63 CO + .37 CH_2OO + .16 OH + .16 HO_2	1.35E-15*EXP(-1270./temp) *.051/(1.-.027)	Wallington et al. (2018)*
G40267b	TrGTerC	BPINENE + O_3 → NOPINOO + CO_2	1.35E-15*EXP(-1270./temp) *.368/(1.-.027)	Nguyen et al. (2009), Wallington et al. (2018)

Table 1: Gas phase reactions (... continued)

#	labels	reaction	rate coefficient	reference
G40267c	TrGTerC	BPINENE + O_3 → NOPINDO2 + CO_2 + OH	1.35E-15*EXP(-1270./temp) *.283/(1.-.027)	Nguyen et al. (2009), Wallington et al. (2018)
G40267d	TrGTerC	BPINENE + O_3 → C8BC + 2 CO_2	1.35E-15*EXP(-1270./temp) *(.104+.167)/(1.-.027)	Nguyen et al. (2009), Wallington et al. (2018)
G40268	TrGTerCN	BPINENE + NO_3 → LNBPINABO2	2.51E-12	Wallington et al. (2018)*
G40269	TrGTerCN	LNBPINABO2 + HO_2 → LNBPINABOOH	k_RO2_HO2(temp,10)	Rickard and Pascoe (2009)
G40270	TrGTerCN	LNBPINABO2 + NO → NOPINONE + HCHO + NO_2 + NO_2	KRO2NO	Rickard and Pascoe (2009)*
G40271	TrGTerCN	LNBPINABO2 + NO_3 → NOPINONE + HCHO + NO_2 + NO_2	KRO2NO3	Rickard and Pascoe (2009)
G40272a	TrGTerCN	LNBPINABO2 → NOPINONE + HCHO + NO_2	k1_RO2tRO2*0.7	Rickard and Pascoe (2009)
G40272b	TrGTerCN	LNBPINABO2 → BPINANO3	k1_RO2tRO2*0.3	Rickard and Pascoe (2009)
G40273	TrGTerCN	LNBPINABOOH + OH → LNBPINABO2	9.58E-12	Rickard and Pascoe (2009)
G40274	TrGTerCN	ROO6R1NO3 + OH → ROO6R3O2 + CH_3COCH_3 + NO_2	9.16E-13	Vereecken and Peeters (2012), Gill and Hites (2002)*
G40275	TrGTerCN	RO6R1NO3 + OH → 9 LCARBON + HCHO + HO_2 + NO_2	9.16E-13	Vereecken and Peeters (2012), Gill and Hites (2002)
G40276	TrGTerC	PINEOL + OH → HCOOH + OH + NORPINAL	k_CH2CHOH_OH_HCOOH	Sander et al. (2019), So et al. (2014)*
G40277	TrGTerC	PINEOL + HCOOH → PINAL + HCOOH	k_CH2CHOH_HCOOH	Sander et al. (2019), da Silva (2010)*
G40278	TrGTerC	PINAL + HCOOH → PINEOL + HCOOH	k_ALD_HCOOH	Sander et al. (2019), da Silva (2010)*
G40279a	TrGC	CARENE + OH → LAPINABO2	8.8E-11*(.50+.25)	Atkinson and Arey (2003)
G40279b	TrGC	CARENE + OH → MENTHEN6ONE + HO_2	8.8E-11*.25*.60	Atkinson and Arey (2003)
G40279c	TrGC	CARENE + OH → ROO6R1O2	8.8E-11*.25*.40	Atkinson and Arey (2003)
G40280a	TrGC	CARENE + O_3 → APINBOO	3.7E-17*.50*.18	Atkinson and Arey (2003)
G40280b	TrGC	CARENE + O_3 → PINONIC	3.7E-17*.50*.16	Atkinson and Arey (2003)
G40280c	TrGC	CARENE + O_3 → OH + NORPINAL + CO + HO_2	3.7E-17*.50*.66	Atkinson and Arey (2003)
G40280d	TrGC	CARENE + O_3 → APINAOO	3.7E-17*.50*.12	Atkinson and Arey (2003)
G40280e	TrGC	CARENE + O_3 → OH + C109O2	3.7E-17*.50*(.22+.66)	Atkinson and Arey (2003)
G40281	TrGCN	CARENE + NO_3 → LNAPINABO2	9.1E-12	Atkinson and Arey (2003)
G40282a	TrGTerC	SABINENE + OH → BPINAO2	1.47E-11*EXP(467./temp) *(0.8326*0.3+0.068)/(0.8326+0.068)	Gill and Hites (2002)*

Table 1: Gas phase reactions (... continued)

#	labels	reaction	rate coefficient	reference
G40282b	TrGTerC	SABINENE + OH → ROO6R1O2	1.47E-11*EXP(467./temp) *0.8326*0.7/(0.8326+0.068)	Vereecken and Peeters (2012), Gill and Hites (2002)*
G40283a	TrGTerC	SABINENE + O_3 → NOPINONE + .63 CO + .37 $HOCH_2OOH$ + .16 OH + .16 HO_2	1.35E-15*EXP(-1270./temp) *.051/(1.-.027)	Wallington et al. (2018)*
G40283b	TrGTerC	SABINENE + O_3 → NOPINOO + CO_2	1.35E-15*EXP(-1270./temp) *.368/(1.-.027)	Nguyen et al. (2009), Wallington et al. (2018)
G40283c	TrGTerC	SABINENE + O_3 → NOPINDO2 + CO_2 + OH	1.35E-15*EXP(-1270./temp) *.283/(1.-.027)	Nguyen et al. (2009), Wallington et al. (2018)
G40283d	TrGTerC	SABINENE + O_3 → C8BC + 2 CO_2	1.35E-15*EXP(-1270./temp) *(.104+.167)/(1.-.027)	Nguyen et al. (2009), Wallington et al. (2018)
G40284	TrGTerCN	SABINENE + NO_3 → LNBPINABO2	2.51E-12	Wallington et al. (2018)*
G40285a	TrGTerC	CAMPHENE + OH → BPINAO2	1.47E-11*EXP(467./temp) *(0.8326*0.3+0.068)/(0.8326+0.068)	Gill and Hites (2002)*
G40285b	TrGTerC	CAMPHENE + OH → ROO6R1O2	1.47E-11*EXP(467./temp) *0.8326*0.7/(0.8326+0.068)	Vereecken and Peeters (2012), Gill and Hites (2002)*
G40286a	TrGTerC	CAMPHENE + O_3 → NOPINONE + .63 CO + .37 $HOCH_2OOH$ + .16 OH + .16 HO_2	1.35E-15*EXP(-1270./temp) *.051/(1.-.027)	Wallington et al. (2018)*
G40286b	TrGTerC	CAMPHENE + O_3 → NOPINOO + CO_2	1.35E-15*EXP(-1270./temp) *.368/(1.-.027)	Nguyen et al. (2009), Wallington et al. (2018)
G40286c	TrGTerC	CAMPHENE + O_3 → NOPINDO2 + CO_2 + OH	1.35E-15*EXP(-1270./temp) *.283/(1.-.027)	Nguyen et al. (2009), Wallington et al. (2018)
G40286d	TrGTerC	CAMPHENE + O_3 → C8BC + 2 CO_2	1.35E-15*EXP(-1270./temp) *(.104+.167)/(1.-.027)	Nguyen et al. (2009), Wallington et al. (2018)
G40287	TrGTerCN	CAMPHENE + NO_3 → LNBPINABO2	2.51E-12	Wallington et al. (2018)*
G40400	TrGAroC	LHAROM + OH → .14 TLEPOXMUC + .03 C6H5CH2O2 + .04 CRESOL + .79 TLBIPERO2 + .18 HO_2 + 4 LCARBON	5.67E-11	Rickard and Pascoe (2009)*
G40401	TrGAroCN	LHAROM + NO_3 → C6H5CH2O2 + HNO_3 + 4 LCARBON	2.60E-15	Rickard and Pascoe (2009)*
G6100	UpStTrGCl	Cl + O_3 → ClO + O_2	2.8E-11*EXP(-250./temp)	Atkinson et al. (2007)
G6101	UpStGCl	ClO + $O(^3P)$ → Cl + O_2	2.5E-11*EXP(110./temp)	Atkinson et al. (2007)
G6102a	StTrGCl	ClO + ClO → Cl_2 + O_2	1.0E-12*EXP(-1590./temp)	Atkinson et al. (2007)
G6102b	StTrGCl	ClO + ClO → 2 Cl + O_2	3.0E-11*EXP(-2450./temp)	Atkinson et al. (2007)
G6102c	StTrGCl	ClO + ClO → Cl + OClO	3.5E-13*EXP(-1370./temp)	Atkinson et al. (2007)
G6102d	StTrGCl	ClO + ClO → Cl_2O_2	k_ClO_ClO	Burkholder et al. (2015)

Table 1: Gas phase reactions (... continued)

#	labels	reaction	rate coefficient	reference
G6103	StTrGCl	$Cl_2O_2 \rightarrow ClO + ClO$	k_ClO_ClO/(2.16E-27*EXP(8537./temp))	Burkholder et al. (2015)*
G6200	StGCl	$Cl + H_2 \rightarrow HCl + H$	3.9E-11*EXP(-2310./temp)	Atkinson et al. (2007)
G6201a	StGCl	$Cl + HO_2 \rightarrow HCl + O_2$	4.4E-11-7.5E-11*EXP(-620./temp)	Atkinson et al. (2007)
G6201b	StGCl	$Cl + HO_2 \rightarrow ClO + OH$	7.5E-11*EXP(-620./temp)	Atkinson et al. (2007)
G6202	StTrGCl	$Cl + H_2O_2 \rightarrow HCl + HO_2$	1.1E-11*EXP(-980./temp)	Atkinson et al. (2007)
G6203	StGCl	$ClO + OH \rightarrow .94\ Cl + .94\ HO_2 + .06\ HCl + .06\ O_2$	7.3E-12*EXP(300./temp)	Atkinson et al. (2007)
G6204	StTrGCl	$ClO + HO_2 \rightarrow HOCl + O_2$	2.2E-12*EXP(340./temp)	Atkinson et al. (2007)*
G6205	StTrGCl	$HCl + OH \rightarrow Cl + H_2O$	1.7E-12*EXP(-230./temp)	Atkinson et al. (2007)
G6206	StGCl	$HOCl + OH \rightarrow ClO + H_2O$	3.0E-12*EXP(-500./temp)	Burkholder et al. (2015)
G6300	UpStTrGClN	$ClO + NO \rightarrow NO_2 + Cl$	6.2E-12*EXP(295./temp)	Atkinson et al. (2007)
G6301	StTrGClN	$ClO + NO_2 \rightarrow ClNO_3$	k_3rd_iupac(temp,cair,1.6E-31,3.4,7.E-11,0.,0.4)	Atkinson et al. (2007)
G6302	TrGClN	$ClNO_3 \rightarrow ClO + NO_2$	6.918E-7*EXP(-10909./temp)*cair	Anderson and Fahey (1990)
G6303	StGClN	$ClNO_3 + O(^3P) \rightarrow ClO + NO_3$	4.5E-12*EXP(-900./temp)	Atkinson et al. (2007)
G6304	StTrGClN	$ClNO_3 + Cl \rightarrow Cl_2 + NO_3$	6.2E-12*EXP(145./temp)	Atkinson et al. (2007)
G6400	StTrGCl	$Cl + CH_4 \rightarrow HCl + CH_3$	6.6E-12*EXP(-1240./temp)	Atkinson et al. (2006)
G6401	StTrGCl	$Cl + HCHO \rightarrow HCl + CO + HO_2$	8.1E-11*EXP(-34./temp)	Atkinson et al. (2006)
G6402	StTrGCl	$Cl + CH_3OOH \rightarrow HCHO + HCl + OH$	5.9E-11	Atkinson et al. (2006)*
G6403	StTrGCl	$ClO + CH_3O_2 \rightarrow HO_2 + Cl + HCHO$	1.8E-12*EXP(-600./temp)	Burkholder et al. (2015)
G6404	StGCl	$CCl_4 + O(^1D) \rightarrow LCARBON + ClO + 3\ Cl$	3.3E-10	Burkholder et al. (2015)
G6405	StGCl	$CH_3Cl + O(^1D) \rightarrow 0.1\ CH_3Cl + 0.1\ O(^3P) + 0.46\ ClO + 0.35\ Cl + 0.09\ H + 0.9\ LCARBON + 0.09\ LCHLORINE$	1.65E-10	Burkholder et al. (2015)
G6406	StGCl	$CH_3Cl + OH \rightarrow LCARBON + H_2O + Cl$	1.96E-12*EXP(-1200./temp)	Burkholder et al. (2015)
G6407	StGCCl	$CH_3CCl_3 + O(^1D) \rightarrow 2\ LCARBON + OH + 3\ Cl$	3.25E-10	Burkholder et al. (2015)
G6408	StTrGCCl	$CH_3CCl_3 + OH \rightarrow 2\ LCARBON + H_2O + 3\ Cl$	1.64E-12*EXP(-1520./temp)	Burkholder et al. (2015)
G6409	TrGCCl	$Cl + C_2H_4 \rightarrow HOCH_2CH_2O_2 + HCl$	k_3rd_iupac(temp,cair,1.85E-29,3.3,6.0E-10,0.0,0.4)	Atkinson et al. (2006)*
G6410	TrGCCl	$Cl + CH_3CHO \rightarrow HCl + CH_3C(O)$	8.0e-11	Atkinson et al. (2006)
G6411	TrGCCl	$C_2H_2 + Cl \rightarrow LCARBON + CH_3 + HCl$	k_3rd_iupac(temp,cair,6.1e-30,3.0,2.0e-10,0.,0.6)	Atkinson et al. (2006)
G6412	TrGCCl	$C_2H_6 + Cl \rightarrow C_2H_5O_2 + HCl$	8.3E-11*EXP(-100./temp)	Atkinson et al. (2006)
G6413	StTrGClN	$Cl + CH_3ONO_2 \rightarrow HCl + HCHO + NO_2$	1.3E-11*EXP(-1200./temp)	Burkholder et al. (2015)
G6414	StTrGClN	$Cl + CH_3ONO \rightarrow HCl + HCHO + NO$	2.1E-12	Sokolov et al. (1999)
G6415	StTrGCl	$Cl + CH_3O_2 \rightarrow .5\ ClO + .5\ CH_3O + .5\ HCl + .5\ CH_2OO$	1.6E-10	Burkholder et al. (2015)

Table 1: Gas phase reactions (... continued)

#	labels	reaction	rate coefficient	reference
G6416	TrGCClN	$Cl + CH_3CN \rightarrow NCCH_2O_2 + HCl$	1.6E-11*EXP(-2104./temp)	Tyndall et al. (1996), Tyndall et al. (2001b), Sander et al. (2019)
G6500	StGClF	$CF_2Cl_2 + O(^1D) \rightarrow LCARBON + 2\ LFLUORINE + ClO + Cl$	1.4E-10	Burkholder et al. (2015)
G6501	StGClF	$CFCl_3 + O(^1D) \rightarrow LCARBON + LFLUORINE + ClO + 2\ Cl$	2.3E-10	Burkholder et al. (2015)
G7100	StTrGBr	$Br + O_3 \rightarrow BrO + O_2$	1.7E-11*EXP(-800./temp)	Atkinson et al. (2007)
G7101	StGBr	$BrO + O(^3P) \rightarrow Br + O_2$	1.9E-11*EXP(230./temp)	Atkinson et al. (2007)
G7102a	StTrGBr	$BrO + BrO \rightarrow 2\ Br + O_2$	2.7E-12	Atkinson et al. (2007)
G7102b	StTrGBr	$BrO + BrO \rightarrow Br_2 + O_2$	2.9E-14*EXP(840./temp)	Atkinson et al. (2007)
G7200	StTrGBr	$Br + HO_2 \rightarrow HBr + O_2$	7.7E-12*EXP(-450./temp)	Atkinson et al. (2007)
G7201	StTrGBr	$BrO + HO_2 \rightarrow HOBr + O_2$	4.5E-12*EXP(500./temp)	Atkinson et al. (2007)
G7202	StTrGBr	$HBr + OH \rightarrow Br + H_2O$	6.7E-12*EXP(155./temp)	Atkinson et al. (2007)
G7203	StGBr	$HOBr + O(^3P) \rightarrow OH + BrO$	1.2E-10*EXP(-430./temp)	Atkinson et al. (2007)
G7204	StTrGBr	$Br_2 + OH \rightarrow HOBr + Br$	2.0E-11*EXP(240./temp)	Atkinson et al. (2007)
G7300	TrGBrN	$Br + BrNO_3 \rightarrow Br_2 + NO_3$	4.9E-11	Orlando and Tyndall (1996)
G7301	StTrGBrN	$BrO + NO \rightarrow Br + NO_2$	8.7E-12*EXP(260./temp)	Atkinson et al. (2007)
G7302	StTrGBrN	$BrO + NO_2 \rightarrow BrNO_3$	k_BrO_NO2	Atkinson et al. (2007)*
G7303	TrGBrN	$BrNO_3 \rightarrow BrO + NO_2$	k_BrO_NO2/(5.44E-9*EXP(14192./temp)*1.E6*R_gas*temp/(atm2Pa*N_A))	Orlando and Tyndall (1996), Atkinson et al. (2007)*
G7400	StTrGBr	$Br + HCHO \rightarrow HBr + CO + HO_2$	7.7E-12*EXP(-580./temp)	Atkinson et al. (2006)
G7401	TrGBr	$Br + CH_3OOH \rightarrow CH_3O_2 + HBr$	2.6E-12*EXP(-1600./temp)	Kondo and Benson (1984)
G7402	TrGBr	$BrO + CH_3O_2 \rightarrow HOBr + CH_2OO$	2.42E-14*EXP(1617./temp)	Shallcross et al. (2015)
G7403	StTrGBr	$CH_3Br + OH \rightarrow LCARBON + H_2O + Br$	1.42E-12*EXP(-1150./temp)	Burkholder et al. (2015)
G7404	TrGBrC	$Br + C_2H_4 \rightarrow HOCH_2CH_2O_2 + HBr$	2.8E-13*EXP(224./temp)/(1.+1.13E24*EXP(-3200./temp)/C(ind_02))	Atkinson et al. (2006)*
G7405	TrGBrC	$Br + CH_3CHO \rightarrow HBr + CH_3C(O)$	1.8e-11*EXP(-460./temp)	Atkinson et al. (2006)
G7406	TrGBrC	$Br + C_2H_2 \rightarrow LCARBON + CH_3O_2 + HBr$	6.35e-15*EXP(440./temp)	Atkinson et al. (2006)
G7407	TrGBr	$CHBr_3 + OH \rightarrow LCARBON + H_2O + 3\ Br$	9.0E-13*EXP(-360./temp)	Burkholder et al. (2015)*
G7408	TrGBr	$CH_2Br_2 + OH \rightarrow LCARBON + H_2O + 2\ Br$	2.0E-12*EXP(-840./temp)	Burkholder et al. (2015)*
G7600	TrGBrCl	$Br + BrCl \rightarrow Br_2 + Cl$	3.32E-15	Manion et al. (2015)
G7601	TrGBrCl	$Br + Cl_2 \rightarrow BrCl + Cl$	1.10E-15	Dolson and Leone (1987)

Table 1: Gas phase reactions (... continued)

#	labels	reaction	rate coefficient	reference
G7602	TrGBrCl	$Br_2 + Cl \rightarrow BrCl + Br$	2.3E-10*EXP(135./temp)	Bedjanian et al. (1998)
G7603a	StTrGBrCl	$BrO + ClO \rightarrow Br + OClO$	1.6E-12*EXP(430./temp)	Atkinson et al. (2007)
G7603b	StTrGBrCl	$BrO + ClO \rightarrow Br + Cl + O_2$	2.9E-12*EXP(220./temp)	Atkinson et al. (2007)
G7603c	StTrGBrCl	$BrO + ClO \rightarrow BrCl + O_2$	5.8E-13*EXP(170./temp)	Atkinson et al. (2007)
G7604	TrGBrCl	$BrCl + Cl \rightarrow Br + Cl_2$	1.45E-11	Clyne and Cruse (1972)
G7605	TrGBrCl	$CHCl_2Br + OH \rightarrow$ LCARBON + 2 Cl + H_2O + Br	2.0E-12*EXP(-840./temp)	see note*
G7606	TrGBrCl	$CHClBr_2 + OH \rightarrow$ LCARBON + Cl + H_2O + 2 Br	2.0E-12*EXP(-840./temp)	see note*
G7607	TrGBrCl	$CH_2ClBr + OH \rightarrow$ LCARBON + Cl + H_2O + Br	2.1E-12*EXP(-880./temp)	Burkholder et al. (2015)*
G8100	TrGI	$I + O_3 \rightarrow IO + O_2$	2.1E-11*EXP(-830./temp)	Atkinson et al. (2007)
G8102	TrGI	$OIO + OIO \rightarrow$ I(part)	5.E-11	von Glasow et al. (2002)*
G8103	TrGI	IO + IO → .38 OIO + 1.62 I + .62 O_2	5.4E-11*EXP(180./temp)	Atkinson et al. (2007)*
G8200	TrGI	$I + HO_2 \rightarrow HI + O_2$	1.5E-11*EXP(-1090./temp)	Atkinson et al. (2007)
G8201	TrGI	$IO + HO_2 \rightarrow HOI + O_2$	1.4E-11*EXP(540./temp)	Atkinson et al. (2007)
G8202	TrGI	$HI + OH \rightarrow I + H_2O$	1.6E-11*EXP(440./temp)	Atkinson et al. (2007)
G8203	TrGI	$OIO + OH \rightarrow HIO_3$	2.2E-10*EXP(243./temp)	Plane et al. (2006)
G8204	TrGI	$I_2 + OH \rightarrow HOI + I$	2.1E-10	Atkinson et al. (2007)
G8205	TrGI	$HOI + OH \rightarrow IO + H_2O$	5.0E-12	Riffault et al. (2005)
G8300	TrGIN	$I + NO_2 \rightarrow INO_2$	k_I_NO2	Atkinson et al. (2007)*
G8301	TrGIN	$I + NO_3 \rightarrow IO + NO_2$	1.E-10	Dillon et al. (2008)
G8302	TrGIN	$IO + NO \rightarrow I + NO_2$	7.15E-12*EXP(300./temp)	Atkinson et al. (2007)
G8303	TrGIN	$IO + NO_2 \rightarrow INO_3$	k_3rd_iupac(temp,cair,7.7E-31, 5.,1.6E-11,0.,0.4)	Atkinson et al. (2007)
G8304	TrGIN	$OIO + NO \rightarrow NO_2 + IO$	1.1E-12*EXP(542./temp)	Atkinson et al. (2007)
G8305	TrGIN	$INO_2 \rightarrow I + NO_2$	k_I_NO2/(3.7E-7*EXP(9568./temp) *1.E6*R_gas*temp/(atm2Pa*N_A))	van den Bergh and Troe (1976), Atkinson et al. (2007)*
G8306	TrGIN	$INO_3 \rightarrow IO + NO_2$	2.1e15*EXP(-13670./temp)	Kaltsoyannis and Plane (2008)
G8307	TrGIN	$I_2 + NO_3 \rightarrow I + INO_3$	1.5E-12	Atkinson et al. (2007)
G8308	TrGIN	$IO + NO_3 \rightarrow OIO + NO_2$	9.E-12	Dillon et al. (2008)
G8309	TrGIN	$I + INO_3 \rightarrow I_2 + NO_3$	9.1E-11*EXP(-146./temp)	Kaltsoyannis and Plane (2008)
G8400	TrGCI	$CH_3CHICH_3 + OH \rightarrow$ 2 LCARBON + CH_3O_2 + I	1.22E-12	Carl and Crowley (2001)
G8401	TrGI	$CH_3O_2 + IO \rightarrow$ .4 I + .6 OIO + HCHO + HO_2	2.E-12	Dillon et al. (2006b), Bale et al. (2005)*
G8402	TrGIN	$CH_3I + NO_3 \rightarrow HNO_3 + HCHO + IO$	3.4E-17	Wayne et al. (1991)*
G8600	TrGCII	IO + ClO → .2 ICl + .25 Cl + .55 OClO + .8 I + .45 O_2	4.7E-12*EXP(280./temp)	Atkinson et al. (2007)
G8700	TrGBrI	$I + BrO \rightarrow IO + Br$	1.2E-11	Burkholder et al. (2015)

Table 1: Gas phase reactions (... continued)

#	labels	reaction	rate coefficient	reference
G8701	TrGBrI	IO + BrO → Br + .8 OIO + .2 I + .2 O_2	1.5E-11*EXP(510./temp)	Atkinson et al. (2007)*
G8702	TrGBrI	IBr + OH → .84 HOI + .84 Br + .16 HOBr + .16 I	1.4E-10	Riffault et al. (2005)
G8703	TrGBrI	IO + Br → I + BrO	2.3E-11	Bedjanian et al. (1997)
G8704	TrGBrI	$I_2 + Br \rightarrow IBr + I$	1.2E-10	Bedjanian et al. (1997)
G9200	StTrGS	$SO_2 + OH \rightarrow H_2SO_4 + HO_2$	k_3rd(temp,cair,3.3E-31,4.3, 1.6E-12,0.,0.6)	Burkholder et al. (2015)
G9400a	TrGCS	$DMS + OH \rightarrow CH_3SO_2 + HCHO$	1.13E-11*EXP(-253./temp)	Atkinson et al. (2004)*
G9400b	TrGCS	$DMS + OH \rightarrow DMSO + HO_2$	k_DMS_OH	Atkinson et al. (2004)*
G9401	TrGCNS	$DMS + NO_3 \rightarrow CH_3SO_2 + HNO_3 + HCHO$	1.9E-13*EXP(520./temp)	Atkinson et al. (2004)
G9402	TrGCS	DMSO + OH → .6 SO_2 + HCHO + .6 CH_3 + .4 HO_2 + .4 CH_3SO_3H	1.E-10	Hynes and Wine (1996)*
G9403	TrGS	$CH_3SO_2 \rightarrow SO_2 + CH_3$	1.8E13*EXP(-8661./temp)	Barone et al. (1995)
G9404	TrGS	$CH_3SO_2 + O_3 \rightarrow CH_3SO_3$	3.E-13	Barone et al. (1995)
G9405	TrGS	$CH_3SO_3 + HO_2 \rightarrow CH_3SO_3H$	5.E-11	Barone et al. (1995)
G9408	StTrGS	$CH_2OO + SO_2 \rightarrow H_2SO_4 + HCHO$	k_CH2OO_SO2	Welz et al. (2012), Stone et al. (2014)*
G9409	TrGTerCS	NOPINOO + SO_2 → NOPINONE + H_2SO_4	7.E-14	Rickard and Pascoe (2009)
G9410	TrGTerCS	APINAOO + SO_2 → PINAL + H_2SO_4	7.00E-14	Rickard and Pascoe (2009)
G9411	TrGTerCS	APINBOO + SO_2 → PINAL + H_2SO_4	7.00E-14	Rickard and Pascoe (2009)
G9412	TrGTerCS	MBOOO + SO_2 → IBUTALOH + H_2SO_4	7.00E-14	Rickard and Pascoe (2009)
G9600	TrGCClS	$DMS + Cl \rightarrow CH_3SO_2 + HCl + HCHO$	3.3E-10	Atkinson et al. (2004)
G9700	TrGBrCS	$DMS + Br \rightarrow CH_3SO_2 + HBr + HCHO$	9.E-11*EXP(-2386./temp)	Jefferson et al. (1994)
G9701	TrGBrCS	$DMS + BrO \rightarrow DMSO + Br$	4.4E-13	Ingham et al. (1999)
G9800	TrGCIS	$DMS + IO \rightarrow DMSO + I$	3.2E-13*EXP(-925./temp)	Dillon et al. (2006a)
G10100	TrGHg	$Hg + O_3 \rightarrow HgO + O_2$	3.0E-20	Hall (1995)
G10200	TrGHg	$Hg + OH \rightarrow HgO + H$	3.55E-14*EXP(294./temp)	Pal and Ariya (2004)
G10201	TrGHg	$Hg + H_2O_2 \rightarrow HgO + H_2O$	8.5E-19	Tokos et al. (1998)*
G10600	TrGClHg	$Hg + Cl \rightarrow HgCl$	1.0E-11	Ariya et al. (2002)
G10601	TrGClHg	$Hg + Cl_2 \rightarrow HgCl_2$	2.6E-18	Ariya et al. (2002)
G10700	TrGBrHg	$Hg + Br \rightarrow HgBr$	3.0E-13	Donohoue et al. (2006)
G10701	TrGBrHg	$HgBr + Br \rightarrow HgBr_2$	2.5E-10*(temp/298.)**(-0.57)	Goodsite et al. (2004)
G10702	TrGBrHg	$Hg + Br_2 \rightarrow HgBr_2$	9.0E-17	Ariya et al. (2002)
G10703	TrGBrHg	$Hg + BrO \rightarrow HgO + Br$	1.0E-15	Raofie and Ariya (2003)
G10704	TrGBrHg	$HgBr + BrO \rightarrow BrHgOBr$	3.0E-12	Calvert and Lindberg (2003)
G10705	TrGBrClHg	$HgCl + BrO \rightarrow ClHgOBr$	3.0E-12	Calvert and Lindberg (2003)

Table 1: Gas phase reactions (... continued)

#	labels	reaction	rate coefficient	reference
G10706	TrGBrClHg	HgBr + Cl → ClHgBr	3.0E-12	Calvert and Lindberg (2003)
G10707	TrGBrClHg	HgCl + Br → ClHgBr	3.0E-12	Calvert and Lindberg (2003)

General notes

Three-body reactions

Rate coefficients for three-body reactions are defined via the function `k_3rd`(T, M, k_0^{300}, n, k_{inf}^{300}, m, f_c). In the code, the temperature T is called `temp` and the concentration of "air molecules" M is called `cair`. Using the auxiliary variables $k_0(T)$, $k_{\mathrm{inf}}(T)$, and k_{ratio}, `k_3rd` is defined as:

$$k_0(T) = k_0^{300} \times \left(\frac{300\mathrm{K}}{T}\right)^n \quad (1)$$

$$k_{\mathrm{inf}}(T) = k_{\mathrm{inf}}^{300} \times \left(\frac{300\mathrm{K}}{T}\right)^m \quad (2)$$

$$k_{\mathrm{ratio}} = \frac{k_0(T)M}{k_{\mathrm{inf}}(T)} \quad (3)$$

$$\texttt{k\_3rd} = \frac{k_0(T)M}{1+k_{\mathrm{ratio}}} \times f_c^{\left(\frac{1}{1+(\log_{10}(k_{\mathrm{ratio}}))^2}\right)} \quad (4)$$

A similar function, called `k_3rd_iupac` here, is used by Wallington et al. (2018) for three-body reactions. It has the same function parameters as `k_3rd` and it is defined as:

$$k_0(T) = k_0^{300} \times \left(\frac{300\mathrm{K}}{T}\right)^n \quad (5)$$

$$k_{\mathrm{inf}}(T) = k_{\mathrm{inf}}^{300} \times \left(\frac{300\mathrm{K}}{T}\right)^m \quad (6)$$

$$k_{\mathrm{ratio}} = \frac{k_0(T)M}{k_{\mathrm{inf}}(T)} \quad (7)$$

$$N = 0.75 - 1.27 \times \log_{10}(f_c) \quad (8)$$

$$\texttt{k\_3rd\_iupac} = \frac{k_0(T)M}{1+k_{\mathrm{ratio}}} \times f_c^{\left(\frac{1}{1+(\log_{10}(k_{\mathrm{ratio}})/N)^2}\right)} \quad (9)$$

Structure-Activity Relationships (SAR)

Some unmeasured rate coefficients are estimated with structure-activity relationships, using the following parameters and substituent factors:

k for H-abstraction by OH in $\mathrm{cm^3 s^{-1}}$	
k_p	$4.49 \times 10^{-18} \times (T/\mathrm{K})^2 \exp(-320\,\mathrm{K}/T)$
k_s	$4.50 \times 10^{-18} \times (T/\mathrm{K})^2 \exp(253\,\mathrm{K}/T)$
k_t	$2.12 \times 10^{-18} \times (T/\mathrm{K})^2 \exp(696\,\mathrm{K}/T)$
k_ROHRO	$2.1 \times 10^{-18} \times (T/\mathrm{K})^2 \exp(-85\,\mathrm{K}/T)$
k_CO2H	$0.7 \times k_{\mathrm{CH_3CO_2H+OH}}$
k_ROOHRO	$0.6 \times k_{\mathrm{CH_3OOH+OH}}$
f_alk	1.23
f_sOH	3.44
f_tOH	2.68
f_sOOH	8.
f_tOOH	8.
f_ONO2	0.04
f_CH2ONO2	0.20
f_cpan	0.25
f_allyl	3.6
f_CHO	0.55
f_CO2H	1.67
f_CO	0.73
f_O	8.15
f_pCH2OH	1.29
f_tCH2OH	0.53

k for OH-addition to double bonds in $\mathrm{cm^3 s^{-1}}$	
k_adp	$4.5 \times 10^{-12} \times (T/300\,\mathrm{K})^{-0.85}$
k_ads	$1/4 \times (1.1 \times 10^{-11} \times \exp(485\,\mathrm{K}/T) + 1.0 \times 10^{-11} \times \exp(553\,\mathrm{K}/T))$
k_adt	$1.922 \times 10^{-11} \times \exp(450\,\mathrm{K}/T) - k_{\mathrm{ads}}$
k_adsecprim	3.0×10^{-11}
k_adtertprim	5.7×10^{-11}
a_PAN	0.56
a_CHO	0.31
a_COCH3	0.76
a_CH2OH	1.7
a_CH2OOH	1.7
a_COH	2.2
a_COOH	2.2
a_CO2H	0.25
a_CH2ONO2	0.64

RO_2 self and cross reactions

The self and cross reactions of organic peroxy radicals are treated according to the permutation reaction formalism as implemented in the MCM (Rickard and Pascoe, 2009), as decribed by Jenkin et al. (1997). Every organic peroxy radical reacts in a pseudo-first-order reaction with a rate constant that is expressed as $k^{1\mathrm{st}} = 2 \times \sqrt{k_{\mathrm{self}} \times \texttt{k\_CH3O2}} \times [\mathrm{RO_2}]$ where k_{self} = second-order rate coefficient of the self reaction of the organic peroxy radical, `k_CH3O2` = second-order rate coefficient of the self reaction of CH_3O_2, and $[\mathrm{RO_2}]$ = sum of the concentrations of all organic peroxy radicals.

Specific notes

G1002a: The path leading to 2 $O(^3P)$ + O_2 results in a null cycle regarding odd oxygen and is neglected.

G2110: The rate coefficient is: `k_HO2_HO2 = (3.0E-13*EXP(460./temp)+2.1E-33*EXP(920./temp)*cair)*(1.+1.4E-21*EXP(2200./temp)*C(ind_H2O))`.

G2117: Converted to Kc [molec-1 cm3]= Kp*R*T/NA, where R is 82.05736 [cm3atmK1mol1].

G2118: Assuming fast equilibrium.

G3109: The rate coefficient is: `k_NO3_NO2 = k_3rd(temp,cair,2.4E-30,3.0,1.6E-12,-0.1,0.6)`.

G3110: The rate coefficient is defined as backward reaction divided by equilibrium constant.

G3203: The rate coefficient is: `k_NO2_HO2 = k_3rd(temp,cair,1.9E-31,3.4,4.0E-12,0.3,0.6)`.

G3206: The rate coefficient is: `k_HNO3_OH = 1.32E-14 * EXP(527/temp) + 1 / ( 1 / (7.39E-32 * EXP(453/temp)*cair) + 1 / (9.73E-17 * EXP(1910/temp)) )`

G3207: The rate coefficient is defined as backward reaction divided by equilibrium constant.

G3227: Backward reaction divided by equilibrium constant from Burkholder et al. (2015).

G3228: Same as for OH + HNO_4.

G4104b: Methyl nitrate yield according to Banic et al. (2003) but reduced by a factor of 10 according to the upper limit derived from measurements by Munger et al. (1999).

G4109: Same temperature dependence as for CH_3CHO+NO_3 assumed.

G4115: The rate coefficient is defined as backward reaction divided by equilibrium constant.

G4116: Same value as for PAN + OH.

G4126: Same as for G4104 but scaled to match the recommeded value at 298K.

G4127: Same as for CH3O2 + NO3 in G4105.

G4130a: SAR for H-abstraction by OH.

G4130b: SAR for H-abstraction by OH.

G4132: SAR for H-abstraction by OH.

G4133: Lower limit of the rate constant. Products uncertain but CH_3OH can be excluded because of a likely high energy barrier (L. Vereecken, pers. comm.). CH_2OO production cannot be excluded.

G4134: Estimate based on the decomposition lifetime of 3 s (Olzmann et al., 1997) and a 20 kcal/mol energy barrier (Vereecken and Francisco, 2012).

G4135: Rate constant for CH_2OO + NO_2 (G4138) multiplied by the factor from Ouyang et al. (2013).

G4136: Average of two measurements.

G4137: Upper limit.

G4138: Average of 7.E-12 and 1.5E-12.

G4141: $HOOCH_2OCHO$ forms and then decomposes to formic anhydride (Gruzdev et al., 1993) which hydrolyses in the humid atmosphere (Conn et al., 1942).

G4142: High-pressure limit.

G4143: Generic estimate for reaction with alcohols.

G4144: Generic estimate for reaction with RO_2.

G4148: Same value as for NO_2+CH_3O_2.

G4149: Barnes et al. (1985) estimated a decomposition rate equal to that of $CH_3O_2NO_2$.

G4150: Value for $CH_3O_2NO_2$ + OH, H-abstraction enhanced by the HO-group by f_sOH.

G4154: Products assumed to be CH_3O_2 + O_2 (could also be HCHO + O_2 + OH).

G4160b: Half of the H-yield is attributed to fast secondary chemistry.

G4160c: The NH + CO channel is also significant but neglected here.

G4161: No studies below 450 K and only the major channel is considered.

G4164: Upper limit. Dominant pathway under atmospheric conditions.

G42001: The product distribution is from Rickard and Pascoe (2009), after substitution of the energized Criegee intermediate, CH_2OO, by its decomposition products and reaction of the stabilized CI with the water dimer.

G42010: Only major channel considered as the end products are essentially the same.

G42013: The rate coefficient is: `k_CH3CO3_NO2 = k_3rd(temp,cair,9.7E-29,5.6,9.3E-12,1.5,0.6)`.

G42018: The rate coefficient is the same as for the CH_3 channel in G4107 (CH_3OOH+OH).

G42021: The rate coefficient is `k_PAN_M = k_CH3CO3_NO2/9.0E-29*EXP(-14000./temp)`, i.e. the rate coefficient is defined as backward reaction divided by equilibrium constant.

G42022a: Quantum yields and products are from Glowacki et al. (2012).

G42022b: Quantum yields and products are from Glowacki et al. (2012).

G42024a: Rate constant is the high-pressure limit as recommended by Atkinson et al. (2006).

G42024b: Rate constant is the high-pressure limit as recommended by Atkinson et al. (2006).

G42047: Orlando et al. (1998) estimated that about 25% of the $HOCH_2CH_2O$ in this reaction is produced with sufficient excess energy that it decomposes

promptly. The decomposition products are 2 HCHO + HO_2.

G42051a: Same as for the CH_3O_2 channel in G4107: CH_3OOH+OH.

G42058b: The aldehydic H is assumed to be like the analogous H of $HOCH_2CHO$.

G42074a: Factor of 3 to match the estimate of k = 1.E-11 molec/cm3/s by Paulot et al. (2009a).

G42074b: Factor of 3 to match the estimate of k = 1.E-11 molec/cm3/s by Paulot et al. (2009a).

G42075: $NO_3CH_2CO_2H$ and $NO_3CH_2CO_3H$ neglected.

G42078: $NO_3CH_2CO_2H$ neglected.

G42082: Same rate constant as for PAN + OH.

G42083a: Rate constant is the high-pressure limit as recommended by Atkinson et al. (2006).

G42083b: Rate constant is the high-pressure limit as recommended by Atkinson et al. (2006).

G42085a: Uncertainties on the kinetics at pressures < 0.1 bar.

G42085b: Channel proposed by Hynes and Wine 1991, OH + HCHO + HOCN, could not be confirmed by Tyndall et al. (2001b). There is no alternative mechanism at the moment. Products assumed to be OH + CH3CO3 + NO

G42086b: Assuming HCN is from channel 2h, HCO + H + HCN. HCO is replaced by H + CO.

G42086c: Assuming exothermic channels 2b and 2d are equally important.

G42087: HCOCN is produced but replaced here by its likely oxidation products (HCN + CO_2) as studied by Tyndall et al. (2001b). The rate constant for a typical RO_2 + NO reaction is used.

G42088: $NCCH_2OOH$ is produced but replaced here by its likely oxidation products (HCN + CO_2) as studied by Tyndall et al. (2001b). The rate constant for a typical RO_2 + HO_2 reaction is used.

G42089a: The minor channel with k=5.2E-12 is combined with the major one producing HCOOH.

G42090: Theoretical keto-enol tautomerization catalyzed by formic acid (Grenfell et al., 2006).

G42091: Theoretical keto-enol tautomerization catalyzed by formic acid (Grenfell et al., 2006).

G43001a: Branching ratios according to Rickard et al. (1999).

G43001b: Branching ratios according to Rickard et al. (1999).

G43004: The value for the generic RO_2 + HO_2 reaction from Atkinson (1997) is used here.

G43008: The value for the generic RO_2 + HO_2 reaction from Atkinson (1997) is used here.

G43011: Strong positive deviation of k below 240 K compared to the expression recommended by JPL (Burkholder et al., 2015).

G43015a: The same value as for G4107 (CH_3OOH + OH) is used, multiplied by the branching ratio of the CH_3O_2 channel.

G43028: Alkyl nitrate formation neglected. (also not considered in MCM).

G43037: Alkyl nitrate formation neglected. (also not considered in MCM).

G43040a: Rate coefficient estimated with SAR (Taraborrelli, 2010).

G43040b: Rate coefficient estimated with SAR (Taraborrelli, 2010).

G43044: Alkyl nitrate formation neglected.

G43045c: Rate coefficient assumed to equal to the one of hydroxyacetone (ACETOL) for this channel.

G43048: Using the high-pressure limit.

G43049: The pressure fall-off between 1000 and 100 mbar is only 3% (Kirchner et al., 1999).

G43050: Value for $CH_3O_2NO_2$ + OH, H-abstraction enhanced by the CH_3CO-group by f_CO.

G43051c: Products approximated with C_2H_5CHO + HO_2.

G43052: Only major H-abstraction channel considered.

G43059: Products approximated with the major end-product CH_3CHO.

G43060b: Products approximated with the major end-product CH_3CHO.

G43061: Products approximated with the likely end-product CH_3CHO.

G43065: As for $HCOCO_3$.

G43070a: Branching ratios estimated with SAR for H-abstraction rate constants by OH.

G43070b: Branching ratios estimated with SAR for H-abstraction rate constants by OH.

G43071a: Only this channel considered as the intermediate radical is likely more stable than $CHCH(OH)_2$.

G43072: Theoretical keto-enol tautomerization catalyzed by formic acid (Grenfell et al., 2006).

G43073: Theoretical keto-enol tautomerization catalyzed by formic acid (Grenfell et al., 2006).

G43074: HCOCOCHO would be produced but undergoes fast photolysis (faster than MGLYOX) and is substituted with its products.

G43223: Products simplified

G43419: KDEC C3DIALO → GLYOX + CO + HO2

G43420: KDEC C3DIALO → GLYOX + CO + HO2

G43421: Permutation reaction (minor channels removed).

G44000: The $LC_4H_9O_2$ composition ($nC_4H_9O_2$:$sC_4H_9O_2$ ratio) is assumed to be equal to the ratio of the production rates at 298K: k_p/(k_p+k_s) = 0.1273 and k_s/(k_p+k_s) = 0.8727.

G44001b: $sC_4H_9O_2$ products are substituted with 0.636 MEK + HO_2 and 0.364 CH_3CHO + $C_2H_5O_2$ at 1 bar and 298 K.

G44003c: The alkyl nitrate yield is the weighted average yield for the two isomers forming from $nC_4H_9O_2$ and $sC_4H_9O_2$.

G44010b: H-abstraction from primary C and substitution of the resulting peroxy radical with its products from the reaction with NO.

G44011: H-abstraction from primary C and substitution of the resulting peroxy radical with its products from the reaction with NO.

G44015b: Products assumed to be only from H-abstraction from a secondary C bearing the -OOH group.

G44016: Products assumed to be only from H-abstraction from a secondary C bearing the -ONO_2 group.

G44018: LHMVKABO2 is 0.12 HMVKAO2 + 0.88 HMVKBO2.

G44019: LMEKO2 represents 0.62 MEKBO2 + 0.38 MEKAO2.

G44021a: The products of MEKAO are substituted with HCHO + CO_2 + $HOCH_2CH_2O_2$.

G44023a: Products from H-abstraction from the tertiary carbon bearing the ONO_2 group.

G44023b: Products from H-abstraction from the secondary carbon bearing the ONO_2 group.

G44025: Same value as for PAN.

G44026: Products as in G4415. Only the main channels for each isomer are considered. Weighted average for the isomers.

G44035: Rate constant replaced with the one of beta hydroxy RO_2.

G44046b: Using value for secondary nitrate (88% of total).

G44061a: Using value for secondary nitrate (88% of total).

G44061b: Using value for secondary nitrate (88% of total).

G44062a: Simplified products.

G44062b: Simplified products.

G44066: Alkyl nitrate formation neglected.

G44070: Alkyl nitrate formation neglected.

G44076: Alkyl nitrate formation neglected.

G44078: Other channel neglected.

G44081: Alkyl nitrate formation neglected.

G44082: Other channel neglected.

G44085: k for CH_3CHCO from Hatakeyama et al. (1985) adjusted.

G44086: Simplified product distribution.

G44089: The nitrated RO_2 is replaced by its products upon reaction with NO.

G44096: Both LBUT1ENO2 isomers mostly C_2H_5CHO.

G44097a: Branching ratios according to Rickard et al. (1999). CH_3CHO_2CHO is replaced with its major products CH_3CHO + CO + HO_2.

G44097b: Branching ratios according to Rickard et al. (1999).

G44098: The nitrated RO_2 is replaced by its products upon reaction with NO.

G44103b: MEKCOH replaced by its major oxidation products.

G44104: Carbonyl nitrate replaced by its major oxidation products.

G44106: CH3CHOOA products as from C_3H_6 + O_3 reaction.

G44107: The nitrated RO_2 is replaced by its products upon reaction with NO.

G44110: The nitrated RO_2 is replaced by its products upon reaction with NO.

G44124b: Skipping intermediate steps mostly leading to acetone.

G44126: Skipping intermediate steps mostly leading to acetone.

G44127: Only this channel considered as the intermediate radical is likely more stable than $CHCH(OH)_2$.

G44128: Theoretical keto-enol tautomerization catalyzed by formic acid (Grenfell et al., 2006).

G44129: Theoretical keto-enol tautomerization catalyzed by formic acid (Grenfell et al., 2006).

G44130: Only this channel considered as the intermediate radical is likely more stable than $CHCH(OH)_2$.

G44131: Theoretical keto-enol tautomerization catalyzed by formic acid (Grenfell et al., 2006).

G44132: Theoretical keto-enol tautomerization catalyzed by formic acid (Grenfell et al., 2006).

G44133: Only this channel considered as the intermediate radical is likely more stable than $CHCH(OH)_2$.

G44134: Theoretical keto-enol tautomerization catalyzed by formic acid (Grenfell et al., 2006).

G44135: Theoretical keto-enol tautomerization catalyzed by formic acid (Grenfell et al., 2006).

G44136: Only this channel considered as the intermediate radical is likely more stable than $CHCH(OH)_2$.

G44137: Theoretical keto-enol tautomerization catalyzed by formic acid (Grenfell et al., 2006).

G44138: Theoretical keto-enol tautomerization catalyzed by formic acid (Grenfell et al., 2006).

G44139: Simplified oxidation.

G44140: Simplified oxidation.

G44141: Simplified oxidation.

G44142: Simplified oxidation.

G44202: Alkyl nitrate formation neglected.

G44203a: Rate coefficient estimated with SAR (Taraborrelli, 2010).

G44205: Alkyl nitrate formation neglected.

G44210: Alkyl nitrate formation neglected.

G44221: Same k as for MGLYOX + OH (Tyndall et al., 1995).

G44402: KDEC NC4DCO2→ MALANHY + NO2

G44406c: KDEC MALDIALCO2 → 0.6 MALANHY + HO2 + 0.4 GLYOX + 0.4 CO + 0.4 CO2

G44407: KDEC MALDIALCO2 → 0.6 MALANHY + HO2 + 0.4 GLYOX + 0.4 CO + 0.4 CO2

G44409: KDEC MALDIALCO2 → 0.6 MALANHY + HO2 + 0.4 GLYOX + 0.4 CO + 0.4 CO2

G44410: KDEC MALDIALCO2 → 0.6 MALANHY + HO2 + 0.4 GLYOX + 0.4 CO + 0.4 CO2

G44412: KDEC BZFUONOOA → 0.5 BZFUONOO + 0.5 CO + 0.5 CO2 + 0.5 HCOCH2O2 + 0.5 OH and BZFUONOO → 0.625 CO14O3CO2H + 0.375 CO14O3CHO + 0.375 H2O2

G44421: Only major channel.

G44424: KDEC: GLYOOA → 0.125 HCHO + 0.18 GLYOO + 0.82 HO2 + 0.57 OH + 1.265 CO + 0.25 CO2 and H2O substitution GLYOO → 0.625 HCOCO2H + 0.375 GLYOX + 0.375 H2O2

G44425: Merged equations.

G44430: KDEC MALANHYO → HCOCOHCO3

G44431: KDEC MALANHYO → HCOCOHCO3

G44432: Only major channel. KDEC MALANHYO → HCOCOHCO3

G44436: KDEC NBZFUO → 0.5 CO14O3CHO + 0.5 NO2 + 0.5 NBZFUONE + 0.5 HO2

G44437: KDEC NBZFUO → 0.5 CO14O3CHO + 0.5 NO2 + 0.5 NBZFUONE + 0.5 HO2

G44438: KDEC NBZFUO → 0.5 CO14O3CHO + 0.5 NO2 + 0.5 NBZFUONE + 0.5 HO2 and RO2 Only major channel.

G44439: KDEC MALDIALCO2 → 0.6 MALANHY + HO2 + 0.4 GLYOX + 0.4 CO + 0.4 CO2

G44443: KDEC MECOACETO → CH3CO3 + HCHO

G44444: KDEC MECOACETO → CH3CO3 + HCHO

G44445: KDEC MECOACETO → CH3CO3 + HCHO

G44450: KDEC BZFUO → CO14O3CHO + HO2

G44451: KDEC BZFUO → CO14O3CHO + HO2

G44452: KDEC BZFUO → CO14O3CHO + HO2. Only major channel.

G44457: KDEC MALDIALO → GLYOX + GLYOX + HO2

G44458: KDEC MALDIALO → GLYOX + GLYOX + HO2

G44459: KDEC MALDIALO → GLYOX + GLYOX + HO2. Only major channel.

G44461: KBPAN → k_PAN_M

G45019d: Delta-1 and delta-2 LIEPOX are not considered and replaced by beta-LIEPOX formed by ISOPBOOH and ISOPDOOH.

G45021: SAR estimate within uncertainty range of the experimentally determined rate constant by Solberg et al. (1997), 1.1E-11.

G45037: SAR estimate within uncertainty range of the experimentally determined rate constant by Solberg et al. (1997), 4.2E-11.

G45040: Alkyl nitrate formation neglected.

G45043: Old MCM rate constant 4.16E-11.

G45047: Alkyl nitrate formation neglected.

G45055: Alkyl nitrate formation neglected.

G45071: Alkyl nitrate formation neglected.

G45074: Formic acid production consistent with results of Bates et al. (2014). Here, the high yields of formic acid and hydroxycarbonyls at low NO from oxidation of cis-beta-LIEPOX (the most abundant isomer) are approximated with the production of DB1O which undergo both the Dibble double H-transfer to DB2O2 and HOCH2 elimination yielding HVMK and HMAC (keto-vinyl alcohol potentially arising from decomposition of the alkoxy radical resulting from the ring opening after H-abstraction). The rate constant is from Paulot et al. (2009b) and adjusted based on Bates et al. (2014) that determined the single rate constants for the cis- and trans- beta isomer.

G45080: Alkyl nitrate formation neglected.

G45092a: C4MDIAL = CM4DIAL in MCM only from aromatics.

G45092b: Only one acyl peroxy radical considered.

G45093: Two aldehydic sites reacting with NO_3 but only one isomer product considered.

G45095: Alkyl nitrate formation neglected.

G45098: Alkyl nitrate formation neglected.

G45100: Alkyl nitrate formation neglected.

G45104a: DB1OOH is a hydroperoxide bearing a vinyl alcohol moiety that upon reaction with OH yields HCOOH (Davis et al., 1998).

G45107: OH production here is to take into account the hydroperoxidic function formed by the shift of the enolic hydrogen and not present in DB2O2. This approximation leads to spurious HO_2 production.

G45108a: Consistent with the results of Bates et al. (2014).

G45108b: Consistent with the results of Bates et al. (2014). Assuming that the enol alkoxy radical partly decomposes yielding a substitute vinyl alcohol.

G45111: Alkyl nitrate formation neglected.

G45114b: Here, formic acid is mechanistically produced by the OH-addition to the vinyl alcohol which, upon RO_2-to-RO conversion (skipped here), yields the HOCHOH fragment which in turn reacts with O_2 forming HCOOH + HO_2. Along $CH_3COCHOOHCHO$ should be produced but not in the mechanism. Only CH_3COCHO_2CHO. The rate constant is consistent with predictions by Ganzeveld et al. (2006) for ENOL. OH-addition to the OH-bearing carbon is considered the dominant channel as it is already for the ENOL (Ganzeveld et al., 2006).

G45115: Theoretical keto-enol tautomerization catalyzed by formic acid (Grenfell et al., 2006). The product should be C1ODC3OOHC4OD but it is neglected in the mechanism.

G45116: As for DB1OOH + OH.

G45117: Additional sinks for DB2OOH are neglected.

G45121b: Nitrate assumed to be major isomer that is mostly similar to products of ISOPDO2-chemistry.

G45128: Rate constant by Liljegren and Stevens (2013). A lumped RO_2 that upon conversion to RO yields 100% 2-methyl-butenedial (C4MDIAL) although Aschmann et al. (2014) quantified a 38% yield of the Z/E mixture.

G45129: As for 3METHYLFURAN + OH but with additional NO_2 production for mass conservation.

G45131: Alkyl nitrate formation neglected.

G45132: Hydroperoxide formation neglected.

G45134b: ZCO2HC23DBCOD formation is neglected. However, it is produced in MCM and in aromatic-related reactions under the name of MC3ODBCO2H.

G45139: LZCPANC23DBCOD is assumed to react like LC5PAN1719.

G45201: Alkyl nitrate formation neglected.

G45207: Alkyl nitrate formation neglected.

G45214: Alkyl nitrate formation neglected.

G45217: Alkyl nitrate formation neglected.

G45225: Alkyl nitrate formation neglected.

G45236: LMBOABO2 = 0.67 MBOAO2 + 0.33 MBOBO2

G45247: Alkyl nitrate formation neglected.

G45400: KDEC NC4MDCO2 → MMALANHY + NO2

G45404: KDEC NTLFUO → ACCOMECHO + NO2

G45405: KDEC NTLFUO → ACCOMECHO + NO2

G45406: KDEC NTLFUO → ACCOMECHO

G45409: KBPAN → k_PAN_M(renaming)

G45413: KFPAN → k_CH3CO3_NO2 (renaming)

G45422: KDEC MMALANHYO→CO2H3CO3

G45423: KDEC MMALANHYO→CO2H3CO3

G45424: KDEC MMALANHYO→CO2H3CO3 and Only major channel.

G45429: KBPAN → k_PAN_M (renamed)

G45430a: KDEC C5CO14CO2 → 0.83 MALANHY + 0.83 CH3 + 0.17 MGLYOX + 0.17 HO2 + 0.17 CO + 0.17 CO2

G45431: KDEC C5CO14CO2 → 0.83 MALANHY + 0.83 CH3 + 0.17 MGLYOX + 0.17 HO2 + 0.17 CO + 0.17 CO2

G45432: KFPAN →k_CH3CO3_NO2 (renaming)

G45433: KDEC C5CO14CO2 → 0.83 MALANHY + 0.83 CH3 + 0.17 MGLYOX + 0.17 HO2 + 0.17 CO + 0.17 CO2

G45434: KDEC C5CO14CO2 → 0.83 MALANHY + 0.83 CH3 + 0.17 MGLYOX + 0.17 HO2 + 0.17 CO + 0.17 CO2 and only major channel.

G45436: KDEC C5CO14CO2 → 0.83 MALANHY + 0.83 CH3 + 0.17 MGLYOX + 0.17 HO2 + 0.17 CO + 0.17 CO2

G45444: KDEC MC3CODBCO2 → 0.35 GLYOX + 0.35 CH3 + 0.35 CO + 0.35 CO2 + 0.65 MMALANHY + 0.65 HO2

G45452: KDEC TLFUONOOA → 0.5 CO + 0.5 OH + 0.5 MECOACETO2 + 0.5 TLFUONOO and H2O subs TLFUONOO → 0.625 C24O3CCO2H + 0.375 ACCOMECHO + 0.375 H2O2

G45456: KFPAN →k_CH3CO3_NO2 (renaming)

G45476b: KDEC NTLFUO → ACCOMECHO + NO2 and reactions with KRO2HO2.

G45477: KDEC NTLFUO → ACCOMECHO + NO2

G45478: KDEC NTLFUO → ACCOMECHO + NO2

G45479: KDEC NTLFUO → ACCOMECHO + NO2

G45486b: KDEC C5DIALO →MALDIAL + CO + HO2 and reactions with KRO2HO2.

G45487: KDEC C5DIALO →MALDIAL

G45488: KDEC C5DIALO →MALDIAL

G45489: KDEC C5DIALO →MALDIAL

G45491b: Reactions with KRO2HO2.

G45492: MGLYOX + GLYOX + HO2 from KDEC substitution

G45493: MGLYOX + GLYOX + HO2 from KDEC substitution

G45494: Permutation reaction (minor channels removed).

G46201: Alkyl nitrate formation neglected.

G46404b: Reactions with KRO2HO2 and KDEC C615CO2O → C5DICARB + CO + HO2.

G46405: KDEC C615CO2O → C5DICARB + CO + HO2

G46406: KDEC C615CO2O → C5DICARB + CO + HO2

G46407: Only major channel.

G46413b: Reactions with KRO2HO2 and KDEC NDNPHENO → NC4DCO2H + HNO3 + CO + CO + NO2.

G46414: KDEC NDNPHENO → NC4DCO2H + HNO3 + CO + CO + NO2

G46415: KDEC NDNPHENO → NC4DCO2H + HNO3 + CO + CO + NO2

G46416: KDEC NDNPHENO → NC4DCO2H + HNO3 + CO + CO + NO2

G46418: KDEC CATECOOA → MALDALCO2H + HCOCO2H + HO2 + OH

G46426: KFPAN →k_CH3CO3_NO2

G46430: KDEC GLYOOA → .125 HCHO + .18 GLYOO + .82 HO2 + .57 OH + 1.265 CO

G46432b: Reactions with KRO2HO2 and KDEC NCATECO → NC4DCO2H + HCOCO2H + HO2

G46433: KDEC NCATECO → NC4DCO2H + HCOCO2H + HO2

G46434: KDEC NCATECO → NC4DCO2H + HCOCO2H + HO2

G46435: KDEC NCATECO → NC4DCO2H + HCOCO2H + HO2

G46437b: Reactions with KRO2HO2 and KDEC NPHENO → MALDALCO2H + GLYOX + NO2

G46438: KDEC NPHENO → MALDALCO2H + GLYOX + NO2

G46439: KDEC NPHENO → MALDALCO2H + GLYOX + NO2

G46440: KDEC NPHENO → MALDALCO2H + GLYOX + NO2

G46441: Merged equations.

G46447b: reactions with KRO2HO2 and KDEC NNCATECO → NC4DCO2H + HCOCO2H + NO2

G46448: KDEC NNCATECO → NC4DCO2H + HCOCO2H + NO2

G46449: KDEC NNCATECO → NC4DCO2H + HCOCO2H + NO2

G46450: KDEC NNCATECO → NC4DCO2H + HCOCO2H + NO2

G46457: Merged equations.

G46458: Merged equations.

G46461b: Reactions with KRO2HO2 and KDEC PHENO → 0.71 MALDALCO2H + 0.71 GLYOX + 0.29 PBZQONE + HO2

G46462: KDEC PHENO → 0.71 MALDALCO2H + 0.71 GLYOX + 0.29 PBZQONE + HO2

G46463: KDEC PHENO → 0.71 MALDALCO2H + 0.71 GLYOX + 0.29 PBZQONE + HO2

G46464: KDEC PHENO → 0.71 MALDALCO2H + 0.71 GLYOX + 0.29 PBZQONE + HO2 and Only major channel.

G46468: KFPAN →k_CH3CO3_NO2

G46472b: new channel

G46476: HOC6H4NO2 is a nitro-phenol

G46480b: Reactions with KRO2HO2 and KDEC PBZQO →C5CO2OHCO3

G46481: KDEC PBZQO →C5CO2OHCO3

G46482: KDEC PBZQO →C5CO2OHCO3

G46483: KDEC PBZQO →C5CO2OHCO3 and Only major channel.

G46485b: Reactions with KRO2HO2 and KDEC DNPHENO → NC4DCO2H + HCOCO2H + NO2

G46486: KDEC DNPHENO → NC4DCO2H + HCOCO2H + NO2

G46487: KDEC DNPHENO → NC4DCO2H + HCOCO2H + NO2

G46488: KDEC DNPHENO → NC4DCO2H + HCOCO2H + NO2

G46490b: Reactions with KRO2HO2 and KDEC BZEMUCO → 0.5 EPXC4DIAL + 0.5 GLYOX + 0.5 HO2 + 0.5 C3DIALO2 + 0.5 C32OH13CO.

G46491b: KDEC BZEMUCO → 0.5 EPXC4DIAL + 0.5 GLYOX + 0.5 HO2 + 0.5 C3DIALO2 + 0.5 C32OH13CO.

G46492: KDEC BZEMUCO → 0.5 EPXC4DIAL + 0.5 GLYOX + 0.5 HO2 + 0.5 C3DIALO2 + 0.5 C32OH13CO

G46493: KDEC BZEMUCO → 0.5 EPXC4DIAL + 0.5 GLYOX + 0.5 HO2 + 0.5 C3DIALO2 + 0.5 C32OH13CO and Only major channel.

G46499b: Reactions with KRO2HO2 and KDEC NBZQO → C6CO4DB + NO2.

G46500: KDEC NBZQO → C6CO4DB + NO2

G46501: KDEC NBZQO → C6CO4DB + NO2

G46502: KDEC NBZQO → C6CO4DB + NO2

G46505b: New channel.

G46515: Only major channel.

G46522b: In analogy to TLBIPERO2 from toluene (Birdsall et al., 2010).

G46523b: KDEC BZBIPERO → GLYOX + HO2 + 0.5 BZFUONE + 0.5 BZFUONE

G46524: KDEC BZBIPERO → GLYOX + HO2 + 0.5 BZFUONE + 0.5 BZFUONE

G46525: KDEC BZBIPERO → GLYOX + HO2 + 0.5 BZFUONE + 0.5 BZFUONE and Only major channel.

G47210: Alkyl nitrate formation neglected.

G47214: Alkyl nitrate formation neglected.

G47218: Alkyl nitrate formation neglected.

G47222: Alkyl nitrate formation neglected.

G47223: ROO6R3OOH produced but no sink for it.

G47225: ROO6R4P produced but no sink for it.

G47226: ROO6R5P produced but no sink for it

G47400: Merged.

G47402a: KROPRIM*O2 fast reaction C6H5CH2O = BENZAL + HO2.

G47402b: KROPRIM*O2 fast reaction C6H5CH2O = BENZAL + HO2.

G47403: KROPRIM*O2 fast reaction C6H5CH2O = BENZAL + HO2.

G47404: KROPRIM*O2 fast reaction C6H5CH2O = BENZAL + HO2. C6H5CH2OH replaced by its oxidation product BENZAL.

G47405: Merged.

G47406: Merged.

G47407b: According to Birdsall et al. (2010), the branching ratio rbipero2_oh is set to 0.4 in order to take into account the OH-recycling and summed yield of butendial and methylbutendial.

G47408a: KDEC TLBIPERO → 0.6 GLYOX + 0.4 MGLYOX + HO2 + 0.2 C4MDIAL + 0.2 C5DICARB + 0.2 TLFUONE + 0.2 BZFUONE + 0.2 MALDIAL

G47408b: KDEC TLBIPERO → 0.6 GLYOX + 0.4 MGLYOX + HO2 + 0.2 ZCODC23DB COD + 0.2 C5DICARB + 0.2 TLFUONE + 0.2 BZFUONE + 0.2 MALDIAL

G47409: KDEC TLBIPERO → 0.6 GLYOX + 0.4 MGLYOX + HO2 + 0.2 ZCODC23DB COD + 0.2 C5DICARB + 0.2 TLFUONE + 0.2 BZFUONE + 0.2 MALDIAL

G47410: Only major channel and KDEC TLBIPERO → 0.6 GLYOX + 0.4 MGLYOX + HO2 + 0.2 ZCODC23DB COD + 0.2 C5DICARB + 0.2 TLFUONE + 0.2 BZFUONE + 0.2 MALDIAL

G47412: KDEC MGLOOB → 0.125 CH3CHO + 0.695 CH3CO + 0.57 CO + 0.57 OH + 0.125 HO2 + 0.18 MGLOO + 0.25 CO2

G47413: Merged.

G47418b: Reactions with KRO2HO2 and KDEC CRESO → 0.68 C5CO14OH + 0.68 GLYOX + HO2 + 0.32 PTLQONE.

G47419: KDEC CRESO → 0.68 C5CO14OH + 0.68 GLYOX + HO2 + 0.32 PTLQONE

G47420: KDEC CRESO → 0.68 C5CO14OH + 0.68 GLYOX + HO2 + 0.32 PTLQONE

G47421: KDEC CRESO → 0.68 C5CO14OH + 0.68 GLYOX + HO2 + 0.32 PTLQONE and Only major channel.

G47422b: Reactions with KRO2HO2 and KDEC NCRESO → C5CO14OH + GLYOX + NO2

G47423: KDEC NCRESO → C5CO14OH + GLYOX + NO2

G47424: KDEC NCRESO → C5CO14OH + GLYOX + NO2

G47425: KDEC NCRESO → C5CO14OH + GLYOX + NO2 and Only major channel.

G47426: TOL1OHNO2 is a nitro-phenol

G47429: KDEC MCATECOOA → MC3ODBCO2H + HCOCO2H + HO2 + OH

G47436: KFPAN →k_CH3CO3_NO2

G47438: Only major channel.

G47439b: Reactions with KRO2HO2 and KDEC TLEMUCO→ 0.5 C3DIALO2 + 0.5 CO2H3CHO + 0.5 EPXC4DIAL + 0.5 MGLYOX + 0.5 HO2

G47440b: KDEC TLEMUCO→ 0.5 C3DIALO2 + 0.5 CO2H3CHO + 0.5 EPXC4DIAL + 0.5 MGLYOX + 0.5 HO2

G47441: KDEC TLEMUCO→ 0.5 C3DIALO2 + 0.5 CO2H3CHO + 0.5 EPXC4DIAL + 0.5 MGLYOX + 0.5 HO2

G47442: KDEC TLEMUCO→ 0.5 C3DIALO2 + 0.5 CO2H3CHO + 0.5 EPXC4DIAL + 0.5 MGLYOX + 0.5 HO2 and Only major channel.

G47445: KFPAN →k_CH3CO3_NO2

G47447: Only major channel.

G47454: New channel.

G47479: New channel.

G47482b: Reactions with KRO2HO2 and KDEC NPTLQO → C7CO4DB + NO2

G47483: KDEC NPTLQO → C7CO4DB + NO2

G47484: KDEC NPTLQO → C7CO4DB + NO2

G47485: KDEC NPTLQO → C7CO4DB + NO2

G47486b: Reactions with KRO2HO2 and KDEC PTLQO → C6CO2OHCO3

G47487: KDEC PTLQO → C6CO2OHCO3

G47488: KDEC PTLQO → C6CO2OHCO3

G47489: Only major channel. KDEC PTLQO → C6CO2OHCO3.

G47494: New channel.

G47497b: Reactions with KRO2HO2 and KDEC MNCATECO → NC4MDCO2H + HCOCO2H + NO2

G47498: KDEC MNNCATECO → NC4MDCO2H + HCOCO2H + NO2

G47499: KDEC MNNCATECO → NC4MDCO2H + HCOCO2H + NO2

G47501b: Reactions with KRO2HO2 and KDEC MNCATECO → NC4MDCO2H + HCOCO2H + HO2

G47502: KDEC MNCATECO → NC4MDCO2H + HCOCO2H + HO2

G47503: KDEC MNCATECO → NC4MDCO2H + HCOCO2H + HO2

G47504: KDEC MNCATECO → NC4MDCO2H + HCOCO2H + HO2

G47509b: Reactions with KRO2HO2 and KDEC NDNCRESO → NC4MDCO2H + HNO3 + CO + CO + NO2

G47510: KDEC NDNCRESO → NC4MDCO2H + HNO3 + CO + CO + NO2

G47511: KDEC NDNCRESO → NC4MDCO2H + HNO3 + CO + CO + NO2

G47512: KDEC NDNCRESO → NC4MDCO2H + HNO3 + CO + CO + NO2

G47513b: Reactions with KRO2HO2 and KDEC DNCRESO → NC4MDCO2H + HCOCO2H + NO2

G47514: KDEC DNCRESO → NC4MDCO2H + HCOCO2H + NO2

G47515: KDEC DNCRESO → NC4MDCO2H + HCOCO2H + NO2

G47516: KDEC DNCRESO → NC4MDCO2H + HCOCO2H + NO2

G48202: Alkyl nitrate formation neglected.

G48205: Alkyl nitrate formation neglected.

G48210: Alkyl nitrate formation neglected.

G48212: Alkyl nitrate formation neglected.

G48216: Alkyl nitrate formation neglected.

G48222: Alkyl nitrate formation neglected.

G48400a: Same products as for toluene. Assuming a 1:1:1 proportion in xylenes emissions the analogous toluene product is produced with a rate constant equal to (1.36E-11*0.24 + 2.31E-11*0.29 + 1.43E-11*0.155)/3, where k and coefficients are for the single isomers ortho, meta and para from MCM.

G48400b: Same products as for toluene. Assuming a 1:1:1 proportion in xylenes emissions the analogous toluene product is produced with a rate constant equal to (1.36E-11*0.05 + 2.31E-11*0.04 + 1.43E-11*0.10)/3, where k and coefficients are for the single isomers ortho, meta and para from MCM.

G48400c: Same products as for toluene. Assuming a 1:1:1 proportion in xylenes emissions the analogous toluene product is produced with a rate constant equal to (1.36E-11*0.16 + 2.31E-11*0.17 + 1.43E-11*0.12)/3, where k and coefficients are for the single isomers ortho, meta and para from MCM.

G48400d: Same products as for toluene. Assuming a 1:1:1 proportion in xylenes emissions the analogous toluene product is produced with a rate constant equal to (1.36E-11*0.55 + 2.31E-11*0.50 + 1.43E-11*0.625)/3, where k and coefficients are for the single isomers ortho, meta and para from MCM.

G48401: Same products as for toluene. The rate constant is the average of m, p, o k=(4.10E-16+2.60E-16+5.00E-16)/3 = 3.9E-16.

G48402: merged under same rate constant

G48403: Same products as for toluene

G48405: KDEC CH2OOB → 0.24 CH2OO + 0.40 CO + 0.36 HO2 + 0.36 CO + 0.36 OH and H2O + PHCHOO → 0.625 PHCOOH + 0.375 BENZAL + 0.375 H2O2 + 0.2 CO2

G48408: KDEC NSTYRENEO → NO2 + HCHO + BENZAL

G48409: KDEC NSTYRENEO → NO2 + HCHO + BENZAL

G48410: KDEC NSTYRENEO → NO2 + HCHO + BENZAL

G48412b: KDEC STYRENO → HO2 + HCHO + BENZAL and reactions with KRO2HO2.

G48413: KDEC STYRENO → HO2 + HCHO + BENZAL

G48414: KDEC STYRENO → HO2 + HCHO + BENZAL

G48415: KDEC STYRENO → HO2 + HCHO + BENZAL

G49207: Alkyl nitrate formation neglected.

G49238: Alkyl nitrate formation neglected.

G49246: Only this channel considered as the intermediate radical is likely more stable than

$CHCH(OH)_2$.Instead of the (lacking) carbonyl a product of further degradation is assumed.

G49247: Theoretical keto-enol tautomerization catalyzed by formic acid (Grenfell et al., 2006).

G49248: Theoretical keto-enol tautomerization catalyzed by formic acid (Grenfell et al., 2006).

G49400a: Same products as for toluene. Assuming a 1:1:1 proportion in xylenes emissions the analogous toluene product is produced with a rate constant equal to (3.27E-11*0.21 + 3.25E-11*0.30 + 5.67E-11*0.14)/3, where k and coefficients are for the single isomers 1,2,3-, 1,3,4- and 1,3,5- from MCM.

G49400b: Same products as for toluene. Assuming a 1:1:1 proportion in xylenes emissions the analogous toluene product is produced with a rate constant equal to (3.27E-11*0.06 + 3.25E-11*0.06 + 5.67E-11*0.03)/3, where k and coefficients are for the single isomers 1,2,3-, 1,3,4- and 1,3,5- from MCM.

G49400c: Same products as for toluene. Assuming a 1:1:1 proportion in xylenes emissions the analogous toluene product is produced with a rate constant equal to (3.27E-11*0.03 + 3.25E-11*0.03 + 5.67E-11*.04)/3, where k and coefficients are for the single isomers 1,2,3-, 1,3,4- and 1,3,5- from MCM.

G49400d: Same products as for toluene. Assuming a 1:1:1 proportion in xylenes emissions the analogous toluene product is produced with a rate constant equal to (3.27E-11*0.70 + 3.25E-11*0.61 + 5.67E-11*0.79)/3, where k and coefficients are for the single isomers 1,2,3-, 1,3,4- and 1,3,5- from MCM.

G49401: Same products as for toluene. The rate constant is the average of m, p, o k=(1.90+1.80+0.88)E-15/3=1.52E-15.

G40200: Products from Vereecken et al. (2007). LAPINABO2 = 0.65 APINAO2 + 0.35 APINBO2

G40203: Weighted average for isomers A and B, `k = 0.33*9.20E-14+0.67*8.80E-13`.

G40204: Weighted average for isomers A and B, `k = 0.35*1.83E-11+0.65*3.28E-11`.

G40205: Weighted average for isomers A and B, `k = 0.35*5.50E-12+0.65*3.64E-12`.

G40206: SAR-estimated rate constant, `(kads+kadt)*acoch3 = 6.46E-11` where `kads = 3.0E-11`, `kadt = 5.5E-11`, `acoch3 = 0.76`

G40207: Alkyl nitrate formation neglected.

G40211: Products from Rickard and Pascoe (2009).

G40212: Products from Rickard and Pascoe (2009).

G40232: Products from Capouet et al. (2008).

G40242: Alkyl nitrate formation neglected.

G40246: Products from Rickard and Pascoe (2009).

G40248: Alkyl nitrate formation neglected.

G40252a: Products from Vereecken and Peeters (2012).

G40252b: Products from Vereecken and Peeters (2012).

G40259: ROO6R1OOH is produced but no sink for it.

G40262: RO6R1OOH is produced but no sink for it.

G40266: Rate constant modified according to MCM protocol.

G40267a: Products from Nguyen et al. (2009).

G40268: Products from Rickard and Pascoe (2009).

G40270: Alkyl nitrate neglected.

G40274: As for RO6R1NO3 in G4085.

G40276: Only this channel considered as the intermediate radical is likely more stable than $CHCH(OH)_2$.

G40277: Theoretical keto-enol tautomerization catalyzed by formic acid (Grenfell et al., 2006).

G40278: Theoretical keto-enol tautomerization catalyzed by formic acid (Grenfell et al., 2006).

G40282a: Products from Vereecken and Peeters (2012).

G40282b: Products from Vereecken and Peeters (2012).

G40283a: Products from Nguyen et al. (2009).

G40284: Products from Rickard and Pascoe (2009).

G40285a: Products from Vereecken and Peeters (2012).

G40285b: Products from Vereecken and Peeters (2012).

G40286a: Products from Nguyen et al. (2009).

G40287: Products from Rickard and Pascoe (2009).

G40400: DIET35TOL(from MCM) as representative of higher aromatics

G40401: Same products as for toluene.

G6103: The rate coefficient is defined as backward reaction divided by equilibrium constant.

G6204: At low temperatures, there may be a minor reaction channel leading to O_3+HCl. See Finkbeiner et al. (1995) for details. It is neglected here.

G6402: The initial products are probably HCl and CH_2OOH (Atkinson et al., 2006). It is assumed that CH_2OOH dissociates into HCHO and OH.

G6409: It is assumed that the reaction liberates all Cl atoms in the form of HCl.

G7302: The rate coefficient is: `k_BrO_NO2 = k_3rd(temp,cair,5.2E-31,3.2,6.9E-12,2.9,0.6)`.

G7303: The rate coefficient is defined as backward reaction (Atkinson et al., 2007) divided by equilibrium constant (Orlando and Tyndall, 1996).

G7404: It is assumed that the reaction liberates all Br atoms in the form of HBr.

G7407: It is assumed that the reaction liberates all Br atoms. The fate of the carbon atom is currently not considered.

G7408: It is assumed that the reaction liberates all Br atoms. The fate of the carbon atom is currently not considered.

G7605: Same value as for G7408: CH_2Br_2+OH assumed. It is assumed that the reaction liberates all Br and Cl atoms. The fate of the carbon atom is currently not considered.

G7606: Same value as for G7408: CH_2Br_2+OH assumed. It is assumed that the reaction liberates all Br and Cl atoms. The fate of the carbon atom is currently not considered.

G7607: It is assumed that the reaction liberates all Br and Cl atoms. The fate of the carbon atom is currently not considered.

G8102: Consistent with O'Dowd and Hoffmann (2005), it is assumed that the reaction produces new particles.

G8103: The yield of 38 % OIO is from Atkinson et al. (2007). It is assumed here that the remaining 62 % produce 2 I + O_2.

G8300: The rate coefficient is: `k_I_NO2 = k_3rd_iupac(temp,cair,3.E-31,1.,6.6E-11,0.,0.63)`.

G8305: The rate coefficient is defined as backward reaction (Atkinson et al., 2007) divided by equilibrium constant (van den Bergh and Troe, 1976).

G8401: The rate coefficient is from Dillon et al. (2006b), the yield of I atoms is a lower limit given on page 2170 of Bale et al. (2005).

G8402: The products are from Nakano et al. (2005).

G8701: 80% Br + OIO production is from Atkinson et al. (2007). The remaining channels are assumed to produce Br + I + O_2.

G9400a: For the abstraction path, the assumed reaction sequence (omitting H_2O and O_2 as products) according to Yin et al. (1990) is:

$$\begin{aligned}
DMS + OH &\rightarrow CH_3SCH_2\\
CH_3SCH_2 + O_2 &\rightarrow CH_3SCH_2OO\\
CH_3SCH_2OO + NO &\rightarrow CH_3SCH_2O + NO_2\\
CH_3SCH_2O &\rightarrow CH_3S + HCHO\\
CH_3S + O_3 &\rightarrow CH_3SO\\
CH_3SO + O_3 &\rightarrow CH_3SO_2\\
\hline
DMS + OH + NO + 2O_3 &\rightarrow CH_3SO_2 + HCHO + NO_2
\end{aligned}$$

Neglecting the effect on O_3 and NO_x, the remaining reaction is:

$$DMS + OH + O_3 \rightarrow CH_3SO_2 + HCHO$$

.

G9400b: For the addition path, the rate coefficient is: `k_DMS_OH = 1.0E-39*EXP(5820./temp)*C(ind_02) / (1.+5.0E-30*EXP(6280./temp)*C(ind_02))`.

G9402: Products and yields are not from Hynes and Wine (1996).

G9408: Average of 3.9E-11 and 3.42E-11.

G10201: Upper limit.

Table 2: Photolysis reactions

#	labels	reaction	rate coefficient	reference
J (gas)				
J0001	UpGJ	$O(^3P) \rightarrow O^+ + e^-$	jx(ip_Op_em) +jx(ip_se_Op_em)	Fuller-Rowell (1993)
J0002a	UpGJ	$O_2 \rightarrow O_2^+ + e^-$	jx(ip_O2p_em) +jx(ip_se_O2_b1)	Fuller-Rowell (1993)
J0002b	UpGJ	$O_2 \rightarrow O^+ + O(^3P) + e^-$	jx(ip_Op_O_em) +jx(ip_se_O2_b2)	Fuller-Rowell (1993)
J0003a	UpGJN	$N_2 \rightarrow N_2^+ + e^-$	jx(ip_N2p_em) +jx(ip_se_N2_b1)	Fuller-Rowell (1993)
J0003b	UpGJN	$N_2 \rightarrow N^+ + N + e^-$	jx(ip_Np_N_em) +jx(ip_se_N2_b2)	Fuller-Rowell (1993)
J0003c	UpGJN	$N_2 \rightarrow N^+ + N(^2D) + e^-$	jx(ip_Np_N2D_em)+jx(ip_se_N2_b3)	Fuller-Rowell (1993)
J0003d	UpGJN	$N_2 \rightarrow N + N(^2D)$	jx(ip_N_N2D_em) +jx(ip_se_N2_b4)	Fuller-Rowell (1993)
J1000a	UpStTrGJ	$O_2 + h\nu \rightarrow O(^3P) + O(^3P)$	jx(ip_O2)	Sander et al. (2014)
J1000b	UpGJ	$O_2 + h\nu \rightarrow O(^3P) + O(^1D)$	jx(ip_O3PO1D)	Sander et al. (2014)
J1000c	UpGJ	$O_2 + h\nu \rightarrow O_2^+ + e^-$	jx(ip_O2_b1)	Sander et al. (2014)
J1000d	UpGJ	$O_2 + h\nu \rightarrow O^+ + O(^3P) + e^-$	jx(ip_O2_b2)	Sander et al. (2014)
J1001a	UpStTrGJ	$O_3 + h\nu \rightarrow O(^1D) + O_2$	jx(ip_O1D)	Sander et al. (2014)
J1001b	UpStTrGJ	$O_3 + h\nu \rightarrow O(^3P) + O_2$	jx(ip_O3P)	Sander et al. (2014)
J1002	UpGJ	$O(^3P) + h\nu \rightarrow O^+ + e^-$	jx(ip_O3Pp)	Sander et al. (2014)
J2100a	UpStGJ	$H_2O + h\nu \rightarrow H + OH$	jx(ip_H2O)	Sander et al. (2014)
J2100b	UpGJ	$H_2O + h\nu \rightarrow H_2 + O(^1D)$	jx(ip_H2O1D)	Sander et al. (2014)
J2101	UpStTrGJ	$H_2O_2 + h\nu \rightarrow 2\ OH$	jx(ip_H2O2)	Sander et al. (2014)
J3000a	UpGJN	$N_2 + h\nu \rightarrow N_2^+ + e^-$	jx(ip_N2_b1)	Sander et al. (2014)
J3000b	UpGJN	$N_2 + h\nu \rightarrow N^+ + N + e^-$	jx(ip_N2_b2)	Sander et al. (2014)
J3000c	UpGJN	$N_2 + h\nu \rightarrow N^+ + N(^2D) + e^-$	jx(ip_N2_b3)	Sander et al. (2014)
J3000d	UpGJN	$N_2 + h\nu \rightarrow N + N(^2D)$	jx(ip_NN2D)	Sander et al. (2014)
J3100	UpStGJN	$N_2O + h\nu \rightarrow O(^1D) + N_2$	jx(ip_N2O)	Sander et al. (2014)
J3101	UpStTrGJN	$NO_2 + h\nu \rightarrow NO + O(^3P)$	jx(ip_NO2)	Sander et al. (2014)
J3102a	UpStGJN	$NO + h\nu \rightarrow N + O(^3P)$	jx(ip_NO)	Sander et al. (2014)
J3102b	UpGJN	$NO + h\nu \rightarrow NO^+ + e^-$	jx(ip_NOp)	Sander et al. (2014)
J3103a	UpStTrGJN	$NO_3 + h\nu \rightarrow NO_2 + O(^3P)$	jx(ip_NO2O)	Sander et al. (2014)
J3103b	UpStTrGJN	$NO_3 + h\nu \rightarrow NO + O_2$	jx(ip_NOO2)	Sander et al. (2014)
J3104	StTrGJN	$N_2O_5 + h\nu \rightarrow NO_2 + NO_3$	jx(ip_N2O5)	Sander et al. (2014)
J3200	TrGJN	$HONO + h\nu \rightarrow NO + OH$	jx(ip_HONO)	Sander et al. (2014)
J3201	StTrGJN	$HNO_3 + h\nu \rightarrow NO_2 + OH$	jx(ip_HNO3)	Sander et al. (2014)
J3202	StTrGJN	$HNO_4 + h\nu \rightarrow .667\ NO_2 + .667\ HO_2 + .333\ NO_3 + .333\ OH$	jx(ip_HNO4)	Sander et al. (2014)
J41000	StTrGJ	$CH_3OOH + h\nu \rightarrow CH_3O + OH$	jx(ip_CH3OOH)	Sander et al. (2014)
J41001a	StTrGJ	$HCHO + h\nu \rightarrow H_2 + CO$	jx(ip_COH2)	Sander et al. (2014)

Table 2: Photolysis reactions (... continued)

#	labels	reaction	rate coefficient	reference
J41001b	StTrGJ	$HCHO + h\nu \rightarrow H + CO + HO_2$	jx(ip_CHOH)	Sander et al. (2014)
J41002	StGJ	$CO_2 + h\nu \rightarrow CO + O(^3P)$	jx(ip_CO2)	Sander et al. (2014)
J41003	StGJ	$CH_4 + h\nu \rightarrow .42\ CH_3 + .42\ H + .6912\ H_2 + .0864\ HCHO + .0864\ O(^3P) + .1584\ OH + .1584\ HO_2 + .2112\ CO_2 + .1824\ CO + .024\ H_2O + .10$ LCARBON	jx(ip_CH4)	Sander et al. (2014)*
J41004	StTrGJN	$CH_3ONO + h\nu \rightarrow CH_3O + NO$	jx(ip_CH3ONO)	Sander et al. (2014)
J41005	StTrGJN	$CH_3ONO_2 + h\nu \rightarrow CH_3O + NO_2$	jx(ip_CH3NO3)	Sander et al. (2014)
J41006	StTrGJN	$CH_3O_2NO_2 + h\nu \rightarrow .667\ NO_2 + .667\ CH_3O_2 + .333\ NO_3 + .333\ CH_3O$	jx(ip_CH3O2NO2)	Sander et al. (2014)*
J41007	StTrGJ	$HOCH_2OOH + h\nu \rightarrow HCOOH + OH + HO_2$	jx(ip_CH3OOH)	Sander et al. (2014)
J41008	StTrGJ	$CH_3O_2 + h\nu \rightarrow HCHO + OH$	jx(ip_CH3O2)	Sander et al. (2014)
J41009	StTrGJ	$HCOOH + h\nu \rightarrow CO + HO_2 + OH$	jx(ip_HCOOH)	Sander et al. (2014)
J41010	StTrGJN	$HOCH_2O_2NO_2 + h\nu \rightarrow .667\ NO_2 + .667\ HOCH_2O_2 + .333\ NO_3 + .333\ HCOOH + .333\ HO_2$	jx(ip_CH3O2NO2)	Sander et al. (2014)
J42000	TrGJC	$C_2H_5OOH + h\nu \rightarrow CH_3CHO + HO_2 + OH$	jx(ip_CH3OOH)	von Kuhlmann (2001)
J42001a	TrGJC	$CH_3CHO + h\nu \rightarrow CH_3 + HO_2 + CO$	jx(ip_CH3CHO)	Sander et al. (2014)
J42001b	TrGJC	$CH_3CHO + h\nu \rightarrow CH_2CHOH$	jx(ip_CH3CHO2VINY)	Clubb et al. (2012)
J42002	TrGJC	$CH_3C(O)OOH + h\nu \rightarrow CH_3 + OH + CO_2$	jx(ip_CH3CO3H)	Sander et al. (2014)
J42004	TrGJCN	$PAN + h\nu \rightarrow .7\ CH_3C(O) + .7\ NO_2 + .3\ CH_3 + .3\ CO_2 + .3\ NO_3$	jx(ip_PAN)	Sander et al. (2014)*
J42005a	TrGJC	$HOCH_2CHO + h\nu \rightarrow HCHO + 2\ HO_2 + CO$	jx(ip_HOCH2CHO)*0.83	Sander et al. (2014)*
J42005b	TrGJC	$HOCH_2CHO + h\nu \rightarrow OH + HCOCH_2O_2$	jx(ip_HOCH2CHO)*0.07	Sander et al. (2014)*
J42005c	TrGJC	$HOCH_2CHO + h\nu \rightarrow CH_3OH + CO$	jx(ip_HOCH2CHO)*0.10	Sander et al. (2014)*
J42006	TrGJC	$HOCH_2CO_3H + h\nu \rightarrow HCHO + HO_2 + OH + CO_2$	jx(ip_CH3OOH)	Rickard and Pascoe (2009)
J42007	TrGJCN	$PHAN + h\nu \rightarrow .7\ HOCH2CO + .7\ NO_2 + .3\ HCHO + .3\ HO_2 + .3\ CO_2 + .3\ NO_3$	jx(ip_PAN)	see note*
J42008	TrGJC	$GLYOX + h\nu \rightarrow 2\ CO + 2\ HO_2$	jx(ip_GLYOX)	Sander et al. (2014)
J42009	TrGJC	$HCOCO_2H + h\nu \rightarrow 2\ HO_2 + CO + CO_2$	jx(ip_MGLYOX)	Rickard and Pascoe (2009)
J42010	TrGJC	$HCOCO_3H + h\nu \rightarrow HO_2 + CO + OH + CO_2$	jx(ip_CH3OOH)+jx(ip_HOCH2CHO)	Rickard and Pascoe (2009)
J42011	TrGJC	$HYETHO2H + h\nu \rightarrow HOCH_2CH_2O + OH$	jx(ip_CH3OOH)	Rickard and Pascoe (2009)
J42012	TrGJCN	$ETHOHNO3 + h\nu \rightarrow HO_2 + 2\ HCHO + NO_2$	j_IC3H7NO3	Rickard and Pascoe (2009)
J42013	TrGJC	$HOOCH2CO3H + h\nu \rightarrow OH + HCHO + CO_2 + OH$	2.*jx(ip_CH3OOH)	Sander et al. (2019)
J42014	TrGC	$HOOCH2CO2H + h\nu \rightarrow OH + HCHO + HO_2 + CO_2$	jx(ip_CH3OOH)	Sander et al. (2019)
J42015	TrGC	$CH2CO + h\nu \rightarrow .4\ CO_2 + .8\ H + .34\ CO + .34\ OH + .34\ HO_2 + .16\ HCHO + .16\ O(^3P) + .1\ HCOOH + CO$	j_ketene*0.36	Sander et al. (2019)

Table 2: Photolysis reactions (... continued)

#	labels	reaction	rate coefficient	reference
J42016	TrGC	$CH3CHOHOOH + h\nu \rightarrow CH_3 + HCOOH + OH$	jx(ip_CH3OOH)	Sander et al. (2019)
J42017	TrGJCN	$NO_3CH2CHO + h\nu \rightarrow HO_2 + CO + HCHO + NO_2$	(jx(ip_C2H5NO3)+jx(ip_CH3CHO)) *(jx(ip_NOA)+1E-10)/(0.59*j_ IC3H7NO3+jx(ip_CH3COCH3)+1E-10)	Sander et al. (2019)*
J42018	TrGJC	$HOOCH2CHO + h\nu \rightarrow OH + HCHO + CO + HO_2$	jx(ip_CH3OOH)+jx(ip_HOCH2CHO)	Sander et al. (2019)
J42019	TrGJCN	$C_2H_5ONO_2 + h\nu \rightarrow CH_3CHO + HO_2 + NO_2$	jx(ip_C2H5NO3)	Sander et al. (2019)
J42020	TrGJCN	$NO_3CH2CHO + h\nu \rightarrow .7\ NO_3CH2CO_3 + .7\ NO_2 + .3\ HCHO + .3\ NO_2 + .3\ CO_2 + .3\ NO_3$	jx(ip_PAN)	Sander et al. (2019)*
J42021	StTrGJCN	$C_2H_5O_2NO_2 + h\nu \rightarrow .667\ NO_2 + .667\ C_2H_5O_2 + .333\ NO_3 + .333\ CH_3CHO + .333\ HO_2$	jx(ip_CH3O2NO2)	Sander et al. (2019)*
J43000	TrGJC	$iC_3H_7OOH + h\nu \rightarrow CH_3COCH_3 + HO_2 + OH$	jx(ip_CH3OOH)	von Kuhlmann (2001)
J43001	TrGJC	$CH_3COCH_3 + h\nu \rightarrow CH_3C(O) + CH_3$	jx(ip_CH3COCH3)	Sander et al. (2014)
J43002	TrGJC	$CH_3COCH_2OH + h\nu \rightarrow .5\ CH_3C(O) + .5\ HCHO + .5\ HO_2 + .5\ HOCH2CO + .5\ CH_3$	j_ACETOL	Sander et al. (2014)*
J43003	TrGJC	$MGLYOX + h\nu \rightarrow CH_3C(O) + CO + HO_2$	jx(ip_MGLYOX)	Sander et al. (2014)
J43004	TrGJC	$CH_3COCH_2O_2H + h\nu \rightarrow CH_3C(O) + HCHO + OH$	jx(ip_CH3OOH)+j_ACETOL	Rickard and Pascoe (2009)
J43005	TrGJC	$HOCH2COCH2OOH + h\nu \rightarrow HOCH2CO + HCHO + OH$	jx(ip_CH3OOH)+j_ACETOL	Sander et al. (2019)
J43006	TrGJCN	$iC_3H_7ONO_2 + h\nu \rightarrow CH_3COCH_3 + NO_2 + HO_2$	j_IC3H7NO3	von Kuhlmann et al. (2003)*
J43007	TrGJCN	$NOA + h\nu \rightarrow CH_3C(O) + HCHO + NO_2$	jx(ip_NOA)	Barnes et al. (1993)
J43009	TrGJC	$HYPROPO2H + h\nu \rightarrow CH_3CHO + HCHO + HO_2 + OH$	jx(ip_CH3OOH)	Rickard and Pascoe (2009)
J43010	TrGJCN	$PR2O2HNO3 + h\nu \rightarrow NOA + HO_2 + OH$	jx(ip_CH3OOH)	Rickard and Pascoe (2009)
J43011	TrGJC	$HOCH2COCHO + h\nu \rightarrow HOCH2CO + CO + HO_2$	jx(ip_MGLYOX)	Rickard and Pascoe (2009)
J43012	TrGJC	$HCOCOCH_2OOH + h\nu \rightarrow HCOCO + HCHO + OH$	jx(ip_CH3OOH)+j_ACETOL	Sander et al. (2019)
J43013	TrGJC	$HCOCOCH_2OOH + h\nu \rightarrow HOOCH_2CO_3 + CO + HO_2$	jx(ip_MGLYOX)	Sander et al. (2019)
J43014	TrGJTerC	$HCOCH2CHO + h\nu \rightarrow HCOCH_2O_2 + HO_2 + CO$	jx(ip_HOCH2CHO)*2.	Rickard and Pascoe (2009)
J43015	TrGJTerC	$HCOCH2CO2H + h\nu \rightarrow HCOCH_2O_2 + CO_2 + HO_2$	jx(ip_HOCH2CHO)	Rickard and Pascoe (2009)
J43016	TrGJTerC	$HOC2H4CO3H + h\nu \rightarrow HOCH_2CH_2O_2 + CO_2 + OH$	jx(ip_CH3OOH)	Rickard and Pascoe (2009)
J43017	TrGJC	$HCOCOCHO + h\nu \rightarrow HCOCO + HO_2 + CO$	2.*jx(ip_MGLYOX)	Sander et al. (2019)
J43018	TrGJC	$CH_3COCO_2H + h\nu \rightarrow .32\ CH_3CHO + .16\ CH_2CHOH + .54\ CO_2 + .38\ CH_3C(O) + .38\ HO_2 + .38\ CO_2 + .07\ CH_3COOH + .07\ CO + .05\ CH_3C(O) + .05\ CO + .05\ OH$	jx(ip_CH3COCO2H)	Sander et al. (2019)*
J43019	TrGC	$CH_3COCO_3H + h\nu \rightarrow CH_3C(O) + OH + CO_2$	jx(ip_MGLYOX)+jx(ip_CH3OOH)	Sander et al. (2019)
J43020	TrGC	$CH3CHCO + h\nu \rightarrow C_2H_4 + CO$	j_ketene*0.36*2.	Sander et al. (2019)
J43021	TrGCN	$PROPOLNO3 + h\nu \rightarrow HOCH_2CHO + HCHO + HO_2 + NO_2$	j_IC3H7NO3	Sander et al. (2019)

Table 2: Photolysis reactions (... continued)

#	labels	reaction	rate coefficient	reference
J43022	TrGCN	$CH_3COCH_2OONO_2 + h\nu \rightarrow CH_3C(O) + HCHO + NO_3$	jx(ip_CH3O2NO2)+jx(ip_CH3COCH3)	Sander et al. (2019)
J43023	TrGJC	$C_3H_7OOH + h\nu \rightarrow C_2H_5CHO + HO_2 + OH$	jx(ip_CH3OOH)	von Kuhlmann (2001)
J43024	TrGJCN	$C_3H_7ONO_2 + h\nu \rightarrow C_2H_5CHO + NO_2 + HO_2$	0.59*j_IC3H7NO3	see note*
J43025a	TrGJC	$C_2H_5CHO + h\nu \rightarrow C_2H_5O_2 + HO_2 + CO$	jx(ip_C2H5CHO2HCO)	see note*
J43025b	TrGJC	$C_2H_5CHO + h\nu \rightarrow CH_2CHCH_2OH$	jx(ip_C2H5CHO2ENOL)	Andrews et al. (2012), Sander et al. (2019)*
J43026	TrGJCN	$PPN + h\nu \rightarrow .7\ C_2H_5CO_3 + .7\ NO_2 + .3\ C_2H_5O_2 + .3\ CO_2 + .3\ NO_3$	jx(ip_PAN)	Sander et al. (2014)
J43027	TrGJC	$C_2H_5CO_3H + h\nu \rightarrow C_2H_5O_2 + CO_2 + OH$	jx(ip_CH3OOH)	von Kuhlmann (2001)
J43028a	TrGJC	$HCOCOCH_2OOH + h\nu \rightarrow HOOCH_2CO_3 + CO + HO_2$	jx(ip_MGLYOX)	Sander et al. (2019)
J43028b	TrGJC	$HCOCOCH_2OOH + h\nu \rightarrow HCOCO + HCHO + OH$	jx(ip_HOCH2CHO)+jx(ip_CH3OOH)	Sander et al. (2019)
J43200	TrGJTerC	$HCOCH2CO3H + h\nu \rightarrow HCOCH_2O_2 + CO_2 + OH$	jx(ip_HOCH2CHO)+jx(ip_CH3OOH)	Rickard and Pascoe (2009)
J43400	TrGJAroC	$C3DIALOOH + h\nu \rightarrow GLYOX + CO + HO_2 + OH$	jx(ip_HOCH2CHO)*2.+jx(ip_CH3OOH)	Rickard and Pascoe (2009)*
J43401	TrGJAroC	$C32OH13CO + h\nu \rightarrow GLYOX + HO_2 + HO_2 + CO$	jx(ip_HOCH2CHO)*2.	Rickard and Pascoe (2009)
J43402	TrGJAroC	$HCOCOHCO3H + h\nu \rightarrow GLYOX + HO_2 + CO_2 + OH$	jx(ip_CH3OOH)	Rickard and Pascoe (2009)
J44000a	TrGJC	$LC_4H_9OOH + h\nu \rightarrow OH + C_3H_7CHO + HO_2$	jx(ip_CH3OOH)*(k_p/(k_p+k_s))	Rickard and Pascoe (2009), Sander et al. (2019)
J44000b	TrGJC	$LC_4H_9OOH + h\nu \rightarrow OH + .636\ MEK + .636\ HO_2 + .364\ CH_3CHO + .364\ C_2H_5O_2$	jx(ip_CH3OOH)*(k_s/(k_p+k_s))	Rickard and Pascoe (2009), Sander et al. (2019)
J44001	TrGJC	$MVK + h\nu \rightarrow .5\ C_3H_6 + .5\ CH_3C(O) + .5\ HCHO + CO + .5\ HO_2$	jx(ip_MVK)	Sander et al. (2014)
J44002	TrGJC	$MEK + h\nu \rightarrow CH_3C(O) + C_2H_5O_2$	0.42*jx(ip_CHOH)	von Kuhlmann et al. (2003)
J44003	TrGJC	$LMEKOOH + h\nu \rightarrow .62\ CH_3C(O) + .62\ CH_3CHO + .38\ HCHO + .38\ CO_2 + .38\ HOCH_2CH_2O_2 + OH$	jx(ip_CH3OOH)+0.42*jx(ip_CHOH)	Sander et al. (2019)
J44004	TrGJC	$BIACET + h\nu \rightarrow 2\ CH_3C(O)$	2.15*jx(ip_MGLYOX)	see note*
J44005a	TrGJCN	$LC4H9NO3 + h\nu \rightarrow NO_2 + C_3H_7CHO + HO_2$	j_IC3H7NO3*(k_p/(k_p+k_s))	see note*
J44005b	TrGJCN	$LC4H9NO3 + h\nu \rightarrow NO_2 + MEK + HO_2$	j_IC3H7NO3*(k_s/(k_p+k_s))	see note*
J44006	TrGJCN	$MPAN + h\nu \rightarrow .7\ MACO3 + .7\ NO_2 + .3\ MACO2 + .3\ NO_3$	jx(ip_PAN)	see note*
J44007a	TrGJC	$CO2H3CO3H + h\nu \rightarrow MGLYOX + HO_2 + OH + CO_2$	jx(ip_CH3OOH)	Rickard and Pascoe (2009)
J44007b	TrGJC	$CO2H3CO3H + h\nu \rightarrow CH_3C(O) + HO_2 + HCOCO_3H$	j_ACETOL	Rickard and Pascoe (2009)

Table 2: Photolysis reactions (... continued)

#	labels	reaction	rate coefficient	reference
J44008	TrGJC	MACR + hν → .5 MACO3 + .5 $CH_3C(O)$ + .5 HCHO + .5 CO + HO_2	jx(ip_MACR)	Sander et al. (2014)
J44009	TrGJC	MACROOH + hν → MACRO + OH	jx(ip_CH3OOH)+2.77*jx(ip_HOCH2CHO)	Sander et al. (2019)*
J44010	TrGJC	MACROH + hν → CH_3COCH_2OH + CO + HO_2 + HO_2	2.77*jx(ip_HOCH2CHO)	see note*
J44011	TrGJC	MACO3H + hν → MACO2 + OH	jx(ip_CH3OOH)	Sander et al. (2019)
J44012	TrGJC	LHMVKABOOH + hν → .12 MGLYOX + .12 HO_2 + .88 $CH_3C(O)$ + .88 $HOCH_2CHO$ + .12 HCHO + OH	jx(ip_CH3OOH)+j_ACETOL	Sander et al. (2019)
J44013	TrGJC	CO2H3CHO + hν → MGLYOX + CO + HO_2 + HO_2	jx(ip_HOCH2CHO)+j_ACETOL	Sander et al. (2019)
J44014	TrGJC	HO12CO3C4 + hν → $CH_3C(O)$ + $HOCH_2CHO$ + HO_2	j_ACETOL	Rickard and Pascoe (2009)
J44015	TrGJC	BIACETOH + hν → $CH_3C(O)$ + HOCH2CO	2.15*jx(ip_MGLYOX)	see note*
J44016	TrGC	$HCOCCH_3CO$ + hν → .5 OH + .5 CH_3CHO + CO + .5 CH3CHCO + .5 CO	j_ketene	Sander et al. (2019)
J44017a	TrGC	$CH_3COCHCO$ + hν → .0192 CH_3COCO_2H + .1848 H_2O_2 + .2208 MGLYOX + .36 OH + .36 CO + .56 $CH_3C(O)$ + .2 CH_3CHO + .2 CO_2 + .2 HCHO + .2 HO_2 + CO	j_ketene*0.5	Sander et al. (2019),Rickard and Pascoe (2009)*
J44017b	TrGC	$CH_3COCHCO$ + hν → CH3CHCO + CO	j_ketene*0.5	Sander et al. (2019)
J44018a	TrGJC	$CH_3COCOCHO$ + hν → $CH_3C(O)$ + 2 CO + HO_2	jx(ip_MGLYOX)	Sander et al. (2019)
J44018b	TrGJC	$CH_3COCOCHO$ + hν → HCOCO + $CH_3C(O)$	2.15*jx(ip_MGLYOX)	Sander et al. (2019)
J44019	TrGJC	CH3COCOCO2H + hν → $CH_3C(O)$ + CO + CO_2 + HO_2	3.15*jx(ip_MGLYOX)	Sander et al. (2019)
J44020a	TrGJTerC	$CH_3COCOCH_2OOH$ + hν → $CH_3C(O)$ + OH + HCHO + CO	jx(ip_CH3OOH)+j_ACETOL	Rickard and Pascoe (2009)
J44020b	TrGJTerC	$CH_3COCOCH_2OOH$ + hν → $CH_3C(O)$ + HCOCO	2.15*jx(ip_MGLYOX)	Rickard and Pascoe (2009)
J44021	TrGJTerC	C44OOH + hν → HCOCH2CHO + CO_2 + HO_2 + OH	jx(ip_CH3OOH)	Rickard and Pascoe (2009)
J44022	TrGJTerC	C413COOOH + hν → HCOCH2CO3 + HCHO + OH	jx(ip_CH3OOH)+jx(ip_HOCH2CHO)+j_ACETOL	Rickard and Pascoe (2009)
J44023a	TrGJTerC	C4CODIAL + hν → $HCOCOCH_2O_2$ + HO_2 + CO	jx(ip_HOCH2CHO)	Rickard and Pascoe (2009)
J44023b	TrGJTerC	C4CODIAL + hν → HCOCH2CO3 + HO_2 + CO	jx(ip_MGLYOX)	Rickard and Pascoe (2009)
J44024	TrGJTerC	C312COCO3H + hν → $HCOCOCH_2O_2$ + CO_2 + OH	jx(ip_CH3OOH)+jx(ip_MGLYOX)	Rickard and Pascoe (2009)
J44025	TrGJCN	LMEKNO3 + hν → .62 $CH_3C(O)$ + .62 CH_3CHO + .38 HCHO + .38 CO_2 + .38 $HOCH_2CH_2O_2$ + NO_2	jx(ip_MEKNO3)	Barnes et al. (1993), Sander et al. (2019)*
J44026	TrGJCN	MVKNO3 + hν → $CH_3C(O)$ + $HOCH_2CHO$ + NO_2	jx(ip_MEKNO3)	Barnes et al. (1993), Sander et al. (2019)*
J44027	TrGJCN	MACRNO3 + hν → CH_3COCH_2OH + CO + HO_2 + NO_2	(2.84*j_IC3H7NO3+jx(ip_CH3CHO))*(jx(ip_MEKNO3)+1E-10)/(j_IC3H7NO3+0.42*jx(ip_CHOH)+1E-10)	Müller et al. (2014), Sander et al. (2019)*

Table 2: Photolysis reactions (... continued)

#	labels	reaction	rate coefficient	reference
J44028	TrGJCN	TC4H9NO3 + hν → CH_3COCH_3 + CH_3 + NO_2	2.84*j_IC3H7NO3	Sander et al. (2019)
J44029	TrGJC	TC_4H_9OOH + hν → CH_3COCH_3 + CH_3 + OH	jx(ip_CH3OOH)	Sander et al. (2019)
J44030	TrGJCN	IBUTOLBNO3 + hν → CH_3COCH_3 + HCHO + HO_2 + NO_2	2.84*j_IC3H7NO3	Sander et al. (2019)
J44031	TrGJC	IBUTOLBOOH + hν → CH_3COCH_3 + HCHO + HO_2 + OH	jx(ip_CH3OOH)	Sander et al. (2019)
J44032	TrGJC	LBUT1ENOOH + hν → C_2H_5CHO + HCHO + HO_2 + OH	jx(ip_CH3OOH)	Sander et al. (2019)
J44033	TrGJCN	LBUT1ENNO3 + hν → C_2H_5CHO + HCHO + HO_2 + NO_2	j_IC3H7NO3	Sander et al. (2019)
J44034	TrGJC	BUT2OLOOH + hν → 2 CH_3CHO + HO_2 + OH	jx(ip_CH3OOH)	Sander et al. (2019)
J44035	TrGJCN	BUT2OLNO3 + hν → 2 CH_3CHO + HO_2 + NO_2	j_IC3H7NO3	Sander et al. (2019)
J44036	TrGJC	BUT2OLO + hν → $CH_3C(O)$ + HOCH2CO	j_ACETOL	Sander et al. (2019)
J44037a	TrGJC	C_3H_7CHO + hν → $C_3H_7O_2$ + CO + HO_2	jx(ip_C3H7CHO2HCO)	Sander et al. (2019)
J44037b	TrGJC	C_3H_7CHO + hν → C_2H_4 + CH_2CHOH	jx(ip_C3H7CHO2VINY)	Sander et al. (2019)*
J44038	TrGJC	IPRCHO + hν → $iC_3H_7O_2$ + CO + HO_2	jx(ip_IPRCHO2HCO)	Sander et al. (2019)
J44039	TrGJCN	IC4H9NO3 + hν → IPRCHO + NO_2	j_IC3H7NO3	Sander et al. (2019)
J44040	TrGJC	IC_4H_9OOH + hν → IPRCHO + HO_2 + OH	jx(ip_CH3OOH)	Sander et al. (2019)
J44041	TrGJC	PERIBUACID + hν → $iC_3H_7O_2$ + CO_2 + OH	jx(ip_CH3OOH)	Sander et al. (2019)
J44042	TrGJCN	PIPN + hν → .7 IPRCO3 + .7 NO_2 + .3 $iC_3H_7O_2$ + .3 CO_2 + .3 NO_3	jx(ip_PAN)	Sander et al. (2019), Sander et al. (2014)
J44043	TrGJC	HVMK + hν → MGLYOX + CO + 2 OH	jx(ip_PeDIONE24)	Sander et al. (2019), Nakanishi et al. (1977), Messaadia et al. (2015), Yoon et al. (1999)*
J44044	TrGJC	HMAC + hν → $HCOCCH_3CO$ + 2 OH	jx(ip_PeDIONE24)	Sander et al. (2019), Nakanishi et al. (1977), Messaadia et al. (2015), Yoon et al. (1999)*
J44045a	TrGJC	CO2C3CHO + hν → $CH_3COCH_2O_2$ + HO_2 + CO	jx(ip_C2H5CHO2HCO)	Rickard and Pascoe (2009)
J44045b	TrGJC	CO2C3CHO + hν → HVMK	jx(ip_C2H5CHO2ENOL)	Andrews et al. (2012), Sander et al. (2019)
J44046a	TrGJC	IBUTDIAL + hν → CH_3CHO + CO + HO_2 + CO_2 + H_2O	jx(ip_C2H5CHO2HCO)*2.	see note*
J44046b	TrGJC	IBUTDIAL + hν → HMAC	jx(ip_C2H5CHO2ENOL)*2.	Andrews et al. (2012), Sander et al. (2019)
J44200	TrGJTerC	IBUTALOH + hν → CH_3COCH_3 + HO_2 + HO_2 + CO	j_ACETOL	Rickard and Pascoe (2009)
J44201	TrGJTerC	IPRHOCO3H + hν → CH_3COCH_3 + HO_2 + CO_2 + OH	jx(ip_CH3OOH)	Rickard and Pascoe (2009)
J44400a	TrGJAroC	MALDIALOOH + hν → C32OH13CO + CO + OH + HO_2	jx(ip_HOCH2CHO)*2.	Rickard and Pascoe (2009)

Table 2: Photolysis reactions (... continued)

#	labels	reaction	rate coefficient	reference
J44400b	TrGJAroC	MALDIALOOH + hν → GLYOX + GLYOX + HO_2 + OH	jx(ip_CH3OOH)	Rickard and Pascoe (2009)*
J44401	TrGJAroC	BZFUOOH + hν → CO14O3CHO + HO_2 + OH	jx(ip_CH3OOH)	Rickard and Pascoe (2009)*
J44402	TrGJAroC	HOCOC4DIAL + hν → HCOCOHCO3 + HO_2 + CO	jx(ip_MGLYOX)+jx(ip_HOCH2CHO)	Rickard and Pascoe (2009)
J44403	TrGJAroCN	NBZFUOOH + hν → .5 CO14O3CHO + .5 NO_2 + .5 NBZFUONE + .5 HO_2 + OH	jx(ip_CH3OOH)	Rickard and Pascoe (2009)*
J44404a	TrGJAroC	MALDALCO3H + hν → $HCOCO_3H$ + HO_2 + CO + HO_2 + CO	jx(ip_MACR)	Rickard and Pascoe (2009)
J44404b	TrGJAroC	MALDALCO3H + hν → .6 MALANHY + HO_2 + .4 GLYOX + .4 CO + .4 CO_2 + OH	jx(ip_CH3OOH)	Rickard and Pascoe (2009)*
J44405	TrGJAroC	EPXDLCO2H + hν → C3DIALO2 + CO_2 + HO_2	2.77*jx(ip_HOCH2CHO)	Rickard and Pascoe (2009)
J44406	TrGJAroC	MALDIAL + hν → .4 BZFUONE + .6 MALDIALCO3 + .6 HO_2	jx(ip_NO2)*0.14	Rickard and Pascoe (2009)
J44407	TrGJAroC	MALANHYOOH + hν → HCOCOHCO3 + CO_2 + OH	jx(ip_CH3OOH)	Rickard and Pascoe (2009)*
J44408	TrGJAroC	EPXDLCO3H + hν → C3DIALO2 + OH + CO_2	jx(ip_CH3OOH)+2.77*jx(ip_HOCH2CHO)	Rickard and Pascoe (2009)
J44409	TrGJAroC	CO2C4DIAL + hν → CO + CO + HO_2 + HO_2 + CO + CO	jx(ip_MGLYOX)*2.	Rickard and Pascoe (2009)
J44410	TrGJAroC	MALDALCO2H + hν → $HCOCO_2H$ + HO_2 + CO + HO_2 + CO	jx(ip_MACR)	Rickard and Pascoe (2009)
J44411	TrGJAroC	EPXC4DIAL + hν → C3DIALO2 + CO + HO_2	2.77*jx(ip_HOCH2CHO)*2.	Rickard and Pascoe (2009)
J44412	TrGJAroC	CO14O3CHO + hν → HO_2 + CO + $HCOCH_2O_2$ + CO_2	jx(ip_MGLYOX)	Rickard and Pascoe (2009)
J44414	TrGJAroC	MECOACEOOH + hν → $CH_3C(O)$ + HCHO + CO_2 + OH	jx(ip_CH3OOH)	Rickard and Pascoe (2009)*
J45002	TrGJC	LISOPACOOH + hν → LISOPACO + OH	jx(ip_CH3OOH)	Rickard and Pascoe (2009)
J45003	TrGJCN	LISOPACNO3 + hν → LISOPACO + NO_2	0.59*j_IC3H7NO3	see note*
J45004	TrGJC	ISOPBOOH + hν → MVK + HCHO + HO_2 + OH	jx(ip_CH3OOH)	Rickard and Pascoe (2009)
J45005	TrGJCN	ISOPBNO3 + hν → MVK + HCHO + HO_2 + NO_2	2.84*j_IC3H7NO3	see note*
J45006	TrGJC	ISOPDOOH + hν → MACR + HCHO + HO_2 + OH	jx(ip_CH3OOH)	Rickard and Pascoe (2009)
J45007	TrGJCN	ISOPDNO3 + hν → MACR + HCHO + HO_2 + NO_2	j_IC3H7NO3	see note*
J45008	TrGJCN	NISOPOOH + hν → NC4CHO + HO_2 + OH	jx(ip_CH3OOH)	Rickard and Pascoe (2009)
J45009	TrGJCN	NC4CHO + hν → LHC4ACCO3 + NO_2	(.59*j_IC3H7NO3+jx(ip_MACR))*(jx(ip_MEKNO3)+1E-10)/(j_IC3H7NO3+0.42*jx(ip_CHOH)+1E-10)	Müller et al. (2014), Sander et al. (2019)*
J45010	TrGJCN	LNISOOH + hν → NOA + OH + .5 HOCHCHO + .5 CO + .5 HO_2 + .5 CO_2	jx(ip_CH3OOH)	Taraborrelli et al. (2009), Sander et al. (2019)

Table 2: Photolysis reactions (... continued)

#	labels	reaction	rate coefficient	reference
J45011	TrGJC	LHC4ACCHO + hν → .5 LHC4ACCO3 + .5 HO_2 + .5 CO + .5 OH + .25 MACRO2 + .25 LHMVKABO2	jx(ip_MACR)	Sander et al. (2019)
J45012	TrGJC	LC578OOH + hν → .25 CH_3COCH_2OH + .75 MGLYOX + .25 HOCHCHO + .75 $HOCH_2CHO$ + .75 HO_2 + OH	jx(ip_CH3OOH)+ 2.77*jx(ip_HOCH2CHO)	Sander et al. (2019)
J45013	TrGJC	LHC4ACCO3H + hν → OH + .5 MACRO2 + .5 LHMVKABO2 + OH + CO_2	j_HPALD	Sander et al. (2019)
J45014	TrGJCN	LC5PAN1719 + hν → .7 LHC4ACCO3 + .7 NO_2 + .15 MACRO2 + .15 LHMVKABO2 + .3 CO_2 + .3 NO_3	jx(ip_PAN)	Sander et al. (2019)
J45015	TrGJC	HCOC5 + hν → .65 CH_3 + .65 CO + .65 HCHO + .35 OH + .35 $CH_3COCH_2O_2$ + HOCH2CO	0.5*jx(ip_MVK)	Sander et al. (2019)*
J45016	TrGJC	C59OOH + hν → CH_3COCH_2OH + HOCH2CO + OH	j_ACETOL+jx(ip_CH3OOH)	Sander et al. (2019)
J45017	TrGJTerC	C511OOH + hν → $CH_3C(O)$ + HCOCH2CHO + OH	jx(ip_CH3OOH)+jx(ip_HOCH2CHO)	Rickard and Pascoe (2009)
J45018a	TrGJTerC	CO23C4CHO + hν → $CH_3COCOCH_2O_2$ + HO_2 + CO	jx(ip_HOCH2CHO)	Rickard and Pascoe (2009)
J45018b	TrGJTerC	CO23C4CHO + hν → $CH_3C(O)$ + HCOCH2CO3	2.15*jx(ip_MGLYOX)	Rickard and Pascoe (2009)
J45019	TrGJTerC	CO23C4CO3H + hν → $CH_3COCOCH_2O_2$ + CO_2 + OH	jx(ip_CH3OOH)+jx(ip_HOCH2CHO)	Rickard and Pascoe (2009)
J45020	TrGJTerC	C512OOH + hν → C513O2 + OH	jx(ip_CH3OOH)+jx(ip_HOCH2CHO)	Rickard and Pascoe (2009)
J45021	TrGJTerC	CO13C4CHO + hν → CHOC3COO2 + CO + HO_2	jx(ip_HOCH2CHO)*2.	Rickard and Pascoe (2009)
J45022	TrGJTerC	C513OOH + hν → GLYOX + $HOC_2H_4CO_3$ + OH	jx(ip_CH3OOH)+jx(ip_HOCH2CHO)	Rickard and Pascoe (2009)
J45023	TrGJTerC	C513CO + hν → $HOC_2H_4CO_3$ + HO_2 + CO + CO	jx(ip_MGLYOX)+2.15*jx(ip_MGLYOX)	Rickard and Pascoe (2009)
J45024	TrGJTerC	C514OOH + hν → CO13C4CHO + HO_2 + OH	jx(ip_CH3OOH)+jx(ip_HOCH2CHO)*2.	Rickard and Pascoe (2009)
J45025	TrGJTerCN	C514NO3 + hν → CO13C4CHO + HO_2 + NO_2	j_IC3H7NO3+jx(ip_HOCH2CHO)*2.	Rickard and Pascoe (2009)
J45026a	TrGJC	LZCODC23DBCOOH + hν → OH + CO + HVMK + OH	j_HPALD*0.6*0.5	Sander et al. (2019), Jenkin et al. (2015), Peeters et al. (2014)
J45026b	TrGJC	LZCODC23DBCOOH + hν → OH + CO + $CH_3C(O)$ + $HOCH_2CHO$	j_HPALD*0.6*0.5	Sander et al. (2019), Jenkin et al. (2015), Peeters et al. (2014)
J45026c	TrGJC	LZCODC23DBCOOH + hν → OH + CO + HMAC + OH	j_HPALD*0.4*0.5	Sander et al. (2019), Jenkin et al. (2015), Peeters et al. (2014)
J45026d	TrGJC	LZCODC23DBCOOH + hν → OH + CO + CO + CH_3COCH_2OH + HO_2	j_HPALD*0.4*0.5	Sander et al. (2019), Jenkin et al. (2015), Peeters et al. (2014)
J45027	TrGJC	LZCO3HC23DBCOD + hν → .62 EZCH3CO2CHCHO + .38 EZCHOCCH3CHO2 + OH + CO_2	j_HPALD	Sander et al. (2019)

Table 2: Photolysis reactions (... continued)

#	labels	reaction	rate coefficient	reference
J45028a	TrGJC	C1OOHC2OOHC4OD + hν → $CH_3COCH_2O_2H$ + OH + 2 CO + HO_2	2.77*jx(ip_HOCH2CHO)	Sander et al. (2019)
J45028b	TrGJC	C1OOHC2OOHC4OD + hν → .5 $CH_3COCH_2O_2H$ + .5 HOCHCHO + .5 CO2H3CHO + .5 HCHO + 1.5 OH	2.*jx(ip_CH3OOH)	Sander et al. (2019)
J45029	TrGC	DB1OOH + hν → DB1O2 + OH	jx(ip_CH3OOH)	Sander et al. (2019)
J45030	TrGC	DB2OOH + hν → .48 CH_3COCH_2OH + .52 $HOCH_2CHO$ + .52 MGLYOX + .48 GLYOX + HO_2 + OH	jx(ip_CH3OOH)	Sander et al. (2019)
J45031a	TrGJC	C1ODC2OOHC4OD + hν → MGLYOX + HOCHCHO + OH	jx(ip_CH3OOH)	Sander et al. (2019)
J45031b	TrGJC	C1ODC2OOHC4OD + hν → CO2H3CHO + CO + HO_2 + OH	2.*2.77*jx(ip_HOCH2CHO)	Sander et al. (2019)
J45032	TrGJC	C4MDIAL + hν → .5 $CH_3COCHCO$ + .5 $HCOCCH_3CO$ + CO + HO_2 + OH	jx(ip_NO2)*0.1*0.5	Sander et al. (2019)*
J45033	TrGCN	DB1NO3 + hν → DB1O2 + NO_2	j_IC3H7NO3	Sander et al. (2019)
J45034	TrGJTerC	CHOC3COOOH + hν → CHOC3COO2 + CO_2 + OH	jx(ip_CH3OOH)+jx(ip_HOCH2CHO) +j_ACETOL	Rickard and Pascoe (2009)
J45200a	TrGJTerC	LMBOABOOH + hν → $HOCH_2CHO$ + CH_3COCH_3 + HO_2 + OH	jx(ip_CH3OOH)*.67	Rickard and Pascoe (2009), Sander et al. (2019)
J45200b	TrGJTerC	LMBOABOOH + hν → IBUTALOH + HCHO + HO_2 + OH	jx(ip_CH3OOH)*.33	Rickard and Pascoe (2009), Sander et al. (2019)
J45201	TrGJTerC	MBOACO + hν → HCHO + HO_2 + IPRHOCO3	j_ACETOL	Rickard and Pascoe (2009)
J45202	TrGJTerC	MBOCOCO + hν → CO + HO_2 + IPRHOCO3	jx(ip_MGLYOX)	Rickard and Pascoe (2009)
J45203a	TrGJTerCN	LNMBOABOOH + hν → $NO_3CH2CHO$ + CH_3COCH_3 + HO_2 + OH	jx(ip_CH3OOH)*.65	Rickard and Pascoe (2009), Sander et al. (2019)
J45203b	TrGJTerCN	LNMBOABOOH + hν → IBUTALOH + HCHO + NO_2 + OH	jx(ip_CH3OOH)*.35	Rickard and Pascoe (2009), Sander et al. (2019)
J45204	TrGJTerCN	NC4OHCO3H + hν → IBUTALOH + CO_2 + NO_2 + OH	jx(ip_CH3OOH)	Rickard and Pascoe (2009)
J45400	TrGJAroC	C54CO + hν → HO_2 + CO + CO + CO + $CH_3C(O)$	jx(ip_MGLYOX)+2.15*jx(ip_MGLYOX) *2.	Rickard and Pascoe (2009)
J45401	TrGJAroC	C5134CO2OH + hν → $CH_3COCOCHO$ + HO_2 + CO + HO_2	jx(ip_HOCH2CHO)+2.15*jx(ip_ MGLYOX)	Rickard and Pascoe (2009)
J45402	TrGJAroC	C5DIALOOH + hν → MALDIAL + CO + HO_2 + OH	jx(ip_CH3OOH)+jx(ip_MACR)	Rickard and Pascoe (2009)*

Table 2: Photolysis reactions (... continued)

#	labels	reaction	rate coefficient	reference
J45406	TrGJAroC	C5CO14OH + hν → $CH_3C(O)$ + $HCOCO_2H$ + HO_2 + CO	jx(ip_MVK)	Rickard and Pascoe (2009)
J45407	TrGJAroC	C5DICARB + hν → .6 C5CO14O2 + .6 HO_2 + .4 TLFUONE	jx(ip_NO2)*0.2	Rickard and Pascoe (2009)*
J45408	TrGJAroC	MC3ODBCO2H + hν → CH_3COCO_2H + HO_2 + CO + HO_2 + CO	jx(ip_MACR)	Rickard and Pascoe (2009)
J45409	TrGJAroC	ACCOMECHO + hν → MECOACETO2 + HO_2 + CO	jx(ip_HOCH2CHO)	Rickard and Pascoe (2009)
J45410	TrGJAroC	MMALNHYOOH + hν → CO2H3CO3 + CO_2 + OH	jx(ip_CH3OOH)	Rickard and Pascoe (2009)*
J45411	TrGJAroC	C5DICAROOH + hν → MGLYOX + GLYOX + HO_2 + OH	jx(ip_CH3OOH)+jx(ip_HOCH2CHO) +j_ACETOL	Rickard and Pascoe (2009)*
J45412	TrGJAroCN	NTLFUOOH + hν → ACCOMECHO + NO_2 + OH	jx(ip_CH3OOH)	Rickard and Pascoe (2009)*
J45414	TrGJAroC	C5CO14OOH + hν → .83 MALANHY + .83 CH_3 + .17 MGLYOX + .17 HO_2 + .17 CO + .17 CO_2 + OH	jx(ip_CH3OOH)	Rickard and Pascoe (2009)*
J45415	TrGJAroC	TLFUOOH + hν → ACCOMECHO + HO_2 + OH	jx(ip_CH3OOH)	Rickard and Pascoe (2009)*
J45417	TrGJAroC	ACCOMECO3H + hν → MECOACETO2 + CO_2 + OH	jx(ip_CH3OOH)	Rickard and Pascoe (2009)
J45418	TrGJAroC	C5DIALCO + hν → MALDIALCO3 + CO + HO_2	jx(ip_MGLYOX)+jx(ip_MACR)	Rickard and Pascoe (2009)
J46200	TrGJTerCN	C614NO3 + hν → CO23C4CHO + HCHO + HO_2 + NO_2	2.15*jx(ip_MGLYOX)	Rickard and Pascoe (2009)
J46201	TrGJTerC	C614OOH + hν → CO23C4CHO + HCHO + HO_2 + OH	jx(ip_CH3OOH)+2.15*jx(ip_MGLYOX)	Rickard and Pascoe (2009)
J46202	TrGJTerC	CO235C5CHO + hν → CO23C4CO3 + CO + HO_2	jx(ip_MGLYOX)	Rickard and Pascoe (2009)
J46203	TrGJTerC	CO235C6OOH + hν → CO23C4CO3 + HCHO + OH	jx(ip_CH3OOH)+2.15*jx(ip_MGLYOX)	Rickard and Pascoe (2009)
J46400	TrGJAroC	PHENOOH + hν → .71 MALDALCO2H + .71 GLYOX + .29 PBZQONE + HO_2 + OH	jx(ip_CH3OOH)	Rickard and Pascoe (2009)*
J46401	TrGJAroC	C6CO4DB + hν → C4CO2DBCO3 + HO_2 + CO	jx(ip_MGLYOX)*2.	Rickard and Pascoe (2009)
J46402	TrGJAroC	C5CO2DCO3H + hν → $CH_3C(O)$ + HCOCOCHO + CO_2 + OH	jx(ip_CH3OOH)+jx(ip_MGLYOX)	Rickard and Pascoe (2009)
J46403	TrGJAroCN	NDNPHENOOH + hν → NC4DCO2H + HNO_3 + CO + CO + NO_2 + OH	jx(ip_CH3OOH)	Rickard and Pascoe (2009)*
J46404	TrGJAroCN	BZBIPERNO3 + hν → GLYOX + HO_2 + .5 BZFUONE + .5 BZFUONE + NO_2	j_IC3H7NO3	Rickard and Pascoe (2009)*
J46405	TrGJAroCN	HOC6H4NO2 + hν → HONO + CPDKETENE	jx(ip_HOC6H4NO2)	Chen et al. (2011)*
J46406	TrGJAroC	CPDKETENE + hν → CO_2 + CO + 2 HO_2 + MALDIAL	j_ketene	see note*
J46407	TrGJAroC	C5COOHCO3H + hν → HOCOC4DIAL + HO_2 + CO + CO_2 + OH	jx(ip_CH3OOH)	Rickard and Pascoe (2009)

Table 2: Photolysis reactions (... continued)

#	labels	reaction	rate coefficient	reference
J46408	TrGJAroC	BZEPOXMUC + hν → .5 C5DIALO2 + 1.5 HO_2 + 1.5 CO + .5 MALDIAL	4.E3*jx(ip_MVK)*0.1	Rickard and Pascoe (2009)
J46409	TrGJAroCN	NPHEN1OOH + hν → NPHEN1O + OH	jx(ip_CH3OOH)	Rickard and Pascoe (2009)
J46410	TrGJAroC	BZEMUCCO + hν → HCOCOHCO3 + C3DIALO2	jx(ip_HOCH2CHO)*2.+j_ACETOL	Rickard and Pascoe (2009)
J46411	TrGJAroC	BZEMUCCO2H + hν → C5DIALO2 + CO_2 + HO_2	jx(ip_MACR)	Rickard and Pascoe (2009)
J46412	TrGJAroCN	NNCATECOOH + hν → NC4DCO2H + $HCOCO_2H$ + NO_2 + OH	jx(ip_CH3OOH)	Rickard and Pascoe (2009)*
J46413	TrGJAroC	C615CO2OOH + hν → C5DICARB + CO + HO_2 + OH	jx(ip_MVK)+jx(ip_CH3OOH)	Rickard and Pascoe (2009)
J46414	TrGJAroCN	NPHENOOH + hν → MALDALCO2H + GLYOX + OH + NO_2	j_IC3H7NO3 + jx(ip_CH3OOH)	Rickard and Pascoe (2009)
J46415	TrGJAroCN	NCATECOOH + hν → NC4DCO2H + $HCOCO_2H$ + HO_2 + OH	jx(ip_CH3OOH)	Rickard and Pascoe (2009)*
J46416	TrGJAroC	PBZQOOH + hν → C5CO2OHCO3 + OH	jx(ip_CH3OOH)	Rickard and Pascoe (2009)*
J46417	TrGJAroC	BZOBIPEROH + hν → MALDIALCO3 + GLYOX + HO_2	j_ACETOL	Rickard and Pascoe (2009)
J46418	TrGJAroC	BZBIPEROOH + hν → GLYOX + HO_2 + .5 BZFUONE + .5 BZFUONE + OH	jx(ip_CH3OOH)	Rickard and Pascoe (2009)*
J46419	TrGJAroCN	NBZQOOH + hν → C6CO4DB + NO_2 + OH	jx(ip_CH3OOH)	Rickard and Pascoe (2009)*
J46420	TrGJAroC	CATEC1OOH + hν → CATEC1O + OH	jx(ip_CH3OOH)	Rickard and Pascoe (2009)
J46421	TrGJAroC	C6125CO + hν → C5CO14O2 + CO + HO_2	jx(ip_MGLYOX)+jx(ip_MVK)	Rickard and Pascoe (2009)
J46422	TrGJAroCN	DNPHENOOH + hν → NC4DCO2H + $HCOCO_2H$ + NO_2 + OH	jx(ip_CH3OOH)	Rickard and Pascoe (2009)*
J46423	TrGJAroC	BZEMUCCO3H + hν → C5DIALO2 + CO_2 + OH	jx(ip_CH3OOH)+jx(ip_MACR)	Rickard and Pascoe (2009)
J46424	TrGJAroC	C6H5OOH + hν → C6H5O + OH	jx(ip_CH3OOH)	Rickard and Pascoe (2009)
J46425	TrGJAroC	BZEMUCOOH + hν → .5 EPXC4DIAL + .5 GLYOX + .5 HO_2 + .5 C3DIALO2 + .5 C32OH13CO + OH	jx(ip_CH3OOH)+jx(ip_HOCH2CHO)*2.	Rickard and Pascoe (2009)*
J46427	TrGJAroCN	BZEMUCNO3 + hν → EPXC4DIAL + NO_2 + GLYOX + HO_2	2.77*jx(ip_HOCH2CHO)	Rickard and Pascoe (2009)
J46428	TrGJAroCN	DNPHEN + hν → HONO + NCPDKETENE	jx(ip_HOC6H4NO2)	Sander et al. (2019)
J46429	TrGJAroCN	NCPDKETENE + hν → CO_2 + CO + 2 HO_2 + NC4DCO2H	j_ketene	see note*
J47200	TrGJTerC	CO235C6CHO + hν → CHOC3COCO3 + $CH_3C(O)$	2.15*jx(ip_MGLYOX)	Rickard and Pascoe (2009)
J47201	TrGJTerC	C235C6CO3H + hν → CO235C6O2 + CO_2 + OH	jx(ip_CH3OOH)+2.15*jx(ip_MGLYOX)	Rickard and Pascoe (2009)
J47202	TrGJTerC	C716OOH + hν → CO13C4CHO + $CH_3C(O)$ + OH	jx(ip_CH3OOH)+jx(ip_HOCH2CHO)	Rickard and Pascoe (2009)
J47203	TrGJTerC	C721OOH + hν → C722O2 + OH	jx(ip_CH3OOH)	Rickard and Pascoe (2009)
J47204	TrGJTerC	C722OOH + hν → CH_3COCH_3 + C44O2 + OH	jx(ip_CH3OOH)	Rickard and Pascoe (2009)

96

Table 2: Photolysis reactions (... continued)

#	labels	reaction	rate coefficient	reference
J47400	TrGJAroC	TLEPOXMUC + hν → .5 C615CO2O2 + HO_2 + CO + .5 EPXC4DIAL + .5 $CH_3C(O)$	4.E3*jx(ip_MVK)*0.1	Rickard and Pascoe (2009)
J47401	TrGJAroC	C6H5CH2OOH + hν → BENZAL + HO_2 + OH	jx(ip_CH3OOH)	Rickard and Pascoe (2009)*
J47402	TrGJAroCN	C6H5CH2NO3 + hν → BENZAL + HO_2 + NO_2	0.59*j_IC3H7NO3	Rickard and Pascoe (2009)*
J47403	TrGJAroC	BENZAL + hν → HO_2 + CO + C6H5O2	jx(ip_BENZAL)	Wallington et al. (2018)
J47404	TrGJAroC	TLBIPEROOH + hν → .6 GLYOX + .4 MGLYOX + HO_2 + .2 C4MDIAL + .2 C5DICARB + .2 TLFUONE + .2 BZFUONE + .2 MALDIAL + OH	jx(ip_CH3OOH)	Rickard and Pascoe (2009)*
J47405	TrGJAroCN	TLBIPERNO3 + hν → .6 GLYOX + .4 MGLYOX + HO_2 + .2 C4MDIAL + .2 C5DICARB + .2 TLFUONE + .2 BZFUONE + .2 MALDIAL + NO_2	j_IC3H7NO3	Rickard and Pascoe (2009)*
J47406	TrGJAroC	TLOBIPEROH + hν → C5CO14O2 + GLYOX + HO_2	j_ACETOL	Rickard and Pascoe (2009)
J47407	TrGJAroC	CRESOOH + hν → .68 C5CO14OH + .68 GLYOX + HO_2 + .32 PTLQONE + OH	jx(ip_CH3OOH)	Rickard and Pascoe (2009)*
J47408a	TrGJAroCN	NCRESOOH + hν → .68 C5CO14OH + .68 GLYOX + HO_2 + .32 PTLQONE + OH + NO_2	j_IC3H7NO3	Rickard and Pascoe (2009)*
J47408b	TrGJAroCN	NCRESOOH + hν → C5CO14OH + GLYOX + NO_2 + OH	jx(ip_CH3OOH)	Rickard and Pascoe (2009)*
J47409	TrGJAroCN	TOL1OHNO2 + hν → HONO + MCPDKETENE	jx(ip_HOPh3Me2NO2)	see note*
J47410	TrGJAroC	TLEMUCCO2H + hν → C615CO2O2 + CO_2 + HO_2	jx(ip_MACR)	Rickard and Pascoe (2009)
J47411	TrGJAroC	TLEMUCCO3H + hν → C615CO2O2 + CO_2 + OH	jx(ip_CH3OOH)+jx(ip_MACR)	Rickard and Pascoe (2009)
J47412	TrGJAroC	TLEMUCOOH + hν → .5 C3DIALO2 + .5 CO2H3CHO + .5 EPXC4DIAL + .5 MGLYOX + .5 HO_2 + OH	jx(ip_CH3OOH)+2.77*jx(ip_HOCH2CHO)+j_ACETOL	Rickard and Pascoe (2009)*
J47413	TrGJAroCN	TLEMUCNO3 + hν → EPXC4DIAL + NO_2 + $CH_3C(O)$ + CO + HO_2	2.77*jx(ip_HOCH2CHO)+j_ACETOL	Rickard and Pascoe (2009)
J47414	TrGJAroC	TLEMUCCO + hν → $CH_3C(O)$ + EPXC4DIAL + CO + HO_2	2.77*jx(ip_HOCH2CHO)+2.15*jx(ip_MGLYOX)	Rickard and Pascoe (2009)
J47415	TrGJAroC	C6H5CO3H + hν → C6H5O2 + CO_2 + OH	jx(ip_CH3OOH)	Rickard and Pascoe (2009)
J47416	TrGJAroC	OXYL1OOH + hν → TOL1O + OH	jx(ip_CH3OOH)	Rickard and Pascoe (2009)
J47417	TrGJAroCN	MNCATECH + hν → HONO + MCPDKETENE	jx(ip_HOPh3Me2NO2)	see note*
J47418	TrGJAroC	MCPDKETENE + hν → CO_2 + CO + 2 HO_2 + C4MDIAL	j_ketene	see note*
J47419	TrGJAroCN	DNCRES + hν → HONO + MNCPDKETENE	jx(ip_HOPh3Me2NO2)	see note*

97

Table 2: Photolysis reactions (... continued)

#	labels	reaction	rate coefficient	reference
J47420	TrGJAroCN	MNCPDKETENE + hν → CO_2 + CO + 2 HO_2 + NC4MDCO2HN	j_ketene	see note*
J47421	TrGJAroC	MCATEC1OOH + hν → MCATEC1O + OH	jx(ip_CH3OOH)	Rickard and Pascoe (2009)
J47422	TrGJAroCN	NPTLQOOH + hν → C7CO4DB + NO_2 + OH	jx(ip_CH3OOH)	Rickard and Pascoe (2009)*
J47423	TrGJAroC	PTLQOOH + hν → C6CO2OHCO3 + OH	jx(ip_CH3OOH)	Rickard and Pascoe (2009)*
J47424	TrGJAroCN	NCRES1OOH + hν → NCRES1O + OH	jx(ip_CH3OOH)	Rickard and Pascoe (2009)
J47425	TrGJAroCN	MNNCATCOOH + hν → NC4MDCO2HN + $HCOCO_2H$ + NO_2 + OH	jx(ip_CH3OOH)	Rickard and Pascoe (2009)*
J47426	TrGJAroCN	MNCATECOOH + hν → NC4MDCO2HN + $HCOCO_2H$ + HO_2 + OH	jx(ip_CH3OOH)	Rickard and Pascoe (2009)*
J47427	TrGJAroC	C7CO4DB + hν → C5CO2DBCO3 + HO_2 + CO	jx(ip_MGLYOX)*2.	Rickard and Pascoe (2009)
J47428	TrGJAroCN	NDNCRESOOH + hν → NC4MDCO2HN + HNO_3 + CO + CO + NO_2 + OH	jx(ip_CH3OOH)	Rickard and Pascoe (2009)*
J47429	TrGJAroCN	DNCRESOOH + hν → NC4MDCO2HN + $HCOCO_2H$ + NO_2 + OH	jx(ip_CH3OOH)	Rickard and Pascoe (2009)*
J47430	TrGJAroC	C6COOHCO3H + hν → C5134CO2OH + HO_2 + CO + CO_2 + OH	jx(ip_CH3OOH)	Rickard and Pascoe (2009)
J48200	TrGJTerC	C86OOH + hν → C511O2 + CH_3COCH_3 + OH	jx(ip_CH3OOH)+ jx(ip_HOCH2CHO)	Rickard and Pascoe (2009)
J48201	TrGJTerC	C812OOH + hν → C813O2 + OH	jx(ip_CH3OOH)	Rickard and Pascoe (2009)
J48202	TrGJTerC	C813OOH + hν → CH_3COCH_3 + C512O2 + OH	jx(ip_CH3OOH)+jx(ip_MGLYOX)	Rickard and Pascoe (2009)
J48203	TrGJTerC	C721CHO + hν → C721O2 + CO + HO_2	jx(ip_HOCH2CHO)	Rickard and Pascoe (2009)
J48204	TrGJTerC	C721CO3H + hν → C721O2 + CO_2 + OH	jx(ip_CH3OOH)	Rickard and Pascoe (2009)
J48205	TrGJTerC	C8BCOOH + hν → C89O2 + OH	jx(ip_CH3OOH)	Rickard and Pascoe (2009)
J48206	TrGJTerC	C89OOH + hν → C810O2 + OH	jx(ip_CH3OOH)+jx(ip_HOCH2CHO)	Rickard and Pascoe (2009)
J48207	TrGJTerCN	C89NO3 + hν → C810O2 + NO_2	jx(ip_CH3OOH)+jx(ip_HOCH2CHO)	Rickard and Pascoe (2009)
J48208	TrGJTerC	C810OOH + hν → CH_3COCH_3 + C514O2 + OH	jx(ip_CH3OOH)+jx(ip_HOCH2CHO)	Rickard and Pascoe (2009)
J48209	TrGJTerCN	C810NO3 + hν → CH_3COCH_3 + C514O2 + NO_2	2.84*j_IC3H7NO3+jx(ip_HOCH2CHO)	Rickard and Pascoe (2009)
J48210	TrGJTerCN	C8BCNO3 + hν → C89O2 + NO_2	j_IC3H7NO3	Rickard and Pascoe (2009)
J48211	TrGJTerC	C85OOH + hν → C86O2 + OH	jx(ip_CH3OOH)+j_ACETOL	Rickard and Pascoe (2009)
J48400	TrGJAroC	STYRENOOH + hν → HO_2 + HCHO + BENZAL + OH	jx(ip_CH3OOH)	Rickard and Pascoe (2009)*
J49200	TrGJTerC	C96OOH + hν → C97O2 + OH	jx(ip_CH3OOH)+j_ACETOL	Rickard and Pascoe (2009)
J49201	TrGJTerC	C97OOH + hν → C98O2 + OH	jx(ip_CH3OOH)+j_ACETOL	Rickard and Pascoe (2009)

Table 2: Photolysis reactions (... continued)

#	labels	reaction	rate coefficient	reference
J49202	TrGJTerC	C98OOH + hν → C614O2 + CH_3COCH_3 + OH	(jx(ip_CH3OOH)+2.15*jx(ip_MGLYOX))	Rickard and Pascoe (2009)
J49203a	TrGJTerC	NORPINAL + hν → C85O2 + CO + HO_2	jx(ip_PINAL2HCO)	Rickard and Pascoe (2009), Sander et al. (2019)
J49203b	TrGJTerC	NORPINAL + hν → NORPINENOL	jx(ip_PINAL2ENOL)	Sander et al. (2019), Andrews et al. (2012)
J49204	TrGJTerC	C85CO3H + hν → C85O2 + CO_2 + OH	jx(ip_CH3OOH)+j_ACETOL	Rickard and Pascoe (2009)
J49205	TrGJTerC	C89CO2H + hν → .8 C811CO3 + .2 C89O2 + .2 CO_2 + HO_2	jx(ip_HOCH2CHO)	Rickard and Pascoe (2009)
J49206	TrGJTerC	C89CO3H + hν → .8 C811CO3 + .2 C89O2 + .2 CO_2 + OH	jx(ip_CH3OOH)+jx(ip_HOCH2CHO)	Rickard and Pascoe (2009)
J49207	TrGJTerC	C811CO3H + hν → C811O2 + CO_2 + OH	jx(ip_CH3OOH)	Rickard and Pascoe (2009)
J49208	TrGJTerC	NOPINDOOH + hν → C89CO3 + OH	jx(ip_CH3OOH)	Rickard and Pascoe (2009)
J40200	TrGJTerC	LAPINABOOH + hν → PINAL + HO_2 + OH	jx(ip_CH3OOH)	Rickard and Pascoe (2009)
J40201	TrGJTerC	MENTHEN6ONE + hν → RO6R1O2 + OH	jx(ip_CH3OOH)	Vereecken et al. (2007)
J40202	TrGJTerC	2OHMENTHEN6ONE + hν → 10 LCARBON + OH	jx(ip_CH3OOH)	Vereecken et al. (2007)
J40203a	TrGJTerC	PINAL + hν → C96O2 + CO + HO_2	jx(ip_PINAL2HCO)	Rickard and Pascoe (2009)
J40203b	TrGJTerC	PINAL + hν → PINEOL	jx(ip_PINAL2ENOL)	Sander et al. (2019), Andrews et al. (2012)*
J40204	TrGJTerC	PERPINONIC + hν → C96O2 + CO_2 + OH	jx(ip_CH3OOH)+j_ACETOL	Rickard and Pascoe (2009)
J40205	TrGJTerC	PINALOOH + hν → C106O2 + OH	jx(ip_CH3OOH)+jx(ip_HOCH2CHO)	Rickard and Pascoe (2009)
J40206	TrGJTerCN	PINALNO3 + hν → C106O2 + NO_2	j_IC3H7NO3+jx(ip_HOCH2CHO)	Rickard and Pascoe (2009)
J40207	TrGJTerC	C106OOH + hν → C716O2 + CH_3COCH_3 + OH	jx(ip_CH3OOH)+jx(ip_HOCH2CHO)	Rickard and Pascoe (2009)
J40208	TrGJTerCN	C106NO3 + hν → C716O2 + CH_3COCH_3 + NO_2	j_IC3H7NO3+ jx(ip_HOCH2CHO)	Rickard and Pascoe (2009)
J40209	TrGJTerC	C109OOH + hν → C89CO3 + HCHO + OH	jx(ip_CH3OOH)+jx(ip_HOCH2CHO)	Rickard and Pascoe (2009)
J40210	TrGJTerC	C109CO + hν → C89CO3 + CO + HO_2	jx(ip_MGLYOX)+jx(ip_HOCH2CHO)	Rickard and Pascoe (2009)
J40211	TrGJTerCN	LNAPINABOOH + hν → PINAL + NO_2 + OH	jx(ip_CH3OOH)	Rickard and Pascoe (2009)
J40212	TrGJTerC	BPINAOOH + hν → NOPINONE + HCHO + HO_2 + OH	jx(ip_CH3OOH)	Rickard and Pascoe (2009)
J40213	TrGJTerCN	LNBPINABOOH + hν → NOPINONE + HCHO + NO_2 + OH	jx(ip_CH3OOH)	Rickard and Pascoe (2009)
J40214	TrGJTerCN	ROO6R1NO3 + hν → ROO6R3O2 + CH_3COCH_3 + NO_2	2.84*j_IC3H7NO3+jx(ip_CH3OOH)	Sander et al. (2019)
J40215	TrGJTerCN	RO6R1NO3 + hν → 9 LCARBON + HCHO + HO_2 + NO_2	2.84*j_IC3H7NO3	Sander et al. (2019)
J6000	StTrGJCl	Cl_2 + hν → Cl + Cl	jx(ip_Cl2)	Sander et al. (2014)
J6100	StTrGJCl	Cl_2O_2 + hν → 2 Cl	jx(ip_Cl2O2)	Sander et al. (2014)
J6101	StTrGJCl	OClO + hν → ClO + $O(^3P)$	jx(ip_OClO)	Sander et al. (2014)
J6200	StGJCl	HCl + hν → Cl + H	jx(ip_HCl)	Sander et al. (2014)
J6201	StTrGJCl	HOCl + hν → OH + Cl	jx(ip_HOCl)	Sander et al. (2014)

Table 2: Photolysis reactions (... continued)

#	labels	reaction	rate coefficient	reference
J6300	TrGJClN	$ClNO_2 + h\nu \rightarrow Cl + NO_2$	jx(ip_ClNO2)	Sander et al. (2014)
J6301a	StTrGJClN	$ClNO_3 + h\nu \rightarrow Cl + NO_3$	jx(ip_ClNO3)	Sander et al. (2014)
J6301b	StTrGJClN	$ClNO_3 + h\nu \rightarrow ClO + NO_2$	jx(ip_ClONO2)	Sander et al. (2014)
J6400	StGJCl	$CH_3Cl + h\nu \rightarrow Cl + CH_3$	jx(ip_CH3Cl)	Sander et al. (2014)
J6401	StGJCl	$CCl_4 + h\nu \rightarrow$ LCARBON + 4 Cl	jx(ip_CCl4)	Sander et al. (2014)
J6402	StGJCCl	$CH_3CCl_3 + h\nu \rightarrow$ 2 LCARBON + 3 Cl	jx(ip_CH3CCl3)	Sander et al. (2014)
J6500	StGJClF	$CFCl_3 + h\nu \rightarrow$ LCARBON + LFLUORINE + 3 Cl	jx(ip_CFCl3)	Sander et al. (2014)*
J6501	StGJClF	$CF_2Cl_2 + h\nu \rightarrow$ LCARBON + 2 LFLUORINE + 2 Cl	jx(ip_CF2Cl2)	Sander et al. (2014)*
J7000	StTrGJBr	$Br_2 + h\nu \rightarrow Br + Br$	jx(ip_Br2)	Sander et al. (2014)
J7100	StTrGJBr	$BrO + h\nu \rightarrow Br + O(^3P)$	jx(ip_BrO)	Sander et al. (2014)
J7200	StTrGJBr	$HOBr + h\nu \rightarrow Br + OH$	jx(ip_HOBr)	Sander et al. (2014)
J7300	TrGJBrN	$BrNO_2 + h\nu \rightarrow Br + NO_2$	jx(ip_BrNO2)	Sander et al. (2014)
J7301	StTrGJBrN	$BrNO_3 + h\nu \rightarrow .85\ Br + .85\ NO_3 + .15\ BrO + .15\ NO_2$	jx(ip_BrNO3)	Sander et al. (2014)*
J7400	StGJBr	$CH_3Br + h\nu \rightarrow Br + CH_3$	jx(ip_CH3Br)	Sander et al. (2014)
J7401	TrGJBr	$CH_2Br_2 + h\nu \rightarrow$ LCARBON + 2 Br	jx(ip_CH2Br2)	Sander et al. (2014)
J7402	TrGJBr	$CHBr_3 + h\nu \rightarrow$ LCARBON + 3 Br	jx(ip_CHBr3)	Sander et al. (2014)
J7500	StGJBrF	$CF_3Br + h\nu \rightarrow$ LCARBON + 3 LFLUORINE + Br	jx(ip_CF3Br)	Sander et al. (2014)
J7600	StTrGJBrCl	$BrCl + h\nu \rightarrow Br + Cl$	jx(ip_BrCl)	Sander et al. (2014)
J7601	StGJBrClF	$CF_2ClBr + h\nu \rightarrow$ LCARBON + 2 LFLUORINE + Br + Cl	jx(ip_CF2ClBr)	Sander et al. (2014)
J7602	TrGJBrCl	$CH_2ClBr + h\nu \rightarrow$ LCARBON + Br + Cl	jx(ip_CH2ClBr)	Sander et al. (2014)
J7603	TrGJBrCl	$CHCl_2Br + h\nu \rightarrow$ LCARBON + Br + 2 Cl	jx(ip_CHCl2Br)	Sander et al. (2014)
J7604	TrGJBrCl	$CHClBr_2 + h\nu \rightarrow$ LCARBON + 2 Br + Cl	jx(ip_CHClBr2)	Sander et al. (2014)
J8000	TrGJI	$I_2 + h\nu \rightarrow I + I$	jx(ip_I2)	Sander et al. (2014)
J8100	TrGJI	$IO + h\nu \rightarrow I + O(^3P)$	jx(ip_IO)	Sander et al. (2014)
J8200	TrGJI	$HOI + h\nu \rightarrow I + OH$	jx(ip_HOI)	Sander et al. (2014)
J8300	TrGJIN	$INO_2 + h\nu \rightarrow I + NO_2$	jx(ip_INO2)	Sander et al. (2014)
J8301	TrGJIN	$INO_3 + h\nu \rightarrow I + NO_3$	jx(ip_INO3)	Sander et al. (2014)
J8400	TrGJI	$CH_2I_2 + h\nu \rightarrow 2\ I + 2\ HO_2 + CO$	jx(ip_CH2I2)	Sander et al. (2014)
J8401	TrGJI	$CH_3I + h\nu \rightarrow I + CH_3$	jx(ip_CH3I)	Sander et al. (2014)
J8402	TrGJCI	$CH_3CHICH_3 + h\nu \rightarrow$ 2 LCARBON + I + CH_3	jx(ip_C3H7I)	Sander et al. (2014)
J8403	TrGJClI	$CH_2ClI + h\nu \rightarrow I + Cl + 2\ HO_2 + CO$	jx(ip_CH2ClI)	Sander et al. (2014)
J8600	TrGJClI	$ICl + h\nu \rightarrow I + Cl$	jx(ip_ICl)	Sander et al. (2014)
J8700	TrGJBrI	$IBr + h\nu \rightarrow I + Br$	jx(ip_IBr)	Sander et al. (2014)
PH (aqueous)				
PH3200_a01	TrAa01JN	$NO_3^-(aq) + h\nu \rightarrow NO_2(aq) + OH(aq) + OH^-(aq)$	xaer(01)*jx(ip_NO2) * 1.4E-4	see note*

Table 2: Photolysis reactions (... continued)

#	labels	reaction	rate coefficient	reference
PH10200_a01	TrAa01JHg	$Hg(OH)_2(aq) + h\nu \rightarrow Hg(aq)$	xaer(01)*6E-5*jx(ip_NO2)	see note*
PH11000_a01	TrAa01JFe	$FeOH^{2+}(aq) + h\nu \rightarrow Fe^{2+}(aq) + OH(aq)$	xaer(01)*4.51E-3*0.312	Herrmann et al. (2000)
PH11001_a01	TrAa01JFe	$Fe(OH)_2^+(aq) + h\nu \rightarrow Fe^{2+}(aq) + OH(aq) + OH^-(aq)$	xaer(01)*5.77E-3*0.255	Herrmann et al. (2000)
PH11003_a01	TrAa01JFeS	$FeSO_4^+(aq) + h\nu \rightarrow Fe^{2+}(aq) + SO_4^-(aq)$	xaer(01)*6.43E-3*7.9E-3	Herrmann et al. (2000)

General notes

j-values are calculated with an external module (e.g., JVAL) and then supplied to the MECCA chemistry.

Values that originate from the Master Chemical Mechanism (MCM) by Rickard and Pascoe (2009) are translated according in the following way:
j(11) → jx(ip_COH2)
j(12) → jx(ip_CHOH)
j(15) → jx(ip_HOCH2CHO)
j(18) → jx(ip_MACR)
j(22) → jx(ip_ACETOL)
j(23)+j(24) → jx(ip_MVK)
j(31)+j(32)+j(33) → jx(ip_GLYOX)
j(34) → jx(ip_MGLYOX)
j(41) → jx(ip_CH3OOH)
j(53) → j(isopropyl nitrate)
j(54) → j(isopropyl nitrate)
j(55) → j(isopropyl nitrate)
j(56)+j(57) → jx(ip_NOA)

Specific notes

J41003: CH_3- and CH_2-channels are considered only and with their branching ratios being 0.42 and 0.48, respectively (Gans et al., 2011). CH-production is neglected. CH_2 is assumed to react only with O2 yielding 1.44 H_2 + 0.18 HCHO + 0.18 $O(^3P)$ + 0.33 OH + 0.33 HO_2 + 0.44 CO_2 + 0.38 CO + 0.05 H_2O as assumed in the WACCM model by J. Orlando (Doug Kinnison, pers. comm. with D. Taraborrelli).

J41006: product distribution as for HNO4

J42004: Quantum yields from Burkholder et al. (2015).

J42005a: Quantum yields from Burkholder et al. (2015).

J42005b: Quantum yields from Burkholder et al. (2015).

J42005c: Quantum yields from Burkholder et al. (2015).

J42007: It is assumed that J(PHAN) is the same as J(PAN).

J42017: Enhancement of j according to Müller et al. (2014).

J42020: It is assumed that j(NO_3CH2CHO) is the same as j(PAN).

J42021: In analogy to what is assumed for $CH_3O_2NO_2$ photolysis as in (Sander et al., 2014).

J43002: Following von Kuhlmann et al. (2003), we use j(CH_3COCH_2OH) = 0.11*jx(ip_CHOH). As an additional factor, the quantum yield of 0.65 is taken from Orlando et al. (1999a).

J43006: Following von Kuhlmann et al. (2003), we use J($iC_3H_7ONO_2$) = 3.7*jx(ip_PAN).

J43018: One third of the acetaldehyde channel is considered to be CH2CHOH according to Hjorth (2002) EUPHORE Report.

J43024: Assuming J($C_3H_7ONO_2$) = 0.59 × J($iC_3H_7ONO_2$), consistent with the photolysis rate coefficients used in the MCM (Rickard and Pascoe, 2009).

J43025a: Photolysis frequencies very similar to the ones of CH_3CHO.

J43025b: Photolysis frequencies very similar to the ones of CH_3CHO.

J43400: KDEC C3DIALO → GLYOX + CO + HO2

J44004: It is assumed that J(BIACET) is 2.15 times larger than J(MGLYOX), consistent with the photolysis rate coefficients used in the MCM (Rickard and Pascoe, 2009).

J44005a: It is assumed that J(LC4H9NO3) is the same as J($iC_3H_7ONO_2$).

J44005b: It is assumed that J(LC4H9NO3) is the same as J($iC_3H_7ONO_2$).

J44006: It is assumed that J(MPAN) is the same as J(PAN).

J44009: It is assumed that J(MACROOH) is 2.77 times larger than J($HOCH_2CHO$), consistent with the photolysis rate coefficients used in the MCM (Rickard and Pascoe, 2009).

J44010: It is assumed that J(MACROH) is 2.77 times larger than J($HOCH_2CHO$), consistent with the photolysis rate coefficients used in the MCM (Rickard and Pascoe, 2009).

J44015: It is assumed that J(BIACETOH) is 2.15 times larger than J(MGLYOX), consistent with the photolysis rate coefficients used in the MCM (Rickard and Pascoe, 2009).

J44017a: CO-channel yielding CH_3COCH which upon reaction with O_2 produces an excited Criegee Intermediate assumed to be similar to MGLOOA in MCM. MGLOOA is produced also in other reactions and is substituted by its decomposition products. Furthermore, the stabilized Criegge Intermediate is assumed to solely react with water.

J44025: J values only for the secondary nitrate.

J44026: Like for LMEKNO3 photolysis

J44027: 2.84*J_IC3H7NO3 like for other tertiary alkyl nitrates (see J4505). Enhancement of J according to Müller et al. (2014).

J44037b: Channel which produces just vinyl alcohol and not a larger enol via keto-enol phototautomerization.

J44043: The resulting vinyl peroxy radical is assumed to mostly form with HO_2 a labile hydroperoxide (see ketene formation). The products are further simplified.

J44044: 1,5-H-shift for the resulting vinyl peroxy radical assumed to be dominant.

J44046a: Simplified oxidation.

J44400b: KDEC MALDIALO → GLYOX + GLYOX + HO2

J44401: KDEC BZFUO → CO14O3CHO + HO2

J44403: KDEC NBZFUO → 0.5 CO14O3CHO + 0.5 NO2 + 0.5 NBZFUONE + 0.5 HO2

J44404b: KDEC MALDIALCO2 → 0.6 MALANHY + HO2 + 0.4 GLYOX + 0.4 CO

J44407: KDEC MALANHYO → HCOCOHCO3

J44414: KDEC MECOACETO → CH3CO3 + HCHO

J45003: It is assumed that J(LISOPACNO3) = 0.59 × J($iC_3H_7ONO_2$), consistent with the photolysis rate coefficients used in the MCM (Rickard and Pascoe, 2009).

J45005: It is assumed that J(ISOPBNO3) = 2.84 × J($iC_3H_7ONO_2$), consistent with the photolysis rate coefficients used in the MCM (Rickard and Pascoe, 2009).

J45007: It is assumed that J(ISOPDNO3) is the same as J($iC_3H_7ONO_2$).

J45009: 0.59*J_IC3H7NO3 like for other primary alkyl nitrates (see J4503). Enhancement of J according to Müller et al. (2014).

J45015: Consistent with the MCM (Rickard and Pascoe, 2009), we assume that J(HCOC5) is half as large as J(MVK). With exeption of HOCH2CO the products of MACO2 decomposition without CO_2.

J45032: approximation with 4-oxo-pentenal photolysis combining results of Thner et al(2004) and Xiang et al(2007)

J45402: KDEC C5DIALO → MALDIAL + CO + HO2

J45407: KDEC TLFUONE → 0.6 C5CO14O2 + 0.6 HO2 + 0.4 TLFUONE

J45410: KDEC MMALANHYO → CO2H3CO3

J45411: KDEC C5DICARBO → MGLYOX + GLYOX + HO2

J45412: KDEC NTLFUO → ACCOMECHO + NO2

J45414: KDEC C5CO14CO2 → 0.83 MALANHY + 0.83 CH3 + .17 MGLYOX + .17 HO2 + .17 CO + .17 CO2

J45415: KDEC TLFUO → ACCOMECHO + HO2

J46400: KDEC PHENO → 0.71 MALDALCO2H + 0.71 GLYOX + 0.29 PBZQONE + HO2

J46403: KDEC NDNPHENO → NC4DCO2H + HNO3 + CO + CO + NO2

J46404: KDEC BZBIPERO → GLYOX + HO2 + 0.5 BZFUONE + 0.5 BZFUONE

J46405: new channel created for nitrophenol decomposition

J46406: new channel created for nitrophenol decomposition

J46412: KDEC NNCATECO → NC4DCO2H + HCOCO2H + NO2

J46415: KDEC NCATECO → NC4DCO2H + HCOCO2H + HO2

J46416: KDEC PBZQO → C5CO2OHCO3

J46418: KDEC BZBIPERO → GLYOX + HO2 + 0.5 BZFUONE + 0.5 BZFUONE

J46419: KDEC NBZQO → C6CO4DB + NO2

J46422: KDEC DNPHENO → NC4DCO2H + HCOCO2H + NO2

J46425: KDEC BZEMUCO → 0.5 EPXC4DIAL + .5 GLYOX + .5 HO2 + .5 C3DIALO2 + .5 C32OH13CO

J46429: new channel

J47401: KROPRIM*O2 fast reaction C6H5CH2O = BENZAL + HO2

J47402: KROPRIM*O2 fast reaction C6H5CH2O = BENZAL + HO2

J47404: KDEC TLBIPERO → 0.6 GLYOX + 0.4 MGLYOX + HO2 + 0.2 C4MDIAL + 0.2 C5DICARB + 0.2 TLFUONE + 0.2 BZFUONE + 0.2 MALDIAL

J47405: KDEC TLBIPERO → 0.6 GLYOX + 0.4 MGLYOX + HO2 + 0.2 C4MDIAL + 0.2 C5DICARB + 0.2 TLFUONE + 0.2 BZFUONE + 0.2 MALDIAL

J47407: KDEC CRESO → 0.68 C5CO14OH + 0.68 GLYOX + HO2 + 0.32 PTLQONE

J47408a: KDEC CRESO → 0.68 C5CO14OH + 0.68 GLYOX + HO2 + 0.32 PTLQONE

J47408b: KDEC NCRESO → C5CO14OH + GLYOX + NO2

J47409: Using J for 3-methyl-2-nitrophenol.

J47412: KDEC TLEMUCO → 0.5 C3DIALO2 + 0.5 CO2H3CHO + 0.5 EPXC4DIAL + 0.5 MGLYOX + 0.5 HO2

J47417: Using J for 3-methyl-2-nitrophenol.

J47418: new channel

J47419: Using J for 3-methyl-2-nitrophenol.

J47420: new channel

J47422: KDEC NPTLQO → C7CO4DB + NO2

J47423: KDEC PTLQO → C6CO2OHCO3

J47425: KDEC MNNCATECO → NC4MDCO2H + HCOCO2H + NO2

J47426: KDEC MNCATECO → NC4MDCO2H + HCOCO2H + HO2

J47428: KDEC NDNCRESO → NC4MDCO2H + HNO3 + CO + CO + NO2

J47429: KDEC DNCRESO → NC4MDCO2H + HCOCO2H + NO2

J48400: KDEC STYRENO → HO2 + HCHO + BENZAL

J40203b: Substituted vinyl alcohol in analogy to CH_3CHO photolysis.

J6500: Even though the elementary reaction produces only 1 Cl atom (Felder and Demuth, 1993), it is assumed here that eventually all Cl atoms are released in secondary reactions.

J6501: Even though the elementary reaction probably produces only 1 Cl atom (as for $CFCl_3$), it is assumed here that eventually all Cl atoms are released in secondary reactions.

J7301: The quantum yields are recommended by Burkholder et al. (2015) for $\lambda > 300$nm and used here for the entire spectrum.

PH3200_a01: Scaled to J(NO_2) so that its lifetime is about 10.5 days, as suggested by Zellner et al. (1990).

PH10200_a01: Scaled to J(NO_2) so that it produces about 3.0×10^{-7}.

Table 3: Reversible (Henry's law) equilibria and irreversible ("heterogenous") uptake

#	labels	reaction	rate coefficient	reference
H1000f_a01	TrAa01Sc	$O_2 \rightarrow O_2(aq)$	k_exf(01,ind_O2)	see general notes*
H1000b_a01	TrAa01Sc	$O_2(aq) \rightarrow O_2$	k_exb(01,ind_O2)	see general notes*
H1001f_a01	TrAa01MblScScm	$O_3 \rightarrow O_3(aq)$	k_exf(01,ind_O3)	see general notes*
H1001b_a01	TrAa01MblScScm	$O_3(aq) \rightarrow O_3$	k_exb(01,ind_O3)	see general notes*
H2100f_a01	TrAa01Sc	$OH \rightarrow OH(aq)$	k_exf(01,ind_OH)	see general notes*
H2100b_a01	TrAa01Sc	$OH(aq) \rightarrow OH$	k_exb(01,ind_OH)	see general notes*
H2101f_a01	TrAa01Sc	$HO_2 \rightarrow HO_2(aq)$	k_exf(01,ind_HO2)	see general notes*
H2101b_a01	TrAa01Sc	$HO_2(aq) \rightarrow HO_2$	k_exb(01,ind_HO2)	see general notes*
H2102f_a01	TrAa01MblScScm	$H_2O_2 \rightarrow H_2O_2(aq)$	k_exf(01,ind_H2O2)	see general notes*
H2102b_a01	TrAa01MblScScm	$H_2O_2(aq) \rightarrow H_2O_2$	k_exb(01,ind_H2O2)	see general notes*
H3101f_a01	TrAa01ScN	$NO_2 \rightarrow NO_2(aq)$	k_exf(01,ind_NO2)	see general notes*
H3101b_a01	TrAa01ScN	$NO_2(aq) \rightarrow NO_2$	k_exb(01,ind_NO2)	see general notes*
H3102f_a01	TrAa01ScN	$NO_3 \rightarrow NO_3(aq)$	k_exf(01,ind_NO3)	see general notes*
H3102b_a01	TrAa01ScN	$NO_3(aq) \rightarrow NO_3$	k_exb(01,ind_NO3)	see general notes*
H3200f_a01	TrAa01MblScScmN	$NH_3 \rightarrow NH_3(aq)$	k_exf(01,ind_NH3)	see general notes*
H3200b_a01	TrAa01MblScScmN	$NH_3(aq) \rightarrow NH_3$	k_exb(01,ind_NH3)	see general notes*
H3201_a01	TrAa01MblScScmN	$N_2O_5 \rightarrow HNO_3(aq) + HNO_3(aq)$	k_exf_N2O5(01)*C(ind_H2O_a01)	Behnke et al. (1994), Behnke et al. (1997)
H3202f_a01	TrAa01ScN	$HONO \rightarrow HONO(aq)$	k_exf(01,ind_HONO)	see general notes*
H3202b_a01	TrAa01ScN	$HONO(aq) \rightarrow HONO$	k_exb(01,ind_HONO)	see general notes*
H3203f_a01	TrAa01MblScScmN	$HNO_3 \rightarrow HNO_3(aq)$	k_exf(01,ind_HNO3)	see general notes*
H3203b_a01	TrAa01MblScScmN	$HNO_3(aq) \rightarrow HNO_3$	k_exb(01,ind_HNO3)	see general notes*
H3204f_a01	TrAa01ScN	$HNO_4 \rightarrow HNO_4(aq)$	k_exf(01,ind_HNO4)	see general notes*
H3204b_a01	TrAa01ScN	$HNO_4(aq) \rightarrow HNO_4$	k_exb(01,ind_HNO4)	see general notes*
H4100f_a01	TrAa01MblScScm	$CO_2 \rightarrow CO_2(aq)$	k_exf(01,ind_CO2)	see general notes*
H4100b_a01	TrAa01MblScScm	$CO_2(aq) \rightarrow CO_2$	k_exb(01,ind_CO2)	see general notes*
H4101f_a01	TrAa01ScScm	$HCHO \rightarrow HCHO(aq)$	k_exf(01,ind_HCHO)	see general notes*
H4101b_a01	TrAa01ScScm	$HCHO(aq) \rightarrow HCHO$	k_exb(01,ind_HCHO)	see general notes*
H4102f_a01	TrAa01Sc	$CH_3O_2 \rightarrow CH_3OO(aq)$	k_exf(01,ind_CH3O2)	see general notes*
H4102b_a01	TrAa01Sc	$CH_3OO(aq) \rightarrow CH_3O_2$	k_exb(01,ind_CH3O2)	see general notes*
H4103f_a01	TrAa01ScScm	$HCOOH \rightarrow HCOOH(aq)$	k_exf(01,ind_HCOOH)	see general notes*
H4103b_a01	TrAa01ScScm	$HCOOH(aq) \rightarrow HCOOH$	k_exb(01,ind_HCOOH)	see general notes*
H4104f_a01	TrAa01ScScm	$CH_3OOH \rightarrow CH_3OOH(aq)$	k_exf(01,ind_CH3OOH)	see general notes*
H4104b_a01	TrAa01ScScm	$CH_3OOH(aq) \rightarrow CH_3OOH$	k_exb(01,ind_CH3OOH)	see general notes*

Table 3: Reversible (Henry's law) equilibria and irreversible ("heterogenous") uptake

#	labels	reaction	rate coefficient	reference
H6000f_a01	TrAa01MblScCl	$Cl_2 \rightarrow Cl_2(aq)$	k_exf(01,ind_Cl2)	see general notes*
H6000b_a01	TrAa01MblScCl	$Cl_2(aq) \rightarrow Cl_2$	k_exb(01,ind_Cl2)	see general notes*
H6200f_a01	TrAa01MblScScmCl	$HCl \rightarrow HCl(aq)$	k_exf(01,ind_HCl)	see general notes*
H6200b_a01	TrAa01MblScScmCl	$HCl(aq) \rightarrow HCl$	k_exb(01,ind_HCl)	see general notes*
H6201f_a01	TrAa01MblScCl	$HOCl \rightarrow HOCl(aq)$	k_exf(01,ind_HOCl)	see general notes*
H6201b_a01	TrAa01MblScCl	$HOCl(aq) \rightarrow HOCl$	k_exb(01,ind_HOCl)	see general notes*
H6300_a01	TrAa01MblClN	$N_2O_5 + Cl^-(aq) \rightarrow ClNO_2 + NO_3^-(aq)$	k_exf_N2O5(01) * 5.E2	Behnke et al. (1994), Behnke et al. (1997)
H6301_a01	TrAa01MblClN	$ClNO_3 \rightarrow HOCl(aq) + HNO_3(aq)$	k_exf_ClNO3(01) * C(ind_H2O_a01)	see general notes*
H6302_a01	TrAa01MblClN	$ClNO_3 + Cl^-(aq) \rightarrow Cl_2(aq) + NO_3^-(aq)$	k_exf_ClNO3(01) * 5.E2	see general notes*
H7000f_a01	TrAa01MblScBr	$Br_2 \rightarrow Br_2(aq)$	k_exf(01,ind_Br2)	see general notes*
H7000b_a01	TrAa01MblScBr	$Br_2(aq) \rightarrow Br_2$	k_exb(01,ind_Br2)	see general notes*
H7200f_a01	TrAa01MblScScmBr	$HBr \rightarrow HBr(aq)$	k_exf(01,ind_HBr)	see general notes*
H7200b_a01	TrAa01MblScScmBr	$HBr(aq) \rightarrow HBr$	k_exb(01,ind_HBr)	see general notes*
H7201f_a01	TrAa01MblScBr	$HOBr \rightarrow HOBr(aq)$	k_exf(01,ind_HOBr)	see general notes*
H7201b_a01	TrAa01MblScBr	$HOBr(aq) \rightarrow HOBr$	k_exb(01,ind_HOBr)	see general notes*
H7300_a01	TrAa01MblBrN	$N_2O_5 + Br^-(aq) \rightarrow BrNO_2 + NO_3^-(aq)$	k_exf_N2O5(01) * 3.E5	Behnke et al. (1994), Behnke et al. (1997)
H7301_a01	TrAa01MblBrN	$BrNO_3 \rightarrow HOBr(aq) + HNO_3(aq)$	k_exf_BrNO3(01) * C(ind_H2O_a01)	see general notes*
H7302_a01	TrAa01MblBrN	$BrNO_3 + Br^-(aq) \rightarrow Br_2(aq) + NO_3^-(aq)$	k_exf_BrNO3(01) * 3.E5	see general notes*
H7600f_a01	TrAa01MblScBrCl	$BrCl \rightarrow BrCl(aq)$	k_exf(01,ind_BrCl)	see general notes*
H7600b_a01	TrAa01MblScBrCl	$BrCl(aq) \rightarrow BrCl$	k_exb(01,ind_BrCl)	see general notes*
H7601_a01	TrAa01MblBrClN	$ClNO_3 + Br^-(aq) \rightarrow BrCl(aq) + NO_3^-(aq)$	k_exf_ClNO3(01) * 3.E5	see general notes*
H7602_a01	TrAa01MblBrClN	$BrNO_3 + Cl^-(aq) \rightarrow BrCl(aq) + NO_3^-(aq)$	k_exf_BrNO3(01) * 5.E2	see general notes*
H8000f_a01	TrAa01ScI	$I_2 \rightarrow I_2(aq)$	k_exf(01,ind_I2)	see general notes*
H8000b_a01	TrAa01ScI	$I_2(aq) \rightarrow I_2$	k_exb(01,ind_I2)	see general notes*
H8100f_a01	TrAa01MblScI	$IO \rightarrow IO(aq)$	k_exf(01,ind_IO)	see general notes*
H8100b_a01	TrAa01MblScI	$IO(aq) \rightarrow IO$	k_exb(01,ind_IO)	see general notes*
H8101_a01	TrAa01I	$OIO \rightarrow HOI(aq) + HO_2(aq)$	k_exf(01,ind_OIO)	see general notes*
H8102_a01	TrAa01I	$I_2O_2 \rightarrow HOI(aq) + H^+(aq) + IO_2^-(aq)$	k_exf(01,ind_I2O2)	see general notes*
H8200f_a01	TrAa01MblScI	$HOI \rightarrow HOI(aq)$	k_exf(01,ind_HOI)	see general notes*
H8200b_a01	TrAa01MblScI	$HOI(aq) \rightarrow HOI$	k_exb(01,ind_HOI)	see general notes*
H8201_a01	TrAa01MblScI	$HI \rightarrow H^+(aq) + I^-(aq)$	$k_{mt}(HI) \cdot lwc$	see general notes*
H8202_a01	TrAa01ScI	$HIO_3 \rightarrow IO_3^-(aq) + H^+(aq)$	$k_{mt}(HIO_3) \cdot lwc$	see general notes*
H8300_a01	TrAa01IN	$INO_2 \rightarrow HOI(aq) + HONO(aq)$	k_exf(01,ind_INO2)	see general notes*

Table 3: Reversible (Henry's law) equilibria and irreversible ("heterogenous") uptake

#	labels	reaction	rate coefficient	reference
H8301_a01	TrAa01MblIN	$INO_3 \rightarrow HOI(aq) + HNO_3(aq)$	k_exf(01,ind_INO3)	see general notes*
H8600f_a01	TrAa01MblScClI	$ICl \rightarrow ICl(aq)$	k_exf(01,ind_ICl)	see general notes*
H8600b_a01	TrAa01MblScClI	$ICl(aq) \rightarrow ICl$	k_exb(01,ind_ICl)	see general notes*
H8700f_a01	TrAa01MblScBrI	$IBr \rightarrow IBr(aq)$	k_exf(01,ind_IBr)	see general notes*
H8700b_a01	TrAa01MblScBrI	$IBr(aq) \rightarrow IBr$	k_exb(01,ind_IBr)	see general notes*
H9100f_a01	TrAa01MblScScmS	$SO_2 \rightarrow SO_2(aq)$	k_exf(01,ind_SO2)	see general notes*
H9100b_a01	TrAa01MblScScmS	$SO_2(aq) \rightarrow SO_2$	k_exb(01,ind_SO2)	see general notes*
H9200_a01	TrAa01MblScScmS	$H_2SO_4 \rightarrow H_2SO_4(aq)$	xnom7sulf*k_exf(01,ind_H2SO4)	see general notes*
H9400f_a01	TrAa01CS	$DMSO \rightarrow DMSO(aq)$	k_exf(01,ind_DMSO)	see general notes*
H9400b_a01	TrAa01CS	$DMSO(aq) \rightarrow DMSO$	k_exb(01,ind_DMSO)	see general notes*
H9401_a01	TrAa01MblS	$CH_3SO_3H \rightarrow CH_3SO_3^-(aq) + H^+(aq)$	k_exf(01,ind_CH3SO3H)	see general notes*
H9402f_a01	TrAa01CS	$DMS \rightarrow DMS(aq)$	k_exf(01,ind_DMS)	see general notes*
H9402b_a01	TrAa01CS	$DMS(aq) \rightarrow DMS$	k_exb(01,ind_DMS)	see general notes*
H10000f_a01	TrAa01Hg	$Hg \rightarrow Hg(aq)$	k_exf(01,ind_Hg)	see general notes*
H10000b_a01	TrAa01Hg	$Hg(aq) \rightarrow Hg$	k_exb(01,ind_Hg)	see general notes*
H10100f_a01	TrAa01Hg	$HgO \rightarrow HgO(aq)$	k_exf(01,ind_HgO)	see general notes*
H10100b_a01	TrAa01Hg	$HgO(aq) \rightarrow HgO$	k_exb(01,ind_HgO)	see general notes*
H10600f_a01	TrAa01ClHg	$HgCl_2 \rightarrow HgCl_2(aq)$	k_exf(01,ind_HgCl2)	see general notes*
H10600b_a01	TrAa01ClHg	$HgCl_2(aq) \rightarrow HgCl_2$	k_exb(01,ind_HgCl2)	see general notes*
H10700f_a01	TrAa01BrHg	$HgBr_2 \rightarrow HgBr_2(aq)$	k_exf(01,ind_HgBr2)	see general notes*
H10700b_a01	TrAa01BrHg	$HgBr_2(aq) \rightarrow HgBr_2$	k_exb(01,ind_HgBr2)	see general notes*
H10701f_a01	TrAa01BrClHg	$ClHgBr \rightarrow ClHgBr(aq)$	k_exf(01,ind_ClHgBr)	see general notes*
H10701b_a01	TrAa01BrClHg	$ClHgBr(aq) \rightarrow ClHgBr$	k_exb(01,ind_ClHgBr)	see general notes*
H10702f_a01	TrAa01BrHg	$BrHgOBr \rightarrow BrHgOBr(aq)$	k_exf(01,ind_BrHgOBr)	see general notes*
H10702b_a01	TrAa01BrHg	$BrHgOBr(aq) \rightarrow BrHgOBr$	k_exb(01,ind_BrHgOBr)	see general notes*
H10703f_a01	TrAa01BrClHg	$ClHgOBr \rightarrow ClHgOBr(aq)$	k_exf(01,ind_ClHgOBr)	see general notes*
H10703b_a01	TrAa01BrClHg	$ClHgOBr(aq) \rightarrow ClHgOBr$	k_exb(01,ind_ClHgOBr)	see general notes*

General notes

The forward (k_exf) and backward (k_exb) rate coefficients are calculated in subroutine mecca_aero_calc_k_ex in the file messy_mecca_aero.f90 using accommodation coefficients and Henry's law constants from chemprop (see chemprop.pdf).

For uptake of X (X = N_2O_5, $ClNO_3$, or $BrNO_3$) and subsequent reaction with H_2O, Cl^-, and Br^- in H3201, H6300, H6301, H6302, H7300, H7301, H7302, H7601, and H7602, we define:

$$k_{\mathrm{exf}}(\mathrm{X}) = \frac{k_{\mathrm{mt}}(\mathrm{X}) \times \mathrm{LWC}}{[\mathrm{H_2O}] + 5 \times 10^2 [\mathrm{Cl^-}] + 3 \times 10^5 [\mathrm{Br^-}]}$$

Here, k_{mt} = mass transfer coefficient, and LWC = liquid water content of the aerosol. The total uptake rate of X is only determined by k_{mt}. The factors only affect

the branching between hydrolysis and the halide reactions. The factor $5{\times}10^2$ was chosen such that the chloride reaction dominates over hydrolysis at about $[Cl^-] > 0.1$ M (see Fig. 3 in Behnke et al. (1997)), i.e. when the ratio $[H_2O]/[Cl^-]$ is less than $5{\times}10^2$. The ratio $5{\times}10^2/3{\times}10^5$ was chosen such that the reactions with chloride and bromide are roughly equal for sea water composition (Behnke et al., 1994). These ratios were measured for uptake of N_2O_5. Here, they are also used for $ClNO_3$ and $BrNO_3$.

Table 4: Heterogeneous reactions

#	labels	reaction	rate coefficient	reference
HET200	StHetN	$N_2O_5 + H_2O \rightarrow 2\ HNO_3$	khet_St(ihs_N2O5_H2O)	see general notes*
HET201	TrHetN	$N_2O_5 \rightarrow 2\ NO_3^-(cs) + 2\ H^+(cs)$	khet_Tr(iht_N2O5)	see general notes*
HET410	StHetCl	$HOCl + HCl \rightarrow Cl_2 + H_2O$	khet_St(ihs_HOCl_HCl)	see general notes*
HET420	StHetClN	$ClNO_3 + HCl \rightarrow Cl_2 + HNO_3$	khet_St(ihs_ClNO3_HCl)	see general notes*
HET421	StHetClN	$ClNO_3 + H_2O \rightarrow HOCl + HNO_3$	khet_St(ihs_ClNO3_H2O)	see general notes*
HET422	StHetClN	$N_2O_5 + HCl \rightarrow ClNO_2 + HNO_3$	khet_St(ihs_N2O5_HCl)	see general notes*
HET510	StHetBr	$HOBr + HBr \rightarrow Br_2 + H_2O$	khet_St(ihs_HOBr_HBr)	see general notes*
HET520	StHetBrN	$BrNO_3 + H_2O \rightarrow HOBr + HNO_3$	khet_St(ihs_BrNO3_H2O)	see general notes*
HET540	StHetBrClN	$ClNO_3 + HBr \rightarrow BrCl + HNO_3$	khet_St(ihs_ClNO3_HBr)	see general notes*
HET541	StHetBrClN	$BrNO_3 + HCl \rightarrow BrCl + HNO_3$	khet_St(ihs_BrNO3_HCl)	see general notes*
HET542	StHetBrCl	$HOCl + HBr \rightarrow BrCl + H_2O$	khet_St(ihs_HOCl_HBr)	see general notes*
HET543	StHetBrCl	$HOBr + HCl \rightarrow BrCl + H_2O$	khet_St(ihs_HOBr_HCl)	see general notes*
HET1001	StTrHetHg	$Hg \rightarrow Hg(cs)$	khet_Tr(iht_Hg) + khet_St(ihs_Hg)	see general notes*
HET1002	StTrHetHg	$HgO \rightarrow Hg(cs)$	khet_Tr(iht_RGM) + khet_St(ihs_RGM)	see general notes*
HET1003	StTrHetClHg	$HgCl \rightarrow Hg(cs) + LCHLORINE$	khet_Tr(iht_RGM) + khet_St(ihs_RGM)	see general notes*
HET1004	StTrHetClHg	$HgCl_2 \rightarrow Hg(cs) + 2\ LCHLORINE$	khet_Tr(iht_RGM) + khet_St(ihs_RGM)	see general notes*
HET1005	StTrHetBrHg	$HgBr \rightarrow Hg(cs) + LBROMINE$	khet_Tr(iht_RGM) + khet_St(ihs_RGM)	see general notes*
HET1006	StTrHetBrHg	$HgBr_2 \rightarrow Hg(cs) + 2\ LBROMINE$	khet_Tr(iht_RGM) + khet_St(ihs_RGM)	see general notes*
HET1007	StTrHetBrClHg	$ClHgBr \rightarrow Hg(cs) + LCHLORINE + LBROMINE$	khet_Tr(iht_RGM) + khet_St(ihs_RGM)	see general notes*
HET1008	StTrHetBrHg	$BrHgOBr \rightarrow Hg(cs) + 2\ LBROMINE$	khet_Tr(iht_RGM) + khet_St(ihs_RGM)	see general notes*
HET1009	StTrHetBrClHg	$ClHgOBr \rightarrow Hg(cs) + LCHLORINE + LBROMINE$	khet_Tr(iht_RGM) + khet_St(ihs_RGM)	see general notes*

General notes

Heterogeneous reaction rates are calculated with an external module (e.g., MECCA_KHET) and then supplied to the MECCA chemistry (see www.messy-interface.org for details)

Table 5: Acid-base and other equilibria

#	labels	reaction	$K_0[M^{m-n}]$	$-\Delta H/R[K]$	reference
EQ20_a01	TrAa01Sc	$HO_2 \rightleftharpoons O_2^- + H^+$	1.6E-5		Weinstein-Lloyd and Schwartz (1991)
EQ21_a01	TrAa01MblScScm	$H_2O \rightleftharpoons H^+ + OH^-$	1.0E-16	-6716	Chameides (1984)
EQ30_a01	TrAa01MblScScmN	$NH_4^+ \rightleftharpoons H^+ + NH_3$	5.88E-10	-2391	Chameides (1984)
EQ31_a01	TrAa01ScN	$HONO \rightleftharpoons H^+ + NO_2^-$	5.1E-4	-1260	Schwartz and White (1981)
EQ32_a01	TrAa01MblScScmN	$HNO_3 \rightleftharpoons H^+ + NO_3^-$	15	8700	Davis and de Bruin (1964)
EQ33_a01	TrAa01ScN	$HNO_4 \rightleftharpoons NO_4^- + H^+$	1.E-5		Warneck (1999)
EQ40_a01	TrAa01MblScScm	$CO_2 \rightleftharpoons H^+ + HCO_3^-$	4.3E-7	-913	Chameides (1984)*
EQ41_a01	TrAa01ScScm	$HCOOH \rightleftharpoons H^+ + HCOO^-$	1.8E-4		Weast (1980)
EQ60_a01	TrAa01Cl	$Cl_2^- \rightleftharpoons Cl + Cl^-$	7.3E-6		Yu (2004)
EQ61_a01	TrAa01MblScScmCl	$HCl \rightleftharpoons H^+ + Cl^-$	1.7E6	6896	Marsh and McElroy (1985)
EQ62_a01	TrAa01ScCl	$HOCl \rightleftharpoons H^+ + ClO^-$	3.2E-8		Lax (1969)
EQ70_a01	TrAa01Br	$Br_2^- \rightleftharpoons Br + Br^-$	2.54E-6	-2256	Liu et al. (2002)
EQ71_a01	TrAa01MblScScmBr	$HBr \rightleftharpoons H^+ + Br^-$	1.0E9		Lax (1969)
EQ72_a01	TrAa01ScBr	$HOBr \rightleftharpoons H^+ + BrO^-$	2.3E-9	-3091	Kelley and Tartar (1956)*
EQ73_a01	TrAa01MblBrCl	$BrCl + Cl^- \rightleftharpoons BrCl_2^-$	3.8	1191	Wang et al. (1994)
EQ74_a01	TrAa01MblBrCl	$BrCl + Br^- \rightleftharpoons Br_2Cl^-$	1.8E4	7457	Wang et al. (1994)
EQ75_a01	TrAa01MblBrCl	$Br_2 + Cl^- \rightleftharpoons Br_2Cl^-$	1.3	0	Wang et al. (1994)
EQ76_a01	TrAa01MblBrCl	$Br^- + Cl_2 \rightleftharpoons BrCl_2^-$	4.2E6	14072	Wang et al. (1994)
EQ80_a01	TrAa01MblScClI	$ICl + Cl^- \rightleftharpoons ICl_2^-$	7.7E1		Wang et al. (1989)
EQ81_a01	TrAa01MblScBrI	$IBr + Br^- \rightleftharpoons IBr_2^-$	2.9E2		Troy and Margerum (1991)
EQ82_a01	TrAa01MblScBrClI	$ICl + Br^- \rightleftharpoons IBr + Cl^-$	3.3E2		see note*
EQ90_a01	TrAa01MblScScmS	$SO_2 \rightleftharpoons H^+ + HSO_3^-$	1.7E-2	2090	Chameides (1984)
EQ91_a01	TrAa01MblScScmS	$HSO_3^- \rightleftharpoons H^+ + SO_3^{2-}$	6.0E-8	1120	Chameides (1984)
EQ92_a01	TrAa01MblScScmS	$HSO_4^- \rightleftharpoons H^+ + SO_4^{2-}$	1.2E-2	2720	Seinfeld and Pandis (1998)
EQ93_a01	TrAa01MblScScmS	$H_2SO_4 \rightleftharpoons H^+ + HSO_4^-$	1.0E3		Seinfeld and Pandis (1998)
EQ100_a01	TrAa01Hg	$Hg^{2+} + OH^- \rightleftharpoons HgOH^+$	4.0E10		Ammann and Pöschl (2007)
EQ101_a01	TrAa01Hg	$HgOH^+ + OH^- \rightleftharpoons Hg(OH)_2$	1.58E11		Ammann and Pöschl (2007)
EQ102_a01	TrAa01ClHg	$Hg^{2+} + Cl^- \rightleftharpoons HgCl^+$	5.8E6		Ammann and Pöschl (2007)
EQ103_a01	TrAa01ClHg	$HgCl^+ + Cl^- \rightleftharpoons HgCl_2$	2.5E6		Ammann and Pöschl (2007)
EQ104_a01	TrAa01ClHg	$HgOH^+ + Cl^- \rightleftharpoons Hg(OH)Cl$	2.69E7		Ammann and Pöschl (2007)
EQ105_a01	TrAa01BrHg	$Hg^{2+} + Br^- \rightleftharpoons HgBr^+$	1.1E9		Raofie and Ariya (2004)
EQ106_a01	TrAa01BrHg	$HgBr^+ + Br^- \rightleftharpoons HgBr_2$	2.5E8		Raofie and Ariya (2004)
EQ107_a01	TrAa01HgS	$Hg^{2+} + SO_3^{2-} \rightleftharpoons HgSO_3$	2.E13		van Loon et al. (2001)
EQ108_a01	TrAa01HgS	$HgSO_3 + SO_3^{2-} \rightleftharpoons Hg(SO_3)_2^{2-}$	1.E10		van Loon et al. (2001)

Table 5: Acid-base and other equilibria

#	labels	reaction	$K_0[M^{m-n}]$	$-\Delta H/R[K]$	reference
EQ110_a01	TrAa01Fe	$Fe^{3+} \rightleftharpoons FeOH^{2+} + H^+$	2.34E-3		de Laat and Le (2006)*
EQ111_a01	TrAa01Fe	$FeOH^{2+} \rightleftharpoons Fe(OH)_2^+ + H^+$	2E-4		de Laat and Le (2006)*
EQ112_a01	TrAa01Fe	$Fe^{3+} + H_2O_2 \rightleftharpoons FeHO_2^{2+} + H^+$	3.1E-3		de Laat and Le (2006)
EQ113_a01	TrAa01Fe	$FeOH^{2+} + H_2O_2 \rightleftharpoons Fe(OH)(HO_2)^+ + H^+$	2E-4		de Laat and Le (2006)
EQ114_a01	TrAa01ClFe	$Fe^{3+} + Cl^- \rightleftharpoons FeCl^{2+}$	6.61		de Laat and Le (2006)*
EQ115_a01	TrAa01ClFe	$FeCl^{2+} + Cl^- \rightleftharpoons FeCl_2^+$	1.6		de Laat and Le (2006)*
EQ116_a01	TrAa01FeS	$Fe^{3+} + SO_4^{2-} \rightleftharpoons FeSO_4^+$	120		Brand and van Eldik (1995)*
EQ117_a01	TrAa01FeS	$FeOH^{2+} + HSO_3^- \rightleftharpoons FeSO_3^+$	8.25E2		Warneck (2018)*
EQ118_a01	TrAa01FeS	$Fe^{2+} + SO_3^- \rightleftharpoons FeSO_3^+$	1.6E7		Warneck (2018)

Specific notes

EQ40_a01: For $pK_a(CO_2)$, see also Dickson and Millero (1987).

EQ72_a01: For $pK_a(HOBr)$, see also Keller-Rudek et al. (1992).

EQ82_a01: Thermodynamic calculations on the IBr/ICl equilibrium according to the data tables from Wagman et al. (1982):

ICl	+	Br^-	$\rightleftharpoons$	IBr	+	Cl^-
-17.1		-103.96	=	-4.2		-131.228

$$\frac{\Delta G}{[\mathrm{kJ/mol}]} = -4.2 - 131.228 - (-17.1 - 103.96) = -14.368$$

$$K = \frac{[\mathrm{IBr}] \times [\mathrm{Cl}^-]}{[\mathrm{ICl}] \times [\mathrm{Br}^-]} = \exp\left(\frac{-\Delta G}{RT}\right) = \exp\left(\frac{14368}{8.314 \times 298}\right) = 330$$

This means we have equal amounts of IBr and ICl when the $[Cl^-]/[Br^-]$ ratio equals 330.

EQ110_a01: See also K values listed in Tab. 2.5 of Brand and van Eldik (1995).

EQ111_a01: Equilibrium calculated from K_1 and K_2 in Tab. 1 of de Laat and Le (2006). Rate constant for back reaction assumed. See also K values listed in Tab. 2.5 of Brand and van Eldik (1995).

EQ114_a01: See also K values listed in Tab. 2.5 of Brand and van Eldik (1995).

EQ115_a01: Equilibrium calculated from K_{29} and K_{30} in Tab. 2 of de Laat and Le (2006). Rate constant for forward reaction assumed. See also K values listed in Tab. 2.5 of Brand and van Eldik (1995).

EQ116_a01: Equilibrium at $I = 1$ M. Rate constant for back reaction assumed.

EQ117_a01: Rate of equilibration assumed.

Table 6: Aqueous phase reactions

#	labels	reaction	k_0 $[M^{1-n}s^{-1}]$	$-E_a/R[K]$	reference
A1000_a01	TrAa01Sc	$O_3 + O_2^- \rightarrow OH + OH^-$	1.5E9		Sehested et al. (1983)
A2100_a01	TrAa01Sc	$OH + O_2^- \rightarrow OH^-$	1.0E10		Sehested et al. (1968)
A2101_a01	TrAa01Sc	$OH + OH \rightarrow H_2O_2$	5.5E9		Buxton et al. (1988)
A2102_a01	TrAa01Sc	$HO_2 + O_2^- \rightarrow H_2O_2 + OH^-$	1.0E8	-900	Christensen and Sehested (1988)
A2103_a01	TrAa01Sc	$HO_2 + OH \rightarrow H_2O$	7.1E9		Sehested et al. (1968)
A2104_a01	TrAa01Sc	$HO_2 + HO_2 \rightarrow H_2O_2$	9.7E5	-2500	Christensen and Sehested (1988)
A2105_a01	TrAa01Sc	$H_2O_2 + OH \rightarrow HO_2$	2.7E7	-1684	Christensen et al. (1982)
A3100_a01	TrAa01ScN	$NO_2^- + O_3 \rightarrow NO_3^-$	5.0E5	-6950	Damschen and Martin (1983)
A3101_a01	TrAa01ScN	$NO_2 + NO_2 \rightarrow HNO_3 + HONO$	1.0E8		Lee and Schwartz (1981)
A3102_a01	TrAa01ScN	$NO_4^- \rightarrow NO_2^-$	8.0E1		Warneck (1999)
A3200_a01	TrAa01ScN	$NO_2 + HO_2 \rightarrow HNO_4$	1.8E9		Warneck (1999)
A3201_a01	TrAa01ScN	$NO_2^- + OH \rightarrow NO_2 + OH^-$	1.0E10		Wingenter et al. (1999)
A3202_a01	TrAa01ScN	$NO_3 + OH^- \rightarrow NO_3^- + OH$	8.2E7	-2700	Exner et al. (1992)
A3203_a01	TrAa01ScN	$HONO + OH \rightarrow NO_2$	1.0E10		Barker et al. (1970)
A3204_a01	TrAa01ScN	$HONO + H_2O_2 + H^+ \rightarrow HNO_3 + H^+$	4.6E3	-6800	Damschen and Martin (1983)
A4100_a01	TrAa01Sc	$CO_3^- + O_2^- \rightarrow HCO_3^- + OH^-$	6.5E8		Ross et al. (1992)
A4101_a01	TrAa01Sc	$CO_3^- + H_2O_2 \rightarrow HCO_3^- + HO_2$	4.3E5		Ross et al. (1992)
A4102_a01	TrAa01Sc	$HCOO^- + CO_3^- \rightarrow 2\ HCO_3^- + HO_2$	1.5E5		Ross et al. (1992)
A4103_a01	TrAa01Sc	$HCOO^- + OH \rightarrow OH^- + HO_2 + CO_2$	3.1E9	-1240	Chin and Wine (1994)
A4104_a01	TrAa01Sc	$HCO_3^- + OH \rightarrow CO_3^-$	8.5E6		Ross et al. (1992)
A4105_a01	TrAa01Sc	$HCHO + OH \rightarrow HCOOH + HO_2$	7.7E8	-1020	Chin and Wine (1994)
A4106_a01	TrAa01Sc	$HCOOH + OH \rightarrow HO_2 + CO_2$	1.1E8	-991	Chin and Wine (1994)
A4107_a01	TrAa01Sc	$CH_3OO + O_2^- \rightarrow CH_3OOH + OH^-$	5.0E7		Jacob (1986)
A4108_a01	TrAa01Sc	$CH_3OO + HO_2 \rightarrow CH_3OOH$	4.3E5		Jacob (1986)
A4109_a01	TrAa01Sc	$CH_3OH + OH \rightarrow HCHO + HO_2$	9.7E8		Buxton et al. (1988)
A4110a_a01	TrAa01Sc	$CH_3OOH + OH \rightarrow CH_3OO$	2.7E7	-1715	Jacob (1986)
A4110b_a01	TrAa01Sc	$CH_3OOH + OH \rightarrow HCHO + OH$	1.1E7	-1715	Jacob (1986)
A6000_a01	TrAa01Cl	$Cl + Cl \rightarrow Cl_2$	8.8E7		Wu et al. (1980)
A6001_a01	TrAa01Cl	$Cl_2^- + Cl_2^- \rightarrow Cl_2 + 2\ Cl^-$	3.5E9		Yu (2004)
A6100_a01	TrAa01Cl	$Cl^- + O_3 \rightarrow ClO^-$	3.0E-3		Hoigné et al. (1985)
A6101_a01	TrAa01Cl	$Cl_2 + O_2^- \rightarrow Cl_2^-$	1.0E9		Bjergbakke et al. (1981)
A6102_a01	TrAa01Cl	$Cl_2^- + O_2^- \rightarrow 2\ Cl^-$	1.0E9		Jacobi (1996)*
A6200_a01	TrAa01Cl	$Cl \rightarrow H^+ + ClOH^-$	1.8E5		Yu (2004)
A6201_a01	TrAa01Cl	$Cl + H_2O_2 \rightarrow HO_2 + Cl^- + H^+$	2.7E7	-1684	Christensen et al. (1982)

Table 6: Aqueous phase reactions (...continued)

#	labels	reaction	k_0 $[M^{1-n}s^{-1}]$	$-E_a/R[K]$	reference
A6202_a01	TrAa01Cl	$Cl^- + OH \rightarrow ClOH^-$	4.2E9		Yu (2004)
A6203_a01	TrAa01Cl	$Cl_2 + HO_2 \rightarrow Cl_2^- + H^+$	1.0E9		Bjergbakke et al. (1981)
A6204_a01	TrAa01MblCl	$Cl_2 \rightarrow Cl^- + HOCl + H^+$	21.8	-8012	Wang and Margerum (1994)
A6205_a01	TrAa01Cl	$Cl_2^- + HO_2 \rightarrow 2\ Cl^- + H^+$	1.3E10		Jacobi (1996)
A6206_a01	TrAa01Cl	$HOCl + O_2^- \rightarrow Cl + OH^-$	7.5E6		Long and Bielski (1980)
A6207_a01	TrAa01Cl	$HOCl + HO_2 \rightarrow Cl$	7.5E6		Long and Bielski (1980)
A6208_a01	TrAa01MblCl	$HOCl + Cl^- + H^+ \rightarrow Cl_2$	2.2E4	-3508	Wang and Margerum (1994)
A6209_a01	TrAa01Cl	$ClOH^- \rightarrow Cl^- + OH$	6.0E9		Yu (2004)
A6210_a01	TrAa01Cl	$ClOH^- + H^+ \rightarrow Cl$	2.4E10		Yu (2004)
A6300_a01	TrAa01ClN	$Cl + NO_3^- \rightarrow NO_3 + Cl^-$	1.0E8		Buxton et al. (1999b)
A6301_a01	TrAa01ClN	$Cl^- + NO_3 \rightarrow NO_3^- + Cl$	3.4E8		Buxton et al. (1999b)*
A6302_a01	TrAa01ClN	$Cl_2^- + NO_2^- \rightarrow 2\ Cl^- + NO_2$	6.0E7		Jacobi et al. (1996)
A6400_a01	TrAa01Cl	$Cl_2^- + CH_3OOH \rightarrow 2\ Cl^- + H^+ + CH_3OO$	5.0E4		Jacobi et al. (1996)
A7000_a01	TrAa01Br	$Br_2^- + Br_2^- \rightarrow 2\ Br^- + Br_2$	1.9E9		Ross et al. (1992)
A7100_a01	TrAa01Br	$Br^- + O_3 \rightarrow BrO^-$	2.1E2	-4450	Haag and Hoigné (1983)
A7101_a01	TrAa01Br	$Br_2 + O_2^- \rightarrow Br_2^-$	5.6E9		Sutton and Downes (1972)
A7102_a01	TrAa01Br	$Br_2^- + O_2^- \rightarrow 2\ Br^-$	1.7E8		Wagner and Strehlow (1987)
A7200_a01	TrAa01Br	$Br^- + OH \rightarrow BrOH^-$	1.1E10		Zehavi and Rabani (1972)
A7201_a01	TrAa01Br	$Br_2 + HO_2 \rightarrow Br_2^- + H^+$	1.1E8		Sutton and Downes (1972)
A7202_a01	TrAa01MblBr	$Br_2 \rightarrow Br^- + HOBr + H^+$	9.7E1	-7457	Beckwith et al. (1996)
A7203_a01	TrAa01Br	$Br_2^- + HO_2 \rightarrow Br_2 + H_2O_2 + OH^-$	4.4E9		Matthew et al. (2003)
A7204_a01	TrAa01Br	$Br_2^- + H_2O_2 \rightarrow 2\ Br^- + H^+ + HO_2$	1.0E5		Jacobi (1996)
A7205_a01	TrAa01Br	$HOBr + O_2^- \rightarrow Br + OH^-$	3.5E9		Schwarz and Bielski (1986)
A7206_a01	TrAa01Br	$HOBr + HO_2 \rightarrow Br$	1.0E9		Herrmann et al. (1999)
A7207_a01	TrAa01Br	$HOBr + H_2O_2 \rightarrow Br^- + H^+$	1.2E6		Bichsel and von Gunten (1999)
A7208_a01	TrAa01MblBr	$HOBr + Br^- + H^+ \rightarrow Br_2$	1.6E10		Beckwith et al. (1996)
A7209a_a01	TrAa01Br	$BrOH^- \rightarrow Br^- + OH$	3.3E7		Zehavi and Rabani (1972)
A7209b_a01	TrAa01Br	$BrOH^- \rightarrow Br + OH^-$	4.2E6		Zehavi and Rabani (1972)
A7210_a01	TrAa01Br	$BrOH^- + H^+ \rightarrow Br$	4.4E10		Zehavi and Rabani (1972)
A7300_a01	TrAa01BrN	$Br^- + NO_3 \rightarrow Br + NO_3^-$	4.0E9		Neta and Huie (1986)
A7301_a01	TrAa01BrN	$Br_2^- + NO_2^- \rightarrow 2\ Br^- + NO_2$	1.7E7	-1720	Shoute et al. (1991)
A7400_a01	TrAa01Br	$Br_2^- + CH_3OOH \rightarrow 2\ Br^- + H^+ + CH_3OO$	1.0E5		Jacobi (1996)*
A7601_a01	TrAa01BrCl	$Br^- + ClO^- + H^+ \rightarrow BrCl + OH^-$	3.7E10		Kumar and Margerum (1987)
A7602_a01	TrAa01MblBrCl	$Br^- + HOCl + H^+ \rightarrow BrCl$	1.32E6		Kumar and Margerum (1987)

Table 6: Aqueous phase reactions (...continued)

#	labels	reaction	k_0 $[M^{1-n}s^{-1}]$	$-E_a/R[K]$	reference
A7603_a01	TrAa01MblBrCl	$HOBr + Cl^- + H^+ \rightarrow BrCl$	2.3E10		Liu and Margerum (2001)*
A7604_a01	TrAa01MblBrCl	$BrCl \rightarrow Cl^- + HOBr + H^+$	3.0E6		Liu and Margerum (2001)
A8100_a01	TrAa01MblI	$I^- + O_3 \rightarrow HOI + OH^-$	4.2E9	-9311	Magi et al. (1997)
A8101_a01	TrAa01MblI	$IO + IO \rightarrow HOI + IO_2^- + H^+$	1.5E9		Buxton et al. (1986)
A8200_a01	TrAa01MblI	$IO_2^- + H_2O_2 \rightarrow IO_3^-$	6.0E1		Furrow (1987)
A8201_a01	TrAa01I	$HOI + IO_2^- \rightarrow IO_3^- + I^- + H^+$	6.0E2		Chinake and Simoyi (1996)
A8202_a01	TrAa01MblI	$HOI + I^- + H^+ \rightarrow I_2$	4.4E12		Eigen and Kustin (1962)
A8203_a01	TrAa01MblI	$IO_2^- + I^- + H^+ \rightarrow 2\ HOI + OH^-$	2.0E10		Edblom et al. (1987)
A8600_a01	TrAa01MblClI	$ICl \rightarrow HOI + Cl^- + H^+$	2.4E6		Wang et al. (1989)
A8601_a01	TrAa01MblClI	$I^- + HOCl + H^+ \rightarrow ICl$	3.5E11		Nagy et al. (1988)
A8602_a01	TrAa01ClI	$IO_2^- + HOCl \rightarrow IO_3^- + Cl^- + H^+$	1.5E3		Lengyel et al. (1996)
A8603_a01	TrAa01MblClI	$HOI + Cl^- + H^+ \rightarrow ICl$	2.9E10		Wang et al. (1989)
A8604_a01	TrAa01ClI	$HOI + Cl_2 \rightarrow IO_2^- + 2\ Cl^- + 3H^+$	1.0E6		Lengyel et al. (1996)
A8605_a01	TrAa01ClI	$HOI + HOCl \rightarrow IO_2^- + Cl^- + 2\ H^+$	5.0E5		Citri and Epstein (1988)
A8606_a01	TrAa01ClI	$ICl + I^- \rightarrow I_2 + Cl^-$	1.1E9		Margerum et al. (1986)
A8700_a01	TrAa01MblBrI	$IBr \rightarrow HOI + H^+ + Br^-$	8.0E5		Troy et al. (1991)
A8701_a01	TrAa01MblBrI	$I^- + HOBr \rightarrow IBr + OH^-$	5.0E9		Troy and Margerum (1991)
A8702_a01	TrAa01BrI	$IO_2^- + HOBr \rightarrow IO_3^- + Br^- + H^+$	1.0E6		Chinake and Simoyi (1996)
A8703_a01	TrAa01MblBrI	$HOI + Br^- + H^+ \rightarrow IBr$	3.3E12		Troy et al. (1991)
A8704_a01	TrAa01BrI	$HOI + HOBr \rightarrow IO_2^- + Br^- + 2\ H^+$	1.0E6		Chinake and Simoyi (1996)
A8705_a01	TrAa01BrI	$IBr + I^- \rightarrow I_2 + Br^-$	2.0E9		Faria et al. (1993)
A9100_a01	TrAa01ScS	$SO_3^- + O_2 \rightarrow SO_5^-$	1.5E9		Huie and Neta (1987)
A9101_a01	TrAa01MblScScmS	$SO_3^{2-} + O_3 \rightarrow SO_4^{2-}$	1.5E9	-5300	Hoffmann (1986)
A9102_a01	TrAa01ScS	$SO_4^- + O_2^- \rightarrow SO_4^{2-}$	3.5E9		Jiang et al. (1992)
A9103_a01	TrAa01ScS	$SO_4^- + SO_3^{2-} \rightarrow SO_3^- + SO_4^{2-}$	4.6E8		Huie and Neta (1987)
A9104_a01	TrAa01ScS	$SO_5^- + O_2^- \rightarrow HSO_5^- + OH^-$	2.3E8		Buxton et al. (1996)
A9105_a01	TrAa01S	$SO_5^- + SO_3^{2-} \rightarrow .72\ SO_4^- + .72\ SO_4^{2-} + .28\ SO_3^- + .28\ HSO_5^- + .28\ OH^-$	1.3E7		Huie and Neta (1987), Deister and Warneck (1990)*
A9106_a01	TrAa01S	$SO_5^- + SO_5^- \rightarrow O_2 + SO_4^{2-} + LSULFUR$	1.0E8		Ross et al. (1992)*
A9200_a01	TrAa01ScS	$SO_3^{2-} + OH \rightarrow SO_3^- + OH^-$	5.5E9		Buxton et al. (1988)
A9201_a01	TrAa01ScS	$SO_4^- + OH \rightarrow HSO_5^-$	1.0E9		Jiang et al. (1992)
A9202_a01	TrAa01ScS	$SO_4^- + HO_2 \rightarrow SO_4^{2-} + H^+$	3.5E9		Jiang et al. (1992)
A9203_a01	TrAa01ScS	$SO_4^- + H_2O \rightarrow SO_4^{2-} + H^+ + OH$	1.1E1	-1110	Herrmann et al. (1995)
A9204_a01	TrAa01ScS	$SO_4^- + H_2O_2 \rightarrow SO_4^{2-} + H^+ + HO_2$	1.2E7		Wine et al. (1989)

Table 6: Aqueous phase reactions (...continued)

#	labels	reaction	k_0 $[M^{1-n}s^{-1}]$	$-E_a/R[K]$	reference
A9205_a01	TrAa01ScS	$HSO_3^- + O_2^- \rightarrow SO_4^{2-} + OH$	3.0E3		see note*
A9206_a01	TrAa01MblScScmS	$HSO_3^- + O_3 \rightarrow SO_4^{2-} + H^+$	3.7E5	-5500	Hoffmann (1986)
A9207_a01	TrAa01ScS	$HSO_3^- + OH \rightarrow SO_3^-$	4.5E9		Buxton et al. (1988)
A9208_a01	TrAa01ScS	$HSO_3^- + HO_2 \rightarrow SO_4^{2-} + OH + H^+$	3.0E3		see note*
A9209_a01	TrAa01MblScScmS	$HSO_3^- + H_2O_2 \rightarrow SO_4^{2-} + H^+$	5.2E6	-3650	Martin and Damschen (1981)
A9210_a01	TrAa01ScS	$HSO_3^- + SO_4^- \rightarrow SO_3^- + SO_4^{2-} + H^+$	8.0E8		Huie and Neta (1987)
A9211_a01	TrAa01S	$HSO_3^- + SO_5^- \rightarrow .75\ SO_4^- + .75\ SO_4^{2-} + .75\ H^+ + .25\ SO_3^- + .25\ HSO_5^-$	1.0E5		Huie and Neta (1987)
A9212_a01	TrAa01ScS	$HSO_3^- + HSO_5^- + H^+ \rightarrow 2\ HSO_4^- + H^+$	7.1E6		Betterton and Hoffmann (1988)
A9301_a01	TrAa01ScNS	$SO_4^- + NO_3^- \rightarrow SO_4^{2-} + NO_3$	5.0E4		Exner et al. (1992)
A9302_a01	TrAa01ScNS	$SO_4^{2-} + NO_3 \rightarrow NO_3^- + SO_4^-$	1.0E5		Løgager et al. (1993)
A9304_a01	TrAa01ScNS	$HSO_3^- + NO_3 \rightarrow SO_3^- + NO_3^- + H^+$	1.4E9	-2000	Exner et al. (1992)
A9305_a01	TrAa01ScNS	$HSO_3^- + HNO_4 \rightarrow HSO_4^- + NO_3^- + H^+$	3.1E5		Warneck (1999)
A9400_a01	TrAa01ScS	$SO_3^{2-} + HCHO \rightarrow CH_2OHSO_3^- + OH^-$	1.4E4		Boyce and Hoffmann (1984)*
A9401_a01	TrAa01ScS	$SO_3^{2-} + CH_3OOH + H^+ \rightarrow SO_4^{2-} + H^+ + CH_3OH$	1.6E7	-3800	Lind et al. (1987)
A9402_a01	TrAa01ScS	$HSO_3^- + HCHO \rightarrow CH_2OHSO_3^-$	4.3E-1		Boyce and Hoffmann (1984)*
A9403_a01	TrAa01ScS	$HSO_3^- + CH_3OOH + H^+ \rightarrow HSO_4^- + H^+ + CH_3OH$	1.6E7	-3800	Lind et al. (1987)
A9404_a01	TrAa01ScS	$CH_2OHSO_3^- + OH^- \rightarrow SO_3^{2-} + HCHO$	3.6E3		Seinfeld and Pandis (1998)
A9600_a01	TrAa01ClS	$SO_3^{2-} + Cl_2^- \rightarrow SO_3^- + 2\ Cl^-$	6.2E7		Jacobi et al. (1996)
A9601_a01	TrAa01MblClS	$SO_3^{2-} + HOCl \rightarrow Cl^- + HSO_4^-$	7.6E8		Fogelman et al. (1989)
A9602_a01	TrAa01ClS	$SO_4^- + Cl^- \rightarrow SO_4^{2-} + Cl$	2.5E8		Buxton et al. (1999a)
A9603_a01	TrAa01ClS	$SO_4^{2-} + Cl \rightarrow SO_4^- + Cl^-$	2.1E8		Buxton et al. (1999a)
A9604_a01	TrAa01ClS	$HSO_3^- + Cl_2^- \rightarrow SO_3^- + 2\ Cl^- + H^+$	4.7E8	-1082	Shoute et al. (1991)
A9605_a01	TrAa01MblClS	$HSO_3^- + HOCl \rightarrow Cl^- + HSO_4^- + H^+$	7.6E8		see note*
A9606_a01	TrAa01ClS	$HSO_5^- + Cl^- \rightarrow HOCl + SO_4^{2-}$	1.8E-3	-7352	Fortnum et al. (1960)
A9700_a01	TrAa01BrS	$SO_3^{2-} + Br_2^- \rightarrow 2\ Br^- + SO_3^-$	2.2E8	-649	Shoute et al. (1991)
A9701_a01	TrAa01BrS	$SO_3^{2-} + BrO^- \rightarrow Br^- + SO_4^{2-}$	1.0E8		Troy and Margerum (1991)
A9702_a01	TrAa01MblBrS	$SO_3^{2-} + HOBr \rightarrow Br^- + HSO_4^-$	5.0E9		Troy and Margerum (1991)
A9703_a01	TrAa01BrS	$SO_4^- + Br^- \rightarrow Br + SO_4^{2-}$	2.1E9		Jacobi (1996)
A9704_a01	TrAa01BrS	$HSO_3^- + Br_2^- \rightarrow 2\ Br^- + H^+ + SO_3^-$	6.3E7	-782	Shoute et al. (1991)
A9705_a01	TrAa01MblBrS	$HSO_3^- + HOBr \rightarrow Br^- + HSO_4^- + H^+$	5.0E9		see note*
A9706_a01	TrAa01BrS	$HSO_5^- + Br^- \rightarrow HOBr + SO_4^{2-}$	1.0E0	-5338	Fogelman et al. (1989)
A9800_a01	TrAa01IS	$HSO_3^- + I_2 \rightarrow 2\ I^- + HSO_4^- + 2\ H^+$	1.7E9		Yiin and Margerum (1990)
A10100_a01	TrAa01Hg	$Hg + O_3 \rightarrow HgO + O_2$	4.7E7		Munthe (1992)

Table 6: Aqueous phase reactions (...continued)

#	labels	reaction	k_0 $[M^{1-n}s^{-1}]$	$-E_a/R[K]$	reference
A10200_a01	TrAa01Hg	$HgO + H^+ \rightarrow Hg^{2+} + OH^-$	1.0E10		Pleijel and Munthe (1995)
A10201_a01	TrAa01Hg	$Hg + OH \rightarrow Hg^+ + OH^-$	2.0E9		Lin and Pehkonen (1997)
A10202_a01	TrAa01Hg	$Hg^+ + OH \rightarrow Hg^{2+} + OH^-$	1.0E10		Lin and Pehkonen (1997)
A10203_a01	TrAa01Hg	$Hg^{2+} + HO_2 \rightarrow Hg^+ + O_2 + H^+$	1.7E4		Enami et al. (2007)
A10204_a01	TrAa01Hg	$Hg^+ + HO_2 \rightarrow Hg + O_2 + H^+$	1.0E10		Lin and Pehkonen (1997)
A10600_a01	TrAa01ClHg	$Hg + HOCl \rightarrow Hg^{2+} + Cl^- + OH^-$	2.09E6		Lin and Pehkonen (1998)
A10601_a01	TrAa01ClHg	$Hg + ClO^- \rightarrow Hg^{2+} + Cl^- + 2\ OH^-$	1.99E6		Lin and Pehkonen (1998)
A10700_a01	TrAa01BrHg	$Hg + HOBr \rightarrow Hg^{2+} + Br^- + OH^-$	0.279		Wang and Pehkonen (2004)
A10701_a01	TrAa01BrHg	$Hg + BrO^- \rightarrow Hg^{2+} + Br^- + 2\ OH^-$	0.273		Wang and Pehkonen (2004)
A10702_a01	TrAa01BrHg	$Hg + Br_2 \rightarrow Hg^{2+} + 2\ Br^-$	0.196		Wang and Pehkonen (2004)
A10900_a01	TrAa01HgS	$HgSO_3 \rightarrow Hg + HSO_4^- + H^+$	0.0106		van Loon et al. (2000)
A11101_a01	TrAa01Fe	$Fe^{2+} + O_2^- \rightarrow Fe^{3+} + HO2^- + OH^-$	1E7		de Laat and Le (2006)
A11102_a01	TrAa01Fe	$Fe^{3+} + O_2^- \rightarrow O_2 + Fe^{2+}$	5E7		de Laat and Le (2006)
A11103_a01	TrAa01Fe	$Fe^{2+} + O_3 \rightarrow FeO^{2+} + O_2$	8.2E5		Løgager et al. (1992)
A11201a_a01	TrAa01Fe	$Fe^{2+} + OH \rightarrow Fe^{3+} + OH^-$	2.7E8		de Laat and Le (2006)
A11201b_a01	TrAa01Fe	$FeOH^+ + OH \rightarrow Fe^{3+} + 2\ OH^-$	2.7E8		de Laat and Le (2006)
A11202a_a01	TrAa01Fe	$Fe^{2+} + H_2O_2 \rightarrow Fe^{3+} + OH + OH^-$	5.5E1		de Laat and Le (2006)
A11202b_a01	TrAa01Fe	$FeOH^+ + H_2O_2 \rightarrow Fe^{3+} + OH + 2\ OH^-$	5.9E6		de Laat and Le (2006)
A11203_a01	TrAa01Fe	$FeHO_2^{2+} \rightarrow Fe^{2+} + HO_2$	2.3E-3		de Laat and Le (2006)
A11204_a01	TrAa01Fe	$Fe(OH)(HO_2)^+ \rightarrow Fe^{2+} + HO_2 + OH^-$	2.3E-3		de Laat and Le (2006)
A11206_a01	TrAa01Fe	$Fe^{2+} + HO_2 \rightarrow Fe^{3+} + HO2^-$	1.2E6		de Laat and Le (2006)
A11208a_a01	TrAa01Fe	$FeOH^{2+} + O_2^- \rightarrow Fe^{2+} + O_2 + OH^-$	1.5E8		Rush and Bielski (1985)
A11208b_a01	TrAa01Fe	$Fe(OH)_2^+ + O_2^- \rightarrow Fe^{2+} + O_2 + 2\ OH^-$	1.5E8		Rush and Bielski (1985)
A11209_a01	TrAa01Fe	$Fe^{2+} + O_2^- \rightarrow Fe^{3+} + H_2O_2 + 2\ OH^-$	1.0E7		Rush and Bielski (1985)
A11210_a01	TrAa01Fe	$Fe^{2+} + OH \rightarrow FeOH^{2+}$	4.3E8		Christensen and Sehested (1981)
A11211_a01	TrAa01Fe	$FeO^{2+} + H_2O_2 \rightarrow Fe^{3+} + HO_2 + OH^-$	9.5E3		Løgager et al. (1992)
A11212_a01	TrAa01Fe	$FeO^{2+} \rightarrow Fe^{3+} + OH + OH^-$	1.3E-2		Løgager et al. (1992)
A11213_a01	TrAa01Fe	$FeO^{2+} + HO_2 \rightarrow Fe^{3+} + O_2 + OH^-$	2.0E6		Løgager et al. (1992)
A11214_a01	TrAa01Fe	$FeO^{2+} + OH \rightarrow Fe^{3+} + HO2^-$	1.0E7		Løgager et al. (1992)
A11215_a01	TrAa01Fe	$FeO^{2+} + Fe^{2+} \rightarrow 2\ Fe^{3+} + 2\ OH^-$	1.4E5		Løgager et al. (1992)
A11216_a01	TrAa01Fe	$FeO^{2+} + Fe^{2+} \rightarrow Fe(OH)_2Fe^{4+}$	1.8E4		Jacobsen et al. (1997)
A11217_a01	TrAa01Fe	$Fe(OH)_2Fe^{4+} + H^+ \rightarrow 2\ Fe^{3+} + OH^-$	2.0		Jacobsen et al. (1997)
A11218_a01	TrAa01Fe	$Fe(OH)_2Fe^{4+} \rightarrow 2\ Fe^{3+} + 2\ OH^-$	0.49		Jacobsen et al. (1997)
A11301_a01	TrAa01FeN	$FeO^{2+} + HONO \rightarrow Fe^{3+} + NO_2 + OH^-$	1.1E4		Jacobsen et al. (1998)
A11302_a01	TrAa01FeN	$Fe^{2+} + NO_3 \rightarrow Fe^{3+} + NO_3^-$	8.0E6		Herrmann et al. (2000)*

Table 6: Aqueous phase reactions (...continued)

#	labels	reaction	k_0 $[M^{1-n_s}s^{-1}]$	$-E_a/R[K]$	reference
A11601_a01	TrAa01ClFe	$Fe^{2+} + Cl \rightarrow Fe^{3+} + Cl^-$	5.9E9		Jayson et al. (1973)
A11602a_a01	TrAa01ClFe	$Fe^{2+} + Cl_2^- \rightarrow Fe^{3+} + 2\ Cl^-$	1E7		Thornton and Laurence (1973)
A11602b_a01	TrAa01ClFe	$Fe^{2+} + Cl_2^- \rightarrow FeCl^{2+} + Cl^-$	4E6		Thornton and Laurence (1973)
A11603a_a01	TrAa01ClFe	$FeCl^+ + HO_2 \rightarrow Fe^{3+} + Cl^- + HO2^-$	1.2E6		de Laat and Le (2006)
A11603b_a01	TrAa01ClFe	$FeCl^+ + O_2^- \rightarrow Fe^{3+} + Cl^- + HO2^- + OH^-$	1E7		de Laat and Le (2006)
A11604a_a01	TrAa01ClFe	$FeCl^{2+} + HO_2 \rightarrow Fe^{2+} + Cl^- + O_2 + H^+$	2E4		de Laat and Le (2006)
A11604b_a01	TrAa01ClFe	$FeCl_2^+ + HO_2 \rightarrow Fe^{2+} + 2\ Cl^- + O_2 + H^+$	2E4		de Laat and Le (2006)
A11604c_a01	TrAa01ClFe	$FeCl^{2+} + O_2^- \rightarrow Fe^{2+} + Cl^- + O_2$	5E7		de Laat and Le (2006)
A11604d_a01	TrAa01ClFe	$FeCl_2^+ + O_2^- \rightarrow Fe^{2+} + 2\ Cl^- + O_2$	5E7		de Laat and Le (2006)
A11605_a01	TrAa01ClFe	$FeO^{2+} + Cl^- \rightarrow Fe^{3+} + Cl + 2\ OH^-$	1E2		Jacobsen et al. (1998)*
A11701_a01	TrAa01BrFe	$Fe^{2+} + Br_2^- \rightarrow Fe^{3+} + 2\ Br^-$	3.6E6		Thornton and Laurence (1973)
A11901_a01	TrAa01FeS	$FeO^{2+} + SO_2 \rightarrow Fe^{3+} + SO_3^-$	4.5E5		Jacobsen et al. (1998)*
A11902_a01	TrAa01FeS	$FeO^{2+} + HSO_3^- \rightarrow Fe^{3+} + SO_3^- + OH^-$	2.5E5		Jacobsen et al. (1998)*
A11903_a01	TrAa01FeS	$FeOH^{2+} + HSO_3^- \rightarrow Fe^{2+} + SO_3^- + H_2O$	30		Ziajka et al. (1994)
A11904_a01	TrAa01FeS	$Fe^{2+} + SO_5^- \rightarrow FeOH^{2+} + HSO_5^-$	8E5		Ziajka et al. (1994)*
A11905_a01	TrAa01FeS	$Fe^{2+} + HSO_5^- \rightarrow FeOH^{2+} + SO_4^-$	3.0E4		Gilbert and Stell (1990)
A11906_a01	TrAa01FeS	$Fe^{2+} + SO_4^- \rightarrow FeSO_4^+$	3.6E7		McElroy and Waygood (1990)*
A11907_a01	TrAa01FeS	$FeOH^{2+} + SO_3^- \rightarrow Fe^{2+} + HSO_4^-$	3E7		Warneck (2018)
A11908_a01	TrAa01FeS	$FeSO_3^+ + SO_3^- \rightarrow Fe^{2+} + SO_4^{2-} + SO_2$	2.16E6		Warneck (2018)*

Specific notes

A6102_a01: Jacobi (1996) found an upper limit of 6E9 and cite an upper limit from another study of 2E9. Here, we set the rate coefficient to 1E9.

A6301_a01: There is also an earlier study by Exner et al. (1992) which found a smaller rate coefficient but did not consider the back reaction.

A7400_a01: Assumed to be the same as for Br_2^- + H_2O_2.

A7603_a01: The rate coefficient is defined as backward reaction divided by equilibrium constant.

A9105_a01: The rate coefficient for the sum of the paths (leading to either HSO_5^- or SO_4^{2-}) is from Huie and Neta (1987), the ratio 0.28/0.72 is from Deister and Warneck (1990).

A9106_a01: See also: (Huie and Neta, 1987; Warneck, 1991). If this reaction produces a lot of SO_4^-, it will have an effect. However, we currently assume only the stable $S_2O_8^{2-}$ as product. Since $S_2O_8^{2-}$ is not treated explicitly in the mechanism, SO_4^{2-} is used as a proxy and the second sulfur atom is put into the lumped LSULFUR.

A9205_a01: D. Sedlak, pers. comm. (1993).

A9208_a01: D. Sedlak, pers. comm. (1993).

A9400_a01: Product $2.48 \times 10^7 \times 5.5 \times 10^{-4}$ considering the hydrated form of HCHO.

A9402_a01: Product $790 \times 5.5 \times 10^{-4}$ considering the hydrated form of HCHO.

A9605_a01: Assumed to be the same as for SO_3^{2-} + HOCl.

A9705_a01: Assumed to be the same as for SO_3^{2-} + HOBr.

A11302_a01: value from Pikaev et al. (1974)

A11605_a01: products assumed

A11901_a01: products assumed

A11902_a01: products assumed

A11904_a01: Assumed. Note that CAPRAM 2.4 lists k=4.3E7 from Herrmann Air Pollution Research Report 57 and it also lists k= 2.65E7 from Williams PhD 1996 http://lib.leeds.ac.uk/record=b1835184~S5. Brand and van Eldik (1995) also list k=3.56E4 from Waygood EUROTRAC 1992 report.

A11906_a01: 3E8*6500/(48000+6500)

A11908_a01: Assuming that the intermediate $S_2O_6^{2-}$ dissociates quickly.

References

Albaladejo, J., Jiménez, E., Notario, A., Cabañas, B., and Martínez, E.: CH_3O yield in the $CH_3 + O_3$ reaction using the LP/LIF technique at room temperature, J. Phys. Chem. A, 106, 2512–2519, doi:10.1021/jp012249o, 2002.

Amedro, D., Berasategui, M., Bunkan, A. J. C., Pozzer, A., Lelieveld, J., and Crowley, J. N.: Kinetics of the OH + NO_2 reaction: effect of water vapour and new parameterization for global modelling, Atmos. Chem. Phys., 20, 3091–3105, doi:10.5194/acp-20-3091-2020, 2020.

Ammann, M. and Pöschl, U.: Kinetic model framework for aerosol and cloud surface chemistry and gas-particle interactions - Part 2: exemplary practical applications and numerical simulations, Atmos. Chem. Phys., 7, 6025–6045, doi:10.5194/ACP-7-6025-2007, 2007.

Anderson, L. C. and Fahey, D. W.: Studies with $ClONO_2$: Thermal dissociation rate and catalytic conversion to NO using an NO/O_3 chemiluminescence detector, J. Phys. Chem., 94, 644–652, doi:10.1021/J100365A027, 1990.

Andrews, D. U., Heazlewood, B. R., Maccarone, A. T., Conroy, T., Payne, R. J., Jordan, M. J. T., and Kable, S. H.: Photo-tautomerization of acetaldehyde to vinyl alcohol: a potential route to tropospheric acids, Science, 337, 1203–1206, doi:10.1126/science.1220712, 2012.

Ariya, P. A., Khalizov, A., and Gidas, A.: Reactions of gaseous mercury with atomic and molecular halogens: Kinetics, product studies, and atmospheric implications, J. Phys. Chem. A, 106, 7310–7320, doi:10.1021/JP020719O, 2002.

Aschmann, S. M., Nishino, N., Arey, J., and Atkinson, R.: Products of the OH radical-initiated reactions of furan, 2- and 3-methylfuran, and 2,3- and 2,5-dimethylfuran in the presence of NO, J. Phys. Chem. A, 118, 457–466, doi:10.1021/jp410345k, 2014.

Atkinson, R.: Gas-phase tropospheric chemistry of volatile organic compounds: 1. Alkanes and alkenes, J. Phys. Chem. Ref. Data, 26, 215–290, doi:10.1063/1.556012, 1997.

Atkinson, R.: Kinetics of the gas-phase reactions of OH radicals with alkanes and cycloalkanes, Atmos. Chem. Phys., 3, 2233–2307, doi:10.5194/ACP-3-2233-2003, 2003.

Atkinson, R. and Arey, J.: Atmospheric degradation of volatile organic compounds, Chem. Rev., 103, 4605–4638, doi:10.1021/cr0206420, 2003.

Atkinson, R., Baulch, D. L., Cox, R. A., Crowley, J. N., Hampson, R. F., Hynes, R. G., Jenkin, M. E., Rossi, M. J., and Troe, J.: Evaluated kinetic and photochemical data for atmospheric chemistry: Volume I – gas phase reactions of O_x, HO_x, NO_x and SO_x species, Atmos. Chem. Phys., 4, 1461–1738, doi:10.5194/ACP-4-1461-2004, 2004.

Atkinson, R., Baulch, D. L., Cox, R. A., Crowley, J. N., Hampson, R. F., Hynes, R. G., Jenkin, M. E., Rossi, M. J., Troe, J., and IUPAC Subcommittee: Evaluated kinetic and photochemical data for atmospheric chemistry: Volume II – gas phase reactions of organic species, Atmos. Chem. Phys., 6, 3625–4055, doi:10.5194/ACP-6-3625-2006, 2006.

Atkinson, R., Baulch, D. L., Cox, R. A., Crowley, J. N., Hampson, R. F., Hynes, R. G., Jenkin, M. E., Rossi, M. J., and Troe, J.: Evaluated kinetic and photochemical data for atmospheric chemistry: Volume III – gas phase reactions of inorganic halogens, Atmos. Chem. Phys., 7, 981–1191, doi:10.5194/ACP-7-981-2007, 2007.

Baeza-Romero, M. T., Glowacki, D. R., Blitz, M. A., Heard, D., Pilling, M. J., Rickard, A. R., and Seakins, P. W.: A combined experimental and theoretical study of the reaction between methylglyoxal and OH/OD radical: OH regeneration, Phys. Chem. Chem. Phys., 9, 4114–4128, doi:10.1039/b702916k, 2007.

Bailey, S. M., Barth, C. A., and Solomon, S. C.: A model of nitric oxide in the lower thermosphere, J. Geophys. Res., 107, doi:10.1029/2001JA000258, 2002.

Bale, C. S. E., Canosa-Mas, C. E., Shallcross, D. E., and Wayne, R. P.: A discharge-flow study of the kinetics of the reactions of IO with CH_3O_2 and CF_3O_2, Phys. Chem. Chem. Phys., 7, 2164–2172, doi:10.1039/B501903F, 2005.

Banic, C. M., Beauchamp, S. T., Tordon, R. J., Schroeder, W. H., Steffen, A., Anlauf, K. A., and Wong, H. K. T.: Vertical distribution of gaseous elemental mercury in Canada, J. Geophys. Res., 108D, 4264, doi:10.1029/2002JD002116, 2003.

Barker, G. C., Fowles, P., and Stringer, B.: Pulse radiolytic induced transient electrical conductance in liquid solutions, Trans. Faraday Soc., 66, 1509–1519, doi:10.1039/TF9706601509, 1970.

Barnes, I., Becker, K. H., Fink, E. H., Reimer, A., Zabel, F., and Niki, H.: FTIR spectroscopic study of the gas-phase reaction of HO_2 with H_2CO, Chem. Phys. Lett., 115, 1–8, doi:10.1016/0009-2614(85)80091-9, 1985.

Barnes, I., Becker, K. H., and Zhu, T.: Near UV absorption-spectra and photolysis products of difunctional organic nitrates – possible importance as NO_x reservoirs, J. Atmos. Chem., 17, 353–373, doi:10.1007/BF00696854, 1993.

Barone, S. B., Turnipseed, A. A., and Ravishankara, A. R.: Role of adducts in the atmospheric oxidation of dimethyl sulfide, Faraday Discuss., 100, 39–54, doi:10.1039/FD9950000039, 1995.

Barth, C. A.: Nitric oxide in the lower thermosphere, Planet. Space Sci., 40, 315–336, doi:10.1016/0032-0633(92)90067-X, 1992.

Bates, K. H., Crounse, J. D., St. Clair, J. M., Bennett, N. B., Nguyen, T. B., Seinfeld, J. H., Stoltz, B. M., and Wennberg, P. O.: Gas phase production and loss of isoprene epoxydiols, J. Phys. Chem. A, 118, 1237–1246, doi:10.1021/jp4107958, 2014.

Baulch, D. L., Bowman, C. T., Cobos, C. J., Cox, R. A., Just, T., Kerr, J. A., Pilling, M. J., Stocker, D., Troe, J., Tsang, W., Walker, R. W., and Warnatz, J.: Evaluated kinetic data for combustion modeling: Supplement II, J. Phys. Chem. Ref. Data, 34, 757–1397, doi:10.1063/1.1748524, 2005.

Becker, K. H., Kurtenbach, R., Schmidt, F., and Wiesen, P.: Kinetics of the NCO radical reacting with atoms and selected molecules, Combust. Flame, 120, 570–577, doi:10.1016/S0010-2180(99)00108-X, 2000.

Beckwith, R. C., Wang, T. X., and Margerum, D. W.: Equilibrium and kinetics of bromine hydrolysis, Inorg. Chem., 35, 995–1000, doi:10.1021/IC950909W, 1996.

Bedjanian, Y., Le Bras, G., and Poulet, G.: Kinetic study of the Br + IO, I + BrO and Br + I_2 reactions. Heat of formation of the BrO radical, Chem. Phys. Lett., 266, 233–238, doi:10.1016/S0009-2614(97)01530-3, 1997.

Bedjanian, Y., Laverdet, G., and Le Bras, G.: Low-pressure study of the reaction of Cl atoms with isoprene, J. Phys. Chem. A, 102, 953–959, doi:10.1021/JP973336C, 1998.

Behnke, W., Scheer, V., and Zetzsch, C.: Production of $BrNO_2$, Br_2 and $ClNO_2$ from the reaction between sea spray aerosol and N_2O_5, J. Aerosol Sci., 25, S277–S278, doi:10.1016/0021-8502(94)90369-7, 1994.

Behnke, W., George, C., Scheer, V., and Zetzsch, C.: Production and decay of $ClNO_2$ from the reaction of gaseous N_2O_5 with NaCl solution: Bulk and aerosol experiments, J. Geophys. Res., 102D, 3795–3804, doi:10.1029/96JD03057, 1997.

Betterton, E. A. and Hoffmann, M. R.: Oxidation of aqueous SO_2 by peroxymonosulfate, J. Phys. Chem., 92, 5962–5965, doi:10.1021/J100332A025, 1988.

Beyersdorf, A. J., Blake, D. R., Swanson, A., Meinardi, S., Rowland, F. S., and Davis, D.: Abundances and variability of tropospheric volatile organic compounds at the South Pole and other Antarctic locations, Atmos. Environ., 44, 4565–4574, doi:10.1016/j.atmosenv.2010.08.025, 2010.

Bichsel, Y. and von Gunten, U.: Oxidation of iodide and hypoiodous acid in the disinfection of natural waters, Environ. Sci. Technol., 33, 4040–4045, doi:10.1021/ES990336C, 1999.

Birdsall, A. W., Andreoni, J. F., and Elrod, M. J.: Investigation of the role of bicyclic peroxy radicals in the oxidation mechanism of toluene, J. Phys. Chem. A, 114, 10 655–10 663, doi:10.1021/jp105467e, 2010.

Bjergbakke, E., Navartnam, S., Parsons, B. J., and Swallow, A. J.: Reaction between HO_2· and chlorine in aqueous solution, J. Am. Chem. Soc., 103, 5926–5928, doi:10.1021/JA00409A059, 1981.

Bossolasco, A., Faragó, E. P., Schoemaecker, C., and Fittschen, C.: Rate constant of the reaction between CH_3O_2 and OH radicals, Chem. Phys. Lett., 593, 7–13, doi:10.1016/j.cplett.2013.12.052, 2014.

Boyce, S. D. and Hoffmann, M. R.: Kinetics and mechanism of the formation of hydroxymethanesulfonic acid at low pH, J. Phys. Chem., 88, 4740–4746, doi:10.1021/j150664a059, 1984.

Brand, C. and van Eldik, R.: Transition metal-catalyzed oxidation of sulfur(IV)oxides. Atmospheric relevant processes and mechanisms, Chem. Rev., 95, 119–190, doi:10.1021/cr00033a006, 1995.

Buras, Z. J., Elsamra, R. M. I., and Green, W. H.: Direct determination of the simplest Criegee intermediate (CH_2OO) self reaction rate, J. Phys. Chem. Lett., 5, 2224–2228, doi:10.1021/jz5008406, 2014.

Burkholder, J. B., Sander, S. P., Abbatt, J., Barker, J. R., Huie, R. E., Kolb, C. E., Kurylo, M. J., Orkin, V. L., Wilmouth, D. M., and Wine, P. H.: Chemical Kinetics and Photochemical Data for Use in Atmospheric Studies, Evaluation No. 18, JPL Publication 15-10, Jet Propulsion Laboratory, Pasadena, `http://jpldataeval.jpl.nasa.gov`, 2015.

Butkovskaya, N., Kukui, A., and Le Bras, G.: Pressure and temperature dependence of ethyl nitrate formation in the $C_2H_5O_2$ + NO reaction, J. Phys. Chem. A, 114, 956–964, doi:10.1021/jp910003a, 2010.

Butkovskaya, N., Kukui, A., and Le Bras, G.: Pressure and temperature dependence of methyl nitrate forma-

tion in the CH_3O_2 + NO reaction, J. Phys. Chem. A, 116, 5972–5980, doi:10.1021/jp210710d, 2012.

Buxton, G. V., Kilner, C., and Sellers, R. M.: Pulse radiolysis of HOI and IO^- in aqueous solution. Formation and characterization of I(II), Proc. Tihany Symp. Radiat. Chem., 6, 155–159, 1986.

Buxton, G. V., Greenstock, C. L., Helman, W. P., and Ross, A. B.: Critical review of rate constants for reactions of hydrated electrons, hydrogen atoms and hydroxyl radicals ($\cdot OH/\cdot O^-$) in aqueous solution, J. Phys. Chem. Ref. Data, 17, 513–886, doi:10.1063/1.555805, 1988.

Buxton, G. V., McGowan, S., Salmon, G. A., Williams, J. E., and Wood, N. D.: A study of the spectra and reactivity of oxysulphur-radical anions involved in the chain oxidation of S(IV): A pulse and γ-radiolysis study, Atmos. Environ., 30, 2483–2493, doi:10.1016/1352-2310(95)00473-4, 1996.

Buxton, G. V., Bydder, M., and Salmon, G. A.: The reactivity of chlorine atoms in aqueous solution: Part II. The equilibrium $SO_4^{\cdot-} + Cl^- \rightleftharpoons Cl\cdot + SO_4^{2-}$, Phys. Chem. Chem. Phys., 1, 269–273, doi:10.1039/A807808D, 1999a.

Buxton, G. V., Salmon, G. A., and Wang, J. Q.: The equilibrium $NO_3 + Cl^- \rightleftharpoons NO_3^- + Cl\cdot$: A laser flash photolysis and pulse radiolysis study of the reactivity of NO_3 with chloride ion in aqueous solution, Phys. Chem. Chem. Phys., 1, 3589–3593, doi:10.1039/A903286J, 1999b.

Calvert, J. G. and Lindberg, S. E.: A modeling study of the mechanism of the halogen-ozone-mercury homogeneous reactions in the troposphere during the polar spring, Atmos. Environ., 37, 4467–4481, doi:10.1016/J.ATMOSENV.2003.07.001, 2003.

Canosa-Mas, C. E., King, M. D., Lopez, R., Percival, C. J., Wayne, R. P., Shallcross, D. E., Pyle, J. A., and Daele, V.: Is the reaction between $CH_3(O)O_2$ and NO_3 important in the night-time troposphere?, J. Chem. Soc. Faraday Trans., 92, 2211–2222, doi:10.1039/FT9969202211, 1996.

Capouet, M., Müller, J.-F., Ceulemans, K., Compernolle, S., Vereecken, L., and Peeters, J.: Modeling aerosol formation in alpha-pinene photo-oxidation experiments, J. Geophys. Res., 113D, doi:10.1029/2007JD008995, 2008.

Carl, S. A. and Crowley, J. N.: 298 K rate coefficients for the reaction of OH with i$-C_3H_7I$, n$-C_3H_7I$ and C_3H_8, Atmos. Chem. Phys., 1, 1–7, doi:10.5194/acp-1-1-2001, 2001.

Chai, J., Hu, H., Dibble, T. S., Tyndall, G. S., and Orlando, J. J.: Rate constants and kinetic isotope effects for methoxy radical reacting with NO_2 and O_2, J. Phys. Chem. A, 118, 3552–3563, doi:10.1021/jp501205d, 2014.

Chameides, W. L.: The photochemistry of a remote marine stratiform cloud, J. Geophys. Res., 89D, 4739–4755, doi:10.1029/JD089ID03P04739, 1984.

Chao, W., Hsieh, J.-T., Chang, C.-H., and Lin, J. J.-M.: Direct kinetic measurement of the reaction of the simplest Criegee intermediate with water vapor, Science, 347, 751–754, doi:10.1126/science.1261549, 2015.

Chen, J., Wenger, J. C., and Venables, D. S.: Near-ultraviolet absorption cross sections of nitrophenols and their potential influence on tropospheric oxidation capacity, J. Phys. Chem. A, 115, 12 235–12 242, doi:10.1021/jp206929r, 2011.

Chin, M. and Wine, P. H.: A temperature-dependent competitive kinetics study of the aqueous-phase reactions of OH radicals with formate, formic acid, acetate, acetic acid, and hydrated formaldehyde, in: Aquatic and Surface Photochemistry, edited by Helz, G. R., Zepp, R. G., and Crosby, D. G., pp. 85–96, A. F. Lewis, NY, 1994.

Chinake, C. R. and Simoyi, R. H.: Kinetics and mechanism of the complex bromate-iodine reaction, J. Phys. Chem., 100, 1643–1656, doi:10.1021/JP951956C, 1996.

Christensen, H. and Sehested, K.: Pulse radiolysis at high temperatures and high pressures, Radiat. Phys. Chem., 18, 723–231, doi:10.1016/0146-5724(81)90195-3, 1981.

Christensen, H. and Sehested, K.: HO_2 and O_2^- radicals at elevated temperatures, J. Phys. Chem., 92, 3007–3011, doi:10.1021/J100321A060, 1988.

Christensen, H., Sehested, K., and Corfitzen, H.: Reactions of hydroxyl radicals with hydrogen peroxide at ambient and elevated temperatures, J. Phys. Chem., 86, 1588–1590, doi:10.1021/J100206A023, 1982.

Citri, O. and Epstein, I. R.: Mechanistic study of a coupled chemical oscillator: the bromate-chlorite-iodide reaction, J. Phys. Chem., 92, 1865–1871, doi:10.1021/J100318A034, 1988.

Clubb, A. E., Jordan, M. J. T., Kable, S. H., and Osborn, D. L.: Photoautomerization of acetaldehyde to vinyl alcohol: a primary process in UV-irradiated acetaldehyde from 295 to 335 nm, J. Phys. Chem. Lett., 3, 3522–3526, doi:10.1021/jz301701x, 2012.

Clyne, M. A. A. and Cruse, H. W.: Atomic resonance fluorescence spectrometry for the rate constants of

rapid bimolecular reactions. Part 2. Reactions Cl + BrCl, Cl + Br_2, Cl + ICl, Br + IBr, Br + ICl, J. Chem. Soc. Faraday Trans. 2, 68, 1377–1387, doi:10.1039/F29726801377, 1972.

Conn, J. B., Kistiakowsky, G. B., Roberts, R. M., and Smith, E. A.: Heats of organic reactions. XIII. Heats of hydrolysis of some acid anhydrides, Journal of the American Chemical Society, 64, 1747–1752, doi:10.1021/ja01260a001, 1942.

da Silva, G.: Carboxylic acid catalyzed keto-enol tautomerizations in the gas phase, Angew. Chem., 122, 7685–7687, doi:10.1002/ange.201003530, 2010.

Damschen, D. E. and Martin, L. R.: Aqueous aerosol oxidation of nitrous acid by O_2, O_3 and H_2O_2, Atmos. Environ., 17, 2005–2011, doi:10.1016/0004-6981(83)90357-8, 1983.

Davis, D., Chen, G., Kasibhatla, P., Jefferson, A., Tanner, D., Eisele, F., Lenschow, D., Neff, W., and Berresheim, H.: DMS oxidation in the Antarctic marine boundary layer: Comparison of model simulations and field observations of DMS, DMSO, $DMSO_2$, H_2SO_4(g), MSA(g), and MSA(p), J. Geophys. Res., 103D, 1657–1678, doi:10.1029/97JD03452, 1998.

Davis, Jr., W. and de Bruin, H. J.: New activity coefficients of 0-100 per cent aqueous nitric acid, J. Inorg. Nucl. Chem., 26, 1069–1083, doi:10.1016/0022-1902(64)80268-2, 1964.

de Laat, J. and Le, T. G.: Effects of chloride ions on the iron(III)-catalyzed decomposition of hydrogen peroxide and on the efficiency of the Fenton-like oxidation process, Appl. Catal. B: Environ., 66, 137–146, doi:10.1016/j.apcatb.2006.03.008, 2006.

Deister, U. and Warneck, P.: Photooxidation of SO_3^{2-} in aqueous solution, J. Phys. Chem., 94, 2191–2198, doi:10.1021/J100368A084, 1990.

Dickson, A. G. and Millero, F. J.: A comparison of the equilibrium constants for the dissociation of carbonic acid in seawater media, Deep-Sea Res. A, 34, 1733–1743, 1987.

Dillon, T. J., Karunanandan, R., and Crowley, J. N.: The reaction of IO with CH_3SCH_3: Products and temperature dependent rate coefficients by laser induced fluorescence, Phys. Chem. Chem. Phys., 8, 847–855, doi:10.1039/B514718B, 2006a.

Dillon, T. J., Tucceri, M. E., and Crowley, J. N.: Laser induced fluorescence studies of iodine oxide chemistry. Part II. The reactions of IO with CH_3O_2, CF_3O_2 and O_3, Phys. Chem. Chem. Phys., 8, 5185–5198, doi:10.1039/B611116E, 2006b.

Dillon, T. J., Tucceri, M. E., Sander, R., and Crowley, J. N.: LIF studies of iodine oxide chemistry, part 3. Reactions IO + NO_3 $\rightarrow$ OIO + NO_2, I + NO_3 $\rightarrow$ IO + NO_2, and $CH_2I + O_2$ $\rightarrow$ (products): Implications for the chemistry of the marine atmosphere at night., Phys. Chem. Chem. Phys., 10, 1540–1554, doi:10.1039/B717386E, 2008.

Dolson, D. A. and Leone, S. R.: A reinvestigation of the laser-initiated chlorine/hydrogen bromide chain reaction: absolute rate constants and the v = 2/v = 1 ratio from chlorine atom + hydrogen bromide $\rightarrow$ hydrogen chloride(v) + bromine atom, J. Phys. Chem., 91, 3543–3550, doi:10.1021/J100297A016, 1987.

Donohoue, D. L., Bauer, D., Cossairt, B., and Hynes, A. J.: Temperature and pressure dependent rate coefficients for the reaction of Hg with Br and the reaction of Br with Br: a pulsed laser photolysis-pulsed laser induced fluorescence study, J. Phys. Chem. A, 110, 6623–6632, doi:10.1021/JP054688J, 2006.

Duff, J. W., Dothe, H., and Sharma, R. D.: On the rate coefficient of the $N(^2D)+O_2 \rightarrow NO+O$ reaction in the terrestrial thermosphere, Geophys. Res. Lett., 30, 1259–1263, 2003.

Dulitz, K., Amedro, D., Dillon, T. J., Pozzer, A., and Crowley, J. N.: Temperature (208–318 K) and pressure (18–696 Torr) dependent rate coefficients for the reaction between OH and HNO_3, Atmos. Chem. Phys., 18, 2381–2394, doi:10.5194/acp-18-2381-2018, 2018.

Edblom, E. C., Györgyi, L., Orbán, M., and Epstein, I. R.: A mechanism for dynamical behavior in the Landolt reaction with ferrocyanide, J. Am. Chem. Soc., 109, 4876–4880, doi:10.1021/JA00250A020, 1987.

Eigen, M. and Kustin, K.: The kinetics of halogen hydrolysis, J. Am. Chem. Soc., 84, 1355–1361, doi:10.1021/JA00867A005, 1962.

Enami, S., Hoshino, Y., and Kawasaki, M.: A kinetic study of the gas-phase reactions of OIO with NO, NO_2, and Cl_2, Int. J. Chem. Kinet., 39, 688–693, doi:10.1002/KIN.20283, 2007.

Espinosa-Garcia, J. and Garcia-Bernáldez, J. C.: Analytical potential energy surface for the $CH_4 + O(^3P)$ $\rightarrow$ CH_3 + OH reaction. Thermal rate constants and kinetic isotope effects, Phys. Chem. Chem. Phys., 2, 2345–2351, doi:10.1039/b001038n, 2000.

Exner, M., Herrmann, H., and Zellner, R.: Laser-based studies of reactions of the nitrate radical in aqueous solution, Ber. Bunsenges. Phys. Chem., 96, 470–477, doi:10.1002/BBPC.19920960347, 1992.

Faria, R. B., Lengyel, I., Epstein, I. R., and Kustin, K.: Combined mechanism explaining nonlinear dynamics in bromine(III) and bromine(V) oxidations of iodide ion, J. Phys. Chem., 97, 1164–1171, doi:10.1021/J100108A011, 1993.

Feierabend, K. J., Zhu, L., Talukdar, R. K., and Burkholder, J. B.: Rate coefficients for the OH + HC(O)C(O)H (glyoxal) raction between 210 and 390 K, J. Phys. Chem. A, 112, 73–82, doi:10.1021/JP0768571, 2008.

Felder, P. and Demuth, C.: Photodissociation of $CFCl_3$ at 193 nm investigated by photofragment translational spectroscopy, Chem. Phys. Lett., 208, 21–26, doi:10.1016/0009-2614(93)80070-6, 1993.

Fell, C., Steinfeld, J. I., and Miller, S.: Quenching of $N(^2D)$ by $O(^3P)$, J. Chem. Phys., 92, 4768–4777, doi:10.1063/1.457694, 1990.

Finkbeiner, M., Crowley, J. N., Horie, O., Müller, R., Moortgat, G. K., and Crutzen, P. J.: Reaction between HO_2 and ClO: Product formation between 210 and 300 K, J. Phys. Chem., 99, 16 264–16 275, doi:10.1021/J100044A011, 1995.

Flocke, F., Atlas, E., Madronich, S., Schauffler, S. M., Aikin, K., Margitan, J. J., and Bui, T. P.: Observations of methyl nitrate in the lower stratosphere during STRAT: implications for its gas phase production mechanisms, Geophys. Res. Lett., 25, 1891–1894, doi:10.1029/98GL01417, 1998.

Fogelman, K. D., Walker, D. M., and Margerum, D. W.: Non-metal redox kinetics: Hypochlorite and hypochlorous acid reactions with sulfite, Inorg. Chem., 28, 986–993, doi:10.1021/IC00305A002, 1989.

Fortnum, D. H., Battaglia, C. J., Cohen, S. R., and Edwards, J. O.: The kinetics of the oxidation of halide ions by monosubstituted peroxides, J. Am. Chem. Soc., 82, 778–782, doi:10.1021/JA01489A004, 1960.

Francisco-Marquez, M., Alvarez-Idaboy, J. R., Galano, A., and Vivier-Bunge, A.: Theoretical study of the initial reaction between OH and isoprene in tropospheric conditions, Phys. Chem. Chem. Phys., 5, 1392–1399, doi:10.1039/B211185C, 2003.

Fuller-Rowell, T. J.: Modeling the solar cycle change in nitric oxide in the thermosphere and upper mesosphere, J. Geophys. Res., 98A, 1559–1570, doi:10.1029/92JA02201, 1993.

Furrow, S.: Reactions of iodine intermediates in iodate-hydrogen peroxide oscillators, J. Phys. Chem., 91, 2129–2135, doi:10.1021/J100292A031, 1987.

Gans, B., Boyé-Peronne, S., Broquier, M., Delsaut, M., Douin, S., Fellows, C. E., Halvick, P., Loison, J.-C., Lucchese, R. R., and Gauyacq, D.: Photolysis of methane revisited at 121.6 nm and at 118.2 nm: quantum yields of the primary products, measured by mass spectrometry, Phys. Chem. Chem. Phys., 13, 8140–8152, doi:10.1039/c0cp02627a, 2011.

Ganzeveld, L., Klemm, O., Rappenglück, B., and Valverde-Canossa, J.: Evaluation of meteorological parameters over a coniferous forest in a single-column chemistry-climate model, Atmos. Environ., 40, S21–S27, doi:10.1016/J.ATMOSENV.2006.01.061, 2006.

Garton, D. J., Minton, T. K., Troya, D., Pascual, R., and Schatz, G. C.: Hyperthermal reactions of $O(^3P)$ with alkanes: Observations of novel reaction pathways in crossed-beams and theoretical studies, J. Phys. Chem. A, 107, 4583–4587, doi:10.1021/jp0226026, 2003.

Gilbert, B. C. and Stell, J. K.: Mechanisms of peroxide decomposition. An ESR study of the reactions of the peroxomonosulphate anion (HOOSO3$^-$) with TiIII, FeII, and α-oxygen-substituted radicals, J. Chem. Soc. Perkin Trans. 2, pp. 1281–1288, doi:10.1039/P29900001281, 1990.

Gill, K. J. and Hites, R. A.: Rate constants for the gas-phase reactions of the hydroxyl radical with isoprene, α- and β-pinene, and limonene as a function of temperature, J. Phys. Chem. A, 106, 2538–2544, doi:10.1021/jp013532q, 2002.

Glowacki, D. R., Lockhart, J., Blitz, M. A., Klippenstein, S. J., Pilling, M. J., Robertson, S. H., and Seakins, P. W.: Interception of excited vibrational quantum states by O_2 in atmospheric association reactions, Science, 337, 1066–1069, doi:10.1126/science.1224106, 2012.

Goodsite, M., Plane, J. M. C., and Skov, H.: A theoretical study of the oxidation of Hg^0 to $HgBr_2$ in the troposphere, Environ. Sci. Technol., 38, 1772–1776, doi:10.1021/ES034680S, 2004.

Grenfell, J. L., Lehmann, R., Mieth, P., Langematz, U., and Steil, B.: Chemical reaction pathways affecting stratospheric and mesospheric ozone, J. Geophys. Res., 111D, doi:10.1029/2004JD005713, 2006.

Groß, C. B. M., Dillon, T. J., Schuster, G., Lelieveld, J., and Crowley, J. N.: Direct kinetic study of OH and O_3 formation in the reaction of $CH_3C(O)O_2$ with HO_2, J. Phys. Chem. A, 1, 974–985, doi:10.1021/jp412380z, 2014.

Gruzdev, A. N., Elokhov, A. S., Makarov, O. V., and Mokhov, I. I.: Some recent results of Russian measurements of surface ozone in Antarctica. A meteorological interpretation, Tellus, 45B, 99–105, doi:10.3402/TELLUSB.V45I2.15584, 1993.

Haag, W. R. and Hoigné, J.: Ozonation of bromide-containing waters: Kinetics of formation of hypobromous acid and bromate, Environ. Sci. Technol., 17, 261–267, doi:10.1021/ES00111A004, 1983.

Hall, B.: The gas phase oxidation of elemental mercury by ozone, Water Air Soil Pollut., 80, 301–315, doi:10.1007/BF01189680, 1995.

Hatakeyama, S., Honda, S., and Akimoto, H.: Rate constants and mechanism for reactions of ketenes with OH radicals in air at 299±2 K, Bull. Chem. Soc. Jpn., 58, 2157–2162, doi:10.1246/BCSJ.58.2157, 1985.

Hermans, I., Müller, J.-F., Nguyen, T. L., Jacobs, P. A., and Peeters, J.: Kinetics of α-hydroxy-alkylperoxyl radicals in oxidation processes. HO_2-initiated oxidation of ketones/aldehydes near the tropopause, J. Phys. Chem. A, 109, 4303–4311, doi:10.1021/jp044080v, 2005.

Herrmann, H., Reese, A., and Zellner, R.: Time resolved UV/VIS diode array absorption spectroscopy of SO_x^- (x=3, 4, 5) radical anions in aqueous solution, J. Mol. Struct., 348, 183–186, doi:10.1016/0022-2860(95)08619-7, 1995.

Herrmann, H., Ervens, B., Nowacki, P., Wolke, R., and Zellner, R.: A chemical aqueous phase radical mechanism for tropospheric chemistry, Chemosphere, 38, 1223–1232, doi:10.1016/S0045-6535(98)00520-7, 1999.

Herrmann, H., Ervens, B., Jacobi, H.-W., Wolke, R., Nowacki, P., and Zellner, R.: CAPRAM2.3: A chemical aqueous phase radical mechanism for tropospheric chemistry, J. Atmos. Chem., 36, 231–284, doi:10.1023/A:1006318622743, 2000.

Hoffmann, M. R.: On the kinetics and mechanism of oxidation of aquated sulfur dioxide by ozone, Atmos. Environ., 20, 1145–1154, doi:10.1016/0004-6981(86)90147-2, 1986.

Hoigné, J., Bader, H., Haag, W. R., and Staehelin, J.: Rate constants of reactions of ozone with organic and inorganic compounds in water – III Inorganic compounds and radicals, Wat. Res., 19, 993–1004, doi:10.1016/0043-1354(85)90368-9, 1985.

Huie, R. E. and Neta, P.: Rate constants for some oxidations of S(IV) by radicals in aqueous solutions, Atmos. Environ., 21, 1743–1747, doi:10.1016/0004-6981(87)90113-2, 1987.

Hynes, A. J. and Wine, P. H.: The atmospheric chemistry of dimethylsulfoxide (DMSO) kinetics and mechanism of the OH + DMSO reaction, J. Atmos. Chem., 24, 23–37, doi:10.1007/BF00053821, 1996.

Ingham, T., Bauer, D., Sander, R., Crutzen, P. J., and Crowley, J. N.: Kinetics and products of the reactions BrO + DMS and Br + DMS at 298 K, J. Phys. Chem. A, 103, 7199–7209, doi:10.1021/JP9905979, 1999.

Jacob, D. J.: Chemistry of OH in remote clouds and its role in the production of formic acid and peroxymonosulfate, J. Geophys. Res., 91D, 9807–9826, doi:10.1029/JD091ID09P09807, 1986.

Jacobi, H.-W.: Kinetische Untersuchungen und Modellrechnungen zur troposphärischen Chemie von Radikalanionen und Ozon in wäßriger Phase, Ph.D. thesis, Universität GH Essen, Germany, 1996.

Jacobi, H.-W., Herrmann, H., and Zellner, R.: Kinetic investigation of the Cl_2^- radical in the aqueous phase, in: Air Pollution Research Report 57: Homogeneous and heterogeneous chemical Processes in the Troposphere, edited by Mirabel, P., pp. 172–176, Office for official Publications of the European Communities, Luxembourg, 1996.

Jacobsen, F., Holcman, J., and Sehested, K.: Activation parameters of ferryl ion reactions in aqueous acid solutions, Int. J. Chem. Kinet., 29, 17–24, doi:10.1002/(SICI)1097-4601(1997)29:1⟨17::AID-KIN3⟩3.0.CO;2-O, 1997.

Jacobsen, F., Holcman, J., and Sehested, K.: Reactions of the ferryl ion with some compounds found in cloud water, Int. J. Chem. Kinet., 30, 215–221, doi:10.1002/(SICI)1097-4601(1998)30:3⟨215::AID-KIN7⟩3.0.CO;2-V, 1998.

Jagiella, S. and Zabel, F.: Reaction of phenylperoxy radicals with NO_2 at 298 K, Phys. Chem. Chem. Phys., 9, 5036–5051, doi:10.1039/B705193J, 2007.

Jayson, G. G., Parsons, B. J., and Swallow, A. J.: Some simple, highly reactive, inorganic chlorine derivatives in aqueous solution, J. Chem. Soc. Faraday Trans. 1, 69, 1597–1607, doi:10.1039/F19736901597, 1973.

Jefferson, A., Nicovich, J. M., and Wine, P. H.: Temperature-dependent kinetics studies of the reactions $Br(^2P_{3/2})$ + CH_3SCH_3 ↔ CH_3SCH_2 + HBr. Heat of formation of the CH_3SCH_2 radical, J. Phys. Chem., 98, 7128–7135, doi:10.1021/J100080A006, 1994.

Jenkin, M., Saunders, S. M., and Pilling, M. J.: The tropospheric degradation of volatile organic compounds: A protocol for mechanism development, Atmos. Environ., 31, 81–104, doi:10.1016/S1352-2310(96)00105-7, 1997.

Jenkin, M. E., Young, J. C., and Rickard, A. R.: The MCM v3.3.1 degradation scheme for isoprene, Atmos. Chem. Phys., 15, 11 433–11 459, doi:10.5194/acp-15-11433-2015, 2015.

Jiang, P.-Y., Katsumura, Y., Nagaishi, R., Domae, M., Ishikawa, K., Ishigure, K., and Yoshida, Y.: Pulse radiolysis study of concentrated sulfuric acid solutions. Formation mechanism, yield and reactivity of sulfate radicals, J. Chem. Soc. Faraday Trans., 88, 1653–1658, doi:10.1039/FT9928801653, 1992.

Kaltsoyannis, N. and Plane, J. M. C.: Quantum chemical calculations on a selection of iodine-containing species (IO, OIO, INO_3, $(IO)_2$, I_2O_3, I_2O_4 and I_2O_5) of importance in the atmosphere, Phys. Chem. Chem. Phys., 10, 1723–1733, doi:10.1039/B715687C, 2008.

Keller-Rudek, H., Koschel, D., Merlet, P., Ohms-Bredemann, U., Wagner, J., and Wietelmann, A.: Gmelin Handbook of Inorganic and Organometallic Chemistry, 8th Edition, Br, Bromine, Supplement Volume B2, Compounds with Oxygen and Nitrogen, Springer Verlag, Berlin, 1992.

Kelley, C. M. and Tartar, H. V.: On the system: bromine-water, J. Am. Chem. Soc., 78, 5752–5756, doi:10.1021/JA01603A010, 1956.

Kirchner, F., Mayer-Figge, A., Zabel, F., and Becker, K. H.: Thermal stability of peroxynitrates, Int. J. Chem. Kinet., 31, 127–144, doi:10.1002/(SICI)1097-4601(1999)31:2⟨127::AID-KIN6⟩3.0.CO;2-L, 1999.

Kleinböhl, A., Toon, G. C., Sen, B., Blavier, J.-F. L., Weisenstein, D. K., Strekowski, R. S., Nicovich, J. M., Wine, P. H., and Wennberg, P. O.: On the stratospheric chemistry of hydrogen cyanide, Geophys. Res. Lett., 33, doi:10.1029/2006GL026015, 2006.

Kohlmann, J.-P. and Poppe, D.: The tropospheric gas-phase degradation of NH_3 and its impact on the formation of N_2O and NO_x, J. Atmos. Chem., 32, 397–415, doi:10.1023/A:1006162910279, 1999.

Kondo, O. and Benson, S. W.: Kinetics and equilibria in the system $Br + CH_3OOH \rightleftharpoons HBr + CH_3OO$. An upper limit for the heat of formation of the methylperoxy radical, J. Phys. Chem., 88, 6675–6680, doi:10.1021/J150670A034, 1984.

Kumar, K. and Margerum, D. W.: Kinetics and mechanism of general-acid-assisted oxidation of bromide by hypochlorite and hypochlorous acid, Inorg. Chem., 26, 2706–2711, doi:10.1021/IC00263A030, 1987.

Lax, E.: Taschenbuch für Chemiker und Physiker, Springer Verlag, Berlin, 1969.

Lee, Y.-N. and Schwartz, S. E.: Reaction kinetics of nitrogen dioxide with liquid water at low partial pressure, J. Phys. Chem., 85, 840–848, doi:10.1021/J150607A022, 1981.

Lengyel, I., Li, J., Kustin, K., and Epstein, I. R.: Rate constants for reactions between iodine- and chlorine-containing species: A detailed mechanism of the chlorine dioxine/chlorite reaction, J. Am. Chem. Soc., 118, 3708–3719, doi:10.1021/JA953938E, 1996.

Lewis, T. R., Blitz, M. A., Heard, D. E., and Seakins, P. W.: Direct evidence for a substantive reaction between the Criegee intermediate, CH_2OO, and the water vapour dimer, Phys. Chem. Chem. Phys., 17, 4859–4863, doi:10.1039/C4CP04750H, 2015.

Liljegren, J. A. and Stevens, P. S.: Measurements of the kinetics of the reaction of OH radicals with 3-methylfuran at low pressure, Int. J. Chem. Kinet., 45, 787–794, doi:10.1002/KIN.20814, 2013.

Lin, C.-J. and Pehkonen, S. O.: Aqueous free radical chemistry of mercury in the presence of iron oxides and ambient aerosol, Atmos. Environ., 31, 4125–4137, doi:10.1016/S1352-2310(97)00269-0, 1997.

Lin, C.-J. and Pehkonen, S. O.: Oxidation of elemental mercury by aqueous chlorine ($HOCl/OCl^-$): Implications for tropospheric mercury chemistry, J. Geophys. Res., 103D, 28 093–28 102, doi:10.1029/98JD02304, 1998.

Lind, J. A., Lazrus, A. L., and Kok, G. L.: Aqueous phase oxidation of sulfur(IV) by hydrogen peroxide, methylhydroperoxide, and peroxyacetic acid, J. Geophys. Res., 92D, 4171–4177, doi:10.1029/JD092ID04P04171, 1987.

Liu, Q. and Margerum, D. W.: Equilibrium and kinetics of bromine chloride hydrolysis, Environ. Sci. Technol., 35, 1127–1133, doi:10.1021/ES001380R, 2001.

Liu, Y., Pimentel, A. S., Antoku, Y., Giles, B. J., and Barker, J. R.: Temperature-dependent rate and equilibrium constants for $Br \cdot (aq) + Br^-(aq) \rightleftharpoons Br_2^- \cdot (aq)$, J. Phys. Chem. A, 106, 11 075–11 082, doi:10.1021/JP0255536, 2002.

Lockhart, J., Blitz, M., Heard, D., Seakins, P., and Shannon, R.: Kinetic study of the OH + glyoxal reaction: experimental evidence and quantification of direct OH recycling, J. Phys. Chem. A, 117, 11 027–11 037, doi:10.1021/jp4076806, 2013.

Lockwood, A. L., Shepson, P. B., Fiddler, M. N., and Alaghmand, M.: Isoprene nitrates: preparation, separation, identification, yields, and atmospheric chemistry, Atmos. Chem. Phys., 10, 6169–6178, doi:10.5194/acp-10-6169-2010, 2010.

Løgager, T., Holcman, J., Sehested, K., and Pedersen, T.: Oxidation of ferrous ions by ozone in acidic solutions, Inorg. Chem., 31, 3523–3529, doi:10.1021/ic00043a009, 1992.

Løgager, T., Sehested, K., and Holcman, J.: Rate constants of the equilibrium reactions $SO_4 + HNO_3 \rightleftharpoons HSO_4^- + NO_3$ and $SO_4 + NO_3 \rightleftharpoons SO_4^{2-} + NO_3$, Radiat. Phys. Chem., 41, 539–543, doi:10.1016/0969-806X(93)90017-O, 1993.

Long, C. A. and Bielski, B. H. J.: Rate of reaction of superoxide radical with chloride-containing species, J. Phys. Chem., 84, 555–557, doi:10.1021/J100442A023, 1980.

Magi, L., Schweitzer, F., Pallares, C., Cherif, S., Mirabel, P., and George, C.: Investigation of the uptake rate of ozone and methyl hydroperoxide by water surfaces, J. Phys. Chem. A, 101, 4943–4949, doi:10.1021/JP970646M, 1997.

Manion, J. A., Huie, R. E., Levin, R. D., Burgess, Jr., D. R., Orkin, V. L., Tsang, W., McGivern, W. S., Hudgens, J. W., Knyazev, V. D., Atkinson, D. B., Chai, E., Tereza, A. M., Lin, C.-Y., Allison, T. C., Mallard, W. G., Westley, F., Herron, J. T., Hampson, R. F., and Frizzell, D. H.: NIST Chemical Kinetics Database, NIST Standard Reference Database 17 (Web Version), `http://kinetics.nist.gov`, 2015.

Margerum, D. W., Dickson, P. N., Nagy, J. C., Kumar, K., Bowers, C. P., and Fogelman, K. D.: Kinetics of the iodine monochloride reaction with iodide measured by the pulsed-accelerated-flow method, Inorg. Chem., 25, 4900–4904, doi:10.1021/IC00247A025, 1986.

Marsh, A. R. W. and McElroy, W. J.: The dissociation constant and Henry's law constant of HCl in aqueous solution, Atmos. Environ., 19, 1075–1080, doi:10.1016/0004-6981(85)90192-1, 1985.

Martin, L. R. and Damschen, D. E.: Aqueous oxidation of sulfur dioxide by hydrogen peroxide at low pH, Atmos. Environ., 15, 1615–1621, doi:10.1016/0004-6981(81)90146-3, 1981.

Matthew, B. M., George, I., and Anastasio, C.: Hydroperoxyl radical (HO2·) oxidizes dibromide radical anion ($\cdot Br_2^-$) to bromine (Br_2) in aqueous solution: Implications for the formation of Br_2 in the marine boundary layer, Geophys. Res. Lett., 30, doi:10.1029/2003GL018572, 2003.

McCabe, D. C., Gierczak, T., Talukdar, R. K., and Ravishankara, A. R.: Kinetics of the reaction OH + CO under atmospheric conditions, Geophys. Res. Lett., 28, 3135–3138, doi:10.1029/2000GL012719, 2001.

McElroy, W. J. and Waygood, S. J.: Kinetics of the reactions of the SO_4^- radical with SO_4^-, $S_2O_8^{2-}$, H_2O and Fe^{2+}, J. Chem. Soc. Faraday Trans., 86, 2557–2564, doi:10.1039/FT9908602557, 1990.

Mellouki, A. and Mu, Y.: On the atmospheric degradation of pyruvic acid in the gas phase, J. Photochem. Photobiol. A: Chem., 157, doi:10.1016/S1010-6030(03)00070-4, 2003.

Messaadia, L., Dib, G. E., Ferhati, A., and Chakir, A.: UV-visible spectra and gas-phase rate coefficients for the reaction of 2,3-pentanedione and 2,4-pentanedione with OH radicals, Chem. Phys. Lett., 626, 73–79, doi:10.1016/j.cplett.2015.02.032, 2015.

Müller, J.-F., Peeters, J., and Stavrakou, T.: Fast photolysis of carbonyl nitrates from isoprene, Atmos. Chem. Phys., 14, 2497–2508, doi:10.5194/acp-14-2497-2014, 2014.

Munger, J. W., Jacob, D. J., Fan, S.-M., Colman, A. S., and Dibb, J. E.: Concentrations and snow-atmosphere fluxes of reactive nitrogen at Summit, Greenland, J. Geophys. Res., 104D, 13 721–13 734, doi:10.1029/1999JD900192, 1999.

Munthe, J.: The aqueous oxidation of elemental mercury by ozone, Atmos. Environ., 26A, 1461–1468, doi:10.1016/0960-1686(92)90131-4, 1992.

Nagy, J. C., Kumar, K., and Margerum, D. W.: Non-metal redox kinetics: Oxidation of iodide by hypochlorous acid and by nitrogen trichloride measured by the pulsed-accelerated-flow method, Inorg. Chem., 27, 2773–2780, doi:10.1021/IC00289A007, 1988.

Nakanishi, H., Morita, H., and Nagakura, S.: Electronic structures and spectra of the keto and enol forms of acetylacetone, Bull. Chem. Soc. Jpn., 50, 2255–2261, doi:10.1246/bcsj.50.2255, 1977.

Nakano, Y., Ishiwata, T., and Kawasaki, M.: Rate constants of the reaction of NO_3 with CH_3I measured with use of cavity ring-down spectroscopy, J. Phys. Chem. A, 109, 6527–6531, doi:10.1021/JP051817N, 2005.

Neta, P. and Huie, R. E.: Rate constants for reactions of NO_3 radicals in aqueous solutions, J. Phys. Chem., 90, 4644–4648, doi:10.1021/J100410A035, 1986.

Nguyen, T. L., Peeters, J., and Vereecken, L.: Theoretical study of the gas-phase ozonolysis of β-pinene ($C_{10}H_{16}$), Phys. Chem. Chem. Phys., 11, 5643–5656, doi:10.1039/b822984h, 2009.

Nielsen, O. J., Sidebottom, H. W., Donlon, M., and Treacy, J.: Rate constants for the gas-phase reactions of OH radicals and Cl atoms with n-alkyl nitrites at atmospheric pressure and 298 K, Int. J. Chem. Kinet., 23, 1095–1109, doi:10.1002/kin.550231204, 1991.

O'Dowd, C. D. and Hoffmann, T.: Coastal new particle formation: a review of the current state-of-the-art, Environ. Chem., 2, 245–255, doi:10.1071/EN05077, 2005.

Ogryzlo, E. A., Paltenghi, R., and Bayes, K. D.: The rate of reaction of methyl radicals with ozone, Int. J. Chem. Kinet., 13, 667–675, doi:10.1002/kin.550130707, 1981.

Olzmann, M., Kraka, E., Cremer, D., Gutbrod, R., and Andersson, S.: Energetics, kinetics, and product distributions of the reactions of ozone with ethene and 2,3-dimethyl-2-butene, J. Phys. Chem. A, 101, 9421–9429, doi:10.1021/JP971663E, 1997.

Orlando, J. J. and Tyndall, G. S.: Rate coefficients for the thermal decomposition of $BrONO_2$ and the heat of formation of $BrONO_2$, J. Phys. Chem., 100, 19 398–19 405, doi:10.1021/JP9620274, 1996.

Orlando, J. J. and Tyndall, G. S.: The atmospheric chemistry of the HC(O)CO radical, Int. J. Chem. Kinet., 33, 149–156, doi:10.1002/1097-4601(200103)33:3⟨149::AID-KIN1008⟩3.0.CO;2-1, 2001.

Orlando, J. J. and Tyndall, G. S.: Laboratory studies of organic peroxy radical chemistry: an overview with emphasis on recent issues of atmospheric significance, Chem. Soc. Rev., 41, 6294–6317, doi:10.1039/C2CS35166H, 2012.

Orlando, J. J., Tyndall, G. S., Bilde, M., Ferronato, C., Wallington, T. J., Vereecken, L., and Peeters, J.: Laboratory and theoretical study of the oxy radicals in the OH- and Cl-initiated oxidation of ethene, J. Phys. Chem. A, 102, 8116–8123, doi:10.1021/JP981937D, 1998.

Orlando, J. J., Tyndall, G. S., Fracheboud, J. M., Estupinan, E. G., Haberkorn, S., and Zimmer, A.: The rate and mechanism of the gas-phase oxidation of hydroxyacetone, Atmos. Environ., 33, 1621–1629, doi:10.1016/S1352-2310(98)00386-0, 1999a.

Orlando, J. J., Tyndall, G. S., and Paulson, S. E.: Mechanism of the OH-initiated oxidation of methacrolein, Geophys. Res. Lett., 26, 2191–2194, doi:10.1029/1999GL900453, 1999b.

Orlando, J. J., Tyndall, G. S., Bertman, S. B., Chen, W., and Burkholder, J. B.: Rate coefficient for the reaction of OH with CH_2=C(CH_3)C(O)ONO_2 (MPAN), Atmos. Environ., 36, 1895–1900, doi:10.1016/S1352-2310(02)00090-0, 2002.

Ouyang, B., McLeod, M. W., Jones, R. L., and Bloss, W. J.: NO_3 radical production from the reaction between the Criegee intermediate CH_2OO and NO_2, Phys. Chem. Chem. Phys., 15, 17 070–17 075, doi:10.1039/c3cp53024h, 2013.

Pal, B. and Ariya, P. A.: Gas-phase HO-initiated reactions of elemental mercury: Kinetics, product studies, and atmospheric implications, Environ. Sci. Technol., 38, 5555–5566, doi:10.1021/ES0494353, 2004.

Paulot, F., Crounse, J. D., Kjaergaard, H. G., Kroll, J. H., Seinfeld, J. H., and Wennberg, P. O.: Isoprene photooxidation: new insights into the production of acids and organic nitrates, Atmos. Chem. Phys., 9, 1479–1501, doi:10.5194/ACP-9-1479-2009, 2009a.

Paulot, F., Crounse, J. D., Kjaergaard, H. G., Kürten, A., St. Clair, J. M., Seinfeld, J. H., and Wennberg, P. O.: Unexpected epoxide formation in the gas-phase photooxidation of isoprene, Science, 325, 730–733, doi:10.1126/science.1172910, 2009b.

Paulot, F., Wunch, D., Crounse, J. D., Toon, G. C., Millet, D. B., DeCarlo, P. F., Vigouroux, C., Deutscher, N. M., González Abad, G., Notholt, J., Warneke, T., Hannigan, J. W., Warneke, C., de Gouw, J. A., Dunlea, E. J., De Mazière, M., Griffith, D. W. T., Bernath, P., Jimenez, J. L., and Wennberg, P. O.: Importance of secondary sources in the atmospheric budgets of formic and acetic acids, Atmos. Chem. Phys., 11, 1989–2013, doi:10.5194/acp-11-1989-2011, 2011.

Peeters, J. and Nguyen, T. L.: Unusually fast 1,6-H shifts of enolic hydrogens in peroxy radicals: formation of the first-generation C_2 and C_3 carbonyls in the oxidation of isoprene, J. Phys. Chem. A, 116, 6134–6141, doi:10.1021/jp211447q, 2012.

Peeters, J., Müller, J.-F., Stavrakou, T., and Nguyen, V. S.: Hydroxyl radical recycling in isoprene oxidation driven by hydrogen bonding and hydrogen tunneling: the upgraded LIM1 mechanism, J. Phys. Chem. A, 118, 8625–8643, doi:10.1021/jp5033146, 2014.

Plane, J. M. C., Joseph, D. M., Allan, B. J., Ashworth, S. H., and Francisco, J. S.: An experimental and theoretical study of the reactions OIO + NO and OIO + OH, J. Phys. Chem. A, 110, 93–100, doi:10.1021/JP055364Y, 2006.

Platz, J., Nielsen, O. J., Wallington, T. J., Ball, J. C., Hurley, M. D., Straccia, A. M., Schneider, W. F., and Sehested, J.: Atmospheric chemistry of the phenoxy radical, $C_6H_5O(\cdot)$: UV spectrum and kinetics of its reaction with NO, NO_2, and O_2, J. Phys. Chem. A, 102, 7964–7974, doi:10.1021/jp982221l, 1998.

Pleijel, K. and Munthe, J.: Modelling the atmospheric mercury cycle – Chemistry in fog droplets, Atmos. Environ., 29, 1441–1457, doi:10.1016/1352-2310(94)00323-D, 1995.

Raofie, F. and Ariya, P. A.: Kinetics and products study of the reaction of BrO radicals with gaseous mercury, J. Phys. IV France, 107, 1119–1121, doi:10.1051/JP4:20030497, 2003.

Raofie, F. and Ariya, P. A.: Product study of the gas-phase BrO-initiated oxidation of Hg^0: Evidence for stable Hg^{1+} compounds, Environ. Sci. Technol., 38, 4319–4326, doi:10.1021/ES035339A, 2004.

Rickard, A. and Pascoe, S.: The Master Chemical Mechanism (MCM), `http://mcm.leeds.ac.uk`, 2009.

Rickard, A. R., Johnson, D., McGill, C. D., and Marston, G.: OH yields in the gas-phase reactions of ozone with alkenes, J. Phys. Chem. A, 103, 7656–7664, doi:10.1021/JP9916992, 1999.

Riffault, V., Bedjanian, Y., and Poulet, G.: Kinetic and mechanistic study of the reactions of OH with IBr and HOI, J. Photochem. Photobiol. A: Chem., 176, 155–161, doi:10.1016/j.jphotochem.2005.09.002, 2005.

Roble, R. G.: Energetics of the mesosphere and thermosphere, in: The upper Mesosphere and Lower Thermosphere: A Review of Experiment and Theory, Geophysical Monograph 87, edited by Johnson, R. M. and Killeen, T. L., pp. 1–23, American Geophysical Union, Washington, DC, USA, 1995.

Ross, A. B., Mallard, W. G., Helman, W. P., Bielski, B. H. J., Buxton, G. V., Cabelli, D. E., Greenstock, C. L., Huie, R. E., and Neta, P.: NDRL-NIST Solution Kinetics Database: - Ver. 1, National Institute of Standards and Technology, Gaithersburg, MD, 1992.

Roth, E., Chakir, A., and Ferhati, A.: Study of a benzoylperoxy radical in the gas phase: ultraviolet spectrum and $C_6H_5C(O)O_2$ + HO_2 reaction between 295 and 357 K, J. Phys. Chem. A, 114, 10 367–10 379, doi:10.1021/jp1021467, 2010.

Rush, J. D. and Bielski, B. H. J.: Pulse radiolytic studies of the reaction of HO_2/O_2^- with Fe(II)/Fe(III) ions. The reactivity of HO_2/O_2^- with ferric ions and its implication on the occurrence of the Haber-Weiss reaction, J. Phys. Chem., 89, 5062–5066, doi:10.1021/j100269a035, 1985.

Sander, R., Jöckel, P., Kirner, O., Kunert, A. T., Landgraf, J., and Pozzer, A.: The photolysis module JVAL-14, compatible with the MESSy standard, and the JVal PreProcessor (JVPP), Geosci. Model Dev., 7, 2653–2662, doi:10.5194/GMD-7-2653-2014, 2014.

Sander, R., Baumgaertner, A., Cabrera-Perez, D., Frank, F., Gromov, S., Grooß, J.-U., Harder, H., Huijnen, V., Jöckel, P., Karydis, V. A., Niemeyer, K. E., Pozzer, A., Riede, H., Schultz, M. G., Taraborrelli, D., and Tauer, S.: The community atmospheric chemistry box model CAABA/MECCA-4.0, Geosci. Model Dev., 12, 1365–1385, doi:10.5194/gmd-12-1365-2019, 2019.

Sander, S. P., Finlayson-Pitts, B. J., Friedl, R. R., Golden, D. M., Huie, R. E., Kolb, C. E., Kurylo, M. J., Molina, M. J., Moortgat, G. K., Orkin, V. L., and Ravishankara, A. R.: Chemical Kinetics and Photochemical Data for Use in Atmospheric Studies, Evaluation Number 14, JPL Publication 02-25, Jet Propulsion Laboratory, Pasadena, CA, 2003.

Schwartz, S. E. and White, W. H.: Solubility equilibria of the nitrogen oxides and oxyacids in dilute aqueous solution, in: Advances in Environmental Science and Engineering, edited by Pfafflin, J. R. and Ziegler, E. N., vol. 4, pp. 1–45, Gordon and Breach Science Publishers, NY, 1981.

Schwarz, H. A. and Bielski, B. H. J.: Reactions of HO_2 and O_2^- with iodine and bromine and the I_2^- and I atom reduction potentials, J. Phys. Chem., 90, 1445–1448, doi:10.1021/J100398A045, 1986.

Scribano, Y., Goldman, N., Saykally, R. J., and Leforestier, C.: Water dimers in the atmosphere III: Equilibrium constant from a flexible potential, J. Phys. Chem. A, 110, 5411–5419, doi:10.1021/jp056759k, 2006.

Sehested, J., Christensen, L. K., Nielsen, O. J., Bilde, M., Wallington, T. J., Schneider, W. F., Orlando, J. J., and Tyndall, G. S.: Atmospheric chemistry of acetone: Kinetic study of the $CH_3C(O)CH_2O_2$ + NO/NO_2 reactions and decomposition of $CH_3C(O)CH_2O_2NO_2$, Int. J. Chem. Kinet., 30, 475–489, doi:10.1002/(SICI)1097-4601(1998)30:7⟨475::AID-KIN4⟩3.0.CO;2-P, 1998.

Sehested, K., Rasmussen, O. L., and Fricke, H.: Rate constants of OH with HO_2, O_2^-, and $H_2O_2^+$ from hydrogen peroxide formation in pulse-irradiated oxygenated water, J. Phys. Chem., 72, 626–631, doi:10.1021/J100848A040, 1968.

Sehested, K., Holcman, J., and Hart, E. J.: Rate constants and products of the reactions of e_{aq}^-, O_2^- and H with ozone in aqueous solutions, J. Phys. Chem., 87, 1951–1954, doi:10.1021/J100234A024, 1983.

Seinfeld, J. H. and Pandis, S. N.: Atmospheric Chemistry and Physics, John Wiley & Sons, Inc., 1998.

Shallcross, D. E., Leather, K. E., Bacak, A., Xiao, P., Lee, E. P. F., Ng, M., Mok, D. K. W., Dyke, J. M., Hossaini, R., Chipperfield, M. P., Khan, M. A. H., and Percival, C. J.: Reaction between CH_3O_2 and BrO radicals: a new source of upper troposphere lower stratosphere hydroxyl radicals, J. Phys. Chem. A, 119, 4618–4632, doi:10.1021/JP5108203, 2015.

Shoute, L. C. T., Alfassi, Z. B., Neta, P., and Huie, R. E.: Temperature dependence of the rate constants

for reaction of dihalide and azide radicals with inorganic reductants, J. Phys. Chem., 95, 3238–3242, doi:10.1021/J100161A050, 1991.

Sivakumaran, V., Hölscher, D., Dillon, T. J., and Crowley, J. N.: Reaction between OH and HCHO: temperature dependent rate coefficients (202-399 K) and product pathways (298 K), Phys. Chem. Chem. Phys., 5, 4821–4827, doi:10.1039/B306859E, 2003.

So, S., Wille, U., and da Silva, G.: Atmospheric chemistry of enols: a theoretical study of the vinyl alcohol + OH + O_2 reaction mechanism, Environ. Sci. Technol., 48, 6694–6701, doi:10.1021/es500319q, 2014.

Sokolov, O., Hurley, M. D., Ball, J. C., Wallington, T. J., Nelsen, W., Barnes, I., and Becker, K. H.: Kinetics of the reactions of chlorine atoms with CH_3ONO and CH_3ONO_2, Int. J. Chem. Kinet., 31, 357–359, doi:10.1002/(SICI)1097-4601(1999)31:5⟨357::AID-KIN5⟩3.0.CO;2-6, 1999.

Solberg, S., Stordal, F., and Hov, Ø.: Tropospheric ozone at high latitudes in clean and polluted air masses, a climatological study, J. Atmos. Chem., 28, 111–123, doi:10.1023/A:1005766612853, 1997.

Stone, D., Blitz, M., Daubney, L., Howes, N. U. M., and Seakins, P.: Kinetics of CH_2OO reactions with SO_2, NO_2, NO, H_2O and CH_3CHO as a function of pressure, Phys. Chem. Chem. Phys., 16, 1139–1149, doi:10.1039/c3cp54391a, 2014.

Strekowski, R. S., Nicovich, J. M., and Wine, P. H.: Kinetic and mechanistic study of the Reactions of $O(^1D_2)$ with HCN and CH_3CN, Chem. Phys. Chem., 11, 3942–3955, doi:10.1002/cphc.201000550, 2010.

Sutton, H. C. and Downes, M. T.: Reactions of the HO_2 radical in aqueous solution with bromine and related compounds, J. Chem. Soc. Faraday Trans. 1, 68, 1498–1507, doi:10.1039/F19726801498, 1972.

Swaminathan, P. K., Strobel, D. F., Kupperman, D. G., Acton, L., DeMajistre, R., Yee, J.-H., Paxton, L., Anderson, D. E., Strickland, D. J., and Duff, J. W.: Nitric oxide abundance in the mesosphere/lower thermosphere region: Roles of solar soft X rays, suprathermal $N(^4S)$ atoms, and vertical transport, J. Geophys. Res., 103A, 11 579–11 594, doi:10.1029/97JA03249, 1998.

Tao, Z. and Li, Z.: A kinetics study on reactions of C_6H_5O with C_6H_5O and O_3 at 298 K, Int. J. Chem. Kinet., 31, 65–72, doi:10.1002/(SICI)1097-4601(1999)31:1⟨65::AID-KIN8⟩3.0.CO;2-J, 1999.

Taraborrelli, D.: Isoprene oxidation and its impacts on the atmospheric composition, Ph.D. thesis, Johannes Gutenberg-Universität, Mainz, Germany, http://d-nb.info/1003538770/34, 2010.

Taraborrelli, D., Lawrence, M. G., Butler, T. M., Sander, R., and Lelieveld, J.: Mainz Isoprene Mechanism 2 (MIM2): an isoprene oxidation mechanism for regional and global atmospheric modelling, Atmos. Chem. Phys., 9, 2751–2777, doi:10.5194/ACP-9-2751-2009, 2009.

Thornton, A. T. and Laurence, G. S.: Kinetics of oxidation of transition-metal ions by halogen radical anions. Part I. The oxidation of iron(II) by dibromide and dichloride ions generated by flash photolysis, J. Chem. Soc. Dalton Trans., pp. 804–813, doi:10.1039/DT9730000804, 1973.

Tokos, J. J. S., Hall, B., Calhoun, J. A., and Prestbo, E. M.: Homogeneous gas-phase reaction of Hg^0 with H_2O_2, O_3, CH_3I, and $(CH_3)_2S$: Implications for atmospheric Hg cycling, Atmos. Environ., 32, 823–827, doi:10.1016/S1352-2310(97)00171-4, 1998.

Troy, R. C. and Margerum, D. W.: Non-metal redox kinetics: Hypobromite and hypobromous acid reactions with iodide and with sulfite and the hydrolysis of bromosulfate, Inorg. Chem., 30, 3538–3543, doi:10.1021/IC00018A028, 1991.

Troy, R. C., Kelley, M. D., Nagy, J. C., and Margerum, D. W.: Non-metal redox kinetics: Iodine monobromide reaction with iodide ion and the hydrolysis of IBr, Inorg. Chem., 30, 4838–4845, doi:10.1021/IC00025A030, 1991.

Tyndall, G. S., Staffelbach, T. A., Orlando, J. J., and Calvert, J. G.: Rate coefficients for the reactions of OH radicals with methylglyoxal and acetaldehyde, Int. J. Chem. Kinet., 27, 1009–1020, doi:10.1002/KIN.550271006, 1995.

Tyndall, G. S., Orlando, J. J., Wallington, T. J., Sehested, J., and Nielsen, O. J.: Kinetics of the reactions of acetonitrile with chlorine and fluorine atoms, J. Phys. Chem., 100, 660–668, doi:10.1021/jp9521417, 1996.

Tyndall, G. S., Cox, R. A., Granier, C., Lesclaux, R., Moortgat, G. K., Pilling, M. J., Ravishankara, A. R., and Wallington, T. J.: The atmospheric chemistry of small organic peroxy radicals, J. Geophys. Res., 106D, 12 157–12 182, doi:10.1029/2000JD900746, 2001a.

Tyndall, G. S., Orlando, J. J., Wallington, T. J., and Hurley, M. D.: Products of the chlorine-atom- and hydroxyl-radical-initiated oxidation of CH_3CN, J. Phys. Chem. A, 105, 5380–5384, doi:10.1021/jp004318p, 2001b.

van den Bergh, H. and Troe, J.: Kinetic and thermodynamic properties of INO and INO_2 intermediate complexes in iodine recombination, J. Chem. Phys., 64, 736–742, doi:10.1063/1.432220, 1976.

van Loon, L., Mader, E., and Scott, S. L.: Reduction of the aqueous mercuric ion by sulfite: UV spectrum of $HgSO_3$ and its intramolecular redox reaction, J. Phys. Chem. A, 104, 1621–1626, doi:10.1021/JP994268S, 2000.

van Loon, L. L., Mader, E. A., and Scott, S. L.: Sulfite stabilization and reduction of the aqueous mercuric ion: Kinetic determination of sequential formation constants, J. Phys. Chem. A, 105, 3190–3195, doi:10.1021/JP003803H, 2001.

Vereecken, L. and Francisco, J. S.: Theoretical studies of atmospheric reaction mechanisms in the troposphere, Chem. Soc. Rev., 41, 6259–6293, doi:10.1039/c2cs35070j, 2012.

Vereecken, L. and Peeters, J.: A theoretical study of the OH-initiated gas-phase oxidation mechanism of β-pinene ($C_{10}H_{16}$): first generation products, Phys. Chem. Chem. Phys., 14, 3802–3815, doi:10.1039/c2cp23711c, 2012.

Vereecken, L., Müller, J.-F., and Peeters, J.: Low-volatility poly-oxygenates in the OH-initiated atmospheric oxidation of α-pinene: impact of non-traditional peroxyl radical chemistry, Phys. Chem. Chem. Phys., 9, 5241–5248, doi:10.1039/b708023a, 2007.

Vereecken, L., Harder, H., and Novelli, A.: The reaction of Criegee intermediates with NO, RO_2, and SO_2, and their fate in the atmosphere, Phys. Chem. Chem. Phys., 14, 14 682–14 695, doi:10.1039/c2cp42300f, 2012.

Vereecken, L., Harder, H., and Novelli, A.: The reactions of Criegee intermediates with alkenes, ozone, and carbonyl oxides, Phys. Chem. Chem. Phys., 16, 4039–4049, doi:10.1039/c3cp54514h, 2014.

von Glasow, R., Sander, R., Bott, A., and Crutzen, P. J.: Modeling halogen chemistry in the marine boundary layer, 1. Cloud-free MBL, J. Geophys. Res., 107D, 4341, doi:10.1029/2001JD000942, 2002.

von Kuhlmann, R.: Tropospheric photochemistry of ozone, its precursors and the hydroxyl radical: A 3D-modeling study considering non-methane hydrocarbons, Ph.D. thesis, Johannes Gutenberg-Universität, Mainz, Germany, 2001.

von Kuhlmann, R., Lawrence, M. G., Crutzen, P. J., and Rasch, P. J.: A model for studies of tropospheric ozone and nonmethane hydrocarbons: Model description and ozone results, J. Geophys. Res., 108D, 4294, doi:10.1029/2002JD002893, 2003.

Wagman, D. D., Evans, W. H., Parker, V. B., Schumm, R. H., Halow, I., Bailey, S. M., Churney, K. L., and Nuttall, R. L.: The NBS tables of chemical thermodynamic properties; Selected values for inorganic and C_1 and C_2 organic substances in SI units, J. Phys. Chem. Ref. Data, 11, suppl. 2, 1982.

Wagner, I. and Strehlow, H.: On the flash photolysis of bromide ions in aqueous solution, Ber. Bunsenges. Phys. Chem., 91, 1317–1321, doi:10.1002/BBPC.19870911203, 1987.

Wallington, T. J., Ammann, M., Cox, R. A., Crowley, J. N., Herrmann, H., Jenkin, M. E., McNeill, V., Mellouki, A., Rossi, M. J., and Troe, J.: IUPAC Task group on atmospheric chemical kinetic data evaluation: Evaluated kinetic data, http://iupac.pole-ether.fr, 2018.

Wang, T. X. and Margerum, D. W.: Kinetics of reversible chlorine hydrolysis: Temperature dependence and general-acid/base-assisted mechanisms, Inorg. Chem., 33, 1050–1055, doi:10.1021/IC00084A014, 1994.

Wang, T. X., Kelley, M. D., Cooper, J. N., Beckwith, R. C., and Margerum, D. W.: Equilibrium, kinetic, and UV-spectral characteristics of aqueous bromine chloride, bromine, and chlorine species, Inorg. Chem., 33, 5872–5878, doi:10.1021/IC00103A040, 1994.

Wang, Y. L., Nagy, J. C., and Margerum, D. W.: Kinetics of hydrolysis of iodine monochloride measured by the pulsed-accelerated-flow method, J. Am. Chem. Soc., 111, 7838–7844, doi:10.1021/JA00202A026, 1989.

Wang, Z. and Pehkonen, S. O.: Oxidation of elemental mercury by aqueous bromine: atmospheric implications, Atmos. Environ., 38, 3675–3688, doi:10.1016/J.ATMOSENV.2004.02.059, 2004.

Warneck, P.: Chemical reactions in clouds, Fresenius J. Anal. Chem., 340, 585–590, doi:10.1007/BF00322434, 1991.

Warneck, P.: The relative importance of various pathways for the oxidation of sulfur dioxide and nitrogen dioxide in sunlit continental fair weather clouds, Phys. Chem. Chem. Phys., 1, 5471–5483, doi:10.1039/A906558J, 1999.

Warneck, P.: The oxidation of sulfur(IV) by reaction with iron(III): a critical review and data analysis, Phys. Chem. Chem. Phys., 20, 4020–4037, doi:10.1039/c7cp07584g, 2018.

Wayne, R. P., Barnes, I., Biggs, P., Burrows, J. P., Canosa-Mas, C. E., Hjorth, J., Le Bras, G., Moortgat, G. K., Perner, D., Poulet, G., Restelli, G., and

Sidebottom, H.: The nitrate radical: Physics, chemistry, and the atmosphere, Atmos. Environ., 25A, 1–203, doi:10.1016/0960-1686(91)90192-A, 1991.

Weast, R. C., ed.: CRC Handbook of Chemistry and Physics, 61st Edition, CRC Press, Inc., Boca Raton, FL, 1980.

Weinstein-Lloyd, J. and Schwartz, S. E.: Low-intensity radiolysis study of free-radical reactions in cloudwater: H_2O_2 production and destruction, Environ. Sci. Technol., 25, 791–800, doi:10.1021/ES00016A027, 1991.

Welz, O., Savee, J. D., Osborn, D. L., Vasu, S. S., Percival, C. J., Shallcross, D. E., and Taatjes, C. A.: Direct kinetic measurements of Criegee intermediate (CH_2OO) formed by reaction of CH_2I with O_2, Science, 335, 204–207, doi:10.1126/science.1213229, 2012.

Welz, O., Eskola, A. J., Sheps, L., Rotavera, B., Savee, J. D., Scheer, A. M., Osborn, D. L., Lowe, D., Booth, A. M., Xiao, P., Khan, M. A. H., Percival, C. J., Shallcross, D. E., and Taatjes, C. A.: Rate coefficients of C1 and C2 Criegee intermediate reactions with formic and acetic acid near the collision limit: Direct kinetics measurements and atmospheric implications, Angew. Chem., 126, 4635–4638, doi:10.1002/ange.201400964, 2014.

Wine, P. H., Tang, Y., Thorn, R. P., Wells, J. R., and Davis, D. D.: Kinetics of aqueous phase reactions of the SO_4^- radical with potential importance in cloud chemistry, J. Geophys. Res., 94D, 1085–1094, doi:10.1029/JD094ID01P01085, 1989.

Wingenter, O. W., Sive, B. C., Blake, N. J., and Rowland, F. S.: Atomic chlorine concentrations determined from ethane and hydroxyl measurements made over the Central Pacific Ocean, Eos, Trans. AGU (Abstract Supplement), 80, F149–F150, 1999.

Wu, D., Wong, D., and Di Bartolo, B.: Evolution of Cl_2^- in aqueous NaCl solutions, J. Photochem., 14, 303–310, doi:10.1016/0047-2670(80)85102-1, 1980.

Yiin, B. S. and Margerum, D. W.: Nonmetal redox kinetics: reactions of iodine and triiodide with sulfite and hydrogen sulfite and the hydrolysis of iodosulfate, Inorg. Chem., 29, 1559–1564, doi:10.1021/IC00333A023, 1990.

Yin, F., Grosjean, D., and Seinfeld, J. H.: Photooxidation of dimethyl sulfide and dimethyl disulfide. I: Mechanism development, J. Atmos. Chem., 11, 309–364, doi:10.1007/BF00053780, 1990.

Yoon, M.-C., Choi, Y. S., and Kim, S. K.: The OH production from the $\pi - \pi^*$ transition of acetylacetone, Chem. Phys. Lett., 300, 207–212, doi:10.1016/S0009-2614(98)01373-6, 1999.

Yu, X.-Y.: Critical evaluation of rate constants and equilibrium constants of hydrogen peroxide photolysis in acidic aqueous solutions containing chloride ions, J. Phys. Chem. Ref. Data, 33, 747–763, doi:10.1063/1.1695414, 2004.

Zehavi, D. and Rabani, J.: The oxidation of aqueous bromide by hydroxyl radicals. A pulse radiolytic investigation, J. Phys. Chem., 76, 312–319, doi:10.1021/J100647A006, 1972.

Zellner, R., Hartmann, D., Karthäuser, J., Rhäsa, D., and Weibring, G.: A laser photolysis/LIF study of the reactions of $O(^3P)$ atoms with CH_3 and CH_3O_2 radicals, J. Chem. Soc. Faraday Trans. 2, 84, 549–568, doi:10.1039/f29888400549, 1988.

Zellner, R., Exner, M., and Herrmann, H.: Absolute OH quantum yield in the laser photolysis of nitrate, nitrite and dissolved H_2O_2 at 308 and 351 nm in the temperature range 278-353 K, J. Atmos. Chem., 10, 411–425, doi:10.1007/BF00115783, 1990.

Ziajka, J., Beer, F., and Warneck, P.: Iron-catalysed oxidation of bisulphit aqueous solution: evidence for free radical chain mechanism, Atmos. Environ., 28, 2549–2552, doi:10.1016/1352-2310(94)90405-7, 1994.

C. Datasheets

Ø273 µm Core TECS-Coated Multimode Optical Fiber

Item #	Wavelength Range	Hydroxyl Content	Core Diameter	Cladding Diameter	Coating Diameter	Buffer Diameter	Core/ Cladding	Coating[a]	Buffer	Proof Test
FG273UEC	250 - 1200 nm[b]	High OH	273 ± 10 µm	300 ± 6 µm	330 ± 10 µm	400 ± 30 µm	Pure Silica / Fluorine-Doped Silica	TECS Hard Fluoropolymer	Tefzel	≥100 kpsi
FG273LEC	400 - 2200 nm	Low OH								

Item #	NA	Max Power Capability		Max Attenuation @ 808 nm	Max Core-Cladding Offset	Max Core-TECS Offset	Bend Radius		Operating Temperature	Strip Tool	Core Index	Cladding Index
		Pulsed[c]	CW[d]				Short Term	Long Term				
FG273UEC	0.22 ± 0.02	1.87 MW	0.37 kW	10 dB/km	4 µm	7 µm	16 mm	32 mm	-60 to 125 °C	T14S18[e]	See Table in *Overview* Tab	Proprietary[f]
FG273LEC												

a. This coating acts as a second cladding with an NA of 0.39, which is calculated from the index difference between the TECS coating to the core, rather than between the silica cladding and the TECS coating/second cladding.
b. Solarization may occur at wavelengths below 300 nm. We also offer solarization-resistant multimode fiber.
c. Based on 5 GW/cm^2 for 1064 nm Nd:YAG laser with 10 ns pulse length and input spot size equal to 80% of the core diameter.
d. Based on 1 MW/cm^2 for 1064 nm Nd:YAG laser and input spot size equal to 80% of the core diameter.
e. This tool will strip off the buffer for termination to the coating.
f. We regret that we cannot provide this proprietary information.

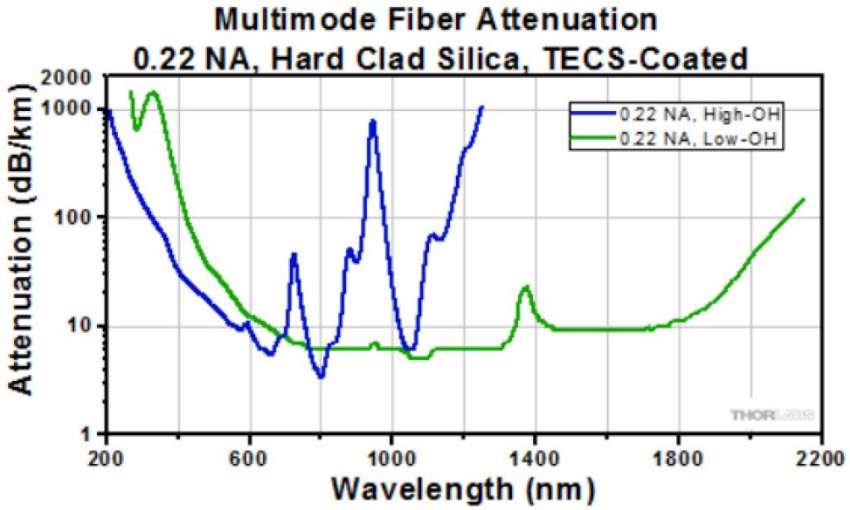

Figure C.1 Specifications of coated silica fiber used for transittance of 308 nm light through the HORUS instrument. (Information taken from specification listings, Thorlabs GmbH, Europe, Germany, www.thorlabs.de)

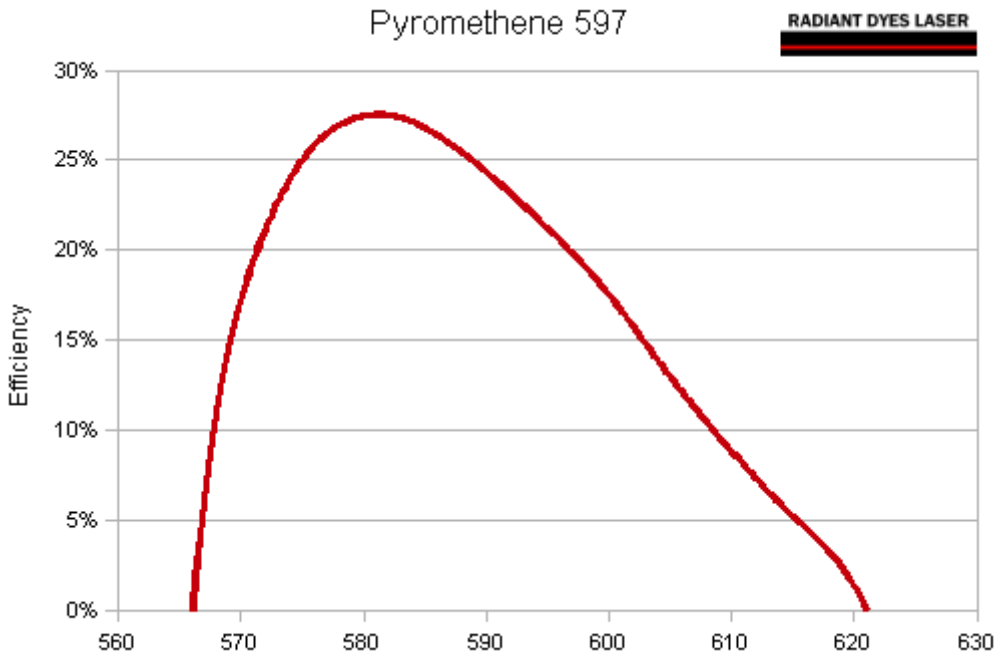

Figure C.2 Laser Dye, Pyrromethane-597 used in tunable dye laser powered by a diode-pumped Nd:YAG laser emitting 532 nm light. (Information taken from www.radiant-dyes.com)

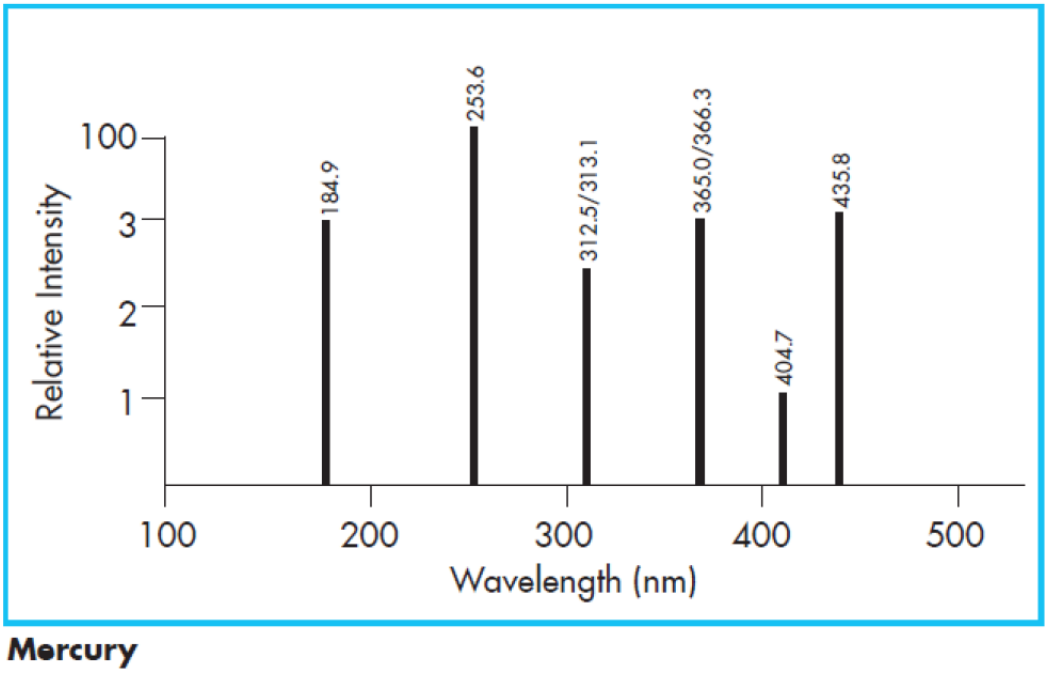

Figure C.3 Spectrum of the Pen-Ray line source used for the calibration of the HORUS instrument (Taken from manual, LOT-QuantumDesign, Europe, www.lot-qd.com)